ALFRED-WEGENER-INSTITUT
HELMHOLTZ-ZENTRUM FÜR POLAR- UND MEERESFORSCHUNG

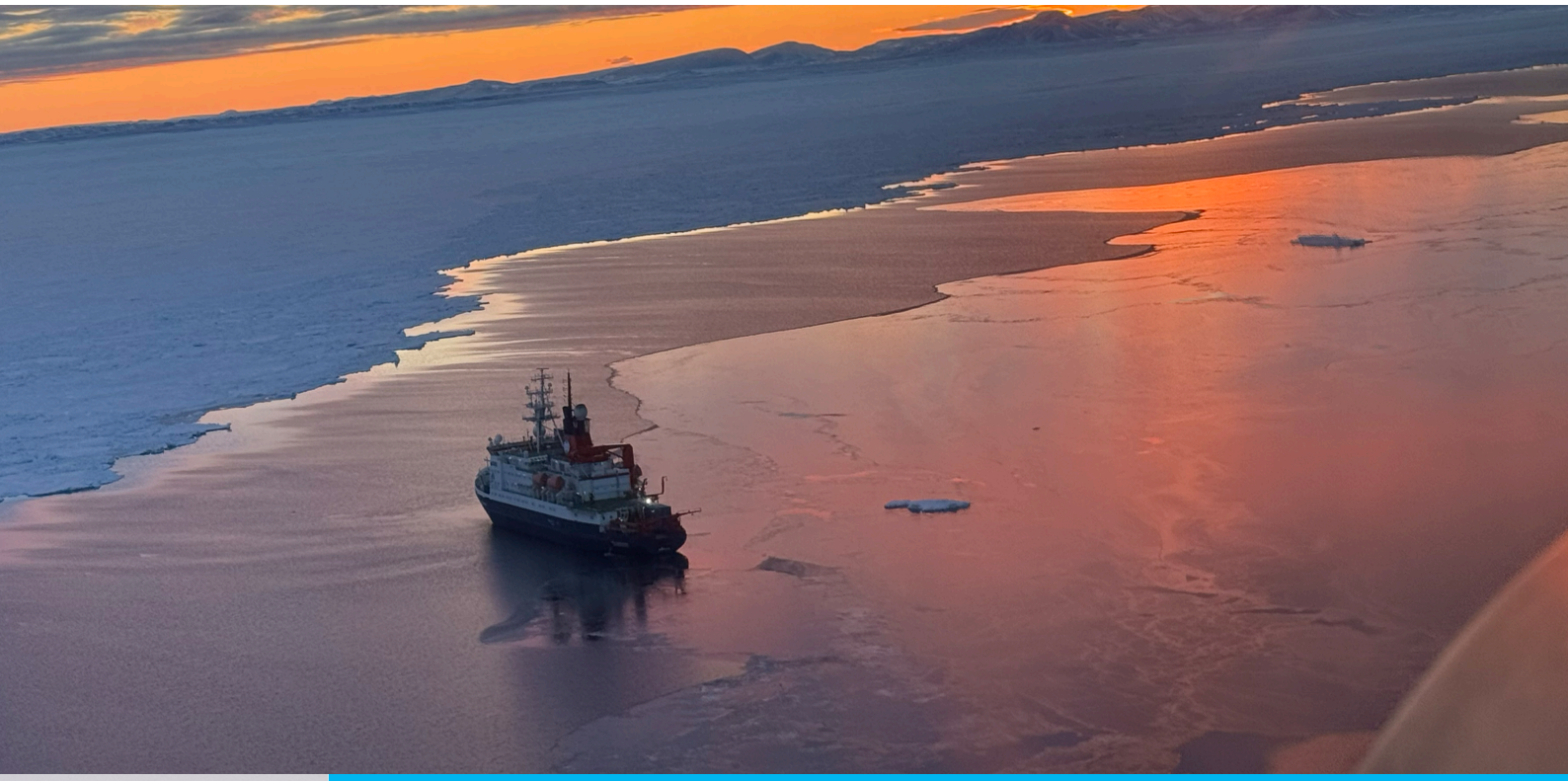

809
2026

Berichte
zur Polar- und Meeresforschung
Reports on Polar and Marine Research

The Expedition PS150 of the Research Vessel POLARSTERN to the Arctic Ocean in 2025

Edited by
Torsten Kanzow

with contributions of the participants

HELMHOLTZ

Die Berichte zur Polar- und Meeresforschung werden vom Alfred-Wegener-Institut, Helmholtz-Zentrum für Polar- und Meeresforschung (AWI) in Bremerhaven, Deutschland, in Fortsetzung der vormaligen Berichte zur Polarforschung herausgegeben. Sie erscheinen in unregelmäßiger Abfolge.

Die Berichte zur Polar- und Meeresforschung enthalten Darstellungen und Ergebnisse der vom AWI selbst oder mit seiner Unterstützung durchgeführten Forschungsarbeiten in den Polargebieten und in den Meeren.

Die Publikationen umfassen Expeditionsberichte der vom AWI betriebenen Schiffe, Flugzeuge und Stationen, Forschungsergebnisse (inkl. Dissertationen) des Instituts und des Archivs für deutsche Polarforschung, sowie Abstracts und Proceedings von nationalen und internationalen Tagungen und Workshops des AWI.

Die Beiträge geben nicht notwendigerweise die Auffassung des AWI wider.

Herausgeber
Dr. Horst Bornemann

Redaktionelle Bearbeitung und Layout
Susan Amir Sawadkuhi

Alfred-Wegener-Institut
Helmholtz-Zentrum für Polar- und Meeresforschung
Am Handelshafen 12
27570 Bremerhaven
Germany

www.awi.de
www.awi.de/reports

The Reports on Polar and Marine Research are issued by the Alfred Wegener Institute, Helmholtz Centre for Polar and Marine Research (AWI) in Bremerhaven, Germany, succeeding the former Reports on Polar Research. They are published at irregular intervals.

The Reports on Polar and Marine Research contain presentations and results of research activities in polar regions and in the seas either carried out by the AWI or with its support.

Publications comprise expedition reports of the ships, aircrafts, and stations operated by the AWI, research results (incl. dissertations) of the Institute and the Archiv für deutsche Polarforschung, as well as abstracts and proceedings of national and international conferences and workshops of the AWI.

The papers contained in the Reports do not necessarily reflect the opinion of the AWI.

Editor
Dr. Horst Bornemann

Editorial editing and layout
Susan Amir Sawadkuhi

Alfred-Wegener-Institut
Helmholtz-Zentrum für Polar- und Meeresforschung
Am Handelshafen 12
27570 Bremerhaven
Germany

www.awi.de
www.awi.de/en/reports

Titel:*An der Mündung des Independence Fjords, Nordgrönland. Foto: Torsten Kanzow, AWI*

Title: *At the mouth of Independence Fjord, North Greenland. Photo: Torsten Kanzow, AWI*

The Expedition PS150 of the Research Vessel POLARSTERN to the Arctic Ocean in 2025

Edited by

Torsten Kanzow
with contributions of the participants

Please cite or link this publication using the identi iers

https://epic.awi.de/id/eprint/60780/
https://doi.org/10.57738/BzPM_0809_2026

ISSN 1866-3192

PS150 / EGC Sources

4 September 2025 – 23 October 2025

Longyearbyen – Bremerhaven

Chief scientist
Torsten Kanzow

Coordinator
Ingo Schewe

Contents

1. ÜBERBLICK UND EXPEDITIONSVERLAUF

Torsten Kanzow DE.AWI

Am Abend des 4. September 2025 verließ das Forschungsschiff *Polarstern* Longyearbyen und startete damit die EGC-Sources-Expedition (PS150) bei ruhigen Wetterbedingungen. Das Schiff navigierte zunächst westwärts durch den Isfjorden, bevor es nach Norden entlang der rauen Küste Svalbards abbog und Kurs auf das Untersuchungsgebiet nahm. Das 45-köpfige Team aus Wissenschaftler:innen, Techniker:innen und Studierenden begann sofort mit den Vorbereitungen der Instrumente für die anstehenden Arbeiten. Ziel der Expedition war es, die Quellen des Ostgrönlandstroms entlang der Küste Nordost- und Nordgrönlands zu erforschen – eine entscheidende Route für arktische Wassermassen, die in das Europäische Nordmeer einströmen und den Wärmetransport zu Grönlands Gletschern beeinflussen. Dazu zählen sowohl kaltes, süßes Polarwasser (PW) an der Meeresoberfläche als auch wärmeres, salzhaltigeres Wasser in mittleren Tiefen, hier als Atlantisches Wasser (AW) bezeichnet. Trotz der Bedeutung dieser Region ist sie nur unzureichend erforscht, und historische ozeanographische Messdaten sind rar. Die *EGC-Sources* Expedition verfolgt wichtige Ziele des „Erde und Umwelt" Programms POF IV der Helmholtz-Gemeinschaft.

Nach einer Teststation am 5. September wurde am Morgen des 6. September eine Langzeitverankerung am westlichen Hang des Yermak-Plateaus geborgen. Diese war drei Jahre zuvor von der Universität Bergen während der Expedition PS131 ausgebracht worden. Ihre Daten sollen das Verständnis interner Wellen und Vermischungsprozesse in diesem „Hotspot“ des Arktischen Ozeans verbessern.

Zwischen dem 7. September und 11. September konzentrierte sich die Expedition auf einen hochauflösenden hydrographischen Transekt, der nordost-südwestlich quer durch das Randstromsystem vor der Flade-Isblink-Eiskappe (Nordostgrönland) verlief. Ursprünglich mit einer Auflösung von 5 Seemeilen geplant, wurde der Transekt über der Kontinentalschelfkante auf 2,5 Seemeilen verfeinert. Zum Einsatz kamen eine CTD-Rosette (Conductivity-Temperature-Depth), ein MultiNet-Zooplankton-Probennehmer, ein Lichtprofiler und ein Mikrostruktur-Turbulenzprofiler (MSS). Das 80 Seemeilen lange Transekt erstreckte sich vom offenen Ozean über die Schelfkante bis in die Küstenzone, wobei dichtes Packeis nahe der Küste eine südliche Abweichung von der geplanten Linie erforderlich machte. Trotz dieser Herausforderung war der Abschnitt sehr erfolgreich und lieferte wichtige ozeanographische Daten, darunter den Nachweis eines starken südwärts gerichteten Küstenstroms, der möglicherweise mit Strömungen im nahegelegenen Independence-Fjord zusammenhängt. Während dieser Phase war die Neubildung von Eis deutlich sichtbar – ein Phänomen, das die gesamte Reise entlang der grönländischen Küste begleitete. Zudem führten die Wissenschaftler:innen helikoptergestützte EM-Bird-Vermessungen zur Eisdickenmessung durch und testeten ein autonomes Oberflächenfahrzeug auf dem Kontinentalschelf.

Am 11. September erreichte die *Polarstern* den breiten Schelf vor dem Independence-Fjord, wo das Team Ozeanbodenseismometer (OBS) ausbrachte. Festes Eis blockierte jedoch den Zugang zum Fjord, sodass auf bathymetrische und hydrographische Untersuchungen der Fjordmündung ausgewichen wurde. Gleichzeitig ermöglichte der Helikopter CTD-Messungen im Independence-Fjord und im benachbarten Hagen-Fjord, um Austauschprozesse zwischen Fjord und Ozean zu studieren. Im gesamten Fjordsystem wurden warme, atlantische Wassermassen in mittleren Tiefen nachgewiesen. Nach Abschluss der Arbeiten im Fjordsystem setzte die Expedition ihre Fahrt nordwestwärts auf dem Schelf in Richtung

Wandelmeer fort. Auf dem Weg zum nächsten hydrographischen Schnitt führte das Team am 13. September eine achtstündige Eistation durch, die physikalische, ozeanographische, biogeochemische und biologische Probenahmen umfasste.

Am 14. September begann ein 80 Seemeilen langer hydrographischer Transekt von der Küste über die Schelfkante in den offenen Ozean des Wandelmeers, mit einer ähnlichen räumlichen Auflösung wie beim Flade-Isblink-Transekt. Ein 10 Seemeilen langer Küstenabschnitt blieb jedoch aufgrund von Festeis unzugänglich, sodass helikoptergestützte CTD-Einsätze notwendig waren, um den Transekt bis zur Küste zu verlängern. Hier zeigte das schiffsgebundene ADCP einen eher schwachen Küstenstrom und eine südwärts gerichtete Oberflächen- und Tiefenströmung an der Schelfkante.

Bis zum 18. September war der Transekt abgeschlossen, und die *Polarstern* setzte ihre Fahrt nordwestwärts im offenen Ozean in Richtung Morris-Jesup-Rücken (MJR) fort – eine submarine Erhebung, die vom Schelf vor Peary Land in den Ozean ragt und als bedeutendes Hindernis für das Randstromsystem gilt. Am 19. September begann ein hydrographisches Profil vom tiefen Ozean bis zum Kamm des MJR, um die Zirkulation von AW und PW entlang des südlichen Hangs des MJR zu untersuchen. An diesem Tag wurde zudem eine weitere EM-Bird-Vermessung durchgeführt. Am 20. September setzten Helikopter-CTDs die vorherige Wandelmeer-Sektion weiter seewärts fort.

Bis zum 21. September war die schiffsbasierte MJR-Sektion abgeschlossen, und eine weitere multidisziplinäre Eistation fand statt. Die Expedition folgte dann dem Kamm des MJR in Richtung des grönländischen Schelfs und begann am 22. September einen weiteren hydrographischen Transekt zur Küste von Peary Land nahe Kap Morris Jesup, der am 23. September abgeschlossen wurde. Ziel war es, die Wassermassen zu untersuchen, die über die submarine Erhebung auf dem Schelf und entlang der Schelfkante strömen. Zwei küstennahe Stationen mussten aufgrund von Festeis gestrichen werden. Die Messungen zeigten einen intensiven nordwestwärts gerichteten Küstenstrom (nachgewiesen durch das schiffsmontierte ADCP) und relativ salzhaltiges Wasser nahe der Küste (im Vergleich zu weiter seewärts), was auf eine geostrophische Strömung in dieser Richtung hindeutet. Um die Beständigkeit dieses Stroms über die Zeit zu untersuchen, wurden zwei Mini-Verankerungen auf dem Schelf ausgebracht (eine mit CTD, eine mit CTD und Strömungsmesser), die im folgenden Jahr geborgen werden sollen.

Bemerkenswert ist, dass die beobachtete Küstenströmung entgegengesetzt zu der am Flade-Isblink-Transekt verlief. Der Helikopter führte erneut EM-Bird- und CTD-Arbeiten durch und konnte zwei von fünf geplanten Landungen am seewärtigen Ende des Morris-Jesup-Rückens durchführen, das für das Schiff nicht erreichbar war. Während dieser Phase stellten dichtes Eis und große Schollen eine Herausforderung für das Messprogramm dar. Teilweise waren Eisaufklärungsflüge notwendig, doch schließlich fand sich eine Passage. Es schien, als würden windgetriebene, divergente Eisschollen häufig Rinnen öffnen. Ob dies ein typisches Phänomen in der Region oder nur ein glücklicher Zufall war, bleibt unklar.

Nach Abschluss der Küstenabschnitte bei Kap Morris Jesup verschlechterte sich die Eissituation nach Westen hin zusehends, und Satellitenbilder zeigten kaum offenes Wasser. Daher wurde beschlossen, nicht weiter westwärts in die Lincolnsee vorzudringen, um einen weiteren hydrographischen Schnitt vor West-Peary-Land durchzuführen. Stattdessen wurde eine einzige tiefe Multigeräte-Station („Almost Lincoln“) knapp westlich des MJR an der Schelfkante durchgeführt, um Wasser- und Netzproben aus dem stromaufwärts gelegenen hydrographischen Regime zu gewinnen. Die Eisbedingungen erschwerten den Schiffstransit erheblich und verursachten Verzögerungen.

In Erwartung der notwendigen Gebietsgenehmigungen wurde am 23. September eine Voraberkundung für die Installation eines Landseismometers im Gebiet von Kap Skagen durchgeführt. Am 24. September erteilten die grönländischen Behörden die Genehmigungen, und bis zum 25. September waren die Landstationen eingerichtet: Seismometer an zwei Standorten (eines auf Peary Land, eines auf Kap Skagen) sowie eine zusätzliche GNSS-

Station auf Peary Land. Gute Flugbedingungen ermöglichten es dem Team zusätzlich, weit nach Westen zu fliegen und eine 6-Stationen-XCTD-Vermessung über die Schelfkante hinweg bei 33°W durchzuführen. Abschließend wurde eine achstündige Eistation (die dritte der Expedition) südlich des Morris-Jesup-Rückens abgeschlossen. Hierbei wurde ein eisverankerter Ozeanprofiler (TOP) ausgesetzt, um mit dem Eis entlang des Kontinentalhangs nach Süden zu driften. Diese Station beendete die Arbeiten im nördlichsten Einsatzgebiet, und die anschließende Transitphase bot Gelegenheit für ein Grillfest.

Bis zum 28. September hatte die Expedition sich südwärts entlang des Schelfs bewegt und eine Lücke in der bathymetrischen Kartierung vor dem Independence-Fjord geschlossen. Hierbei wurde ein Trog von der Schelfkante zum Fjord entdeckt. Ein hydrographischer Transekt mit sieben Stationen über die Kontinentalschelfkante vor dem Independence-Fjord wurde abgeschlossen, begleitet von einem weiteren EM-Bird-Flug und helikoptergestützter Probenahme im Fasteis des äußeren Fjords. Zudem wurde eine Mini-Verankerung auf der nördlichen Schulter des Trogs ausgebracht – dem wahrscheinlichsten Weg für atlantische Wassermassen in den Independence-Fjord, wie durch Strömungsmessungen durch das schiffgebundene ADCP nahegelegt. Die Ausbringung erfolgte von einer Eisscholle aus, logistisch unterstützt durch den Helikopter.

Bis zum 30. September war eine ozeanographische Boje im Fasteis auf dem inneren (südlichen) Schelf vor dem Independence-Fjord installiert worden, die die weiter nördlich liegende Mini-Verankerung ergänzte. Zwei weitere Verankerungen wurden auf dem Schelf vor dem Flade-Isblink-Eisschild ausgebracht, entlang desselben „Flade-Isblink“-Transekts, das auf der Anreise nach Norden bereits mit einem engmaschig beprobten hydrographischen Schnitt untersucht worden war. Das Meereis behinderte den Transit in diesem Gebiet besonders (mehrstündiger Maschinenstopp) und war deutlich kompakter als beim ersten Besuch, sodass Eisaufklärung notwendig wurde. Bis zum 2. Oktober waren alle sechs Verankerungen ausgebracht, begleitet von nächtlichen hydrographischen (Multigeräte-) Stationen. Die Ausbringung einer Verankerung in steilem Gelände an der Schelfkante war besonders anspruchsvoll, aber letztlich erfolgreich. Zwei EM-Bird-Vermessungen wurden durchgeführt, womit die Feldarbeiten in Nordgrönland abgeschlossen waren. Eine geplante Eistation nach Abschluss der Verankerungsarbeiten musste aufgrund von starkem Wind und schlechter Sicht abgesagt werden.

Bis zum 4. Oktober waren vier ozeanbodenseismische Messgeräte in den tiefen Gewässern der nördlichen Framstraße ausgebracht worden. Das Meereis in diesem Gebiet bestand aus sehr kleinen Schollen, die offenbar durch Dünung zertrümmert worden waren. Daher wurden Eisstationsarbeiten verschoben, und das Team begann stattdessen mit der Bergung von eisgebundenen Messgeräten, die während der Expedition PS149 nördlich von Grönland installiert worden waren. Die ursprüngliche Scholle war inzwischen in mehrere Teile zerbrochen, die durch den Ostgrönlandstrom nach Süden vertrieben worden waren und nun über 100 Meilen voneinander entfernt lagen. Die Expedition folgte dem Ostgrönlandstrom südwärts und hatte bis zur Nacht vom 5. auf den 6. Oktober alle Bergungen abgeschlossen. Eine Kameraboje, ein ADCP und Reste einer Schneeboje konnten u.a. erfolgreich geborgen werden, während andere Geräte nicht gefunden wurden.

Entlang 78°10’N, in eisfreien Gewässern, fuhr die Expedition weit auf den inneren Schelf bis zum Norske-Trog, wo die Arbeiten im letzten Expeditionsgebiet begannen. In der Nacht zum 7. Oktober, bei schnell zunehmenden Winden, wurde die IdF-3_2-Verankerung geborgen, die 2022 im Atlantischen-Wasser-Zuflussweg zum 79°N-Gletscher ausgebracht worden war. Ursprünglich war ein Multigeräte-Transekt mit acht Stationen quer über den Norske-Trog von Nordost nach Südwest (Ile-de-France) geplant. Aufgrund eines herannahenden Sturms konnten jedoch nur die drei östlichen Stationen um die Verankerungsposition mit CTDs beprobt werden, während andere Geräte (z. B. Netze, MSS) nicht zum Einsatz kamen. Um dem schwersten Teil des Sturms an der grönländischen Küste zu entgehen, fuhr die *Polarstern* ostwärts bis 12°W und anschließend nordwärts durch Schneesturm und dichtes Eis über die Belgica-Bank in Richtung Westwind-Trog. Schweres Eisbrechen war erforderlich,

und an einem Punkt mussten die Maschinen abgestellt werden, da kein Vorankommen möglich war.

Bis zum 10. Oktober war der „Flade-Schelf“-Transekt abgeschlossen, der nordwärts über den Westwind-Trog führte (wobei der Fortschritt durch das Eis weiterhin langsam war). Die Expedition bewegte sich dann westwärts entlang der Küstenpolynya, die sich durch die nordöstlichen Sturmwinde geöffnet hatte, führte eine MUC-Station durch und beendete die vierte Eistation auf einer mehrere Kilometer langen Scholle aus ehemaligem Festeis. Das Team barg zudem eine GNSS-Station vom Holm Land-Standort und richtete ein landgestütztes seismisches Netzwerk mit drei Stationen ein (Kap Anna Bistrup, Norske Øer und die Südküste des 79°N-Gletschers). Gute Flugbedingungen ermöglichten eine Vorabinspektion des Meereises nahe der Kalbungsfront des 79N-Gletschers für eine mögliche Verankerungs-/Bojen-Ausbringung.

In den folgenden Tagen wurde ein kurzer Transekt vor Holm Land durchgeführt, der den westlichen Teil des Westwind-Trogs abdeckte. Die zentralen und östlichen Abschnitte in Richtung Belgica-Bank blieben aufgrund von dickem, dichtem Eis („Porridgeeis“, wie es die nautische Crew nannte) unzugänglich. Per Helikopter brachte das Team eine Mini-Verankerung und eine ozeanographische Boje im Festeis direkt an der Kalbungsfront des 79N-Gletschers aus. Vom Holm-Transekt aus fuhr das Schiff südwärts, passierte die Einfahrt zum 79N-Fjord, wo eine MUC-Station erfolgreich geborgen wurde und installierte/wartete in einem weiteren Helikoptereinsatz eine geodätische GNSS-Station auf Lambert Land (LAMW). Die Expedition erreichte dann die Nordspitze von Norske Øer, von wo aus ein weiterer Transektversuch ostwärts über den Norske-Trog unternommen wurde. Nach drei Stationen musste die Arbeit jedoch wegen dichtem Eis eingestellt werden. Hier wurde eine Verankerung ausgebracht, um den Zustrom von Atlantischem Wasser zum 79°N-Gletscher zu erfassen. Gegen Mitternacht des 12. Oktober wurden die Stationsarbeiten abgeschlossen. In diesen Tagen behinderte das Meereis die Schiffsbewegung zunehmend, und die Tageslichtperiode wurde immer kürzer.

Während eines weiteren Sturms mit Schnee am 13. Oktober kehrte die *Polarstern* nach Norden in Richtung Westwind-Trog zurück. Es dauerte zwei volle Tage, um Holm Land (70 Seemeilen direkte Entfernung) zu erreichen, und erst in den Morgenstunden des 17. Oktober konnte das Schiff das Eis verlassen, nachdem es den Ostgrönlandstrom bei 80°N überquert hatte. Nach einem Zwischenstopp in Longyearbyen am 18. Oktober, um die „Grönlandgewehre“ (Kaliber 30.06) an den Händler zurückzugeben, setzte die Expedition ihre Rückreise nach Bremerhaven fort, durchquerte am 19. Oktober einen weiteren Sturm und traf dort am 24. Oktober – einen Tag später als geplant – ein.

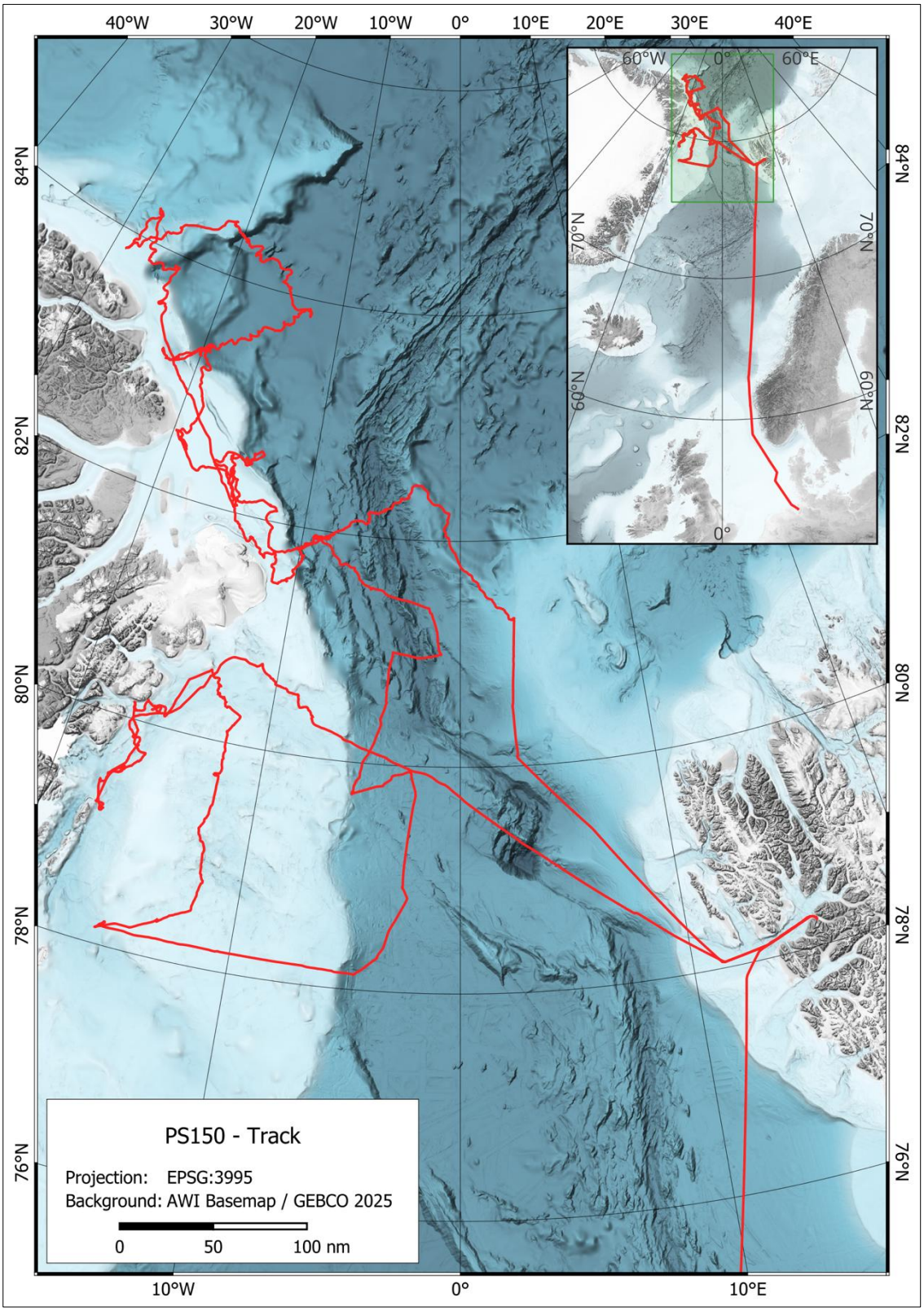

Abb. 1: Route der Expedition PS150. Siehe https://doi.pangaea.de/10.1594/PANGAEA.987832 des master tracks in Verbindung mit der Stationsliste der Expedition PS150.

Fig. 1: Track of expedition PS150. See https://doi.pangaea.de/10.1594/PANGAEA.987832 to display the master track in conjunction with the station list of expedition PS150.

SUMMARY AND ITINERARY

On the evening of 4 September 2025, the research vessel *Polarstern* departed from Longyearbyen, marking the start of the EGC-Sources expedition (PS150) under calm weather conditions. The vessel navigated westward through Isfjorden before turning north along Svalbard's rugged coastline, setting course for the study area. The onboard team of 45 scientists, technicians, and students immediately began preparing instruments for the upcoming operations. This expedition aimed to investigate the sources of the East Greenland Current (EGC) along the coast of Northeast and North Greenland, a critical pathway for Arctic-derived water masses entering the Nordic Seas and influencing heat transport to Greenland's glaciers. This includes both cold, fresh Polar Waters (PW) at the sea surface and intermediate-depth warmer, saline waters, referred to here as Atlantic Waters (AW). Despite its significance, this remote region remains poorly sampled, with few historical oceanographic measurements available. The *EGC-Sources* expedition addressed important goals of the program POF IV of the research field "Earth and Environment" of the Helmholtz Association.

After conducting a test station on 5 September, the team recovered a long-term mooring on the morning of 6 September from the western flank of the Yermak Plateau. This mooring had been deployed three years earlier by the University of Bergen during the expedition PS131. Its data will contribute to understanding internal waves and mixing in this Arctic Ocean hotspot.

Between 7 and 11 September, the expedition focused on a high-resolution hydrographic transect, oriented northeast-southwest across the boundary current system off Flade Isblink ice cap (Northeast Greenland). Originally designed with a 5-nautical-mile resolution, the transect was refined to 2.5 nautical miles across the continental shelf break. The survey employed a CTD (Conductivity-Temperature-Depth) rosette, a MultiNet zooplankton sampling system, a light profiler, and a microstructure turbulence profiler (MSS). The 80-nautical-mile transect extended from the open ocean across the shelf break to the coastal zone, though dense pack ice near the coast required a southward deviation from the planned survey line. Despite this challenge, the section proved highly successful in capturing critical oceanographic data, revealing, among other things, a strong southward coastal current, possibly related to ocean currents in the nearby Independence Fjord. Throughout this period, new ice formation was clearly visible – a phenomenon that would accompany the voyage along the coast of Greenland. During this time, the team also conducted helicopter-supported EM-Bird surveys to measure sea-ice thickness, while an autonomous surface vehicle underwent initial testing on the continental shelf.

On 11 September, *Polarstern* arrived on the wide shelf off Independence Fjord, where the team deployed ocean-bottom seismometers (OBS). However, fast ice blocked the ship's passage into the fjord, prompting a shift to bathymetric and hydrographic surveys of the fjord mouth. Meanwhile, the helicopter facilitated CTD casts within Independence Fjord and the adjacent Hagen Fjord to study fjord-ocean exchange processes. Warm subsurface Arctic Atlantic waters were encountered throughout the fjord system. Upon completing operations in the fjord system, the expedition proceeded northwestward on the shelf toward the Wandel Sea. *En route* to the next hydrographic survey line on 13 September, the team conducted an 8-hour ice station, integrating ice physics, physical oceanography, and biogeochemical and biological sampling.

On 14 September, the expedition initiated an 80-nautical-mile hydrographic survey from the coast across the shelf break toward the open ocean in the Wandel Sea, using a similar spatial

resolution as on the Flade Isblink transect. However, a 10-nautical-mile coastal segment remained inaccessible due to consolidated sea ice, necessitating helicopter-assisted CTD deployments to extend the transect to the shoreline. Here, the VMADCP revealed a rather weak coastal flow and a southward surface and subsurface flow off the shelf edge.

By 18 September, the survey was completed, and *Polarstern* began transiting northwestward in the open ocean toward Morris Jesup Rise (MJR), a submarine escarpment protruding into the ocean from the shelf off Peary Land. This topographic feature is thought to be a major obstacle for the boundary current system in this area, routing both PW and AW around it. A hydrographic section from the deep ocean toward the crest of MJR commenced on 19 September, aiming to observe AW and PW circulation bands moving onshore along the southern slope of MJR. Another EM-Bird survey was conducted on the same day. On 20 September, helicopter-assisted CTDs were deployed to extend the previous Wandel section further offshore.

By 21 September, the vessel-based MJR section was completed, and another multidisciplinary ice station took place. The expedition then followed the crest of MJR toward the shelf of Greenland, commencing another hydrographic section to the coast of Peary Land near Cape Morris Jesup on 22 September, which was finished on 23 September. The aim was to survey the waters passing over the submarine rise on the shelf and near the shelf break. The two near-coastal stations were canceled due to landfast ice. Observations revealed an intense northwestward coastal current from the vessel-mounted ADCP and rather saline waters near the coast (compared to further offshore), supporting a geostrophic flow in this direction. The decision was made to deploy two mini-moorings on the shelf (one equipped with a CTD, the other with a CTD and current meter) to investigate the persistence of this flow over time, with the moorings to be recovered the following year. Notably, the observed coastal flow was in the opposite direction to that found at the Flade Isblink line. Again, the helicopter was busy with EM-Bird and CTD work, completing two out of five planned landings at the offshore tip of Morris Jesup Rise, which was not accessible by ship. Throughout this period, dense ice cover and large floes posed challenges to the measurement program. At times, ice reconnaissance flights were necessary, but eventually, a passage was found. It appeared that wind-driven, divergent ice floes frequently opened up leads. Whether this is a usual phenomenon in the area or just a fortunate coincidence remains unclear.

Upon completing the onshore Cape Morris Jesup section, it became apparent that the ice situation to the west was worsening, with satellite-based ice imagery revealing little open water. Therefore, the decision was made not to attempt to proceed significantly further west (into the Lincoln Sea) to perform another hydrographic line off western Peary Land. Instead, one single deep multi-gear station was conducted just west of MJR, close to the shelf break, allowing water and net samples to be obtained from an upstream hydrographic regime. The ice conditions proved challenging for the ship's transit, causing major delays.

In anticipation of receiving the necessary area allotments, a pre-site survey was conducted on 23 September for the installation of a land seismometer in the Cape Skagen area. On 24 September, the allotments were finally granted by the Greenlandic authorities. By 25 September, the land station installations were completed. Seismometers were set up at two sites–one on Peary Land and the other on Cape Skagen – with an additional GNSS station installed at the Peary Land site. Excellent flight conditions allowed the team to fly far to the west to conduct a six-station (X)CTD survey across the shelf break near 33°W. Finally, an eight-hour ice station (the third of the expedition) was completed off the shelf south of Morris Jesup Rise. On this occasion, an ice-tethered mooring profiler (TOP) was deployed, to drift south with the ice along the continental slope. This station concluded the work in the northernmost area, and the subsequent transit provided an ideal opportunity for a barbecue.

By 28 September, the expedition had moved south along the shelf and closed a gap in the bathymetric charting off Independence Fjord, revealing a trough from the shelf edge to the fjord. A hydrographic section across the continental shelf break (seven stations) was completed off Independence Fjord, along with another EM-Bird flight and helicopter-supported

sampling in the fast ice of the outer fjord. Additionally, a mini-mooring was deployed on the northern shoulder of the trough – the most likely pathway for Atlantic waters to enter Independence Fjord, as suggested by the VMADCP. This deployment was carried out from an ice floe, again supported by helicopter.

By 30 September, an oceanographic buoy had been installed in the fast ice on the inner (southern) shelf off Independence Fjord, complementing the mini-mooring further north. Two mooring deployments were also completed on the shelf off Flade Isblink Ice Cap, along the same ("Flade Isblink") section where a densely spaced hydrographic section had been conducted on the northward journey. Sea ice particularly challenged progress in this area, with engines stopped for several hours, and appeared much more compact than during the first visit, necessitating ice reconnaissance. By 2 October, all six moorings had been deployed, accompanied by hydrographic station work (CTD, etc.) during the night hours. The deployment of one mooring – in steep terrain off the shelf break–was particularly challenging but ultimately successful. Two EM-Bird surveys were also conducted, concluding the North Greenland fieldwork of the expedition. One ice station that had been planned upon completion of the mooring work needed to be cancelled due to high wind and low visibility.

By 4 October, four ocean-bottom seismometers had been deployed in the deep waters of the northern Fram Strait. Sea ice in this area consisted of very small floes, apparently crushed by ocean swell. Ice station work was therefore postponed, and the team instead began recovering ice-borne instrumentation from a floe that had been installed during PS149 north of Greenland. The floe had subsequently broken into several pieces, which had been advected south by the East Greenland Current, spreading apart by 100 miles. Consequently, the expedition proceeded south along the East Greenland Current, and by the night of 5–6 October, had completed the recoveries. A camera buoy, an ADCP, and remains of a snow buoy were successfully retrieved, though some equipment could not be found.

Along 78°10'N, in ice-free waters, the expedition then proceeded far onto the inner shelf until reaching Norske Trough, commencing operations in the final working area. In the night of 7 October, with rapidly increasing winds, the team recovered the IdF-3_2 mooring, which had been deployed in 2022 in the Atlantic Water inflow pathway toward the 79°N Glacier. The original plan had been to carry out a multi-gear section with 8 stations across Norske Trough from northeast to southwest (Ile-de-France). However, with a major storm approaching, only the three eastern stations around the mooring location were covered by CTDs, while several other gears (e.g., nets, MSS) were canceled. To avoid the most severe part of the storm along the Greenland coast, *Polarstern* moved east to 12°W and subsequently north through snowstorms and dense ice across Belgica Bank toward Westwind Trough. Heavy ice breaking was required, and at one point, the engines were shut down as no progress was possible.

By the end of 10 October, the "Flade Shelf" section had been completed, finishing northward across Westwind Trough (with progress still slow through the ice). The expedition then moved westward along the coastal polynya that northerly storm winds had opened, carried out a MUC, and completed a fourth ice station on a several-kilometer-long floe composed of former fast ice. The team also recovered a GNSS station from the Holm Land site and set up a land-based seismic network consisting of three stations (Cape Anna Bistrup, Norske Øer, and the southern coast of the 79°N Glacier). Excellent flight conditions allowed for a pre-inspection of the sea ice next to the calving front of the 79°N Glacier for a possible mooring/buoy deployment.

In the following days, a short section off Holm Land covered the western part of Westwind Trough. The central and eastern parts toward Belgica Bank were inaccessible due to thick, dense sea ice (referred to as "porridge ice" by the nautical staff). By helicopter, the team deployed a mini-mooring and an oceanographic buoy in the fast ice right at the calving front of the 79°N Glacier. From the Holm section, the ship headed south, passing the entrance of the 79°N Fjord, where a MUC was successfully recovered. In another helicopter operation, a geodetic GNSS site was installed/serviced at Lambert Land (LAMW). The expedition then proceeded to the northern tip of Norske Øer, from where an attempt was made to carry out another section eastward across Norske Trough. However, after three stations, the operation

was halted due to dense ice cover. Here, a mooring was deployed to capture the inflow of Atlantic Water toward the 79°N Glacier. Near midnight on 12 October, the station work was finalized. Throughout these days, sea ice increasingly limited the ship transit, and the daylight period grew shorter.

During another storm with snow on 13 October, *Polarstern* then returned north toward Westwind Trough. It took two full days to reach Holm Land (a direct distance of 70 nautical miles), and only in the morning hours of 17 October the ship was able to leave the sea ice, having crossed the East Greenland Current near 80°N. After a stopover in Longyearbyen on 18 October to return the “Greenland rifles” (30.06 caliber) to the shop from which they had been obtained, the expedition continued its transit to Bremerhaven, passing through another storm on 19 October and arriving on 24 October – one day later than originally planned.

WEATHER CONDITIONS DURING PS150

Patrick Suter DE.DWD

Longyearbyen – Northern Fram Strait – Flade Section (NE Greenland)

In the late afternoon of 4 September 2025, *Polarstern* started from Longyearbyen in calm and cloudy conditions. A large low-pressure zone extended from the south northwards across the Fram Strait. On its way to the Yermak Plateau, *Polarstern* sailed just west of Svalbard, still somewhat sheltered. During the day, the northeasterly wind increased to 5 to 6 Bft. Moist air was also brought in close to the ground, leading to fog in the late afternoon. The waves reached a maximum of 1.5 m. From 6 September, the low-pressure zone moved eastward. The north wind subsided, but the supercooled fog remained in the increasingly dense sea ice.

Polarstern continued northwestward and began the so-called Flade Section work near Northeast Greenland on 7 September. Another low-pressure system moved northwards from the Fram Strait just east of the ship. Behind the low, the weather improved significantly on 8 September with a drier westsouthwesterly flow. However, the improvement was only temporary. With another low from the Fram Strait, foggy air spread again on 9 September. During the course of the day, there was a seamless transition to frontal Nimbostratus cloud cover, with freezing rain and drizzle. Another low-pressure system moved eastwards from eastern Greenland just south of the research area before a high-pressure ridge established itself over Northeast Greenland on 11 September. This, combined with the inflow of colder air, led to a hesitant improvement in the weather.

NE-Greenland: Independence Fjord – Wandel Section

After completing the Flade Section, the ship continued northwestward and remained east of Peary Land and the ice-covered Independence Fjord until 12 September. Meanwhile, the ridge had strengthened into a high-pressure system and lay east of the ship. With weak winds and cold-dry air, conditions were quite sunny. Due to a strong surface inversion, very shallow fog formed on 13 September. This broke up during the day. Thus, during the first so-called ice station, shallow fog fields accompanied the scientific measurements on an ice floe, in addition to sunshine.

With the start of the Wandel Section on 14 September, the above-mentioned high remained over northern Greenland. However, an upper-level low brought more moisture, which led to light snow in some areas and, from late afternoon onwards, deep stratus clouds and temporarily fog. With a low-pressure zone south of Svalbard, the air pressure differences increased and the northwesterly wind picked up to 7 Bft on 15 September. This, combined with light snow and snow drifts, led to a snowstorm at times. A ridge of the high-pressure system over northern Greenland subsequently moved eastwards over the research area. This brought a decrease in wind speed and, especially on the Greenland coast, larger cloud-free areas in the otherwise low-lying stratus and stratocumulus clouds. In the course of 17 September, there was a significant decrease in cloud cover. From 18 September onwards, embedded in the low-pressure zone far to the east, two lows moved from the North Pole into the northern Barents Sea. This brought strong northwesterly winds (6 Bft) and, during the final work of the Wandel Section, very low stratus clouds and freezing fog once again dominated.

North of NE-Greenland: Nearby Cape Morris – Jesup

After a tough transit northward through dense sea ice, work began on the first Morris Jesup Section on 19 September, with strong northwesterly to westerly winds and frequently low cloud cover. A high-pressure system then moved from northern Greenland to the North Pole and slowly towards Siberia over the next few days. On the southern flank of the high, the weakening winds shifted to easterly directions. Until 22 September, with temperatures often below -10°C, sunny phases alternated with recurring fog patches and occasional stratus and stratocumulus clouds. Between the first and second Cape Morris Jesup Sections, a second ice station was established on 21 September. Meanwhile, *Polarstern* reached the northernmost position of the expedition: near 84°30´N 20°W. During the second Section near Cape Morris Jesup, a low-pressure system just east of Svalbard pushed the remnants of a frontal system into the area on 23 September. With little wind, this again brought temporarily increased cloud cover and brief fog before the clouds bases lifted in the afternoon and slowly thinned out.

On 24 September, a low-pressure zone approached from the Canadian Arctic and a ground trough formed over northern Greenland. With an increasing air pressure gradient, strong to near-gale southeasterly to easterly winds arose, with 6 to 7 Bft during the day and gusts up to 8 Bft. The strong winds caused snow drifts, which led to floating ice crystals in the air, temporarily moderate visibility and so-called 'diamond dust' which created a halo around the sun. The ground trough, and with it the wind, weakened again on 25 September. This created an air mass boundary in a small area: This contained cloudy and less cold air, which was brought in from the Fram Strait. By the morning, significantly colder and drier continental air from northeast Greenland had prevailed near the coast. It pushed the more humid air northwards, resulting in the third ice station on 25 September taking place with little cloudiness and plenty of sunshine.

Transit to the Southeast to Independence Fjord and Mooring Works at Flade Section

While the ship was heading southeast towards Independence Fjord, further station work took place away from the ship on 26 September using helicopter flights. Fog repeatedly set in, which required very precise planning of the flights. On 27 September, a low-pressure system moved northwards from the Fram Strait. The northwesterly wind increased to 5 to 6 Bft off Independence Fjord and fog returned in the morning, often with dense stratus and stratocumulus clouds above. Afterwards, a high-pressure ridge moved from the Fram Strait to northeastern Greenland, bringing a significant improvement in the weather on 28 September. By 29 September, a new low was approaching from the Fram Strait, but veered off towards Svalbard. With moderate to fresh west to northwesterly winds, a frontal system initially brought fog on 29 September, followed by Nimbostratus clouds and snow during the course of the day.

On 30 September, *Polarstern* reached the Flade Section again and mooring work followed. The high-pressure ridge described above, which had regained strength, brought calm but cloudy conditions. However, the cloud ceiling was lifted significantly again and the snow had stopped.

From the beginning of October, there was a sustained change in the general weather pattern. Active low pressure took over. From 1 October, a strong low approached from the south and an easterly flow gained strength. The low initially caused in the middle and upper air layers with strong warm air advection, resulting in fairly dense mid-level clouds. With strong to stormy north-easterly winds, a warm front brought moist and significantly milder air until 2 October. This led to Nimbostratus clouds, fog and snow. The air temperature rose from just below -10°C to above 0°C on 2 October, resulting in a transition to freezing rain and then rain during the course of the day.

Transit to the Fram Strait: Deployment of 4 OBS and collecting Devices from PS149

From the evening of 2 October, *Polarstern* headed south, deploying OBS devices on the ocean floor at several locations north of the Fram Strait. The aforementioned low-pressure system moved northwards, with its core passing over *Polarstern* during the course of 3 October. Due to the proximity to the low-pressure core, northwesterly winds with colder air around -3°C alternated with southeasterly winds with milder air and temperatures above 0°C. This was accompanied by dense cloud cover, fog, snow, rain and drizzle. From the afternoon onwards, the ship finally reached the rear side of the northwards moving low, and the weather improved until 4 October with the influx of colder and drier air.

During the previous PS149 expedition, various measuring instruments were left on an ice floe for further measurements. To recover these, the ship continued south into the Fram Strait on 5 October. As it approached the marginal sea ice zone, swells could also be observed in the ice. These increased to 2 to 3 m at the sea ice boundary. Meanwhile, a storm complex southeast of Jan Mayen brought another warm front and moist air into the Fram Strait from 5 October onwards. The continuous supply of moist air marked the beginning of a prolonged period of poor weather.

Western and Northwestern Fram Strait and 79°N-Glacier

After collecting the scattered measuring devices, *Polarstern* headed west into the western Fram Strait on 6 October. With the storm complex, a northerly current gradually increased and it became stormy. Another low-pressure system joined from Iceland. It was steered northwards by the low-pressure complex via Jan Mayen, while deepening into a storm. The maximum wind speed was measured during the night to 8 October with a 10-minute average wind speed of 45 kt (9 Bft) and gusts of 58 kt (11 Bft). Despite the adverse weather conditions, station work was successfully carried out from the ship during the night of 7 October. *Polarstern* then moved north through ice that was heavily compressed by the storm and already very thick, as the Arctic autumn progressed.

On 9 October, the storm moved northwards. While a veritable snowstorm prevailed in the morning, the weather improved rapidly in the afternoon. With only light winds, the clouds cleared and there were only local snow showers left. This allowed work to begin on the Flade Shelf Section and the first flights to the Greenland mainland to take place. Starting from a high-pressure zone over Greenland, a ridge settled over the research area and, with winds coming from Greenland, the clouds were pushed eastwards from 10 October onwards. This opened up an optimal weather window for extensive helicopter operations at the 79°N glacier and surrounding area, as well as for a fourth ice station on 10 October. The air continued to cool, and on 11 October, large areas of fog formed along the Greenland coast. In order to avoid being swallowed up by the fog and to maintain flight operations, *Polarstern* found a fog-free spot at the entrance to the ice-covered Dijmphna Sound on 11 October. There, an outflow of dry, cold air kept the fog away.

On 12 October, *Polarstern* moved slightly southwards to Naroke Oes Island. The lowest temperature of the expedition was recorded at this point: -20.0°C. Meanwhile, the high-pressure zone over Greenland had weakened. Two low-pressure systems were approaching, one from the south and one from Greenland. After a cloudless morning, cirrus clouds approached from the south. Around midday, as warm air advection progressed, there was a sharp transition to dense and very low stratus clouds. This expected deterioration in the weather once again required very precise planning of flight operations.

Transit Northwestern Fram Strait – Longyearbyen – Bremerhaven

The two lows merged and formed a storm over the Fram Strait by 13 October. Northerly winds of around 8 Bft and a snowstorm made it impossible to conduct a final ice station. *Polarstern* began its return transit on the evening of 13 October. The storm moved to the north of Svalbard and the wind quickly subsided behind the low. The remaining clouds also moved eastward on 14 October. The ship made very slow progress through the dense sea ice. Repeated ice reconnaissance flights were made by the helicopter to find the easiest route possible. A weak high-pressure ridge ensured fairly calm conditions and little cloudiness, although daylight hours were already quite short.

During the night of 17 October, *Polarstern* left the sea ice and headed towards Svalbard. A powerful storm extended from the Barents Sea to north of Franz Josef Land. As a result, the northwesterly current picked up speed over the eastern Fram Strait and reached 7 Bft by the afternoon of 17 October. At the same time, humidity increased and the stratocumulus clouds became denser. The storm moved close to Svalbard. Protected from the stormy northwesterly wind, weather conditions on 18 October in the Isfjord and during the stopover in Longyearbyen were significantly calmer. Thanks to slight lee effects, the cloud cover also broke up at times. Upon leaving the Isfjord, *Polarstern* once again encountered the stormy northwesterly flow from the afternoon of 18 October, which was now blowing at 7 to 8 Bft and causing severe gale gusts (9 Bft). The wind-driven wind sea and swell from the northwest quickly increased to 4 to 5 m, with individual waves even higher. Snow also set in and the air mass became increasingly unstable as the ship headed south. This led to dynamic showery weather with snow and sometimes small hail until 20 October.

On 20 October, the wind and the waves in the northern part of the Norwegian Sea calmed down under the influence of an intermediate high-pressure ridge. From 21 October onwards, a storm north of Scotland brought another temporary gale-force increase in wind from northeast to east, reaching 7 to 8 Bft. With swells from the north and considerable wind waves, the wave height increased to around 4 m. The storm moved northwestward and on 22 October, while steering a trough with rain northward over the sailing area with southerly winds. The southerly winds temporarily reached 6 Bft.

Despite a temporary decrease in wind speed, the low-pressure activity continued. A developing severe storm (‘Benjamin’) moved southwest of England through the English Channel into the North Sea by 23 October. North of this, gale-force east to northeasterly winds and a frontal system developed west of Denmark on 23 October. *Polarstern* then continued southwards just east of the low-pressure core with less wind. Due to the storm development, the ship had already accelerated from 22 October onwards. This was an attempt to avoid the southern flank of the low-pressure system. This was predicted to bring full storm force and hurricane-force gusts (12 Bft) from the west to the inner German Bight during the course of 24 October. On the morning of 24 October, *Polarstern* arrived in Bremerhaven in stormy conditions, bringing the PS150 expedition to an end.

In the research area (05.09. to 17.10.25), air pressure fluctuated between 970.6 hPa and 1031.7 hPa. At the same time, wind speed of 7 Bft or more was recorded on 9 days and over the entire journey on 14 days. Gusts of 9 Bft or more were measured on 4 days in the research area and on a total on 7 days. The average temperature in the research area was -6.4°C, with a maximum of 3.7°C and a minimum of -20.0°C. On 28 of the 43 days of research operations, a so-called fog-day with visibility of less than 1 km was recorded.

2. PHYSICAL OCEANOGRAPHY

Torsten Kanzow[1*], Wilken-Jon von Appen[1], Francois Challet[2], Nele Eggers[3], Carina Engicht[1], Mario Hoppmann[1], John Mortensen[4], Andreas Münchow[5], Ufuk Özkan[1], Manuel Franco Pire[6], Quentin Rauschenbach[1], Clemens Rohling[7], Claudia Wekerle[1], Andreas Welsch[7]

Not on board: Femke de Jong[8], Laura de Steur[9], Zoé König[10], Rebecca McPherson[1], Sandra Tippenhauer[1], Jacob Allerholt[1], Ke-Hsien Fu[11], Ying-Chi Fang[11], Jeff O'Brien[12], Sylvia Cole[12], John Toole[12], Don Perovich[13], Olivier Desprez de Gesincourt[14], Sébastien Pere[14], Jean Rabault[15]

* torsten.kanzow@awi.de

[1]DE.AWI
[2]FR.LOCEAN
[3]DE.Uni-Potsdam
[4]GL.NATUR
[5]US.Uni-Delaware
[6]DE.Uni-Kiel
[7]DE.Uni-Hamburg
[8]NL.NIOZ
[9]NO.NPI
[10]NO.Uni-Tromsø
[11]TW.NSYSU
[12]US.WHOI
[13]US.Dartmouth
[14]FR.SHOM
[15]NO.MET-NO

Grant-No. AWI_PS150_01

Objectives

The East Greenland Current (EGC) is widely known for exporting fresh Polar Surface Waters (PSW) and sea ice from the Arctic Ocean and has recently shown major changes. The EGC also exports rather warm and saline, subsurface Arctic Atlantic Water (AAW)–supplied to the Arctic Ocean by the inflow of warm Atlantic Water (AW)–which is steered along both the continental slopes of Eurasia and Canada and along mid-oceanic ridges. We lack a good understanding of the closure of the Arctic-wide circulation in the Last Ice Area north of Greenland, where AAW drives the melt of major glaciers. First, we attempted to determine the circulation of AAW and PSW on the shelf and continental slope north of Greenland, and its downstream connection to the EGC. We further attempted to investigate how the ocean-driven melt of major, retreating glaciers is affected by AAW and AW, and how the meltwater drives shelf currents.

The Arctic Ocean is undergoing rapid change with the ongoing Atlantification (Polyakov et al. 2017), meaning the subsurface inflow of warm Atlantic Water is gaining importance in limiting the growth of sea ice in the Eurasian Basin of the Arctic Ocean as it is no longer strictly subsurface in the Eurasian Basin. Simultaneously, multi-year sea ice has all but disappeared in the fraction of sea ice that is exported out of the Arctic Ocean within the East Greenland Current (EGC) in Fram Strait (Sumata et al. 2023) after the year of 2007.

Atlantic Water (AW) is warm saline water of subtropical origin that flows along the eastern Nordic Seas to the Arctic Ocean. Some of the AW enters the Arctic Ocean through the Barents Sea Opening as well as the West Spitsbergen Current (WSC) on the eastern side of Fram Strait. Analysis of mooring observations suggests that the AW in the WSC has warmed by >0.5°C over the past 2.5 decades (McPherson et al. in press). The surface of the Arctic Ocean is occupied by cold and fresh Polar Surface Water (PSW) of Pacific, riverine, and sea ice melt

origin. A strong halocline separates the PSW from the AW below. As the AW travels through the Arctic Ocean for years to decades, it gets transformed to colder (<2°C) Arctic Atlantic Water (AAW). The AAW, PSW and sea ice exit the Arctic Ocean through the western side of Fram Strait. As not all AW (>2°C) enters the Arctic Ocean, some of it "recirculates" from the eastern to the western side of Fram Strait. This recirculating AW and the AAW join and form the East Greenland Current (EGC) which flows southward along the East Greenland shelfbreak in Fram Strait. When the mixture of AW and AAW in the EGC moves southward and onto the Greenland shelf, we call it Atlantic Intermediate Water (AIW).

The East Greenland Current (EGC) represents the major export route of liquid freshwater and sea ice from the Arctic Ocean. It has long been established that the EGC is fed by Polar Surface Water (PSW) by the Transpolar Drift (Carmack et al. 2016), which provides an upstream connection to the Laptev Sea, a major formation region of sea ice (Krumpen et al. 2019) affected by Atlantification (Polyakov et al. 2017). The amount of Pacific origin water in the PSW exiting the Arctic Ocean through Fram Strait changes on interannual time scales (Dodd et al. 2012). In hydrographic sections along the EGC south of Fram Strait to Denmark Strait, (Håvik et al. 2017) demonstrate the presence of AIW below the PSW above. Thereby the EGC is found to be split into 3 branches, a shelfbreak EGC, an outer EGC further offshore and a jet transporting PSW inshore of the shelfbreak. Based on sections across the shelfbreak within Fram Strait, both Falck et al. (2005) and Richter et al. (2018) show that AW recirculating westward from the WSC across Fram Strait is not present at the East Greenland shelfbreak north of ~79.5°N. Rather, in northern Fram Strait, below the PSW, there is a broad outflow of AAW returning from its long journey around the Arctic Ocean proper. How the circulation connects to the flow of AAW further upstream within the Arctic is not known for lack of observations. We hypothesized that a boundary current exists along the northeastern and northern shelfbreak of Greenland. It likely feeds an important contribution to the East Greenland Current in Fram Strait. The structure, strength, variability, and the properties carried by this boundary current were unknown to this cruise, having presented a blank space of lacking oceanographic knowledge on the map.

The inflow of AW into the Arctic Ocean and along the Eurasian continental slope is well known in terms of its dynamics, strength, and variability from mooring array-based observations north of Svalbard at 30°E (Pérez-Hernández et al. 2019), Zervernaya Semlya at 95°E (Ruiz-Castillo, et al. 2022), and in the Laptev Sea at 126°E (Pnyushkov et al. 2021). Aksenov et al. (2011) described an Arctic Ocean Boundary Current of both AAW and halocline waters around the entire rim of the Arctic Ocean. However, the evolution of the Atlantic Water flow east of 126°E is less clear, where it may split into three branches, along Lomonosov and Mendeleyev Ridges (Woodgate et al. 2001) across the central Arctic Ocean toward North Greenland, and along the continental slope of the Canada Basin into the Lincoln Sea (Karcher et al. 2012; Newton & Sotirin 1997; Rudels et al. 1994). The partitioning into the three branches is related (besides topographic steering) to the large-scale wind forcing (Smith et al. 2021). As one approaches the Greenland shelf in the Lincoln Sea, the situation is less clear, as the eastward flow in the boundary current system reaches a speed maximum in the AW layer but not in the halocline waters above (Aksenov et al. 2011; Newton & Sotirin 1997). Using satellite altimetry, Doglioni et al. (2023) describe a coherent wintertime strengthening of the entire Arctic boundary current between Barents Sea and Alaska, but they found no such signal north of Greenland.

The above discussion indicates a boundary current north of Greenland that feeds AAW into the East Greenland current, e.g. de Steur et al. (2014) detect AAW in long-term observations of Fram Strait moorings. To this cruise, however, nobody had observed the strength, structure, or variability of this boundary current. It was thus unclear whether the AAW flow north of Greenland constitutes a well-defined boundary current or a diffusive circulation branch. The flow structure impacts the residence time of AAW in the Arctic Ocean and thus affects how the Arctic Ocean heat content varies.

In order to diagnose the potential circulation north of Greenland, we conducted and assessed a model simulation using the global ocean-sea ice model FESOM2.1 at 4.5 km horizontal

resolution in the Arctic Ocean (McPherson et al. 2023). It shows a coherent, narrow, and eastward moving boundary current within the AAW layer at 295-m depth. This boundary current feeds into the Fram Strait EGC after it is strengthened by additional supply of AAW from the Lomonosov Ridge and after it is steered offshore around Morris Jesup Rise. In contrast, the surface layer circulation at 60 m appears less impacted by bottom topography. Surface waters along the Lomonosov Ridge move eastward as a broad flow toward Morris Jesup Rise, where the waters move onto the shelf to feed a coastal current that enters Nares Strait (Münchow, 2016) while there also exists evidence that fresh PSW is fed to Fram Strait from north of Greenland (Dmitrenko et al. 2019).

We expected large shelf-slope exchanges as observed to the west off Svalbard (Kolås et al. 2020). For example, an Ekman bottom boundary layer over the slope may advect buoyant water across the slope (Kolås & Fer, 2018) resulting in unstable vertical stratification and mixing. Alternatively, baroclinic instability may form eddies of EGC shelf waters (Koenig et al. 2018). While such processes are observed on Arctic shelves, we knew little on dominant processes on the northern shelf of Greenland. Investigating such exchange processes, we attempted to understand the dynamics and water mass transformation along the flow's path towards the EGC in Fram Strait. Mixing will influence both biogeochemical cycles and ecosystem dynamics.

One prominent example of rapid glacier retreat in Northeast Greenland is the collapse of the floating ice tongue of Zachariæ Isstrøm (ZI) (Mouginot et al. 2015). The largest remaining floating ice tongue of Greenland is the neighboring Nioghalvfjerdsfjorden Glacier which is also known as the 79 North Glacier (79NG). Together, ZI and 79NG drain the Northeast Greenland Ice Stream (NEGIS) – encompassing 15% of the total area of the Greenland ice sheet. Continuous thinning of the 79NG tongue by up to 30% has occurred over the past 20 years (Mayer et al. 2018), caused by increased melting along the ice tongue base (Mayer et al. 2018; Wilson et al. 2017), driven by ocean heat fluxes. Münchow et al. (2020) demonstrated the existence of a year-round, subsurface pathway of warm saline AIW from the shelfbreak following Norske Trough all the way to the 79NG. Consistent with the decadal warming of AW in the WSC, the AIW on the shelf close to 79NG has warmed by 0.5°C and there has been a vertical redistribution of principal water masses on the shelf (Gjelstrup et al. 2022). Once reaching the calving front of the 79NG, the inflow of AIW into the cavity of the 79NG is hydraulically controlled by a local bathymetric sill-system (Schaffer et al. 2020). This means, the height of the layer of AIW above the sill ultimately controls the ocean heat transport into the cavity and thus the melting of the glacier from below, which we can explicitly resolve with the FESOM2.1 model. Using annual-mean, mooring-based estimates of ocean heat transport into the cavity, the basal melt rates below the floating ice tongue of 79NG were estimated to be 10.4±3.1 m/yr (Schaffer et al. 2020) which compare favorably with a snap-shot melt rate estimate of 8.6±1.4 m/yr by Huhn et al. (2021), based on water samples of noble gas concentrations using helium (He) and neon (Ne).

The first ever hydrographic measurements close to the calving front of the ZI (Schaffer et al. 2020) revealed that it is exposed to warm AIW just like 79NG. We thus suspect the increased ocean heat supply to have caused the collapse of the ZI. Using numerical modeling based on the FESOM model, McPherson et al. (2023) showed that temperatures on the shelf of Northeast Greenland correlate with those in the WSC with a 3-year lag. In addition, wind forcing anomalies over the Barents Sea significantly strengthen both the AW flow within the WSC and the recirculation branches on interannual time scales, while the export of AAW along the shelfbreak is weakened. Regional wind patterns may thus control the relative contributions of warm AW and colder AAW to the AIW. Despite an emerging long-term warming of the AIW on the shelf of Northeast Greenland, neither the interannual temperature variability of AIW nor the role of AAW, AW and PSW to drive it were known. Our analysis of mooring-based observations at the calving front of the 79NG since 2016 revealed a cooling of the AIW since 2018 exceeding 0.5°C, and goes along with marked weakening of the heat transport into the cavity. PS150

EGC-Sources attempted to conduct observations that will explain how changes in the AW branches and AAW outflow affect basal melt of the 79NG.

Only two other outlet glaciers of the Greenland Ice sheet retain major floating ice tongues: They are Petermann Glacier which drains 4% of the Greenland Ice sheet area and Ryder Glacier. Both are located within fjords on the coast of North Greenland and are thus affected by water masses in the Lincoln Sea. There is strong evidence that they are exposed to the inflow of AAW (Jakobsson et al. 2020; Münchow et al. 2016). The sill-controlled inflow of AAW appears to be particularly critical for determining the basal melt rate of Ryder Glacier (Nilsson et al. 2023), who emphasize that an increase in AAW interface height in the Lincoln Sea increases the basal melt rate. Petermann Glacier, unlike the other glaciers, appears to be in a melt controlled rather than a hydraulically controlled state with basal melt rates sensitive to rising AAW temperature. Another major marine terminating glacier of Northeast Greenland is the Flade Isblink Ice Cap near Wandel Sea. It is the largest peripheral ice mass of Greenland and exhibits a small floating ice tongue (Bendtsen et al. 2017). Here, however, the bottom water interacting with the ice tongues is PSW close to the freezing point, so that melting is controlled by seasonal warming of the surface water during sea ice retreat in the summer. PS150 EGC-Sources attempted to determine both of these control parameters (AAW temperature and interface height, PSW properties) in the Lincoln Sea and Wandel Sea.

Ocean-glacier interaction also concerns the impact of the meltwater on the ocean. Huhn et al. (2021) showed that the basal meltwater from the 79NG stays at a depth range of 100-200 m, i.e. roughly at the interface of AIW and PSW while it dilutes from the calving front towards the shelfbreak and the EGC. We thus expected the melt rates to play a significant role for circulation close to the Greenlandic coast, but not within the EGC. The light and hardly soluble noble gasses helium (He) and neon (Ne) provide a unique tool to identify submarine meltwater, to quantify its fractions, and to trace its further pathways inside the ocean (e.g. Huhn et al. 2021). So far, noble gas observations in the northern part of Greenland had been restricted to shelf regions around the 79NG. The PS150 EGC-Sources attempted to explore the meltwater signatures of the other North Greenland floating ice tongues to the EGC.

Work at sea

We deployed the CTD-rosette with lowered-ADCP attached at as many stations as possible given the encountered sea ice conditions. We operated the vessel-mounted ADCP throughout the cruise. At selected stations, we deployed a microstructure probe. Where ice conditions did not allow operation of the regular CTD and from the helicopter, we deployed XCTDs and a small RBR concerto CTD attached to a fishing rod. We deployed a mooring array north of the Flade Isblink and we also deployed five further moorings in other locations. We recovered 2 moorings deployed during PS131 in 2022. We performed measurements during four ice stations. We deployed various oceanographic ice tethered instruments during sea ice stations. Figure 2.1 gives an overview of the cruise track and the achieved oceanographic sections (for more details for how they are defined, see the Expected Results at the end of this chapter).

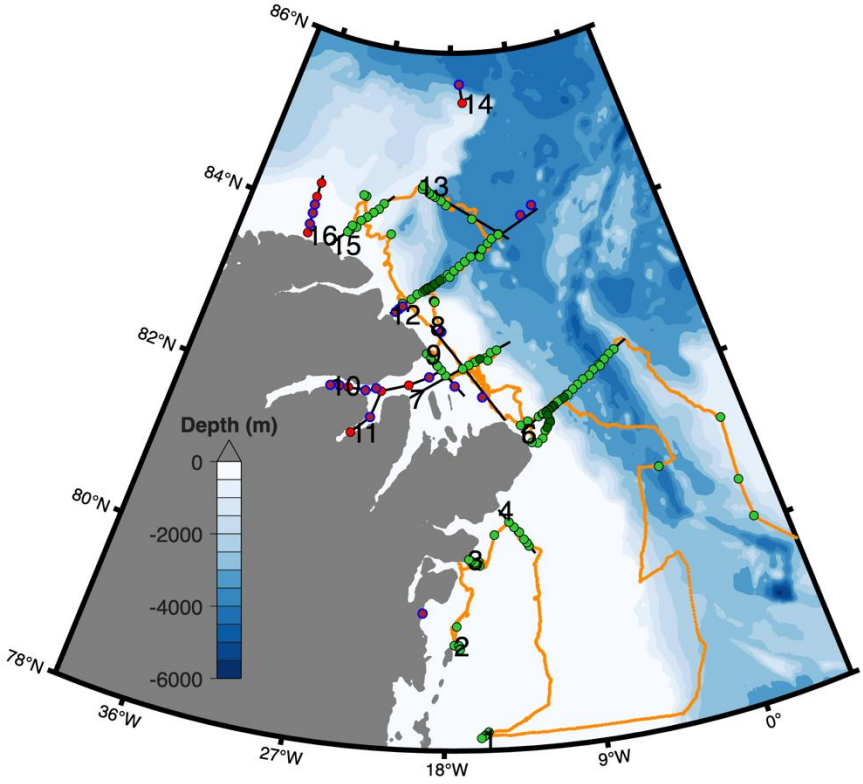

Fig. 2.1: Map of the study area with cruise track (orange), ship stations with CTD (light green) and XCTD (dark green) measurements and measurements via helicopter (fishing rod CTD in purple and XCTD in red). Along the cruise track, velocity measurements from the ship ADCP are available. Black lines indicate the 16 sections.

Overview of helicopter operations of the physical oceanography team

There were 10 helicopter flights during PS150 in which the physical oceanography group participated (Fig. 2.2). Table 2.1 presents an overview of the activities during those flights and assigns station names to the activities. Note that station and cast numbering does not automatically occur for work that is not carried out from the ship. Therefore, for working with our own data, we assigned station names along the naming pattern PS150_heli_OZE_XXX_YY where XXX is the station number (with leading zeros) and YY is the cast number (with leading zeros) at that station.

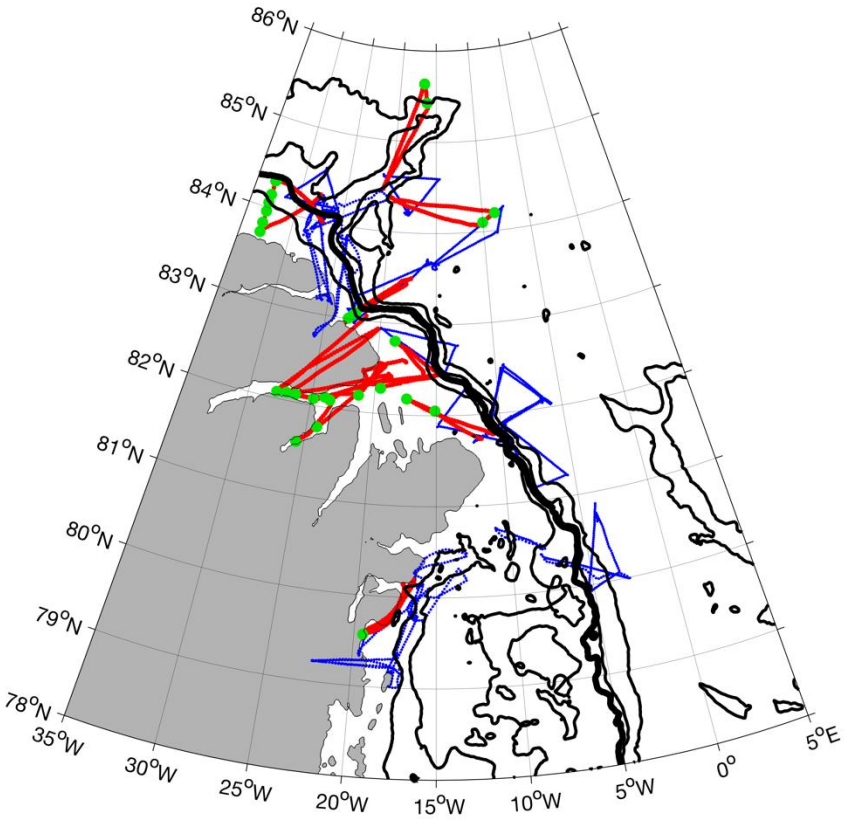

Fig. 2.2: Map of all helicopter flights during PS150 (blue) and of all the helicopter flights that the physical oceanography team participated in (red). Those flights lead to the green locations which is where the activities listed in Tab. 2.1 took place.

Tab. 2.1: Table of all helicopter activities of the physical oceanography team

Event label OZE	Event label	Optional label	Event type (number)	Date/Time start	Date/Time end	Latitude	Longitude	Device ID (in Registry)	Description	Water depth	Source Water depth	Cast depth	Station	Cast	Gear	Latitude degree	Latitude minute	Longitude degree	Longitude minute
PS150_heli_OZE_001_01	PS150_heli-CTD_48M_1495-01	Independence Fjord Station 1	187	2025-09-12T11:52:00		82.0733	-27.8093	6470	water depth: 865 m (Simrad Echosounder)	865	Echosounder	800	1	1	S&S	82	4.40	27	48.56
PS150_heli_OZE_001_02	PS150_heli-rbr_concerto_210909-01	Independence Fjord Station 1	187	2025-09-12T13:00:00		82.0733	-27.8093	11142	water depth: 865 m (Simrad Echosounder)	865	Echosounder		1	2	RBR	82	4.40	27	48.56
PS150_heli_OZE_002_01	PS150_heli-XCTD_MK150_1-01	Independence Fjord Station 2	187	2025-09-12T14:09:00		82.0856	-26.2927	5079	deployed from hovering heli; instrument depth: ~420 m (to bottom)	420	XCTD	420	2	1	XCTD_hovering	82	5.14	26	17.56
PS150_heli_OZE_003_01	PS150_heli-rbr_concerto_210909-02	Independence Fjord Station 3	187	2025-09-12T14:46:00		82.1104	-23.9614	11142	water depth: 640 m (Simrad Echosounder)	640	Echosounder		3	1	RBR	82	6.63	23	57.68
PS150_heli_OZE_004_01	PS150_heli-XCTD_MK150_1-02	Independence Fjord Station 4	187	2025-09-12T16:18:00		82.1798	-21.2795	5079	deployed from hovering heli; instrument depth: ~550 m (to bottom)	550	XCTD	550	4	1	XCTD_hovering	82	10.79	21	16.77
PS150_heli_OZE_005_01	PS150_heli-XCTD_MK150_1-03	Hagen Fjord Station 2	187	2025-09-12T19:03:00		81.5775	-25.5986	5079	deployed from hovering heli; instrument depth: ~375 m; cut off early	390	XCTD	375	5	1	XCTD_hovering	81	34.65	25	35.92
PS150_heli_OZE_005_02	PS150_heli-XCTD_MK150_1-04	Hagen Fjord Station 2	187	2025-09-12T19:06:00		81.5775	-25.5986	5079	deployed from hovering heli; instrument depth: ~390 m (to bottom)	390	XCTD	390	5	2	XCTD_hovering	81	34.65	25	35.92
PS150_heli_OZE_006_01	PS150_heli-rbr_concerto_210909-03	Hagen Fjord Station 3	187	2025-09-12T19:41:00		81.7736	-24.2095	11142	water depth: 592 m (Simrad Echosounder)	592	Echosounder		6	1	RBR	81	46.41	24	12.57
PS150_heli_OZE_007_01	PS150_heli-XCTD_MK150_1-05	Hagen Fjord Station 4	187	2025-09-12T21:01:00		82.0863	-23.5132	5079	deployed from hovering heli; instrument depth: ~300 m (to bottom)	300	XCTD	300	7	1	XCTD_hovering	82	5.18	23	30.79
PS150_heli_OZE_008_01	PS150_heli-rbr_concerto_210909-04	Wandel Section Southwest middle cast 1	187	2025-09-16T17:03:00		83.0414	-22.6340	11142	water depth: 138 m (Simrad Echosounder)	138	Echosounder	138	8	1	RBR	83	2.48	22	38.04
PS150_heli_OZE_008_02	PS150_heli-rbr_concerto_210909-05	Wandel Section Southwest middle cast 2	187	2025-09-16T17:17:00		83.0414	-22.6340	11142	water depth: 138 m (Simrad Echosounder)	138	Echosounder	138	8	2	RBR	83	2.48	22	38.04
PS150_heli_OZE_009_01	PS150_heli-rbr_concerto_210909-06	Wandel Section Southwest far cast 1	187	2025-09-16T18:14:00		83.0053	-22.9504	11142	water depth: 105 m (Simrad Echosounder)	105	Echosounder	105	9	1	RBR	83	0.32	22	57.02
PS150_heli_OZE_009_02	PS150_heli-rbr_concerto_210909-07	Wandel Section Southwest far cast 2	187	2025-09-16T18:23:00		83.0053	-22.9504	11142	water depth: 105 m (Simrad Echosounder)	105	Echosounder	105	9	2	RBR	83	0.32	22	57.02
PS150_heli_OZE_010_01	PS150_heli-rbr_concerto_210909-08	Wandel Section Southwest close cast 1	187	2025-09-16T19:20:00		83.0764	-22.3334	11142	water depth: 216 m (Simrad Echosounder)	216	Echosounder	216	10	1	RBR	83	4.58	22	20.00
PS150_heli_OZE_010_02	PS150_heli-rbr_concerto_210909-09	Wandel Section Southwest close cast 2	187	2025-09-16T19:33:00		83.0764	-22.3334	11142	water depth: 216 m (Simrad Echosounder)	216	Echosounder	216	10	2	RBR	83	4.58	22	20.00
PS150_heli_OZE_011_01	PS150_heli-rbr_concerto_210909-10	Wandel Section Northeast Point 3	187	2025-09-20T06:30:00		84.1965	-8.6559	11142	winch to 750 m; CTD to 350 m		not available	350	11	1	RBR	84	11.79	8	39.35
PS150_heli_OZE_011_02	PS150_heli-S1000Heli-01	Wandel Section Northeast Point 3	187	2025-09-20T06:55:00	2025-09-20T07:27:00	84.1965	-8.6559	11809	ADCP; 32 mins data		not available	0	11	2	S1000	84	11.79	8	39.35
PS150_heli_OZE_012_01	PS150_heli-S1000Heli-02	Wandel Section Northeast Point 2	187	2025-09-20T08:03:00	2025-09-20T09:09:00	84.1005	-10.0270	11809	ADCP; 66 mins data		not available	0	12	1	S1000	84	6.03	10	1.62
PS150_heli_OZE_012_02	PS150_heli-rbr_concerto_210909-11	Wandel Section Northeast Point 2	187	2025-09-20T08:08:00		84.1005	-10.0270	11142	winch to 900 m; CTD to 412 m		not available	412	12	2	RBR	84	6.03	10	1.62
PS150_heli_OZE_013_01	PS150_heli-rbr_concerto_210909-12	Morris Jesup Rise 1	187	2025-09-21T14:42:00		85.6400	-16.6613	11142	winch to 740 m		not available		13	1	RBR	85	38.40	16	39.68
PS150_heli_OZE_013_02	PS150_heli-S1000Heli-03	Morris Jesup Rise 1	187	2025-09-21T14:50:00	2025-09-21T15:42:00	85.6400	-16.6613	11809	ADCP; 58 mins data		not available	0	13	2	S1000	85	38.40	16	39.68
PS150_heli_OZE_014_01	PS150_heli-XCTD_MK150_1-06	Morris Jesup Rise 2	187	2025-09-21T16:18:00		85.4300	-16.2367	5079	deployed from hovering heli		not available	1085	14	1	XCTD_hovering	85	25.80	16	14.20
PS150_heli_OZE_015_01	PS150_heli-XCTD_MK150_1-07	Lincoln Sea transect LS0	187	2025-09-24T10:58:00		83.7203	-32.9769	5079	deployed from hovering heli; cut off immediately after launch	47	XCTD	2	15	1	XCTD_hovering	83	43.22	32	58.61
PS150_heli_OZE_015_02	PS150_heli-XCTD_MK150_1-08	Lincoln Sea transect LS0	187	2025-09-24T11:00:00		83.7203	-32.9766	5079	deployed from hovering heli; repeated cast; instrument depth: 47 m (to bottom)	47	XCTD	47	15	2	XCTD_hovering	83	43.22	32	58.60
PS150_heli_OZE_016_01	PS150_heli-rbr_concerto_210909-13	Lincoln Sea transect LS1	187	2025-09-24T11:29:00		83.8267	-32.9991	11142	water depth: 106 m (Simrad Echosounder); winch to 146 m; ice thickness: ~2 m	106	Echosounder	106	16	1	RBR	83	49.60	32	59.95
PS150_heli_OZE_017_01	PS150_heli-rbr_concerto_210909-14	Lincoln Sea transect LS2	187	2025-09-24T12:16:00		83.9563	-32.9845	11142	water depth: 175 m (Simrad Echosounder); winch to 228 m; ice thickness: > 2 m	175	Echosounder	175	17	1	RBR	83	57.38	32	59.07
PS150_heli_OZE_018_01	PS150_heli-rbr_concerto_210909-15	Lincoln Sea transect LS3	187	2025-09-24T13:01:00		84.0538	-33.0201	11142	water depth: 443 m (Simrad Echosounder); winch to 609 m; ice thickness: ~1.5 m	443	Echosounder	443	18	1	RBR	84	3.23	33	1.21
PS150_heli_OZE_019_01	PS150_heli-XCTD_MK150_1-09	Lincoln Sea transect LS4	187	2025-09-24T14:01:00		84.1479	-33.0179	5079	instrument depth: 878 m (to bottom)	878	XCTD	878	19	1	XCTD	84	8.88	33	1.07
PS150_heli_OZE_019_02	PS150_heli-buoy-01	Lincoln Sea transect LS4	187	2025-09-24T14:36:00		84.3023	-33.0240	12839	MetOcean SVP-I-BXGS-AP 2025P345; IMEI 300534067122450; ice thickness > 2m;	878	XCTD	0	19	2	Buoy	84	18.14	33	1.44
PS150_heli_OZE_020_01	PS150_heli-XCTD_MK150_1-10	Lincoln Sea transect LS5	187	2025-09-24T14:56:00		84.3125	-32.9509	5079	instrument depth: 805 m (to bottom)	805	XCTD	805	20	1	XCTD	84	18.75	32	57.05
PS150_heli_OZE_021_01	PS150_heli-XCTD_MK150_1-11	Independence Fjord Station 1.5	187	2025-09-26T15:13:00		82.0862	-27.0423	5079	instrument depth: 631 m (to bottom); ice thickness: ~1 m	631	XCTD	631	21	1	XCTD	82	5.17	27	2.54
PS150_heli_OZE_021_02	PS150_heli-rbr_concerto_210909-16	Independence Fjord Station 1.5	187	2025-09-26T15:23:00		82.0862	-27.0423	11142	instrument depth: 293 m; deep Niskin cast, fall rate suboptimal, not full water depth	631	XCTD	293	21	2	RBR	82	5.17	27	2.54
PS150_heli_OZE_021_03	PS150_heli-Niskin_2L-01	Independence Fjord Station 1.5	187	2025-09-26T15:23:00		82.0862	-27.0423	11811	1 Niskin, closed at around 300m depth	631	XCTD	293	21	3	Niskin	82	5.17	27	2.54
PS150_heli_OZE_021_04	PS150_heli-rbr_concerto_210909-17	Independence Fjord Station 1.5	187	2025-09-26T16:00:00		82.0862	-27.0423	11142	instrument depth: 55 m; shallow Niskin cast, fall rate suboptimal, not full water depth	631	XCTD	55	21	4	RBR	82	5.17	27	2.54
PS150_heli_OZE_021_05	PS150_heli-Niskin_2L-02	Independence Fjord Station 1.5	187	2025-09-26T16:00:00		82.0862	-27.0423	11811	3 Niskins, closed at around 5, 25, 50m depth	631	XCTD	55	21	5	Niskin	82	5.17	27	2.54
PS150_heli_OZE_022_01	PS150_heli-XCTD_MK150_1-12	Independence Fjord Station 2.5	187	2025-09-26T17:10:00		82.0742	-24.8379	5079	instrument depth: 561 m (to bottom); ice thickness: ~1 m	561	XCTD	561	22	1	XCTD	82	4.45	24	50.28
PS150_heli_OZE_022_02	PS150_heli-rbr_concerto_210909-18	Independence Fjord Station 2.5	187	2025-09-26T17:17:00		82.0742	-24.8379	11142	instrument depth: 55 m; shallow Niskin cast, fall rate suboptimal, not full water depth	561	XCTD	55	22	2	RBR	82	4.45	24	50.28
PS150_heli_OZE_022_03	PS150_heli-Niskin_2L-03	Independence Fjord Station 2.5	187	2025-09-26T17:17:00		82.0742	-24.8379	11811	3 Niskins, closed at around 5, 25, 50m depth	561	XCTD	55	22	3	Niskin	82	4.45	24	50.28
PS150_heli_OZE_023_01	PS150_heli-XCTD_MK150_1-13	5nm SE of planned Independence Fjord Station 6	187	2025-09-28T13:03:00		82.2789	-19.5589	5079	instrument depth: 580 m (to bottom); ice thickness: ~1.6 m	580	XCTD	580	23	1	XCTD	82	16.73	19	33.53
PS150_heli_OZE_023_02	PS150_heli-rbr_concerto_210909-19	5nm SE of planned Independence Fjord Station 6	187	2025-09-28T13:10:00		82.2789	-19.5589	11142	instrument depth: 55 m; shallow Niskin cast, fall rate suboptimal, not full water depth	580	XCTD	55	23	2	RBR	82	16.73	19	33.53
PS150_heli_OZE_023_03	PS150_heli-Niskin_2L-04	5nm SE of planned Independence Fjord Station 6	187	2025-09-28T13:10:00		82.2789	-19.5589	11811	4 Niskins, closed at around 5, 15, 25, 50m depth	580	XCTD	55	23	3	Niskin	82	16.73	19	33.53
PS150_heli_OZE_024_01	PS150_heli-rbr_concerto_210909-20	Independence Heli mooring	187	2025-09-28T15:41:00		82.8052	-18.6087	11142	water depth: 296 m (Simrad Echosounder); winch to 373 m; data file also contains previous deployment	296	Echosounder	296	24	1	RBR	82	48.31	18	36.52
PS150_heli_OZE_024_02	PS150_heli-mooring-01	Independence Heli mooring	187	2025-09-28T16:15:00		82.8052	-18.6087	13319	IT1-1; deployed through new ice at floe edge	296	Echosounder	0	24	2	Moor	82	48.31	18	36.52
PS150_heli_OZE_025_01	PS150_heli-rbr_concerto_210909-21	Independence Outflow Heli CTD buoy on fast ice	187	2025-09-30T15:25:00		82.0508	-15.1093	11142	water depth: 114 m (Simrad Echosounder)	114	Echosounder	114	25	1	RBR	82	3.05	15	6.56
PS150_heli_OZE_025_02	PS150_heli-buoy-02	Independence Outflow Heli CTD buoy on fast ice	187	2025-09-30T16:15:00		82.0508	-15.1093	12970	PacificGyre AWI-SVP5S-0006 (2025O34); IMEI 300234068514740; ice thickness 1.3 m; FB 0.12 m; snow 0.04	114	Echosounder	100	25	2	Buoy	82	3.05	15	6.56
PS150_heli_OZE_026_01	PS150_heli-rbr_concerto_210909-22	Independence Outflow CTD on fast ice	187	2025-09-30T17:03:00		82.1779	-17.3935	11142	water depth: 148 m (Simrad Echosounder)	148	Echosounder	148	26	1	RBR	82	10.67	17	23.61
PS150_heli_OZE_027_01	PS150_heli-rbr_concerto_210909-23	79NG Heli mooring on fast ice	187	2025-10-11T11:17:00		79.5697	-19.4627	11142	water depth: 475 m (Simrad Echosounder); winch to 580 m	475	Echosounder	475	27	1	RBR	79	34.18	19	27.76
PS150_heli_OZE_027_02	PS150_heli-mooring-02	79NG Heli mooring on fast ice	187	2025-10-11T13:14:00		79.5697	-19.4627	8868	79N2-3; deployed through hole	475	Echosounder	0	27	2	Moor	79	34.18	19	27.76
PS150_heli_OZE_027_03	PS150_heli-buoy-03	79NG Heli mooring on fast ice	187	2025-10-11T14:00:00		79.5697	-19.4627	12969	PacificGyre AWI-SVP5S-0012 (2025O33); IMEI 300534064368480; ice thickness 1.3 m; FB 0.05 m; snow 0.4	475	Echosounder	200	27	3	Buoy	79	34.18	19	27.76
PS150_heli_OZE_027_04	PS150_heli-buoy-04	79NG Heli mooring on fast ice	187	2025-10-11T14:45:00		79.5697	-19.4627	12784	SIMBA AWI11-01	475	Echosounder	0	27	4	Buoy	79	34.18	19	27.76

Oceanographic work on the ice stations

During PS150 several oceanographic tasks have been conducted on the four ice stations. Detailed descriptions of the ice floe characteristics and general conditions can be found in the Sea Ice Physics Section. On all stations MSS profiles (see below) have been taken, a CTD Upriser Transect (see below) was conducted and a 300kHz ADCP were deployed under the ice (see below). The S1000 ADCP (see below) has been deployed on stations 2,3 and 4. On ice station 3 additionally 2 ice buoys (TOP016, SIMB3 2025F) have been deployed on the floes and left for measuring (see below).

The following figures (Fig. 2.3 to 2.6) give an overview over the different ice floes and localise the different deployment sites on all ice stations. They can be used to locate the Upriser Transect relative to the ice edge, which is crucial to characterize horizontal gradients of under ice hydrography. Included are the ship Heading at the time of image acquisition and an approximate length scale based on *Polarstern*.

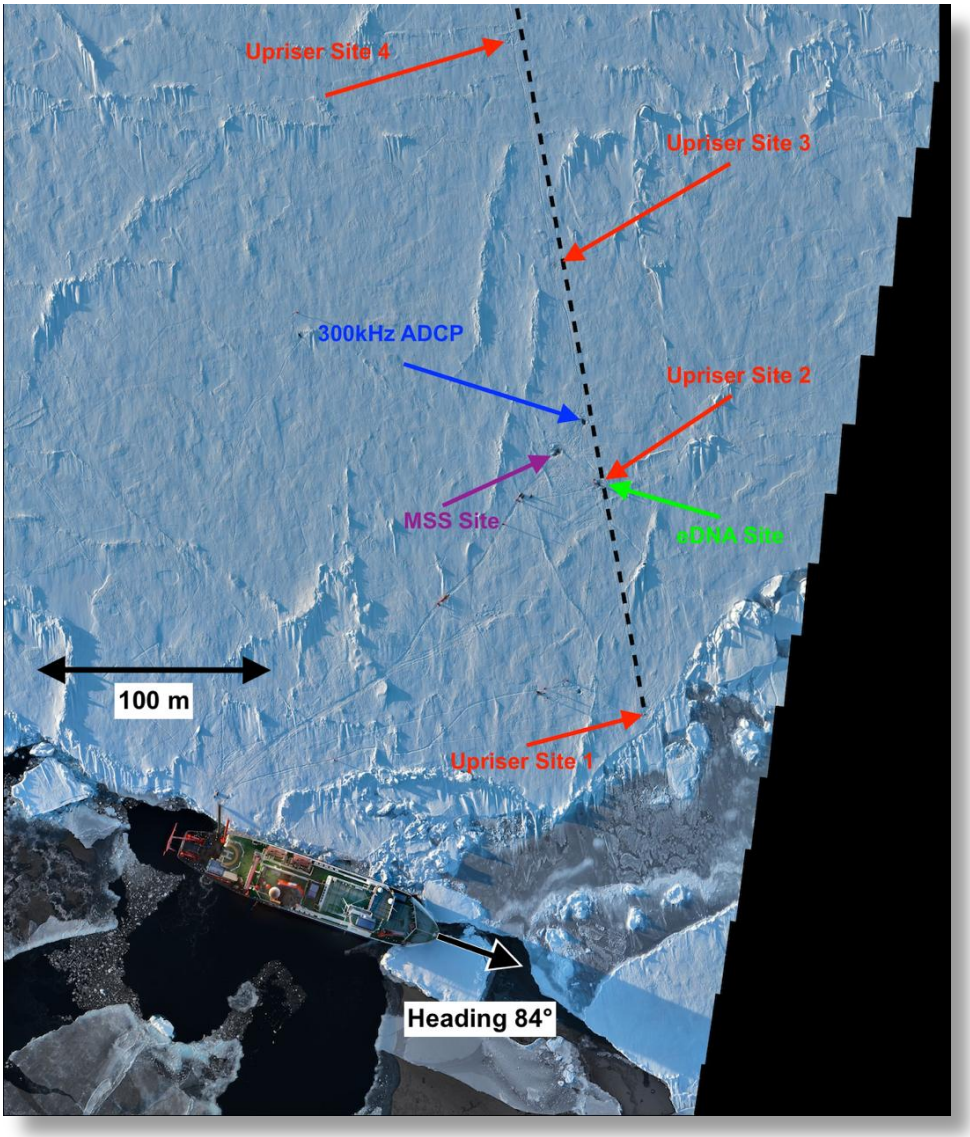

Fig. 2.3: Photomosaic from ice station 1 with labels of relevant sites, obtained from a set of photos taken by a DJI Mavic drone at 130 m altitude. Photomosaic by Marcel Nicolaus and Bernhard Schmitz, modified by Clemens Rohling.

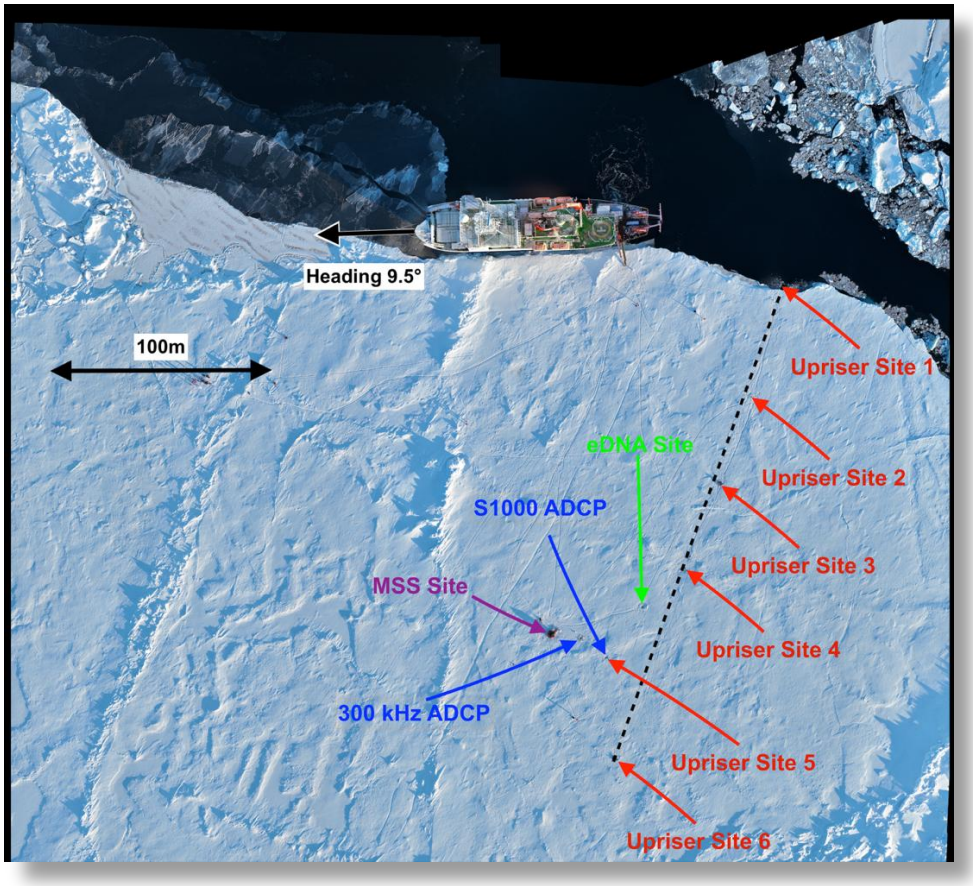

Fig. 2.4: Photomosaic from ice station 2 with labels of relevant sites, obtained from a set of photos taken by a DJI Mavic drone at 130 m altitude. Photomosaic by Marcel Nicolaus and Bernhard Schmitz, modified by Clemens Rohling.

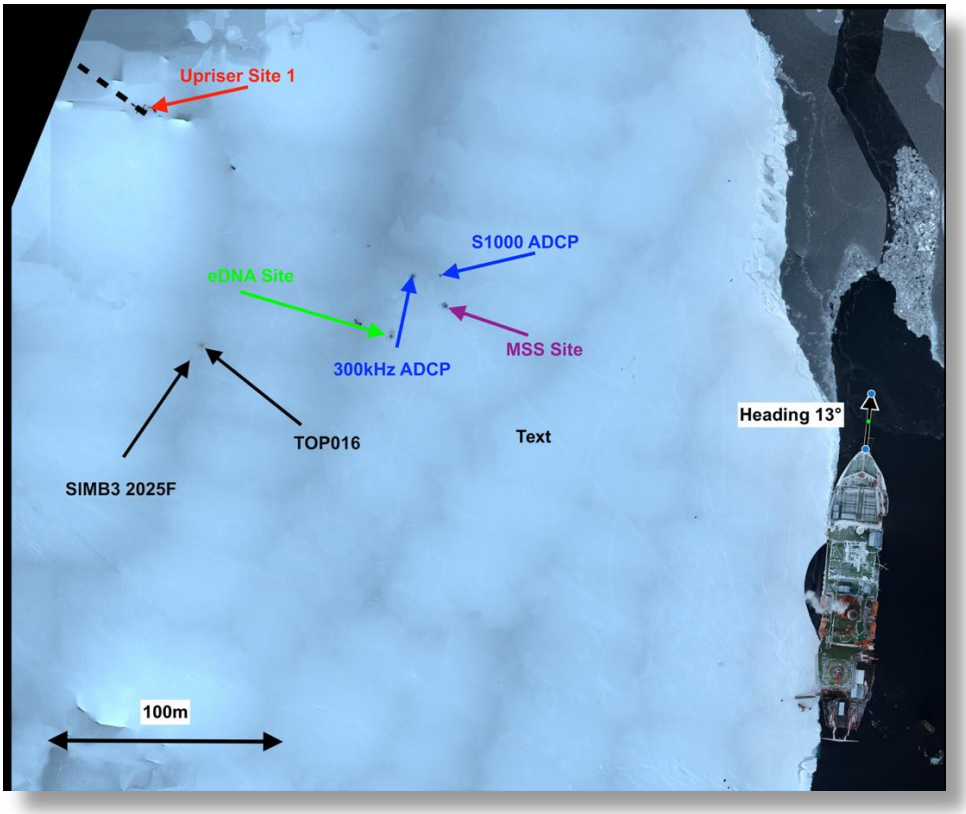

Fig. 2.5: Photomosaic from ice station 3 with labels of relevant sites, obtained from a set of photos taken by a DJI Mavic drone at 70 m altitude. Photomosaic by Marcel Nicolaus and Bernhard Schmitz, modified by Clemens Rohling.

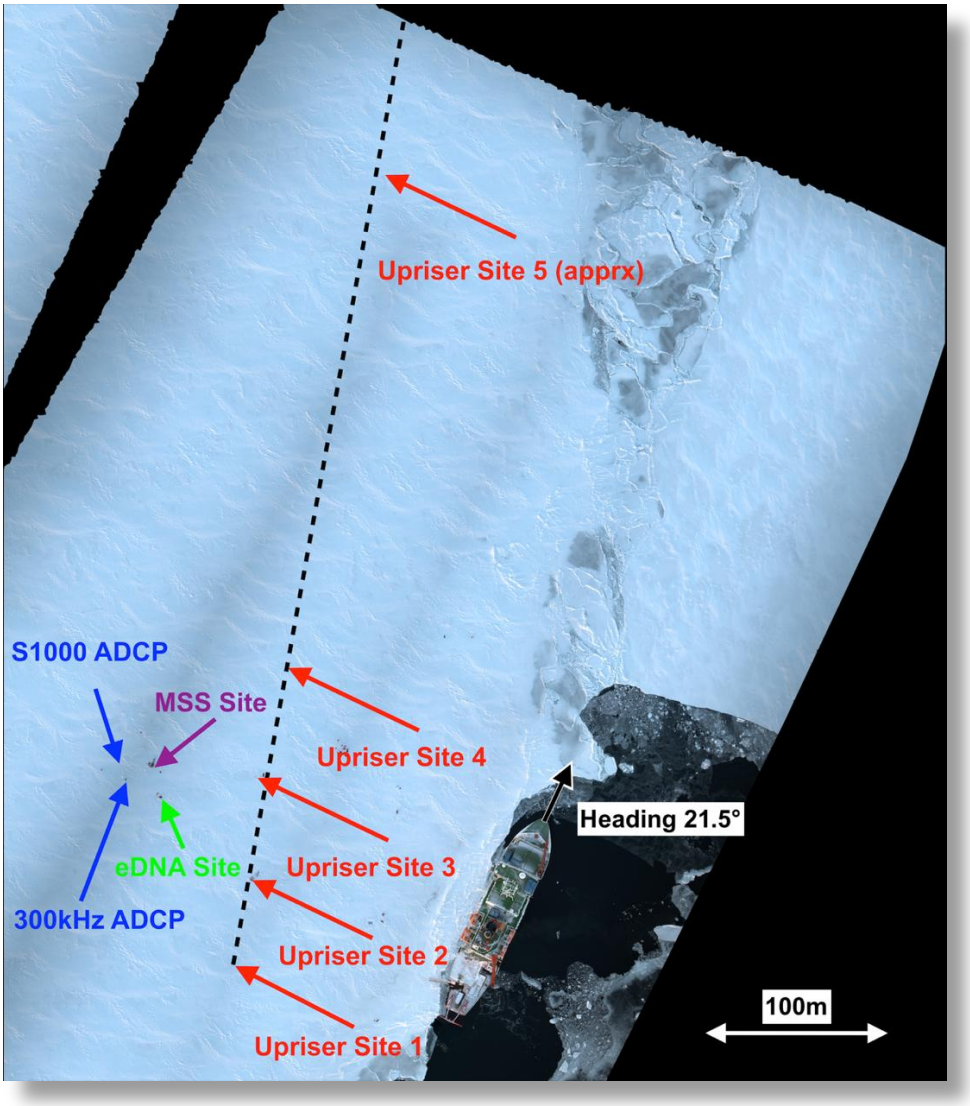

Fig. 2.6: Photomosaic from ice station 4 with labels of relevant sites, obtained from a set of photos taken by a DJI Mavic drone at 130 m altitude. Photomosaic by Marcel Nicolaus and Bernhard Schmitz, modified by Clemens Rohling.

Lowered Conductivity Temperature Depth (CTD) rosette and mounted sensors

During PS150, the OZE CTD/rosette (shortname CTD_SBE9plus_287, “Piglet") was equipped with a standard SeaBird SBE911plus setup, and operated with double sensors for temperature, salinity, and oxygen on two separate pumped seawater ducts. Additionally, sensors for seawater pressure, Chl-*a* fluorescence (WET Labs ECO-AFL/FL), fluorescence of colored dissolved organic matter (CDOM, WETLabs ECO CDOM), yellow substance fluorescence (BackScat *in situ* Fluorometer Series 1100, Dr. Haardt), beam transmission (WETLabs C-Star), photosynthetically active radiation (PAR/Logarithmic, Satlantic), and surface photosynthetically active radiation (SPAR/Linear, Satlantic) were installed. The C-Star transmissometer was calibrated in May 2025 following the procedure described in Seabird application-note-07. In addition, 24 12-liter Niskin bottles (OTE, USA) for water sampling were attached to the CTD/rosette. Initially, a Teledyne Benthos 916 altimeter was mounted to the bottom of the frame to monitor the distance to the seafloor. Since the altimeter was only able to detect the seafloor at a distance smaller than 30 m, it was replaced by a Valeport VA500

altimeter after cast 12. Even though this new altimeter exhibited pronounced spiking with oscillatory characteristics, it had a significantly better performance, consistently detecting the seafloor at a distance of 90 – 100 m. The Valeport altimeter was used for the remainder of the expedition. We recommend to exclusively use this model in the future.

Tab. 2.2: Sensor configuration (conf1) for the ship-based CTD/rosette used during PS150. The instrument shortname was CTD_SBE9plus_287 ("Piglet"), and is a property of the AWI Physical Oceanography section. The configuration remained unchanged throughout the cruise, except the exchange of the altimeter between the 12 and 13th CTD cast for performance reasons (see text).

Parameter	SN	Calibration Date	Channel	Sensor type
CTD deck unit	525	-	deck unit	SBE11plus
CTD underwater unit	287	14 November 2017	underwater unit	SeaBird SBE 911plus
Carousel water sampler	55	11 August 2021	-	SBE32
24 x 12l Niskin bottles	-	-	-	Niskin 12l, OTE
Temperature 1	5112	11 August 2021	F1	SeaBird SBE3plus
Conductivity 1	3570	10 August 2021	F2	SeaBird SBE4c
Pressure	287	14 November 2017	F3	SeaBird SBE9
Temperature 2	5115	16 January 2024	F4	SeaBird SBE3plus
Conductivity 2	3290	09 January 2024	F5	SeaBird SBE4c
Oxygen 1	4305	13 July 2023	V0	SeaBird SBE43
Oxygen 2	4303	11 July 2023	V1	SeaBird SBE43
Pump	0845	-	-	SeaBird SBE5T
Pump	4316	-	-	SeaBird SBE5T
Altimeter (before cast 13)	51533	-	V2	Teledyne Benthos PSA916
Altimeter (after cast 12)	86344	-	V2	Valeport VA500
CDOM fluorescence	7239	21 December 2023	V3	WETLabs ECO CDOM Fluorometer
Chl-a fluorescence	8103	20 April 2023	V4	WETLabs ECO_AFL
Beam Transmission	1220	07 September 2022	V5	WETLabs C-Star Transmissometer
Yellow substance fluorescence	3	-	V6	Dr Haardt BackScat 1100
PAR	2197	30 November 2021	V7	PAR logarithmic, Satlantic
Surface PAR	2335	09 January 2024	SPAR	SPAR linear, Satlantic
Additional sensors:				
Current velocity	23293/ 23292	-	-	2 x RDI Workhorse 300kHz ADCPs
Nitrate	1166	tbd	power only	Deep SUNA V2, Satlantic
Underwater Vision Profiler	202	-	-	UVP Hydroptic

The configuration report for SBE 911plus system operated throughout PS150 as exported from the SeaSave software was

```
Configuration report for SBE 911plus/917plus CTD
------------------------------------------------

Frequency channels suppressed : 0
Voltage words suppressed      : 0
Computer interface            : RS-232C
Deck unit                     : SBE11plus Firmware Version >= 5.0
Scans to average              : 1
NMEA position data added      : Yes
NMEA depth data added         : No
NMEA time added               : Yes
NMEA device connected to      : PC
Surface PAR voltage added     : Yes
Scan time added               : Yes
```

```
1) Frequency 0, Temperature
   Serial number : 5112
   Calibrated on : 11-Aug-21
   G             : 4.37912040e-003
   H             : 6.41671949e-004
   I             : 2.19205819e-005
   J             : 1.97553836e-006
   F0            : 1000.000
   Slope         : 1.00000000
   Offset        : 0.0000

2) Frequency 1, Conductivity
   Serial number : 3570
   Calibrated on : 10-Aug-21
   G             : -9.81144980e+000
   H             : 1.21489535e+000
   I             : -1.49288698e-003
   J             : 1.62338152e-004
   CTcor         : 3.2500e-006
   CPcor         : -9.57000000e-008
   Slope         : 1.00000000
   Offset        : 0.00000

3) Frequency 2, Pressure, Digiquartz with TC
   Serial number : 0287
   Calibrated on : 14-Nov-17
   C1            : -3.790306e+004
   C2            : 9.794570e-002
   C3            : 1.354010e-002
   D1            : 4.020500e-002
   D2            : 0.000000e+000
   T1            : 3.035689e+001
   T2            : -2.122140e-004
   T3            : 4.413970e-006
   T4            : 3.212790e-009
   T5            : 0.000000e+000
   Slope         : 0.99989540
   Offset        : -4.21890
   AD590M        : 1.167000e-002
   AD590B        : -7.948920e+000

4) Frequency 3, Temperature, 2
   Serial number : 5115
   Calibrated on : 16-Jan-24
   G             : 4.33203430e-003
   H             : 6.38681269e-004
   I             : 2.19019858e-005
   J             : 2.06107407e-006
   F0            : 1000.000
   Slope         : 1.00000000
   Offset        : 0.0000
```

5) Frequency 4, Conductivity, 2
   Serial number : 3290
   Calibrated on : 09-Jan-24
   G   : -9.84519897e+000
   H   : 1.51594258e+000
   I   : 4.33780327e-004
   J   : 7.24364513e-005
   CTcor   : 3.2500e-006
   CPcor   : -9.57000000e-008
   Slope   : 1.00000000
   Offset   : 0.00000

6) A/D voltage 0, Oxygen, SBE 43
   Serial number : 4305
   Calibrated on : 13-Jul-23
   Equation   : Sea-Bird
   Soc   : 4.99610e-001
   Offset   : -4.83900e-001
   A   : -3.74710e-003
   B   : 1.88080e-004
   C   : -2.95430e-006
   E   : 3.60000e-002
   Tau20   : 1.35000e+000
   D1   : 1.92634e-004
   D2   : -4.64803e-002
   H1   : -3.30000e-002
   H2   : 5.00000e+003
   H3   : 1.45000e+003

7) A/D voltage 1, Oxygen, SBE 43, 2
   Serial number : 4303
   Calibrated on : 11-Jul-23
   Equation   : Sea-Bird
   Soc   : 5.01560e-001
   Offset   : -5.17200e-001
   A   : -4.58240e-003
   B   : 2.12870e-004
   C   : -2.79860e-006
   E   : 3.60000e-002
   Tau20   : 1.91000e+000
   D1   : 1.92634e-004
   D2   : -4.64803e-002
   H1   : -3.30000e-002
   H2   : 5.00000e+003
   H3   : 1.45000e+003

8) A/D voltage 2, Altimeter
   Serial number : 51533
   Calibrated on :
   Scale factor : 15.000
   Offset   : 0.000

9) A/D voltage 3, Fluorometer, WET Labs ECO CDOM
   Serial number : 7239
   Calibrated on : 21-Dez-2023
   Dark output   : 0.021
   Scale factor : 103.000

```
10) A/D voltage 4, Fluorometer, WET Labs ECO-AFL/FL
    Serial number : 8103
    Calibrated on : 20-April-2023
    Dark output   : 0.0180
    Scale factor  : 2.40000000e+001

11) A/D voltage 5, Transmissometer, WET Labs C-Star
    Serial number : 1220
    Calibrated on : 07-Sep-2022
    M             : 22.3083
    B             : -0.1278
    Path length   : 0.250

12) A/D voltage 6, Fluorometer, Dr. Haardt Yellow Sub.
    Serial number     : 03
    Calibrated on     :
    Gain range switch : None
    A0                : 0.00000000
    A1                : 1.00000000
    B0                : 0.00000000
    B1                : 1.00000000

13) A/D voltage 7, PAR/Logarithmic, Satlantic
    Serial number        : 2197
    Calibrated on        : 30-Nov-2021
    a0                   : 1.04100000
    a1                   : 0.80687000
    Im                   : 1.35890000
    Conversion units     : umol photons/m^2/sec
    Multiplier           : 1.00000000

14) SPAR voltage, Unavailable

15) SPAR voltage, SPAR/Linear, Satlantic
    Serial number     : 2335
    Calibrated on     : 9-Jan-2024
    a0                : 0.12892000
    a1                : 581.29170000
    Im                : 1.00000000
    Conversion units  : umol photons/m^2/sec
    Conversion factor : 1.00000000
    Ratio multiplier  : 1.00000000
```

Two 300 kHz RDI Workhorse up- and downward-looking ADCPs were mounted on the CTD/rosette to act as lowered ADCPs (LADCP): ADCP SN 23293 (sw1309) as master, looking down and ADCP SN 23292 (sw1258) as slave, looking up. The LADCP assembly was powered by a separate battery container, and interconnected by a star-type cable. The ADCPs were operated using the GUI of the LADCP tool V1.7 from GEOMAR. LADCP measurements were conducted at all CTD stations. The battery was changed twice after 2.5 weeks of operation, the last time on 06 October. See the subsection on the LADCP for additional details.

A SUNA nitrate sensor (SN 1166, depth rating 2000 m) was installed on the CTD/rosette during all casts shallower than its depth rating, to obtain high-resolution nitrate profiles. The instrument was powered by the SBE911plus system, and recorded its data internally. The data were retrieved from the instrument's internal memory and the instrument time was synchronized to UTC on a regular basis using a PC. For additional details on the SUNA, refer to the section of the chemistry team.

An Underwater Vision Profiler (UVP) was attached to the rosette to continuously record plankton and particle images during the CTD downcast. For additional details, refer to Section UVP. The initial configuration (*conf1*) of the SBE911+ CTD on the rosette remained unchanged throughout the cruise. The sensor configuration is summarized in Table 2.2.

Finally, a set of 4 small plastic pieces were attached to the CTD with cable ties on 10 September to test their durability in Arctic waters (Fig. 2.7). These were provided by the German Hydrographic Institute BSH (Hamburg, Germany), and intended to be included on their ArgoFloats. They were attached to the CTD on 10 September, and removed on 19 October 2025. In total, they remained on the CTD for 104 casts (see Tab. 2.3).

Fig. 2.7: POM parts provided by the BSH for their ArgoFloats attached to the CTD. Photo by Mario Hoppmann.

Furthermore, a Satlantics/SeaBird SUNA nitrate sensor (SN 1166) was installed on the rosette during most casts. As this sensor has a depth rating of 2,000 m, it was only attached during casts shallower than that. The device was programmed to start sampling – and recording the data internally – as soon as power is supplied. Power was supplied by the SBE11plus, so that data acquisition starts when the CTD is turned on.

During the CTD profiles (see Tab. 2.3), water samples were collected at all stations except 44_01_01, 44_01_02, 44_01_03, 44_01_04, 44_01_05, **87_01**. The Niskin bottles were fired during the upcast, with a 20-second pause before each firing to allow the sensors to stabilize and to ensure sampling of the ambient water mass. These water samples were analyzed by different groups participating in the expedition. The Physical Oceanography group used them to calibrate salinity and oxygen measurements. The salinometry results are presented below, and the oxygen titration results are shown in the section of the chemistry team**.**

Tab. 2.3 (next pages): Overview of the CTD-rosette stations showing times and locations, as well as the LADCP file names, the section names (see final section of this chapter), and any comments on unusual aspects during the respective stations.

Station	LADCP	Time(UTC)	Lat(N)	Lon(E)	Actual Depth[m]	Cast Depth[m]	Description	Comments
001_01	002	'05-Sep-2025 10:55:00'	80.084	2.929	2356	2325	Test	Altimeter did not work. Transmission signal indicated that we are at bottom boundary layer.
002_01	004	'05-Sep-2025 18:55:06'	80.542	2.8262	1518	1516	Test	
003_01	005	'06-Sep-2025 04:10:04'	81.28	3.1407	791	788	Test	25 meter from the
005_01	006	'07-Sep-2025 02:50:33'	82.388	-3.4787	2379	2319	Flade_1	1000 and 2000 m for calibration.
006_01	007_01	'07-Sep-2025 08:47:04'	82.35	-3.9852	3308	1000	Flade_1	
007_01	008	'07-Sep-2025 12:28:24'	82.3	-4.4927	3533	1001	Flade_1	
008_01	009	'07-Sep-2025 15:00:31'	82.253	-5.0245	3381	3135	Flade_1	any signal. CTD stopped according to Hydrosweep
008_04	10	'07-Sep-2025 20:38:03'	82.237	-4.9427	2742	751	Flade_1	
009_01	11	'08-Sep-2025 01:19:35'	82.212	-5.5763	4032	4030	Flade_1	fired 4 bottles at 2000 m. Needed second cast.
009_04		'08-Sep-2025 05:51:48'	82.215	-5.4858	4253	100	Flade_1	Shallow cast to 100 meter to get water samples.
010_01	12	'08-Sep-2025 08:03:31'	82.155	-6.017	3565	1001	Flade_1	Two bottles were not closed correctly.
011_01	13	'08-Sep-2025 11:01:58'	82.124	-6.5967	3385	3404	Flade_1	
012_03	14	'08-Sep-2025 19:42:10'	82.077	-7.1372	3344	1001	Flade_1	
013_01	15	'08-Sep-2025 23:24:41'	82.033	-7.5845	3403	1000	Flade_1	
014_01	16	'09-Sep-2025 01:51:31'	81.984	-8.1427	3098	3057	Flade_1	
015_01	17	'09-Sep-2025 06:14:53'	81.941	-8.6377	2789	1001	Flade_1	
016_01	18	'09-Sep-2025 08:49:52'	81.887	-9.2245	2596	1001	Flade_1	
018_01	19	'09-Sep-2025 12:59:37'	81.876	-9.3978	2338	2286	Flade_1	
020_01	20	'09-Sep-2025 19:12:00'	81.852	-9.6328	2303	1001	Flade_1	
022_01	21	'09-Sep-2025 22:49:13'	81.827	-9.8928	2166	1900	Flade_1	The plan was 1300 m, hence suna was on. Hydrosweep indicated
024_01	22	'10-Sep-2025 01:46:42'	81.807	-10.108	1161	1111	Flade_1	
025_01	23	'10-Sep-2025 09:31:36'	81.724	-9.7868	577	551	Flade_1	No hydrosweep. (Narwhal zone)
027_01	24	'10-Sep-2025 12:34:08'	81.684	-9.9238	551	535	Flade_1	
029_01	25	'10-Sep-2025 15:27:44'	81.613	-10.274	329	353	Flade_1	Bottle 10 did not close.
030_01	26	'10-Sep-2025 20:47:05'	81.523	-10.546	147	148	Flade_1	
031_01	27_1	'11-Sep-2025 00:00:26'	81.479	-10.963	74	74	Flade_1	
032_01	28	'11-Sep-2025 01:55:12'	81.49	-11.41	53	58	Flade_1	
036_01	29	'12-Sep-2025 06:29:06'	82.305	-18.163	120	121	Independence Mouth	
037_01	30	'12-Sep-2025 07:56:06'	82.366	-18.555	379	372	Independence Mouth	
038_01	30	'12-Sep-2025 09:46:19'	82.429	-18.957	495	503	Independence Mouth	037_01 and 038_01 is the same LADCP file as 030.
039_01	31	'12-Sep-2025 13:46:35'	82.48	-19.405	466	457	Independence Mouth	
040_01	32	'12-Sep-2025 17:02:49'	82.548	-19.85	118	137	Independence Mouth	We stopped when the altimeter was 20 m since it was already below the depth from hydrosweep.
041_01	33	'12-Sep-2025 18:56:42'	82.495	-19.481	489	491	Independence Mouth	
042_01	34	'12-Sep-2025 21:14:05'	82.412	-18.869	526	516	Independence Mouth	
044_02	35	'13-Sep-2025 12:16:19'	83.158	-19.421	1052	1045	Ice station 1	The filename is 044_01_01. LADCP file '35' contains first and second cast.
044_02	35	'13-Sep-2025 13:12:45'	83.156	-19.403	1073	1072	Ice station 2	The filename is 044_01_02.

044_04	36	'13-Sep-2025 15:15:40'	83.152	-19.357	1070	1060	Ice station 3	The filename is 044_01_03. LADCP file '36' contains last four cast for the ice station.
044_04	36	'13-Sep-2025 16:11:09'	83.15	-19.337	1067	1084	Ice station 4	The filename is 044_01_04.
044_04	36	'13-Sep-2025 17:02:33'	83.148	-19.319	1087	1073	Ice station 5	The filename is 044_01_05. 10 bottles are closed.
044_04	36	'13-Sep-2025 17:57:20'	83.145	-19.301	1076	1056	Ice station 6	The filename is 044_01_06.
045_01	37	'14-Sep-2025 11:05:11'	83.109	-22.37	218	216	Wandel	Bottle 10 did not close.
046_01	38	'14-Sep-2025 13:35:17'	83.165	-21.579	226	221	Wandel	
047_01	40	'14-Sep-2025 18:29:54'	83.227	-21.047	203	205	Wandel	Temperature, salinity and oxygen had larger values in the upcast. 0,4 C at 110 meter, 0,6 PSU at 35 m, and maximum difference for oxygen at 60 m.
048_01	41	'14-Sep-2025 20:13:14'	83.258	-20.472	237	235	Wandel	
050_01	42	'14-Sep-2025 23:14:07'	83.282	-20.133	1076	1073	Wandel	
050_06	43	'15-Sep-2025 06:55:38'	83.29	-20.126	1154	1164	Wandel	
052_01	44	'15-Sep-2025 12:56:50'	83.31	-19.903	1854	1946	Wandel	Chl max dropped to 0,4 from 0,8 mg/m3 and moved to 75 m in the upcast.
054_01	45	'15-Sep-2025 16:57:09'	83.335	-19.545	2988	2922	Wandel	Cast started at 18:00 in shiplog. Chl max at 90 m associated with lower beam transmission, temperature and oxygen changes.
056_01	46	'15-Sep-2025 23:57:51'	83.362	-19.211	3113	3107	Wandel	
058_01	47	'16-Sep-2025 05:13:35'	83.411	-18.669	3125	1000	Wandel	
059_01	48	'16-Sep-2025 09:49:54'	83.465	-18.11	3174	1001	Wandel	
059_07	49	'16-Sep-2025 16:22:18'	83.435	-17.869	3096	1001	Wandel	
060_01	050	'16-Sep-2025 19:01:46'	83.508	-17.477	3195	1001	Wandel	
061_01	051	'16-Sep-2025 22:29:00'	83.56	-16.892	3233	3229	Wandel	Salinity difference is not 0 but constant.
062_01	52	'17-Sep-2025 03:00:48'	83.613	-16.335	3405	1000	Wandel	
063_01	53	'17-Sep-2025 06:03:15'	83.665	-15.732	3486	1001	Wandel	
064_01	54	'17-Sep-2025 13:47:09'	83.663	-14.783	3528	1001	Wandel	
065_01	not running	'17-Sep-2025 17:47:19'	83.75	-14.534	3563	101	Wandel	
065_02	55	'17-Sep-2025 18:54:02'	83.749	-14.529	3558	3558	Wandel	Ctd stopped at 3045 due to winch operation.
066_01	56	'18-Sep-2025 00:43:05'	83.813	-13.874	3651	1000	Wandel	
067_01	57	'18-Sep-2025 04:54:11'	83.859	-13.429	3777	1000	Wandel	Strong increase in temperature in upcast.
068_01	58_2	'18-Sep-2025 09:21:40'	83.911	-12.649	3851	3850	Moris Jesup Rise	Bottle 5 did not close.
068_03	60	'18-Sep-2025 19:15:12'	83.904	-12.675	3855	1001	Moris Jesup Rise	
069_01	not running	'19-Sep-2025 03:31:01'	84.096	-15.465	3762	1000	Moris Jesup Rise	
070_01	62	'19-Sep-2025 15:22:05'	84.259	-18.367	3150	1001	Moris Jesup Rise	LADCP restarted due to conncection problems via COM ports.
071_01	63	'19-Sep-2025 21:41:46'	84.307	-18.941	3335	1001	Moris Jesup Rise	No uplooker file for LADCP.
072_01	64	'20-Sep-2025 02:30:24'	84.351	-19.64	3320	3316	Moris Jesup Rise	Chl max was nearly 1 mg/m3(way higher than usual). Strong temperature max difference between upcast and downcast.

073_01	68_2	'20-Sep-2025 09:54:47'	84.377	-20.121	1079	1091	Moris Jesup Rise	CTD needed to go out of water due to re-parking the ship. The new cast named as 073_01_02. Bottle 5 did not close. COM5 did not work while starting LADCP.
074_01	69	'20-Sep-2025 13:21:22'	84.37	-19.911	2437	2389	Moris Jesup Rise	Bottle 5 did not close.
075_01	71_1	'20-Sep-2025 18:22:23'	84.39	-20.345	790	789	Moris Jesup Rise	
076_01	72	'20-Sep-2025 22:20:51'	84.427	-20.768	762	784	Moris Jesup Rise	
077_01	73	'21-Sep-2025 02:29:01'	84.436	-21.146	719	719	Moris Jesup Rise	
078_03	74	'21-Sep-2025 13:00:41'	84.471	-21.04	738	734	Moris Jesup Rise	Filename is 078_01.
079_01	75_1	'22-Sep-2025 07:07:35'	84.222	-25.396	621	610	Cape Morris Jesup	Bottle 1 imploded and bottle 2 got a crack.
080_01	77(?)	'22-Sep-2025 12:54:41'	84.153	-25.872	616	601	Cape Morris Jesup	
081_01		'22-Sep-2025 19:21:41'	84.104	-26.421	600	581	Cape Morris Jesup	
082_01	80	'22-Sep-2025 23:00:52'	84.044	-27.059	547	530	Cape Morris Jesup	
083_01	81	'23-Sep-2025 02:58:37'	83.991	-27.677	379	368	Cape Morris Jesup	
084_01	82	'23-Sep-2025 05:45:15'	83.908	-28.025	266	261	Cape Morris Jesup	
085_01	83	'23-Sep-2025 12:09:45'	83.858	-28.67	84	93	Cape Morris Jesup	
085_06	84	'23-Sep-2025 14:46:44'	83.858	-28.69	95	93	Cape Morris Jesup	
086_01	85	'23-Sep-2025 16:11:48'	83.837	-28.841	79	83	Cape Morris Jesup	
088_01	86	'23-Sep-2025 18:59:02'	83.919	-28.496	207	214	Cape Morris Jesup	filename is 087_01
089_01	87	'24-Sep-2025 03:47:42'	84.276	-27.535	1061	1062		
089_07	88	'24-Sep-2025 10:18:04'	84.289	-27.829	1015	1015		Bottle 11 did not close well, however, it was samplable.
090_03	90	'25-Sep-2025 12:55:12'	83.887	-24.234	2491	2498		
091_01	92	'27-Sep-2025 10:50:22'	82.454	-15.653	188	177	Independence Shelfbreak	There are spikes in beam tranmission in first 20 m at the downcast.
093_01	93	'27-Sep-2025 16:09:26'	82.502	-14.621	1335	1202	Independence Shelfbreak	
093_05	94	'27-Sep-2025 19:29:26'	82.467	-14.516	808	731	Independence Shelfbreak	Bottle 5 did not close. Strong drift. Ctd started at 808 m depth but it moved to 730 m when it was at depth.
094_01	95	'27-Sep-2025 22:38:09'	82.554	-14.213	2115	1948	Independence Shelfbreak	CTD stopped during the downcast because of the ice closing. Stopped when the altimeter shows 40 m because of upslope drift.
095_01	96	'28-Sep-2025 02:17:42'	82.579	-13.673	2320	2178	Independence Shelfbreak	Filename is 095_01_01. Software crushed in downcast. Station restarted.
096_01	97	'28-Sep-2025 17:41:13'	82.422	-16.166	189	187	Independence Shelfbreak	
097_01	98_01	'28-Sep-2025 19:15:37'	82.38	-16.708	163	165	Independence Shelfbreak	
098_03	99	'30-Sep-2025 08:42:37'	81.699	-12.139	129	124	Flade_2	
099_01	100	'30-Sep-2025 12:59:19'	81.737	-11.562	178	177	Flade_2	Bottle 5 did not close. Navlot depth correction: depth_flade_corrected.xlsx
100_02	102	'30-Sep-2025 17:37:55'	81.776	-10.651	201	201	Flade_2	
101_02	103	'30-Sep-2025 20:29:48'	81.8	-10.342	584	571	Flade_2	Bottle 5 did not close.
102_01	104	'30-Sep-2025 22:17:48'	81.834	-9.9208	2198	2144	Flade_2	Stopped at 60 m in altimeter. The signal was not decreasing steadily. Strong gradient in bathymetry.

103_01	105	'01-Oct-2025 01:03:19'	81.811	-10.253	939	1004	Flade_2	
104_01	106	'01-Oct-2025 11:03:19'	81.841	-9.7387	2264	2201	Flade_2	
105_01	108	'01-Oct-2025 17:51:19'	81.886	-9.3225	2504	1001	Flade_2	
106_01	109	'01-Oct-2025 21:56:12'	81.921	-8.9538	2712	2642	Flade_2	
107_02	110	'02-Oct-2025 09:09:44'	81.978	-8.0577	3035	1001	Flade_2	
113_01	111	'03-Oct-2025 23:42:16'	80.955	-2.345	4277	4278		The hook is replaced for bottle 23 by Mario. 'Bouncing' when stopping CTD for bottles.
117_01	112	'06-Oct-2025 21:48:52'	78.209	-15.518	249	243	Ile de France	5 angle in cable. 1.3 knot ship speed/drift.
118_01	113	'06-Oct-2025 23:13:12'	78.176	-15.714	361	348	Ile de France	
118_04	114	'07-Oct-2025 00:45:45'	78.165	-15.76	372	363	Ile de France	file name is 118_03.
119_01	115	'07-Oct-2025 02:07:57'	78.142	-15.914	408	406	Ile de France	
120_01	116	'09-Oct-2025 02:41:40'	80.313	-12.332	173	167	Holm	
121_01	117	'09-Oct-2025 04:54:55'	80.354	-12.455	216	206	Holm	
122_01	118	'09-Oct-2025 06:33:47'	80.394	-12.649	257	250	Holm	Aquadop SN12706 calibration cast. Stopped 15 mins at 230 and 200 m.
123_01	119	'09-Oct-2025 15:50:51'	80.485	-12.985	278	272	Holm	
123_06	120	'09-Oct-2025 18:30:06'	80.478	-12.913	280	274	Holm	
124_01	121	'09-Oct-2025 21:12:47'	80.543	-13.285	259	254	Holm	
125_01	122	'09-Oct-2025 23:38:12'	80.604	-13.592	133	133	Holm	Bottle 1 did not close.
126_01	123	'10-Oct-2025 02:23:57'	80.462	-14.664	319	317	Holm	Pronounced mixed layer around 50 m. Very thin ice cover. One noght after the storm.
127_03	124	'10-Oct-2025 14:16:08'	80.136	-16.021	221	218	Holm	Spikes occurred on both temperature and conductivity sensors. Noticed only in processing. Also in raw data -11 C temperature between 5200 and 5207 scan.
127_06	125	'10-Oct-2025 18:30:53'	80.166	-15.807	303	302	Holm	
128_01	126	'11-Oct-2025 00:07:16'	80.115	-15.732	374	363	Holm	Bottle 1 did not close.
129_01	127	'11-Oct-2025 02:28:33'	80.158	-16.042	324	314	Holm	Station name entered 128_01 INSIDE THE FILE uncorrectly.
130_01	128	'11-Oct-2025 06:41:18'	80.177	-16.327	147	148	Holm	
131_01	130	'11-Oct-2025 08:16:52'	80.194	-16.452	149	142	Holm	
132_01	132	'12-Oct-2025 06:12:29'	79.423	-17.304	413	401		
133_01	133	'12-Oct-2025 11:23:20'	79.209	-17.45	153	148	Norske Trough	
134_02	134	'12-Oct-2025 16:15:50'	79.208	-17.172	370	359	Norske Trough	The filename is 134_01.
135_02	135	'12-Oct-2025 19:51:29'	79.169	-17.08	398	387	Norske Trough	CTD waited 5 minutes on deck with syringe on and heater next to it. No freezing. Bottle 1 did not close. Station name is 134_02 INSIDE THE FILE uncorrectly.
135_07	136	'12-Oct-2025 23:06:33'	79.159	-17.096	397	386	Norske Trough	Bottle 1 did not close.

In Table 2.3**,** two different depth values are listed: *cast depth* and *actual depth*. The *cast depth* refers to the maximum depth to which the CTD was lowered, while the *actual depth* corresponds to the bottom depth obtained either from the Hydrosweep or from depth sounding, depending on whether the station was located within the Narwhal area.

Typically, the CTD was lowered until the altimeter indicated a distance of 10 m above the seafloor. At some stations, however, the lowering was stopped earlier due to strong drift or steep topography, such as at **station 102_01**. In a few cases, no altimeter signal was available, and the bottom depth was instead determined from Hydrosweep or depth sounding data, with careful verification of the beam transmission—e.g., at **station 008_01**. In some cases, such as **station 040_01**, the CTD was stopped approximately 20 m above the bottom because it had already exceeded the depth indicated by the Hydrosweep.

During the initial test station, all Niskin bottles closed successfully. The altimeter did not give any signal. Beam transmission signals indicated that the CTD was within the bottom boundary layer, even though it was approximately 30 m shallower than the depth obtained from the Hydrosweep. The two oxygen sensors showed a disagreement of 0.3 ml l^{-1}. The surface Photosynthetically Active Radiation (PAR) sensor was tested at 10:59 during this station.

The originally installed Benthos altimeter did not provide reliable readings until the CTD was approximately 30 m above the bottom. At some casts such as **001_01**, it did not record any signal. Hence, it was substituted by a Valeport altimeter tool was installed after **012_01**, which led to a dramatic improvement in the measurements. With the new tool, altimeter signals consistently began around 90–100 m above the bottom (Fig. 2.8).

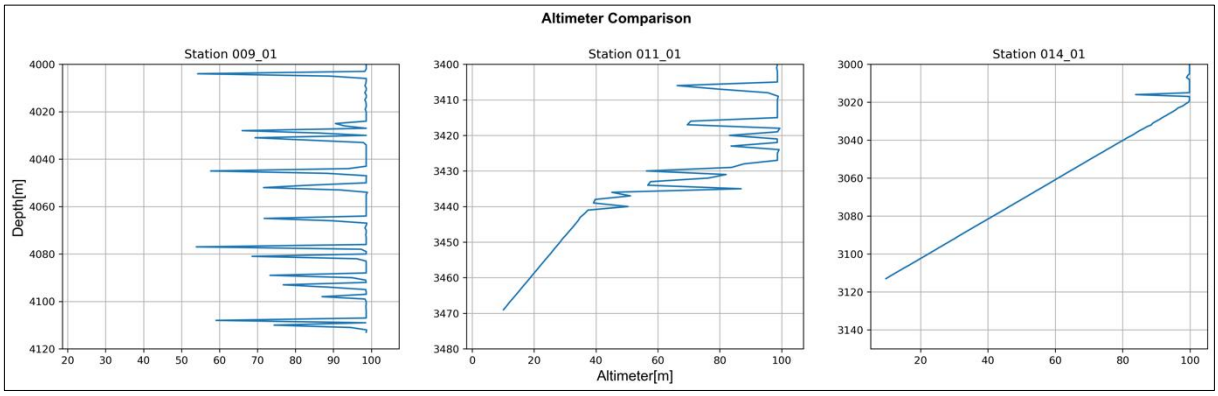

Fig. 2.8: Comparison of the behavior of the different altimeters: left and center panels show casts with the Benthos altimeter and right panel shows a cast with the Valeport altimeter.

The biological working groups targeted the chlorophyll maximum in each profile. The intensity and depth of the chlorophyll maximum occasionally differed between the downcast and upcast, as observed at **station 052_01**, where the chlorophyll maximum decreased from 0.8 to 0.4 mg m^{-3}.

Station and cast numbers occasionally differed between the dataset and the ship's records. To preserve the integrity of the files, these discrepancies have not been corrected. The correct station numbers and their corresponding file names are provided in Table 2.4.

Station Number as logged by the ship	Station Number in CTD protocols
009_04	009_03
044_02	044_01_01
044_02	044_01_02
044_04	044_01_03
044_04	044_01_04
044_04	044_01_05
044_04	044_01_06
078_03	078_01
088_01	087_01
134_02	134_01

Tab. 2.4: Matching of incorrectly assigned file and protocol names to the correct station numbers as in DShip.

The temperature sensors did not exhibit any noticeable offset, whereas the oxygen sensors showed differences ranging from 0.2 to 0.4 ml l^{-1}. The salinity sensors agreed well up to approximately sample number 50,000; however, beyond this point, a slight negative tilt was observed, indicating that the primary sensor recorded lower values than the secondary sensor (Fig. 2.9).

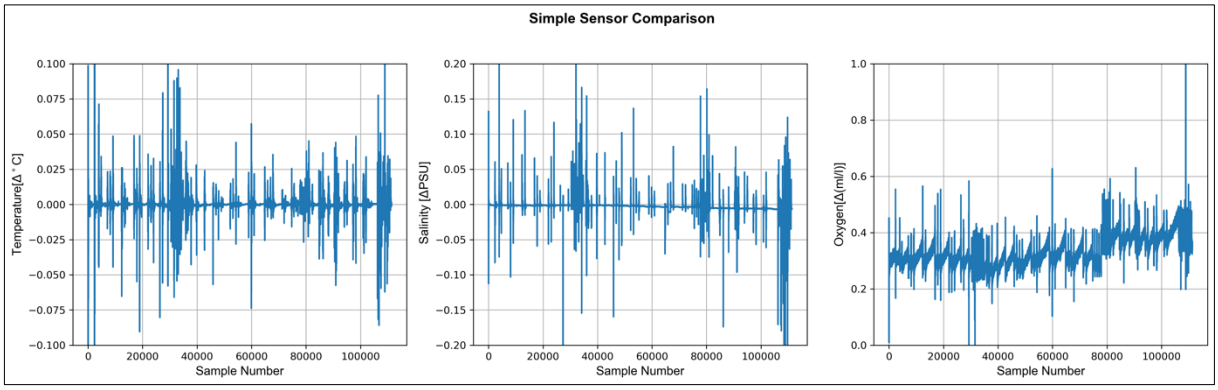

Fig. 2.9: Comparison of primary and secondary sensors for temperature, salinity (calculated from temperature and conductivity sensors), and oxygen (calculated from temperature, conductivity, and oxygen sensors).

LADCP measurements (lowered acoustic Doppler current profiler)

Lowered LADCP measurements were conducted at all CTD stations. Table 2.7 lists the CTD stations and associated LADCP casts. In some casts the uplooker (slave) did not work, and data was only recorded by the downlooker (master). The processing was conducted with the LDEO LADCP software (Version IX_15). Folder *raw_unsorted* contains all LADCP raw data, while folder *raw* contains the raw data copied from *raw_unsorted* used for data processing. Folder *processed* contains the output of the processing with the LDEO LADCP software (the filename contains the CTD station name).

In order to save ship time, many CTD casts in deep water were conducted only to 1000m depth and therefore, the casts did not reach the bottom. In the beginning of the cruise, the altimeter did not work properly and we thus stopped much earlier than 10 m above the sea floor, whereas a number of casts in the deep ocean were conducted only until 1,000 m water depth. These profiles created problems during processing, as no bottom information was available. This resulted in unrealistically high velocities at depth.

During the entire cruise, the settings documented in Table 2.5 and Table 2.6 were used. Specifically, they use a bin size of 10 m, a maximum range of 200 m, beam coordinates, no blanking after transmission, narrow band processing, and timing of the master and slave such that the acoustic energy of the master is separated by 0.55 seconds from the acoustic energy of the slave.

The Slave (upward-looking) and Master (downward looking) data file names consist of the LADCP cast number (three digit), an abbreviation indicating the viewing direction (UP for upward and DN for downward) and a running number with three digits beginning with 000, representing the file number. In some cases, with multiple files, running numbers can be higher value such as 001 and 002. These files are stored according to LADCP cast number. Please, note that LADCP cast number and station number are not the same numbers. Sometimes also log files documenting all actions conducted as starting (with configurations), stopping, and downloading was kept, but since the files were not downloaded after every cast, and sometimes these log files are not available for all stations.

After the 58th cast, the LADCP started to have connection problems. Both of the cables were changed, in addition to that, the underwater plug for the Master at the rim of the CTD-rosette was changed. There are no cast files between 64 and 68, because these were test casts for the changed cables and connector. However, there were still major issues with the connection of the ADCPs and the computer in the winch room. During several CTD casts only one of the ADCP was recording (e.g. 071 LADCP cast), or there are some stations during which LADCP did not record anything (e.g. 124 LADCP cast). After several CTD casts, the stop and download command did not work, in which files were needed to be downloaded manually (e.g. 115 LADCP cast) (Tab. 2.7).

Data processing was carried out with the LDEO LADCP Software Version IX.15 which is executed in Matlab. The software combines, if available, data from the LADCP, CTD, navigational data, and vessel-mounted ADCP to conduct the velocity inversion method.

Tab. 2.5: Start protocol of the Master LADCP used during PS150

[BREAK Wakeup A]
WorkHorse Broadband ADCP Version 50.40
Teledyne RD Instruments (c) 1996-2010
All Rights Reserved.
SB0 Writing Channel B Break State [DISABLED].
CR1
[Parameters set to FACTORY defaults]
SB0 Writing Channel B Break State [DISABLED].
TS yy/mm/dd,hh:MM:ss
WM15 ; LADCP water ping mode 15
WV250 ; ambiguity velocity
WN20 ; 20 bins
WS1000 ; 10 m bins
WF0 ; no blank after transmit
WB1 ; narrow band
EZ0111101 ; fixed speed of sound
EX00111 ; beam coordinates, use pitch/roll, 3 beam solution, bin mapping
CF11101 ; allow serial output
WP1 ; single ping data
TP 00:00.00 ; ping length of <0.00 seconds

TE 00:00:01.20 ; ensemble length of 1.2 seconds
SM1 ; Master
SI0 ; sync pulse on every ping, n/a for Slave, but needs ST0200
SA011 ; sync pulse before every ensemble
SW5500 ; wait 0.55 seconds, n/a for Slave
CQ255 ;
RN (three-digit cast no.)DN ; file name
CK
[Parameters saved as USER defaults]
SA = 011 ---------- Synch Before/After Ping/Ensemble Bottom/Water/Both
SI = 00000 ---------- Synch Interval (0-65535)
SM = 1 ---------- Mode Select (0=OFF,1=MASTER,2=SLAVE,3=NEMO)
SS = 0 ---------- RDS3 Sleep Mode (0=No Sleep)
ST = 00000 ---------- Slave Timeout (seconds,0=indefinite)
SW = 05500 ---------- Synch Delay (1/10 msec)
T?
Available Commands:
*TB 00:00:00.00 TC 00000 TE 00:00:01.20 TF **/**/**,**:**:** TG ****/**/**,**:**:** TP 00:00.00 TS yy/mm/dd,hh:MM:ss ---------- Time per Burst (hrs:min:sec.sec/100)*
---------- Ensembles Per Burst (0-65535)
---------- Time per Ensemble (hrs:min:sec.sec/100)
---------- Time of First Ping (yr/mon/day,hour:min:sec)
---------- Time of First Ping (CCYY/MM/DD,hh:mm:ss)
---------- Time per Ping (min:sec.sec/100)
---------- Time Set (yr/mon/day,hour:min:sec)
TT yyyy/mm/dd,hh:MM:ss ---------- Time Set (CCYY/MM/DD,hh:mm:ss)
TX 00:00:00 ---------- Buffer Output Period: (hh:mm:ss)
T? ---------- Display Time Help
W?
Available Commands:
WD 111100000 ---------- Data Out (Vel;Cor;Amp PG;St;P0 P1;P2;P3)
WF 0000 WG 000 WN 020 WP 00001 WS 1000 WV 250 WZ 010 ---------- Blank After Transmit (cm)
---------- Percent Good Minimum (1-100%)
---------- Number of depth cells (1-255)
---------- Pings per Ensemble (0-16384)
---------- Depth Cell Size (cm)
---------- Mode 1 Ambiguity Vel (cm/s radial)
---------- Mode 5 Ambiguity Velocity (cm/s radial)
W? ---------- Display Water-Profile Help
E?
EA = +00000 EB = +00000 ED = 00000 ES = 35 EX = 00111 EZ = 0111101 ---------- Heading Alignment (1/100 deg)
---------- Heading Bias (1/100 deg)

---------- Transducer Depth (0 - 65535 dm)
---------- Salinity (0-40 pp thousand)
---------- Coord Transform (Xform:Type; Tilts; 3Bm; Map)
---------- Sensor Source (C;D;H;P;R;S;T)
CS ; start pinging

Tab. 2.6: Start protocol of the Slave LADCP used during PS131

[BREAK Wakeup A]
WorkHorse Broadband ADCP Version 50.40
Teledyne RD Instruments (c) 1996-2010
All Rights Reserved.
SB0 Writing Channel B Break State [DISABLED].
43***PS131***
CR1
[Parameters set to FACTORY defaults]
SB0 Writing Channel B Break State [DISABLED].
TS yy/mm/dd,hh:MM:ss
WM15 ; LADCP water ping mode 15
WV250 ; ambiguity velocity
WN20 ; 20 bins
WS1000 ; 10 m bins
WF0 ; no blank after transmit
WB1 ; narrow band
EZ0111101 ; fixed speed of sound
EX00111 ; beam coordinates, use pitch/roll, 3 beam solution, bin mapping
CF11101 ; allow serial output
WP1 ; single ping data
TP 00:00.00 ; ping length of <0.00 seconds
TE 00:00:01.20 ; ensemble length of 1.2 seconds
SM2 ; Slave
SA011 ; sync pulse before every ensemble
ST200 ; slave timout 200 seconds, n/a for Master, but needs SI0
CQ255 ;
RN (three-digit cast no.)UP ; file name
CK
[Parameters saved as USER defaults]
S?
SA = 011 ---------- Synch Before/After Ping/Ensemble Bottom/Water/Both
SI = 00000 ---------- Synch Interval (0-65535)
SM = 2 ---------- Mode Select (0=OFF,1=MASTER,2=SLAVE,3=NEMO)
SS = 0 ---------- RDS3 Sleep Mode (0=No Sleep)
ST = 00200 ---------- Slave Timeout (seconds,0=indefinite)
SW = 00000 ---------- Synch Delay (1/10 msec)

T?

Available Commands:

*TB 00:00:00.00 TC 00000 TE 00:00:01.20 TF **/**/**,**:**:** TG ****/**/**,**:**:** TP 00:00.00 TS yy/mm/dd,hh:MM:ss TT yyyy/mm/dd,hh:MM:ss TX 00:00:00 ---------- Time per Burst (hrs:min:sec.sec/100)*

---------- Ensembles Per Burst (0-65535)

---------- Time per Ensemble (hrs:min:sec.sec/100)

---------- Time of First Ping (yr/mon/day,hour:min:sec)

---------- Time of First Ping (CCYY/MM/DD,hh:mm:ss)

---------- Time per Ping (min:sec.sec/100)

---------- Time Set (yr/mon/day,hour:min:sec)

---------- Time Set (CCYY/MM/DD,hh:mm:ss)

---------- Buffer Output Period: (hh:mm:ss)

T? ---------- Display Time Help

W?

Available Commands:

WD 111100000 ---------- Data Out (Vel;Cor;Amp PG;St;P0 P1;P2;P3)

WF 0000 WG 000 WN 020 WP 00001 WS 1000 WV 250 WZ 010 ---------- Blank After Transmit (cm)

---------- Percent Good Minimum (1-100%)

---------- Number of depth cells (1-255)

---------- Pings per Ensemble (0-16384)

---------- Depth Cell Size (cm)

---------- Mode 1 Ambiguity Vel (cm/s radial)

---------- Mode 5 Ambiguity Velocity (cm/s radial)

W? ---------- Display Water-Profile Help

E?

EA = +00000 EB = +00000 ED = 00000 ES = 35 EX = 00111 EZ = 0111101 CS

---------- Heading Alignment (1/100 deg)

---------- Heading Bias (1/100 deg)

---------- Transducer Depth (0 - 65535 dm)

---------- Salinity (0-40 pp thousand)

---------- Coord Transform (Xform:Type; Tilts; 3Bm; Map)

---------- Sensor Source (C;D;H;P;R;S;T)

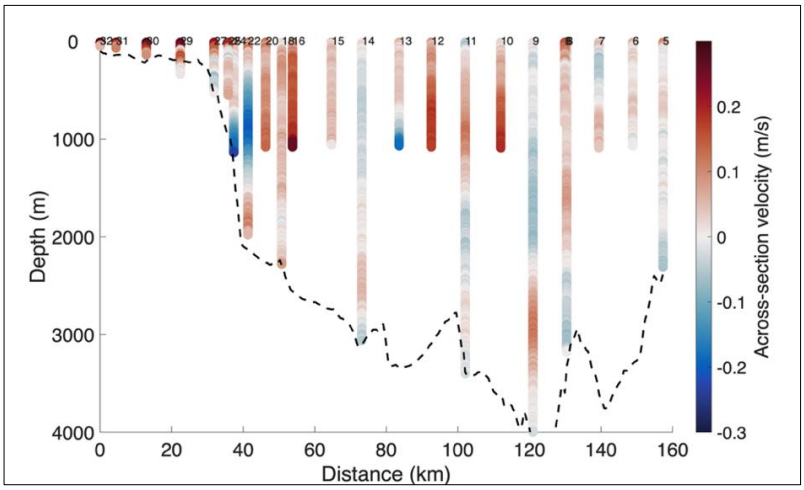

Fig. 2.10: Profiles of across-section velocity (positive out of the page) at the Flade section obtained from LADCP data. Some casts stopped at 1000 m water depth, and showed unrealistically high velocities at depth.

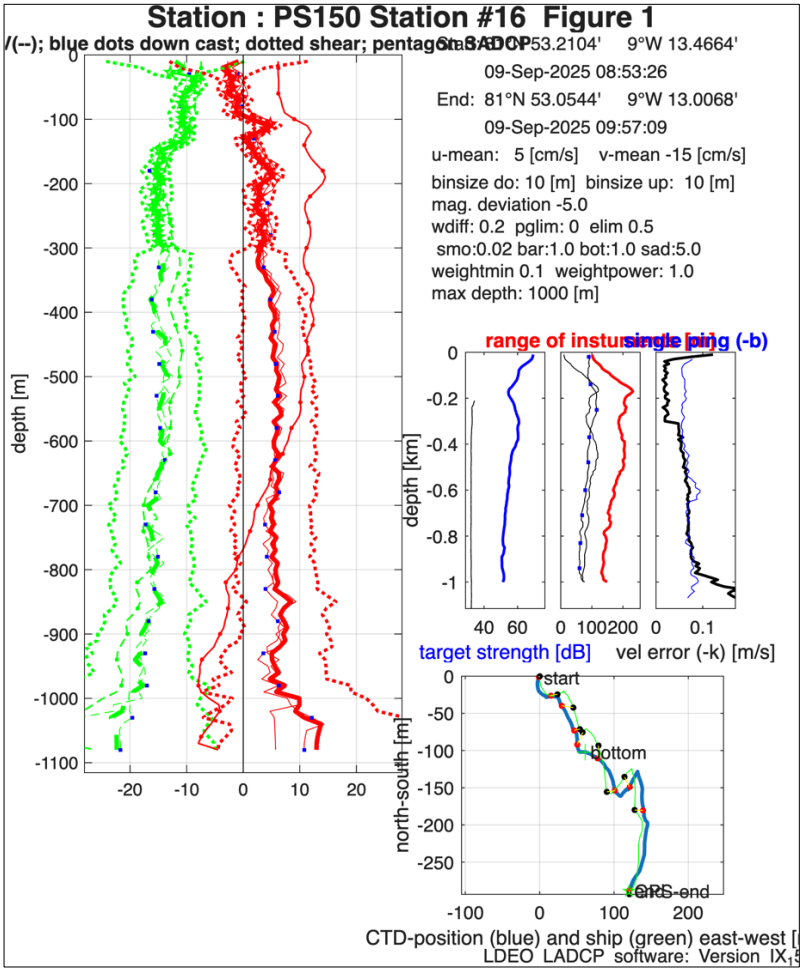

Fig. 2.11: Exemplary output of the LADCP processing software LDEO LADCP. The cast did not reach the bottom.

Tab. 2.7: CTD cast number and the corresponding LACDP casts

CTD cast no.	LADCP profile no.	DOWN	UP	cast reaches bottom	Comments
001_01	2	x	x	y	
002_01	4	x	x	y	
003_01	5	x	x	y	
005_01	6	x	x	y	
006_01	7	x	x	n	
007_01	8	x	x	y	
008_01	9	x	x	y	
008_04	10	x	x	n	
009_01	11	x	x	y	
010_01	12	x	x	n	
011_01	13	x	x	y	
012_03	14	x	x	n	
013_01	15	x	x	n	
014_01	16	x	x	y	
015_01	17	x	x	n	
016_01	18	x	x	n	
018_01	19	x	x	y	
020_01	20	x	x	n	
022_01	21	x	x	n	
024_01	22	x	x	y	
025_01	23	x	x	y	
027_01	24	x	x	y	
029_01	25	x	x	y	
030_01	26	x	x	y	
031_01	27	x	x	y	LADCP files are in folder 027_1
032_01	28	x	x	y	
036_01	29	x	x	y	
037_01	30	x	x	y	
038_01	30	x	x	y	
039_01	31	x	x	y	
040_01	32	x	x	y	
041_01	33	x	x	y	
042_01	34	x	x	y	
044_01_01	35	x	x	y	Two casts saved in one LADCP file
044_01_02	35	x	x	y	Two casts saved in one LADCP file
044_01_03	36	x	x	y	Four casts saved in one LADCP file
044_01_04	36	x	x	y	Four casts saved in one LADCP file
044_01_05	36	x	x	y	Four casts saved in one LADCP file
044_01_06	36	x	x	y	Four casts saved in one LADCP file
045_01	37	x	x	y	
046_01	38	x	x	y	
047_01	40	x	x	y	
048_01	41	x	x	y	
050_01	42	x	x	y	
050_06	43	x	x	y	
052_01	44	x	x	y	

054_01	45	x	x	y	
056_01	46	x	x	y	
058_01	47	x	x	n	
059_01	48	x	x	n	
059_07	49	x	x	n	
060_01	50	x	x	n	
061_01	51	x	x	y	
062_01	52	x	x	n	
063_01	53	x	x	n	
064_01	54	x	x	n	
065_02	55	x	x	y	
066_01	56	x	x	n	
067_01	57	x	x	n	
068_01	58	x	x	y	LADCP files are in folder 058_2
068_03	60	x	x	n	
070_01	62	x	x	n	
071_01	63	x		n	
072_01	64	x	x	y	
073_01_02	68	x	x	y	
074_01	69	x	x	y	
075_01	71	x	x	y	Processing not working
076_01	72	x	x	y	Processing not working
077_01	73	x	x	y	Processing not working
079_01	75	x	x	y	Processing not working
080_01	74	x	x	y	This is written in log sheet but time does not match. LADCP stopped at 11:48. Data files are 400 kb.
081_01	75	x	x	y	
082_01	80	x		y	Processing not working
083_01	81	x		y	
084_01	82	x		y	
085_01	83	x		y	
085_06	84	x		y	
086_01	85	x		y	
087_01	86	x		y	
089_01	87	x		y	
089_07	88	x		n	
090_03	90	x	x	y	
091_01	92	x		y	
093_01	93	x	x	y	
093_05	94	x	x	y	
094_01	95	x	x	y	
095_01	96	x	x	y	Software crash. Went to the 800 m, then back to surface, then do the cast again.
096_01	97	x		y	
097_01	98_01	x	x	y	LADCP did not stopped right away. Download time; 12:58 29th of September
098_03	99	x	x	y	

099_01	100	x	x	y	Processing not working
100_02	102	x	x	y	
101_02	103	x		y	
102_01	104	x		y	
103_01	105	x		y	
104_01	106	x		y	
105_01	108	x		n	
106_01	109	x		y	
107_02	110	x		n	
113_01	111	x		y	
117_01	112	x	x	y	
118_01	113	x	x	y	113UP000.000 is and empty file. Stopped in the middle of download.
118_04	114	x		y	113UP000.000 file can be found in this directory. There is no start log but download log time matches with 114th cast.
119_01	115	x		y	Could not connect to COM6, could not even establish connection via BB talk.
120_01	116	x	x	y	
121_01	117	x	x	y	
122_01	118	x		y	
123_01	119	x		y	
123_06	120	x		y	
124_01	121	x		y	
125_01	122	x		y	
126_01	123	x		y	
127_03	124				files empty
127_06	125				files empty
128_01	126	x		y	
129_01	127	x		y	
130_01	128	x	x	y	
131_01	130	x		y	
132_01	132	x	x	y	
133_01	133	x	x	y	
134_01	134	x	x	y	
135_02	135	x	x	y	
135_07	136	x	x	y	

Additionally, an external attitude/inertial motion unit (“IMP”) provided by A. Thurnherr (Columbia University, USA) was attached close to the upward-looking (Slave) ADCP to record improved attitude (heading, pitch, and roll) data with the aim to enhance the LADCP data (Thurnherr, 2017). It was connected to the slave ADCP with an additional T-type cable, and triggered by an external signal by the master ADCP. In total, external attitude data was obtained during 60 casts (Tab. 2.8). At first, the data was downloaded from the instrument using a USB cable, but it turned out to be much more efficient to open the instrument and retrieve the data directly from the µSD card. The instrument did not record data during a number of casts due to low power.

The settings of the instrument were:

```
     2 --- Sampling Mode (2: burst)
 50.00 --- Sampling Rate (Hz)
     1 --- Trigger Type (0: RTC, 1: external)
     1 --- Trigger Interval (s)
 2.000 --- Burst Duration (s)
     1 --- New File on Wakeup (0: no, 1: yes)
  3.50 --- Low Battery Voltage (V)
     0 --- Delay After Trigger (ms)
```

An overview of all files containing external attitude data is presented in Table 2.8.

Tab. 2.8: Filename (including date and time as mmdd_HHMM), duration (minutes) and battery voltage at start and end for each of 60 successful IMP cast.

Filename	Duration in min	Start voltage	End voltage
0917_1830.001	107.7	4.02	3.83
0917_2346.002	61.5	3.87	3.77
0918_0444.002	43.6	3.79	3.73
0918_0841.001	118.7	3.75	3.69
0918_1719.001	2.1	4.1	4.09
0918_1901.002	45	4.08	4
0919_0532.002	0.2	4.09	4.08
0919_1515.002	37.8	4.07	3.99
0919_1639.001	0.2	4.01	4
0920_0222.002	93.4	4.07	3.89
0920_0849.001	0.6	3.92	3.91
0920_0901.001	0.7	3.92	3.91
0920_0910.002	2.4	3.91	3.9
0920_0918.002	62.4	3.91	3.82
0920_1315.001	73.9	3.85	3.75
0920_1633.002	1.8	3.76	3.76
0920_1816.002	36.7	3.76	3.72
0920_2211.002	15.8	3.74	3.72
0920_2319.002	25	3.73	3.71
0921_0215.002	0.6	3.73	3.72
0921_0318.002	2	3.72	3.71
0921_1243.001	0.9	3.73	3.72
0921_1355.001	0.7	3.72	3.71
0922_0639.002	10.8	4.03	4.01
0922_0807.002	1.1	4	4
0922_1057.002	0.7	4.01	4
0922_1133.001	6.5	4	3.98
0922_1239.002	33.8	3.99	3.91
0922_1912.002	34	3.93	3.86
0926_1121.002	22.7	3.99	3.94
0927_1559.002	43	3.91	3.83

Filename	Duration in min	Start voltage	End voltage
0927_1920.002	33.4	3.86	3.79
0927_2216.001	69.9	3.81	3.73
0928_0111.001	95.1	3.75	3.69
0928_1731.001	22.5	3.72	3.68
0928_1906.003	18.8	3.7	3.67
0930_0829.001	21.4	4.02	3.96
0930_1252.002	22.1	3.98	3.91
0930_1730.002	19	3.93	3.88
0930_2019.003	33.4	3.91	3.84
0930_2207.001	64.1	3.87	3.77
1001_1045.002	71.9	3.78	3.72
1001_1737.002	1.2	3.74	3.73
1001_1742.002	37.1	3.74	3.71
1001_2139.001	82.2	3.73	3.66
1002_0900.002	45.9	3.67	3.62
1009_0205.002	31.8	4.05	3.99
1009_0435.002	27.8	4	3.92
1009_0626.002	131.7	3.94	3.79
1009_1545.001	26.6	3.79	3.75
1009_1817.002	25.5	3.77	3.73
1009_2058.002	25	3.75	3.72
1009_2324.001	20.1	3.74	3.71
1010_0210.001	25	3.73	3.71
1010_1404.001	22.8	3.73	3.7
1010_1821.002	22.4	3.71	3.68
1011_0001.002	22.7	3.69	3.66
1011_0209.001	30	3.68	3.63
1011_0619.002	26.7	3.64	3.61
1011_0728.002	14.2	3.62	3.5

Salinometry

High precision salinity measurements were obtained with an Optimare Precision Salinometer (OPS) for potential recalibration of the Seabird SBE11+ CTD conductivity sensors. Water samples were taken from Niskin bottles on all deep casts, with standard sampling depths of 1,000 and 2,000 m. Given the lack of deep casts in the last part of the cruise, 6 samples were taken from water depths shallower than 300 m. Two samples were always taken for the same depth. Sample bottles were rinsed three times before sampling and sealed with an aluminium cap after sampling.

Two salinometers were present on board: SN006 and SN007. Initial tests with SN006 yielded unsatisfactory results (for example constant negative slope in the measured salinity curve or erratic behaviour with many sudden jumps), so the system was cleaned 2 times following manual recommendations by the Labor-ELO. Work was then planned to continue on SN007. Initial tests with SN007 deemed the instrument fit for measurement, but after standardisation and measurement of the first samples the behaviour was suboptimal and some samples could not be satisfactorily measured. At this moment, direct comparison of SN006 and SN007 by

consecutively measuring the same sample with both instruments suggested that SN006 was operating normally again, while SN007 showed the same problems previously documented for SN006. The rest of samples were measured with SN006 in three sessions of 21, 18 and 16 samples. 6 samples were measured with SN007 and N samples could not be measured due to problems with SN007. Table 2.9 contains an overview of all measured samples and an overview of the salinometry results.

The measuring session was conducted as follows. At least a day before each session, the salinity bottles were heated in a water bath to approximately 30 degrees for at least an hour to remove gas micro bubbles. After the water bath the bottles were flipped once and overpressure was removed by inserting a needle through the rubber cap. The bottles were then stored in the salinity room, where they cooled down to room temperature. The measurement session started by calibrating the OPS using standard seawater (SSW). During the expedition batch 168 of SSW was used, with a K15 value of 0.99993. Before calibration, a test sample consisting of old SSW was measured twice to ensure correct instrument operation. After calibration, the SSW bottle was sealed again and kept aside to be measured again at the end of the session. This last measurement allows to check for instrument drift during the session. In all sessions this final SSW measurement was ~0.001-0.002 units higher than during calibration. This increase is expected due to evaporation, and confirms that the OPS operated correctly throughout the session. Before measuring salinity, each sample was shaken with the bottle shaker for ~10 minutes. The metal inlet tube of the OPS was cleaned with a Kim-wipe before inserting each bottle and the bottles were sealed with parafilm during measuring to minimize evaporation.

Preliminary comparison of the OPS salinity measurements with the CTD sensors suggests that the absolute differences of both salinity sensors were generally smaller than 0.005 (Fig. 2.12). The collection of samples shallower than 350 meters occurred on 2025-10-12 and was undertaken with knowledge of its potentially limited usability. Given the large differences in bias with respect to CTD sensors and the lack of other shallow samples they have not been taken into account to asses sensor performance. With respect to the rest of the samples, sal00 consistently shows a negative bias during the whole cruise. A time dependent bias can be appreciated in both sensors. The bias of sal11 changes sign between the 2025-10-15 and 2025-10-20. The bias of sal00 increased in magnitude between the 2025-10-20 and the 25th of September. The time evolution of these deviations is consistent with the time series of median daily differences between sal00 and sal11 (Fig. 2.13). The mean absolute error of sal00 0.0032 and of sal11 0.0019. Overall, the magnitude of the absolute difference to OPS measurements is sufficient for the planned scientific analysis. Recalibration of the conductivity sensors to minimize these biases is still possible and could be conducted in the future.

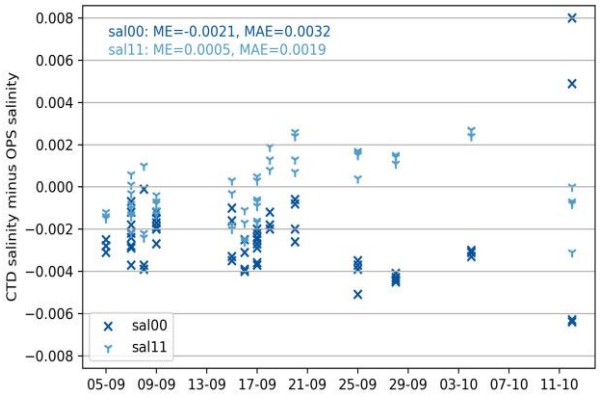

Fig. 2.12: Timeseries of the difference of CTD salinity measurements to OPS measurements from the primary sensor (sal00, dark blue) and the secondary sensor (sal11, light blue). Mean errors (ME) and mean absolute errors (MAE) for the whole timeseries for each sensor are shown on the upper left corner. The samples from the 12th of October are shallower than 350 and are discarded from the MAE calculations.

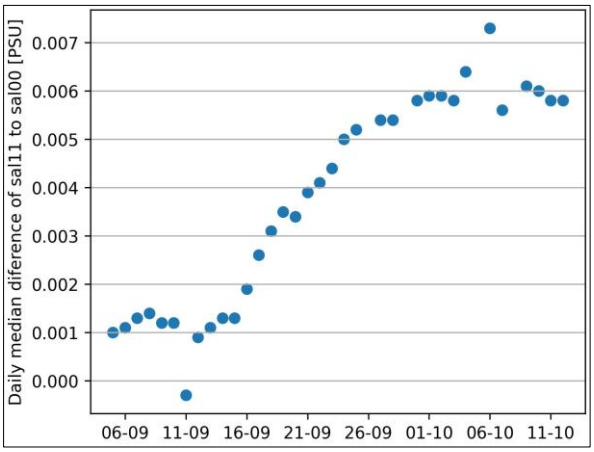

Fig. 2.13: Timeseries of the daily median difference of sal11 vs sal00 measurements. Only downcast readings are included in the calculation.

Tab. 2.9: Results from OPS salinity measurements

Station No.	Niskin bottle	Sample depth	Date of sampling	OPS Salinity [PSU]	Sal00 salinity [PSU]	Sal11 salinity [PSU]	OPS SN
001_01	2	1000	2025-09-05	34.9085	34.9054	34.9070	007
002_01	7	1400	2025-09-05	34.9141	34.9116	34.9129	006
002_01	13	1000	2025-09-05	34.9123	34.9095	34.9109	006
002_01	13	1000	2025-09-05	34.9123	34.9095	34.9109	006
005_01	5	2000	2025-09-07	34.9169	34.9151	34.9166	006
005_01	5	2000	2025-09-07	34.9179	34.9151	34.9166	006
005_01	8	1000	2025-09-07	34.9065	34.9036	34.9051	006
005_01	8	1000	2025-09-07	34.9073	34.9036	34.9051	006
008_01	12	2000	2025-09-07	34.9218	34.9211	34.9224	006
008_01	12	2000	2025-09-07	34.9223	34.9211	34.9224	006
008_01	16	1000	2025-09-07	34.9045	34.9021	34.9035	006
008_01	16	1000	2025-09-07	34.9043	34.9021	34.9035	007
011_01	9	1000	2025-09-08	34.9016	34.8979	34.8994	007
011_01	9	1000	2025-09-08	34.9018	34.8979	34.8994	007
011_01	5	2000	2025-09-08	34.9201	34.9200	34.9211	007
014_01	8	1000	2025-09-09	34.8930	34.8903	34.8917	007
014_01	4	2000	2025-09-09	34.9273	34.9254	34.9266	006
018_01	3	2000	2025-09-09	34.9249	34.9232	34.9245	006
018_01	3	2000	2025-09-09	34.9252	34.9232	34.9245	006
018_01	7	1000	2025-09-09	34.8803	34.8788	34.8792	006
018_01	7	1000	2025-09-09	34.8800	34.8788	34.8792	006
054_01	5	2000	2025-09-15	34.9248	34.9238	34.9251	006
054_01	5	2000	2025-09-15	34.9254	34.9238	34.9251	006
054_01	9	1000	2025-09-15	34.8852	34.8817	34.8832	006
054_01	9	1000	2025-09-15	34.8850	34.8817	34.8832	006
056_01	8	1000	2025-09-16	34.8889	34.8849	34.8863	006
056_01	8	1000	2025-09-16	34.8880	34.8849	34.8863	006
056_01	4	2000	2025-09-16	34.9275	34.9236	34.9250	006

Station No.	Niskin bottle	Sample depth	Date of sampling	OPS Salinity [PSU]	Sal00 salinity [PSU]	Sal11 salinity [PSU]	OPS SN
056_01	4	2000	2025-09-16	34.9261	34.9236	34.9250	006
061_01	9	1000	2025-09-17	34.8931	34.8894	34.8914	006
061_01	9	1000	2025-09-17	34.8930	34.8894	34.8914	006
061_01	5	2000	2025-09-17	34.9284	34.9259	34.9277	006
061_01	5	2000	2025-09-17	34.9283	34.9259	34.9277	006
065_02	5	2000	2025-09-17	34.9284	34.9262	34.9287	006
065_02	5	2000	2025-09-17	34.9282	34.9262	34.9287	006
065_02	9	1000	2025-09-17	34.8938	34.8911	34.8931	006
065_02	9	1000	2025-09-17	34.8940	34.8911	34.8931	006
068_01	16	2000	2025-09-18	34.9284	34.9264	34.9292	006
068_01	16	2000	2025-09-18	34.8940	34.9264	34.9292	006
068_01	22	1000	2025-09-18	34.8918	34.8906	34.8937	006
068_01	22	1000	2025-09-18	34.8924	34.8906	34.8937	006
072_01	5	2000	2025-09-20	34.9256	34.9250	34.9282	006
072_01	5	2000	2025-09-20	34.9258	34.9250	34.9282	006
072_01	8	1000	2025-09-20	34.8907	34.8887	34.8920	006
072_01	8	1000	2025-09-20	34.8913	34.8887	34.8920	006
090_03	2	2000	2025-09-25	34.9241	34.9202	34.9257	006
090_03	2	2000	2025-09-25	34.9253	34.9202	34.9257	006
090_03	3	1000	2025-09-25	34.8867	34.8830	34.8882	006
090_03	3	1000	2025-09-25	34.8865	34.8830	34.8882	006
095_01	2	2000	2025-09-28	34.9272	34.9228	34.9286	006
095_01	2	2000	2025-09-28	34.9271	34.9228	34.9286	006
095_01	5	1000	2025-09-28	34.8865	34.8824	34.8880	006
095_01	5	1000	2025-09-28	34.8869	34.8824	34.8880	006
113_01	8	2000	2025-10-04	34.9214	34.9183	34.9241	006
113_01	8	2000	2025-10-04	34.9214	34.9183	34.9241	006
113_01	12	1000	2025-10-04	34.8952	34.8919	34.8976	006
113_01	12	1000	2025-10-04	34.8949	34.8919	34.8976	006
134_01	4	300	2025-10-12	34.5831	34.5970	34.6022	006
134_01	4	300	2025-10-12	34.5826	34.5970	34.6022	006
135_07	3	350	2025-10-12	34.8686	34.8623	34.8679	006
135_07	3	350	2025-10-12	34.8687	34.8623	34.8679	006
135_07	4	300	2025-10-12	34.5776	34.5825	34.5745	006
135_07	4	300	2025-10-12	34.5745	34.5825	34.5745	006

Thermosalinograph

Onboard *Polarstern* there are two SBE21 SeaCAT Thermosalinograph with additional external thermometer SBE38 for minimum thermal contamination from the ship. The two systems are operated in parallel on the same seawater intake. The pumped system is equipped with a flow meter and set to pump 60 L/min. Position and time information are added via NMEA telegram. The system is located in the ship's keel with the water intake at about 11 m depth, depending on the ship's draft. During PS150 the system was running continuously without any maintenance or cleaning being necessary. For calibration, salinity samples are taken irregularly, depending on the ice conditions. On average, samples are taken every week and measured with an Optimare Precision Salinometer on board by the ship's laboratory-electrician. The sensors are usually operated for one full season (about half a year, depending on expedition schedule) and changed during time in port in Bremerhaven. After post-cruise calibration of sensors, the data is processed and calibrated by Fielax GmbH and stored in the PANGAEA data repository.

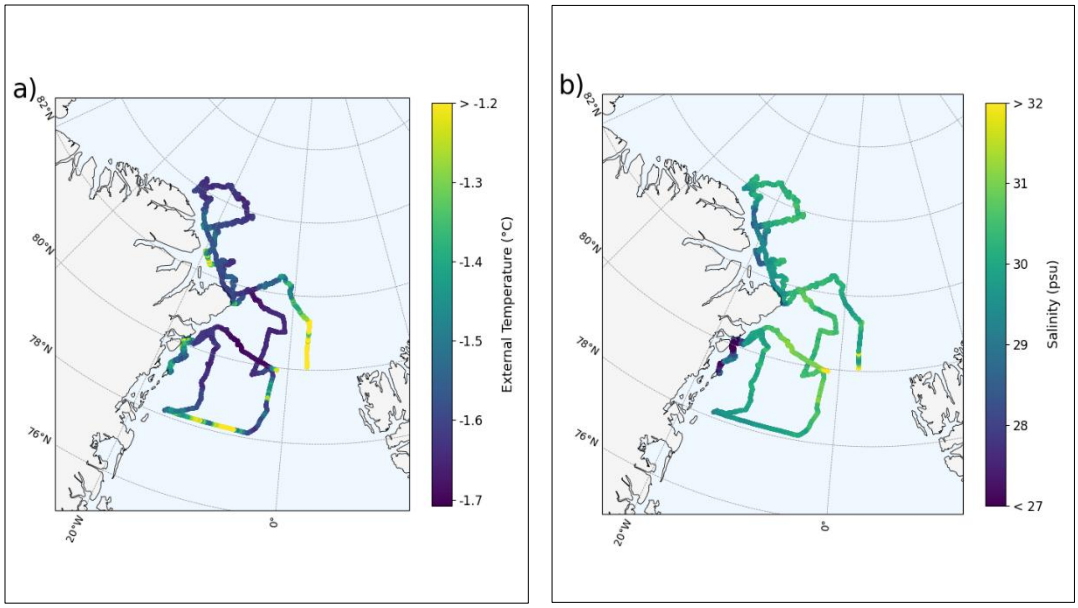

Fig. 2.14: Thermosalinograph 1: Salinity and external temperature data illustrated at their location of measurement

An overview of the temperature measurements from the external thermometer and the salinity data from sensor 1 are shown in Figure 2.14. Surface temperatures were close to the freezing point (between -1.7°C and -1.5°C) for most of the expedition, as the ship was moving through ice-covered regions. Warmer temperatures were only recorded during the transit between Longyearbyen and the start of the Flade section, and on the East Greenland shelf close to 78°N, as the ship was moving over open water. Surface salinities ranged between 29 and 31 for most of the expedition. Lower values were recorded when the ship was closer to the Greenland coast, in particular close to the mouth of the Independence Fjord (around 29 psu) and in the vicinity of the 79N glacier (below 28 psu, with a minimum of around 23.7 psu).

Deviations between sensor 1 and sensor 2 for the external temperature, as well as for the salinity are shown in Figure 2.15. The agreement between the temperature sensors is generally good. However, the salinity sensors can differ by up to 1 psu. In particular, differences between the two salinity sensors were observed when the ship was on station.

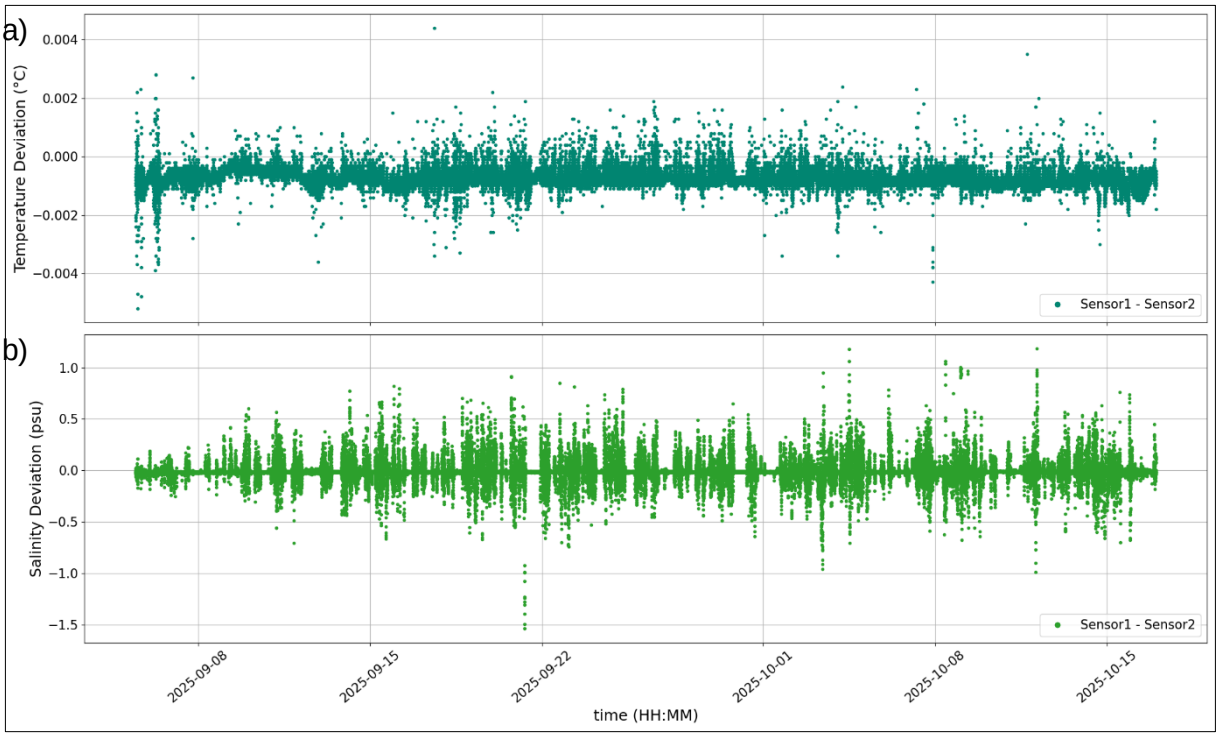

Fig. 2.15: Difference between sensor 1 and sensor 2 for a) external temperature and b) salinity

The surface temperatures recorded by both internal and external temperature sensors were also impacted by the ship's stops at the different stations. Figure 2.16a shows that these values usually increased by 0.05°C every time the ship stopped, likely because of thermal contamination from the ship. As for the salinity, it did not seem to be impacted by the ship's stops: the larger variability visible in Figure 2.16b when the ship is steaming is likely the signature of spatial salinity changes in the area where the ship is moving.

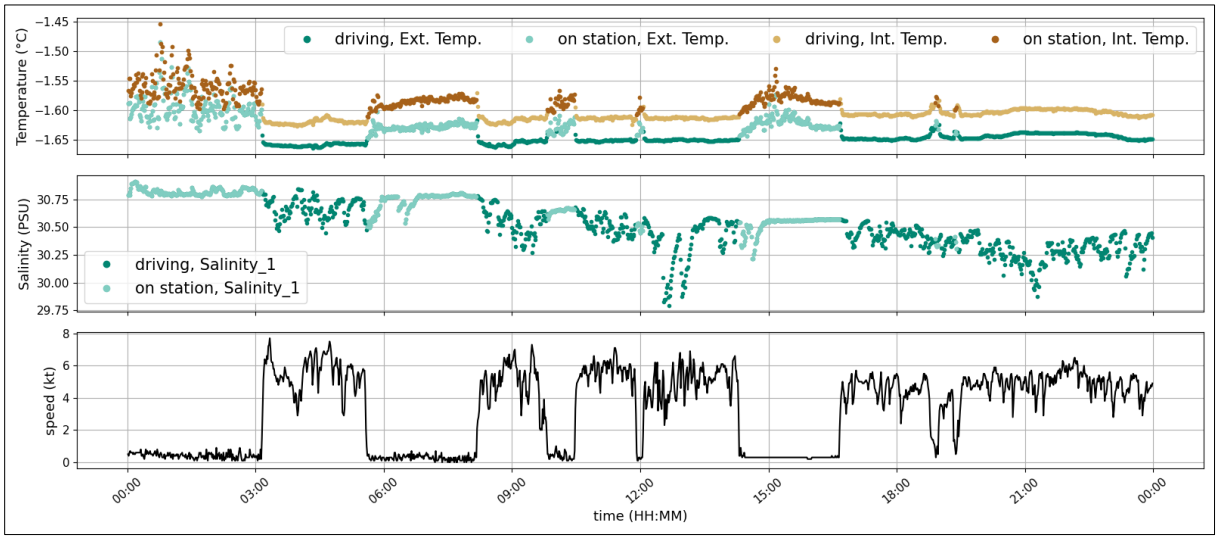

Fig. 2.16: Case study of 04 October 2025 regarding differences in temperature (external and internal) and salinity when the ship was on station (i.e. speed < 1 kt) versus when it was steaming

Vessel mounted ADCP (vmADCP)

Introduction: A vessel-mounted acoustic Doppler Current Profiler (vmADCP) is mounted to the hull of *Polarstern* about 11-m below the sea surface. The vmADCP of Teledyne RDI sends and receives sound near 153 kHz. It generally profiles the water column from below the ship's hull to the about 300-400 m at 8-m vertical bins continuously along the ship track. The vertical profiles of horizontal velocity are measured relative to the moving ship whose velocity vector must be removed in order to measure earth- rather than ship-referenced ocean current vectors. The necessary angles pitch, roll, and heading originate from a Hydrins inertial navigation system (SN PH-1904) manufactured by iXBlue while position data originates from a Trimble R750 GPS system (SN 6236R47098).

Two independent methods exist to accurately estimate the ship's absolute velocity vector: The first uses a specific bottom tracking ping while the second uses the ship's GPS. We compare the ship's velocity vectors from the vmADCP to that of the navigational GPS device, if the bottom-tracking ping correctly detects the bottom, as it does to about almost 760-m. This calibrates the instrument for misalignment alpha and scaling beta of the transducers in the simplest possible way.

The vmADCP collected data from the ADCP (.ENR files, binary), GPS (.N1R files, NMEA ascii), and inertial (.N2R, NMEA ascii) sensors continuously as single ping data in beam co-ordinates. Other files such as useful .ENS or .ENX files derive from the above three data streams that are merged by the data collection software VMDAS. This software also provides a time stamp for the NMEA navigation files to facilitate matching of them with the .ENR files via a "$PADCP" sentence.

We operated the vmADCP in Narrowband mode for both water and bottom tracking pings (WP000), because this mode is (a) more robust, (b) penetrates deeper into the water column, and (c) avoids an ambiguity velocity. For the entire expedition we configured the ADCP with an 8-m vertical bin size (NS0800, resolution), an 8-m blanking interval below the transducers (NF0800), and between 30 (NN030) to 45 (NN045) vertical bins. The center of the first bin (near surface) is about 11-m (hull depth) plus 8-m (blanking) plus 4-m (½ of the 8-m bin size) or about 23-m below the surface. Table 2.10 shows and example file that we used with minor modifications, that is, a setting of BP000 turns off the bottom tracking ping as we did when the ship operated in water deeper than 1000 m.

Tab. 2.10: Sample file to control data collection via VMDAS

```
;-------------------------------------------------------------------------\
; ADCP Command File for use with VmDas software.
;
; ADCP type: 150 Khz Ocean Surveyor
; Setup name: for Polarstern in 6/2014
; Setup type: Low resolution, long range profile (Narrowband)
; NOTE: Any line beginning with a semicolon in the first
; column is treated as a comment and is ignored by
; the VmDas software.
; NOTE: This file is best viewed with a fixed-point font (e.g. courier).
; Modified Last: 12Jun2014 09Sept2025 (a. Muenchow)
;-------------------------------------------------------------------------/
; Restore factory default settings in the ADCP
cr1
; set the data collection baud rate to 9600 bps,
; no parity, one stop bit, 8 data bits
; NOTE: VmDas sends baud rate change command after all other commands in
; this file, so that it is not made permanent by a CK command.
cb411
; Set for narrowband single-ping profile mode (NP), 100 (NN) 4 meter bins (NS),
; 2 meter blanking distance (NF), 390 cm/s ambiguity vel (WV)
WP000
NP001
NN030
```

```
NS0800
NF0800
;WV390
; Disable single-ping bottom track (BP),
; Set maximum bottom search depth to 1200 meters (BX)
BP001
BX10000
; output velocity, correlation, echo intensity, percent good
ND111100000
; Ping as fast as possible
TP000000
; Since VmDas uses manual pinging, TE is ignored by the ADCP
; and should not be set.
;TE0000000
; Set to calculate speed-of-sound, no depth sensor, external synchro heading
; sensor, pitch or roll being used, no salinity sensor, use internal transducer
; temperature sensor
EZ1011101
; Output beam data (rotations are done in software)
EX00000
; Set transducer misalignment (hundredths of degrees).
; Ignored here but set in VmDAS options.
;EA00000
; Set transducer depth (decimeters)
ED00110
; Set Salinity (ppt)
ES35
;set external triggering and output trigger; no trigger
CX0,0
;set external triggering and output trigger
;CX1,3
; save this setup to non-volatile memory in the ADCP
CK
```

Measurements made within about 15% of the bottom must be discarded on account of sidelobe interference of a strong bottom return for the nominal 30 degree beam angle, that is, in 100-m deep water, the maximal profiling range is limited to 85-m or less.

Processing and Calibration

From 4. September through 16 October 2025 we processed all .ENR, .N1R, and .N2R files into 2 minute and 10 minute ensembles. For calibration purposes we used the 2 minute averaged estimates of ADCP-derived bottom-track (BT) and GPS-derived estimates of the ship's velocity vector. The calibration data had to satisfy ALL the following criteria for each bottom tracking ping:

1. Bottom-tracking Error Velocity < 20 mm/s;
2. Bottom-tracking 4-beam solutions only;
3. Bottom-tracking backscatter intensity > 245 counts;

The standard deviation of a single-ping NarrowBand vmADCP velocity measurement in cm/s is dv=160,000/f/D=0.13 m/s where f is the transmit frequency (153,000 Hz) and D is the depth bin (8-m). Averaging N pings. we reduce this error to dv/sqrt(N), if the variable has a Gaussian or Normal probability density distribution. For a Gaussian variable a 2 minute (10 minute) average reduces the standard deviation of the average to about 2 cm/s (1 cm/s) as our set-up results in about N~36 pings (~180 pings). We next describe how we force our 2 or 10 minute ensemble towards a Gaussian distribution that minimizes the effect of outliers.

Data within each ensemble window were sorted prior to averaging from largest to smallest velocity to remove the largest 10% and the smallest 10% of values within each ensemble. The sorting of all variables within an averaging interval was determined by the variable that had the largest variance within the ensemble. Only bottom-tracking east and north as well as GPS-derived east and north velocity components are considered. Muenchow et al (2007) provide more detail on this processing of vmADCP data in a polar environment.

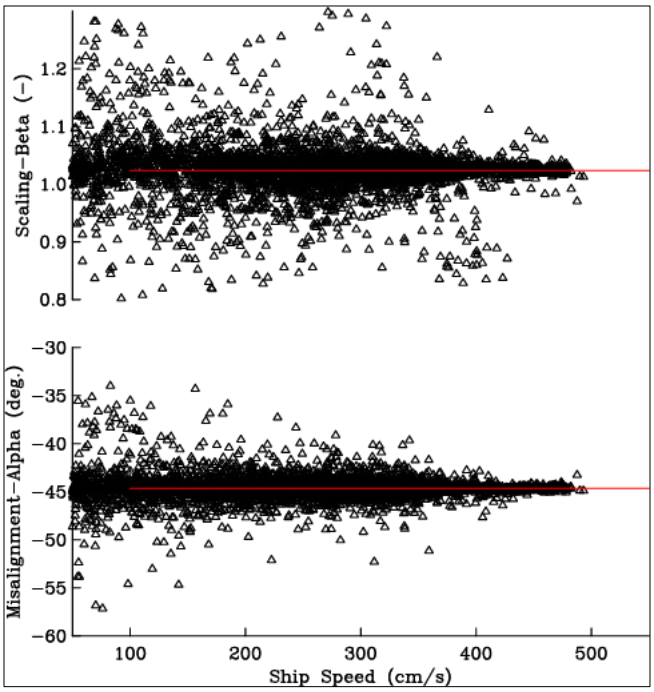

Fig. 2.17: ADCP transducer misalignment angles estimated from all 2-minute averages of GPS- and ADCP-derived estimates of the ship's horizontal velocity vectors. The data are sorted by the ships speed from the GPS.

This processing resulted in about 6750 ensembles of 2-minute screened bottom-tracked data while the ship moved at speeds between 0.5 to 5.5 m/s (Fig. 2.17). From these we find misalignment (alpha) and scaling (beta) factors which were

alpha = -44.647 degrees and beta = 1.023571

Hence the heading hh applied to the heading information contained within the .ENR file Head is

hh = Head - alpha

while the scaling is

*(u,v) = (vx,vy)_{e} * beta*

where (u,v) are corrected and calibrated ship velocity components determined from the earth-referenced horizontal velocity vector (vx,vy)_e which results after all rotational matrices for heading, pitch, and roll are applied. In the absence of bottom tracking, the misalignment angle and scaling constant must be applied to velocity profile data before the GPS-derived ship velocity vector is removed to result in absolute earth-referenced water velocity vectors. Figure 2.18 and Figure 2.19 show almost symmetric distributions of alpha and beta estimates that originated from a wide range of ship speeds and directions.

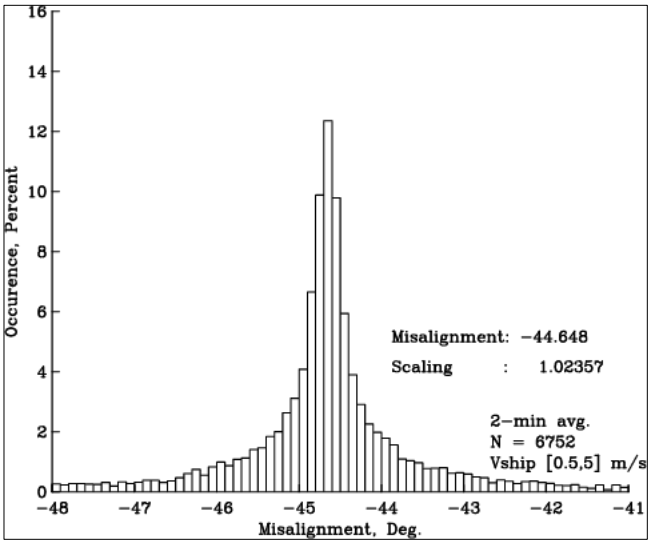

Fig. 2.18: Normalized histogram of the misalignment angle from data shown above.

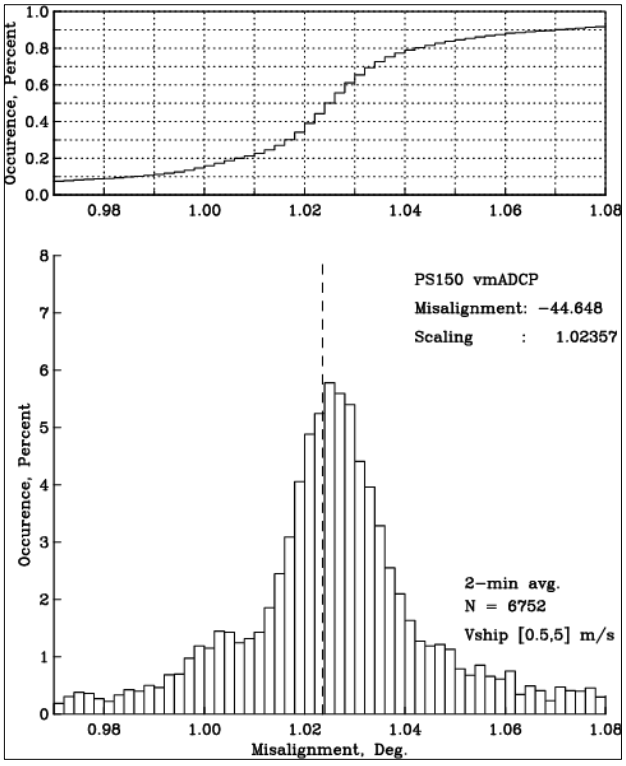

Fig. 2.19: Normalized histogram of the scaling constant (bottom panel) and its integration (top panel). That latter cummulative histogram can be used to boot-strap confidence limits or median values.

The direct comparison of calibrated bottom-tracking (BT) and GPS-derived velocity components suggests a near perfect fit, however, we here display velocity differences in Figure 2.20 as histograms for each velocity component overlaid with its cumulative histogram. The latter enables estimation of confidence limits via boot-strapping.

The distribution peaks near zero velocity difference, however, substantial variance resides in the broad shoulders that dip to +/-9 cm/s about 90% of the time. This velocity difference includes uncertainties of both GPS and ADCP derived velocities. Assuming a GPS position error of about 5 m, we find a GPS velocity error of about 8 cm/s for differencing samples 2 minutes apart.

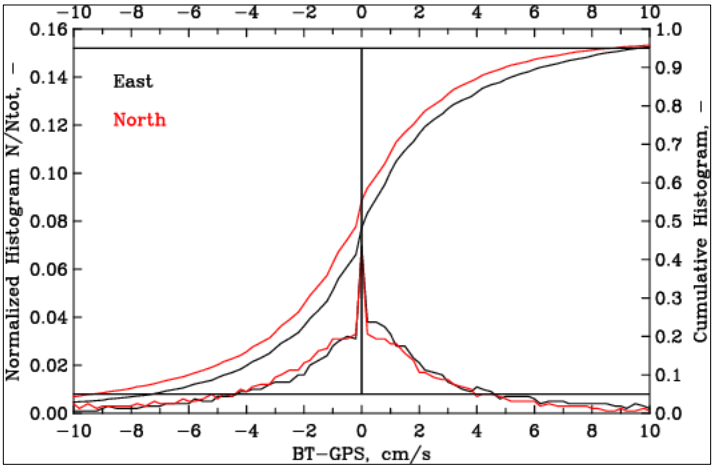

Fig. 2.20: Velocity vector difference between GPS- and Bottom-Track (BT) ship's velocity displayed both a normalized histograms (curves that peak at 0 BT-GPS) and cumulative histograms. Colors represent east (black) and north (red) velocity components.

Results: Daily time series of calibrated 10-minute vmADCP profile data were generated each day along with an ascii data in accessible columnar format for use of the entire science party via the public science server aboard the ship. These data were used to support the processing of the lowered ADCP data as well as the interpretation of MSS microstructure or turbulence profiler data. Furthermore, quality control issues due to poor initial calibrations were identified as large differences of velocity profiles during station works and ship transits emerged that were thus quickly identified and fixed as the processing improved throughout the experiment. Both shell scripting and compiled Fortran codes allow rapid processing of the entire single ping data set of about 5.5 GB in 15 minutes on a 2015 MacBook Pro to a single 10-minute output file of earth-referenced, calibrated, and screened 45 MB ascii data file. Table 2.11 describes the format of this preliminary processed data set.

Tab. 2.11: Format of the processed and calibrated ascii output file for the entire expedition

```
VmADCP Data Output Format from osadcp5.f (muenchow@ude).edu)
Header Line-1 # of Data, # of Profiles, Calibration Coefficients, Date String of
File Creation
Column-1 Year
Column-2 Month
Column-3 Day
Column-4 Hour
Column-5 Minute
Column-6 Longitude, decimal degrees
Column-7 Latitude, decimal degrees
Column-8 Bottom Depth relative to transducer, meters
Column-9 Bin Dpeth relative to transducers, meters
Column-10 Ueast, cm/s
Column-11 Vnorth, cm/s
Column-12 Wvertical, cm/s
Column-13 Eerror, cm/s
Column-14 Vector Uncertainty, cm/s
```

```
Column-15 Percent Good Pings Water Tracking
Column-16 Number of 3-Beam Solutions
Column-17 Uship from Bottom Tracking, cm/s
Column-18 Vship from Bottom Tracking, cm/s
Column-19 Uship from GPS, cm/s
Column-20 Vship from GPS, cm/s
Column-21 Not used, "0.0"
Column-22 Percent Bottom Track (BT) Ship Velocity (0-all GPS, 100-all BT)
Column-23 Percent Good Pings Bottom Tracking
Column-24 Bin Number
Column-25 Profile Number
Column-26 Last Bin Number (ignore in output001)
Column-27 Barotropic Tidal Current East, cm/s (only in .tide files)
Column-28 Barotropic Tidal Current North, cm/s (only in .tide files)
Column-29 Bottom Depth in Barotropic Tidal Model, m (only in .tide files)
```

For example, Figure 2.21 shows all available profiles on 10 September 2025 when we approached the coast of Greenland as part of the Flade-1 section. While the two bottom panels show earth-referenced east and north velocities as a function of depth, the top panel shows the ship's speed during the day from which to infer times of station work and transits. Data until about 15:00 use the GPS navigation to remove the ship's motion from the ADCP data while afterwards the ship's motion was determined from bottom-tracking. We show section data as color-coded dots above the bottom 15% of the bottom depth to remove noise from below the bottom and outside the sidelobe interference from bottom returns. A strong flow to the south (negative Vnorth in red) and west (positive Ueast in blue) emerges over the continental shelf and slope which likely is our first crossing of the East Greenland Current off Flade Isblink at 81.5 N latitude.

The long station in Figure 2.21 between about 1:30 and 7:30 UTC is PS150-024 at 1126 m depth. It includes a massive disturbance between 60 to 100 m depths as two distinct back and forth along with a large vertical velocity component up and down (not shown). While such velocities are unlikely to be ocean currents, they do track a reflecting object (like a false bottom) or indicate a large cloud of scattering particles (like zooplankton) moving in a non-random fashion like a school of fish. We speculate that these signals relate to other sampling with undulating multi-nets or MSS turbulence profilers.

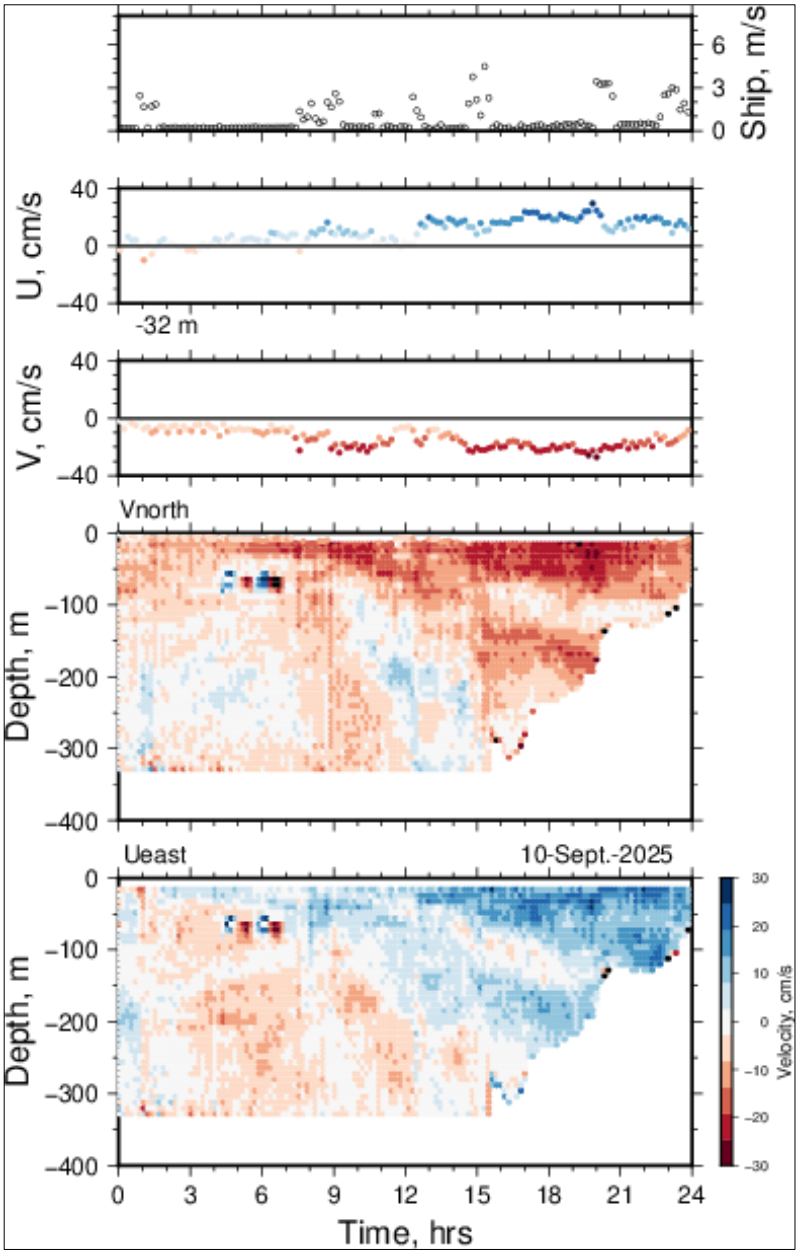

Fig. 2.21: Earth referenced ocean velocities (bottom panels) for 10. September 2025 as we approached the coast of Greenland as 10 minute averages of calibrated but unscreened vmADCP data. The ship's velocity in the top panel of ship's speed allows evaluation of on-station and transit velocity estimates.

The time series information also relates to spatial sections and maps to place ocean circulation into a geographical context. For example, in Figure 2.22 we display the data along the Flade-1 section in a reference frame that is rotated across and along the section as a function of depth and distance from the shelf-break after we remove barotropic tidal current predictions in its Arc5km2018 implementation, that is, we use model coefficients of 12 tidal constituents to estimate the tidal current at the time and (interpolated) location of our observations.

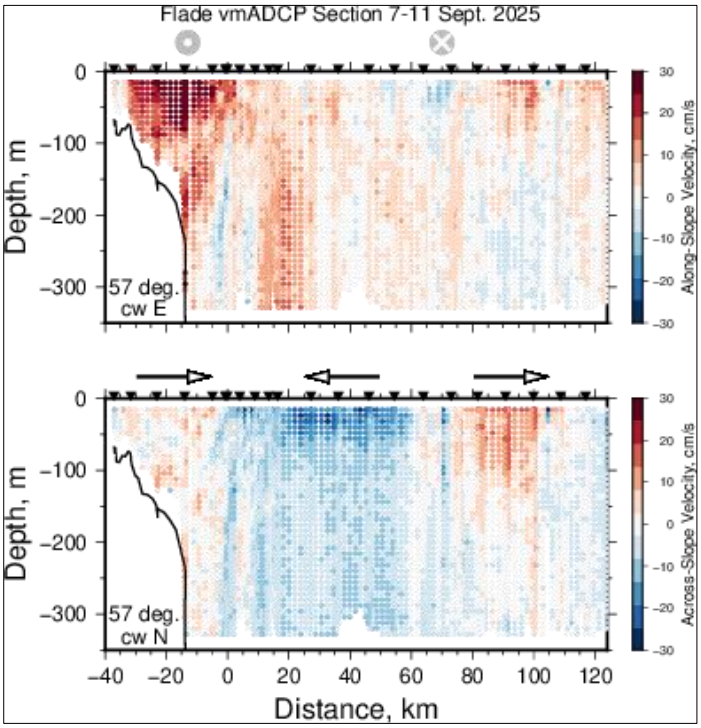

Fig. 2.22: Earth-referenced, calibrated, screened, and detided velocity along the Flade-1 section rotated into velocity components along and across the sloping bottom. The shelfbreak at the origin of the distance.

A strong along-shore flow to the south-west results that represent the East Greenland Current extending onto the sloping continental shelf off Flade Isblink This flow is strongly sheared in both the vertical and horizontal directions as expected for a buoyancy driven current in geostrophic balance. Furthermore, the across-slope velocity component likely contains significant variations as we discern a convergence near the shelf break (Distance 0 km) and a strong divergence about 60 km seaward from the shelfbreak. This statement assumes a 2-dimensional flow without alongshore variability, which will need to be test with additional information and work beyond the scope of this report. We close our discussion of this example with a map of ocean currents at 48 m in Figure 23.

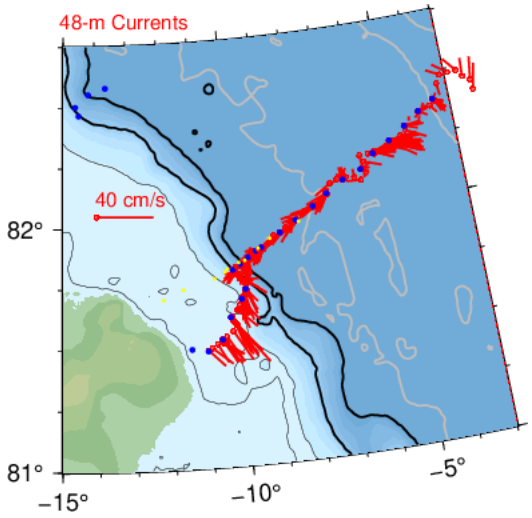

Fig. 2.23: Extraction of the vectors shown in Fig. 2.22 at 48-m depth with bottom bathymetry and PS150 CTD (blue symbols) and XCTD (yellow) locations. The thick contours represent 1000 and 2000 m isobaths

The vmADCP on PS150 performed exceptionally well without major issues. During my almost 40 years of working with and processing vmADCP data I have never had the pleasure to work with such a well-maintained and fine-tuned system as aboard *Polarstern*. For future applications I strongly recommend use of a bottom tracking pulse in water less than 1000 m deep.

XCTD (expendable CTD)

Complementing CTD transects with expendable CTD probes (XCTDs), we deployed 30 XCTDs during PS150 of which 29 returned data. The XCTD profile increase the spatial resolution of across-shelf sections and via helicopter deployments extend sections into fjords. Ship-based XCTD casts were deployed using a hand-held launcher over the ship's starboard or aft deck. Helicopter-based deployments were conducted either while hovering or after landing on sea ice via holes drilled into the ice. Table 2.12 list the 30 XCTD casts of which five failed or terminated prematurely mostly because sea ice cut the thin copper wire. Hence only 28 XCTD locations returned useful data.

We used a TSURUMI-SEIKI MK-150 system to deploy the probes. It consists of a TS-MK 150N deck unit with SN 09922 and SN 8865 for shipboard and helicopter operations, respectively. Initial processing software (MK-150 application version 1.63) converted .RAW files of time, temperature, and conductivity channels with calibration coefficients to engineering units in .CTD ascii files. The latter also include depth estimated from fall rates (Kizu et al., 2008). While these files also include estimates of salinity (calculated from temperature and conductivity), we found discrepancies at times larger than 0.1 psu for MK-150 salinity calculations as compared to Gibbs Seawater (GSW) Oceanographic.

1. Expunge the first 32 scans to remove transient effects (1 scan represents about 0.13m);
2. Move conductivity measurements by 1.1 scans relative to temperature measurements;
3. Remove scans after probe hits bottom via vertical density gradient,
4. Lanczos low-pass filter (2-m half-power point, 8-m filter-width);
5. Remove filter-loss 4-m at top and 4-m at bottom of profile;
6. Sub-sample to 1-m;
7. Write data to ascii .DAT files with latitude and longitude as separate columns for each depth.

The processing Fortran-95 code xctd.f95 is attached for documentation of processing details. It includes the filter (Duchon 1979), but not the TEOS-10 GSW functions whose version 3.03 for Fortran we used here. The output .DAT files have columns

- Column-1 pressure, dbar (estimated from fall rate)
- Column-2 potential temperature, C
- Column-3 practical salinity, psu
- Column-4 density anomaly, kg/m^3
- Column-5 conservative temperature, C
- Column-6 absolute salinity, g/kg
- Column-7 in-situ temperature, C
- Column-8 conductivity, mS/cm
- Column-9 Longitude, decimal degrees East (East positive)
- Column-10 Latitude, decimal degrees (North positive)

Figure 2.24 compares a XCTD cast at station PS150_017 against two adjacent CTD casts PS150_016 and PS150_018 in 2400 deep water offshore on the Flade-1 section where horizontal temperature and salinity variations are small. The XCTD data agree well with the CTD data for temperature but not for salinity. More specifically, we find that the salinity values S could benefit from a constant offset by about 0.025 psu, i.e., Scor = S+0.025 psu. Furthermore, all XCTD data contain large variance below the Atlantic temperature maximum at vertical scales between 5 and 150 vertical meters. We did not investigate the cause of this unrealistic variance that may require additional or revised processing beyond the scope of this report.

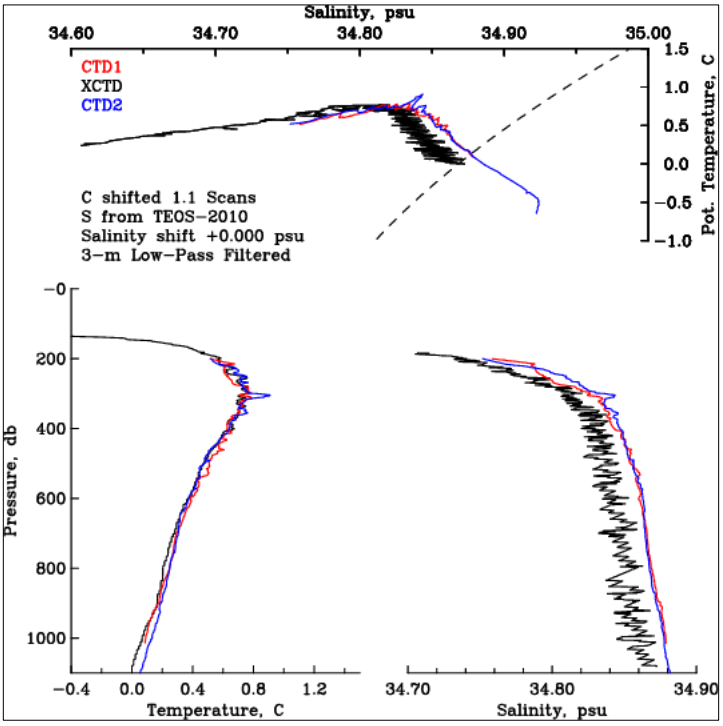

Fig. 2.24: Comparison of XCTD profile from station PS150_017 (black) as compared to adjacent CTD casts from stations PS150-016 (red) and PS150_018 (blue). Scales for potential temperature T and salinity S are chosen to emphasize discrepancies both for vertical profile (bottom panels) as and S-T diagrams (top panel). Notice the almost constant offset of about 0.025 psu of salinity.

Tab. 2.12: Summary of XCTD deployments from ship and helicopter. No sequential cast numbers are given for the ship-based XCTDs, as these were not logged by *Polarstern*.

Station	Platform	Serial Number	File name	Time UTC	Lat [deg N]	Lon [deg E]	Water depth [m]	Source Water depth	cast depth [m]	Comment
PS150_017_01	Polarstern	1N25014434	XCTD-010809092025	20250909T12:21	81.8781	-9.3228	2441	EK80 uncorr	1081	
PS150_019_01	Polarstern	1N25014436	XCTD-010909092025	20250909T18:36	81.8601	-9.5071	2305	EK80 uncorr	1081	
PS150_021_01	Polarstern	1N25014435	XCTD-011009092025	20250909T22:08	81.8377	-9.7493	2247	EK80 uncorr	1081	
PS150_023_01	Polarstern	1N25014433	XCTD-011109102025	20250910T01:03	81.8186	-10.0043	1996	EK80 uncorr	1081	
PS150_026_01	Polarstern	1N25014432	XCTD-011209102025	20250910T07:08	81.7794	-9.9173	1385	EK80 uncorr	1081	
PS150_026_01	Polarstern	1N25014430	XCTD-011309102025	20250910T11:56	81.7004	-9.7802	576	EK80 uncorr	554	
PS150_028_01	Polarstern	1N25014426	XCTD-011409102025	20250910T14:54	81.6413	-10.0670	1128	EK80 uncorr	1081	irregular isobaths -> xCTD deeper than neighboring CTDs
PS150_heli_OZE_002_01	Heli flying	1N25014420	XCTD-011509122025	20250912T14:09	82.0856	-26.2927	436	XCTD at bottom	436	
PS150_heli_OZE_004_01	Heli flying	1N25014431	XCTD-011609122025	20250912T16:18	82.1798	-21.2795	545	XCTD at bottom	545	
PS150_heli_OZE_005_01	Heli flying	1N25014425	XCTD-011709122025	20250912T19:03	81.5775	-25.5986	384	XCTD at bottom	355	cut off early, repeated cast
PS150_heli_OZE_005_02	Heli flying	1N25014441	XCTD-011809122025	20250912T19:06	81.5775	-25.5986	384	XCTD at bottom	384	
PS150_heli_OZE_007_01	Heli flying	1N25014440	XCTD-011909122025	20250912T21:01	82.0863	-23.5132	293	XCTD at bottom	293	
PS150_049_01	Polarstern	1N25014429	XCTD-012009142025	20250914T21:20	83.2786	-20.3165	494	EK80 uncorr	293	aborted prematurely, repeated cast
PS150_049_01	Polarstern	1N25014427	XCTD-012109142025	20250914T21:37	83.2768	-20.3054	509	Hydrosweep	517	
PS150_051_01	Polarstern	1N25014445	XCTD-012209152025	20250915T10:03	83.3016	-20.0297	1504	Hydrosweep	480	cut off early, repeated cast
PS150_051_01	Polarstern		File doesnt exist		NaN	NaN	NaN		0	Cast failed
PS150_051_01	Polarstern	1N25014442	XCTD-012409152025	20250915T10:22	83.2984	-20.0140	1511	Hydrosweep	1081	
PS150_053_01	Polarstern	1N25014443	XCTD-012509152025	20250915T16:02	83.3175	-19.6238	2789	Hydrosweep	1081	
PS150_055_01	Polarstern	1N25014446	XCTD-012609152025	20250915T22:59	83.3519	-19.3690	3046	Hydrosweep	1081	
PS150_057_01	Polarstern	1N25014447	XCTD-012709162025	20250916T04:06	83.3924	-18.8819	3100	Hydrosweep	1081	
PS150_heli_OZE_014_01	Heli on floe	1N24124099	XCTD-012809212025	20250921T16:18	85.4300	-16.2367	NaN		1081	
PS150_heli_OZE_015_01	Heli flying	1N25014438	XCTD-012909242025	20250924T10:58	83.7203	-32.9769	43	XCTD at bottom	0	stopped after a few meters; no processed file
PS150_heli_OZE_015_02	Heli flying	1N25014439	XCTD-013009242025	20250924T11:00	83.7203	-32.9766	43	XCTD at bottom	43	
PS150_heli_OZE_019_01	Heli on floe	1N24124101	XCTD-013109242025	20250924T14:01	84.1479	-33.0179	874	XCTD at bottom	874	deployed through hole in ice
PS150_heli_OZE_020_01	Heli on floe	1N24124108	XCTD-013209242025	20250924T14:56	84.3125	-32.9509	801	XCTD at bottom	801	deployed through hole in ice
PS150_heli_OZE_021_01	Heli on floe	1N24124098	XCTD-013309262025	20250926T15:13	82.0862	-27.0423	631	XCTD at bottom	627	
PS150_heli_OZE_022_01	Heli on floe	1N25014437	XCTD-013409262025	20250926T17:10	82.0742	-24.8379	561	XCTD at bottom	557	
PS150_092_01	Polarstern	1N24124097	XCTD-013509272025	20250927T13:27	82.4887	-15.1741	345	Hydrosweep	351	
PS150_heli_OZE_023_01	Heli on floe	1N24124103	XCTD-013609282025	20250928T13:03	82.2789	-19.5589	580	XCTD at bottom	571	
PS150_108_01	Polarstern	1N24124104	XCTD-013710022025	20251002T11:11	81.9579	-8.4069	2927	EK80 uncorr	1081	

Mooring recoveries and deployments

Two moorings were recovered during PS150 and 12 moorings were deployed (Tab. 2.13). Moorings Y8-1 and IdF3-2 had been deployed in 2022 during PS131 (attempted recoveries during PS137 in 2023 and PS143.2 in 2024 had previously failed due to sea ice conditions). They were both recovered in their entirety as in the drawings with the releasers working upon the first release command. Most sensors collected and returned data as planned.

Tab. 2.13: Mooring operations during PS150

Name	Latitude		Longitude		Depth	Top	Deployment time UTC					Deployment station	Recovery time UTC					Recovery station
	Degrees	Minutes	Degrees	Minutes	Meters	Meters	Year	Month	Day	Hour	Minute		Year	Month	Day	Hour	Minute	
Recoveries																		
Y8-1	81	18.82 N	3	10.31 E	777	16	2022	7	29	5	31	PS131_085_01	2025	9	6	5	48	PS150_004_01
IdF3-2	78	10.73 N	15	43.12 W	351	150	2022	8	7	6	44	PS131_112_01	2025	10	6	20	12	PS150_116_01
Deployments																		
MJ1-1	83	51.52 N	28	39.93 W	95	85	2025	9	23	17	36	PS150_087_01	2026					
MJ2-1	83	55.14 N	28	29.75 W	207	203	2025	9	23	19	24	PS150_088_02	2026					
IT1-1	82	48.31 N	18	36.52 W	299	267	2025	9	28	16	15	PS150_heli_OZE_024_02	2026					
FI0-1	81	41.33 N	12	13.05 W	109	104	2025	9	29	18	47	PS150_098_01	2026					
FI1-1	81	44.04 N	11	32.11 W	186	55	2025	9	30	14	40	PS150_099_02	2026					
FI2-1	81	46.69 N	10	40.08 W	195	48	2025	9	30	17	22	PS150_100_01	2026					
FI3-1	81	48.19 N	10	7.94 W	1023	48	2025	10	1	9	56	PS150_103_03	2026					
FI4-1	81	50.05 N	9	47.33 W	2178	45	2025	10	1	16	11	PS150_104_02	2026					
FI5-1	81	55.47 N	8	55.17 W	2672	46	2025	10	2	15	32	PS150_109_01	2026					
FI6-1	81	59.44 N	8	6.57 W	2999	47	2025	10	2	8	36	PS150_107_01	2026					
79N2-3	79	34.18 N	19	27.76 W	475	444	2025	10	11	13	14	PS150_heli_OZE_027_02	2026					
NT4-1	79	10.40 N	17	2.87 W	400	92	2025	10	12	19	14	PS150_135_01	2026					

Data from a 153 kHz ADCP initially deployed 7 August 2022 filled two of two memory cards completely with single ping data in 80 vertical bins each covering 5 successive meters above the upward-looking transducers every 4 seconds. Decoding the two separate binary files (_RDI_000.000 and _RDI_001.000), we first generated a single binary data file (IdF3.merged) that we subsequently split into files with an integer multiple of an ensemble size. An ensemble for each ping consists of so-called Header, Fixed Leader, Variable Leader, Velocity, Correlation, Echo Intensity, and Percent Good Ping data that are packed into 1,754 bytes. Initial processing trials revealed that not all computers or codes can easily read 2.5 GB easily memory as a single 1-byte binary array. Hence, we split the files via a Unix-like command

split -b 1573999258 -d IdF3.merged adcp

where “1,573,999,258” (bytes) represents 897,377 ensembles, “IdF3.merged” is the input and “adcp” indicates that files with this prefix will be created on output. A compiled Fortran code bin3.f (attached for documentation only) then converts these binary data into ascii data for further processing. For example, the file line1 gives the time string for each ensemble which indicates that

First Ensemble (1)	5 August 2022	15:00:00
Last Ensemble (1312327)	1 February 2025	23:00:31

Combining this with transducer pressure (and/or pitch and/or roll and/or heading) data stored in fie line4 indicates that the transducer were deployed in the water at about 351 m.

In-Water Ensemble (2401)	7 August 2022	07:00:00

North of the Flade Isblink (FI) along the Flade_1 CTD section that was occupied in the beginning of the cruise, we deployed a mooring array containing 7 moorings named FI0-1 (FI = “Flade Isblink”) to FI6-1. The array contains six regular large oceanographic moorings measuring from the sea floor to about 50m below the surface. Thus, they range in length from 130 m (FI1-1) to 2,952 m (FI6-1). These moorings contain extensive sensors distributed to measure temperature, salinity, and velocity from 50 m to 400 m, as well as velocity from 50m to 10m, and temperature and salinity at 750 m. Furthermore, FI1-1 and FI6-1 contain upward looking sonars (ULS) to determine ice thickness. FI2-1 and FI4-1 contain remote access samplers (RAS) and biological and biogeochemical sensor packages at 50 m (both moorings) and at 250 m (FI4-1 only). FI4-1 also contains sediment traps 200 m below the surface and 200 m above the bottom. At FI2-1 and FI5-1, passive acoustic recorders listen to ambient marine mammal associated noise. Finally, deep water temperature and salinity in ~3000m water depth are recorded at FI6-1. Mooring FI0-1 was intended to be as far inshore as possible to measure the salinity signal of the outflow from Independence Fjord along the coast. At the time the ship was there, the sea ice conditions were very severe such that in the end the ship could only drift with the swiftly moving sea ice. As a result, the mooring had to be deployed where the ship was located at the time, which was in 109m water depth such that the mooring now measures temperature and salinity 106m below the surface, i.e. somewhat deeper than originally intended. The mooring itself is also only very short to minimize contact with ice bergs that are assumed to be more prominent in close vicinity to the coast.

At the southern tip of the Morris Jessup Rise along the Cape Morris Jessup CTD section, unexpectedly salty water was found on the upper shelf along with westward VMADCP velocities suggesting a possible westward current there. In order to obtain time series observations of this boundary current, two small moorings (MJ1-1 and MJ2-1) were designed and deployed at short notice. MJ1-1 records temperature, salinity, and velocity at 87m in 95m water depth and MJ2-1 records temperature and salinity at 205 m in 207 m water depth.

Upon having traversed the shelf in front of the Independence Fjord on the way south, it appeared that there may be a trough system on the shelf deep enough to supply dense Arctic Atlantic Water to the fjord. In order to test the deployment of a small mooring from the sea ice and because the ship had already travelled much further south by the time this decision could be taken, mooring IT1-1 was deployed with the assistance of the helicopter. The helicopter transported the mooring equipment and four scientists to the target location where it could land on an ice floe that was moving at ~0.2 knots southward. On the edge of the ice floe, a hole could be pushed into the new ice. The water depth was determined twice with an echosounder both at the start of the operation and immediately after the deployment of the mooring; the second sounding was 299 m. Thus mooring IT1-1 measures temperature, salinity, and velocity at 268 m in 299 m water depth.

The three microcats supplied by the University of Delaware were moored on the short moorings (MJ1-1, MJ2-1, and FI0-1). They had not been pre-cruise manufacturer calibrated which is why they were calibrated on the CTD rosette during station PS150_005_01. Compared to the uncalibrated first salinity (sal00) of the CTD-rosette, the instruments on FI0-1 and MJ1-1 were good with offsets of ~0.01psu (FI0-1 SBE37 SN2909 34.903 psu compared to 34.915psu from the CTD-rosette at 2000 m; MJ1-1, SBE37 SN2907 34.904 psu compared to 34.9115psu from the CTD-rosette at 2000 m). The offset for the instrument on MJ2-1 was more substantial showing salinities ~0.17 psu too fresh compared to the CTD-rosette. This instrument requires a post-recovery calibration and the application of a salinity offset: MJ2-1 SBE37 SN2889 showed salinities of 34.743 psu at 1000 m and 34.736 psu at 2000 m compared to 34.904 psu at 1000 m and 34.915 psu at 2000 m from the CTD-rosette.

The final mooring deployment of PS150 was mooring NT4-1. This is a traditional ship-deployed mooring (mooring length 307m in 400m water depth). However, its location was decided on short notice based on what the ship could reach in difficult ice conditions in the Norske Trough in front of the Norske Øer island.

Mooring with Acoustic Modem

The second to last mooring deployment of PS150 (mooring 79N2-3 was special in that it was deployed from the landfast sea ice in front of the calving front of the 79N glacier. The deployment with the help of the helicopter and through an ice hole was similar to the operation of mooring IT1-1. The second special aspect of this mooring is that it contains an acoustic modem (Evologics S2C R 7/17 Underwater Acoustic Modem). The goal is that the data from the mooring may be retrieved by landing on the sea ice, drilling a hole, and acoustically downloading the data even if the hardware might not be recovered. This scenario could happen if there again is landfast sea ice in front of the glacier calving front during the deployment cruise. Note that this location could be reached by ship during 3 prior attempts (PS100 in 2016, PS109 in 2017, and in 2021). During 3 attempts the embayment was blocked by landfast sea ice (PS114 in 2018, PS131 in 2022, and now PS150 in 2025). In order to reduce the amount of data that would need to be acoustically recovered (and thus the time that operation would take), the Microcat and the Aquadopp were programmed to record one data point only every 6 hours. The data download was tested multiple times on the ship prior to deployment. The following commands should facilitate the data recovery:

[Initiate an acoustic connection between the surface and underwater units]
+++AT&V
+++ATD
+++AT?ZSL
[Communicate with the Microcat]
ds

Stop
Stop
GetSamples:1,N *[here N is the number of samples as determined from ds]*
[Change to communication with the Aquadopp]
+++AT!ZS1
[Communicate with the Aquadopp]
@@@@@@
@@@@@@
@@@@@@ *[Break]*
K1W%!Q *[Break confirmation]*
MC *[Switch to command mode]*
RF *[Ask for the file list, read response in hex encoding]*
[Switch to hex encoding for input]
46430000 *[Download header]*
4443NNNNMMMMOOOOPPPP *[Download data; here N/M/O/P to be determined from the response to RF]*
[Once data download has finished, save as file and convert with Aquadopp DW software]

The final settings of the underwater unit are:
+++AT&V:379:Source Level: 3
Source Level Control: 1
Gain: 0
Carrier Waveform ID: 1
Local Address: 2
Remote Address: 1
Highest Address: 14
Cluster Size: 10
Packet Time: 750
Retry Count: 3
Retry Timeout: 8000
Wake Up Active Time: 20
Wake Up Period: 180
Promiscuous Mode: 1
Sound Speed: 1500
IM Retry Count: 1
Pool Size: 16384 16384 16384
Hold Timeout: 900
Idle Timeout: 900
+++AT?ZSL:127:0 tcp://0.0.0.0:9200:lr|at -c 1
1 tcp://0.0.0.0:9201:lr|at -p 1
7 tcp://0.0.0.0:9207:lr|at -p 7 -l "\n" -f 1 -u 1 -x 1 -a 1

The final settings of the surface unit are:
+++AT&V:376:Source Level: 3

Source Level Control: 0
Gain: 0
Carrier Waveform ID: 0
Local Address: 1
Remote Address: 2
Highest Address: 14
Cluster Size: 10
Packet Time: 750
Retry Count: 3
Retry Timeout: 8000
Wake Up Active Time: 12
Wake Up Period: 12
Promiscuous Mode: 1
Sound Speed: 1500
IM Retry Count: 1
Pool Size: 16384 16384 16384
Hold Timeout: 0
Idle Timeout: 120
+++AT?ZSL:127:0 tcp://0.0.0.0:9200:lr|at -c 1
1 tcp://0.0.0.0:9201:lr|at -p 1
7 tcp://0.0.0.0:9207:lr|at -p 7 -l "\n" -f 1 -u 1 -x 1 -a 1

The Microcat was programmed for a 6 hours measurement interval:
ds
SBE37SM-RS232 v4.1 SERIAL NO. 11422 09 Oct 2025 16:07:09
vMain = 13.29, vLith = 3.07
samplenumber = 3687, free = 555553
not logging, stop command
sample interval = 600 seconds
data format = converted engineering
transmit real-time = no
sync mode = no
pump installed = yes, minimum conductivity frequency = 3143.3
<Executed/>
OutputFormat=1
<Executed/>
TxRealTime=0
<Executed/>
SampleInterval=21600
<Executed/>
SampleNumber=0
this command will modify memory pointers
repeat the command to confirm
<Executed/>

SampleNumber=0
<Executed/>
StartDateTime=10092025180000
<start dateTime = 09 Oct 2025 18:00:00/>
<Executed/>
StartLater
<!--start logging at = 09 Oct 2025 18:00:00, sample interval = 21600 seconds-->
<Executed/>
ds
SBE37SM-RS232 v4.1 SERIAL NO. 11422 09 Oct 2025 16:08:21
vMain = 13.29, vLith = 3.07
samplenumber = 0, free = 559240
not logging, waiting to start at 09 Oct 2025 18:00:00
sample interval = 21600 seconds
data format = converted engineering
transmit real-time = no
sync mode = no
pump installed = yes, minimum conductivity frequency = 3143.3
<Executed/>

The Aquadopp was programmed for a 6 hours measurement interval:
==========
Deployment : AQDMOD
Current time : 10/9/2025 4:30:04 PM
Start at : 10/9/2025 6:00:00 PM
Comment:
Aquadopp SN 12706 programmed for modem at 6 hour interval

Measurement interval (s) : 21600
Average interval (s) : 60
Blanking distance (m) : 0.50
Measurement load (%) : 4
Power level : HIGH
Diagnostics interval(min) : N/A
Diagnostics samples : N/A
Compass upd. rate (s) : 21600
Coordinate System : ENU
Speed of sound (m/s) : MEASURED
Salinity (ppt) : 35
Analog input 1 : NONE
Analog input 2 : NONE
Analog input power out : DISABLED
Raw magnetometer out : OFF
File wrapping : OFF

TellTale : OFF
AcousticModem : OFF
Serial output : OFF
Baud rate : 19200

Assumed duration (days) : 1460.0
Battery utilization (%) : 21.0
Battery level (V) : 11.1
Recorder size (MB) : 9
Recorder free space (MB) : 8.973
Memory required (MB) : 0.2
Vertical vel. prec (cm/s) : 1.4
Horizon. vel. prec (cm/s) : 0.9

Instrument ID : AQD12706
Head ID : A6L 7650
Firmware version : 3.39

Aquadopp Deep Water Version 2.00.02
Copyright (C) Nortek AS
==========

Microstructure

Instrument description

During the whole expedition, we deployed a microstructure profiler (MSS90L, Sea&Sun Technologies, Germany) from the ship and through ice boreholes to measure key physical and biogeochemical parameters—temperature, salinity, dissolved oxygen, chlorophyll-a fluorescence, and shear—to investigate turbulent exchange processes. One profiler unit (serial number 097) was used, equipped with a consistent sensor suite (see Tab. 2.14). This included two parallel airfoil shear probes (type PNS6), a fast-response thermistor (FP07) with a small sensor guard, an accelerometer for detecting instrument vibration, standard CTD sensors (SST) for high-precision measurements, a Turner Designs Cyclops-7 in vivo chlorophyll/blue sensor, and a fast-response optical oxygen sensor (SST). All sensor channels recorded data at a sampling rate of 512 Hz. From the second MSS station onwards, unreliable data was provided by shear number 2 (Sensor SN6204), which was eventually replaced on September 14th (Sensor SN6184). At the beginning of the expedition, the second MSS90L (SN075) had already two broken shear amplifiers, and further analysis showed that SN097 also had one broken shear channel. Several attempts to repair the electronics failed. Therefore, we had to take all measures to reduce the risk of additional failures. All other sensors worked fine throughout the expedition.

Tab. 2.14: Overview of shear sensors mounted on the MSS profiler 097

Sensor	Sensor number SN (if available)	Calibration coefficients					
		A0	A1	A2	A3	A4	A5
Shear 1	c6326 (Casts 001 - 156)	5.191E-4	8.1673E-1	1.189E-2	-2.9319E-4	7.8432E-6	0
Shear 2	c6204* (Casts 001 - 030)	7.09E-4	8.2807E-1	6.995E-3	3.0667E-5	2.4701E-6	0
	c6184* (Casts 031 - 156)	5.731E-4	8.4192E-1	3.9464E-3	2.0116E-4	-1.6398E-7	0
Count	-	0	1	0	0	0	0
NTCHP (fast termperature thermistor)	-	-2.64852E-3	1.18684E-3	-8.679E-5	2.81326E-6	0	0
Press	-	-1.21814E2	1.77293E-2	1.87386E-9	-3.14373E-14	0	0
Temp	-	-2.39217	5.91377E-4	0	0	0	0
Cond	-	-2.72597E-1	1.19769E-3	2.17241E-10	-1.3099E-15	0	0
ACC	-	-3.03778E1	9.29025E-4	0	0	0	0
NTC	-	-1.49485E-5	4.42047E-4	-1.64861E-5	5.97979E-7	0	0
ACCx	-	-1.37131	3.89211E-5	0	0	0	0
ACCy	-	-1.38975	3.89826E-5	0	0	0	0
Chl_A	-	-9.65368E-3	7.66885E-5	0	0	-3.2E-1 (B0)	2.55484E1 (B1)
rawO2	-	8.09025E-1	1.00023E-2	9.99E2	0	6.71 (Spots cal. A0)	1.03278 (Spots cal. A1)
T_iS	-	-9.90689	9.99721E-4	0	1 (B1)	0	0
* : The sensor was replaced, but it remains non-functional due to an amplifier issue							

Profiling from the ship

MSS casts were conducted directly from the starboard side of *Polarstern* at numerous stations (Fig. 2.25). A SWM400 winch (Sea&Sun, Germany) with a 400m-long cable drum was mounted on a pallet tower and a metallic arm was welded on its base to extend the cable from the winch to the outside. All relevant MSS and winch electronics were set up in a small Zarges box. Data recording was done using a standard dedicated Panasonic Toughbook, running the SDA software (Sea&Sun, Germany). An external GPS was connected to the computer as well to include GPS position and time directly in the data files. The MSS was run with the attached cage, to ensure maximum protection against damage. After the first downcast, the connection between the probe and the computer was lost on the way up, and the winch was sent to commissioning, after which it worked correctly.

Because of the keel of the ship, the upper 25 m of each cast were excluded from dissipation estimates. All casts were performed by lowering the winch wire with a remote controller, ensuring that all sensors were pointed downwards. The profiler was deployed at a free-fall speed of 0.6 to 0.8 $m.s^{-1}$. The MSS was typically deployed down to approximately 360 m, unless the water depth was shallower. In that case, the first cast was usually stopped earlier, and used to mark the cable with tape 20 m above the bottom for the next casts.

Profiling during ice stations

Repeated under-ice profiling for microstructure turbulence was done using the MSS. It was operated from the sea ice throughout all four main ice stations, collecting as many subsequent profiles as possible. A typical MSS deployment consisted of the following setup: a SWM400 winch (Sea&Sun, Germany) with approximately 400 m cable for real-time data transmission was mounted on a pallet and strapped onto one end of a Nansen sled. The sled was placed next to a ~0.5 x 0.5 m hole in the ice that was prepared beforehand using standard ice drilling equipment. The site was typically located approximately 200-250 m sideways of the ship, to reduce the risk of entanglement with any ship-based gear in the water. Most of the time, a large pop-up tent was erected as protection from the elements. Similarly to the ship deployment, all electronics were set up in a small Zarges box, the recording was done using the same toughbook, also connecting the external GPS. The MSS was connected to the winch on-site, and both were powered by a 2kW Honda generator placed in some distance to the site.

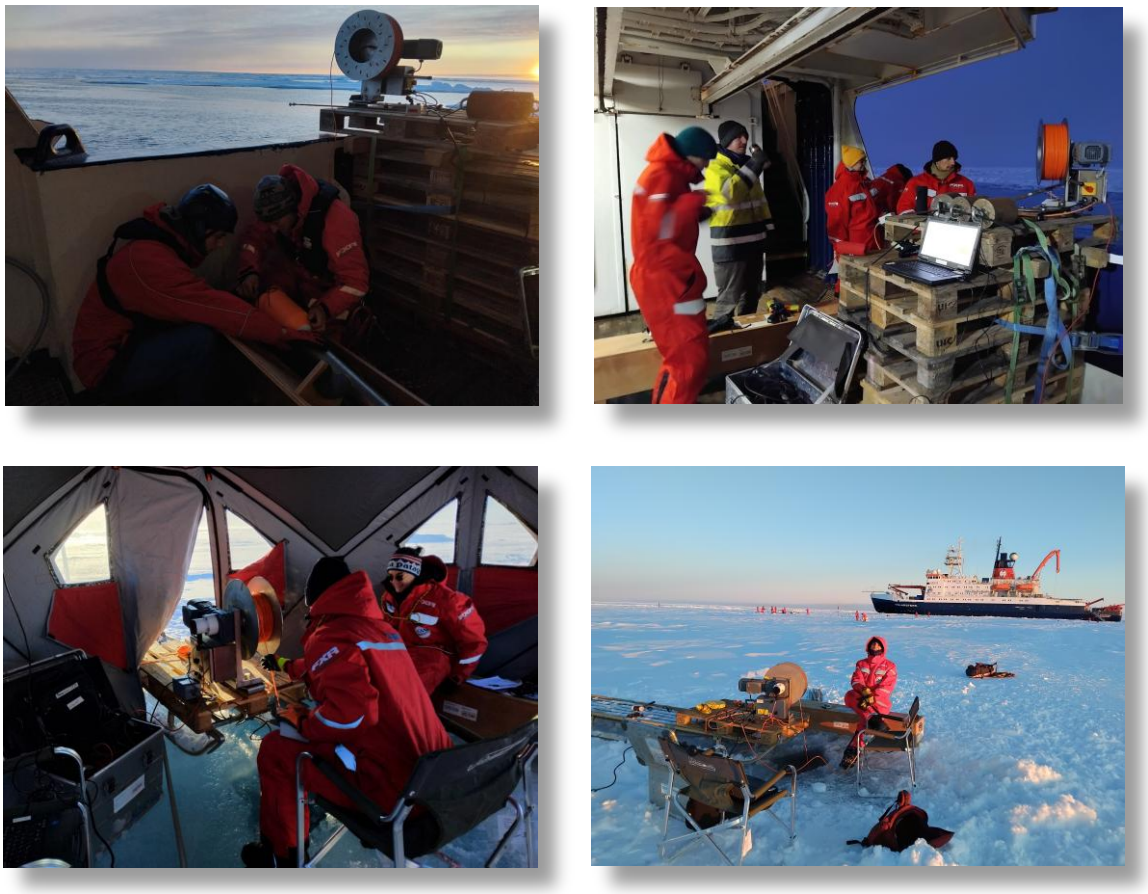

Fig. 2.25: MSS deployment from the ship (top), during Ice Station 1 (bottom left) and Ice Station 4 (bottom right). Photos by François Challet.

We collected profiles down to 350-400 m (depending on ocean currents and ice drift velocities) as frequently as possible. During the ice stations, the MSS was also run with the attached cage and the profiler was always kept in the water between casts. The instrument was deployed as early as possible during each station, and retrieved as late as possible, to obtain a maximum number of casts. Ice station 4 was located in shallower waters, and the water depth changed between 180 m and 270 m during the 5 hours of ice station work due to the floe drift. To adapt to these conditions, tape was added on the cable at depths of 150 m and 200 m and the station coordination provided regular updates on the water depth changes.

Due to the cold air temperatures, it sometimes happened that the shear and conductivity sensors froze before the first cast. When it happened, the recorded conductivity was abnormally low and the shear probes recorded constant values during the first 100 m of the downcast, but all sensors recovered when reaching warmer layers. Data from the following casts was not impacted.

For both ship and ice station profiling, instrument data were pre-processed using the MSP toolbox. The processed files are available as matlab structures (.mat files), whose first element is time, second element is latitude and third element is longitude. The fifth element (*ppd.sensors*) provides the list of parameters derived from the sensor measurements. The processed data for all parameters (temperature, salinity, dissipation rate, chlorophyll, oxygen concentration, etc.) is the fourth element (*ppd.data*). The locations of all MSS stations are shown in Figure 2.26 and a summary of all casts performed both from the ship and during ice

stations is available in Table 2.15. Examples of plots obtained from the dataset are presented in Figure 2.27.

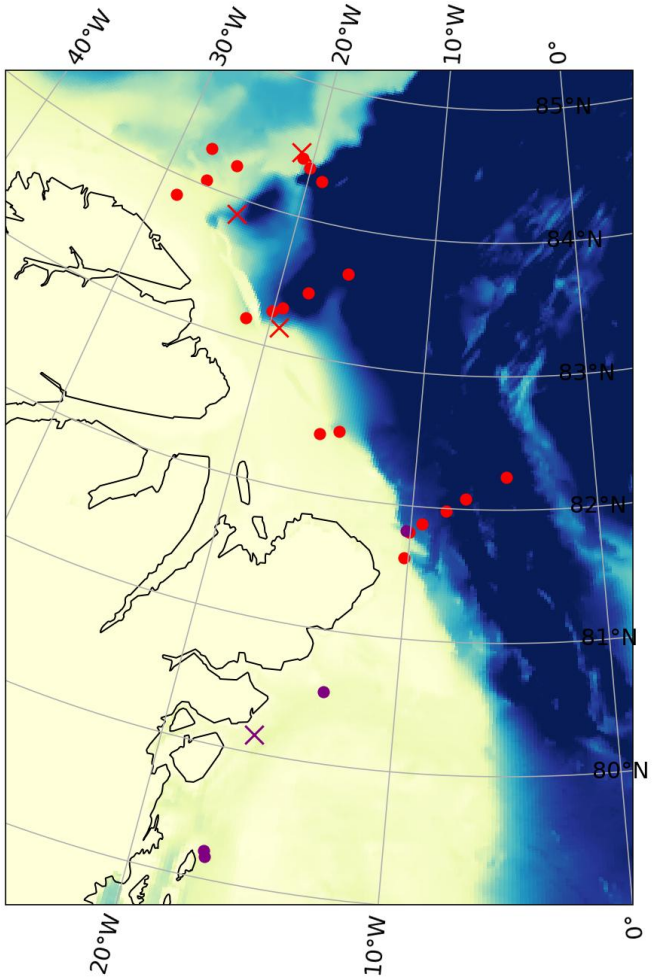

Fig. 2.26: Locations of all MSS stations of PS150. The dots show the locations where profiling was done from the ship and the crosses show the locations of ice stations. Red (resp. purple) symbols indicate the September (resp. October) stations. The background colour shading represents the bathymetry.

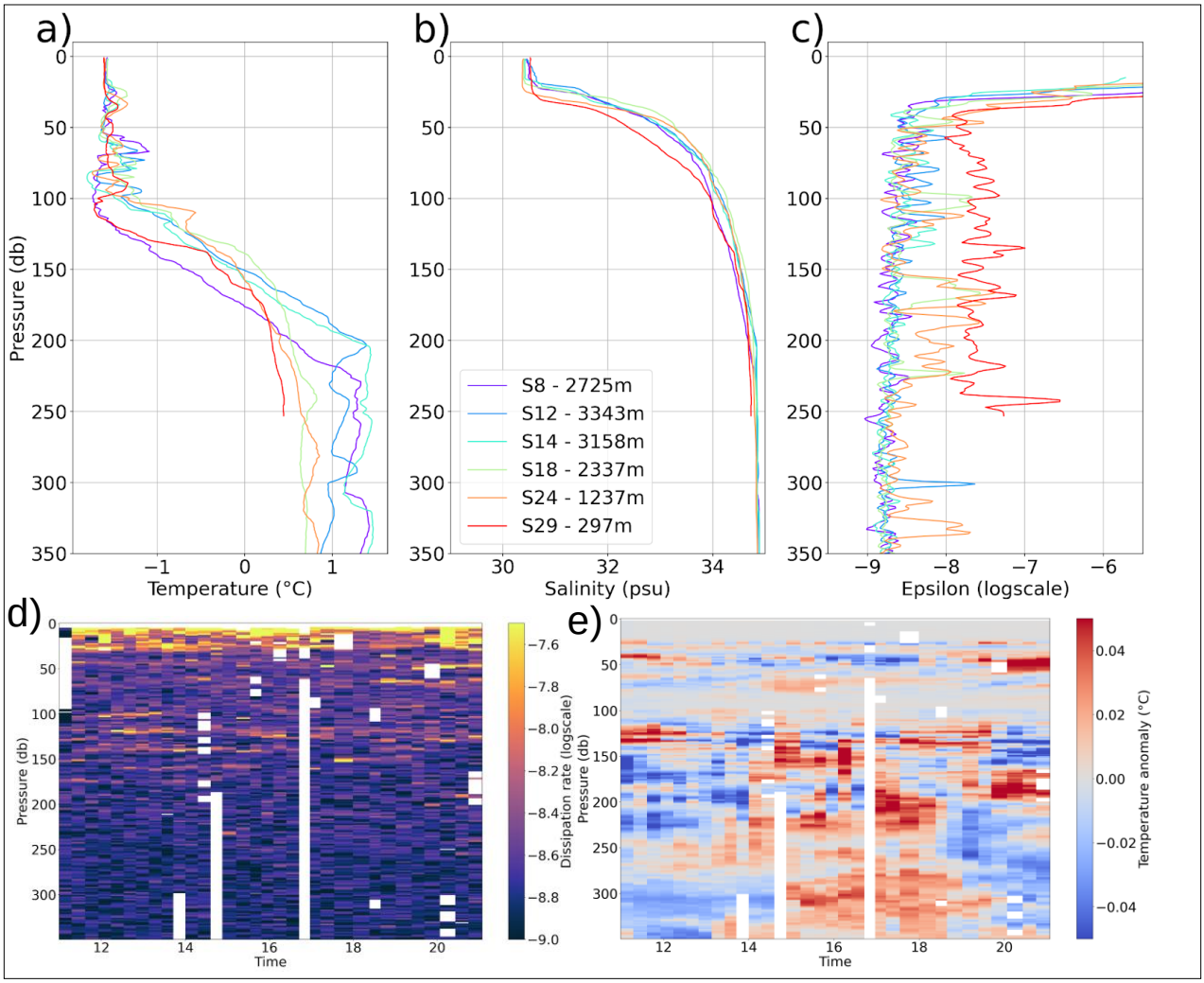

Fig. 2.27: Average a) temperature, b) salinity and c) dissipation rate profiles for each station of the Flade line (stations PS150_008_02 to PS150_029_02). Temporal evolution of d) the dissipation rate and e) the temperature anomaly compared to the mean profile during Ice Station 2.

Tab. 2.15 (next pages): List of MSS profiles obtained during PS150. The latitudes and longitudes are provided by the GPS connected to the MSS computer. The indicated water depth is the uncorrected value given either by the NBS depth sounding or the hydrosweep at the end of the previous CTD cast.

Raw file number (.MRD)	Station number	MSS cast number	Date	Time UTC	Latitude (°N)	Longitude (°E)	Water depth (m)	Depth of the cast (m)	Station type	Comments
1	PS150_008_02	1/1	07/09/2025	17:55	82.2440	-4.9375	2800	365	Ship	Values lost on the way up
2	PS150_012_02	1/3	08/09/2025	21:18	82.0753	-7.1418	3344	382	Ship	
3	PS150_012_02	2/3	08/09/2025	21:34	82.0749	-7.1482	3344	383	Ship	
4	PS150_012_02	3/3	08/09/2025	21:51	82.0730	-7.1534	3344	372	Ship	
5	PS150_014_02	1/2	09/09/2025	04:43	81.9789	-8.2034	3158	388	Ship	
6	PS150_014_02	2/2	09/09/2025	05:03	81.9782	-8.2107	3158	389	Ship	
7	PS150_018_02	1/3	09/09/2025	17:22	81.8717	-9.4194	2337	353	Ship	
8	PS150_018_02	2/3	09/09/2025	17:40	81.8708	-9.4205	2337	394	Ship	
9	PS150_018_02	3/3	09/09/2025	17:56	81.8699	-9.4220	2337	390	Ship	
10	PS150_024_02	1/2	10/09/2025	03:09	81.8003	-10.0558	1237	366	Ship	
11	PS150_024_02	2/2	10/09/2025	03:29	81.7994	-10.0435	1237	365	Ship	
12	PS150_029_02	1/3	10/09/2025	16:38	81.6061	-10.2344	297	245	Ship	Winch went backwards around 90 m
13	PS150_029_02	2/3	10/09/2025	16:58	81.6033	-10.2292	297	253	Ship	
14	PS150_029_02	3/3	10/09/2025	17:10	81.6019	-10.2251	297	232	Ship	
15	PS150_044_01	1/16	13/09/2025	13:15	83.1577	-19.4008	1073	356	Ice station 1	
16	PS150_044_01	2/16	13/09/2025	13:38	83.1569	-19.3928	1073	352	Ice station 1	Connection lost on the way up
17	PS150_044_01	3/16	13/09/2025	14:02	83.1560	-19.3840	1073	352	Ice station 1	Winch went backwards - 10s stop
18	PS150_044_01	4/16	13/09/2025	14:19	83.1555	-19.3778	1073	351	Ice station 1	Winch went backwards - 10s stop
19	PS150_044_01	5/16	13/09/2025	14:36	83.1549	-19.3715	1073	348	Ice station 1	Winch went backwards - 5s stop
20	PS150_044_01	6/16	13/09/2025	14:53	83.1543	-19.3651	1073	348	Ice station 1	
21	PS150_044_01	7/16	13/09/2025	15:16	83.1534	-19.3561	1073	170	Ice station 1	Stopped, entangled wire
22	PS150_044_01	8/16	13/09/2025	15:26	83.1531	-19.3524	1073	353	Ice station 1	
23	PS150_044_01	9/16	13/09/2025	15:43	83.1525	-19.3460	1073	352	Ice station 1	Wire entangled, no stop
24	PS150_044_01	10/16	13/09/2025	16:03	83.1517	-19.3387	1073	351	Ice station 1	
25	PS150_044_01	11/16	13/09/2025	16:21	83.1510	-19.3322	1073	352	Ice station 1	
26	PS150_044_01	12/16	13/09/2025	16:38	83.1503	-19.3260	1073	352	Ice station 1	
27	PS150_044_01	13/16	13/09/2025	16:57	83.1495	-19.3194	1073	349	Ice station 1	Winch went backwards
28	PS150_044_01	14/16	13/09/2025	17:32	83.1481	-19.3081	1073	351	Ice station 1	Frozen cable, had to be pulled sometimes on the way down
29	PS150_044_01	15/16	13/09/2025	18:03	83.1468	-19.2989	1073	354	Ice station 1	Frozen cable, had to be pulled sometimes on the way down
30	PS150_044_01	16/16	13/09/2025	18:21	83.1460	-19.2939	1073	353	Ice station 1	Frozen cable, had to be pulled sometimes on the way down
31	PS150_046_02	1/3	14/09/2025	14:54	83.1624	-21.5616	223	144	Ship	
32	PS150_046_02	2/3	14/09/2025	15:07	83.1620	-21.5562	223	168	Ship	
33	PS150_046_02	3/3	14/09/2025	00:00	83.1613	-21.5508	223	168	Ship	

34	PS150_050_02	1/3	15/09/2025	00:43	83.2671	-20.0662	1115	337	Ship	gps forgotten, the coordinates of the third cast were used
35	PS150_050_02	2/3	15/09/2025	01:03	83.2671	-20.0662	1115	333	Ship	gps forgotten, the coordinates of the third cast were used
36	PS150_050_02	3/3	15/09/2025	01:19	83.2671	-20.0662	1115	326	Ship	
37	PS150_054_02	1/6	15/09/2025	19:53	83.3085	-19.4835	2876	364	Ship	Windy
38	PS150_054_02	2/6	15/09/2025	20:08	83.3062	-19.4758	2876	287	Ship	Windy
39	PS150_054_02	3/6	15/09/2025	20:24	83.3042	-19.4698	2876	372	Ship	Windy
40	PS150_054_02	4/6	15/09/2025	20:37	83.3023	-19.4638	2876	372	Ship	Windy
41	PS150_054_02	5/6	15/09/2025	20:52	83.3006	-19.4565	2876	375	Ship	Windy
42	PS150_054_02	6/6	15/09/2025	21:10	83.2990	-19.4488	2876	373	Ship	Windy
43	PS150_059_02	1/4	16/09/2025	11:32	83.4597	-18.0553	3151	377	Ship	12 hours after storm, winch went backwards early in the cast
44	PS150_059_02	2/4	16/09/2025	11:47	83.4587	-18.0445	3151	377	Ship	12 hours after storm
45	PS150_059_02	3/4	16/09/2025	12:04	83.4577	-18.0346	3151	377	Ship	12 hours after storm
46	PS150_059_02	4/4	16/09/2025	12:22	83.4566	-18.0246	3151	377	Ship	12 hours after storm
47	PS150_063_02	1/2	17/09/2025	08:35	83.6608	-15.7195	3482	394	Ship	
48	PS150_063_02	2/2	17/09/2025	08:55	83.6614	-15.7176	3482	396	Ship	Problem with the winch after pressing the emergency stop, solved by opening it and pressing ok to error message
49	PS150_071_02	1/3	19/09/2025	22:59	84.2984	-18.9527	3338	372	Ship	
50	PS150_071_02	2/3	19/09/2025	23:15	84.2969	-18.9551	3338	375	Ship	
51	PS150_071_02	3/3	19/09/2025	23:31	84.2954	-18.9576	3338	372	Ship	
52	PS150_073_02	1/3	20/09/2025	11:35	84.3750	-20.1484	1166	395	Ship	
53	PS150_073_02	2/3	20/09/2025	11:52	84.3749	-20.1522	1166	395	Ship	
54	PS150_073_02	3/3	20/09/2025	12:12	84.3748	-20.1591	1166	400	Ship	
55	PS150_076_02	1/3	20/09/2025	23:32	84.4281	-20.7890	782	391	Ship	
56	PS150_076_02	2/3	20/09/2025	23:47	84.4283	-20.7931	782	393	Ship	
57	PS150_076_02	3/3	21/09/2025	00:04	84.4284	-20.7964	782	390	Ship	
58	PS150_078_01	1/32	21/09/2025	11:18	84.4703	-21.0405	736	356	Ice station 2	
59	PS150_078_01	2/32	21/09/2025	11:35	84.4705	-21.0447	736	356	Ice station 2	
60	PS150_078_01	3/32	21/09/2025	11:55	84.4707	-21.0491	736	358	Ice station 2	
61	PS150_078_01	4/32	21/09/2025	12:13	84.4709	-21.0525	736	359	Ice station 2	
62	PS150_078_01	5/32	21/09/2025	12:32	84.4710	-21.0551	736	357	Ice station 2	
63	PS150_078_01	6/32	21/09/2025	12:50	84.4711	-21.0574	736	361	Ice station 2	
64	PS150_078_01	7/32	21/09/2025	13:07	84.4712	-21.0591	736	363	Ice station 2	
65	PS150_078_01	8/32	21/09/2025	13:26	84.4712	-21.0605	736	361	Ice station 2	
66	PS150_078_01	9/32	21/09/2025	13:43	84.4712	-21.0615	736	361	Ice station 2	
67	PS150_078_01	10/32	21/09/2025	13:59	84.4712	-21.0621	736	300	Ice station 2	
68	PS150_078_01	11/32	21/09/2025	14:18	84.4710	-21.0631	736	361	Ice station 2	
69	PS150_078_01	12/32	21/09/2025	14:26	84.4709	-21.0640	736	361	Ice station 2	
70	PS150_078_01	13/32	21/09/2025	14:51	84.4706	-21.0651	736	188	Ice station 2	
71	PS150_078_01	14/32	21/09/2025	15:10	84.4704	-21.0664	736	362	Ice station 2	
72	PS150_078_01	15/32	21/09/2025	15:34	84.4698	-21.0694	736	360	Ice station 2	
73	PS150_078_01	16/32	21/09/2025	15:49	84.4694	-21.0717	736	361	Ice station 2	
74	PS150_078_01	17/32	21/09/2025	16:05	84.4690	-21.0750	736	362	Ice station 2	
75	PS150_078_01	18/32	21/09/2025	16:25	84.4685	-21.0789	736	365	Ice station 2	
76	PS150_078_01	19/32	21/09/2025	16:43	84.4679	-21.0837	736	365	Ice station 2	
77	PS150_078_01	20/32	21/09/2025	16:51	84.4674	-21.0879	736	69	Ice station 2	Cast stopped after 70 m
78	PS150_078_01	21/32	21/09/2025	16:59	84.4670	-21.0916	736	363	Ice station 2	
79	PS150_078_01	22/32	21/09/2025	17:13	84.4664	-21.0964	736	362	Ice station 2	
80	PS150_078_01	23/32	21/09/2025	17:30	84.4658	-21.1032	736	361	Ice station 2	
81	PS150_078_01	24/32	21/09/2025	17:53	84.4649	-21.1143	736	358	Ice station 2	

82	PS150_078_01	25/32	21/09/2025	18:23	84.4645	-21.1203	736	359	Ice station 2	
83	PS150_078_01	26/32	21/09/2025	18:38	84.4642	-21.1265	736	357	Ice station 2	
84	PS150_078_01	27/32	21/09/2025	18:53	84.4637	-21.1381	736	358	Ice station 2	
85	PS150_078_01	28/32	21/09/2025	19:23	84.4634	-21.1453	736	358	Ice station 2	
86	PS150_078_01	29/32	21/09/2025	19:41	84.4632	-21.1533	736	360	Ice station 2	
87	PS150_078_01	30/32	21/09/2025	20:25	84.4631	-21.1640	736	353	Ice station 2	
88	PS150_078_01	31/32	21/09/2025	20:44	84.4630	-21.1720	736	356	Ice station 2	
89	PS150_078_01	32/32	21/09/2025	21:03	84.4630	-21.1799	736	355	Ice station 2	
90	PS150_079_02	1/3	22/09/2025	08:27	84.2216	-25.4004	621	354	Ship	
91	PS150_079_02	2/3	22/09/2025	08:43	84.2224	-25.4151	621	375	Ship	
92	PS150_079_02	3/3	22/09/2025	09:08	84.2227	-25.4252	621	352	Ship	
93	PS150_082_02	1/3	23/09/2025	00:11	84.0439	-27.0847	545	395	Ship	
94	PS150_082_02	2/3	23/09/2025	00:28	84.0438	-27.0899	545	393	Ship	
95	PS150_082_02	3/3	23/09/2025	00:45	84.0437	-27.0950	545	396	Ship	
96	PS150_085_02	ot a cast	23/09/2025	12:58	83.8581	-28.6752	87	72	Ship	No free fall: test to mark the cable length to avoid hitting the bottom
97	PS150_085_02	1/3	23/09/2025	13:13	83.8579	-28.6799	87	86	Ship	
98	PS150_085_02	2/3	23/09/2025	13:18	83.8580	-28.6795	87	84	Ship	
99	PS150_085_02	3/3	23/09/2025	13:23	83.8580	-28.6789	87	84	Ship	
100	PS150_089_02	1/3	24/09/2025	05:20	84.2761	-27.5977	1059	376	Ship	
101	PS150_089_02	2/3	24/09/2025	05:35	84.2763	-27.6101	1059	370	Ship	
102	PS150_089_02	3/3	24/09/2025	05:52	84.2765	-27.6239	1059	377	Ship	
103	PS150_090_01	1/19	25/09/2025	10:50	83.8856	-24.2264	2482	355	Ice station 3	
104	PS150_090_01	2/19	25/09/2025	11:06	83.8858	-24.2296	2482	357	Ice station 3	
105	PS150_090_01	3/19	25/09/2025	11:23	83.8860	-24.2330	2482	357	Ice station 3	
106	PS150_090_01	4/19	25/09/2025	11:40	83.8863	-24.2361	2482	355	Ice station 3	
107	PS150_090_01	5/19	25/09/2025	11:59	83.8867	-24.2394	2482	353	Ice station 3	
108	PS150_090_01	6/19	25/09/2025	12:16	83.8870	-24.2422	2482	356	Ice station 3	
109	PS150_090_01	7/19	25/09/2025	12:32	83.8874	-24.2445	2482	356	Ice station 3	
110	PS150_090_01	8/19	25/09/2025	12:49	83.8878	-24.2470	2482	356	Ice station 3	
111	PS150_090_01	9/19	25/09/2025	13:08	83.8883	-24.2493	2482	355	Ice station 3	
112	PS150_090_01	10/19	25/09/2025	13:30	83.8889	-24.2516	2482	354	Ice station 3	
113	PS150_090_01	11/19	25/09/2025	13:46	83.8893	-24.2532	2482	353	Ice station 3	
114	PS150_090_01	12/19	25/09/2025	14:09	83.8899	-24.2548	2482	354	Ice station 3	
115	PS150_090_01	13/19	25/09/2025	14:26	83.8904	-24.2558	2482	353	Ice station 3	
116	PS150_090_01	14/19	25/09/2025	14:42	83.8908	-24.2566	2482	356	Ice station 3	
117	PS150_090_01	15/19	25/09/2025	15:00	83.8911	-24.2575	2482	357	Ice station 3	
118	PS150_090_01	16/19	25/09/2025	15:18	83.8915	-24.2587	2482	358	Ice station 3	
119	PS150_090_01	17/19	25/09/2025	15:33	83.8918	-24.2594	2482	358	Ice station 3	
120	PS150_090_01	18/19	25/09/2025	15:50	83.8920	-24.2605	2482	359	Ice station 3	
121	PS150_090_01	19/19	25/09/2025	16:09	83.8923	-24.2616	2482	358	Ice station 3	
122	PS150_091_02	1/4	27/09/2025	11:48	82.4449	-15.6407	169	111	Ship	Stopped early because of sea ice
123	PS150_091_02	2/4	27/09/2025	11:55	82.4440	-15.6390	169	135	Ship	
124	PS150_091_02	3/4	27/09/2025	12:03	82.4427	-15.6374	169	149	Ship	
125	PS150_091_02	4/4	27/09/2025	12:15	82.4415	-15.6372	169	144	Ship	
126	PS150_093_02	1/4	27/09/2025	17:35	82.4879	-14.5761	970	338	Ship	
127	PS150_093_02	2/4	27/09/2025	17:54	82.4846	-14.5657	970	338	Ship	
128	PS150_093_02	3/4	27/09/2025	18:08	82.4819	-14.5576	970	53	Ship	Power shutdown (?) after 50m in the downcast.
129	PS150_093_02	4/4	27/09/2025	18:12	82.4812	-14.5553	970	328	Ship	
130	PS150_103_02	1/3	01/10/2025	02:30	81.8102	-10.2379	1019	389	Ship	
131	PS150_103_02	2/3	01/10/2025	02:47	81.8103	-10.2367	1019	396	Ship	
132	PS150_103_02	3/3	01/10/2025	03:05	81.8103	-10.2342	1019	394	Ship	
133	PS150_124_02	1/3	09/10/2025	22:05	80.5400	-13.3168	259	222	Ship	
134	PS150_124_02	2/3	09/10/2025	22:16	80.5394	-13.3245	259	221	Ship	
135	PS150_124_02	3/3	09/10/2025	22:25	80.5391	-13.3310	259	229	Ship	
136	PS150_127_01	1/13	10/10/2025	13:48	80.1341	-16.0571	180-270	163	Ice station 4	

137	PS150_127_01	2/13	10/10/2025	14:05	80.1356	-16.0413	180-270	208	Ice station 4	
138	PS150_127_01	no data	10/10/2025	-	-	-	180-270	-	Ice station 4	No data recorded
139	PS150_127_01	3/13	10/10/2025	14:22	80.1373	-16.0247	180-270	206	Ice station 4	
140	PS150_127_01	no data	10/10/2025	-	-	-	180-270	-	Ice station 4	No data recorded
141	PS150_127_01	4/13	10/10/2025	14:38	80.1390	-16.0086	180-270	203	Ice station 4	
142	PS150_127_01	5/13	10/10/2025	14:54	80.1408	-15.9906	180-270	153	Ice station 4	
143	PS150_127_01	6/13	10/10/2025	15:09	80.1426	-15.9736	180-270	168	Ice station 4	
144	PS150_127_01	7/13	10/10/2025	15:24	80.1445	-15.9571	180-270	172	Ice station 4	
145	PS150_127_01	8/13	10/10/2025	15:37	80.1462	-15.9428	180-270	203	Ice station 4	
146	PS150_127_01	9/13	10/10/2025	15:50	80.1479	-15.9292	180-270	180	Ice station 4	
147	PS150_127_01	10/13	10/10/2025	16:03	80.1496	-15.9162	180-270	218	Ice station 4	
148	PS150_127_01	11/13	10/10/2025	16:28	80.1527	-15.8936	180-270	231	Ice station 4	
149	PS150_127_01	12/13	10/10/2025	16:41	80.1543	-15.8835	180-270	197	Ice station 4	
150	PS150_127_01	13/13	10/10/2025	16:52	80.1556	-15.8755	180-270	224	Ice station 4	
151	PS150_134_01	1/3	12/10/2025	14:37	79.2083	-17.1688	370	343	Ship	
152	PS150_134_01	2/3	12/10/2025	15:23	79.2079	-17.1736	370	343	Ship	Frozen sensors in the first 150 m
153	PS150_134_01	3/3	12/10/2025	15:38	79.2080	-17.1739	370	346	Ship	
154	PS150_135_02	1/3	12/10/2025	20:50	79.1670	-17.0824	396	346	Ship	
155	PS150_135_02	2/3	12/10/2025	21:07	79.1666	-17.0834	396	357	Ship	
156	PS150_135_02	3/3	12/10/2025	21:22	79.1660	-17.0838	396	364	Ship	

Helicopter-based hydrographic measurements and instrument deployments

We obtained a number of additional CTD casts, water samples and sea-ice cores far beyond the ship's track during several helicopter flights. We were able to conduct additional hydrographic sections further (north)west towards the Lincoln Sea, to extend the ship-based Wandel Sea transect into both directions without spending additional ship time, and to reach remote locations that were generally inaccessible for *Polarstern* (e.g. deep inside the fast-ice covered Independence and Hagen Fjords (Fig. 2.28), or close to the 79°N glacier). These CTD profiles were either recorded using XCTDs (Tsurumi Seiki, Japan) from the sea ice or directly from the hovering helicopter (see above), or by using a hand-held CTD in conjunction with a motorized fishing rod (Shimano, Japan). The first two fishing-rod CTD casts (at Independence Fjord Station 1) were performed using our standard Sea&Sun CTD48M (SN 1495, depth rating 1,500 m), but the instrument did not record any data on the first cast, and had a data download error in the field on the second cast. The data could be recovered later though, after removing and reinstalling the batteries. Due to these reliability issues, we used a freshly calibrated RBRconcerto CTD (SN 210909, pressure rating 750 dbar) for the rest of the campaign.

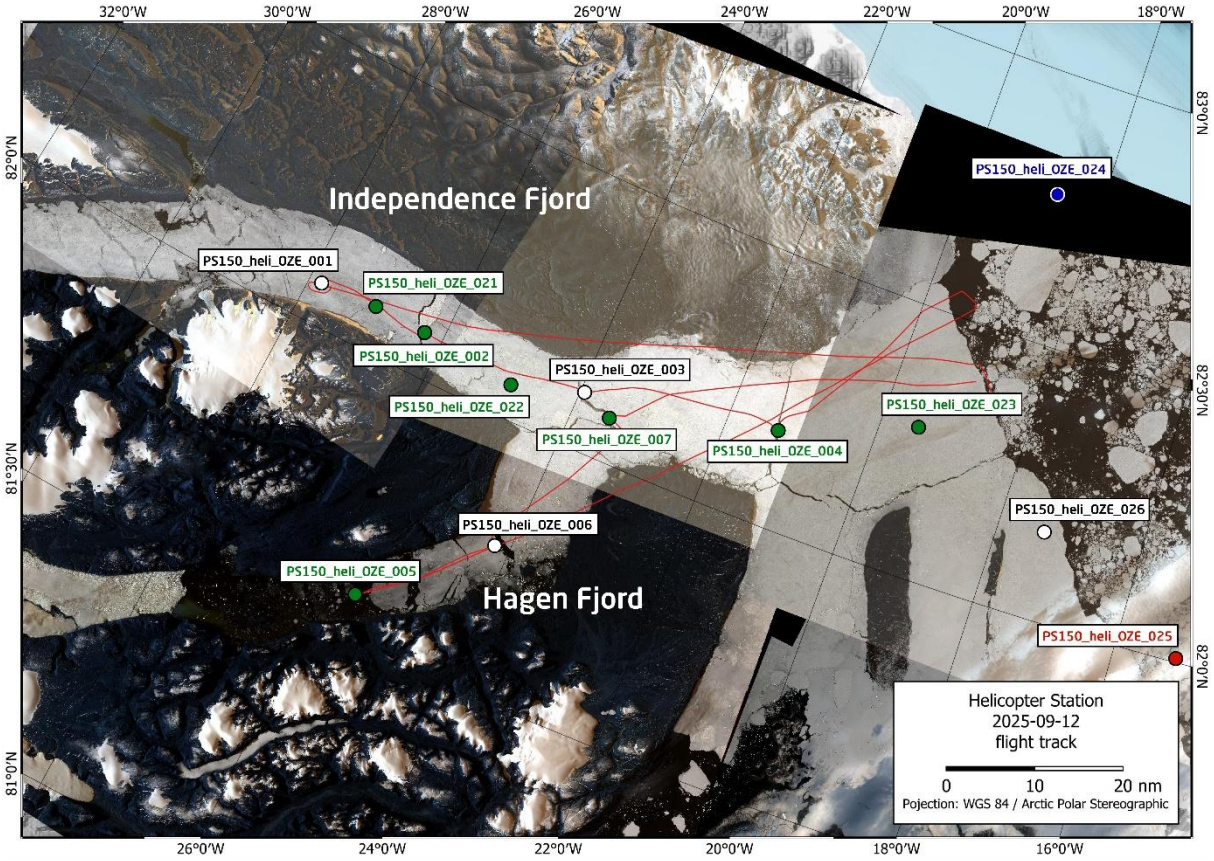

Fig. 2.28: Example of helicopter-based hydrographic stations conducted in Independence Fjord and Hagen Fjord during 5 flights on 12 Sep, 26 Sep, 28 Sep, and 30 Sep 2025. During these stations, hydrographic profiles were obtained using RBRconcerto fishing-rod CTDs (black) and XCTDs (green), water samples were taken for tracer analysis and eDNA measurements, and sea-ice cores were extracted for biological analysis. Furthermore, a helicopter-based mooring (IT1-1) was deployed in the fjord inflow (blue), and CTD buoy AWI-SVP5S-0006 was installed on the newly formed fast ice over the fjord outflow (red).

Before deployment of the fishing-rod CTD, we drilled a 0.25 m hole through the ice, or chose a suitable spot of open water or thin new ice at the edge of a floe. Before deployment of the CTD, water depth was usually measured using a mobile Simrad S2009 Echosounder. Both, the motorized fishing rod and the echosounder were powered by a lead acid battery installed in a pelicase. Both down- und upcasts were recorded internally upon twist activation of the RBRconcerto, and downloaded from the instrument via Wifi upon recovery. The motorized fishing rod also had a real-time display of cable length, which was usually accurate to +- 5 m. It has to be noted though that the paid-out cable length deviated strongly from the instrument depth of the CTD due to the strong currents. Also, the lowering speed of the fishing rod winch was rather slow (~0.5-0.8 m/s), because of the limited weight of the CTD in water. During the first weeks of the campaign, we did not lower the CTD to the ground, but stopped the winch well before the paid-out cable reached the pre-determined water depth. As we got more experienced later in the campaign, we put an additional weight of ~0.5 kg on the CTD to increase its lowering speed, and we lowered the CTD until it touched the ground (as long as the water depth was lower than the instrument's depth rating of 750 dbar). On some occasions, seafloor sediment got stuck on the out- and inside of the inductive cell upon touching the ground, and the following upcast was of low quality. A photo of a typical deployment is shown in Figure 2.29.

Fig. 2.29: An RBRconcerto CTD is deployed through an ice hole during a helicopter-based station using a motorized fishing rod. The Zarges box contains the mobile Simrad Echosounder to determine the water depth beforehand. Photo by Manuel Franco Pire.

A total of 24 casts were conducted using the RBRconcerto CTD SN210909, 4 of which were not deployed via the fishing rod, but attached to the end of a niskin sampling line to provide hydrographic context for the mobile water sampling. Of the remaining 20 casts, 19 were deployed from ice floes reached by helicopter, and one from *Polarstern's* working deck. Table 2.16 contains an overview of all casts. For further metadata on water depth or descriptions of the casts, the reader is referred to the helicopter events table (Tab. 2.1).

Raw instrument data files were converted to ASCII format using the RBR Ruskin Software (https://rbr-global.com/products/software/). From these files, processed upcast and downcast profiles were generated. A 4th order butterworth low-pass filter with a cutoff frequency of 0.4 Hz was applied to remove high-frequency signals, corresponding to a spatial smoothing of approximately 2–3 meters based on typical profiling speeds. The filtered data were then binned into 1 dbar intervals, starting from 3 dbar. The dataset will be archived in three levels: raw files, ASCII files from Ruskin, and manually processed upcast and downcast files. Ruskin provides 4 files after processing raw files: a data file containing a time series of measurements, a metadata file, an events file and an annotations file.

In many profiles the upcast data were considered more reliable due to conductivity sensor misreadings at the beginning of the downcasts. We speculate that these misreadings are likely caused by ice accumulation around the sensor due to very low air/sensor temperatures at deployment. In at least two casts, the upcast data appeared anomalous, potentially due to sediment interfering with the sensors. This preliminary quality control analysis can only carried out when comparing upcast and downcast data, as shown in Figure 2.30. Based on the processed dataset, Table 2.16 contains information on the profiles that are deemed usable for each cast. Future in-depth investigations of the dataset could reach different conclusions. If both upcast and downcast profiles are available, downcast data is recommended for scientific analysis due to optimal and more consistent profiling speeds.

For future operations care should be taken to prevent a very cold instrument from entering the water. This could be achieved by storing it on an insulating container with a heat source (e.g. a warm water flask) or by thoroughly rinsing it with warm water just before deployment. We also recommend careful visual inspection to detect freezing water around the conductivity sensor before deployment.

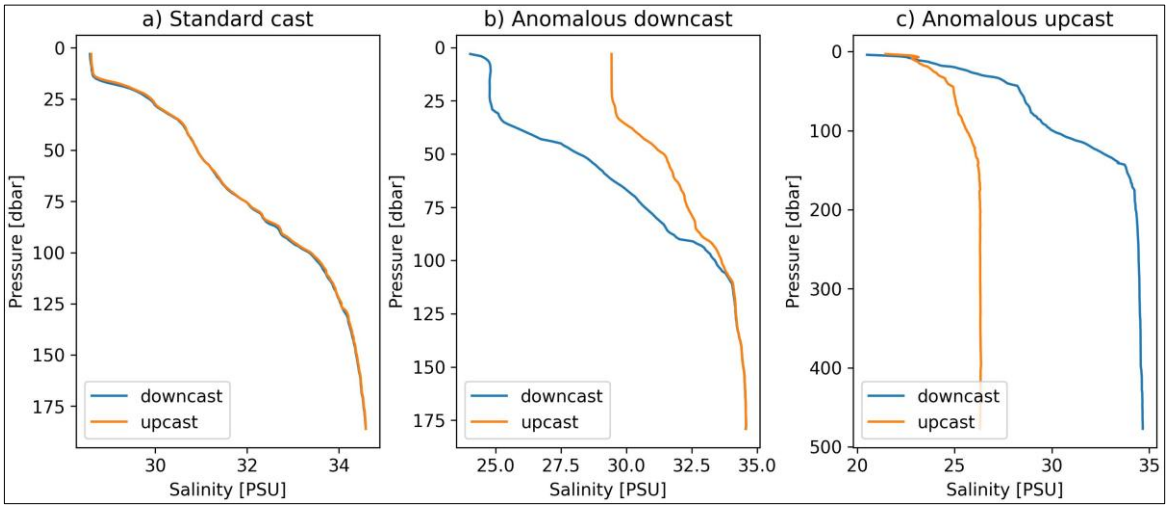

Fig. 2.30: Examples of fishing rod CTD casts using the RBRconcerto CTD with a) good quality upcast and downcast profiles b) salinity misreadings at the beginning of the downcast and c) misreadings during the upcast.

Tab. 2.16: List of fishing-rod CTD deployments. Additional metadata information for the helicopter deployments can be found on the helicopter events table (Tab. 2.1). The *filename* column lists base names. Raw files are named by appending .rsk, and Ruskin files by appending _data.txt, _events.txt, _metadata.txt, and _annotations_profile.txt. Processed files follow station numbering, with the prefixes dRBR_and uRBR_ indicating downcast and upcast profiles respectively. u/d indicates which of the upcast (u) or downcast (d) data is deemed reliable (see e.g. Fig. 2.30) and thus recommended for use.

Station No.	Time	Latitude	Longitude	Cast depth	Raw filename	Recom	Comments
PS150_heli_OZE_001_02	2025-09-12T13:00:00	82.0733	-27.8093	640	210909_20250912_1340_1	u, d	
PS150_heli_OZE_003_01	2025-09-12T14:46:00	82.1104	-23.9614	560	210909_20250912_1530_2	u, d	
PS150_heli_OZE_006_01	2025-09-12T19:41:00	81.7736	-24.2095	525	210909_20250912_2020_3	u, d	
PS150_heli_OZE_008_01	2025-09-16T17:03:00	83.0414	-22.634	138	210909_20250916_1715_1	u, d	
PS150_heli_OZE_008_02	2025-09-16T17:17:00	83.0414	-22.634	138	210909_20250916_1725_1	u, d	
PS150_heli_OZE_009_01	2025-09-16T18:14:00	83.0053	-22.9504	105	210909_20250916_1821_2	u, d	
PS150_heli_OZE_009_02	2025-09-16T18:23:00	83.0053	-22.9504	105	210909_20250916_1832_2	u	
PS150_heli_OZE_010_01	2025-09-16T19:20:00	83.0764	-22.3334	216	210909_20250916_1932_3	u, d	
PS150_heli_OZE_010_02	2025-09-16T19:33:00	83.0764	-22.3334	216	210909_20250916_1945_3	u, d	
PS150_heli_OZE_011_01	2025-09-20T06:30:00	84.1965	-8.6559	350	210909_20250920_0721_1	u, d	
PS150_heli_OZE_012_01	2025-09-20T08:08:00	84.1005	-10.027	412	210909_20250920_0914_2	u, d	
PS150_heli_OZE_013_01	2025-09-21T14:42:00	85.64	-16.6613	575	210909_20250921_1532_1	u, d	
PS150_heli_OZE_016_01	2025-09-24T11:29:00	83.8267	-32.9991	106	210909_20250924_1141_1	u	
PS150_heli_OZE_017_01	2025-09-24T12:16:00	83.9563	-32.9845	175	210909_20250924_1228_2	u	
PS150_heli_OZE_018_01	2025-09-24T13:01:00	84.0538	-33.0201	443	210909_20250924_1329_3	u	
PS150_heli_OZE_021_02	2025-09-26T15:23:00	82.0862	-27.0423	293	210909_20250926_1553_1		deep Niskin cast, fall rate suboptimal, not full water depth
PS150_heli_OZE_021_04	2025-09-26T16:00:00	82.0862	-27.0423	55	210909_20250926_1623_1+shallow		shallow Niskin cast, fall rate suboptimal, not full water depth
PS150_heli_OZE_022_02	2025-09-26T17:17:00	82.0742	-24.8379	55	210909_20250926_1803_2_shallow		shallow Niskin cast, fall rate suboptimal, not full water depth
PS150_heli_OZE_023_02	2025-09-28T13:10:00	82.2789	-19.5589	55	210909_20250928_1339		shallow Niskin cast, fall rate suboptimal, not full water depth
PS150_heli_OZE_024_01	2025-09-28T15:41:00	82.8052	-18.6087	296	210909_20250928_1604	u, d	deployment
PS150_heli_OZE_025_01	2025-09-30T15:25:00	82.0508	-15.1093	114	210909_20250930_1538_1	u	
PS150_heli_OZE_026_01	2025-09-30T17:03:00	82.1779	-17.3935	148	210909_20250930_1831_2		
PS150_098_02	2025-09-30T00:48:00	84.6782	-12.1424	122	210909_20250930_0103	u	shipboard deployment, water depth 122 from Navlot.
PS150_heli_OZE_027_01	2025-10-11T11:17:00	79.5697	-19.4627	475	210909_20251011_2232	d	

In addition to the hydrographic measurements outlined above, two buoys (see below) and two moorings (see above) were deployed using the helicopter.

Autonomous ice-tethered buoys

Ice-tethered profiling buoy TOP016

TOP-type ice-tethered profiling buoy TOP016 (shortname 2025W17) was deployed in the Greenland Sea on 25 September 2025 at 14:30 UTC as part of ice station #3. The length of the tether was 300 m, and the buoy is generally able to profile until just under the sea ice bottom. The profiler is equipped with a Solumetrix 300 m CTD, and also records several engineering parameters. The surface unit additionally records GPS position and basic meteorological parameters, and transfers the data of each profile to a land-based station via the iridium satellite network. Figure 2.31 shows a schematic diagram of the buoy and its components. The GPS coordinates at the time of deployment were 83°53.431'N, 024°15.868'W. Ice thickness was 1.35 m, freeboard was 0.08 m, and snow depth was 0.1 m. The ice floe was probably second year ice, and the area of deployment was very level, although ice thickness did vary. Weather conditions were sunny, and there was almost no wind. Air temperatures were around -15°C. Water depth was around 2,000 m.

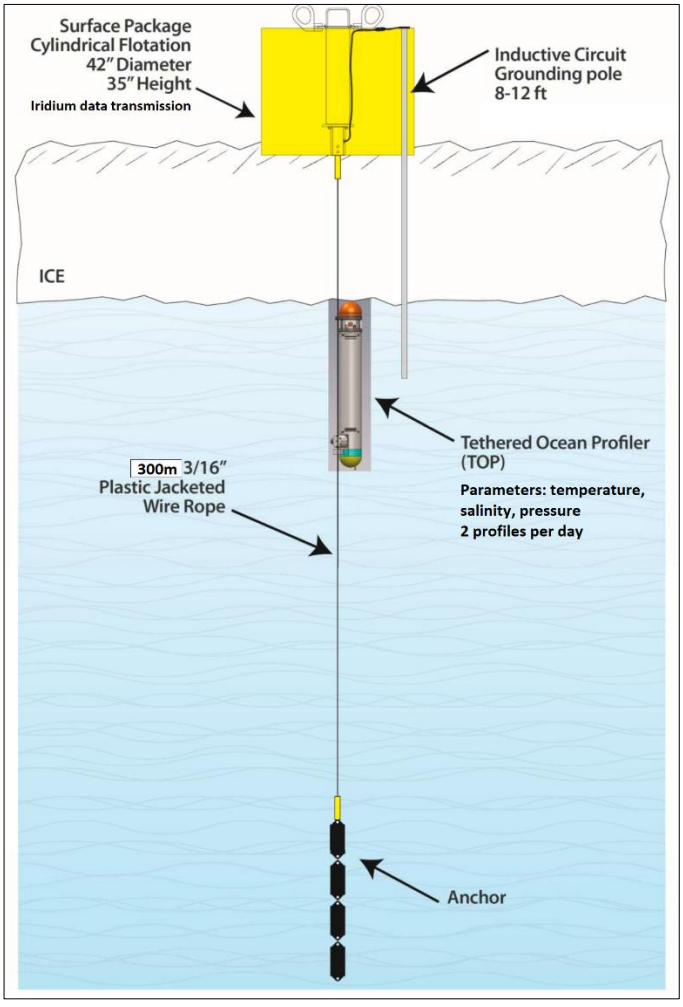

Fig. 2.31: Schematic diagram of TOP016 profiling buoy. Credits: WHOI

The original plan for this deployment was in the fast ice in the 79NG area, but satellite imagery showed that ice conditions would not allow a deployment at any site close to the glaciers. We considered a helicopter deployment, but the risk of bad weather and the conflict with other planned work in the area led us to the decision that another location would be more feasible.

So, we discussed with our WHOI colleagues the alternative plan to deploy the profiler in the pack ice in the Independence Fjord area, which was then generally agreed to.

During deployment, three 0.25 m auger holes were drilled into the ice in a triangular shape. A tripod with a block and 2 chainfalls was installed over the hole, and a deployment winch carrying the 300 m tether was attached to one of the tripod legs. A bottom weight of 80 kg was attached to the tether, which was then lowered into the water over the block. With ~30 m of tether in the water, the profiler was brought from the ship to the site, and installed on the tether with a plate covering the hole (Fig. 2.32). Profiler inductive modem communication was tested using the provided grounding rod inserted into the hole. The profiler was then pushed into water and submerged using a bamboo flag. The rest of the tether was then lowered into the water using the winch and brake, until only ~7 m were left. The tether was then removed from the winch, the surface unit was placed inside the floatation, and the top side of the tether was attached to its bottom connector. The remaining tether was lowered into the water using a yale grip attached to a chainfall, while the second chainfall was used to lift and place the buoy over the hole (Fig. 2.33). Finally, a grounding rod was installed in a 2 inch hole in the ice to close the inductive modem loop. The profiler communication was then tested a second time for final checkout, by connecting the surface unit communication cable to a PC and using the terminal program PuTTy.

During the final checkout test of the buoy, we encountered a problem that required an on-site video conference with the responsible engineer J. O'Brien. The surface buoy did not properly finish the checkout script, and it turned out that it did not recognize the manual wake step as part of the standard test procedure. The likely reason is that it was already awake at that point for its regular daily iridium call, and a code sequence to catch that issue was not present on this particular iteration of the buoy. The problem was solved by rebooting the surface unit by issuing a shutdown command "*~/current# shutdown -h now*", after which it checked out as expected. Fig. 2.34 shows the final deployment setup.

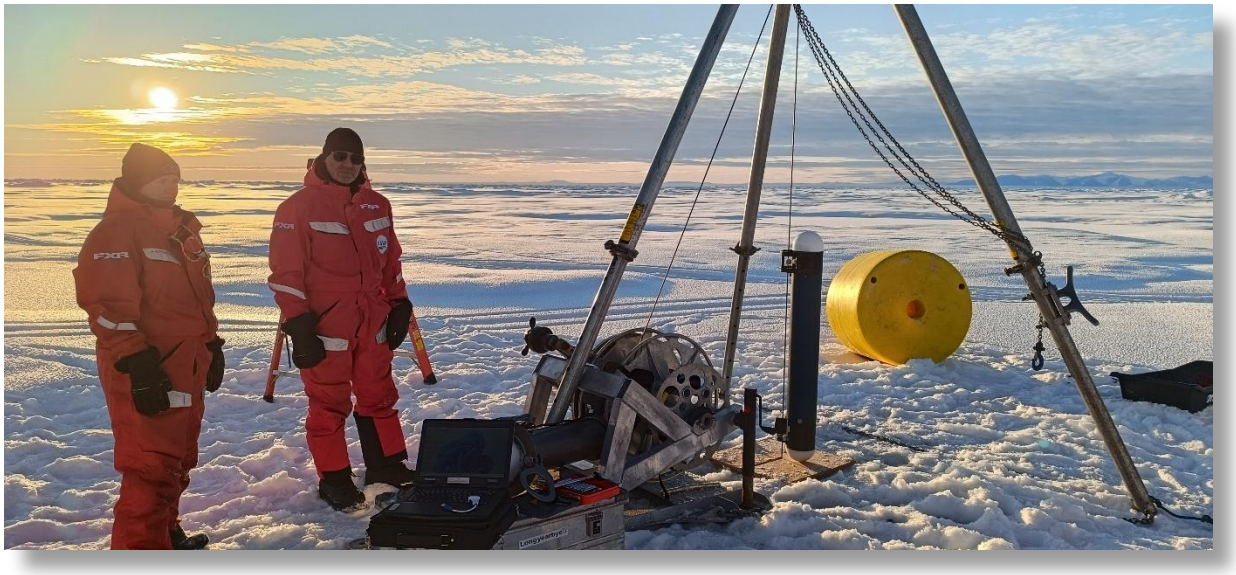

Fig. 2.32: Deployment of ice-tethered profiling buoy TOP016. The photo shows the profiler sitting on top of the hole during the inductive modem communication test. Photo by Mario Hoppmann.

Fig. 2.33: Lifting the surface unit and the floatation package on top of the hole. Photo by Mario Hoppmann.

Fig. 2.34: Photo of ice-tethered profiling buoy TOP016 (2025W17, left) and seasonal ice mass balance buoy 2025F (2025I18, right) during ice station 3 on 25 September 2025. Photo by Mario Hoppmann.

Due to the proximity of the deployment location to the shelf break, where water depths become much shallower (< 300 m, which is also the length of the tether), there is a risk that the buoy would drift over the shelf and that the tether would drag over the seafloor. This happened for example around 06 October 2025. In order to avoid damage to or loss of the profiler, it was remotely reconfigured to only profile to 175 m. The buoy is constantly monitored and reconfigured depending on the water depths, to keep it operational as long as possible. The drift trajectory as of 18 October 2025 is shown in Figure 2.35. Preliminary data plots are provided in Figure 2.36 (contour plot of temperatures), in Figure 2.37 (contour plot of salinities), and in Figure 2.38 (profile history) until 18 October 2025.

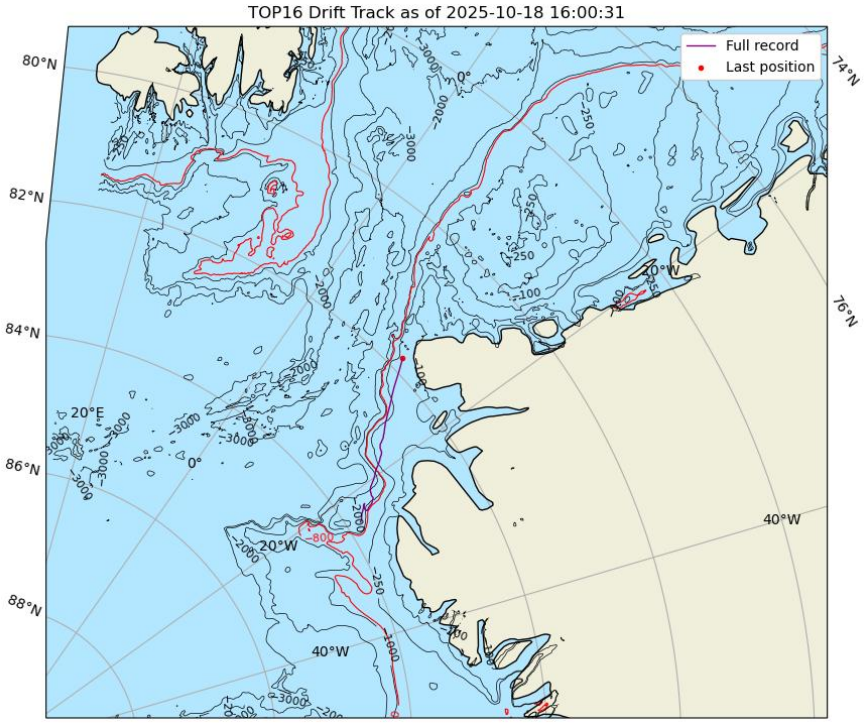

Fig. 2.35: Map of TOP016 drift trajectory. Plot by WHOI automated software

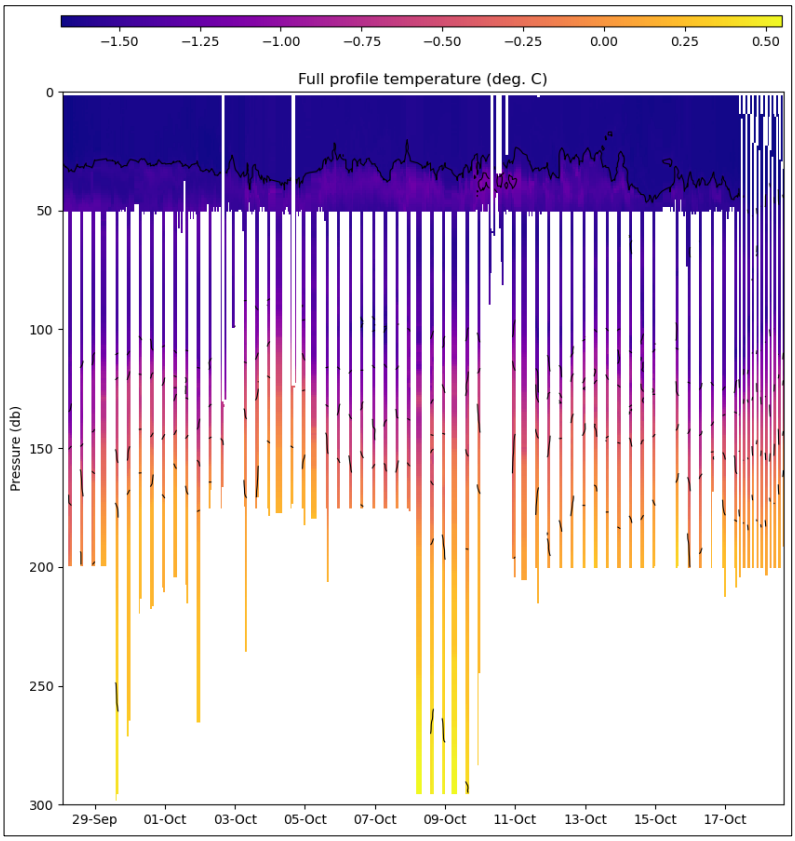

Fig. 2.36: Contour plot of seawater temperature recorded by profiling buoy TOP016. Plot by WHOI automated software

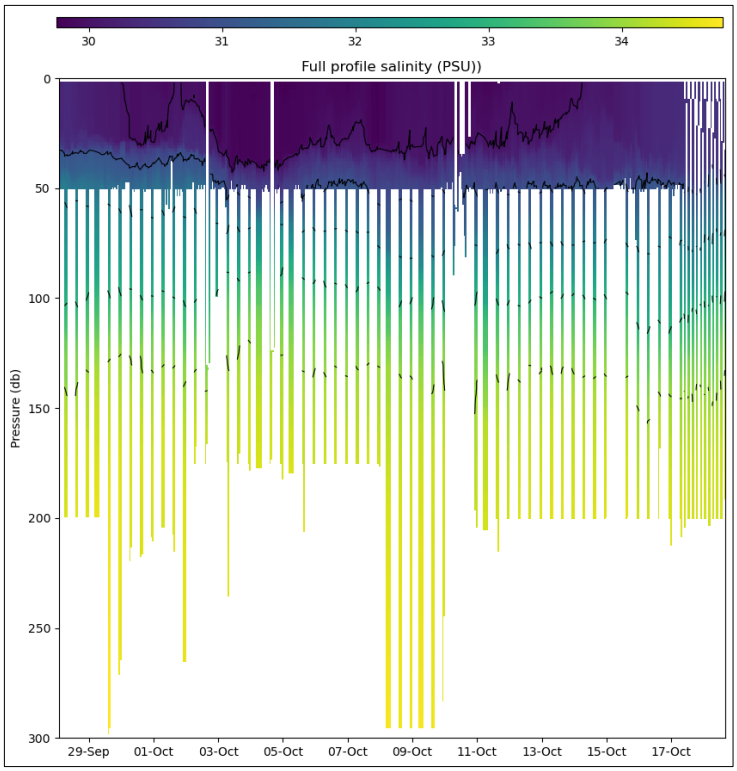

Fig. 2.37: Contour plot of seawater salinity recorded by profiling buoy TOP016. Plot by WHOI automated software

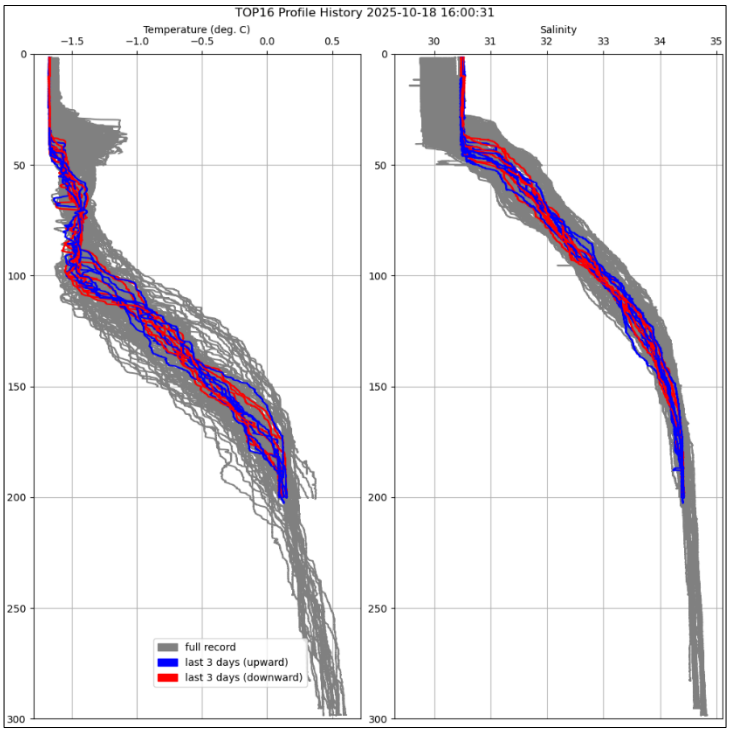

Fig. 2.38: All individual profiles recorded by profiling buoy TOP016. Plot by WHOI

The data can be retrieved with open access from the WHOI ITP website under https://scienceweb.whoi.edu/itp/data/topsys16.

Seasonal Ice Mass balance Buoy (SIMB3) ID 2025F (IMEI 301434060408490, shortname 2025I18) was deployed at the same site on 25 September 2025 at 15:22 UTC, ~10 m from TOP016. Deployment GPS coordinates were 83.8916°N, 24.2675°W. Ice thickness was 1.1 m, freeboard was 0.1 m, and snow depth was 0.08 m. The buoy data is available at https://www.cryosphereinnovation.com/deployment/301434060402490. A deployment photo is shown in Figure 2.34.

CTD buoy at Independence Fjord outflow

SIT-type ice-tethered CTD buoy AWI-SVP5S-0006 (Pacific Gyre, USA), shortname 2025O34, IMEI 300234068514740, was deployed via helicopter on landfast sea ice in the Independence Fjord outflow area on 30 September 2025 at 15:25 UTC. The deployment position was 82.0508°N, 15.1093°W. Water depth was 114 m, as measured by a SIMRAD mobile Echosounder. Ice thickness was 1.30 m, freeboard was 0.12 m, snow depth was 0.04 m. The buoy had a 100 m long tether, a bottom weight of ~ 10kg, and was equipped with 5 SeaBird SBE37IMP CTDs at 10 m (SN 21112), 20 m (SN 21103), 50 m (SN 21113), 75 m (SN 21116), and 100 m (SN 22542). Additionally, a Nortek Aquadopp current meter (SN 401084) was installed at 40 m. The provided fin was not installed. A schematic diagram of the buoy and installed sensors is provided in Figure 2.39.

During deployment, the tether was laid out on the ice, the instruments were installed at pre-determined depths, and then the tether was lowered with the anchor first into a 0.25 m diameter hole in the ice (Fig. 2.40). A warm salt water solution was inserted into the ducts of the pumped CTDs to avoid freezing of the conductivity cells upon entering the relatively fresh surface water. The buoy was placed on a white ablation shield, and then activated by removing a magnet. The data were checked on site via a mobile Starlink system, and were considered ok. The buoy is configured to poll all sensors at an interval of 10 minutes, and send the data as sbd messages to a land-based station via the iridium satellite network.

Preliminary data plots are shown in Figure 2.41 and Figure 2.42. On 18 October 2025, the buoy unexpectedly started to move, changing its location ~ 0.8 nm to the southwest, where it stopped moving again on 20 October. Apparently, the former fast ice broke off, but the ice pressure so far keeps it from moving larger distances. The resulting change in hydrographic properties and currents is also visible in the plots.

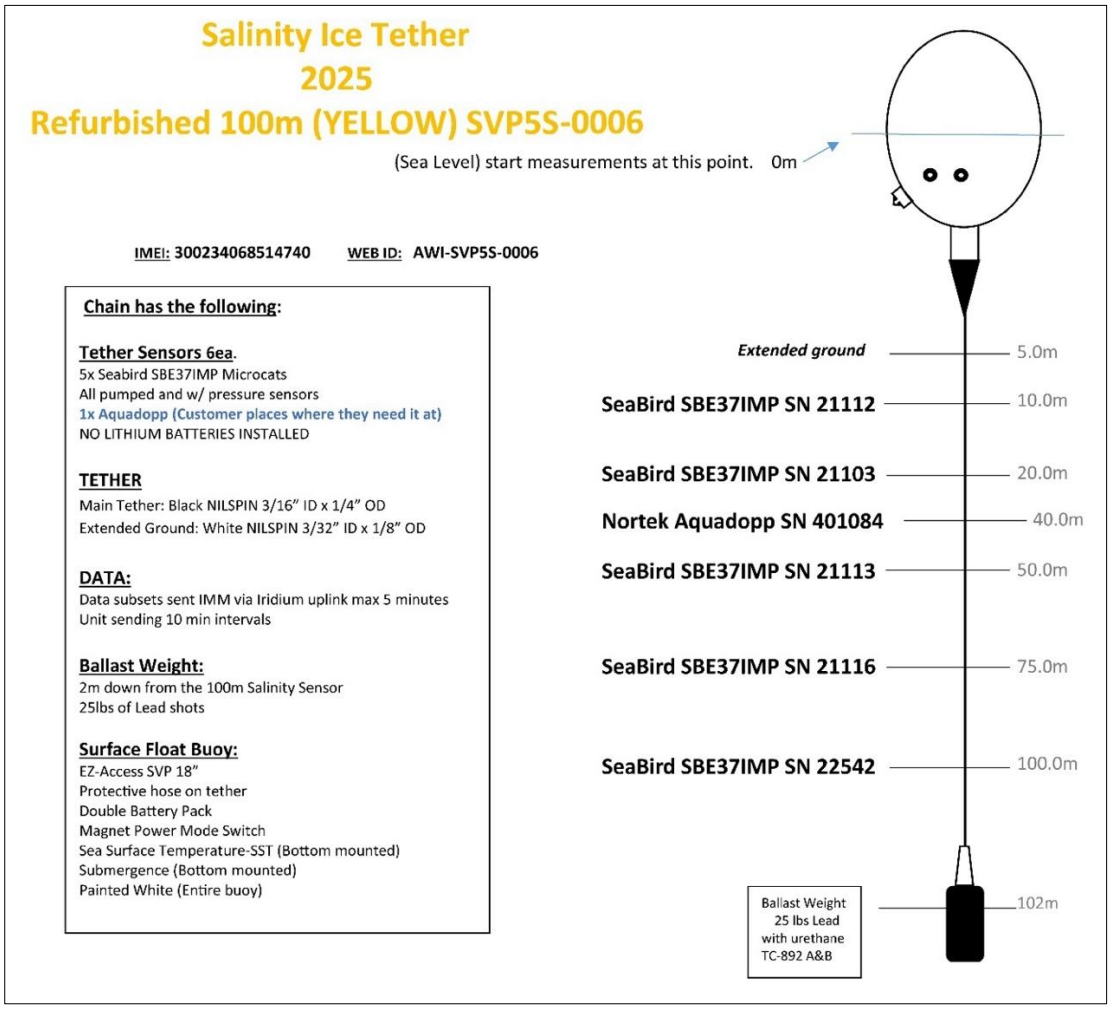

Fig. 2.39: Schematic diagram of CTD buoy AWI-SVP5S-0006 (shortname 2025O34). Modified after Pacific Gyre by Mario Hoppmann

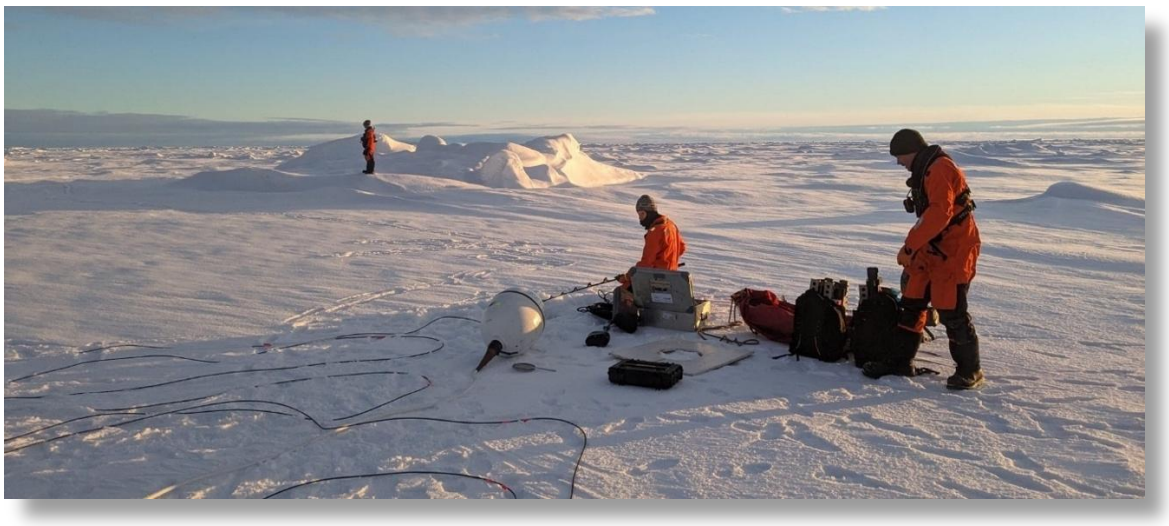

Fig. 2.40: Photo of CTD buoy AWI-SVP5S-0006 (shortname 2025O34) during preparation, while a fishing-rod CTD is conducted in the ice hole prior to deployment. Photo by Manuel Franco Pire

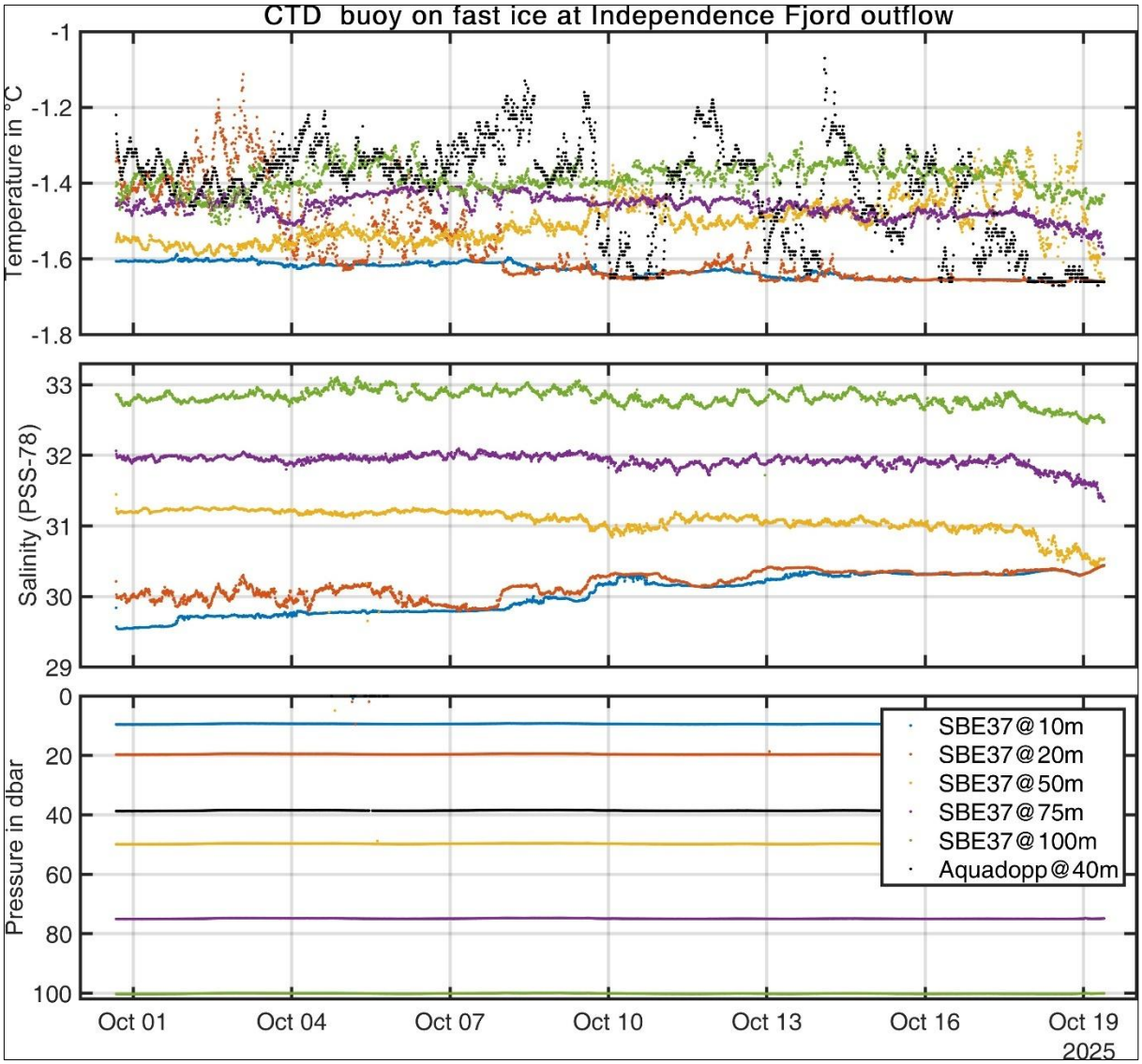

Fig. 2.41: Seawater temperature (top), salinity (middle) and instrument pressure (bottom) of CTD buoy AWI-SVP5S-0006 deployed on the fast ice at the Independence Fjord outflow. Note that the changing properties starting around 17/18 October are likely due to the buoy moving 0.8 nm to the southwest of its initial deployment location. Plot by Mario Hoppmann

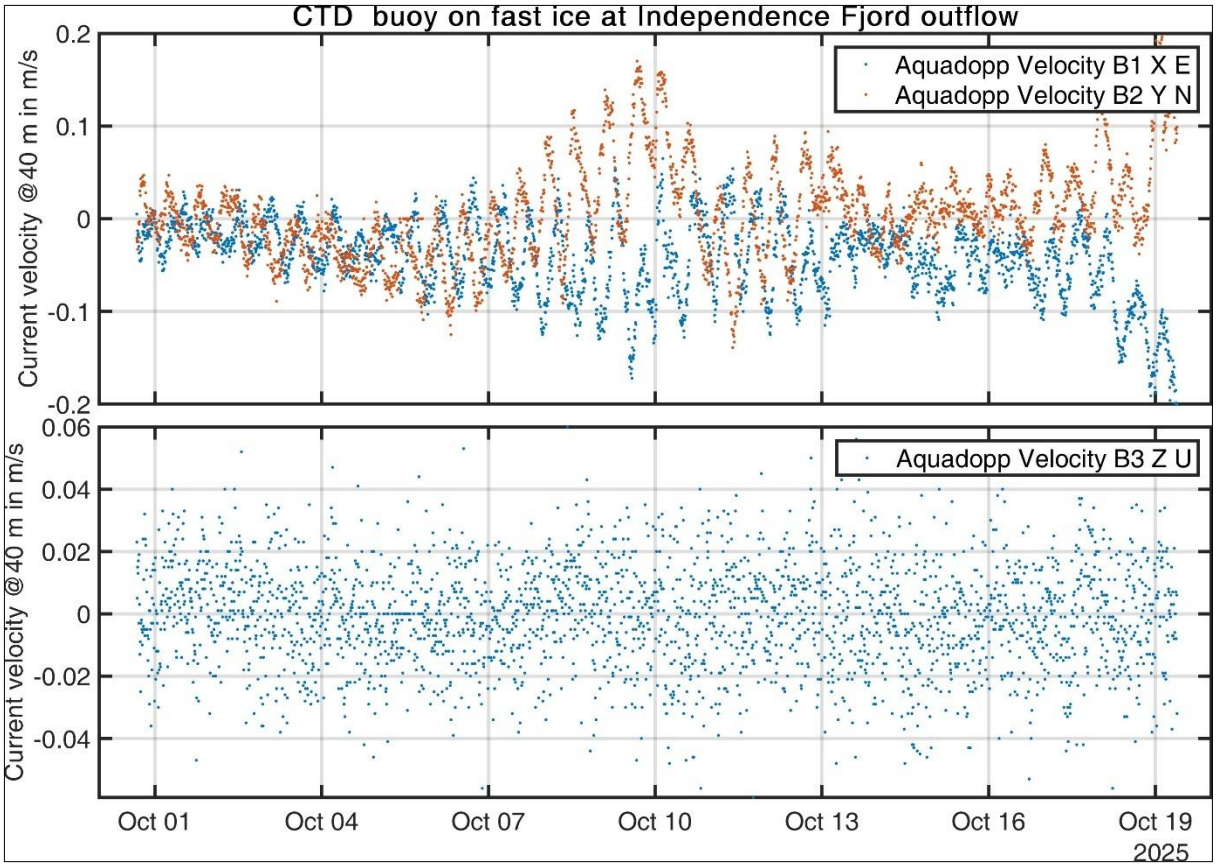

Fig. 2.42: Ocean current velocity at 40 m measured by CTD buoy AWI-SVP5S-0006 deployed on the fast ice at the Independence Fjord outflow. Note that the changing properties starting around 17/18 October are likely due to the buoy moving 0.8 nm to the southwest of its initial deployment location. Plot by Mario Hoppmann

CTD buoy in front of 79°N glacier

SIT-type ice-tethered CTD buoy AWI-SVP7S-0001 (Pacific Gyre, USA), shortname 2025O35, IMEI 300534067621310, was deployed via helicopter on landfast sea ice in front of the 79NG calving front on 11 October 2025 at 14:00 UTC. The deployment position was 79,5697°N, 19,4627°W. Water depth was 475 m, as measured by a SIMRAD mobile Echosounder. Ice thickness was 1.30 m, freeboard was 0.03 m, and snow depth was 0.25 m. The buoy had a 200 m long modular tether, a bottom weight of ~ 8kg, and was equipped with 3 SeaBird SBE37IMP CTDs at 80 m (SN 27621), 120 m (SN 27623), and 190 m (SN 27622), as well as 3 SBE39IM at 40 m (SN 11724), 100 m (SN 11725), and 145 m (SN 11726, including pressure sensor). Additionally, a Nortek Aquadopp current meter (SN 401097) was installed at 135 m. The provided fin was not installed. Finally, 2 deep water buoyancy floats were clamped on the cable at 39 and 99 m. A schematic diagram of the buoy and installed sensors is provided in Figure 2.43. See above for a description of the deployment procedure. Figure 2.44 shows a deployment photo. Preliminary data plots are shown in Figure 2.45 and Figure 2.46.

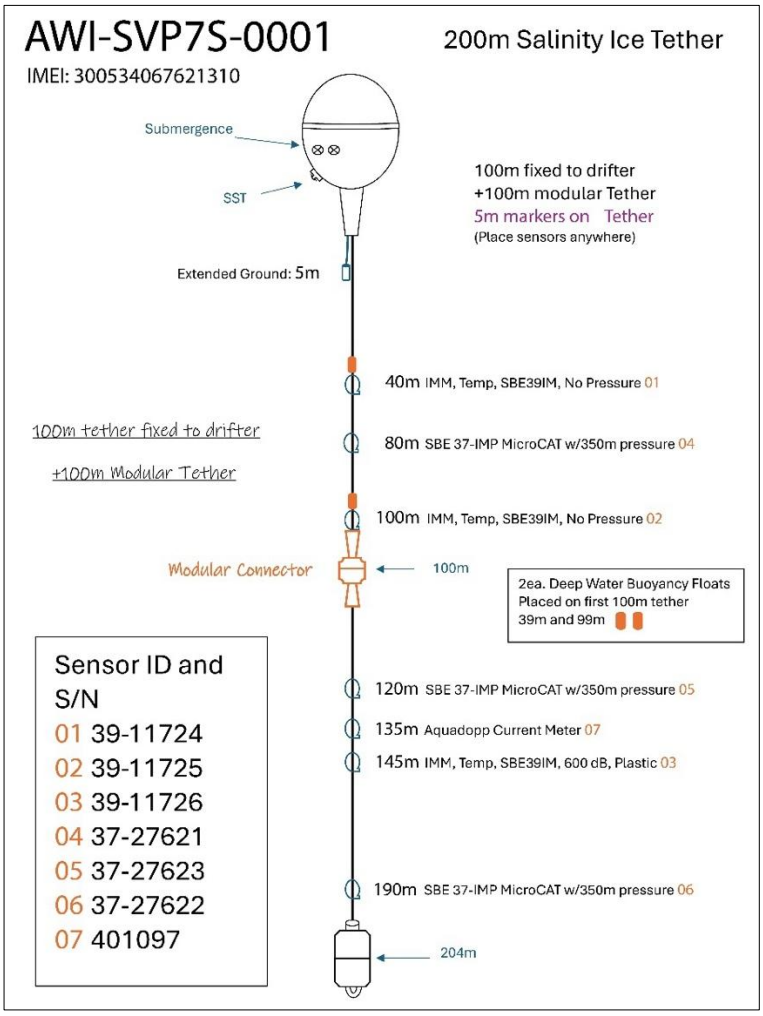

Fig. 2.43: Schematic diagram of SIT-type CTD buoy AWI-SVP7S-0001 (shortname 2025O35). Modified after Pacific Gyre by Mario Hoppmann

Fig. 2.44: Deployment photo of SIT-type CTD buoy AWI-SVP7S-0001 (2025O35) on landfast sea ice close to the 79NG calving front (visible in the background). Photo by Mario Hoppmann

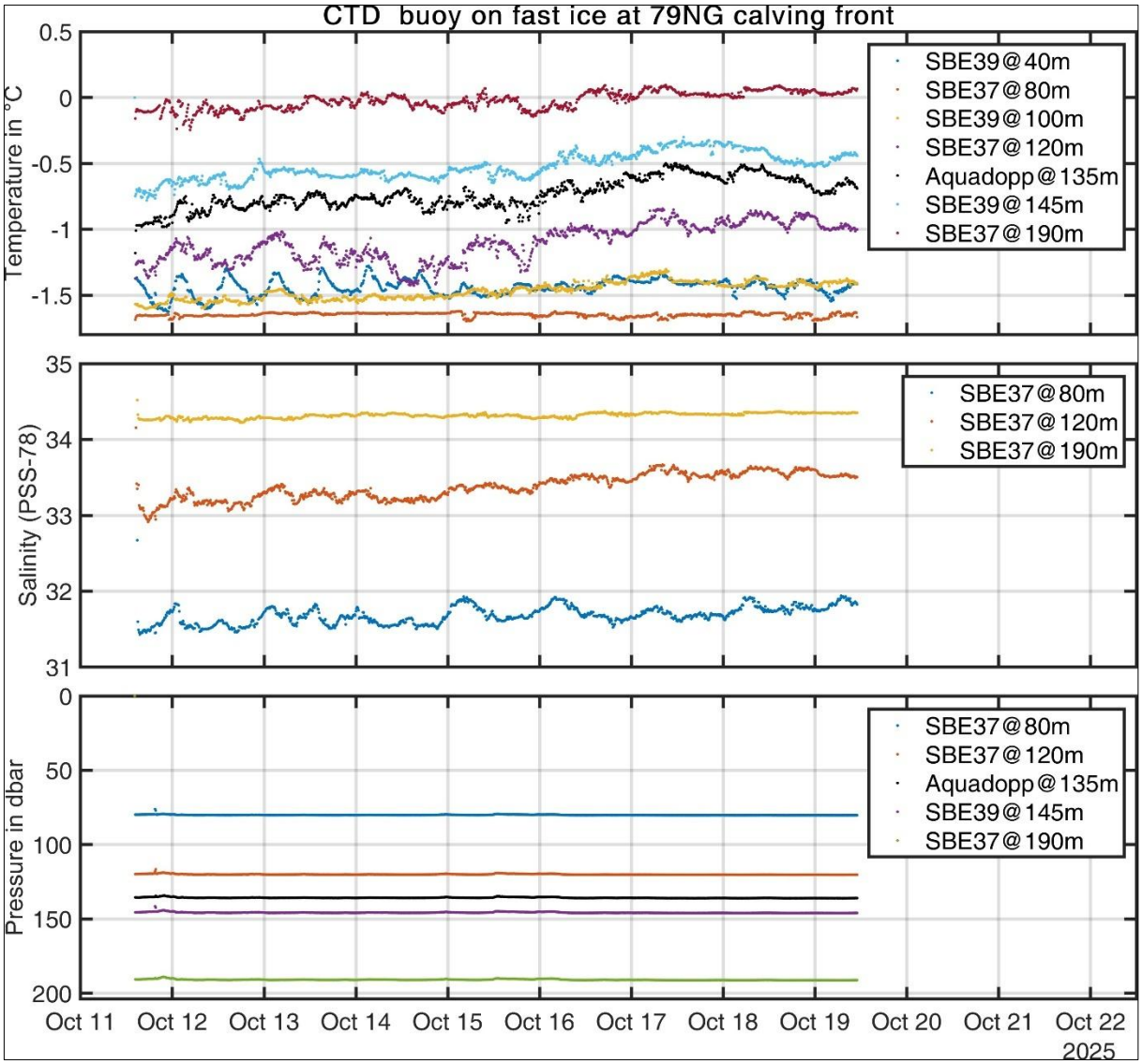

Fig. 2.45: Seawater temperature (top), salinity (middle) and instrument pressure (bottom) of CTD buoy AWI-SVP7S-0001 deployed on the fast ice in front of the 79°N glacier. Plot by Mario Hoppmann

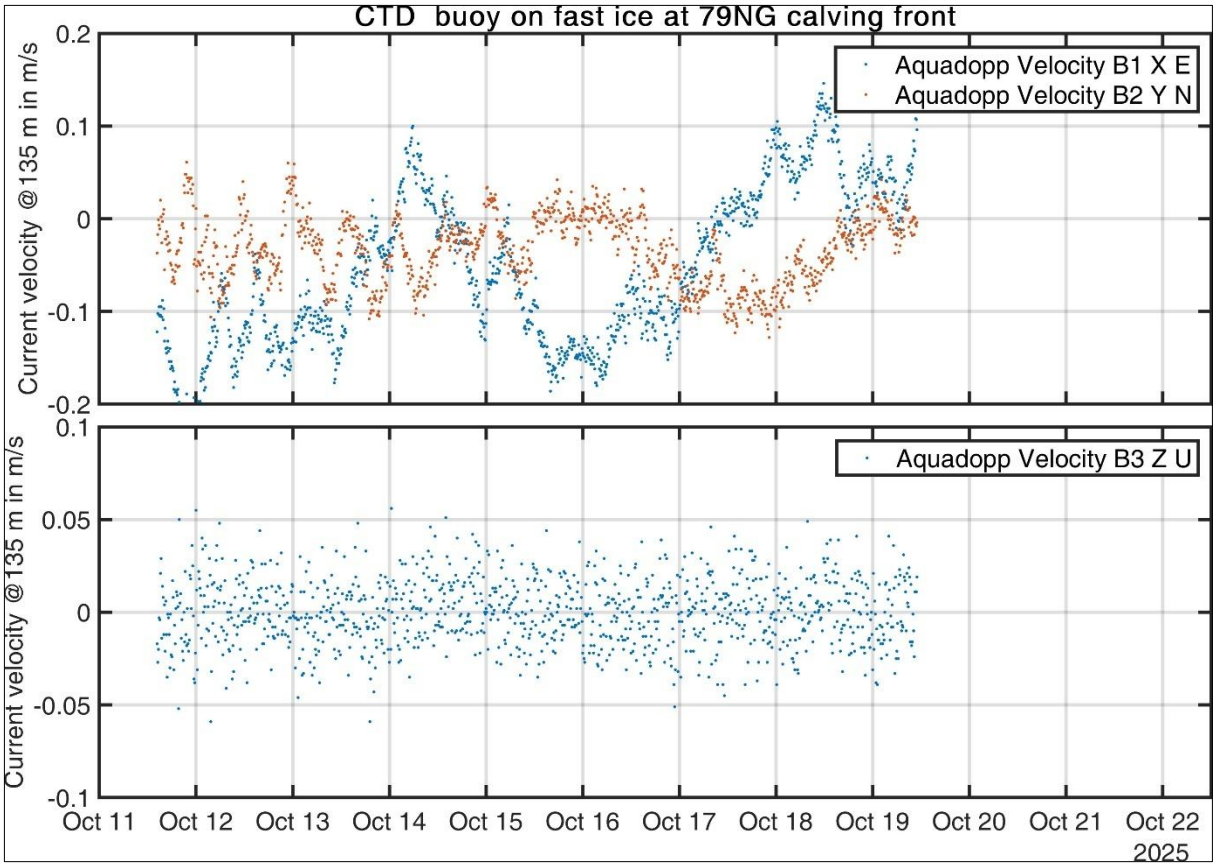

Fig. 2.46: Ocean current velocity at 135 m measured by CTD buoy AWI-SVP7S-0001 deployed on the fast ice in front of the 79°N glacier. Plot by Mario Hoppmann

SIMBA AWI 11-01 (2025T134, IMEI 300534063054440) was co-deployed at the same site, ~ 10 m next to 20205O35, on 11 October 2025 at 14:45UTC. Unfortunately, the buoy was only able to measure one valid temperature profile, before the chain failed and its data became invalid. As apparent from the buoys' tilt data, it was likely flipped over by a polar bear, and the chain was damaged or ripped off in the process. The data contract was deactivated a few days after the failure. Ice thickness in the deployment hole was 1.0 m, freeboard was 0 m, and snow depth was 0.43 m. Thermistor 40 was at the ice surface.

Drifting buoys with barometric pressure

We deployed 2 SVP-Bs (MetOcean, Halifax, Canada) in the northeastern Greenland Sea to obtain a better coverage of in-situ surface temperature and barometric pressure. The buoys were provided by Meteo France in the framework of a collaboration between AWI and SHOM/EUMETNET. The deployment metadata is as follows:

MetOcean SVP-B, type SVP-I-BXGS-AP-16-003, IMEI 300534067419730, Shortname: 2025P347, WMO ID 6301636 was deployed via Helicopter on 21 September 2025 14:48 UTC at 85.6399°N, 16.6613°W. This location was the northernmost location this expedition would reach. Ice thickness was 1.5 m, freeboard 0.01 m, and snow depth 0.04 m. A deployment photo is shown in Figure 2.47.

Fig. 2.47: Photo of SVP-B 2025P347 (IMEI 300534067419730, WMO ID 6301636) deployed on 21 September 2025. Photo by Daniel Scholz

MetOcean SVP-B, type SVP-I-BXGS-AP-16-003, IMEI 300534067122450, Shortname: 2025P345, WMO ID 6301634 was deployed via Helicopter on 24 September 2025 14:46 UTC at 84.3023°N, 33.02402°W by Mario Hoppmann. Ice thickness was >2 m. A deployment photo is shown in Figure 2.48.

Fig. 2.48: Photo of SVP-B 2025P345 (IMEI 300534067122450, WMO ID 6301634) deployed on 24 September 2025. Photo by Mario Hoppmann

OpenMetBuoys from PS149

2 OpenMetBuoys (SN 210294 = 2025X27, SN 210300 = 2025X17) initially deployed during *Polarstern* expedition PS149 were still operational during PS150. The drift trajectories are displayed in Figure 2.49. They recorded pronounced waves (Fig. 2.50, Fig. 2.51) that led to the rapid decay of the ice floes they were initially deployed on. This led to the loss of several instruments that were planned to be recovered during PS150 from PS149 ice floe R3.

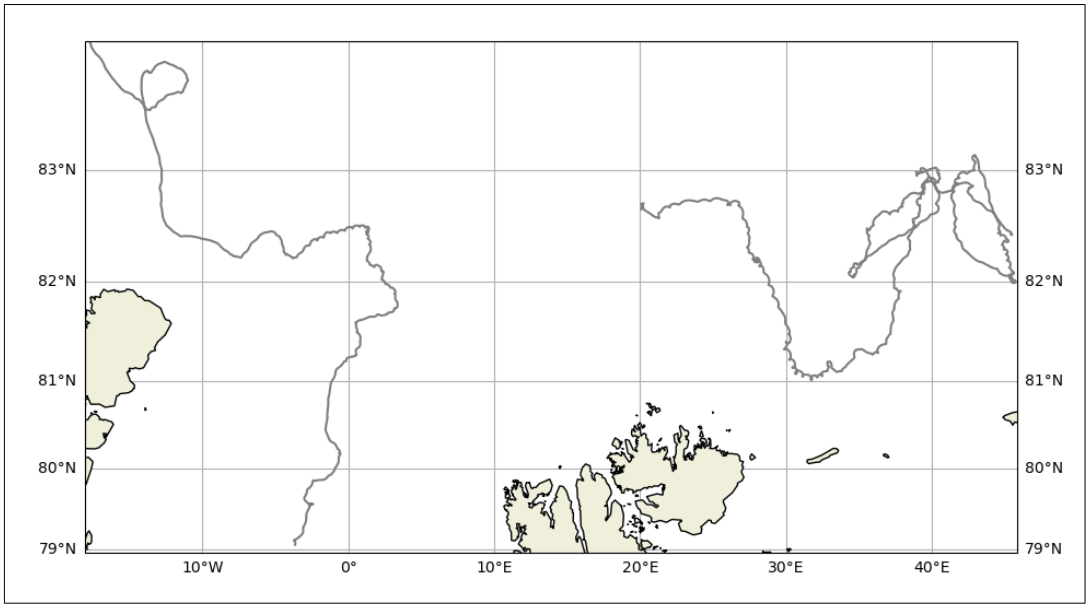

Fig. 2.49: Map showing the drift trajectories of OMBs 2025X27 (right) and 2025X17 (left). Plot by Jean Rabault

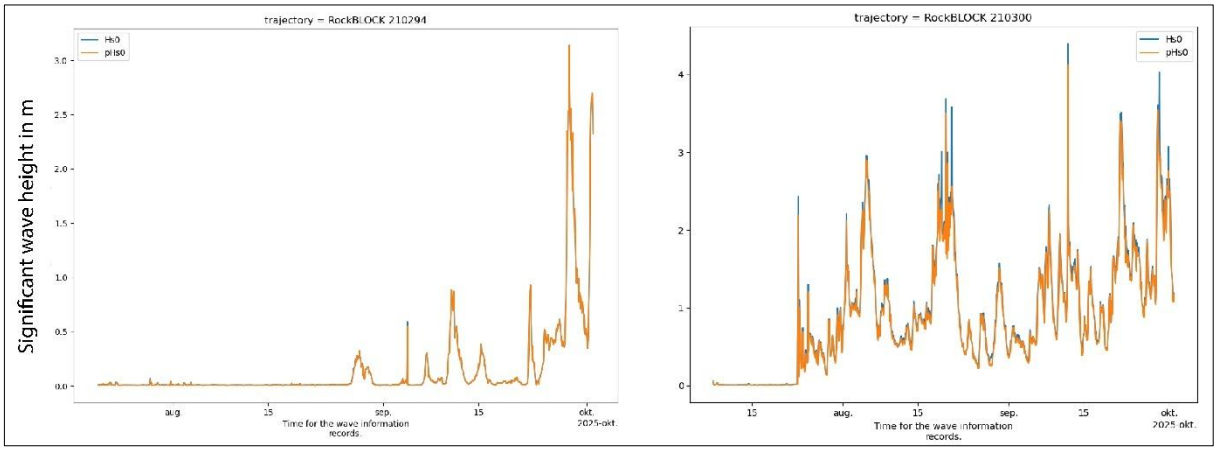

Fig. 2.50: Significant wave height measured by OMBs 2025X27 (left) and 2025X17 (right). Plot by Jean Rabault

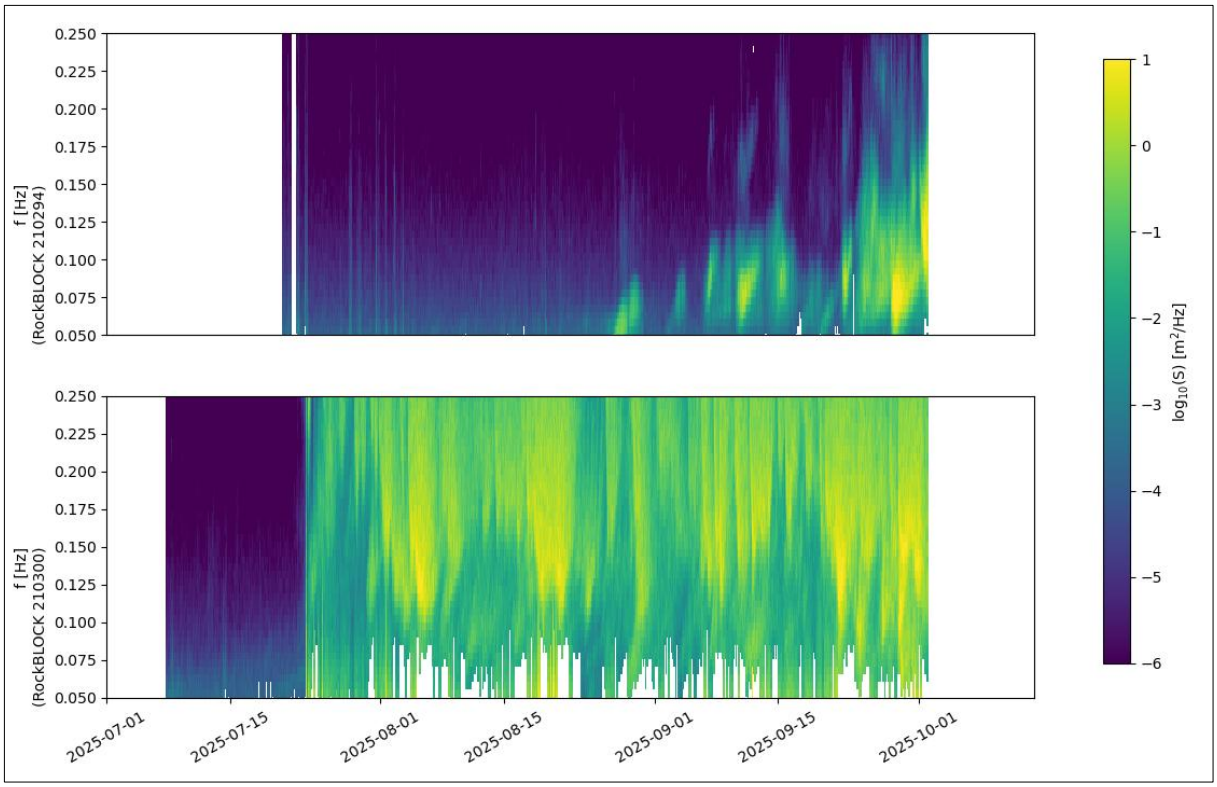

Fig. 2.51: Wave spectra measured by OMBs 2025X27 (top) and 2025X17 (bottom). Plot by Jean Rabault

ADCP buoy recovery

A Nortek S250 ADCP was deployed through a hole in the ice during the fourth visit of ice floe R3 on 27 August 2025 during *Polarstern* expedition PS149. It was recovered during *Polarstern* expedition PS150 in the marginal ice zone on 6 October 2025. The S250 ADCP was configured to take average current measurements in the upper 200 m with a bin size of 2 m, sampling for 120 seconds with an average interval of 15 minutes. Figure 2.52 shows the drift trajectory of the instrument in Aug – Oct 2025. Figure 2.53 shows preliminary plots of the meridional (u) and zonal (v) components of the measured ocean current velocities (corrected for ice drift).

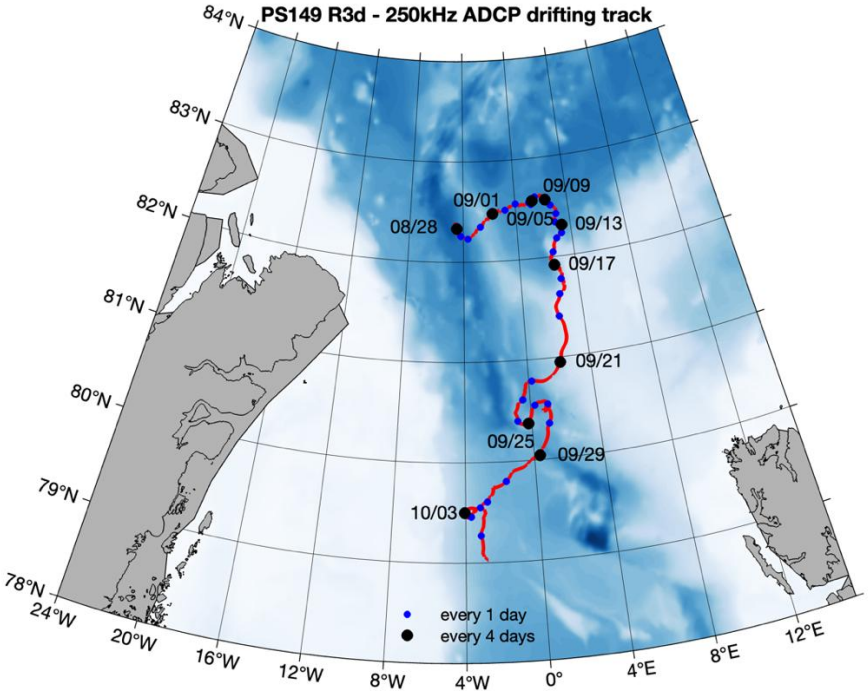

Fig. 2.52: Map showing the drift trajectory of the S250 ADCP. Plot by Ke-Hsien Fu

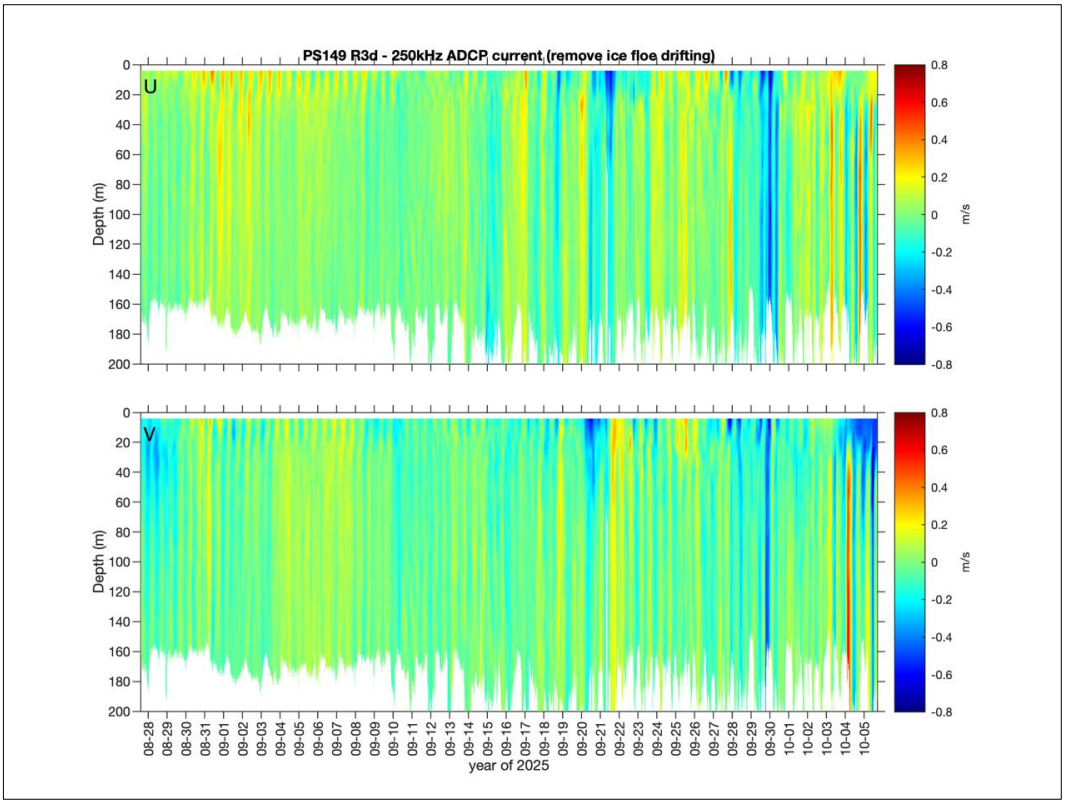

Fig. 2.53: Preliminary plot of the meridional (u) and zonal (v) components of the ocean current velocities measured by the instrument. Plot by Ke-Hsien Fu

Under-ice continuous observations

During all ice stations, an **RDI Workhorse Sentinel 300 kHz ADCP** (Teledyne Marine, USA) was suspended through a separate hole in the ice, typically located at 10-20 m distance from the microstructure profiling site, to obtain ocean current velocity profiles in the upper 100-200 m of the water column. The instrument was configured to sample continuously at 1s intervals, with a 2m vertical bin size. The instrument was suspended right below the ice base, and beam 3 was oriented parallel to the ship, pointing to the front. The instrument was deployed as early as possible during each station, and retrieved as late as possible. As the instrument was deployed close to the MSS site, the profiling of the MSS created some artifacts in the data during the casts. Figure 2.54 shows an exemplary plot of the north- and eastward current velocities as 10-minute averages.

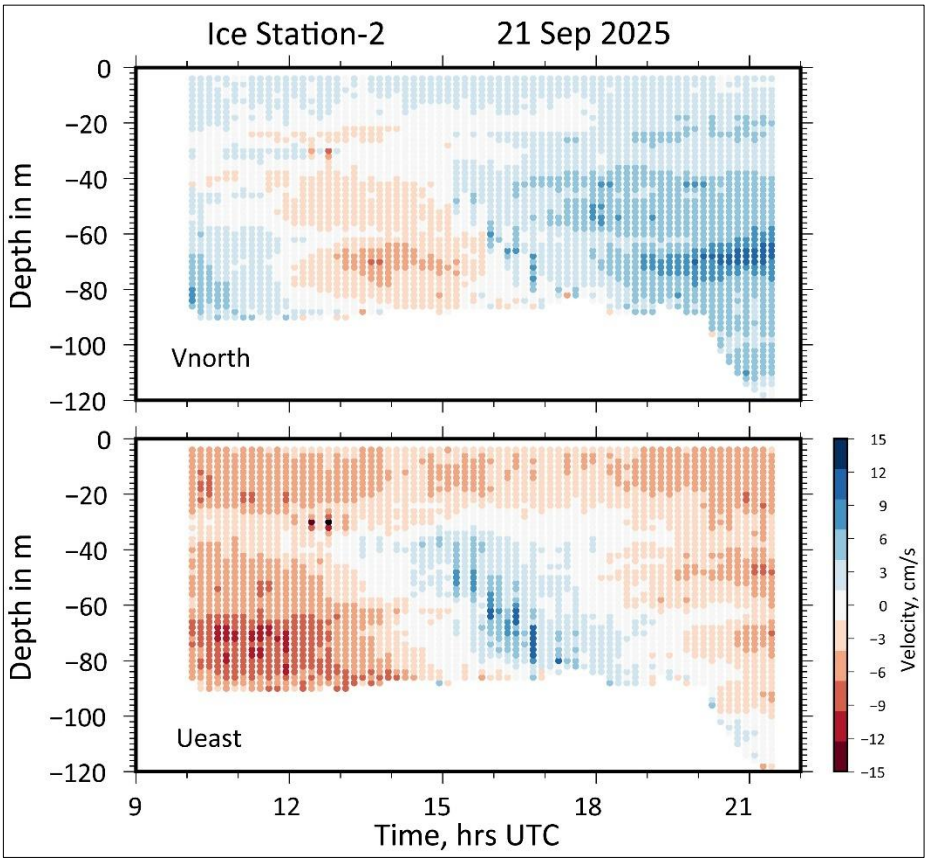

Fig. 2.54: Meridional (u) and zonal (v) components of the ocean current velocities measured by the WH300 ADCP during ice station 2. Plot by Andreas Münchow, modified by Mario Hoppmann

During ice stations 2-4, a **Nortek Signature1000 ADCP** (Nortek, Norway) was also suspended through a separate hole in the ice, typically located at 10-20 m distance from the microstructure profiling and 300 kHz ADCP sites. The instrument's serial number was 107676, and it was equipped with the high-resolution (HR) firmware to measure turbulence. The instrument was configured to record 1-minute average current profiles in the upper 20 m every 2 minutes with a bin size of 1 m, and to continuously record high-resolution "Burst HR1-5" measurements in the upper 2.5 m beneath the ice, with a bin size of 0.05 m. The instrument was suspended right below the ice base, and beam 3 was oriented parallel to the ship, pointing to the front. The instrument was deployed as early as possible during each station, and retrieved as late as possible. The configuration and deployment file for the ice stations were the following:

```
##############################################
## Nortek Configuration file
##############################################
## Filename : S107676A005_PS150.cfg
## Date     : 2025-09-20 22:13:05
## ID       : Signature1000
## SN       : 107676
## Frequency: 1000 kHz
##############################################
$PNOR,SETDEFAULT,CONFIG*00
$PNOR,SETPLAN,MIAVG=120,AVG=1,DIAVG=0,VD=0,MV=10,SA=35.0,BURST=1,MIBURST=60,DIBURST
=0,SV=0.00,FN="S107676A005_PS150.ad2cp",SO=0,FREQ=1000,NSTT=0*3C
$PNOR,SETAVG,NC=19,CS=1.00,BD=0.20,CY="ENU",PL=0.0,AI=60,VP=0.000,VR=2.50,DF=3,NPIN
G=48,NB=4,CH=0,MUX=0,BW="NARROW",ALTI=0,BT=0,ICE=0,ALTISTART=0.10,ALTIEND=30.00,RAW
ALTI=1*53
$PNOR,SETBURST,NC=43,NB=5,CS=0.500,BD=0.100,CY="BEAM",PL=0.0,SR=4,NS=240,VR=2.50,VP
=0.000,DF=3,NPING=1,CH=0,ALTI=0,VR5=2.50,BT=0,DISV=0,ECHO=0,RAWALTI=1,ALTISTART=0.1
0,ALTIEND=30.00,HR=1,HR5=1*38
$PNOR,SETBURSTHR,PROC=1,LAG=2.85,LAG5=2.85,SCORR=6,NC=54,CS=0.0500,BD=0.100,PL=0.0*
4A
$PNOR,SAVE,CONFIG*08
##-------------------------------------------------------------------------------
---------
##           | Temperature | Compass | Average  | Burst    | Average   | Burst
| Burst |
## Time [us] | Pressure    |         | Velocity | Velocity | Altimeter | Altimeter
| Echo  |
##-------------------------------------------------------------------------------
---------
##        0  |      x      |    x    |          |    x     |           |
|       |
##-------------------------------------------------------------------------------
---------
##    62500  |      x      |         |     x    |          |           |
|       |
##-------------------------------------------------------------------------------
---------
##   125000  |      x      |         |          |    x     |           |
|       |
##-------------------------------------------------------------------------------
---------
##   250000  |      x      |         |          |    x     |           |
|       |
##-------------------------------------------------------------------------------
---------
##   375000  |      x      |         |          |    x     |           |
|       |
##-------------------------------------------------------------------------------
---------
##   500000  |      x      |         |          |    x     |           |
|       |
##-------------------------------------------------------------------------------
---------
##   625000  |      x      |         |          |    x     |           |
|       |
##-------------------------------------------------------------------------------
---------
##   750000  |      x      |         |          |    x     |           |
|       |
##-------------------------------------------------------------------------------
---------
##   875000  |      x      |         |          |    x     |           |
|       |
##-------------------------------------------------------------------------------
---------
##  1000000  |             |         |          |          |           |
|       |
```

```
##-------------------------------------------------------------------------------
---------

#$DeployFileVersion,4,c2851d46a2d653ee3a41cadecd76f402
#$SWSource,"Deployment-v4.7.16.1"
#$InstrumentId,{"InstrumentType":"Signature1000","HeadFrequency":1000,"IsDeepWater"
:false,"IsLADCP":false,"FWVersion":"2216.14"$C
#$}
#$DeploymentName,"PS150"
#$Comment,"Suspended from drifting sea ice, just below the ice bottom"
#$ApplicationConfig,[{"Enabled":true,"Application":"Avg, Burst5Beams,
ExtBurstHR","Mounting":"Fixedframe","Orientation":"DownLo$C
#$oking","Geography":"ArcticRegion","SoundVelocity":"Measured","SoundVelocityValue"
:0.0,"Salinity":35.0,"StrongWaves":false,"Pr$C
#$ofileRange":20.0,"InstrumentDepth":20.0,"TidalRange":1.0,"BurstHR":true,"BurstHR5
":true,"WaveProcessing":false},{"Enabled":fa$C
#$lse,"Application":"None","Mounting":"Fixedframe","Orientation":"DownLooking","Geo
graphy":"ArcticRegion","SoundVelocity":"Meas$C
#$ured","SoundVelocityValue":0.0,"Salinity":35.0,"StrongWaves":false,"ProfileRange"
:20.0,"InstrumentDepth":20.0,"TidalRange":1.$C
#$0,"BurstHR":false,"BurstHR5":false,"WaveProcessing":false}]
#$AlternatingRatio,[6,1]
#$DeploymentConfigExtensions,[{"AvgDesiredRange":18.0,"BurstDesiredRange":20.0,"Bur
stHrDesiredRange":2.5,"EchoSounderDesiredRan$C
#$ge":20.0,"AvgEndProfile":19.8,"BurstEndProfile":22.0,"BurstHrEndProfile":2.75,"Ec
hoSounderEndProfile":22.0,"AIStep":1,"RangeS$C
#$tep":0.1,"BurstMeasurementContinuous":true,"AvgMeasurementLoad":8.75,"MinAvgMeasu
rementLoad":0.416666657,"MaxAvgMeasurementLo$C
#$ad":100.0,"AvgAutoMeasurementLoad":true,"AvgMeasurementLoadTick":0.416666657,"Bur
stMeasurementLoad":100.0,"BurstAutoMeasureme$C
#$ntLoad":true,"BurstMeasurementLoadTick":100.0,"PulseDistanceAutoOption":3,"PulseD
istance":3,"DistanceToBottom":2.0,"DistanceT$C
#$oSurface":2.0,"DesiredVelocityRange":0.25,"ValidBurstIntervals":[],"MeasurementIn
tervalAlternate":0},{"AvgDesiredRange":20.0,$C
#$"BurstDesiredRange":20.0,"BurstHrDesiredRange":20.0,"EchoSounderDesiredRange":20.
0,"AvgEndProfile":22.0,"BurstEndProfile":22.$C
#$0,"BurstHrEndProfile":22.0,"EchoSounderEndProfile":22.0,"AIStep":1,"RangeStep":0.
1,"BurstMeasurementContinuous":false,"AvgMea$C
#$urementLoad":100.0,"MinAvgMeasurementLoad":0.0,"MaxAvgMeasurementLoad":100.0,"Av
gAutoMeasurementLoad":true,"AvgMeasurementLo$C
#$adTick":1.0,"BurstMeasurementLoad":100.0,"BurstAutoMeasurementLoad":true,"BurstMe
asurementLoadTick":1.0,"PulseDistanceAutoOpt$C
#$ion":3,"PulseDistance":3,"DistanceToBottom":2.0,"DistanceToSurface":2.0,"DesiredV
elocityRange":0.25,"ValidBurstIntervals":[],$C
#$"MeasurementIntervalAlternate":0}]
#$BatteryItem,null
#$BatteryCombo,{"InternalBattery":{"Name":"Alkaline 90
Wh","Volume":90.0,"Voltage":15.0},"ExternalBattery":{"Name":"None 0 Wh",$C
#$"Volume":0.0,"Voltage":0.0},"Volume":90.0,"Voltage":15.0}
#$RecorderItem,{"Name":"16 GB","Capacity":16000000000}
#$AhrsInstalled,false
#$DeploymentDays,1
SETDEFAULT,ALL
SETPLAN,MIAVG=120,AVG=1,DIAVG=0,VD=0,MV=10,SA=35,BURST=1,MIBURST=60,DIBURST=0,SV=0,
FN="S107676A005_PS150.ad2cp",SO=0,FREQ=1000,NSTT=0
SETAVG,NC=19,CS=1,BD=0.2,CY="ENU",PL=0,AI=60,VR=2.5,DF=3,NPING=21,NB=4,CH=0,MUX=0,B
W="NARROW",ALTI=0,BT=0,ICE=0,ALTISTART=0.1,ALTIEND=30,RAWALTI=1
SETBURST,NC=43,NB=5,CS=0.5,BD=0.1,CY="BEAM",PL=0,SR=4,NS=240,VR=2.5,DF=3,NPING=1,CH
=0,VR5=2.5,ALTI=0,BT=0,DISV=0,ECHO=0,RAWALTI=1,ALTISTART=0.1,ALTIEND=30,HR=1,HR5=1
SETBURSTHR,NC=54,CS=0.05,BD=0.1,PL=0,PROC=1,LAG=2.85,LAG5=2.85,SCORR=6
SETTMAVG,EN=0,CD=1,PD=1,AVG=60,TV=1,TA=1,TC=1,CY="ENU",FO=0,SO=1,DF=100,DISTILT=0,T
PG=0,MAPBINS=0
SAVE,ALL
```

Table 2.17 presents an overview of all ADCP measurements during the four ice stations.

Tab. 2.17: Overview of ADCP deployments duing ice stations

Event label	Date/Time start	Date/Time end	Comment
PS150_44-1-ADCP_WH300_9271-01	2025-09-13T12:08:00	2025-09-13T18:45:00	
PS150_78-1-nortek_s1000_adcp_7575-01	2025-09-21T09:49:00	2025-09-13T18:45:00	ice thickness 1.38 m; transducer 1.5 m from surface
PS150_78-1-ADCP_WH300_9271-01	2025-09-21T10:00:00	2025-09-21T21:35:00	ice thickness 1.24 m; transducer 1.5 m from surface
PS150_90-1-nortek_s1000_adcp_7575-01	2025-09-25T10:25:00	2025-09-25T16:45:00	ice thickness 1.16 m; transducer 1.7 m from surface
PS150_90-1-ADCP_WH300_9271-01	2025-09-25T10:15:00	2025-09-25T16:45:00	ice thickness 1.33 m; transducer 1.52 m from surface
PS150_127-1-nortek_s1000_adcp_7575-01	2025-10-10T13:30:00	2025-10-10T17:10:00	ice thickness 1.1 m; transducer 1.3 m from surface
PS150_127-1-ADCP_WH300_9271-01	2025-10-10T13:30:00	2025-10-10T17:10:00	ice thickness 1.1 m; transducer 1.4 m from surface

"Upriser" CTD transects during ice stations

The "Upriser" CTD is a modification of a regular hand-held profiling CTD, which allows to sample the small-scale boundary layer between the sea ice bottom and the underlying ocean. An RBRconcerto CTD (SN 235669, depth rating 200 dbar) was equipped with a set of small floats around the housing to achieve a moderate positive buoyancy (Fig. 2.55). It was attached to a neutrally buoyant line of ~ 30 m length, with a deployment weight attached to the line a few meters (2 to 6 m, typically) away from the instrument. After being lowered to a depth of 15 – 20 m using the weight on the line, the now buoyant instrument rises upwards upon manually pulling the weight up, until the instrument hits the sea ice underside. Under the influence of ocean currents under the ice / ice drift, the instrument is moved away from the deployment hole, which usually impacts any downcasts done with regular handheld CTDs. As the sensors of the RBRconcerto protrude from the instrument's side (which in this setup is the side facing upwards), data up to 0.02 m below the ice can be collected.

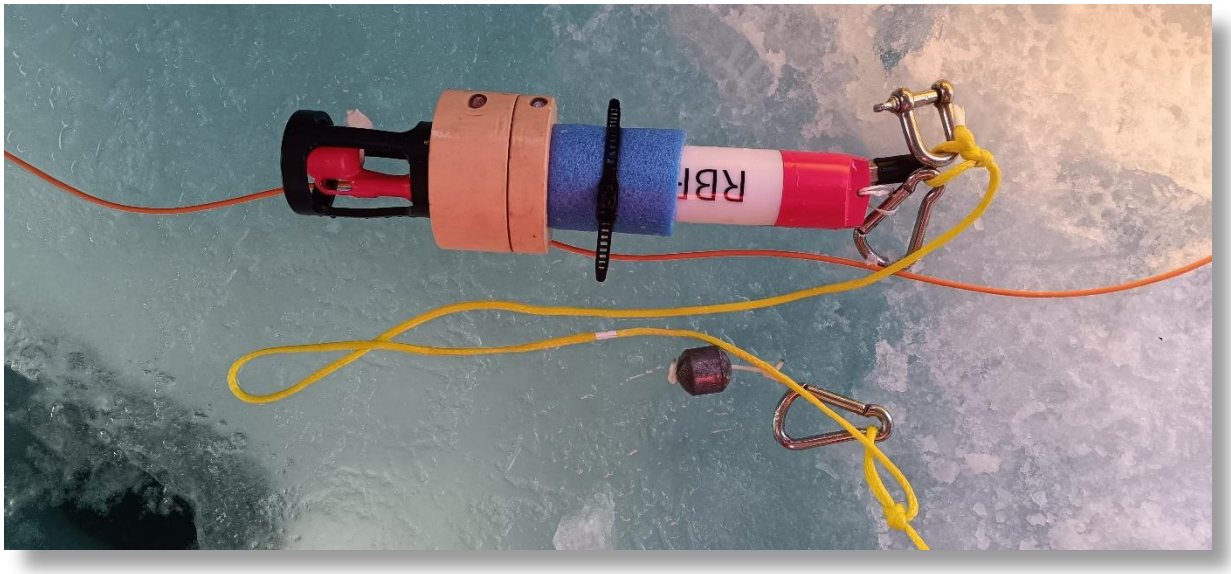

Fig. 2.55: Initial Upriser CTD setup, using different sorts of buoyancy floats, a small weight (shackle)at the bottom of the CTD for additional stabilization, and the deployment weight to lower it to the profile starting depth. Photo by Mario Hoppmann

During all 4 ice stations, Upriser CTD transects were performed along a line in the direction of the mean under-ice ocean current. A comprehensive list of all profiles along these transects can be found in Table 2.18. At each site, multiple casts were recorded to enable intercomparison and better estimation of data quality and variability.

The profiles were analysed on board with a focus on data quality. In a first step, the upcasts conducted at each site were removed from the data. The conductivity sensor exhibited suspicious behaviour once the CTD hit the under-ice boundary. In Figure 2.56 the different behaviour is documented. The plots show the last seconds before the CTD touches the ice bottom and stays at a constant depth level. At Station 1 Site 1 the Salinity drops by ~ 1.5 after hitting the ice underside, before reaching the initial level again. At Station 1 Site 5 the Salinity drops by ~ 1.5 after hitting the ice bottom, and stays constant at the fresher value. At Station 4 Site 1.2 the salinity drops, and temperature increases continuously before the CTD reaches a constant depth underneath the ice. The salinity drops could be explained by the interaction of the CTD with the sea ice. The conductivity is determined using an inductive measurement principle, which induces a current in a volume surrounding the sensor. If sea ice enters this volume, the conductivity drops drastically. In Figure 2.56 this effect is shown by various characteristics in the data:

- In a) the ice enters the measuring volume, but the CTD tilts after some seconds and the measurement returns to the old value.
- In b) the ice stays inside the measurement volume.
- In c) there is a strongly stratified ocean boundary underneath the ice.

To avoid problems associated with the instrument touching the ice all upcasts have been cut 0.5 seconds before the CTD hits the ice underside, determined from acceleration data of the CTD. In Figure 2.56 the data cut is indicated by a horizontal black line. Average rising rates of the CTD were around 0.3m/s, which means that 0.15 m of the under-ice profile is cut in this processing.

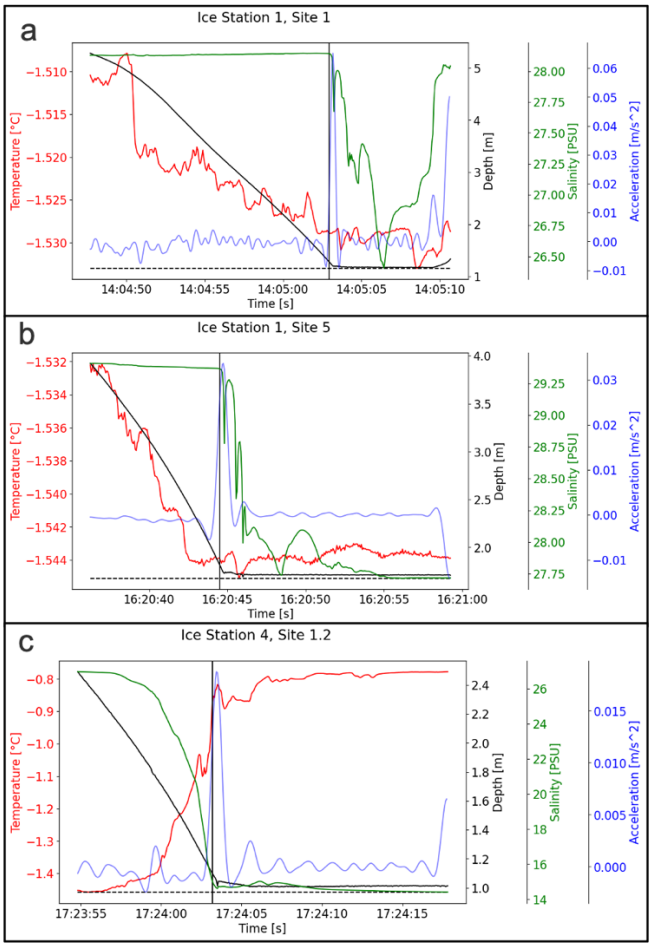

Fig. 2.56: Different behaviour of the CTD at the ice ocean boundary. In a) the salinity drops suddenly and then recovers while the CTD stays at constant depth underneath the ice. In b) the salinity drops suddenly when the CTD stops rising and stays on a fresh level. In c) the salinity drops continuously before the ice underside is reached. Plots by Clemens Rohling.

The upcasts have been filtered after the initial step using a Butterworth filter and a cutoff frequency that excludes variations on scales smaller than 0.2 m, by adapting the filter to the mean rising rate of the sensor. Afterwards, the data was interpolated on a 0.05 m depth grid and exported to .csv files for each profile sorted by ice station and site. (see Tab. 2.18). Some exemplary profiles grouped by ice station and site are displayed in Figure 2.57. Data quality problems are visible in Figure 2.57a) where the first profile shows a 0.4 PSU jump in salinity at 6 m depth. Many profiles show unrealistically fresh water and are not consistent at one sampling site (see Fig. 2.57b). A possible explanation of this behaviour is ice, which forms inside the conductivity coil. During the transect, the CTD was exposed to cold air temperatures (< -5°) for several hours. If the cold CTD comes in contact with the water, ice might form and influence the measurements. When the ice film then suddenly clears from inside the cell in the warmer water during the cast, this may result in a sudden offset in the middle of a cast (see black arrow in Fig. 2.57a).

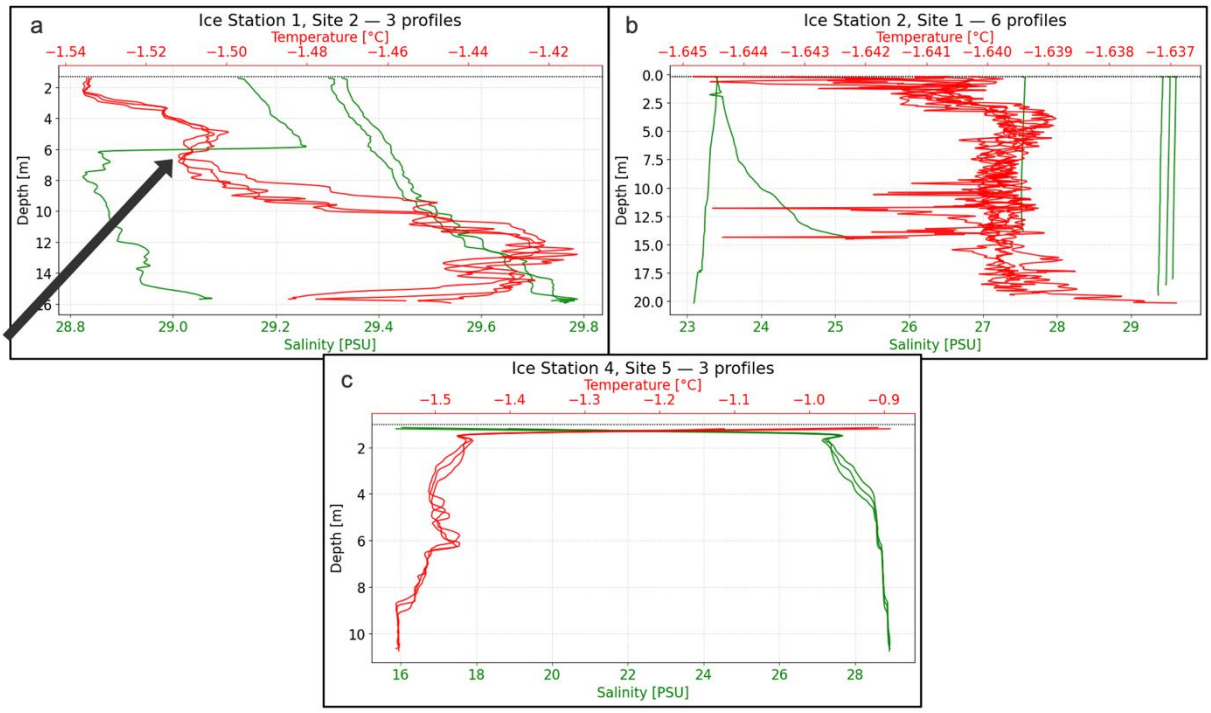

Fig. 2.57: Processed Profiles grouped by ice station and Site. Profiles in a) show problems with data quality and freezing conditions. Profiles in b) show a more consistent salinity signal. c) displays the strong stratification and fresh conditions underneath the ice at ice station 4 close to the coast of Greenland. Plots by Clemens Rohling.

We conclude that the instrument needs to be protected during the ice work, especially during very cold days. We recommend to store the instrument inside an insulation box with a heat source between casts. This has been tested at ice station 4, but the insulation box including a hot water bottle quickly cooled off too quickly. The Profiles of Ice Station 4 already show more consistent data, which could also be due to the strong meltwater layer which can be observed at all sites from ice station 4 (Fig. 2.57c). In summary it should be noted that the data shows significant data quality problems and should be carefully sorted and analysed before it can be used.

Tab. 2.18: Summary of Upriser CTD profiles on the 4 ice stations during PS150. Table compiled by Clemens Rohling

Ice Station	PS150 Station	Site	Nr. of Casts	Along Transect Distance	Raw Data	Processed Data	Comment
1	44	1	10	0	235669_20250913_1419_UpriserTransect_1.rsk	Upriser_CTD_PS150_044_1_[000-009].csv	ice edge close to Polarstern; 2 casts to 18 m; ice thickness 1.06 m, FB 0.01 m, snow 0.17 m
1	44	2	3	100	235669_20250913_1441_UpriserTransect_2.rsk	Upriser_CTD_PS150_044_2_[000-002].csv	in eDNA hole; 3 profiles; ice thickness 1.22 m, FB 0.01 m, snow 0.1 m; 100 m from Site 1; level ice
1	44	3	3	200	235669_20250913_1505_UpriserTransect_3.rsk	Upriser_CTD_PS150_044_3_[000-002].csv	100 m from Site 2; ice thickness 1.36 m, FB 0.1 m, snow 0.09 m; 3 casts to 18 m
1	44	4	6	300	235669_20250913_1539_UpriserTransect_4.rsk	Upriser_CTD_PS150_044_4_[000-005].csv	100 m from Site 3; ice thickness 1.39 m, FB 0.11 m, snow 0.15 m; multiple casts
1	44	5	13	400	235669_20250913_1625_UpriserTransect_5.rsk	Upriser_CTD_PS150_044_5_[000-012].csv	72 m from Site 4; 10 m next to small ridge; ice thickness 1.77 m, FB 0.14 m, snow 0.1 m; several casts for experimenting, especially with increased distance between CTD and weight
2	78				235669_20250921_1141_test.rsk		Test in mss tent
2	78	1	6	0	235669_20250921_1228_1.rsk	Upriser_CTD_PS150_078_1_[000-005].csv	Several tests + 3 casts in the lead behind Polarstern
2	78	2	4	50	235669_20250921_1306_2.rsk	Upriser_CTD_PS150_078_2_[000-003].csv	4 casts - apprx 50 m from lead, ice thickness: 2.10 m, freeboard: 0.25 m
2	78	3	4	100	235669_20250921_1401_3e.rsk	Upriser_CTD_PS150_078_3_[000-003].csv	3 casts - apprx 100 m from lead, ice thickness: 1.97 m, freeboard: 0.12 m
2	78	4	3	150	235669_20250921_1703_4.rsk	Upriser_CTD_PS150_078_4_[000-002].csv	3 casts - apprx 150 m from lead
2	78				235669_20250921_1841_5_6.rsk		sensor did not record, ice thickness: 1.26 m, freeboard: 0.05 m, (ADCP Site)
2	78	5	4	200	235669_20250921_2121_5_S1000b.rsk	Upriser_CTD_PS150_078_5_[000-003].csv	repeat of (ADCP Site) - apprx 200m from lead
2	78	6	3	250	235669_20250921_1841_5_6.rsk	Upriser_CTD_PS150_078_6_[000-002].csv	3 casts - apprx 250 m from lead, ice thickness: 1.38 m, freeboard: 0.06 m
3	90	1	4	-200	235669_20250925_1910.rsk	Upriser_CTD_PS150_090_1_[000-003].csv	Apprx 200 meter in front of the ridge, ice thickness 1.22m, freeboard 7cm, snow ?
3	90	2	4	-24	235669_20250925_1910.rsk	Upriser_CTD_PS150_090_2_[000-003].csv	Apprx 24 meter in front of the ridge, ice thickness 1.76m, freeboard 21cm, snow ?
3	90	3	3	20	235669_20250925_1910.rsk	Upriser_CTD_PS150_090_3_[000-002].csv	Apprx 20 meter behind the ridge, ice thickness 1.37m, freeboard 5cm, snow ?
3	90	4	2	200	235669_20250925_1910.rsk	Upriser_CTD_PS150_090_4_[000-001].csv	Apprx 200 meter behind the ridge, ice thickness 1.55m, freeboard 7cm, snow 16cm
4	127	1	3	0	235669_20251011_0349.rsk	Upriser_CTD_PS150_127_1_[000-002].csv	apprx 120 meter South West of Polarstern, ice thickness: 1.10m , freeboard: 0.0 m, snow: 0.26 m
4	127	2	6	50	235669_20251011_0349.rsk	Upriser_CTD_PS150_127_2_[000-005].csv	50 meter North of Station 1, ice thickness: 1.26m , freeboard: 0.02 m, snow: 0.20 m
4	127	3	3	100	235669_20251011_0349.rsk	Upriser_CTD_PS150_127_3_[000-002].csv	50 meter North of Station 2, ice thickness: 0.84 m , freeboard: 0.03 m, snow: 0.08 m
4	127	4	3	150	235669_20251011_0349.rsk	Upriser_CTD_PS150_127_4_[000-002].csv	50 meter North of Station 3, ice thickness: 0.96m , freeboard: 0.03 m, snow: 0.15 m
4	127	5	3	395	235669_20251011_0349.rsk	Upriser_CTD_PS150_127_5_[000-002].csv	245 meter North of Station 4, ice thickness: 1.37m , freeboard: 0.13 m, snow: 0.08 m
4	127	6	3	645	235669_20251011_0349.rsk	Upriser_CTD_PS150_127_6_[000-002].csv	250 meter North of Station 5, ice thickness: 0.85m , freeboard: 0.00 m, snow: 0.12 m
4	127	1	3	0	235669_20251011_0349.rsk	Upriser_CTD_PS150_127_1.2_[000-002].csv	repeat casts of station 1 to capture temporal variability

Otter Pro Uncrewed Surface Vehicle "Arcturus"

An uncrewed surface vehicle (USV) of the type **Otter Pro** (herein referred to as "Otter") built by Maritime Robotics (Trondheim, Norway) was brought to PS150 to collect physical oceanography and bathymetry data close to some of the main glaciers in the study area of Northeast Greenland, in particular in the Independence/Hagen Fjord system, and the 79°N Glacier area. The scientific payload of the Otter included a Nortek S500 vessel-mounted ADCP, an Autocast profiling winch with an AML-3 CTD attached to a ~130 m cable, a Kongsberg EM20240P multibeam in conjunction with a SeaPath i340 INS unit, and a fixed-depth RBRconcerto CTD (SN 235669, depth rating 200 dbar) attached to the ADCP with cable clamps. In addition to the standard front camera for navigation, the vehicle was also equipped with a SeaSight CL 360° camera plus Lidar system for situational awareness/automatic obstacle avoidance, as well as an AIS class B transceiver. An Insta X3 action camera was installed on the vehicle during the first deployment. The Otter is propelled by 2 electric motors, and powered by 4 Torqueedo 915 Wh lithium-ion batteries. Communication with the Vehicle Control Station (VCS) was maintained via a 5GHz MIMO radio link, with a range of ~2 km. Starlink integration is in progress. An labelled photo of the USV including all major components is shown in Figure 2.58.

Unfortunately, the landfast sea ice still present in the fjord systems and in the 79°N Glacier area made these inaccessible even for *Polarstern*, and as a result, it was impossible to deploy the Otter there for its intended purpose. Instead, we considered to map the shelf areas close to the Northeast Greenland coast, and to opportunistically study the shape and size of individual icebergs, and their interaction with the ocean. However, stormy conditions and, in particular, new ice formation did also not allow us to deploy the vehicle for that purpose in a scientifically useful way. In the end, we deployed the Otter during three stations (Tab. 2.19), to perform extended tests of the instrumentation, and to familiarize ourselves with the controls and mission planning. Some preliminary data plots are shown in Figure 2.59 and Figure 2.60, with additional comments and explanations in the respective figure caption. The bathymetry and current velocity data have not been processed at this point and will be assessed at a later stage.

Tab. 2.19: Overview of Otter Pro USV deployments during PS150. Table by Mario Hoppmann

Station	Date/Time Start (UTC)	Latitude	Longitude	Water depth (m)	Mission
PS150_34-1	11 Sep 2025 12:45	82.1410	-12.4091	225	Initial test
PS150_78-2	21 Sep 2025 11:14	84.4702	-21.0225	735	Test
PS150_127-4	10 Oct 2025 15:08	80.1418	-15.9642	206	Test

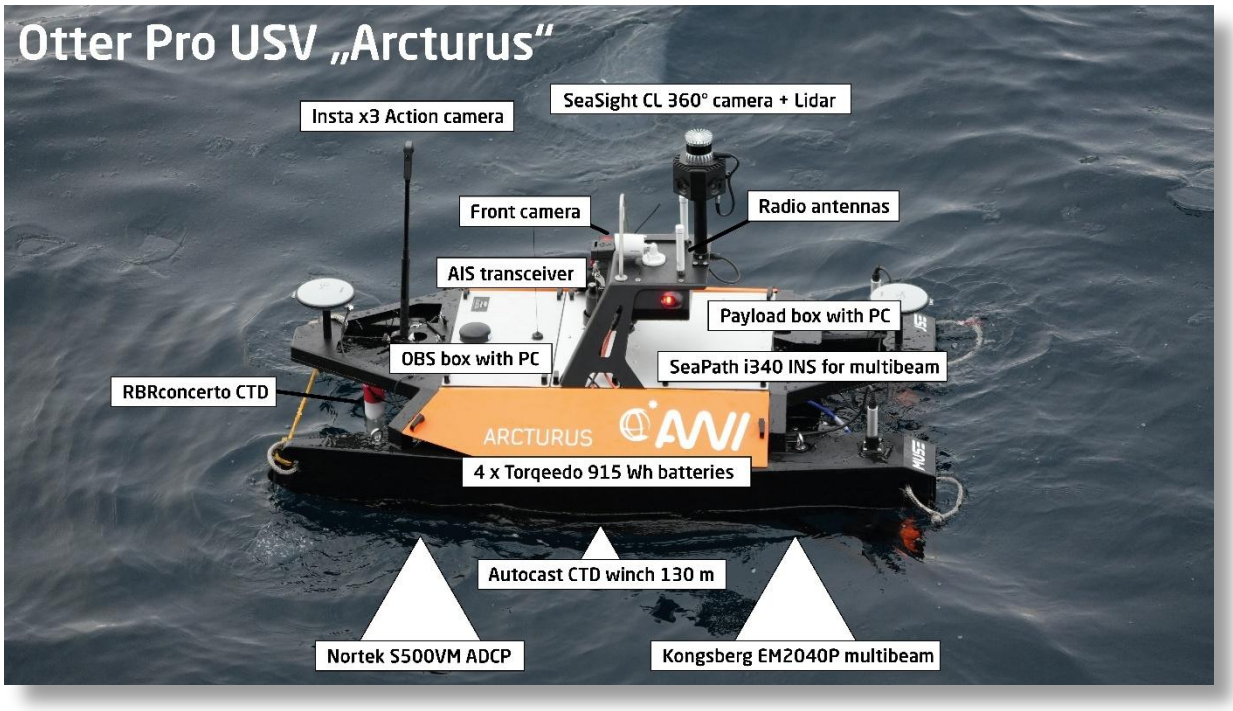

Fig. 2.58: Component overview of the Otter Pro USV (Maritime Robotics, Norway). Figure by Mario Hoppmann.

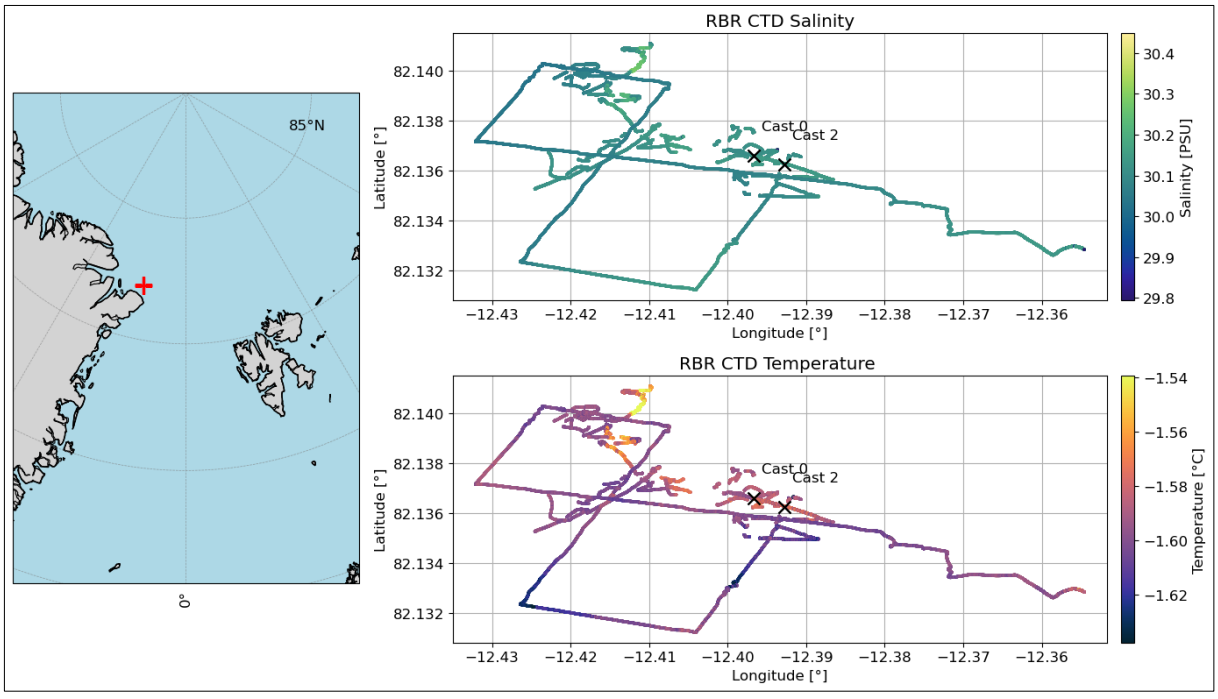

Fig. 2.59: Exemplary plot of temperature and salinity as measured by the RBRconcerto CTD mounted on the Otter during the first deployment on 11 Sep 2025. Cast 0 and Cast 2 refer to profiles obtained from the AML-3 profiling CTD on the Autocast winch, plotted in Figure 2.60. Figure by Clemens Rohling.

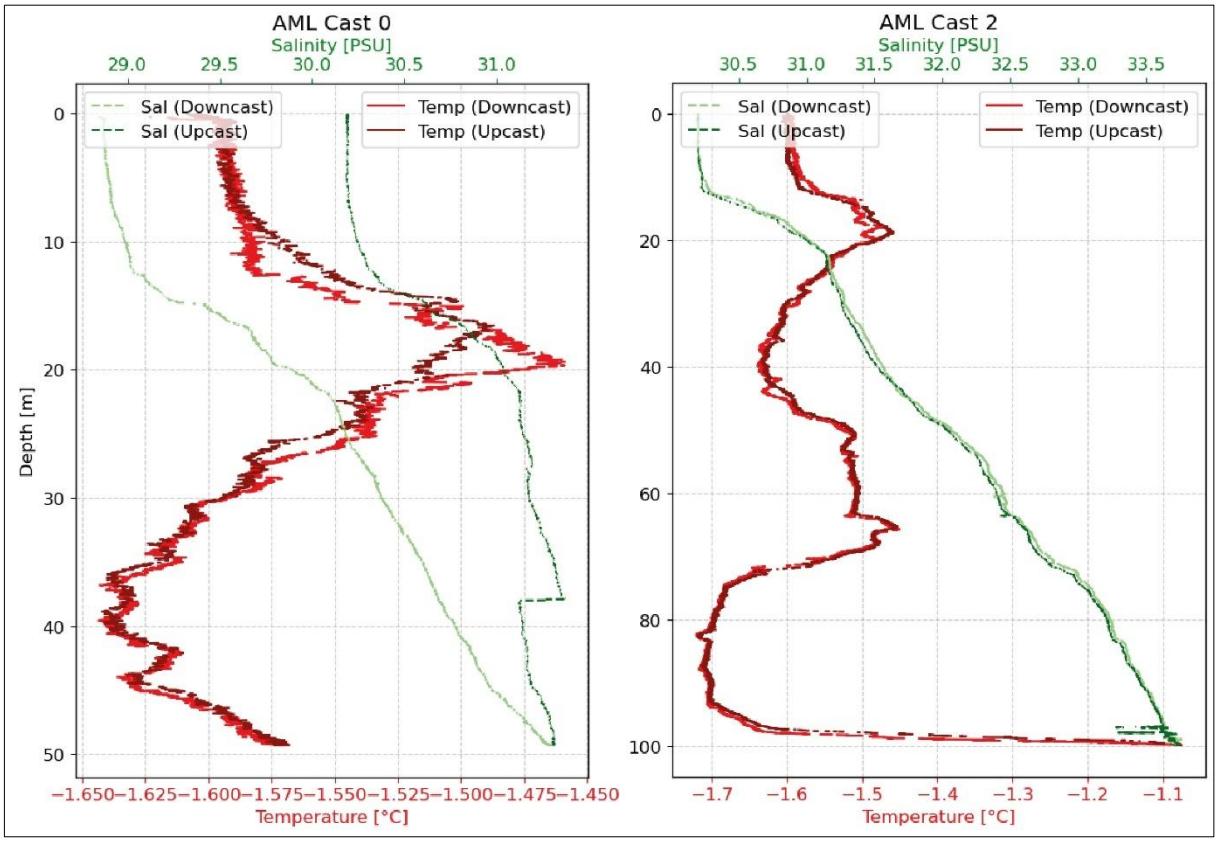

Fig. 2.60: Temperature and salinity profiles obtained by the AML-3 CTD on the Otter's Autocast winch during the first deployment on 11 Sep 2025. Note the difference between down- and upcast during Cast 0 (left), and the jump in salinity at 38 m during the upcast. This was likely caused by a freezing of the exposed instrument due to the low air temperatures during immersion into the seawater. Care needs to be taken when the instrument is used in freezing conditions. Cast 2 data (right) look as expected, with down- and upcast being comparable. Figure by Clemens Rohling.

Expected results

Summary of lessons learnt

Based on our experiences during the cruise, we recommend the following things to be taken into consideration during future cruises:

1. The computer that runs the CTD-rosette software should be restarted regularly, at least once a week.
2. The vmADCP should be used with a bottom tracking pulse in water less than 1000 m depth.
3. The RBR concertos used as uprisers or fishing rod CTDs should be kept in an insulated box with a hot water bottle in order to avoid the formation of ice inside of the conductivity sensor. It should only be removed from the insulated box immediately prior to deployment into the water.

Definition of sections

In order to facilitate comparability between different analyses of the data, we associate the measurements taken during PS150 to 16 sections as shown in Figure 2.61. Note that we count the Flade section twice (5 ,6), since we sampled here in two different time periods. The sections are oriented from the coast or shallow waters into the deep ocean. Table 2.20 associates the ship stations and helicopter stations to these 16 sections. At 11 sections, CTD and XCTD measurements onboard *Polarstern* were conducted, complemented in some cases with measurements via helicopter (section 12). Here ship ADCP data is available. Four sections (10, 11, 14, 16) were only sampled via helicopter. One station is oriented along the ship track, with only ship ADCP data available. Water depth information at these sections was extracted from Dship, and contains GEBCO data, and in some locations bathymetry from previous AWI expeditions and from this expedition.

Tab. 2.20: Definition of the 16 sections (start and end point in longitude/latitude coordinates). Note that sections 10 and 11 are not defined on a straight line.

Section no	Section name	Lat_1	Lon_1	Lat_2	Lon_2	Lat_3	Lon_3	Lat_4	Lon_4	Lat_5	Lon_5	Ship stations	Helicopter stations	Comment
1	Ile_de_France	78.1420	-15.9150	78.2070	-15.5250							117 118 119		
2	Norske_Trough	79.2090	-17.4490	79.2060	-16.8520							133 134 135		
3	Holm	80.1990	-16.5280	80.0860	-15.4950							127 128 129 130 131		
4	Westwind_Trough	80.7520	-14.2850	80.2240	-11.9530							120 121 122 123 124 125		
5	Flade_1	81.6150	-12.1540	82.4710	-2.3017							5 6 7 8 9 10 11 12 13 14 15 16 17 18 19 20 21 22 23 24 25 26 27 28 29 30 31 32		
6	Flade_2	81.6150	-12.1540	82.4710	-2.3017							98 100 101 102 103 104 105 106 107 108		
7	Independence_Shelfbreak	82.0340	-21.1240	82.6640	-12.3930							91 92 93 94 95 96 97		
8	Independence_Midshelf	82.8810	-19.6370	81.7680	-13.3460									
9	Independence_Mouth	82.5530	-19.9040	82.0680	-16.5780							36 37 38 39 40 41 42		
10	Independence_Fjord	82.073	-27.809	82.086	-23.513	82.18	-21.28	83.152	-19.357			37	1 2 4 7 8 21 22 23	section not on a straight line
11	Hagen_Fjord	81.578	-25.599	81.774	-24.209	82.086	-23.513	82.18	-21.28	83.152	-19.357	37	4 5 6 7 23	section not on a straight line
12	Wandel	82.9790	-23.4680	84.1430	-8.0162							45 46 47 48 49 50 51 52 53 54 55 56 57 58 59 60 61 62 63 64 65 66 67 68	8 9 10 11 12	
13	Morris_Jesup_Rise	84.4760	-21.6890	83.8400	-11.5610							68 69 70 71 72 73 74 75 76 77 78		
14	Morris_Jesup_Spit	85.4300	-16.2370	85.6400	-16.6610								13 14	
15	Cape_Morris_Jesup	83.6580	-30.3590	84.3230	-24.3150							79 80 81 82 83 84 85 86 87		
16	Lincoln	83.7000	-33.0000	84.4000	-33.0000								15 16 17 18 19 20	

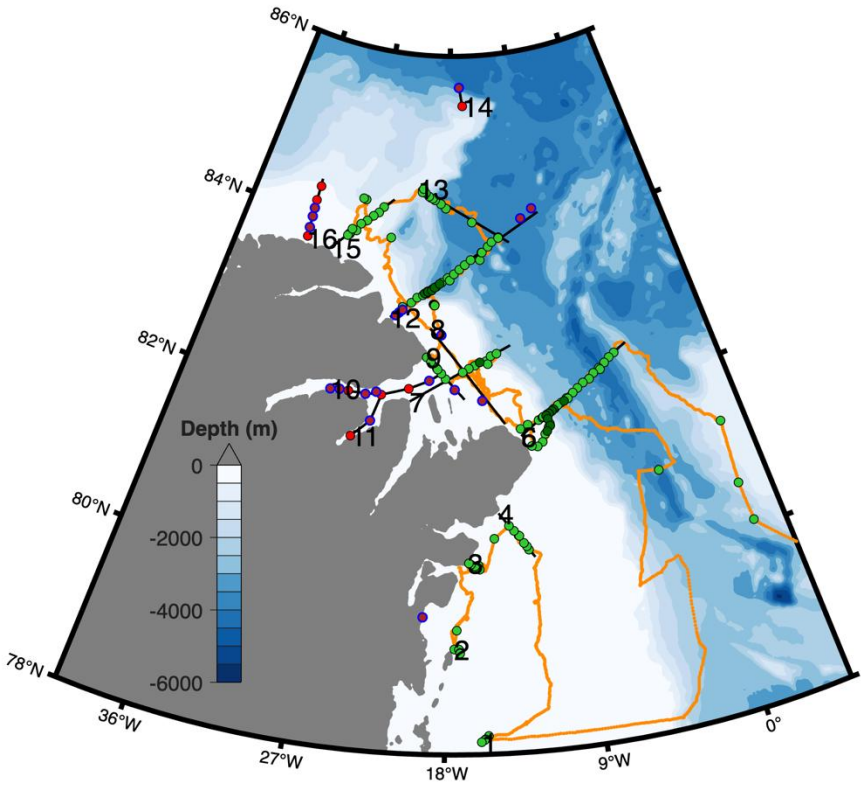

Fig. 2.61: (Same as Fig. 2.1) Map of the study area with cruise track (orange), ship stations with CTD (light green) and XCTD (dark green) measurements and measurements via helicopter (fishing rod CTD in purple and XCTD in red). Along the cruise track, velocity measurements from the ship ADCP are available. Black lines indicate the 16 sections.

Data management

All environmental data obtained during this expedition will be archived, published, and disseminated according to international standards by the World Data Center PANGAEA (Data Publisher for Earth & Environmental Science; https://www.pangaea.de) within two years after the end of the expedition at the latest. Unless specified otherwise, a CC-BY license will apply. Measurements from autonomous systems, which transmit data in near real time via satellite communication, will be made immediately available through the data and information portal meereisportal.de. Any other data will be submitted to an appropriate long-term archive that provides unique and stable identifiers for the datasets and allows open online access to the data.

This expedition was supported by the Helmholtz Research Programme “Changing Earth – Sustaining our Future” Topic 2, Subtopic 2.1.

In all publications based on this expedition, the **Grant No. AWI_PS150_00** will be quoted and the following publication will be cited:

Alfred-Wegener-Institut Helmholtz-Zentrum für Polar- und Meeresforschung (2017) Polar Research and Supply Vessel POLARSTERN Operated by the Alfred-Wegener-Institute. Journal of large-scale research facilities, 3, A119. http://dx.doi.org/10.17815/jlsrf-3-163.

References

Aksenov Y, Ivanov VV, Nurser AJG, Bacon S, Polyakov IV, Coward AC, et al. (2011) The Arctic Circumpolar Boudary Current. Journal of Geophysical Research.

Bendtsen J, Mortensen J., Lennert K, K Ehn J, Boone W, Galindo V, et al. (2017) Sea ice breakup and marine melt of a retreating tidewater outlet glacier in northeast Greenland (81°N). Scientific Reports.

Carmack EC, Yamamoto-Kawai M, Haine TWN, Bacon S, Bluhm BA, Lique C, et al. (2016) Freshwater and its role in the Arctic Marine System: Sources, disposition, storage, export, and physical and biogeochemical consequences in the Arctic and global oceans. Journal of Geophysical Research. Biogeosciences.

Dmitrenko IA, Kirillov SA, Rudels B, Babb DG, Myers PG, Stedmon CA, et al. (2019) Variability of the pacific-derived arctic water over the southeastern Wandel sea shelf (northeast Greenland) in 2015–2016. Journal of Geophysical Research, C: Oceans.

Dodd PA, Rabe B, Hansen E, Falck E, Mackensen A, Rohling E, et al. (2012) The freshwater composition of the Fram Strait outflow derived from a decade of tracer measurements. Journal of Geophysical Research, C: Oceans.

Doglioni F, Ricker R, Rabe B, Barth A, Troupin C & Kanzow T (2023) Sea surface height anomaly and geostrophic current velocity from altimetry measurements over the Arctic Ocean (2011–2020). Earth System Science Data.

Duchon CE (1979) Lanczos filtering in one and two dimensions, J. Appl. Meteorol., 18, 1016-1022.

Falck E, Kattner G & Budéus G (2005) Disappearance of Pacific water in the northwestern Fram Strait. Geophysical Research Letters.

Gjelstrup CVB, Sejr MK, de Steur L, Christiansen JS, Granskog MA. Koch BP., et al (2022) Vertical redistribution of principle water masses on the Northeast Greenland Shelf. Nature Communications.

Håvik L, Våge K, Pickart RS, Harden BE, von Appen W-J, Jónsson S & Osterhus S (2017) Structure and variability of the shelfbreak East Greenland Current north of Denmark Strait. Journal of Physical Oceanography.

Huhn O, Rhein M, Kanzow T, Schaffer J & Sültenfuß J (2021) Submarine meltwater from nioghalvfjerdsbræ (79 north glacier), northeast Greenland. Journal of Geophysical Research.

Jakobsson M, Mayer LA, Nilsson J, Stranne C, Calder B, O'Regan M, et al. (2020) Ryder Glacier in northwest Greenland is shielded from warm Atlantic water by a bathymetric sill. Communications Earth & Environment.

Karcher M, Smith JN, Kauker F, Gerdes R & Smethie WM (2012) Recent changes in Arctic Ocean circulation revealed by iodine-129 observations and modeling. Journal of Geophysical Research.

Kizu, S., H. Onishi, T. Suga, K. Hanawa, T. Watanabe, and H. Iwamiya (2008) Evaluation of the fall rates of the present and developmental XCTDs, Deep Sea Res. Part 1 55(4):571–586.

Koenig Z, Meyer A, Provost C, Sennéchael N, Sundfjord A, Beguery L, et al. (2018) Cooling and Freshening of the West Spitsbergen Current by Shelf-Origin Cold Core Lenses. Journal of Geophysical Research.

Kolås E, & Fer I (2018) Hydrography, transport and mixing of the West Spitsbergen Current: the Svalbard Branch in summer 2015. Ocean Science.

Kolås EH, Koenig Z, Fer I, Nilsen F & Marnela M (2020) Structure and transport of Atlantic water north of Svalbard from observations in summer and fall 2018. Journal of Geophysical Research.

Krumpen T, Belter HJ, Boetius A Damm E, Haas C, Hendricks S, et al. (2019) Arctic warming interrupts the Transpolar Drift and affects long-range transport of sea ice and ice-rafted matter. Scientific Reports.

Mayer C, Schaffer J, Hattermann T, Floricioiu D, Krieger L, Dodd P. A, Kanzow T, et al. (2018) Large ice loss variability at Nioghalvfjerdsfjorden Glacier, Northeast-Greenland. Nature Communications.

McPherson RA, Wekerle C, & Kanzow T (2023, revised) Shifts of the Recirculation Pathways in central Fram Strait drive Atlantic Intermediate Water Variability on Northeast Greenland shelf. https://doi.org/10.22541/essoar.168167222.21218611/v1

McPherson R, von Appen W-J, de Steur L, Kanzow T, Beszczynska-Möller A & Renner A (2025, in press) Decades of Change: Warming Trends and Hydrographic Variability of Atlantic Water as observed in the West Spitsbergen Current (1997–2024), Deep Sea Research II.

Mouginot J, Rignot E, Scheuchl B, Fenty I, Khazendar A, Morlighem M et al. (2015) Fast retreat of Zachariæ Isstrøm, northeast Greenland. Science.

Muenchow A, Falkner K & Melling H (2007) Spatial continuity of measured seawater and tracer fluxes through Nares Strait, a dynamically wide channel bordering the Canadian Archi-pelago. J. Mar. Res. 65:759-788.

Münchow A (2016) Volume and Freshwater Flux Observations from Nares Strait to the West of Greenland at Daily Time Scales from 2003 to 2009. Journal of Physical Oceanography.

Münchow A, Padman L, Washam P & Nicholls KW (2016) The ice shelf of Petermann Gletscher, North Greenland, and its connection to the Arctic and Atlantic Oceans. Oceanography.

Münchow A, Schaffer J & Kanzow T (2020) Ocean Circulation Connecting Fram Strait to Glaciers off North-East Greenland: Mean Flows, Topographic Rossby Waves, and their Forcing. Journal of Physical Oceanography.

Newton JL & Sotirin BJ (1997) Boundary Undercurrent and Water Mass Changes in the Lincoln Sea. Journal of Geophysical Research.

Nilsson J, van Dongen E, Jakobsson M, O'Regan M& Stranne C (2023) Hydraulic suppression of basal glacier melt in sill fjords. The Cryosphere.

Padman, L. and S. Erofeeva (2004) A barotropic inverse tidal model for the Arctic Ocean, Geophys. Res. Let., 31.

Pérez-Hernández MD, Pickart RS, Torres DJ, Bahr F, Sundfjord A, Ingvaldsen R et al. (2019) Structure, Transport, and Seasonality of the Atlantic Water Boundary Current North of Svalbard: Results From a Yearlong Mooring Array. Journal of Geophysical Research.

Pnyushkov AV, Polyakov IV, Alekseev GV, Ashik IM, Baumann TM, Carmack EC, et al. (2021) A Steady Regime of Volume and Heat Transports in the Eastern Arctic Ocean in the Early 21st Century. Frontiers in Marine Science.

Polyakov IV Pnyushkov AV, Alkire MB, Ashik IM, Baumann TM, Carmack EC, Kanzow T, et al. (2017) Greater role for Atlantic inflows on sea-ice loss in the Eurasian Basin of the Arctic Ocean. Science.

Richter M, von Appen W-J & Wekerle C (2018) Does the East Greenland Current exist in northern Fram Strait? Ocean Science.

Rudels B, Jones EP, Anderson LG & Kattner G (1994) On the Intermediate Depth Waters of the Arctic Ocean. Geophysical Monograph Series.

Schaffer J, Kanzow T, von Appen W-J. von Albedyll L, Arndt JE & Roberts DH (2020) Bathymetry constrains ocean heat supply to Greenland's largest glacier tongue. Nature Geoscience.

Smith JN, Karcher M, Casacuberta N, Williams WJ, Kenna T & Smethie WM, Jr (2021) A changing arctic ocean: How measured and modeled129I distributions indicate fundamental shifts in circulation between 1994 and 2015. Journal of Geophysical Research.

de Steur L, Hansen E, Mauritzen C, Beszczynska-Möller A & Fahrbach E (2014) Impact of recirculation on the East Greenland Current in Fram Strait: Results from moored current meter measurements between 1997 and 2009. Deep Sea Research.

Sumata H, de Steur L, Divine DV, Granskog MA & Gerland S (2023) Regime shift in Arctic Ocean sea ice thickness. Nature.

Thurnherr AM, Goszczko I & Bahr F (2017) Improving LADCP Velocity with External Heading, Pitch and Roll. J. Atmos. Oceanic Technol.

Uchida H, Shimada K & Kawano T (2011) A method for data processing to obtain high-quality XCTD data. J. Atmos. Ocean. Tech., 28:816–826.

Wilson N, Straneo F & Heimbach P (2017) Satellite-derived submarine melt rates and mass balance (2011–2015) for Greenland's largest remaining ice tongues. The Cryosphere.

Woodgate RA, Aagaard K, Muench RD, Gunn JT, Bjork G, Rudels B, et al. (2001) The Arctic Ocean Boundary Current along the Eurasian Slope and the Adjacent Lomonosov Ridge: Water Mass Properties, Transports and Transformations from Moored Instruments. Deep-Sea Research.

3. PLANKTON ECOLOGY AND BIOGEOCHEMISTRY IN THE CHANGING ARCTIC OCEAN (PEBCAO GROUP)

Hongyan Xi[1*], Ina Schmidt[1], Ayla Murray[1,2], Rebecca Gorniak[1,2], Christian Detsch[2], Clara Mersch[1,3], Moritz Aehle[4,5], Lisa W. von Friesen[6], Rebecca Duncan[6], Adam Makatun[7]

Not on board: Astrid Bracher[1], Charlotte Havermans[1,2], Morten Iversen[1], Alexandra Kraberg[1], Katja Metfies[1], Barbara Niehoff[1], Ilka Peeken[1], Anja Engel[4], Benjamin Pontiller[4], Hanna Farnelid[6]

* hongyan.xi@awi.de

[1]DE.AWI
[2]DE.UNI-Bremen
[3]DE.UNI-Oldenburg
[4]DE.GEOMAR
[5]DE.UNI-Hamburg
[6]SE.LNU
[7]PL.UNI-Gdański

Grant-No. AWI_PS150_02

Outline

The PEBCAO group (Plankton Ecology and Biogeochemistry in a Changing Arctic Ocean) is a collaboration team between colleagues from AWI and GEOMAR focusing on plankton community ecology and the microbial processes relevant to biogeochemical cycles of the Arctic Ocean (AO). The work of this group is of particular relevance, considering that the Arctic Ocean is currently undergoing considerable environmental change with the pronounced decrease in sea ice and increase in temperature, given the latter being nearly four times faster than the global annual average during the last four decades (Rantanen et al. 2022). This phenomenon, known as the Arctic Amplification (Serreze & Barry 2011), arises primarily from interacting feedbacks such as sea-ice loss that enhances heat absorption, along with changes in atmospheric and ocean heat transport. Arctic amplification leads to prominent changes that impact the biogeochemistry and ecology of the Arctic pelagic system; detailed monitoring of existing conditions is therefore vital.

The PEBCAO group began its studies on Arctic plankton ecology in 1991. Since 2009 it intensified its efforts by accomplishing yearly long-term observations in the framework of the Long-term Ecological Research Site HAUSGARTEN in the Fram Strait. Over the past decade, the regular observations of the PEBCAO-group included a combination of classical bulk measurements of biogeochemical parameters, microscopy, optical methods, satellite observations, and molecular genetic approaches in a holistic approach. By doing so, we have compiled comprehensive information on annual variability in plankton composition, primary production, bacterial activity and zooplankton composition, including key ecosystem processes such as carbon export. The long-term observations and process studies have already given us valuable insights into mechanistic linkages between environmental conditions, biodiversity and ecosystem functionality, and into ongoing change in the marine ecosystem of the Fram Strait (e.g., Nöthig et al. 2015, 2020; Metfies et al. 2016; Engel et al. 2019; von Appen et al. 2021).

Objectives

During the PS150 expedition, we continued these observations and covered an extended area beyond the HAUSGARTEN region by focusing on the Western Fram Strait, Northeast Greenland shelf, North Greenland shelf including the Wandel Sea. Within the PEBCAO and with external international collaborators, observational and experimental research took place by several subgroups, addressing cross-disciplinary topics. In this chapter, we describe the research topics and summarize accordingly their objectives and the work that took place onboard.

I. The role of picophytoplankton in the carbon cycle

Picophytoplankton (<3 µm) are the smallest phytoplankton and often dominate primary producers in the Arctic Ocean (Tremblay et al. 2009; Metfies et al. 2016), especially in nutrient-poor regions (Iversen & Seuthe 2011; Ardyna & Arrigo 2020). They play key roles in the Arctic ecosystem, and a shift from larger taxa such as diatoms to smaller groups has been observed (Li et al. 2009; Nöthig et al. 2015) and is expected to intensify with climate change (Flombaum et al. 2020; Oziel et al. 2025). However, their contribution to the marine carbon cycle –I ncluding carbon fixation, regulation, export, and trophic transfer – remains poorly understood (Bachy et al. 2022). During PS150, we examined the role of picophytoplankton in the autumn carbon cycle by assessing their species composition, abundance, productivity, and associated particle export across environmental gradients. We experimentally quantified carbon transfer from the key species *Micromonas polaris* to grazers and to the microbial loop.

The increasing frequency of autumn phytoplankton blooms (Ardyna & Arrigo 2020) affects the Arctic carbon budget and ecosystem dynamics. In parts of the PS150 study area (Wandel Sea), rapid sea-ice decline enhances wind-driven mixing (Schweiger et al. 2021; Muilwijk et al. 2024). We therefore simulated mixing events to assess resulting changes in phytoplankton productivity and community structure.

The following objectives were addressed:

- Quantify size-fractionated and dissolved primary production using stable-isotope tracing.
- Assess autumn mixing effects and test Rubisco as a productivity proxy.
- Characterize sinking particles with UVP5 and link it to phytoplankton community.
- Trace carbon flow from *Micromonas polaris* to grazers and microbes.
- Isolate Arctic phytoplankton for future ecophysiological studies.

II. Connectivity between sea ice and the upper pelagic during freeze-up

Sea-ice algae are a critical component of polar food webs, contributing up to 60% of primary production in ice-covered waters and providing an important source of nutrition during early zooplankton reproduction (Søreide et al. 2010; Fernández-Méndez et al. 2015). As early-season primary producers, their colonisation during ice formation plays a foundational role in energy flow to the marine ecosystem. Despite this importance, the composition and dynamics of sympagic (ice-associated) and pelagic (open-water) microalgal communities during freeze-up remain poorly understood. Improving our understanding of the connectivity between ice and water column microalgae, including species composition, abundance, physiological condition, nutritional quality, and colonisation mechanisms, is essential for predicting how sea-ice decline will alter trophic dynamics and carbon cycling.

The following objectives were addressed:

- Determine sympagic and pelagic phytoplankton community structure and abundance during the freeze-up period across various sea ice types, including multi-year ice and newly formed ice.
- Investigate the nutritional value of the sympagic and pelagic phytoplankton communities as a whole, and of key taxa at a species-specific resolution, across various sea-ice types.
- Assess the role of EPS in sympagic community colonisation during the freeze-up period, by quantifying EPS concentration in different ice types and environmental conditions.

III. Phytooptics: phytoplankton and dissolved organic matter from highly resolved optical measurements

The contribution of the Phytooptics group is the acquisition of high resolved information on the amount and composition of phytoplankton and its pigments, dissolved organic matter and particles along the cruise transect. These data enable the analysis of long-term trends of these parameters in the East Greenland region via the complementation to satellite and previous field data acquisition. During the expedition, continuous measurements with optical sensors will be taken at the surface water and also at discrete stations with the light profiler.

Time series of phytoplankton community structure have been obtained using *in-situ* data derived from our underway sampling and continuous flow-through system and have revealed remarkable interannual variability in the last decade in the Fram Strait (Bracher et al. 2025, submitted). In addition to that, these *in-situ* data are also beneficial for the model development and validation of satellite products on phytoplankton composition and its distribution (EOF-PFT Xi et al. 2021; PhytoDOAS Bracher et al. 2009; Sadeghi et al. 2012; ML-PhyTAO Xi et al. 2025) and spectral attenuation of underwater light (Dinter et al. 2015; Oelker et al. 2019; Oelker et al. 2022).

At this expedition we focus to broaden our sampling frequency of information on phytoplankton, particulate and chromophoric dissolved organic matter (CDOM) abundance and composition by taking continuous optical measurements which directly give information on inherent and apparent optical properties (IOPs, and AOPs, respectively). The specific objectives of PhytoOptics are to

- Collect a high spatial and temporal resolved data set on phytoplankton (total and composition) and its degradation products at the surface and for the full euphotic zone using continuous optical observations during the cruise and from ocean colour remote sensing calibrated with discrete water sample measurements.
- Develop and validate (global and regional) algorithms and associated radiative transfer models in accordance to the previous objective by using discrete water samples for pigment analysis and absorption measurements.
- Obtain a spectral characterisation of the underwater light field and its interplay with optical constituents, such as phytoplankton and CDOM abundance and composition.
- Improve our cal/val activity within Copernicus Marine Service.

IV. eDNA based analysis of arctic eukaryotic and prokaryotic microbial communities

The distribution, thickness, and melt dynamics of sea ice are key drivers of community composition, productivity, biogeochemical cycling, and pelagic-benthic coupling in the AO, while the biodiversity and composition of eukaryotic microbes of pelagic eukaryotic microbial communities are distinct from sea-ice communities (Hardge et al. 2017). Sea-ice associated microalgae, those living attached to or under the ice e.g. diatoms are important food sources of zooplankton (Kaiser et al. 2025). In Fram Strait, the two major currents harbor distinct microbial communities (Metfies et al. 2016), with sea-ice coverage as a major driver of these differences in community composition. The role of sea-ice and meltwater stratification as a driver of Arctic marine ecosystem functionality and pelagic benthic coupling was highlighted in recent studies accomplished in Fram Strait as part of the FRAM observatory and a number of expeditions to LTER HAUSGARTEN since 1999 (von Appen et al. 2021; Weiss et al. 2024). However, information on eukaryotic microbial community composition and biomass from areas with year-round ice-coverage are scarce, especially for picoeukaryotes. In order to comprehensively capture the biodiversity and Chal a biomass in areas with year-round ice-coverage we will complement the optical surveys with 18S meta-barcoding and fractionated chlorophyll *a* (Chla) measurements. Changes in eukaryotic microbial communities are tightly linked to prokaryotic community composition. The assessment of the biodiversity and biogeography of Arctic eukaryotic microbes, including phytoplankton and their linkages to prokaryotic microbial communities, will be based on analyses of eDNA via 16S and 18S meta-barcoding, and quantitative PCR. A suite of automated sampling devices in addition to classical sampling via Niskin bottles attached to a CTD/Rosette Water Sampler will be used to collect samples for eDNA analyses. This includes the automated filtration device AUTOFIM deployed on *Polarstern* for underway filtration, automated Remote Access water Samplers (RAS) and long-term sediment traps deployed on the FRAM moorings for year-round sampling.

V. ARJEL: Zooplankton

The Arctic Ocean is warming rapidly, and the resulting decline in sea ice represents one of the most pronounced impacts of climate change globally. This shift from an ice-covered to an open-water-dominated system is transforming ecosystem structure and function, nutrient cycling, and carbon export, with potentially cascading effects on regional biodiversity. Sea-ice loss, combined with increasing inflows of warmer Atlantic water, has already altered metazoan community compositions and is driving poleward range-shifts in Atlantic-origin fauna (e.g., Neukermans et al., 2018; Schröter et al., 2019). Zooplankton, a key metazoan group closely linked to temperature and water mass distributions, are among the those shifting northward (e.g., Schröter et al., 2019; Caspó et al., 2021). Gelatinous zooplankton (GZP), in particular, are expected to expand in distribution under continued warming and ice loss, increasing in abundance across the Arctic (Pantiukhin et al., 2023, 2024). Although their ecological roles remain poorly understood, they can substantially affect other plankton populations and can be important prey in high-latitude food webs (Irvine et al., 2025; Dischereit et al., 2024a,b). One region of particular interest is Northeast Greenland, known as the “Last Ice Area” due to its extensive multiyear and landfast sea ice-cover. As Arctic sea ice retreat accelerates across the region, this area is expected to serve as a final refuge for ice-associate biota. However, local biodiversity data and the responses of key metazoan groups remain highly limited. Collecting baseline biodiversity data in this unique ecosystem is essential for measuring the impacts of climate change, as well as creating effective mitigation and conservation strategies to protect it.

Onboard PS150, the ARJEL team collected a combination of molecular (eDNA/eRNA metabarcoding, genetic barcoding) and morphological (zooplankton nets and optical surveys) samples to investigate the biodiversity of marine metazoans across environmental gradients in the Last Ice Area. The main objectives of the ARJEL team were:

- To investigate patterns of pelagic and under-ice metazoan diversity across sea ice and hydrographic gradients in ice-covered waters of NE Greenland, based on eDNA metabarcoding of the mtCOI gene, of seawater and marine sediments.
- Collect zooplankton samples using the Midi Multi-net (MN), Bongo nets (BN), and UVP5 (Underwater Vision Profiler) imagery to assess (macro-) zooplankton communities (with a focus on GZP) and phylogeography.
- Link metazoan biodiversity data to sea-ice and hydrographic gradients to elucidate drivers of species distribution, abundance and community composition.
- Use the collected samples and data to complement ongoing net- and eDNA-based studies on GZP diversity and their ecological roles in the Fram Strait.

VI. Plankton imaging

The goal of the imaging-based plankton work in the PEBCAO group (manual microscopy as well as semi-automatic analyses based on instruments such as the underwater vision profiler and PlanktoScope) is to analyse community structure of the phytoplankton and zooplankton communities in different water masses and in relation to ice conditions. One focus is also to examine associations between planktonic organisms especially diatoms and their protistan parasites but also copepods and their external parasites.

VII. Microbial communities and biogeochemistry

To address the effects of global change and anthropogenic pollution on microbial communities and biogeochemical processes in the Arctic Ocean, the MB team

- Continued monitoring concentrations of dissolved organic carbon, nitrogen, amino acids, and carbohydrates.
- Assessed the abundances of phytoplankton, bacteria, and viruses using flow cytometry.

To better understand the potential risks of microplastics to human and ecosystem health, the team also investigated the microbial communities associated with microplastics. This work focuses on identifying potential pathogens and characterizing their resistance mechanisms (e.g., antibiotics) through a combination of field observations and laboratory experiments.

Contributing to the general scientific aims of PEBCAO, the summarized objectives on EGC Sources (PS150) are:

1. Characterise plankton distribution and biomass both horizontally and vertically at the meso-scale in EG shores.
2. Understand the contribution of the smallest phytoplankton to marine primary production.
3. Investigate the interactions between under-ice water and bottom-ice phytoplankton communities in different ice types and ages, during the freeze-up period.
4. Continue ongoing studies on zooplankton/metazoan diversity, community composition and ecology in relation to differing sea ice and hydrographic gradients.
5. Characterise the underwater light field and its interplay with optical constituents, such as CDOM, phytoplankton abundance and composition.

6. Elucidate cryo-pelagic coupling of eukaryotic microbial communities via eDNA based analysis.
7. Analyse community structure of the phytoplankton and zooplankton in different water masses and in relation to ice conditions.
8. Analysis of biofilm composition, function, and structural variation in relation to microplastic colonization and polymer type.

Work at sea

I. The role of picophytoplankton in the carbon cycle

The objectives were addressed through water collection from the CTD/rosette at 2–5 depths within the upper 100 m (Fig. 3.1 A, 3.2 A). We conducted:

- Size-fractionated primary production measurements (stable isotope tracing using ^{13}C-labelled bicarbonate) from the surface (10 m) and the chlorophyll *a* maximum (if any, otherwise 25 m) (14 stations). We collected samples to measure both particulate primary production (carbon fixed into cells) and dissolved primary production (exuded carbon from the cells). Water was incubated in bottles in an on-deck tank (Fig. 3.2.E) with continuously flowing surface water to mimic *in-situ* temperatures. Samples were collected at time 0 (T0) and after 24 hours (T24) for: elemental analyser isotope ratio mass spectrometry (EA-IRMS), dissolved inorganic carbon (δ^{13}C-DIC), dissolved organic carbon (δ^{13}C-DOC), and DNA (for quantitative PCR of picophytoplankton).
- Flow cytometry (26 stations) for cell abundance measurements of bacteria and pico-/nanoplankton from the five PEBCAO standard depths.
- Mixing experiments (3 stations) simulating wind-induced mixing with nutrient-rich deeper water to test effects on size-fractionated primary productivity.
- RNA-stable isotope tracing using labelled *Micromonas polaris*: one treatment with labelled cells and another with labelled dissolved organic matter (3 stations each) (Fig. 3.2.L).
- Sample collection for fluorescence-activated cell sorting (FACS) and sequencing of individual or population-level photosynthetic picoeukaryotes (6 occasions).
- Quantification of group/species-specific Rubisco alongside primary production measurements (8 stations).
- Isolation of pelagic and sympagic phytoplankton strains.
- Vertical profiling of particles throughout the water column with an Underwater Vision Profiler (see Tab. 3.7 for UVP5 deployments at 71 stations).

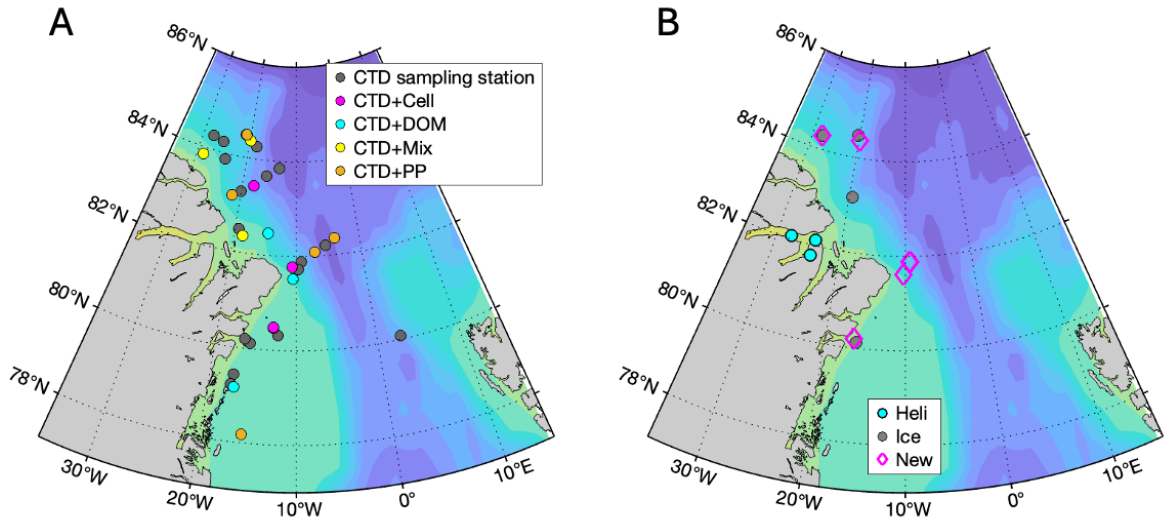

Fig. 3.1: Overview of sampling stations: (A) CTD sampling stations ("PEBCAO" stations) with the additional experiments marked (Cell: Micromonas cell addition, DOM: Micromonas dissolved organic matter addition, Mix: simulated mixing experiment, PP: primary production. (B) Sea ice sampling stations by helicopter (heli), ice stations from Polarstern (ice), and sampling of new ice.

Tab. 3.1: Overview of incubation experiments targeting different aspects of the role of picophytoplankton in the carbon cycle. See Figure 3.1A for the location of stations.

Station	Incubation type	Start date	Region
6	Primary production	2025-09-07	Flade 1
12	Primary production	2025-09-08	Flade 1
30	*M. polaris*, dissolved organic matter	2025-09-10	Flade 1
37	Simulated mixing event	2025-09-12	Independence Mouth
46	Primary production	2025-09-14	Wandel
59	*M. polaris*, cell addition	2025-09-16	Wandel
74	Simulated mixing event	2025-09-21	Morris Jessup Rise
85	Simulated mixing event	2025-09-23	Cape Morris Jessup
89	Primary production	2025-09-24	Towards Lincoln
93	*M. polaris*, dissolved organic matter	2025-09-27	Independence Shelfbreak
100	*M. polaris*, cell addition	2025-09-30	Flade 2
118	Primary production	2025-10-06	Ile de France
123	*M. polaris*, cell addition	2025-10-09	Westwind Trough
135	*M. polaris*, dissolved organic matter	2025-10-12	Norske Trough

II. Connectivity between sea ice and the upper pelagic during freeze-up

The objectives were addressed through sea ice collection at 14 locations capturing various ice types, ages and environmental conditions including multi-year ice, first-year ice, land-fast ice and sea ice in fjords of tidewater glaciers. At each location, between 5 – 16 ice cores were collected, and split into 4 sections (top 30 cm, bottom 10-40 cm, bottom 5 – 10 cm and bottom 5 cm) for biological, chemical, and biogeochemical analyses. With each ice core, snow depth,

ice thickness and free board measurements were taken. Under-ice water from 0.5 m below the ice was sampled with a hand pump and 3 m hose. In addition to the ice coring, new ice was collected at 6 locations, using a bucket sampler operated with the ship's crane (Fig. 3.2 I-J). At 1 location, frost flowers were collected from the new ice surface, using an inflatable boat operated by the ship's crane (Fig. 3.2 G). From sea ice cores, under ice water, new ice (buckets) and frost flowers, samples were collected for analyses of:

- Community Composition (DNA Metabarcoding and qPCR)
- Cell counts (Microscopy)
- Algal biomass and composition (determined by marker pigments and Chla analysis)
- Fatty Acid Composition
- Single Cell Nutritional Value (Synchrotron Fourier Transform Infrared Microspectroscopy (s-FTIR))
- Abundance of microorganisms (Flow Cytometry)
- Biogenic silicate
- Inorganic dissolved nutrients (Nitrate, Silicate, Phosphate, Ammonium)
- Particulate organic carbon: Particulate organic nitrogen (POC:PON)
- Stable isotopes (13 C and 15 N)
- Transparent exopolymer particles (TEP)
- Coomassie stainable particles (CSP)
- Fluorescence-activated cell sorting (FACS) for sequencing of individual cells and/or populations of photosynthetic picoeukaryotes
- Salinity
- Isolation of cells for downstream experiments

Tab. 3.2: Overview of sea ice sampling targeting different aspects of phytoplankton during the freeze-up period. See Figure 3.1 B for the location of stations.

Station	Station Type	Start date	Region
16	New Ice Bucket	2025-09-09	Flade 1
29	New Ice Bucket	2025-09-10	Flade 1
Heli-1	Helicopter	2025-09-12	Independence Fjord
Heli-2	Helicopter	2025-09-12	Independence Fjord
Heli-3	Helicopter	2025-09-12	Hagen Fjord
44	Ship Ice Station	2025-09-13	Wandel Sea
74	New Ice Bucket	2025-09-20	Morris Jessup Rise
78	Ship Ice Station	2025-09-21	Morris Jessup Rise
80	Frost Flower Sampling	2025-09-22	Morris Jessup Rise
89	New Ice Bucket	2025-09-24	Cape Morris Jessup
90	Ship Ice Station	2025-09-25	Towards Lincoln
Heli-4	Helicopter	2025-09-26	Independence Fjord
105	New Ice Bucket	2025-10-01	Flade 2
127	Ship Ice Station	2025-10-10	Westwind Trough
131	New Ice Bucket	2025-10-11	Holm

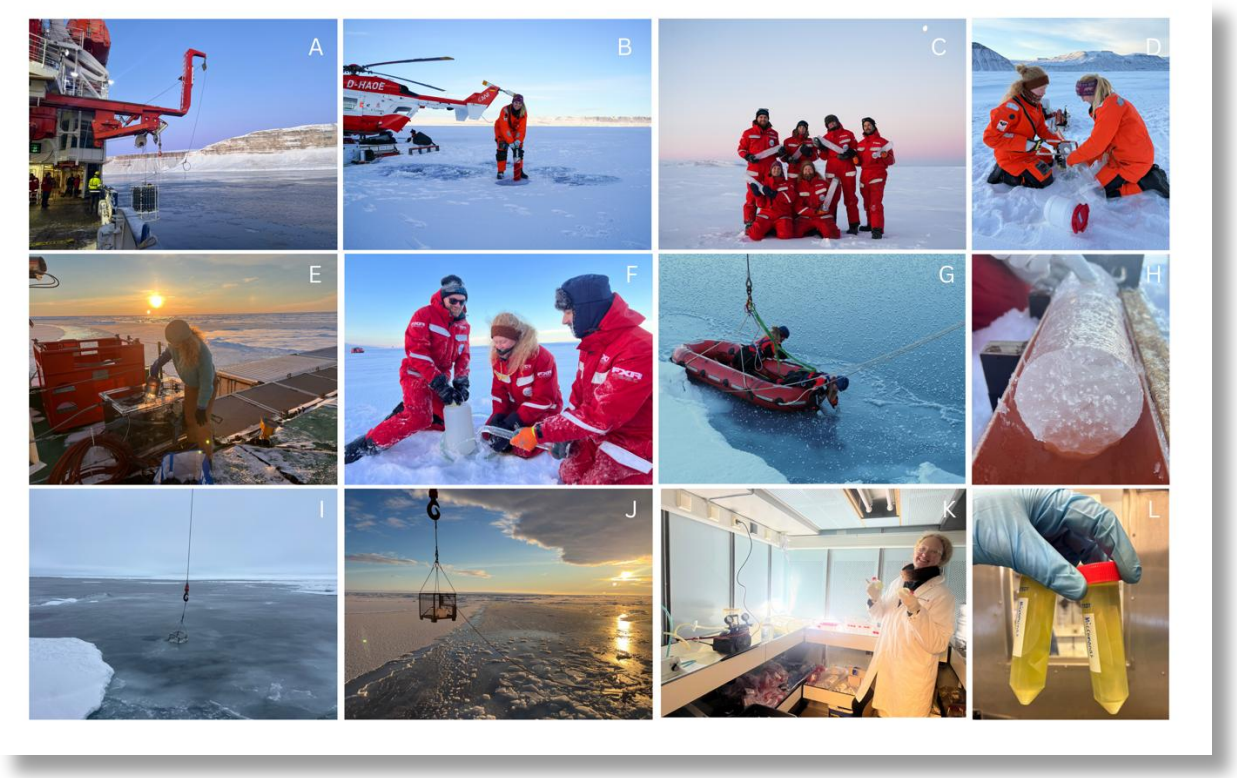

Fig. 3.2: A) CTD Water sampler on the Holm Section, B) Ice coring during a helicopter station, C) sea ice biology coring team, D) collecting sea ice cores in Independence Fjord, E) Primary production bottles being placed into the incubation tank, F) under ice water collection using the hand pump, G) frost flower collection, H) bottom of ice core from Station 127, I-J) new ice collection with the ice buckets, K) ship-based laboratory work, L) M. polaris cultures used in cell addition experiments.

III. Phytooptics: Phytoplankton and dissolved organic matter from highly resolved optical measurements

Active and passive bio-optical measurements for the survey of the underwater light field, specific light attenuation, particle and phytoplankton composition and distribution, have been performed continuously on the surface water but also in the profile during selected CTD stations:

1. Continuous measurements of inherent optical properties (IOPs) with a hyperspectral spectrophotometer: the HyperSpecBox mounted with an *in-situ* spectrophotometer (ACS; Seabird) has been operated in flow-through mode to obtain total and particulate matter attenuation and absorption spectra of surface water (Fig. 3.3). The instrument was connected to a seawater supply taking surface ocean water. A flow-control with a time programmed filter was mounted to the ACS to allow alternating measurements of the total particle absorption and the CDOM absorption of the sea water. Flow-control and debubbler-system ensured water flow through the instrument with no air bubbles. The HyperSpecBox was operated on the seawater supply at the Nasslabor-1, with seawater pumped at Kastenkiel via Spargel with the membrane pump through the Teflon tubing in order to deliver living phytoplankton cells continuously throughout the cruise, also within the ice. However, we have faced big challenges to operate the HyperSpecBox in the dense ice area, because slushy ice was constantly pumped into the pipe and caused pump damage a few times due to too high pressure. Regular water

flow could not be always assured in the ice-covered area. The HyperSpecBox was running during the whole expedition from 18:00 UTC on 4 September 2025 until 10:30 UTC 23 October 2025, except the dock time in Longyearbyen from 17–18 October 2025.

2. Light profiler: Consisting of an ACS instrument mounted on a steel frame together with a depth sensor and a set of hyperspectral radiometers (Ramses sensors from TRIOS), the light profiler has been operated during selected CTD stations during PS150. The profiler has been lowered down to maximal 150 m with a continuous speed of 0.1 m/s or during daylight with additionally stops at 2, 5, 8, 10, 15, 20, 25, 30, 40, 50, 60, 70, 85 and 100 m to allow a better collection of radiometric data. The Apparent Optical Properties of water (AOPs) (surface reflectance and light attenuation through the water column) will be estimated based on downwelling and upwelling irradiance measurements in the surface water profile (down to the 0.1% light depth) from the radiometers calibrated for the incident sunlight with measurements of a radiometer on deck (Fig. 3.4). The ACS measured inherent optical properties in the water profile have also been recorded. During PS150, we have deployed the light profiler at 29 CTD stations (Tab. 3.3, Fig. 3.5) with 27 successful deployments and 2 unsuccessful ones due to failure of the datalogger.
3. Samples for determination of phytoplankton pigment concentrations and composition, IOPs (absorption) were taken a 3-hourly interval from the underway-sampling system during steaming, and from Niskin bottles at 5 depths (surface, Chla-max or 25 m if no Chla-max presented, below Chla max or 35 m, 50 m and 100 m) during selected CTD-stations. Water samples are filtered on board immediately after sampling and the filters for phytoplankton pigments were thermally shocked in liquid nitrogen and were then stored at -80°C. Pigments will be analyzed by High Performance Liquid Chromatography Technique (HPLC) at AWI. Water samples for CDOM absorption analysis were filtered through 0.2 µm filters and stored on board. CDOM will be measured with a 2.5-m path length liquid waveguide capillary cell system (LWCC, WPI) following Lefering et al. (2017) at AWI. Particulate and phytoplankton absorption coefficients (PABs) are determined with the quantitative filter techniques using sample filtered onto glass-fiber filters QFT-ICAM (also stored on board) and will be measured with a portable QFT integrating cavity setup following Röttgers et al. (2016) at AWI. During the PS150, we have collected in total 264 underway samples (Fig. 3.5), and 155 CTD samples at 31 CTD stations across 10 sections (Tab. 3.3, Fig. 3.5).

Fig. 3.3: HyperSpecBox running in the Nasslabor-1

Fig. 3.4: RAMES radiometer sensor mounted above Deck A to measure the sunlight irradiance (left) and the light profiler (right)

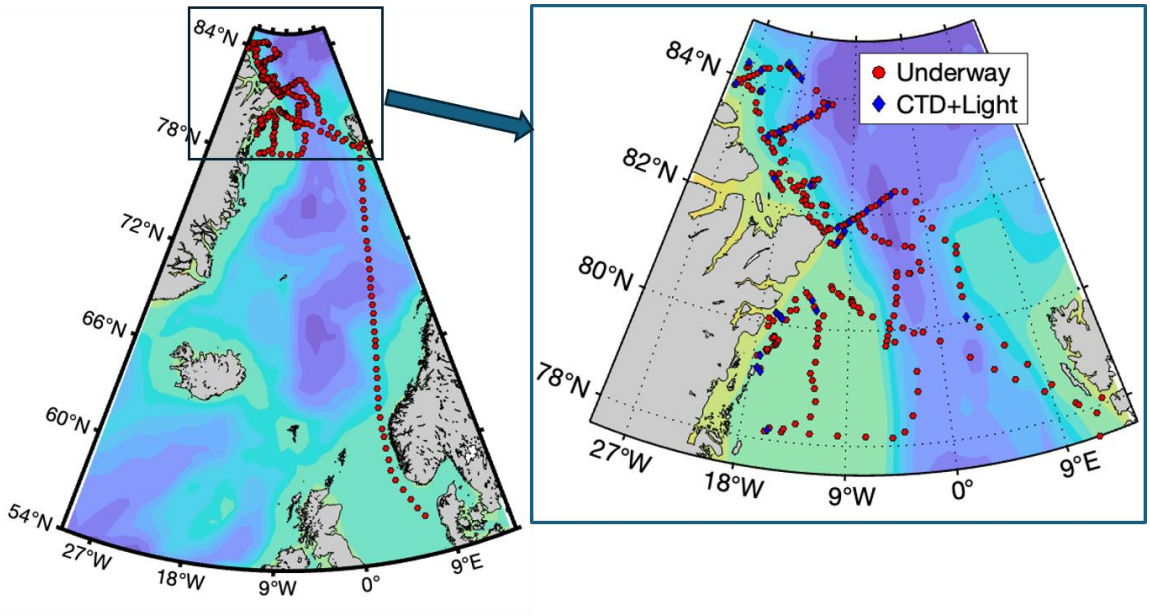

Fig. 3.5: Maps of underway and CTD sampling stations with light profiler deployments (refer to Tab. 3.3).

Tab. 3.3: List of stations with CTD water sampling and light profiler deployments

Station no.	Latitude (°)	Longitude (°)	Sampling parameter			Light Profiler	Region
			HPLC	PABs	CDOM		
001-1	80.0835	2.9302	X	X	X	X	Test station Yarmak
006-1	82.3464	-3.9638	X	X	X	X	Flade 1
009-4	82.2147	-5.4795	X	X	X	X	Flade 1
012-3	82.0770	-7.1313	X	X	X	X	Flade 1
016-1	81.8870	-9.2244	X	X	X	X	Flade 1
025-1	81.7209	-9.7763	X	X	X	X	Flade 1
030-1	81.5213	-10.5365	X	X	X	X	Flade
039-1	82.4800	-19.4047	X	X	X	X	Independence Mouth
044-2	83.1549	-19.3928				X	Ice Station1, Wandel
046-1	83.1646	-21.5737	X	X	X	X	Wandel
050-1	83.2781	-20.1169	X	X	X		Wandel
059-7	83.4319	-17.8545	X	X	X	X	Wandel
063-1	83.6637	-15.7332	X	X	X	XX	Wandel (2 x profiler)
067-1	83.8563	-13.4211	X	X	X	X	Wandel
070-1	84.2568	-18.3715	X	X	X	X	Morris Jesup Rise (MJR)
074-1	84.3691	-19.9145	X	X	X	X	Morris Jesup Rise
078-3	84.4710	-21.0414	X	X	X	X	Ice Station2 (MJR)
079-1	84.2227	-25.3978	X	X	X	X	Cape Morris Jesup
085-1	83.8581	-28.6707	X	X	X	X	Cape Morris Jesup
089-7	84.2909	-27.8439	X	X	X	X	Towards Lincoln

Station no.	Latitude (°)	Longitude (°)	Sampling parameter			Light Profiler	Region
090-3	83.8882	-24.2402	X	X	X	X	Ice Station3, Towards Lincoln
093-5	82.4629	-14.5054	X	X	X	X	transit
100-3	81.7753	-10.6468	X	X	X	X	Transit
118-1	78.1744	-15.7218	X	X	X	X	Ile de France
120-1	80.3114	-12.3304	X	X	X	X	Flade Shelf
123-6	80.4765	-12.9111	X	X	X	X	Flade Shelf
127-3	80.1369	-16.0109	X	X	X	X	Ice Station4, Westwind Trough
128-1	80.1147	-15.7323	X	X	X	X	Holm
131-1	80.1945	-16.4476	X	X	X	X	Holm
132-1	79.4237	-17.3035	X	X	X		79NG
133-1	79.2088	-17.4496	X	X	X	X	Norske Trough
135-7	79.1576	-17.0994	X	X	X		Norske Trough

IV. eDNA based analysis of Arctic eukaryotic and prokaryotic microbial communities

To assess eukaryotic microbial biodiversity along the sections, water samples were collected at 5 depths between the surface and 100 m using the CTD rosette at selected stations (see Tab. 3.4). For eDNA analysis, 2 L of water from each depth were sequentially filtered through 10 µm, 3 µm and 0.4 µm filters. For Chla biomass, 2 L from each depth were sequentially filtered through 3 µm and 0.4 µm filters. In addition, CTD samples (5 L) at each depth for particulate organic carbon and nitrogen (POC, PON) have been collected and filtered; 0.5 – 1.5 L samples were also taken for phytoplankton fixing which will be further analysed at AWI (details see subsection VI).

To obtain high-resolution surface eDNA samples (~10 m), the underway sampling system AUTOFIM filtered 1.5 L of seawater through a 0.4 µm filter approximately every 3 hours (Fig. 3.6). Unfortunately, due to a technical problem that could not be resolved on board, AUTOFIM stopped working on 29 September.

Tab. 3.4: List of stations where CTD rosette samples were taken for different parameters.

Station no.	eDNA	Chla	POC/N	bPSI	Microscopy
PS150_6_1	x	x	x	x	x
PS150_7_1			x		
PS150_8_4			x		
PS150_9_1	x	x	x	x	x
PS150_12_3	x	x	x	x	x
PS150_16_1	x	x	x	x	x
PS150_25_1	x	x	x	x	x
PS150_30_1	x	x	x	x	x
PS150_37_1	x	x	x	x	x
PS150_39_1	x	x	x	x	x
PS150_46_1	x	x	x	x	x
PS150_50_1	x	x	x	x	x

Station no.	eDNA	Chla	POC/N	bPSI	Microscopy
PS150_59_7	x	x	x	x	x
PS150_63_1	x	x	x	x	x
PS150_61_1			x		
PS150_67_1	x	x	x	x	x
PS150_70_1	x	x	x	x	x
PS150_72_1	x	x	x	x	x
PS150_74_1	x	x	x	x	x
PS150_79_1	x	x	x	x	x
PS150_80_1			x		
PS150_85_1	x	x	x	x	x
PS150_89_7	x	x	x	x	x
PS150_93_5	x	x	x	x	x
PS150_100_2	x	x	x	x	x
PS150_113_1			x		
PS150_118_1	x	x	x	x	x
PS150_120_1	x	x	x	x	x
PS150_123_1	x	x	x	x	x
PS150_128_1	x	x	x	x	x
PS150_131_1	x	x	x	x	x
PS150_132_1	x	x	x	x	x
PS150_133_1	x	x	x	x	x
PS150_135_7	x	x	x	x	x

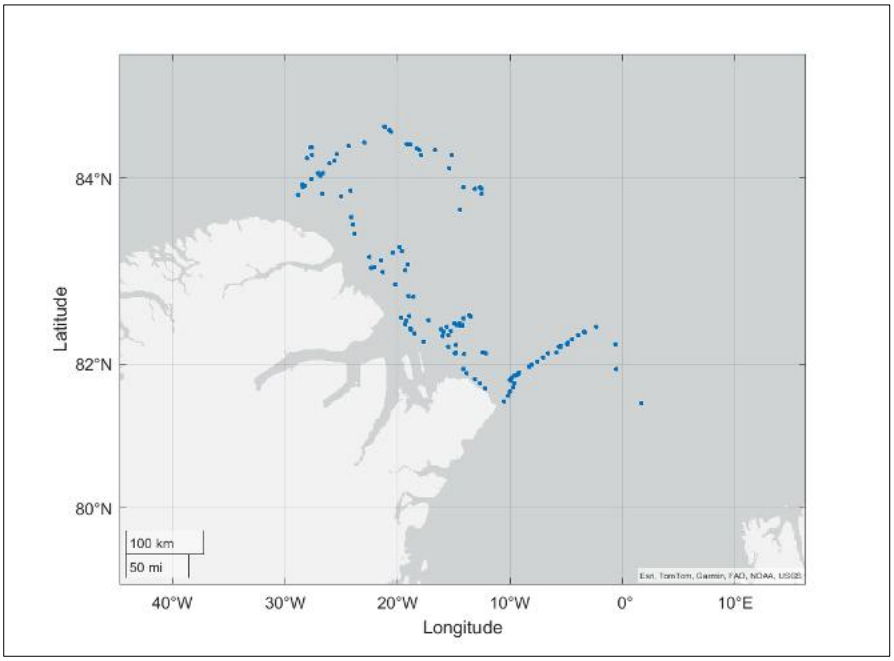

Fig. 3.6: AUTOFIM sample locations northeast of Greenland between 6 September and 29 September

V. ARJEL: Zooplankton

The working area during PS150 consisted of 26 pelagic (water column sampling; Tab. 3.5) and 7 sea ice stations (under-ice water sampling; Tab. 3.6) in the Wandel Sea, Independence Fjord, and 79°N Glacier areas of Northeast Greenland. We deployed plankton nets (MultiNet midi and Bongo nets, Fig. 3.7 A-B and Fig. 3.8), collected water-derived (CTD rosette, hand-Niskin, in-water filtration and passive sampling, Fig. 3.7 C-D and Fig. 3.8) and sediment-derived (MUC cores) eDNA samples and conducted optical surveys of zooplankton (see Tab. 3.7 for UVP5 deployments at 71 stations).

Fig. 3.7: *Gear deployed by the ARJEL team on PS150; (A) Bongo net, (B) Multi-net, (C) PK 1 pump sampler, (D) Yellow submarine sampler. Photo credit: Rebecca Gorniak*

Tab. 3.5: Pelagic and benthic sampling by the ARJEL group onboard PS150

Area	Station	Gear deployed	Maximum sampling depth [m]
Flade_1	008_01	CTD (eDNA)*	3,100
	008_03	MultiNet (zooplankton)	1,500
	008_04	CTD (eDNA)	400
	013_01	CTD (eDNA)*	400
	016_02	MultiNet (zooplankton)	500
	018_02	MultiNet (zooplankton)	1,500
	024_01	CTD (eDNA)	400
	024_04	MultiNet (zooplankton)	1,000
	029_01	CTD (eDNA)*	353
	029_03	MultiNet (zooplankton)	200
	029_05	MUC (eDNA)	234
Independence_Mouth	037_01	CTD (eDNA)*	100
	039_01	CTD (eDNA)*	100
Wandel	046_01	CTD (eDNA)*	200
	046_05	MultiNet (zooplankton)	200
	050_04	MultiNet (zooplankton)	1,000
	050_06	CTD (eDNA)*	400
	058_01	CTD (eDNA)*	400
	058_02	MultiNet (zooplankton)	1,500

Area	Station	Gear deployed	Maximum sampling depth [m]
	063_01	CTD (eDNA)	400
	063_05	MultiNet (zooplankton)	1,500
	064_02	Bongo Net (zooplankton)	-
	068_02	MUC (eDNA)	3,860
	070_04	Bongo Net (zooplankton)	-
Morris_Jesup_Rise	072_02	MultiNet (zooplankton)	1,500
Cape_Morris_Jesup	079_05	Bongo Net (zooplankton)	-
	080_01	CTD (eDNA)*	400
	080_03	MultiNet (zooplankton)	600
	083_01	CTD (eDNA)*	200
	083_02	MultiNet (zooplankton)	300
	089_01	CTD (eDNA)*	400
	089_03	MultiNet (zooplankton)	1,000
Ile_de_France	118_04	CTD (eDNA)*	200
Westwind_Trough	123_01	CTD (eDNA)*	269
	123_05	MultiNet (zooplankton)	350
	126_02	MUC (eDNA)	320
Holm	127_03	CTD (eDNA)	200
	129_03	MultiNet (zooplankton)	250
79NG	132_01	CTD (eDNA)*	401
	132_02	MultiNet (zooplankton)	350
	132_03	MUC (eDNA)	413
Norske_Trough	135_04	MultiNet (zooplankton)	350
	135_07	CTD (eDNA)*	200
UVP also deployed			

Tab. 3.6: Sea ice-based sampling by the ARJEL team onboard PS150

Station type	Station	Gear deployed	Depth
Ice station 1	047_01	Hand Niskin (eDNA)	0m
		PK1 Stick sampler (eDNA)	0m
		Yellow Submarine water sampler (eDNA)	0m
Ice station 2	78_01	Hand Niskin (eDNA)	0m
		PK1 Stick sampler (eDNA)	0m
		Zodiac and Yellow submarine (eDNA)	Surface tow
Ice station 3	90_1	Hand Niskin (eDNA)	0m
		PK1 Stick sampler (eDNA)	0m
		Yellow Submarine water sampler (eDNA)	0m
		Zodiac and Yellow submarine (eDNA)	Surface tow
Ice station 4	127_01	Hand Niskin (eDNA)	0m, 5m
		PK1 Stick sampler (eDNA)	0m (x3)
		Yellow Submarine water sampler (eDNA)	0m, 5m

Station type	Station	Gear deployed	Depth
		Zodiac and Yellow submarine (eDNA)	Surface tow
Helicopter 1	IF_01	Hand Niskin (eDNA)	0m
		PK1 Stick sampler (eDNA)	0m
Helicopter 2	IF_03	Hand Niskin (eDNA)	0m
		PK1 Stick sampler (eDNA)	0m
Helicopter 3	H_03	Hand Niskin (eDNA)	0m
		PK1 Stick sampler (eDNA)	0m

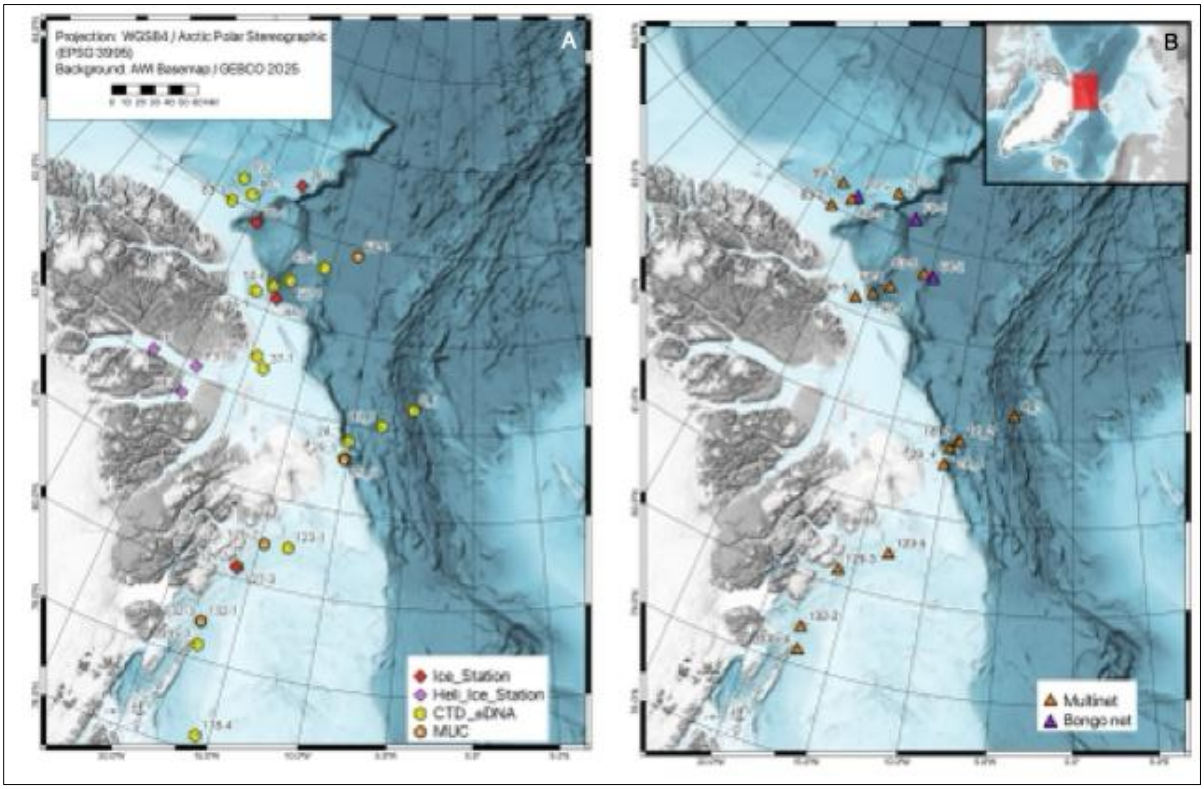

Fig. 3.8: Map of (A) eDNA sampling at pelagic and ice stations and (B) net-based sampling during the ARJEL program on PS150

Tab. 3.7: UVP5 stations onboard PS150

Area	Station	Maximum_cast_depth [m]
Flade_1	006_01	3292
	008_01	3136
	012_03	3343
	013_01	3404
	014_01	3121
	015_01	2790
	018_01	2337
	020_01	2294
	029_01	351
	030_01	150
	031_01	74
	032_01	55
Independence_Mouth	036_01	120
	037_01	380
	038_01	511
	039_01	466
	040_01	122
Wandel	046_01	224
	047_01	205
	048_01	237
	050_06	1159
	052_01	1931
	054_01	2929
	056_01	3106
	058_01	3122
	061_01	3235
	064_01	3534
	065_01	3559
	065_02	3563
Morris_Jesup_Rise	070_01	3156
	071_01	3335
	072_01	3320
	074_01	2448
	075_01	789
	079_01	624

Area	Station	Maximum_cast_depth [m]
Cape_Morris_Jesup	080_01	616
	081_01	597
	082_01	545
	083_01	379
	085_01	84
	089_01	1061
	089_07	1015
Independence_Shelfbreak	093_05	734
	094_01	1955
	095_01	
	095_01	2190
	096_01	187
	097_01	161
Flade_2	105_01	2500
	106_01	2705
	113_01	4271
Ile_de_France	117_01	252
	118_01	357
	118_04	373
	119_01	407
Westwind_Trough	120_01	172
	121_01	211
	122_01	259
	123_01	278
	123_06	282
	124_01	259
	125_01	135
	126_01	320
Holm	128_01	374
	129_01	324
	130_01	154
	131_01	146
79NG	132_01	413
Norske_Trough	133_01	153
	134_02	369
	135_02	396
	135_07	397

VI. Plankton imaging

Phytoplankton*:* Phytoplankton samples were taken from the CTD-Rosette (surface, above the Chla maximum (Chla-max), Chla-max and below Chla-max) and fixed in Lugol iodine solution as well as in Formalin. These samples will be later analysed for phytoplankton abundance and species composition in the home laboratories after the cruise. In addition, live samples were obtained with oblique phytoplankton net hauls (20 µm mesh size), conducted by hand from approx. 20 m to the surface, at 31 stations (Tab. 3.7, Fig. 3.9). These net samples were analyzed immediately after each haul, using the PlanktoScope, a low-cost imaging device for high throughput sample analysis (Fig. 3.10). The resulting images and meta data sets were uploaded to a web-based image analysis platform (EcoTaxa: https://ecotaxa.obs-vlfr.fr/) where the object on each image is currently being identified and taxonomically categorized. The net samples were also analyzed semi-quantitatively using inverted microscopy onboard for comparison with the PlanktoScope results.

Mesozooplankton: The composition of the mesoplankton community and its distribution in the water column were studied using two devices. The MultiNet midi (Hydrobios, Germany) was deployed to analyze the large-scale vertical distribution of the zooplankton in the water column. It was equipped with five nets with a mesh size of 150 µm and collected samples from five depth intervals (1,500-1,000-500-200-50-0 m) at 20 stations (Tab. 3.8, Fig. 3.9). The samples were immediately preserved in hexamethylenetetramine-buffered formalin. These samples will be analysed using the imaging system ZooScan in the AWI laboratories. The ZooScan procedure yield images presenting single organisms; the respective meta data are connected to each image. All images will be uploaded to EcoTaxa, and the zooplankton organisms will be determined to the lowest possible taxonomic level. The resulting data will yield abundances and biomasses at high taxonomical resolution. In addition, the UVP5 was used to determine the distribution patterns of zooplankton taxa in relation to environmental conditions at high vertical resolution. The UVP5 was mounted on the water rosette with a CTD, and continuously took images during the downcast at a rate of approx. 20 frames sec^{-1}. It was, thus, operated during 71 CTD casts from the surface to the sea floor (Tab. 3.7). The UVP5 detects grey-scales and saves images of all objects >200 µm. At AWI, these images will also be uploaded to EcoTaxa, and each object on an image will be categorized. The resulting data will then allow to investigate small scale zooplankton distribution patterns in relation to hydrographical parameters such as temperature and salinity and, thus, water masses.

Tab. 3.8: The list of sampling stations for mesozooplankton and phytoplankton studies

Date	Station	Lat	Lon	Ship_log	Hand Net	MultiNet
06.09.2025	4	81° 17.735' N	003° 01.922' E	PS150_4_2	X	
07.09.2025	5	82° 22.851' N	003° 26.102' W	PS150_5_2		X
07.09.2025	6	82° 20.977' N	003° 59.115' W	PS150_6_3	X	
08.09.2025	9	82° 12.697' N	005° 34.574' W	PS150_9_3	X	
08.09.2025	11	82° 07.636' N	006° 35.986' W	PS150_11_2		X
08.09.2025	12	82° 04.616' N	007° 08.228' W	PS150_12_2	X	
09.09.2025	16	81° 53.221' N	009° 13.467' W	PS150_16_4	X	
10.09.2025	24	81° 47.786' N	010° 01.543' W	PS150_24_3		X
10.09.2025	25	81° 43.427' N	009° 47.240' W	PS150_25_3	X	
10.09.2025	29	81° 35.777' N	010° 11.666' W	PS150_29_4		X
10.09.2025	30	81° 31.380' N	010° 32.737' W	PS150_30_3	X	
12.09.2025	38	82° 25.568' N	018° 55.550' W	PS150_38_2		X
12.09.2025	39	82° 28.787' N	019° 24.265' W	PS150_39_3	X	

Date	Station	Lat	Lon	Ship_log	Hand Net	MultiNet
13.09.2025	42	82° 24.724' N	018° 52.128' W	PS150_42_ICE1	X	
14.09.2025	45	83° 06.450' N	022° 21.985' W	PS150_45_2		X
14.09.2025	46	83° 09.910' N	021° 34.702' W	PS150_46_3	X	
14.09.2025	50	83° 17.377' N	020° 07.564' W	PS150_50_2	X	X
16.09.2025	59	83° 26.072' N	017° 52.092' W	PS150_59_2	X	X
17.09.2025	63	83° 39.875' N	015° 43.915' W	PS150_63_3	X	
18.09.2025	66	83° 48.522' N	013° 50.955' W	PS150_66_2		X
18.09.2025	67	83° 51.506' N	013° 25.727' W	PS150_67_2	X	
19.09.2025	70	84° 15.543' N	018° 22.031' W	PS150_70_2	X	
20.09.2025	74	84° 22.197' N	019° 54.685' W	PS150_74_3	X	
21.09.2025	77	84° 26.074' N	021° 08.812' W	PS150_77_2		X
21.09.2025	78	84° 28.258' N	021° 02.380' W	PS150_78_ICE2	X	
22.09.2025	79	84° 13.341' N	025° 23.648' W	PS150_79_4	X	
22.09.2025	80	84° 09.185' N	025° 53.738' W	PS150_80_2		X
23.09.2025	85	83° 51.485' N	028° 40.215' W	PS150_85_4	X	
23.09.2025	85	83° 51.478' N	028° 41.268' W	PS150_85_5		X
24.09.2025	89	84° 16.550' N	027° 32.065' W	PS150_89_6	X	X
25.09.2025	90	83° 53.199' N	024° 14.032' W	PS150_90_ICE3	X	
27.09.2025	93	82° 30.124' N	014° 37.232' W	PS150_93_2	X	
28.09.2025	95	82° 33.917' N	013° 34.529' W	PS150_95_2		X
30.09.2025	100	81° 46.545' N	010° 39.061' W	PS150_100_4	X	
06.10.2025	118	78° 09.900' N	015° 45.590' W	PS150_118_2	X	
09.10.2025	120	80° 18.748' N	012° 19.953' W	PS150_120_2	X	
09.10.2025	123	80° 29.070' N	012° 59.050' W	PS150_123_2	X	X
10.10.2025	125	80° 36.443' N	013° 35.561' W	PS150_125_2		X
11.10.2025	128	80° 06.890' N	015° 43.909' W	PS150_128_2	X	
11.10.2025	129	80° 09.774' N	016° 01.153' W	PS150_129_2		X
11.10.2025	131	80° 11.621' N	016° 27.092' W	PS150_131_3	X	X
12.10.2025	133	79° 12.534' N	017° 26.965' W	PS150_133_3	X	X
12.10.2025	135	79° 10.143' N	017° 04.801' W	PS150_135_5	X	X

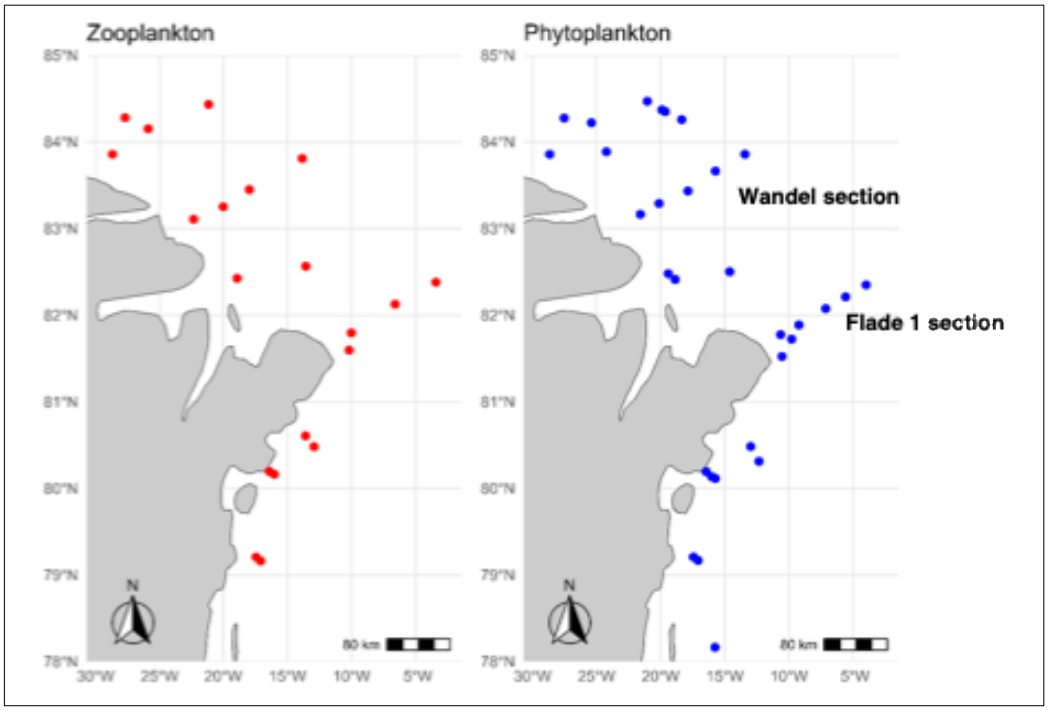

Fig. 3.9: The maps of NE Greenland showing Zooplankton (red) and Phytoplankton (blue) sampling stations.

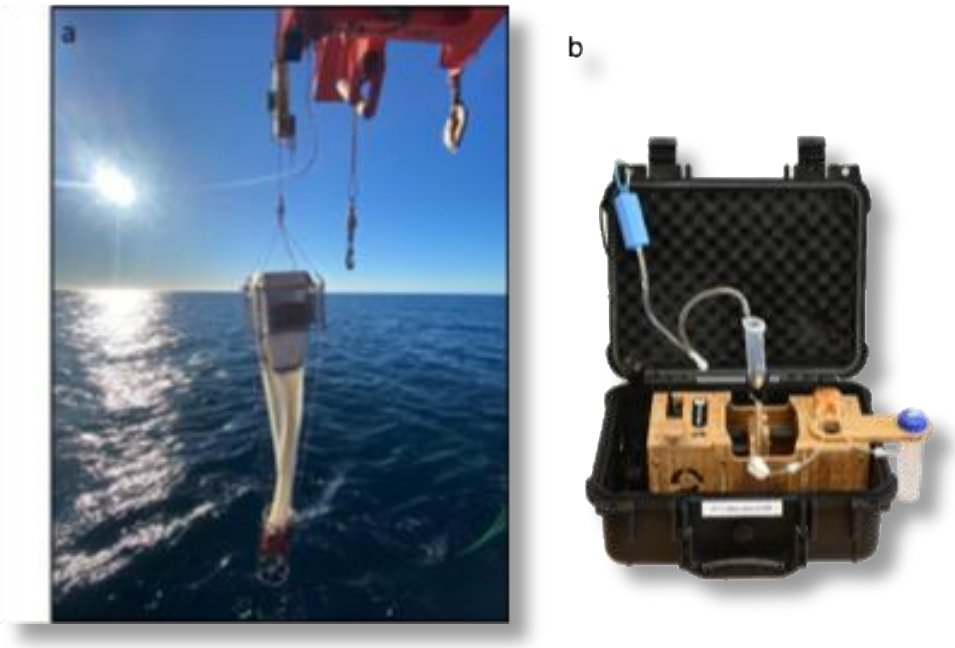

Fig. 3.10: The MultiNet deployment (a) and the PlanktoScope (b)

VII. Microbial communities and biogeochemistry (MB)

To investigate the effects of global change and anthropogenic pollution on microbial communities and biogeochemical processes in the Arctic Ocean, the MB team continued to monitor the concentrations of dissolved organic carbon and nitrogen, as well as dissolved amino acids and carbohydrates. Furthermore, we continued to assess cell abundances via flow cytometry to determine the distribution of phytoplankton, bacteria, and viruses. Additionally, during PS150, we collected microplastic particles (> 300 µm) at selected stations from the surface water via the underway system and analytical sieves. The analysis of the biodiversity and function of plastic-associated microbes as compared to their free-living counterparts is feasible, using 16S rRNA gene amplicon sequencing, metagenomics, and metatranscriptomics. A special focus is given on potential pathogens and their resistance mechanisms. This will allow estimating the potential risks of microplastics to human and ecosystem health. All parameters except microplastic particles were sampled from the water column at 15 stations using a CTD/rosette sampler (Fig. 3.11 and Tab. 3.9). At selected stations, samples for dissolved amino acids and carbohydrate analyses were collected to cover a representative depth distribution to investigate the composition of dissolved organic matter across depth. At all stations, all parameters were sampled at Surface, Chla-max, 50 m, and 100 m. DOM, phytoplankton, bacteria and viruses were also sampled at 200, 500, 750, 1000, 1250 and 2000 m at two selected deep stations. These samples were preserved or frozen at 4°C, -20°C or -80°C and will be analysed in the laboratory at GEOMAR:

- Dissolved organic carbon (DOC)
- Total dissolved nitrogen (TDN)
- Dissolved combined carbohydrates (dCCHO)
- Dissolved hydrolysable amino acids (dHAA)
- Phytoplankton, bacterial, and viral abundance
- Microplastic particles (> 300 µm)
- DNA/RNA

Incubation experiments with environmentally relevant polymers were carried out. Previous sampling attempts of naturally occurring microplastic particles in the Arctic Ocean, drawing water from the ship's "Spargel", have proven to be difficult, as no particles were found during previous cruises (PS143/1 and 2). Therefore, we conducted an incubation experiment with surface water (10 m depth) collected from the CTD rosette. During PS150, we set up the same experiment, using a total of 27 glass jars (1.8 L), filled with surface water, and incubated seven different polymer types in triplicate at 4°C. The experiment was set up during PS150 and was shipped at 4°C to GEOMAR, where biofilms will be collected and DNA and RNA extracted. To investigate the biodiversity and function of plastic-associated bacteria, focusing on potential pathogens and their resistome, we will utilize 16S rRNA gene amplicon sequencing, metagenomics, and metatranscriptomics.

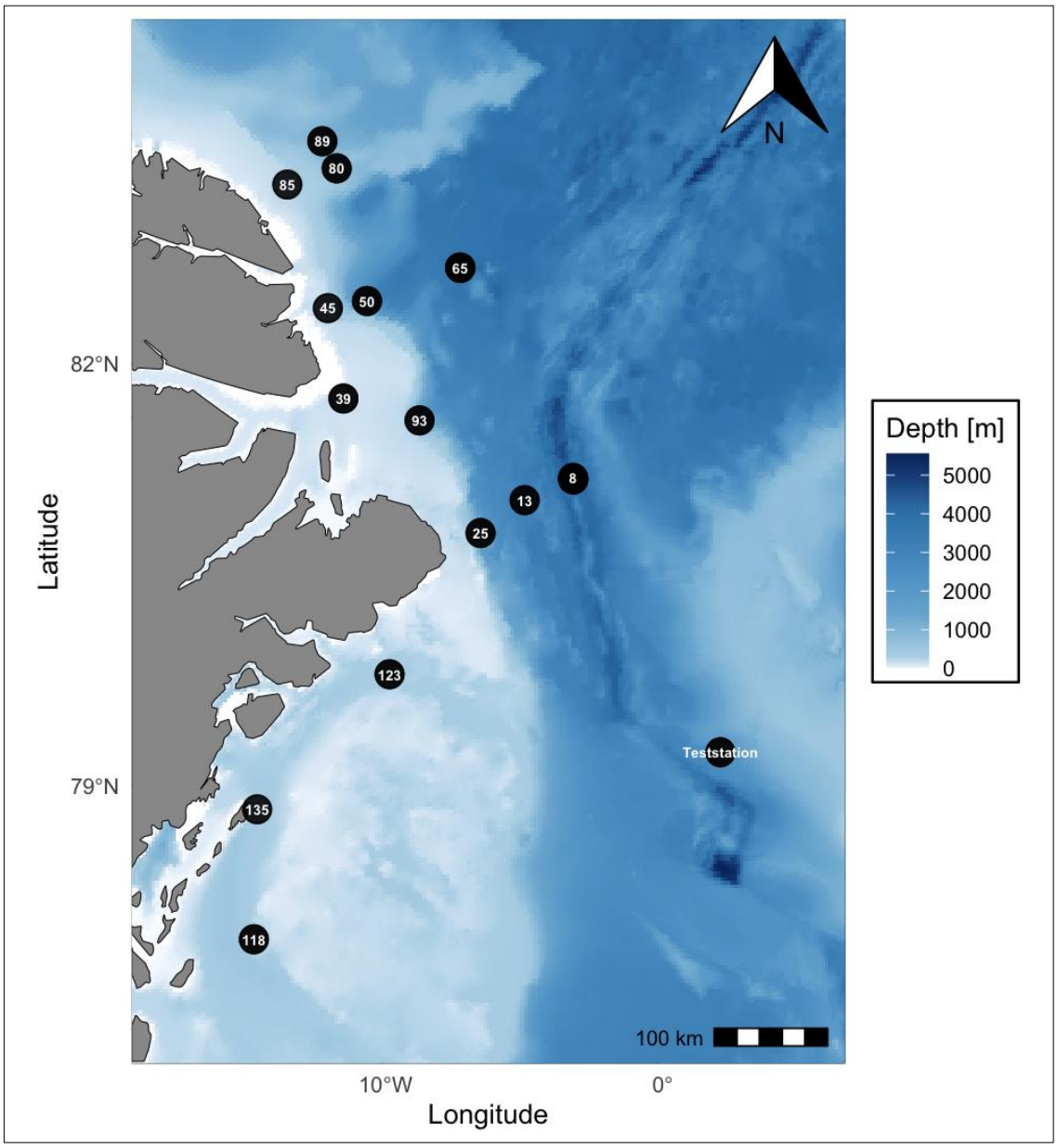

Fig. 3.11: Map of all sampled stations for microbiological and biogeochemical variables during PS150

Tab. 3.9: List of all stations sampled for microbiological and biogeochemical variables during PS150

Station	Latitude	Longitude	Bot-tom depth (m)	Date (UTC)	Time on deck (UTC)	DOC/ DCHO/ DHAA	BA/ PA/ VA	DNA/ RNA
8	82°14,769'N	004°56,038'W	2797.8	9/7/25	17:26:26	X X	X	X X
13	82°01,679'N	007°35,515'W	3403.1	9/9/25	0:32:46	X X	X	X X
25	81°42,994'N	009°45,618'W	578.9	9/10/25	10:28:41	X X	X	X X
39	82°28,800'N	019°24,181'W	465.2	9/12/25	14:31:02	X X	X	X X
45	83°06,467'N	022°22,067'W	221.0	9/14/25	11:38:53	X X	X	X X
50	83°16,433'N	020°05,586'W	1115.0	9/15/25	0:21:04	X X	X	X X
65	83°44,969'N	014°31,928'W	3561.8	9/17/25	18:09:45	X X	X	X X
80	84°09,182'N	025°53,460'W	618.4	9/22/25	13:42:57	X X	X	X X
85	83°51,481'N	028°40,430'W	86.8	9/23/25	12:42:00	X X	X	X X
89	84°17,645'N	027°52,679'W	1009.4	9/24/25	11:20:14	X X	X	X X
93	82°29,439'N	014°35,145'W	1188.5	9/27/25	17:20:19	X X	X	X X
118	78°10,466'N	015°43,724'W	356.5	10/6/25	23:42:37	X X	X	X X
123	80°28,480'N	012°54,648'W	277.8	10/9/25	19:01:54	X X	X	X X
129	80°09,695'N	016,01,528'W	323.6	10/11/25	3:02:43	X X	X	X X
135	79°10,091'N	017°04,825'W	396.7	10/12/25	20:23:36	X X	X	X X

Preliminary (expected) results

The role of picophytoplankton in the carbon cycle

The results are expected to provide a better understanding of i) the size distribution of primary production and the degree of carbon exudation from the cells, ii) the role of picophytoplankton in the autumn carbon cycle, iii) connections between the sympagic and pelagic phytoplankton community structure and function during sea ice formation, and iv) the use of EPS by sympagic microalgae during freeze-up. The results will be published in at least two peer-reviewed scientific articles and presented at international conferences. The collected samples are estimated to be analysed within two years of the end of the expedition.

Connectivity between sea ice and the upper pelagic during freeze-up

The results are expected to provide a better understanding of i) sympagic and pelagic phytoplankton community structure and abundance during the freeze-up period across various sea ice types, including multi-year ice and newly formed ice ii) the nutritional value of the sympagic and pelagic phytoplankton communities as a whole, and of key taxa at a species-specific resolution, across various sea-ice types, ii) the role of EPS in sympagic community colonisation during the freeze-up period. The results will be published in at least two peer-reviewed scientific articles and presented at international conferences. The collected samples are estimated to be analysed within two years after the end of the expedition.

PhytoOptics: phytoplankton biomass from highly resolved optical measurements

The HyperSpecBox data have been preliminarily processed on board to obtain the absorption spectra of particles binned to 1-min temporal resolution from the raw measurements with a 4 Hz frequency. They were then used to derive the phytoplankton biomass based on the

absorption peak line height at 676 nm following the coefficients determined by Bracher et al. (2025) for the measurements collected in the Fram Strait HAUSGARTEN expeditions. In total 48-day (out of 50 expedition days) measurements were collected with 2-day gap from 15 October to 17 October due to the broken pump and a delayed operation of data recording. Absorption spectra and time series of the absorption line height in Figure 3.12 have shown high variability in phytoplankton biomass along the cruise track, which has been reflected in the derived Chla along the cruise track (Fig. 3.13). Much higher biomass indicating the autumn bloom has been identified in the beginning of the expedition from Svalbard to the central Fram Strait. Very low surface Chla has been identified in the Northeast Greenland due to dense ice cover where nutrients and especially light were heavily limited, however slightly higher Chla has been found in the North and below 79°N where open water and thin ice in the beginning of freeze-up period were often seen in these areas. Phytoplankton biomass was much lower on the way back to Svalbard compared to that in the first few days of the expedition. Reduced Chla has been also seen along the cruise track back to Bremerhaven in mid-October which indicates the ending time of blooms in late autumn mainly due to less light availability in such high latitudes. Further refinements in the data processing are still necessary, as thresholds and criterion used in the processing chain should be carefully modified to fit the measuring conditions of this expedition.

Samples and filters for phytoplankton pigments, CDOM and phytoplankton absorption from both underway (264 for each parameter) and 31 CTD depths (155 for each parameter) will be transported and analyzed at AWI in the following months. Optical profiling data successfully recorded at 27 out of 29 light profiler deployments will be processed soon at AWI, including 27 valid casts of ACS absorption profiles and ~20 valid underwater radiometric profiles at stations where light could still penetrate into the water column though signals might be already weak due to low sun elevation during the expedition period.

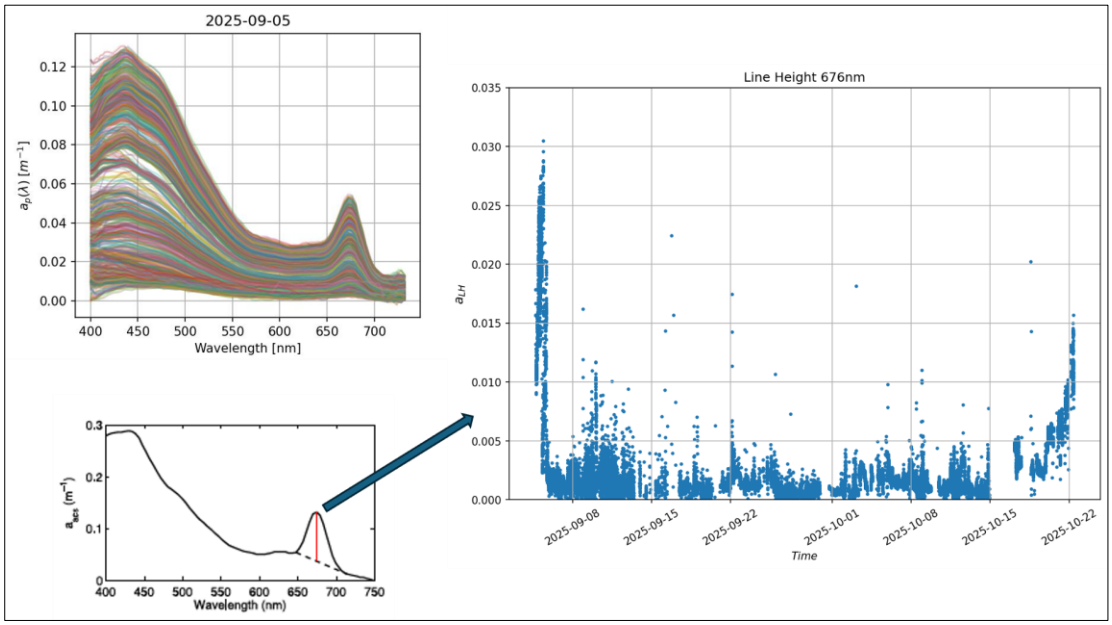

Fig. 3.12: Processed 1-min binned absorption spectra of particles from HyperSpecBox (example spectra on 5 September 2025) and time series of the spectral absorption peak line height at 676 nm that can be used for Chla concentration estimation

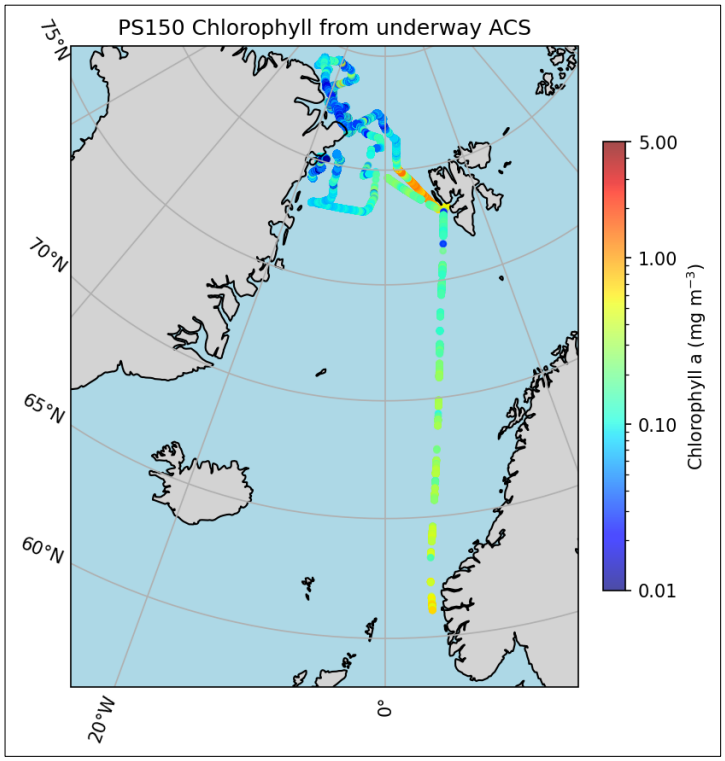

Fig. 3.13: HyperSpecBox derived surface Chla concentrations during the entire expedition (4 September – 23 October 2025).

ARJEL: Zooplankton

Net- and UVP-based zooplankton surveys: Species composition and abundance information from net and UVP data will be linked with oceanographic features and sea ice patterns to identify key drivers of distribution abundance and community composition. The results on diversity and abundances from net catches will also be compared with those obtained with eDNA analyses and optical datasets. We sampled zooplankton from the surface to a maximum depth of 1,500 m. The Multi-net midi (MN, Hydrobios), equipped with five 150 µm nets, was used for depth stratified casts to a maximum depth of 1,500m at a total of 17 stations (Tab. 3.5, Fig. 3.8 B). Oblique surface tows were conducted with the Bongo nets, equipped with a 300 µm and a 500µm net and a maximum line length of 500m, at 3 stations in total (Tab. 3.5, Fig 3.8 B). All net catches were sorted at 4°C on board to the highest taxonomic resolution possible and zooplankton specimens preserved at -80°C or in 96% ethanol. They will be further analysed with both morphological and molecular techniques in the home laboratory. Abundances will be calculated from the MN catches based on the number of individuals per volume of water covered by the depth-stratified MN hauls.

The obtained UVP images will be screened with custom software to extract objects larger than 100 pixels (~0.5 mm; Stemmann et al. 2008). Morphological descriptors (e.g., size) will be calculated using ZooProcess (Gorsky et al. 2010; Vilgrain et al. 2021), and all images, metadata, and descriptors will be archived in EcoTaxa (https://ecotaxa.obs-vlfr.fr/ ; Picheral et al. 2017).

eDNA/eRNA metabarcoding of metazoans: Environmental DNA (eDNA) from water and sediment samples will be processed and analysed in the home lab following Murray et al. (2024, 2025). Metabarcoding will primarily use the mitochondrial COI marker, supplemented by 18S rRNA and 16S where needed, targeting both eukaryotes and metazoans. Diversity indices and community composition will be assessed across depth, sea-ice conditions, and hydrographic gradients, with emphasis on pelagic and sub-ice metazoan communities. Resulting eDNA datasets will be linked with net and optical observations for validation, providing a comprehensive view of biodiversity patterns and community structure in relation to environmental variability.

DNA barcoding and phylogeography of zooplankton specimens: A subset of zooplankton specimens will be genetically barcoded using taxon-specific markers (COI, 16S, 18S rDNA) to expand public reference databases and to conduct phylogeographic analyses of potential indicator species. For widespread taxa, new sequences will be integrated with data from prior Arctic expeditions–HE560 (2020) and HE605 (2022) in Svalbard fjords, PS122 (MOSAiC) in the central Arctic, and PS131 near Northeast Greenland–to support phylogeographic analyses of key Arctic Zooplankton (particularly GZP) species and Atlantic taxa commonly advected into the Arctic Ocean.

Plankton imaging

Phytoplankton: In total, 31 phytoplankton samples were collected with the hand Apstein plankton net (20 µm), either from the ship, or the ice floes. The routine onboard microscopy observations showed considerable phytoplankton diversity. The most abundant ones belonged to genera *Chaetoceros, Protoperidinium, Dictyocha, Thalassiosira, Eucampia,* and *Rhizosolenia* (Fig. 3.14).

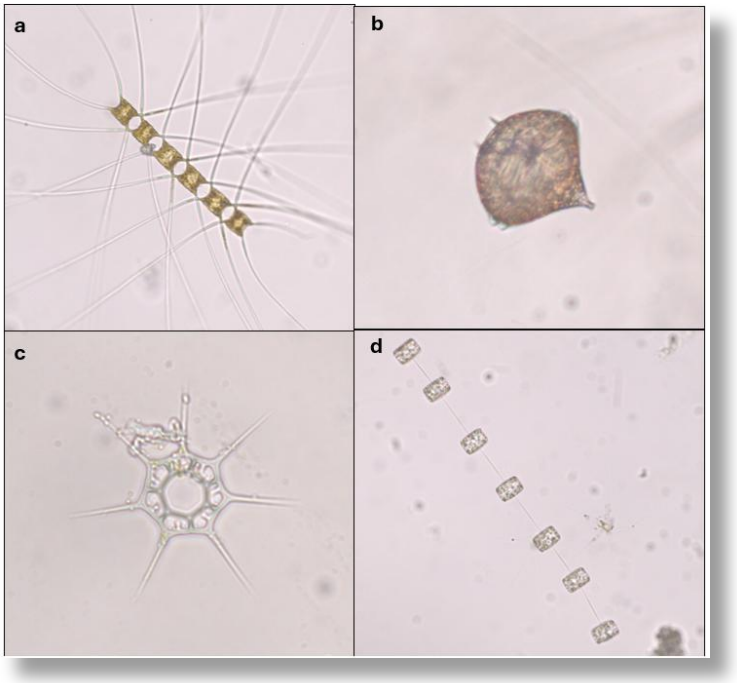

Fig. 3.14: The examples of the most common taxonomic groups found in the research area: a – Chaetoceros sp., b – Protoperidninium sp., c – Dictyocha sp., d- Thalassiosira sp.

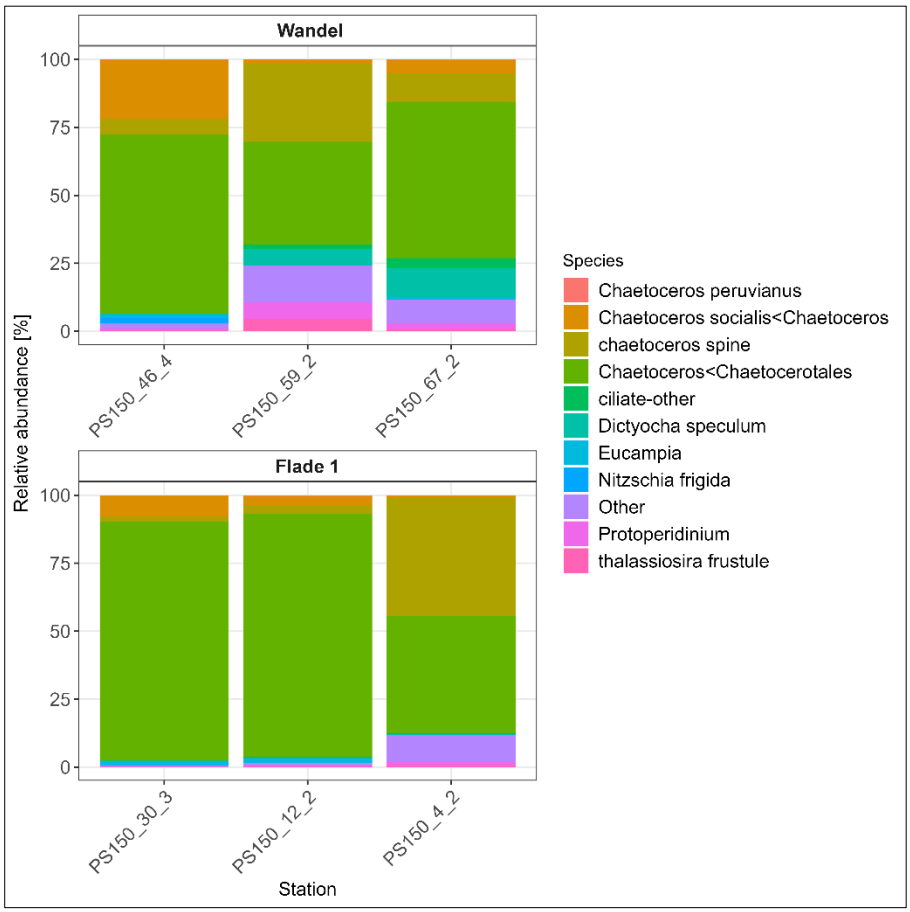

Fig. 3.15: The preliminary results of phytoplankton analysis at stations from Flade 1 and Wandel regions. Figure shows relative abundance of the most common taxa

Zooplankton: During the preservation of MultiNet samples, we observed that the zooplankton community was dominated by calanoid copepods, i.e. *Calanus* spp., *Metridia longa* was usually present below 200 m depth as evidenced by visible blue bioluminescence, along with other regularly occurring non-copepod zooplankton taxa such as chaetognaths, ostracods, amphipods, euphausiids, and jellyfish. Detailed analyses of the MultiNet samples will, however, be carried out later at the AWI laboratories in Bremerhaven using the ZooScan system. The UVP5 data will be appropriately formatted, uploaded to EcoTaxa and evaluated also at AWI Bremerhaven.

Microbial communities and biogeochemistry

At GEOMAR, the structure and function of microbial communities colonising various polymer types will be characterised. This analysis will provide insights into the composition, diversity, and metabolic potential of microorganisms associated with microplastics. The resulting data will enable the assessment of potential ecological and health impacts arising from anthropogenic pollution in the Arctic Ocean, thereby contributing to an improved understanding of the risks that microplastics pose to both ecosystem and human health.

Data management

During PS150, we sampled a large variety of interrelated parameters. Many of the samples will be analyzed at AWI or GEOMAR within approximately one year after the cruise. We plan that the full data set will be available at the latest about two years after the cruise. Samples taken for microscopical and molecular analyses, which cannot be analyzed within two years after the cruise, will be stored at the AWI for at least ten years and will be available upon request to other scientists.

Data will be archived, published, and disseminated according to international standards by the World Data Center PANGAEA Data Publisher for Earth & Environmental Science (www.pangaea.de) within two years after the end of the expedition at the latest. By default, the CC-BY license will be applied. Molecular data (DNA and RNA data) will be archived, published and disseminated within one of the repositories of the International Nucleotide Sequence Data Collaboration (INSDC, www.insdc.org) comprising of EMBL-EBI/ENA, SRA, GenBank and DDBJ). Macrozooplankon samples and eDNA extracts will be kept for long-term storage in the laboratories of Marine Zoology at the University of Bremen. All plankton imagery related to the Planktocope will be archived online in the ecotaxa database (https://ecotaxa.obs-vlfr.fr/).

Any other data will be submitted to an appropriate long-term archive that provides unique and stable identifiers for the datasets and allows open online access to the data.

This expedition was supported by the Helmholtz Research Programme “Changing Earth – Sustaining our Future” Topic 6, Subtopics 6.1 and 6.3, and the Helmholtz Young Investigator Group “ARJEL – Arctic Jellies” with the Grant Number VH-NG-1400.

In all publications based on this expedition, the **Grant No. AWI_PS150_02** will be quoted and the following publication will be cited:

Alfred-Wegener-Institut Helmholtz-Zentrum für Polar- und Meeresforschung (2017) Polar Research and Supply Vessel POLARSTERN Operated by the Alfred-Wegener-Institute. Journal of large-scale research facilities, 3, A119. http://dx.doi.org/10.17815/jlsrf-3-163.

References

Ardyna M & Arrigo KR (2020) Phytoplankton dynamics in a changing Arctic Ocean. Nat Clim Chang 10:892–903. https://doi.org/10.1038/s41558-020-0905-y

Bachy C, Sudek L, Choi C, et al (2022) Phytoplankton Surveys in the Arctic Fram Strait Demonstrate the Tiny Eukaryotic Alga Micromonas and Other Picoprasinophytes Contribute to Deep Sea Export. Microorganisms 10:961. https://doi.org/10.3390/microorganisms10050961

Bracher A, Vountas M, Dinter T, Burrows JP. Röttgers R & Peeken I (2009) Quantitative observation of cyanobacteria and diatoms from space using PhytoDOAS on SCIAMACHY data. Biogeosciences 6: 751–764. https://doi.org/10.5194/bg-6-751-2009

Bracher A, Xi H, von Appen, WJ, Mehdipour E, Metfies K, McPherson R, Zeising M & Nöthig E-M (2025) Resolving the inter-annual variability of phytoplankton community composition in Fram Strait using ship-based high-frequency spectrophotometric measurements from 2015 to 2024. Deep Sea Research Part II, in revision.

Dinter T, Rozanov V, Burrows JP & Bracher A (2015) Retrieval of light availability in ocean waters utilizing signatures of vibrational Raman scattering in hyper-spectral satellite measurements. Ocean Science 11:373–389. https://doi.org/10.5194/os-11-373-2015

Dischereit A, Beermann J, Lebreton B, Wangensteen OS, Neuhaus S & Havermans C (2024a) DNA metabarcoding reveals a diverse, omnivorous diet of Arctic amphipods during the polar night, with jellyfish and fish as major prey. Frontiers in Marine Science 14(11):1327650. https://doi.org/10.3389/fmars.2024.1327650

Dischereit A, Throm JK, Werner KM, Neuhaus S & Havermans C (2024b) A belly full of jelly? DNA metabarcoding shows evidence for gelatinous zooplankton predation by several fish species in Greenland waters. Royal Society Open Science 11(8):240797. https://doi.org/10.1098/rsos.240797

Engel A, Bracher A, Dinter T, Endres S, Grosse J, Metfies K, Peeken I, Piontek J, Salter I & Nöthig EM (2019) Inter-Annual Variability of Organic Carbon Concentration in the Eastern Fram Strait During Summer (2009–2017), Front. Mar. Sci. 6:187. https://doi.org/10.3389/fmars.2019.00187

Fernández-Méndez M, Katlein C, Rabe B, et al (2015) Photosynthetic production in the central Arctic Ocean during the record sea-ice minimum in 2012. Biogeosciences 12:3525–3549. https://doi.org/10.5194/bg-12-3525-2015

Flombaum P, Wang WL, Primeau FW & Martiny AC (2020) Global picophytoplankton niche partitioning predicts overall positive response to ocean warming. Nat Geosci 13:116–120. https://doi.org/10.1038/s41561-019-0524-2

Gorsky G, Ohman MD, Picheral M, et al. (2010) Digital zooplankton image analysis using the ZooScan integrated system. Journal of Plankton Research 32(3):285–303. https://doi.org/10.1093/plankt/fbp124

Hardge K, Peeken I, Neuhaus S, Lange BA, Stock A, Wenisch L& Metfies K (2017) The importance of sea ice for exchange of habitat-specific protist communities in the Central Arctic Ocean. Journal of Marine System 165:124–138. https://doi.org/10.1016/j.jmarsys.2016.10.004

Irvine T, Costello JH, Gemmel BJ, Sutherland KR, Corrales-Ugalde M, Townsend JP & Colin SP (2025) Ctenophores are a highly impactful predatory guild in open oceanic ecosystems. Current Biology 35: 2467–2473. https://doi.org/10.1016/j.cub.2025.04.029

Iversen KR & Seuthe L (2011) Seasonal microbial processes in a high-latitude fjord (Kongsfjorden, Svalbard): I. Heterotrophic bacteria, picoplankton and nanoflagellates. Polar Biol 34:731–749. https://doi.org/10.1007/s00300-010-0929-2

Kaiser P, Hagen W, Schukat A, Metfies K, Biederbick J, Dorschner S & Auel H (2025) Phytoplankton diversity and zooplankton diet across Fram Strait: Spatial patterns with implications for the future Arctic Ocean. Progress in Oceanography 234:103423. https://doi.org/10.1016/j.pocean.2025.103423

Lefering I, Röttgers R, Utschig & McKee D (2017): Uncertainty budgets for liquid waveguide CDOM absorption measurements. Applied Optics 56(22):6357. https://doi.org/10.1364/AO.56.006357

Li WKW, McLaughlin FA, Lovejoy C & Carmack EC (2009) Smallest algae thrive as the Arctic Ocean freshens. Science 326(5952):539. https://doi.org/10.1126/science.1179798

Metfies K, Von Appen WJ, Kilias E, et al (2016) Biogeography and photosynthetic biomass of arctic marine pico-eukaroytes during summer of the record sea ice minimum 2012. PLoS One 11:1–20. https://doi.org/10.1371/journal.pone.0148512

Muilwijk M, Hattermann T, Martin T & Granskog MA (2024) Future sea ice weakening amplifies wind-driven trends in surface stress and Arctic Ocean spin-up. Nat Commun 15. https://doi.org/10.1038/s41467-024-50874-0

Murray A, Priest T, Antich A, von Appen WJ, Neuhaus S & Havermans C (2024) Investigating pelagic biodiversity and gelatinous zooplankton communities in the rapidly changing European Arctic: an eDNA metabarcoding survey. Environmental DNA 6(3):e569. https://doi.org/10.1002/edn3.569

Murray A, Ramondenc S, Reifenberg SF, Jucker M, Neudert M, McPherson R, von Appen WJ & Havermans C (2025) Eukaryotic biodiversity of sub-ice water in the marginal ice zone of the European Arctic: a multi-marker eDNA metabarcoding survey. Science of the Total Environment 968:178840. https://doi.org/10.1016/j.scitotenv.2025.178840

Nöthig E-M, Bracher A, Engel A, et al (2015) Summertime plankton ecology in fram strait-a compilation of long-and short-term observations. Polar Res 34. https://doi.org/10.3402/polar.v34.23349

Nöthig E-M, Ramondenc S, Haas A, Hehemann L, Walter A, Bracher A, Lalande C, Metfies K, Peeken I, Bauerfeind E & Boetius A (2020) Summertime Chlorophyll a and Particulate Organic Carbon Standing Stocks in Surface Waters of the Fram Strait and the Arctic Ocean (1991–2015). Front Mar Sci 7:35. https://doi.org/10.3389/fmars.2020.00350

Oelker J, Losa SN, Richter A & Bracher A (2022) TROPOMI-retrieved underwater light attenuation in three spectral regions in the ultraviolet to blue. Frontiers in Marine Science 9:787992. https://doi.org/10.3389/fmars.2022.787992

Oelker J, Richter A, Dinter T, Rozanov VV, Burrows JP & Bracher A (2019) Global diffuse attenuation coefficient derived from vibrational Raman scattering detected in hyperspectral backscattered satellite spectra. Optics Express 27(12):A829–A855. https://doi.org/10.1364/OE.27.00A829

Oziel L, Gürses Ö, Torres-Valdés S, et al (2025) Climate change and terrigenous inputs decrease the efficiency of the future Arctic Ocean's biological carbon pump. Nat Clim Chang 15. https://doi.org/10.1038/s41558-024-02233-6

Pantiukhin D, Verhaegen G & Havermans C (2024) Pan-Arctic distribution modeling reveals climate-change-driven poleward shifts of major gelatinous zooplankton species. Limnology and Oceanography 69(6):1316–1334. https://doi.org/10.1002/lno.12568

Pantiukhin D, Verhaegen G, Kraan C, Jerosch K, Neitzel P, Hoving HJT & Havermans C (2023) Optical observations and spatio-temporal projections of gelatinous zooplankton in the Fram Strait: a gateway to a changing Arctic Ocean. Frontiers in Marine Science 10:987700. https://doi.org/10.3389/fmars.2023.987700

Rantanen M, Karpechko AY, Lipponen A, Nordling K, Hyvarinen O, Ruosteenoja K, Vihma T & Laaksonen A (2022) The Arctic Has Warmed Nearly Four Times Faster than the Globe since 1979. Communications Earth & Environment 3:168. https://doi.org/10.1038/s43247-022-00498-3

Röttgers R, Doxaran D & Dupouy C (2016) Quantitative filter technique measurements of spectral light absorption by aquatic particles using a portable integrating cavity absorption meter (QFT-ICAM). Opt. Express 24(2):A1–A20. https://doi.org/10.1364/OE.24.0000A1

Sadeghi A, Dinter T, Vountas M, Taylor B, Peeken I, Altenburg Soppa M & Bracher A (2012) Improvements to the PhytoDOAS method for identification of coccolithophores using hyper-spectral satellite data. Ocean Sciences 8 1055–1070. https://doi.org/10.5194/os-8-1055-2012

Schröter F, Havermans C, Kraft A, Knüppel N, Beszczynska-Moeller A, Bauerfeind E & Nöthig E (2019) Pelagic amphipods in the Eastern Fram Strait with continuing presence of *Themisto compressa* based on sediment trap time series. Frontiers in Marine Science 6:311. https://doi.org/10.3389/fmars.2019.00311

Schweiger AJ, Steele M, Zhang J, et al (2021) Accelerated sea ice loss in the Wandel Sea points to a change in the Arctic's Last Ice Area. Commun Earth Environ 2:1–11. https://doi.org/10.1038/s43247-021-00197-5

Serreze MC & Berry RG (2011) Processes and impacts of Arctic amplification: A research synthesis. Global and Planetary Change 77(1-2):85–96. https://doi.org/10.1016/j.gloplacha.2011.03.004

Søreide JE, Leu E, Berge J, et al (2010) Timing of blooms, algal food quality and Calanus glacialis reproduction and growth in a changing Arctic. Glob Chang Biol 16:3154–3163. https://doi.org/10.1111/j.1365-2486.2010.02175.x

Stemmann L, Hosia A, Youngbluth MJ, Soiland H, Picheral M & Gorsky G (2008) Vertical distribution (0–1000 m) of macrozooplankton, estimated using the Underwater Video Profiler, in different hydrographic regimes along the northern portion of the Mid-Atlantic Ridge. Deep Sea Research Part II: Topical Studies in Oceanography 55:94–105. https://doi.org/10.1016/j.dsr2.2007.09.019

Tremblay G, Belzile C, Gosselin M, et al (2009) Late summer phytoplankton distribution along a 3500 km transect in Canadian Arctic waters: Strong numerical dominance by picoeukaryotes. Aquat Microb Ecol 54:55–70. https://doi.org/10.3354/ame01257

Vilgrain L, Maps F, Picheral M, Babin M, Aubry C, Irisson JO & Avata SD (2021) Trait-based approach using *in situ* copepod images reveals contrasting ecological patterns across an Arctic ice melt zone. Limnology & Oceanography. https://doi.org/10.1002/lno.11672

von Appen WJ, Waite AM, Bergmann M, Bienhold C, Boebel O, Bracher A, Cisewski B, Hagemann J, Hoppema M, Iversen MH, Konrad C, Krumpen T, Lochthofen N, Metfies K, Niehoff B, Nöthig EM, Purser A, Salter I, Schaber M, Scholz D, Soltwedel T, Torres-Valdes S, Wekerle C, Wenzhöfer F, Wietz M & Boetius A (2021) Sea-ice derived meltwater stratification slows the biological carbon pump: results from continuous observation. Nature Communications 12(1):7309. https://doi.org/10.1038/s41467-021-26943-z

Xi H, Bretagnon M, Mehdipour E, Demaria J, Mangin A & Bracher A (2025) Consistent long-term observations of surface phytoplankton functional types from space. 9th Copernicus Ocean State Report. State of the Planet. https://doi.org/10.5194/sp-6-osr9-7-2025

Xi H, Losa SN, Mangin A, Garnesson P, Bretagnon M, Demaria J, Soppa MA, d'Andon OHF & Bracher A (2021) Global chlorophyll a concentrations of phytoplankton functional types with detailed uncertainty assessment using multi-sensor ocean color and sea surface temperature satellite products. Journal Geophys. Res.-Oceans 126:e2020JC017127. https://doi.org/10.1029/2020JC017127

4. SEA-ICE PHYSICS

Marcel Nicolaus*[1], Alicia Magdalena Harfst[2], Julia Regnery[1], Bernhard Schmitz[3]
Not on board: Christian Haas[1], Thomas Krumpen[1], Ruzica Dadic[4]
* marcel.nicolaus@awi.de

[1]DE.AWI
[2]DE.Uni-Oldenburg
[3]COM.Driftnoise
[4]CH.WSL

Grant-No. AWI_PS150_06

Outline and objectives

The sea ice in the Last Ice Area, the region north of Greenland, is one of the last regions where multiyear ice may survive summer melt in the future. The recent occurrence of polynyas, both in winter and summer, has raised questions to the state of the sea ice and its survivability. Ice thickness and drift observations are required to distinguish between thermodynamic and dynamic contributions to sea ice changes in the Last Ice Area. In this respect the sea ice physics work during EGC-Sources aimed to

- observe late summer and autumn sea ice thickness variability and gradients in the Last Ice Area across and along the shelf related to different ice origins and deformational histories,
- evaluate relationships between occurrence of polynyas, ice thickness, and drift,
- characterize the physical properties of the sea ice to observe seasonal changes in continuation of observations of previous expeditions (airborne and at sea), including the work of the preceding expedition CONTRASTS (PS149) and IceBird Summer 2025.

Navigation through ice-covered waters is a key topic in the Arctic Ocean, including the realization of each single *Polarstern* expedition. We are currently using various kinds of sea ice information in (near) real time to support navigation and decision making on board. During EGC-Sources, *Polarstern* experienced particularly difficult ice conditions. From the navigation point of view, we visited some of the thickest ice in the Arctic and the expedition reached far into the freeze-up season, including a thick snow pack on new ice. The most important tool for supporting navigation through ice-covered waters is the MapViewer software. This (ice) information and expedition planning tool allows real-time mapping. So, we aimed to

- systematically observe sea ice conditions along the cruise track and relate this to the vessel's performance,
- investigate which data are most suited to support ice navigation,
- improve the MapViewer system by adding advanced possibilities of drift corrections of existing satellite images. This should help the nautical officers to optimize their route selection.

The EGC-Sources expedition started during the summer sea ice extent minimum and experienced the freeze-up of the ice pack and the ocean around this. Following the preceding

CONTRASTS (PS149) expedition, which focusses on the melt season, we aimed to extend these observations into freeze-up, by

- re-visiting some of the same ice already studied during CONTRASTS
- improving our knowledge of atmosphere-ice-ocean interactions, with particular emphasis on thermodynamic processes and sea ice's role as both a habitat and a barrier,
- observing sea ice formation processes as functions of atmospheric and oceanic boundary conditions.
- Enhancing our observational capabilities, testing new instruments and measurement systems in challenging Arctic conditions.

The field activities planned for EGC-Sources can be grouped into five main tasks. Most activities occurred directly on the ice while the vessel is stationary, supplemented by helicopter and drone surveys around the ship. Routine observations and continuous remote-sensing measurements also ran along the transits between stations.

Task 1: Measurements during Ice Stations

We conducted 4 sea ice stations (Tab. 4.0.1, Fig. 4.0.1) and quantifying sea ice and snow properties, as well as their distribution. Melt ponds were all frozen during the ice stations already and were not investigated in particular. These measurements covered all relevant ice types and surface features present at each station.

- Sea ice thickness measurements along surface transects across the floe with GEM-2 electromagnetic sensors. (Section 4.5)
- Snow depth measurements along surface transects across the floe with MagnaProbe sensors. (Section 4.5)
- Snow and sea ice properties and sampling (temperature, salinity, stratigraphy/texture, surface properties). (Sections 4.6 and 4.7)

Task 2: Airborne Measurements

Regional-scale observations of sea ice properties along the East Greenland Current and into the Last Ice Area were carried out with airborne measurements. We observed late summer sea ice thickness variability and gradients for ice regimes from different drift origins, to evaluate relationships between occurrence of polynyas, ice thickness, and drift. The work represented a seasonal continuation of airborne surveys previously conducted in this region during July and August.

- Drone-based photo surveys were conducted at each station floe to map sea ice surface conditions. Images will be stitched for high-resolution surface classification and surface elevation models (digital elevation maps) (Section 4.3)
- Helicopter-based sea ice thickness measurements were realized with the AWI EM-Bird along the cruise track through sea ice. This provides thickness distribution functions on scales of <60 nm around the ship. The data will also help to develop and refine this new EM Bird under various ice conditions. (Section 4.2)

Task 3: Re-visit of CONTRASTS (PS149) sea ice Regime 3

We re-visited the ice Regime 3 of the CONTRSTS expedition, which was equipped with autonomous instruments. At this station, wanted to gather an additional data set later in the season with all possible methods and approaches to observe temporal changes. However, the ice floe disintegrated completely before the re-visit and ended in the marginal ice zone. Hence the remaining task was to

- Recover of autonomous stations and retrieval of data from the stations and to document the ice conditions in the area. (Section 4.8)

Task 4: On-Board Measurements

We continuously observed the sea ice conditions along the cruise track. These data will directly be used to characterize and classify the sea ice and surface conditions. In addition, these data will be used, together with the retrieval of satellite data to actively support the navigation and tactical decisions of the vessel.

- Two panoramic cameras were installed above the crow's nest will capture photographs or short videos. These images were transmitted in near-real time to a project website for outreach and public engagement. (Section 4.1)
- Standardized sea ice observations from the bridge, recording sea ice concentration, floe size, ridging, thickness, plus weather conditions and large fauna, within a ~1.5 nm radius. (Section 4.1)
- Ship-based electromagnetic ice thickness measurements with the Sea Ice Monitoring System (SIMS) to monitor ice thickness along the ship track. (Section 4.4)
- Measurements of solar (spectral) radiation are measured at the ship's bow along track. These data will support different other observations. (Section 4.1)

Tab. 4.0.1: Sea ice stations during EGC-Sources (PS150). A map of all stations is given in Figure 4.0.1. Dates are given in format dd.mm.yyyy.

Station	ID	Start Date	Start Position	End Date	End Position
ICE 1	PS150_44-1	13.09.2025 10:20	83.16 N 019.46 W	13.09.2025 19:43	83.14 N 019.28 W
ICE 2	PS150_78-1	21.09.2025 07:34	84.47 N 020.95 W	21.09.2025 22:13	84.46 N 021.19 W
ICE 3	PS150_90-1	25.09.2025 09:13	83.88 N 024.19 W	25.09.2025 18:45	83.89 N 024.26 W
ICE 4	PS150_127-1	10.10.2025 12:05	80.13 N 016.12 W	10.10.2025 17:49	80.16 N 015.83 W

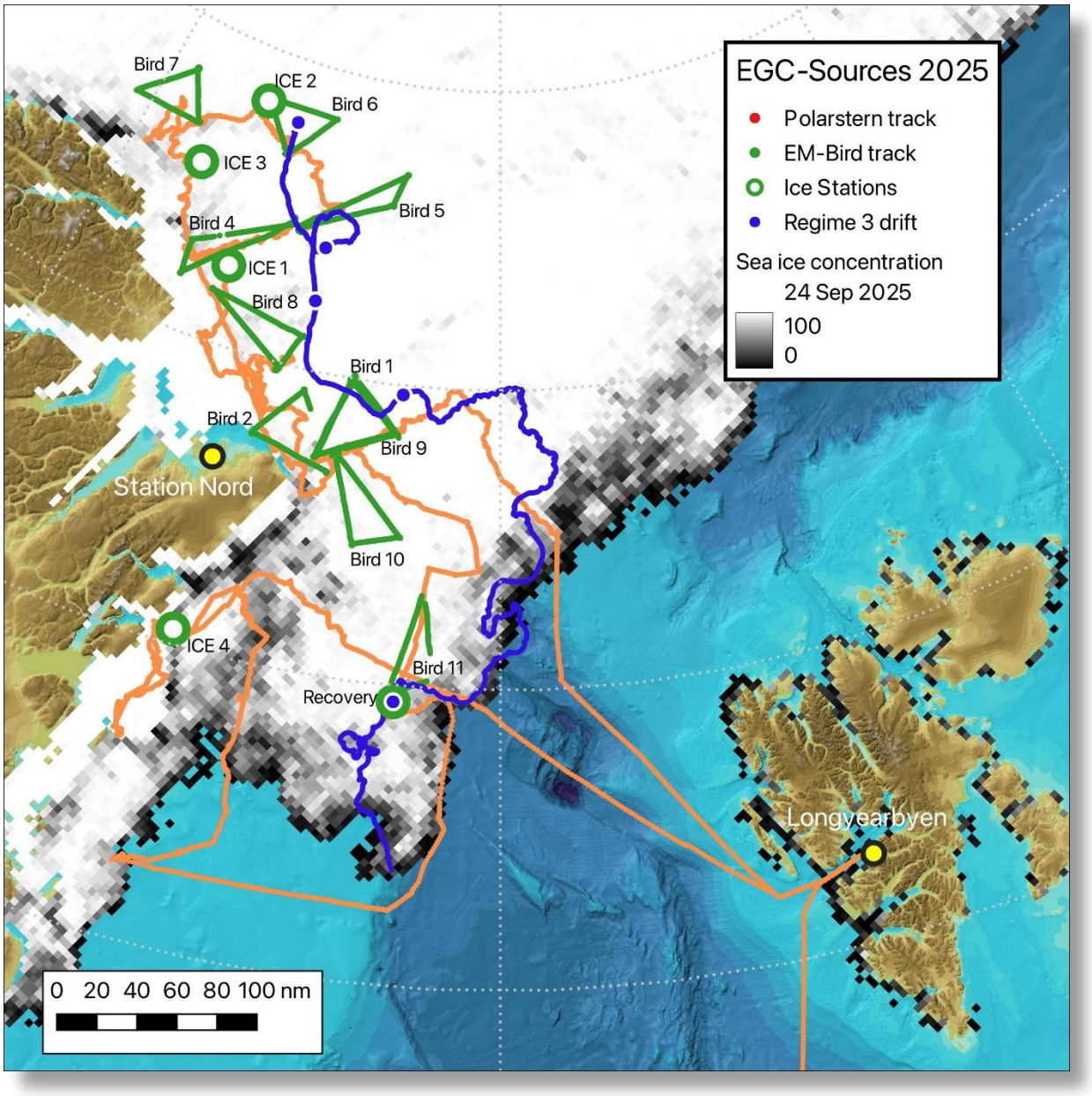

Fig. 4.0.1 Map of the work at sea of the sea ice physics team during EGC-Sources (PS150). A tabositions of the ice stations is given in Table 4.0.1 and a table with the details of the EM-Bird tracks is given in Table 4.2.1. The drift track of Regime 3 refers to instrument deployments of the CONTRASTS (PS149) expedition (see Chapter 4.8).

Work at sea and preliminary (expected) results

The work at sea and expected results are described in each sub-section of this chapter.

4.1 Ship-based sea ice observations and panorama cameras

Work at sea

During the expedition, standardized ice observations were done hourly while *Polarstern* was moving through ice and not on station. The aim of these observations was to describe the surrounding conditions over a ~10-minute period within a radius of 1.5 nautical miles around the vessel. The list of conditions that were recorded is comprehensive, and includes ice concentration, floe size, fraction of ridged ice, ice thickness, amount of ice algae present, melt pond coverage, and other characteristics. In addition, several parameters describing the weather conditions and present macrofauna were included. Due to the subjective nature of the observations, new observers were trained and/or initially paired with people with more experience to ensure consistency throughout the expedition.

In addition, two autonomous panorama cameras were operated continuously over the entire expedition. This record continued the time series from the CONTRASTS (PS149) expedition (Tab. 4.1.1). During EGC-Sources, approx. 1,300 pictures were recorded from each camera. Both provide hourly time laps pictures of the surrounding of the vessel to document ice, snow and weather conditions along the route. The cameras were both mounted above the crow's nest and worked without interruption. Both cameras complement each other in terms of image information. The hourly pictures were transferred to a server on land after recording, through an own Starlink satellite antenna. A small PC-server was installed in the crow's nest controlling the cameras and data transmission.

- The 'Panorama 360°' camera (device short name: Panomax) was operated on different expeditions since MOSAiC in 2019. The camera is based on a rotating line scan camera (type Panomax Roundshot 360°) and each picture consists of 15,680 x 2,048 pixels. This camera has a slightly higher resolution and a complete round view. While moving, the moving ship causes distortions / waves in the resulting image, because the recording of a single round shot takes several minutes, depending on light conditions.
- The 'Panorama 180°' camera (device short name: Panomax180) was operated for the first time during the Arctic season 2025. The camera consists of four individual cameras, which are automatically and directly stitched into one picture. Then each picture consists of 8,192 x 1,728 pixels. The camera also allows the recording and streaming of 4k video streams. In addition to the hourly photos, the camera records internally 20-second interval pictures, which were only used to create daily time-laps videos. The individual high-frequency pictures were not stored or transmitted to land.

Preliminary (expected) results

The minimum of the summer sea ice extent 2025 was reached during the EGC-Sources expedition on 9 September with an area of 4.74 Mio km^2. This was the 12^{th} lowest extent on record. The summer was dominated by high variability, moderate air temperatures and a low drift. The sea ice concentration reached a summer minimum record in the observation area, the Atlantic sector of the Arctic Ocean. This minimum resulted from a divergent ice drift in the region. The re-freezing of the surface and the increase in sea ice concentration and area in September and October was rapid and returned the low values from summer to more average conditions again.

The visual observations of sea ice conditions by ship are an integral part of sea ice monitoring for operational and research support. These observations provide information about sea ice morphology that is not obtainable or ambiguous in remotely-sensed data. The EGC-Sources expedition covered a wide range of sea ice conditions, starting at the end of melt seasons, when large areas of open water were around, to a completely closed ice pack towards the end of the expedition, when new ice and new snow covered the entire area.

Using the panorama cameras, we documented the sea ice, snow and weather conditions through the observation period. Figure 4.1.1 gives examples of these conditions in 8 to 9 days intervals. These pictures are selected as representative views of these days. The cameras turned out to be a most valuable tool to document the changes over time and space of the expedition. They complement the bridge observations and in general to document sea ice and weather conditions.

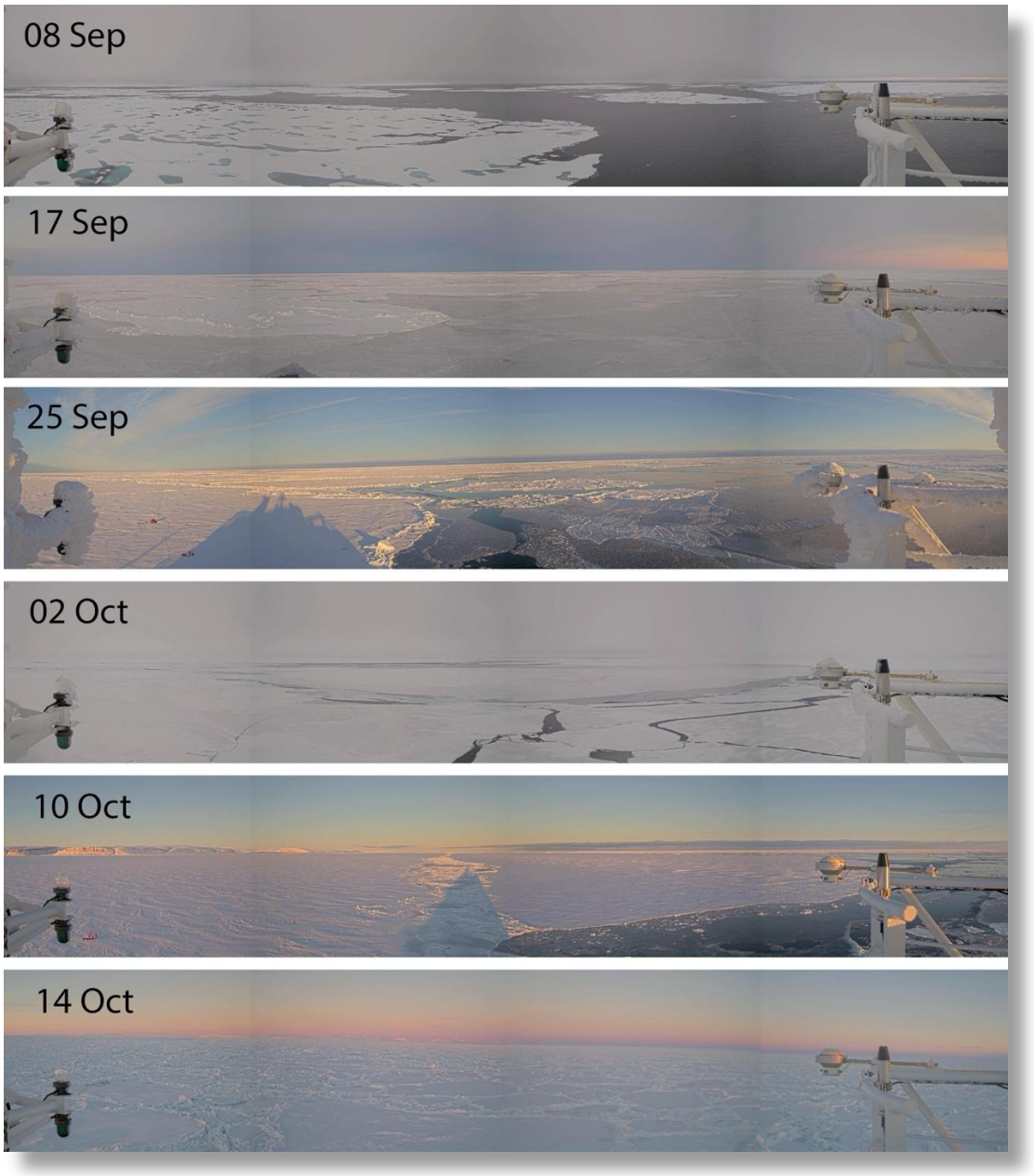

Fig. 4.1.1: Photographs of the 180° panorama camera showing the sea ice and weather conditions during EGC-Sources (PS150). The photos are selected every 8 to 9 days from the full record of the camera (Tab. 4.1.1).

Tab. 4.1.1: Overview of the camera buoys and panorama cameras on *Polarstern*. Dates and times give the first and last photo of the respective camera. The number of photos and videos differs depending on operation times and modes. These observations started during the CONTRASTS expedition and were continued during EGC-Sources. Abbreviation: tbd = to be determined, these cards were not read out yet. Dates are given in format dd.mm.

Camera	First picture date time	Last picture date time	Pictures Web	Pictures SD-card	Videos
Polarstern 180	02.07. 00:58	24.10. 08:50	2719	-	-
Polarstern 360	02.07. 01:00	24.10. 18:00	2282	-	-
Regime 1 surface	12.07. 18:55	05.08. 15:29	3318	3635	-
Regime 1 water	12.07. 18:55	05.08. 15:29	3907	6894	-
Regime 2 surface	17.07. 16:50	24.08. 09:37	5454	tbd	tbd
Regime 2 water	17.07. 16:46	24.08. 09:35	14530	tbd	1080
Regime 3 surface	22.07. 11:47	08.09. 18:02	7550	7106	516
Regime 3 water	22.07. 11:47	08.09. 18:02	12821	7105	516

4.2 Helicopter-borne sea ice thickness and surface roughness

Work at sea

During the expedition, helicopter-borne sea ice thickness surveys were conducted using the Electromagnetic (EM) Bird, a towed sensor system flown at an altitude of 12 to 20 meters above the ice surface. The system measures sea ice thickness by calculating the difference between the EM-derived distance to the ice–water interface and the distance to the snow and ice surface obtained from a single-beam laser altimeter. Ice thickness measurement accuracy is within 0.1 m to drill-hole measurements over level sea ice, while water inclusions within pressure ridges lead to a general underestimation of ridges by as much as 40 % to 50 %. Pressure ridges along flight tracks were detected using range readings from the single beam laser altimeter.

During the expedition a total of 11 EM-Bird flights were performed. Flight 03 has no useful data and was aborted directly after take-off due to a malfunction of a signal amplifier. Table 4.2.1 and Figure 4.2.1 provide the overview of the flights that were conducted. The figure also show the relation of flights connected to the CONTRASTS expedition. A main achievement is that it was possible to survey (partly) identical tracks after several weeks again. These repeat flights include:

- Flight 06 on 19 September repeated a CONTRASTS flight from 21 July
- Flight 08 on 28 September repeated a CONTRASTS flight from 18 August
- Flight 09 on 01 October repeated an EGC-Sources flight on 08 September

Tab. 4.2.1: Overview of EM Bird surveys during EGC-Sources

Event label	Date time yyyy-mm-ddTHH:MM:SS	Surveying activity
PS150_heli-EMBird-01	2025-09-08T14:32:00	Flade section
PS150_heli-EMBird-02	2025-09-10T11:26:00	Towards fast ice area
PS150_heli-EMBird-03	2025-09-14T11:15:00	No useful data, broken amplifier
PS150_heli-EMBird-04	2025-09-17T09:17:00	Flight 1/2 of a long transect
PS150_heli-EMBird-05	2025-09-17T13:23:00	Flight 2/2 of a long transect
PS150_heli-EMBird-06	2025-09-19T13:23:00	Partly repeated survey of 21 July

Event label	Date time yyyy-mm-ddTHH:MM:SS	Surveying activity
PS150_heli-EMBird-07	2025-09-21T15:47:00	Survey furthest to the West
PS150_heli-EMBird-08	2025-09-28T09:16:00	Partly repeated survey of 18 August
PS150_heli-EMBird-09	2025-10-01T10:12:00	Complete repeat of survey of 08 September
PS150_heli-EMBird-10	2025-10-01T12:42:00	Towards East
PS150_heli-EMBird-11	2025-10-04T10:23:00	To recovery sites

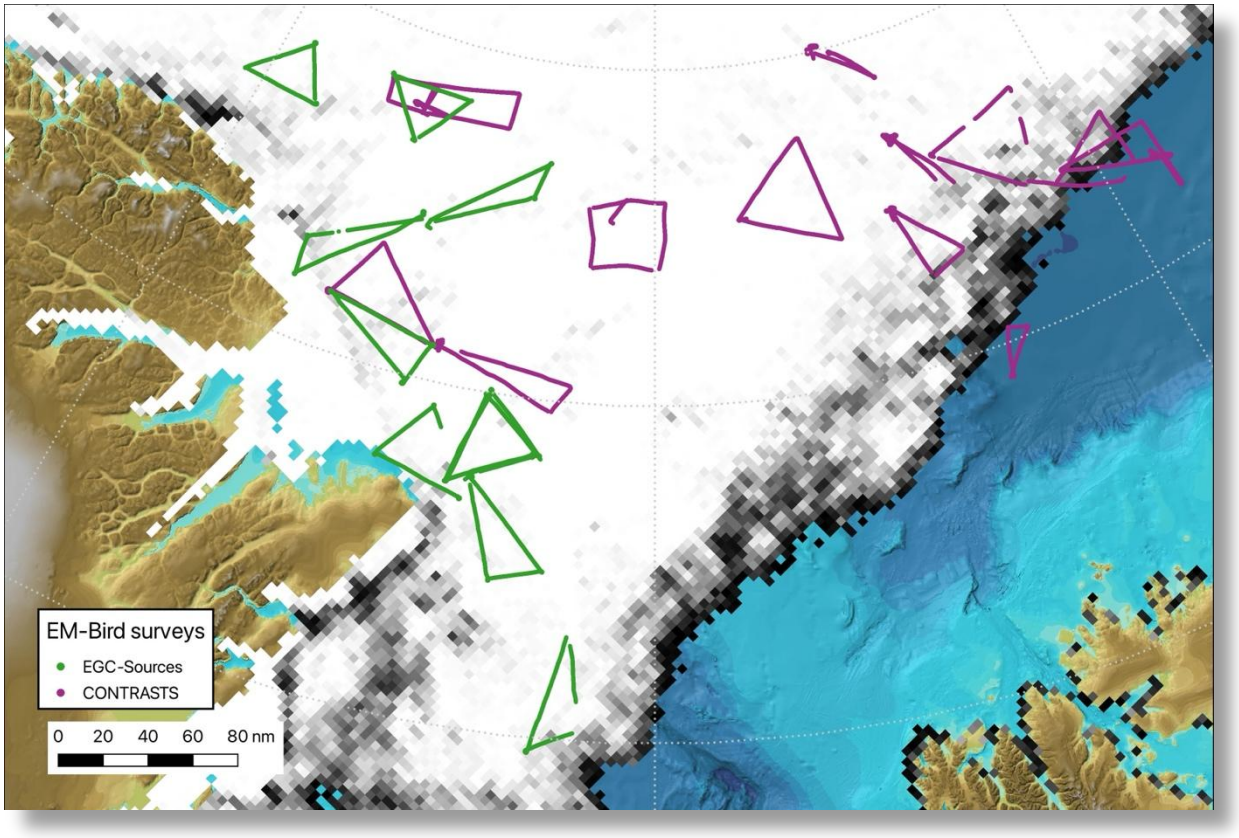

Fig. 4.2.1: Map of the EM-Bird surveys during EGC-Sources and CONTRASTS. Figure 4.0.1 also gives labels for each survey.

Preliminary (expected) results

Figure 4.2.2 shows the comparison of sea ice thickness distributions of the repeat flights. This allows conclusions on the changes of the ice properties in the region, while it must be noted that the same track and not the same ice was surveyed. The ice surveyed during the second flight was further upstream of the ice drift before.

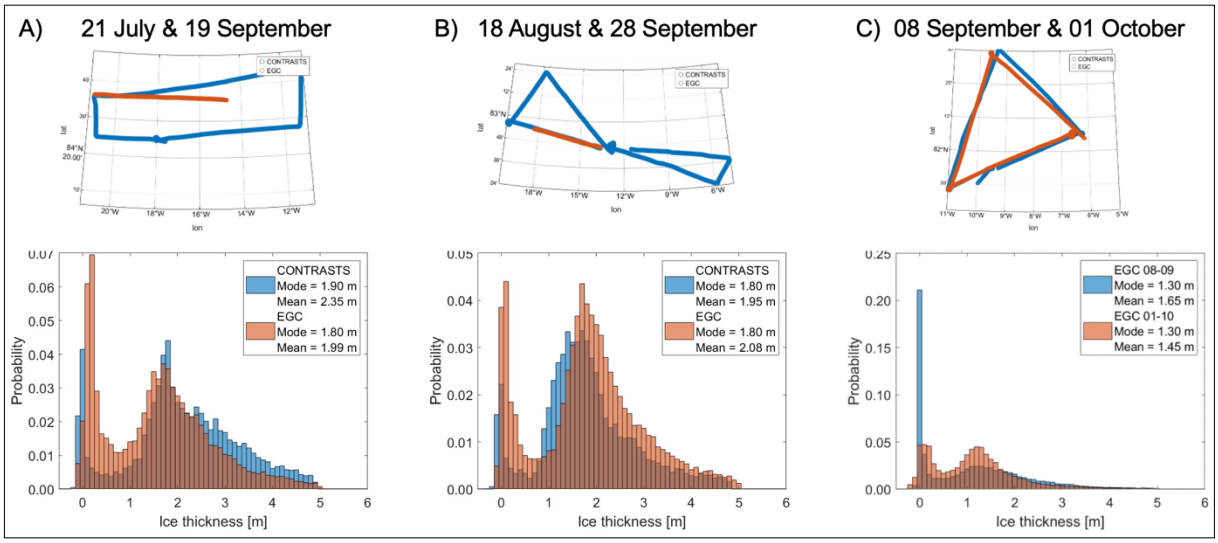

Fig. 4.2.2: Sea ice thickness distributions from EM-Bird surveys during EGC-Sources and CONTRASTS. For each comparison the flight track and the thickness distribution are shown.

4.3 Drone surveys

Work at sea

During the expedition, drone surveys of the ice work area close to *Polarstern* were conducted for each ice station and one additional (test) station before. An overview of all flight events is provided in Table 4.3.1. The observations were performed with a DJI Mavic 3 drone, equipped with an optical camera. The imagery was acquired manually with fixed settings for aperture and exposure time. Afterwards, the photos from each flight were stitched into composites. Later processing is expected to provide digital elevation models (DEMs) with high vertical accuracy.

Tab. 4.3.1: Overview of drone surveys with the DJI Mavic 3 drone. For these flights, photo mosaics of the surface are available. Most stations, flights were performed in two heights.

Event Label	Station/ Area	Date	Time	Altitude	Photos
PS150_drone-Mavic3-01	Otter station	11. Sep 25	16:26	100	204
PS150_drone-Mavic3-02	Station 1 PS150_44-1	13. Sep 25	18:38	80	414
PS150_drone-Mavic3-02	Station 1 PS150_44-1	13. Sep 25	18:54	130	108
PS150_drone-Mavic3-03	Station2 PS150_78-1	21. Sep 25	16:03	80	269
PS150_drone-Mavic3-03	Station2 PS150_78-1	21. Sep 25	16:15	130	156
PS150_drone-Mavic3-04	Station3 PS150_90-1	25. Sep 25	17:01	70	255
PS150_drone-Mavic3-04	Station3 PS150_90-1	25. Sep 25	17:15	130	218
PS150_drone-Mavic3-05	Station4 PS150_127-1	10. Oct 25	15:24	130	181

Preliminary (expected) results

Figure 4.3.1 shows composites from the drone images for each ICE station. Each photo shows an area of 200 m x 200 m.

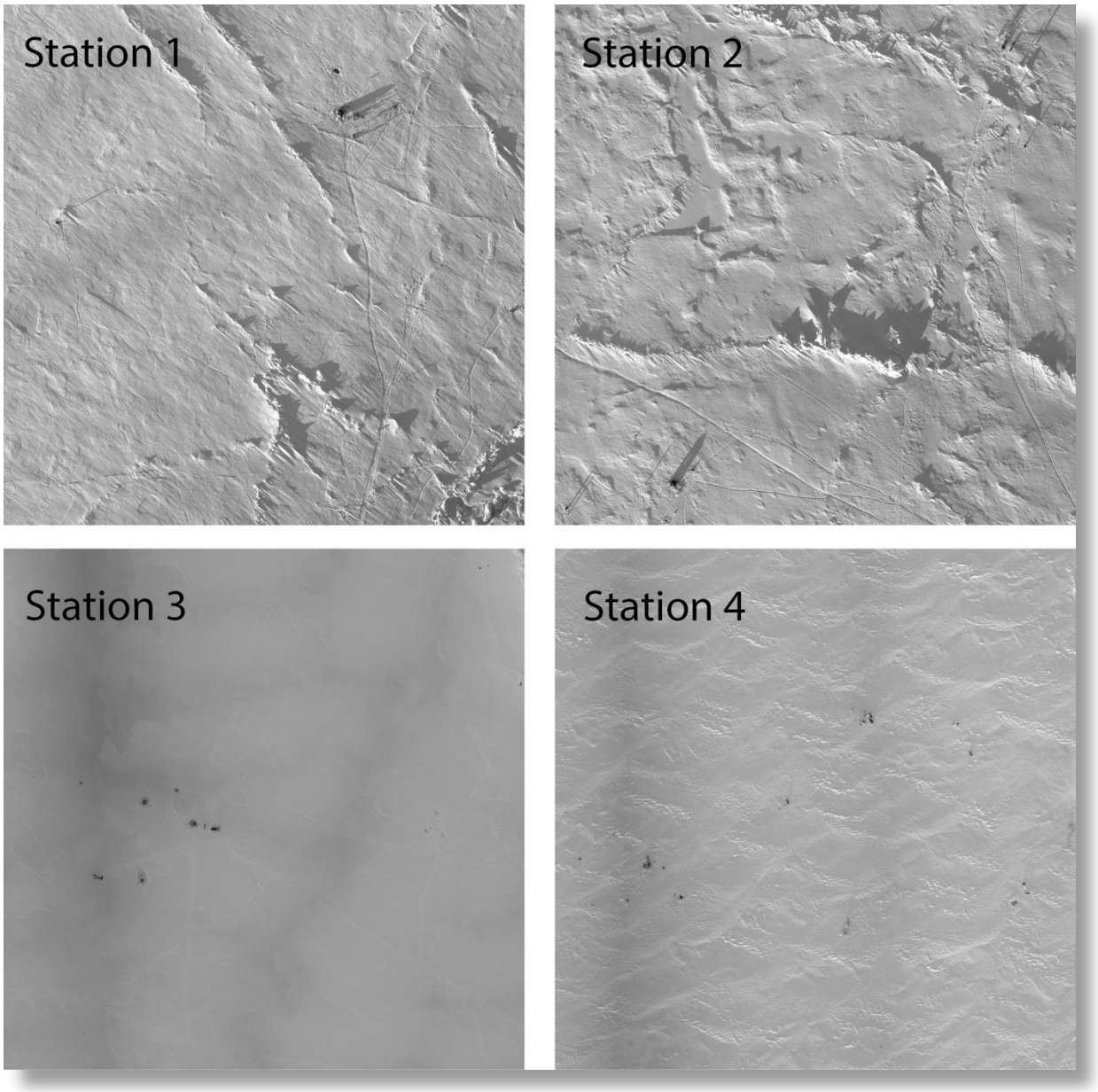

Fig. 4.3.1: Composites of drone images from the four ice stations. Each photo shows an area of 200 m x 200 m.

4.4 Ship-based electromagnetic sea ice thickness monitoring system

Work at sea

An electromagnetic-sounding instrument was used to measure sea ice thickness along the ship track. A sonar detects the distance to the ice surface and an EM31 device measures the distance to the sea surface enabling sea ice thickness calculations. The SIMS is installed at the ship's bow on 6 September. Before starting measurements, a calibration of apparent conductivity $\sigma_a$and height above sea surface h must be carried with the out with the sensors above open water following the equation:

$$\sigma_a = k_0 + k_1 \cdot e^{-k_2 \cdot \mathrm{h}}$$

with k_0, k_1 and k_2 being the calibration coefficients to be determined. The fit is done manually as there are usually many outliers in the calibration data. Calibrations were carried out at the following times coinciding with the file name when discrepancies (~+/- 20 cm) between sonar and EM31 concerning the measured height above open water was observed:

- 2025-09-07 09-37-52
- 2025-09-11 19-00-37
- 2025-09-16 19-09-19
- 2025-09-23 12-54-23.

Finding suitable spots for new calibrations got more difficult when steering north into dense ice with addition of inset of refreezing.

Between two calibrations long-term datasets are collected with the same calibration coefficients saved in the measurement program making real time ice thickness observations possible. First measurements started on 7 September 2025. During measurements the SIMS is brought to a fixed height of about 3-4m above sea surface. Measurement files are saved every 12 hours on a computer located on the bridge which is also used for the calibrations. Periods of long-term measurements are the following where start and end date refer to the last file started in that period:

Tab. 4.4.1: Start and end dates of data sets that follow the same calibration

No. of calibration/ dataset	Start date	End date
1	2025-09-07 09-37-52	2025-09-11 15-26-40
2	2025-09-11 19-16-00	All data not reliable because the antenna broke into two pieces probably right after calibration and therefore the measurements got disturbed
3	2025-09-16 19-19-11	2025-09-23 05-19-19
4	2025-09-23 14-10-07	2025-10-05 06-10-18

During measurements, the ship was occasionally at oceanographic work stationary leading to a bias of the ice thickness. The instrument wasn't switched off during station work and therefore the bias has to be minimized by removing data for low ship speed. The data is also biased as the ship avoids thicker ice whenever possible. After calibration 2 the data of that dataset is not reliable because the antenna broke into two pieces. With support of *Polarstern's* engine workshop we were able to repair and re-install the SIMS again a few days later but still there

is a data gap for same days. After that the SIMS worked fine even without a new calibration for several days.

The last set of measurements (4) was abruptly stopped as we were not able to recover the instrument on time when unexpected high swell came in even into the ice cover and lead to the SIMS losing its antenna again. This time the piece that broke off got lost and the system could not be repaired again. For that reason, SIMS measurements stopped one week earlier than planned.

Preliminary (expected) results

Figure 4.4.1 shows a time-series of the raw sea ice thickness measured by the SIMS during its whole operation time. A 21 and 1001 median filter are added to smooth the data. Typical ice thickness values range between 0 and about 3.5 m according to the smoothed data. Overall high variability in the raw data is observed. The beforehand mentioned data gap due to a broken antenna can be seen between 11 and 16 September. Increasing ice thickness along the ship track going north from the start of the measurements is observed with a peak around 25 September when the ship was north of Cape Morris Jesup. Afterwards a slight decrease is observed again.

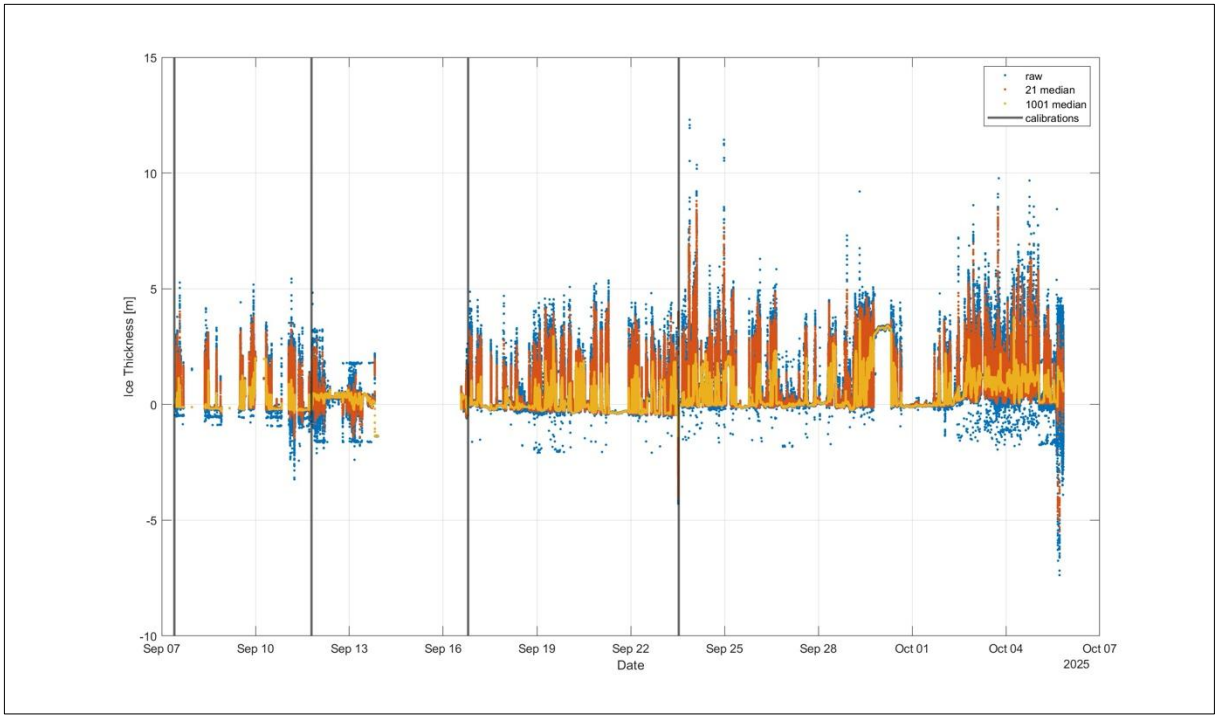

Fig. 4.4.1: Sea ice thickness measured along the Polarstern track with the SIMS in front of the bow. 3 time series are shown, one with the measured raw data, one for each median filter. Vertical grey lines show the times when new calibrations were performed.

Above open water the SIMS usually doesn't show exact agreement of sonar height and EM height but values scatter around zero with a tendency to negative values even shortly after calibration. This is what can be seen in the ice thickness distribution in Figure 4.4.2. Taking data along the whole cruise track into account, two modes can be observed, the first one around zero and the second one at about 0.9 m ice thickness. The lower mode indicates ship movement through open water, but also for thin new ice sheets like Nilas the SIMS shows unrealistic low values similar to measurements above open water. As we went north during start of refreezing period a lot of new ice was observed which is not displayed in the datasets.

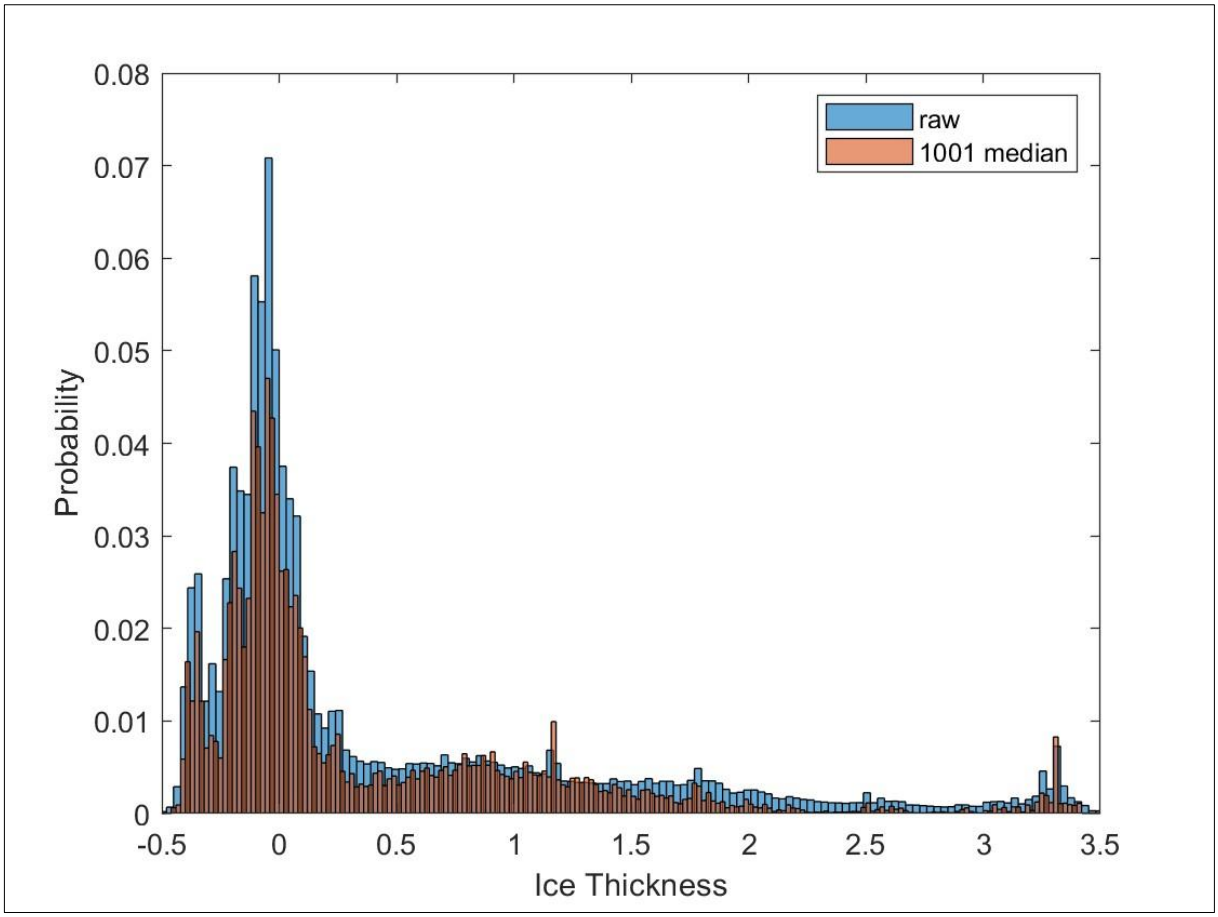

Fig. 4.4.2: Sea ice thickness distribution from the SIMS measurements during EGC-Sources for the raw and the filtered data

4.5 Sea ice thickness and snow depth transects

Work at sea

Sea ice thickness and snow depth were measured along walked transects on each floe where an ice station took place. In the following snow depth refers to the sum of snow depth and surface scattering layer (SSL).

During each transect, total thickness of snow and ice are measured using a GEM instrument (ground electromagnetic induction device, GEM-2 from Geophex Ltd.) pulled behind one person in a pulka sledge. The GEM is based on the great difference in electrical conductivity between sea water and sea ice. A transmitter coil emits a primary electromagnetic signal at 5 frequencies between 1.5 kHz and 93 kHz. This field induces eddy currents in the seawater directly below the bottom of the ice creating a secondary electromagnetic field. The strength of the secondary field decreases exponentially with the distance between transmitter (underside of the sea ice) and the receiver (GEM). With the information, the height of the instrument above the ice-water interface can be determined which corresponds to the total thickness.

For evaluation of these measurements a calibration is needed to find the exponential relationship between the instrument's height above the ice-water interface and the secondary field. Eight measurements are carried out at different known heights on a wooden ladder at each station. Moreover, the ice thickness under and around the ladder is measured by drilling.

Snow depth measurements are carried out with a MagnaProbe device "Anja" (MP; from Snow-Hydro LLC). One person carries the instrument in a rucksack along the transect and every second step tips a rod into the snow down to the ice. A plate that is able to move vertically up the rod remains above the snow. Its position leads to a signal that can be converted to snow depth which is the difference between the tip and the plate. No calibration is needed.

Both instruments are used along almost the same track enabling the calculation of ice thickness as difference between total thickness measured by GEM and snow depth measured by MP. GPS positions are recorded for all measurements. Transects always followed a triangle away and back to the ship where lengths varied depending on floe size and conditions. In addition, the MP was used to measure snow depth and GPS position at several single points as markers for station work. The transects have a length of about 2 to 4 km to obtain data representative for the whole floe (Tab. 4.5.1). During the first transect batteries of MP were empty after walking about half distance and are considered to be broken, so were exchanged for the next stations were everything went well concerning MP. The GEM hat some calibration issues during all floes besides the first one.

Tab. 4.5.1: All GEM and MagnaProbe thickness transects on ICE stations 1 to 4

	Station ICE 1	**Station ICE 2**	**Station ICE 3**	**Station ICE 4**
ID/Date	PS50_44-1/ 2015-09-13	PS50_78-1/ 2025-09-21	PS50_90-1/ 2025-09-25	PS50_127-1/ 2025-10-10
Length	3.0 km	3.9 km	2.2 km	2.5 km
Comment	After 1.2 km MP batteries empty(broken)	Some issue with GEM calibration	Some issue with GEM calibration	Some issue with GEM calibration

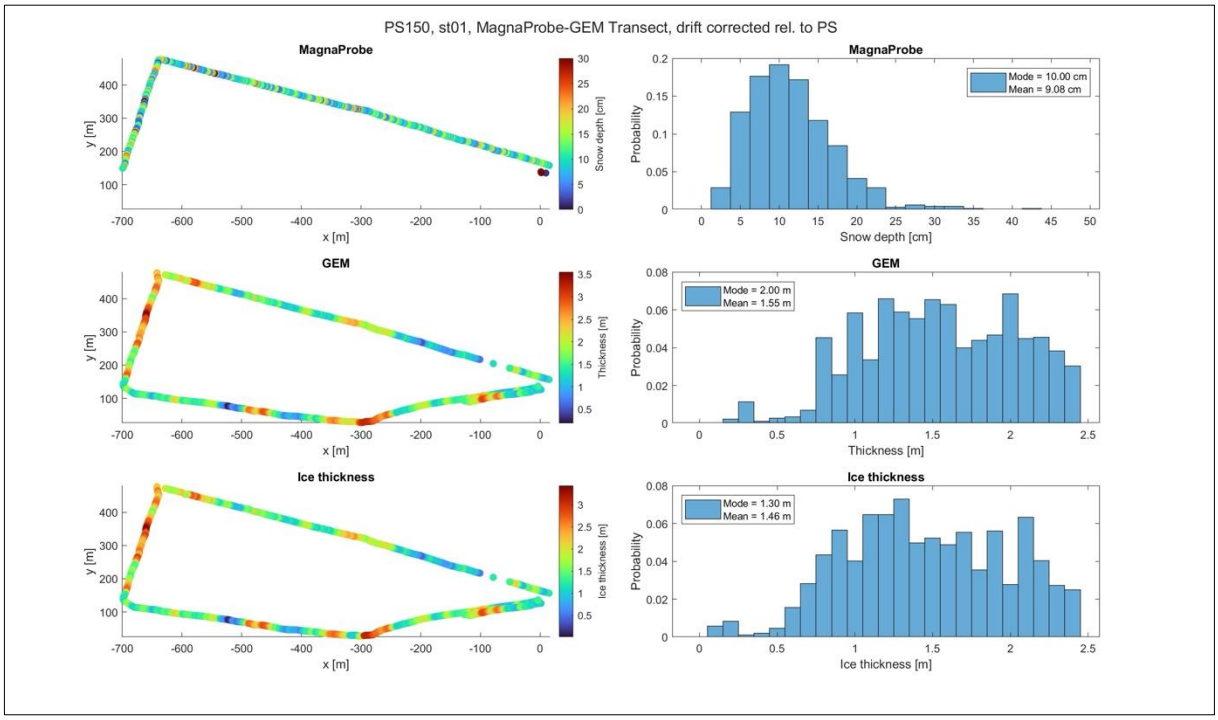

Fig. 4.5.1: Drift corrected tracks and thickness distributions of MagnaProbe and GEM transects for station ICE 1

Tab. 4.5.2: Cleaning times and comments for the 180° panoramic camera, Ramses sensor above crows nest, Sky Camera and Radiometers

Date and time (UTC)	Panomax 180°	Ramses	Sky Camera	Radiometer
2025-09-10 ~15:00-16:00	not cleaned no ice	cleaned little ice	no ice	working
2025-09-14 ~18:40-19:00	cleaned	cleaned little ice	no ice	working
2025-09-16 ~14:45-15:15	Cleaned, still frozen	Not able to clean completely	no ice	working
2025-09-20 ~9:00-9:30	Fully cleaned	Fully cleaned	no ice	working
2025-09-22 ~14:00	Fully cleaned	Fully cleaned	no ice	working
2025-09-27 ~10:50-11:15	Fully cleaned	Fully cleaned	no ice	working

Preliminary (expected) results

At all ICE stations snow depth, total thickness and ice thickness distributions are obtained as shown in Figure 4.5.1 for the first ICE station. Drift corrected tracks relative to *Polarstern* are

shown in the same figure. A part of the MP track is missing as batteries were empty. For floes 2 to 4 some issues with the GEM calibration occurred when checking the data. For that reason, results cannot be presented yet, but this will probably be possible at a later stage.

Overall, there were great differences in snow cover, ridge fraction and ice thickness on the different floes. At station ICE 1 snow thickness ranged approximately between 5 and 20 cm where also some lower and higher values were detected. Total thickness is constant at a high level between about 0.7 and 2.3 m. Subtraction of snow depth from total thickness results in the sea ice thickness which has about the same range with a mode of 1.3 m.

4.6 Physical properties of sea ice from ice coring

Work at sea

Temperature and salinity measurements were performed in collaboration with the ecology Team (Chapter 3).

Two ice cores per station were taken home for further analyses (ARC and TEMP).

Preliminary (expected) results

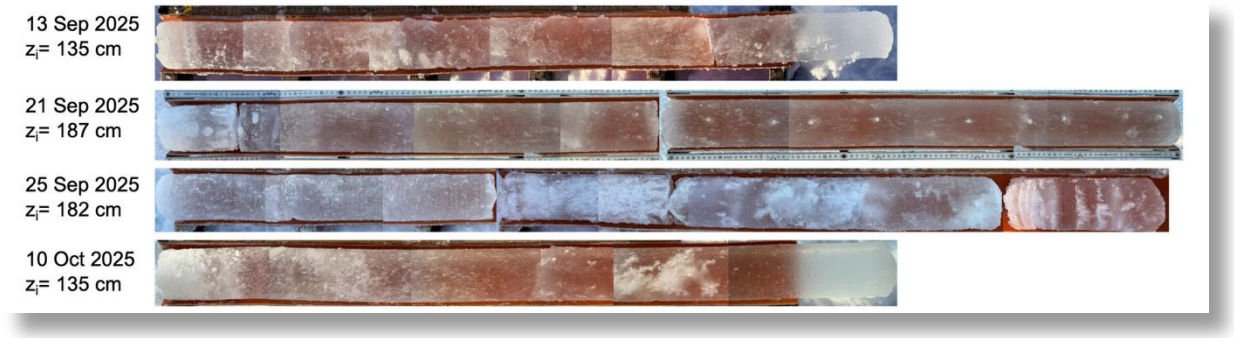

Fig. 4.6.1: Photo composites of the archive core of each ice station. The composites are stitched from photos taken in the field. The picture width is approximately to scale for each core.

4.7 Measurements of snow

Work at sea

Data collection and events

All snow measurement events are recorded as PS150_Stationnumber-1-snowpit_xx. 'Snowpit' is a parent device to all other 'snow' devices. Each 'snowpit' event is shown in Table 4.7.1. All events are recorded as device 'snowpit' (PS150_Stationnumber-1-snowpit_xx).

'Snowpit' measurements were collected on four different ice stations during the 2025 EGC Sources expedition. At each station, an undisturbed area was established for measurements. The measurement site/transect was always close to the coring site.

The measurement consisted of snow imager transects of the surface with different spacings (1-5 m) and different distances (up to 100 m) accompanied by snow depth measurements. In order to obtain the vertical structure of the snowpack additional snow imager photos of vertical snow profiles were taken. In total, 15 events were carried out.

Field instruments

We used the following instruments:

- Wooden ruler (snow height, rectangular square profile of 2 mm x 15 mm)
- Avalanche probe (snow height, cylindrical cone profile with a diameter of 14 mm)
- Camera (mobile phone) for overview pictures
- SnowImager: For taking near infrared reflectance images of a snow surface or profile. It consists of a near infrared (850 nm and 940 nm, separately) illumination system and two cameras to capture the reflected light. The housing of the SnowImager acts as a sun (light) shield. The imageable area is approximately 300 mm x 400 mm. A top and a bottom image of reflectance and dark (no illumination) images from two camaras are captured and stitched together in post processing. (specific surface area + density)

Snow transects

4. Overview pictures of measurement sites
5. SnowImager SSA surface measurements is either every 1 m (if it's a short transect 0-20 m) or every 5 m if it is a long transect (50-100 m).
6. SnowImager density (with grid) measurements of the surface (usually offset by 0.5 or 2.5 m to the SSA transect) (only at selected transects; see comments Tab. 4.7.1)
7. 5 snow heights in each SnowImager footprint, cm-accuracy. With ruler or avalanche probe or both
8. SnowImager measurement of the snow pit wall for SSA (Fig. 4.7.1)

The measurements should also be compared to the MagnaProbe measurements taken on the different ice stations.

Fig. 4.7.1: SnowImager measurement of a snow pit wall (Photo: Marcel Nicolaus, AWI)

Tab. 4.7.1: List of 'snowpit' events that were measured during EGC sources.

Event ID	Date and time	Comments
PS150_42-1-snowpit-01	2025-09-13T13:50:00	SnowImager, 65m transect á 5m, grid 2,5m space between
PS150_42-1-snowpit-02	2025-09-13T15:30:00	SnowImager, vertical profile on ice surface
PS150_42-1-snowpit-03	2025-09-13T15:39:00	SnowImager, vertical profile on frozen pond
PS150_42-1-snowpit-04	2025-09-13T16:01:00	SnowImager, vertical profile on frozen pond
PS150_42-1-snowpit-05	2025-09-13T16:08:00	SnowImager, 10m transect á 1m
PS150_78-1-snowpit-01	2025-09-21T10:00:00	SnowImager, transect 100m á 5m
PS150_78-1-snowpit-02	2025-09-21T11:14:00	SnowImager, vertical profile
PS150_78-1-snowpit-03	2025-09-21T15:59:00	SnowImager, transect 20m á 1m; grid every 0.5m in between
PS150_90-1-snowpit-01	2025-09-25T14:21:00	SnowImager, transect 50m á 5m
PS150_90-1-snowpit-02	2025-09-25T15:05:00	SnowImager, vertical profile on ice surface
PS150_90-1-snowpit-03	2025-09-25T16:11:00	SnowImager, transect 25m á 1m
PS150_90-1-snowpit-04	2025-09-25T16:54:09	SnowImager, vertical profile on frozen pond surface
PS150_127-1-snowpit-01	2025-10-10T13:15:00	SnowImager, transect 50m (1-15m every 1m)
PS150_127-1-snowpit-02	2025-10-10T15:15:00	SnowImager, vertical profile on frozen pond surface
PS150_127-1-snowpit-03	2025-10-10T16:30:00	SnowImager, transect 50m (20-50m every 5m)

Preliminary (expected) results

The objective of the measurements is to quantitatively describe the statistical spatial variability of snow which will be quantified with the SnowImager measurements. However, this needs further processing after the expedition.

The snow height varied between 5-39 cm on the 4 ice stations. The highest snow layer was found on the last ice station (4) on a frozen melt pond. The constitution of the snow changed between ice station 1,2 and 3 compared to 4. On the first three ice stations we found rather fluffy new snow which was still quite soft and on Station 4 a frozen compacted surface (Fig. 4.7.3) and another melt surface layer in the rather big snow pack (Fig. 4.7.2).

Fig. 4.7.2: Snow pit wall on ice station 4 with frozen layer in the middle (Photo: Julia Regnery, AWI)

Fig. 4.7.3: Two different snow surfaces on station 3 (left) and station 4 (right) (Photo: Julia Regnery, AWI)

4.8 Autonomous measurements and seasonal installations

Work at sea

Recoveries of devices for autonomous measurements and seasonal installations were performed during CONTRASTS.

Preliminary (expected) results

Buoy 2025K3 on Floe 3 continued its observation beyond the CONTRASTS expedition and was recovered during the following EGC-Sources (PS150) expedition on 8 September.

See Table 4.1.1 with camera photos.

Station 2025R29 on floe 3 continued its observation beyond the CONTRASTS expedition and is planned to be recovered during the following EGC-Sources (PS150) expedition.

Snow Buoy 2025S133 deployed on 20 July during CONSTRASTS

Fig. 4.8.1: Photographs from the buoy recoveries on 8 September 2025. These buoys were deployed on Regime 3 of the CONTRASTS expedition and recovered at the end of their life time (see Figure 4.0.1): A) sea ice conditions in the marginal ice zone during recovery, B) Camera Buoy 2025K3, C) Acoustic Current Doppler Profiler, D) Snow Buoy 2025S133, E) Radiation station 2025R29, F) position buoy from the former meteorological tower. (Photos: Marcel Nicolaus, AWI)

4.9 Eden – mapping sea ice conditions

Work at sea

The EDEN system is designed to extend the long-term usability of Earth observation data (e.g. TerraSAR-X imagery) and to establish a consistent link between the actual ship position and its position relative to the surrounding sea ice. To accomplish this, ice drift information derived from wind measurements, ice radar, or buoy data is used to refine the georeferencing of the Earth observation data.

When drift correction is applied over extended periods, positional deviations may occur. To address this, during EGC-Sources a functionality was introduced that enables users to manually apply adjustments, which are subsequently integrated with the automatic corrections. This enhancement could further increase the lifetime of the satellite data and improves the usability of the EDEN layer, as it provides a clearer representation of the vessel's current position relative to the ice. Note that these manual adjustments are optional. EDEN remains a system that can operate fully automatic.

Users can use the MapViewer to determine the bearing and distance between the vessel's actual position and its assumed position relative to the ice as displayed within the EDEN layer. This information can then be entered into a new web interface (Figure 4.9.1). Internally, these adjustments are stored in a database and used in future runs of the EDEN software. During the cruise, EDEN generated a new image every four minutes whenever *Polarstern* was within the coverage area of a satellite acquisition.

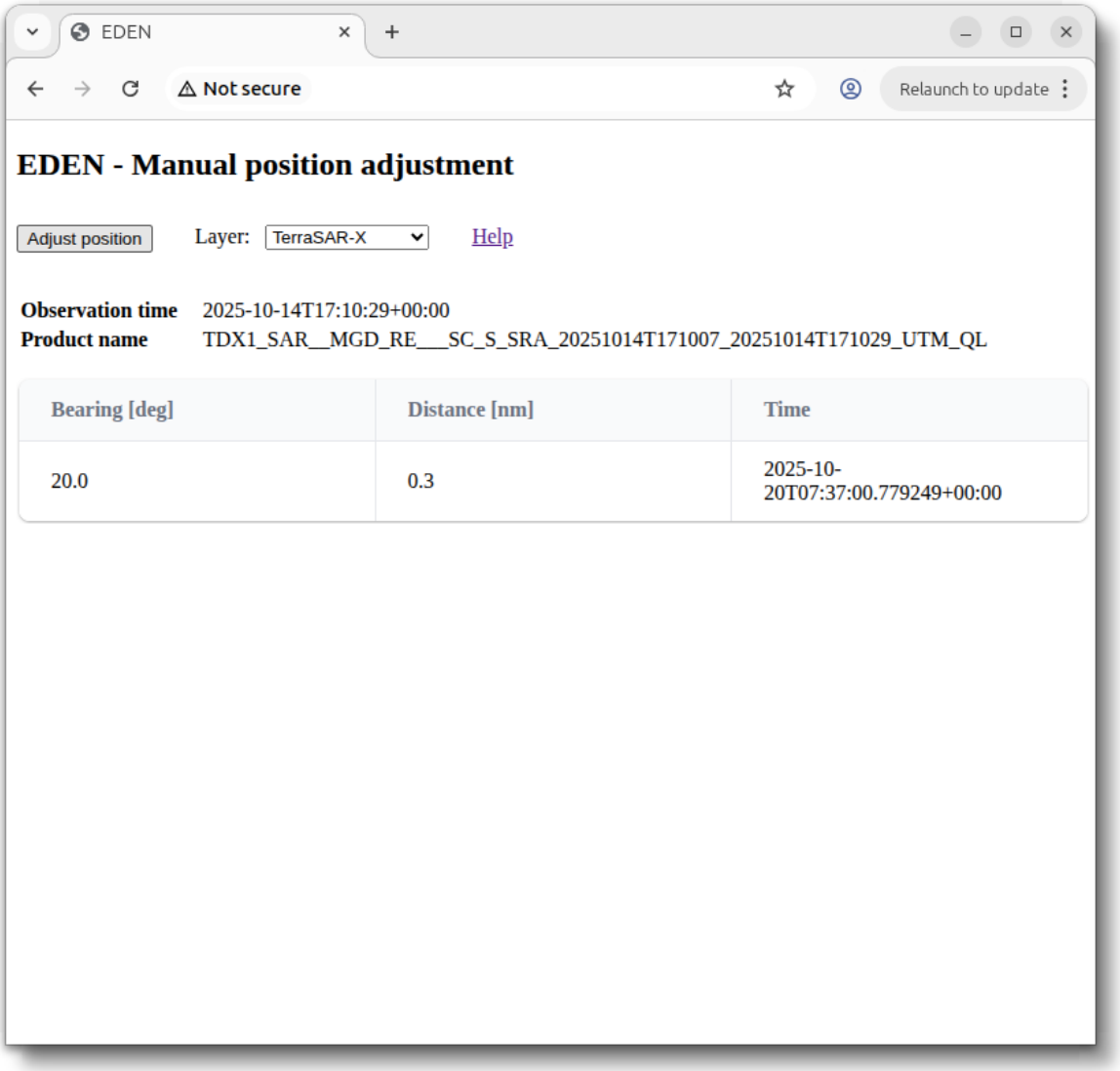

Fig. 4.9.1: User interface for applying manual drift corrections on top of the automatic ones.

Preliminary (expected) results

It proved advantageous to store the adjustments in a database. This database is now also used to maintain metadata of existing satellite images. As a result, the initial data loading process can be significantly accelerated. Moreover, the use of a database facilitates retrospective analysis of the data.

During the expedition, the EDEN system was monitored regarding its robustness and the quality of outputs. Misplacements were measured by manually comparing the satellite image to the data from the ice radar or visual observations.

Data management

All environmental data obtained during this expedition will be archived, published, and disseminated according to international standards by the World Data Center PANGAEA (Data Publisher for Earth & Environmental Science; https://www.pangaea.de) within two years after the end of the expedition at the latest. Unless specified otherwise, a CC-BY license will apply. Measurements from autonomous systems, which transmit data in near real time via satellite communication, will be made immediately available through the data and information portal meereisportal.de. Any other data will be submitted to an appropriate long-term archive that provides unique and stable identifiers for the datasets and allows open online access to the data.

This expedition is supported by the Helmholtz Research Programme “Changing Earth – Sustaining our Future” Topic 2, Subtopic 2.1.

In all publications based on this expedition, the **Grant No. AWI_PS150_06** or, in case of multidisciplinary work, **AWI_PS150_00** will be quoted and the following publication will be cited:

Alfred-Wegener-Institut Helmholtz-Zentrum für Polar- und Meeresforschung (2017) Polar Research and Supply Vessel POLARSTERN Operated by the Alfred-Wegener-Institute. Journal of large-scale research facilities, 3, A119. http://dx.doi.org/10.17815/jlsrf-3-163.

5. GEOPHYSICS AND GEODESY

Vera Schlindwein*[1,2], Matthias Pilot[1], Catalina Gebhardt[1], Simon Dreutter[1], Annie Lemire[1], Johannes Fricke[3];
not on board: Wolfram Geissler[1], Mirko Scheinert[3], Lutz Eberlein[3]
* vera.schlindwein@awi.de

[1]DE.AWI
[2]DE.Uni Bremen
[3]DE.TUD

Grant-No. AWI_PS150_04

5.1 Seismology

Vera Schlindwein*[1,2], Matthias Pilot[1]
not on board: Wolfram Geissler[1]
* vera.schlindwein@awi.de

[1]DE.AWI
[2]DE.Uni Bremen

Objectives

For a geologically old craton, Northeast Greenland shows remarkably strong earthquake activity focussed in three areas (Fig. 5.1.1): 1) seismicity in Peary Land near the Harder Fjord Fault Zone (HFFZ) and the Navarana Fjord Escarpment (NFE), 2) seismicity in the Wandel Sea parallel to the trend of the Trolle Land Fault Zone (TLFZ), and further south 3) the area between 78° and 80°N along the N-S trend of the Caledonian fold belt.

A key debate is, whether the present-day seismicity is a consequence of tectonic stresses induced by the nearby plate boundary in the Lena Trough or is generated by post-glacial and elastic rebound processes due to past and ongoing deglaciation (Chung 2002; Olivieri & Spada 2015). Glacially induced stress may reactivate pre-existing tectonic structures and may even trigger earthquakes with tsunami potential in the North Atlantic (Steffen et al. 2020). The concentration of seismicity along the coasts around Greenland supports the idea of seismicity related to deglaciation processes (Chung 2002).

While seismicity in areas 1 and 2 is likely related to known fault zones, the origin of the seismicity in area 3 between 78°N and 80°N, although following the general trend of the Caledonian orogen, may yet have another explanation: the seismically active area 3 coincides with shallow bathymetry (Arndt et al. 2015) near the Zachariae and 79°N glaciers, with frequent occurrence of weak seismic events at locations with water depths shallower than 200 m (Fig. 5.1.1). Warm ocean currents get access via narrow channels to these glaciers, speeding up disintegration processes (Schaffer et al. 2020), but the ice remains captured between islands and bathymetric highs aligned with the trend of the Caledonian orogen (Henriksen et al. 2000). Ground or mutual contact of icebergs is known to produce considerable seismic energy around Antarctica (Schlindwein 2023).

This highlights that the intraplate seismicity of Greenland is far from being understood, and - with earthquakes exceeding M_w 5-6 - may even pose a considerable seismic hazard (Voss et al. 2007). At the moment, the seismic risk may still be low but as the Arctic is rapidly warming and a blue Arctic Ocean is likely in the next few decades, increased human activities will ultimately result in an augmented exposure to seismic hazards.

Only a single permanent seismic station (NOR, Dahl-Jensen et al. 2010) is located near the three seismically active areas of Northeast Greenland, so little is known about the origin of the earthquakes. In addition, the sparse cover with seismic stations also results in poor locations of earthquake foci along the nearby plate boundary in the Fram Strait. It is therefore not clear where exactly the young plate boundary is situated and whether a magmatic formation of ocean crust has developed here.

DEGLASEIS (Deglaciation seismicity of Northeast Greenland) is an opportunistic project that uses the new technical possibilities of ocean bottom seismometers that can be operated under sea ice and the rare opportunity of two consecutive *Polarstern* cruises to Northeast Greenland to operate an amphibious seismological network there for a year. This network will significantly reduce the detection threshold and improve the location accuracy of earthquakes in a region from Svalbard to North Greenland. DEGLASEIS will use this data set to investigate the following questions:

Is the earthquake activity an expression of the deglaciation of Northeast Greenland? Which geological structures are (re)activated in the process? Are some of the seismic events along large outlet glaciers possibly caused by icebergs? Or is the stress field determined entirely by plate tectonics? Where is the active plate boundary in the Fram Strait, and are tectonic or magmatic processes dominating seafloor spreading here?

Another focus is the mechanical state of the sea ice cover over the course of a year and the effect of storms and swell on the sea ice. These processes leave clear traces in the ambient seismic noise (Schlindwein et al. 2025) and can now for the first time be systematically analysed with seismometers located under the ice.

DEGLASEIS will thus make a concerted effort to better understanding of the deglaciation processes in Greenland and the sea ice disintegration in the Arctic Ocean based on their seismological fingerprints.

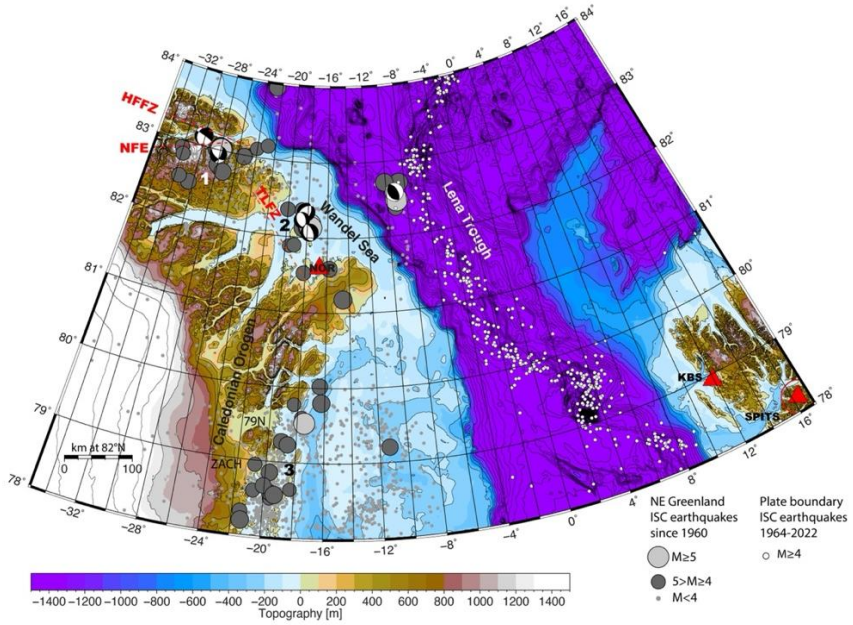

Fig. 5.1.1: Overview over the survey area of DEGLASEIS. Red triangles: permanent seismic stations. See text for abbreviations of geological fault zones. Bathymetry: IBCAO5 (Jakobsson et al. 2024)

Work at sea

DEGLASEIS installed an amphibian seismic network in Northeast Greenland that is planned to record for a period of 12 months seismic events related to deglaciation and tectonic processes. Our network consists of 7 off-shore ocean bottom seismometers (orange circles, DGS01-07, Fig. 5.1.2, Tab. 5.1.1), and 5 seismic stations on land (orange triangles, DGS11-15, Fig. 5.1.2, Tab. 5.1.2).

The OBS are provided by DEPAS (Alfred-Wegener-Institut et al. 2017). They are equipped with Trillium broadband (120 s) 3-component seismometers and a hydrophone. Battery power will allow recording for 12-14 months. Battery power of the release units enables instrument recovery up to 24 months after deployment. Prior to deployment, the release units of the OBS were tested for water tightness and functionality in three tests. OBS were then assembled and deployed in free-fall mode. The USBL positioning system was used to determine the accurate position of the OBS on the seafloor (Tab. 5.1.1).

Land stations are provided by the Geophysical Instrument Pool Potsdam (GIPP). They consist of passive Mark L-4C-3D short period (1 Hz) sensors and low-power consumption data cube loggers. With 2 battery packs per station at a sampling rate of 100 Hz we will achieve a continuous recording period of 12 months. Seismometers were installed on flat-lying bedrock where possible, oriented towards geographic north using compass and known declination (Fig. 5.1.3). The seismic sensor is shielded from wind and precipitation by a white bucket weighed down with bricks and rocks. Recording units and batteries fit in an insulation box that allows transmission of GPS signal (Fig. 5.1.4).

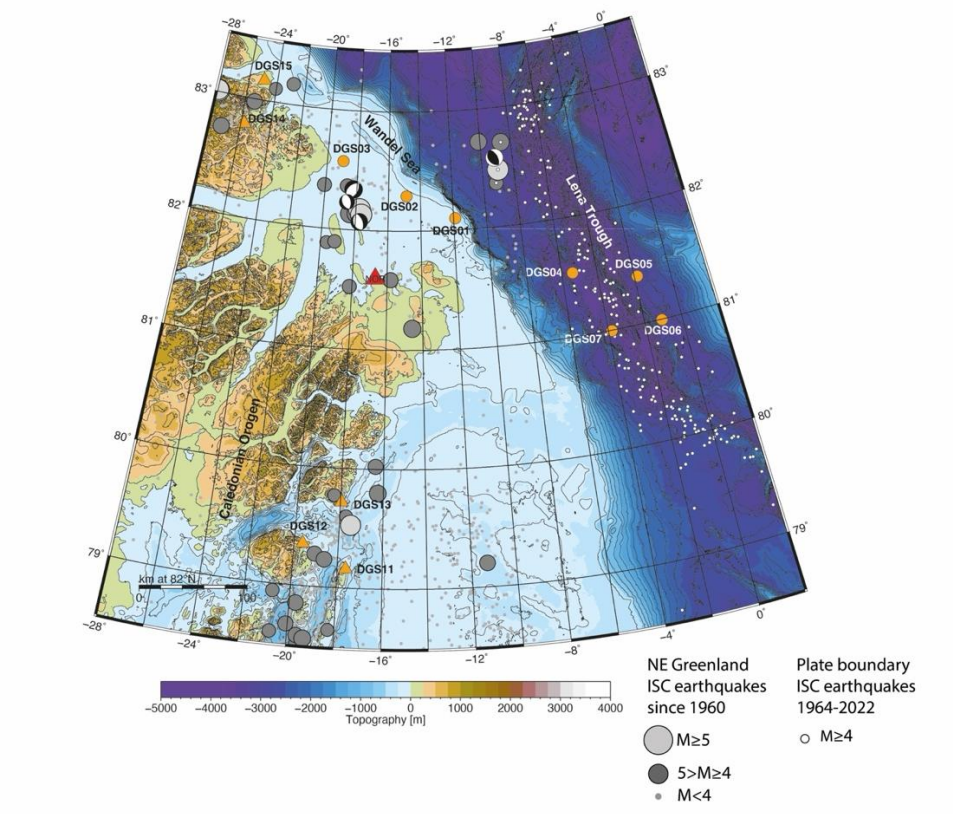

Fig. 5.1.2: Map of the seismic network DEGLASEIS. Orange circles: OBS positions, orange traingles: land seismic stations. Red triangle: permanent seismic station. Bathymetry: IBCAO5 (Jakobsson et al. 2024)

Fig. 5.1.3: Seismometer installed on bedrock

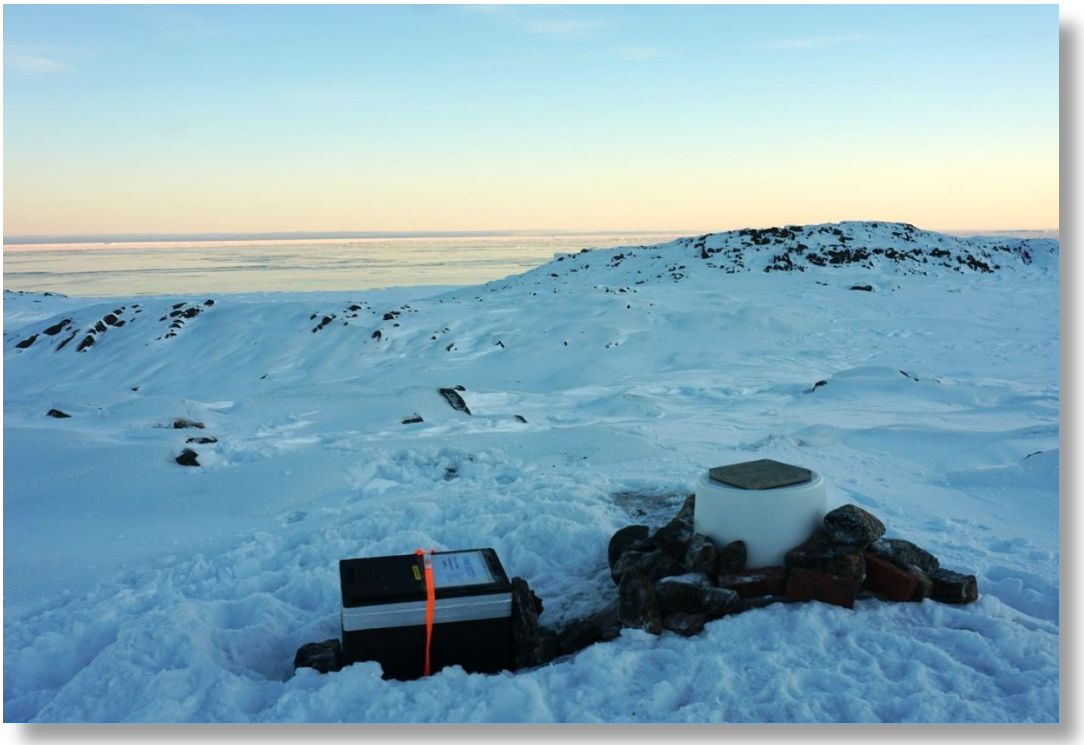

Fig. 5.1.4: Fully mounted seismic station on land. The seismometer is covered by the bucket, data recorder and battery supply are contained in the insulation box.

Preliminary (expected) results

Data will only become accessible upon recovery of the instrumentation during PS156 in 2026.

Tab. 5.1.1: Deployment details of the ocean bottom seismometers

Station	Position at seafloor			Deployment from ship	
	Latitude (°)	Longitude (°)	Depth (m)	Date	Time (UTC)
DGS01	82.0979	-11.9100	254	11.09.2025	10:52
DGS02	82.2916	-14.8772	218	12.09.2025	00:46
DGS03	82.5708	-18.9722	481	13.09.2025	02:22
DGS04	81.5320	-5.3893	3528	03.10.2025	05:02
DGS05	81.3982	-1.8376	3080	03.10.2025	13:13
DGS06	80.9948	-1.0764	3203	03.10.2025	19:23
DGS07	80.9947	-3.8206	3331	04.10.2025	05:40

Tab. 5.1.2: Deployment details of the land seismic stations

Station	Position on land			Deployment time	
	Latitude (°)	Longitude (°)	Elevation (m a.s.l.)	Date	Time (UTC)
DGS11	79.16149	-17.6352	34	10.10.2025	15:00
DGS12	79.35343	-19.6106	212	10.10.2025	11:00
DGS13	79.71693	-17.9487	25	10.10.2025	13:00
DGS14	82.78072	-25.7687	90	25.09.2025	12:00
DGS15	83.16548	-24.9210	176	24.09.2025	18:00

Data management

Raw seismological data will be archived, published, and disseminated according to international standards by the World Data Center **PANGAEA** (Data Publisher for Earth & Environmental Science; https://www.pangaea.de) within **two years** after the end of the expedition at the latest. Unless specified otherwise, a **CC-BY license** will apply. Time-corrected miniseed archives of the seismological data will be submitted to GEOFON from where they are accessible with seismological data base query tools.

This expedition was supported by the Helmholtz Research Programme "Changing Earth – Sustaining our Future" Topic 2, Subtopic 3.

In all publications based on this expedition, the Grant No. **AWI_PS150_04** will be quoted and the following publication will be cited:

Alfred-Wegener-Institut Helmholtz-Zentrum für Polar- und Meeresforschung (2017) Polar Research and Supply Vessel POLARSTERN Operated by the Alfred-Wegener-Institute. Journal of large-scale research facilities, 3, A119. http://dx.doi.org/10.17815/jlsrf-3-163.

For OBS data Alfred-Wegener-Institut Helmholtz-Zentrum für Polar- und Meeresforschung et al. (2017). DEPAS (Deutscher Geräte-Pool für amphibische Seismologie): German Instrument Pool for Amphibian Seismology. Journal of large-scale research facilities, 3, A122. http://dx.doi.org/10.17815/jlsrf-3-165 will be cited.

References

Alfred-Wegener-Institut Helmholtz-Zentrum für Polar- und Meeresforschung et al. (2017). DEPAS (Deutscher Geräte-Pool für amphibische Seismologie): German Instrument Pool for Amphibian Seismology. Journal of large-scale research facilities 3:A122. http://dx.doi.org/10.17815/jlsrf-3-165

Arndt JE, Jokat W, Dorschel B, Myklebust R, Dowdeswell JA & Evans J (2015) A new bathymetry of the Northeast Greenland continental shelf: Constraints on glacial and other processes. Geochemistry, Geophysics, Geosystems 16(10). https://doi.org/10.1002/2015gc005931

Chung W-Y (2002) Earthquakes Along the Passive Margin of Greenland: Evidence for Postglacial Rebound Control. Pure and Applied Geophysics 159:2567–2584.

Dahl-Jensen T, Larsen TB & Voss P (2010) Greenland ice sheet monitoring network (GLISN). Geological Survey of Denmark and Greenland Bulletin 20:55–58.

Henriksen N, Higgins AK, Kalsbeek F & Pulvertaft TCR (2000) Greenland from Archaean to Quaternary: Descriptive text to the Geological Map of Greenland 1:2500000. Geology of Greenland Survey Bulletin 185, 93pp.

Jakobsson M, et al (2024) The International Bathymetric Chart of the Arctic Ocean Version 5.0. Scientific Data 11(1). https://doi.org/10.1038/s41597-024-04278-w

Olivieri M & Spada G (2015) Ice melting and earthquake suppression in Greenland. Polar Science 9(1). https://doi.org/10.1016/j.polar.2014.09.004

Schaffer J, Kanzow T, von Appen W-J, von Albedyll, L, Arndt JE & Roberts DH (2020) Bathymetry constrains ocean heat supply to Greenland's largest glacier tongue. Nature Geoscience 13(3). https://doi.org/10.1038/s41561-019-0529-x

Schlindwein V (2023) Iceberg noise. In G. Bayrakci & F. Klingelhoefer (Eds.), Noisy Oceans: Monitoring Seismic and Acoustic Signals in the Marine Environment, Geophysical Monograph Series 284:83–96.

Schlindwein V, Li S, Kirk H & Schmidt-Aursch MC (2025) Seismic soundscape of the Arctic Ocean: seasonal effects of sea ice and swell on deep-sea ocean bottom seismometer records. Geophysical Journal International, in press. https://doi.org/10.1093/gji/ggaf143

Steffen R, Steffen H, Weiss R, Lecavalier BS, Milne GA, Woodroffe SA & Bennike O (2020) Early Holocene Greenland-ice mass loss likely triggered earthquakes and tsunami. Earth and Planetary Science Letters 546. https://doi.org/10.1016/j.epsl.2020.116443

Voss P, Kildegaard Poulsen S, Bjerregaard Simonsen S & Gregersen S (2007) Seismic hazard assessment of Greenland. Geological Survey of Denmark and Greenland Bulletin 13:57–60.

5.2 Geodetic GNSS Measurements in North-East Greenland

Johannes Fricke[1] [1]DE.TUD

not on board: Mirko Scheinert*[1], Lutz Eberlein[1]

- Mirko.Scheinert@tu-dresden.de

Objectives

The Greenland Ice Sheet (GrIS) is sensitive to changes in atmospheric and oceanic conditions which are triggered by climate change. Meltwater entering the ocean affects both global and regional sea level as well as oceanic circulation patterns. On the contrary, warmer ocean water entering Greenland shelf areas may lead to an increased subglacial melting and, thus, destabilisation of the outlet glaciers. Thus, in the period from 2005 to 2015 the GrIS contributed about 20% to the global mean sea level rise, whereby an acceleration in glacier flow accounts for about 50% of the ice-mass loss (The IMBIE Team 2020, Mouginot et al. 2019). However, ice-mass losses and changes in glacier dynamics vary considerably from region to region. They are determined by the complex interaction of ice, ocean, atmosphere and land (Kanzow et al. 2025). In order to gain a better understanding of these interplays and to arrive at reliable projections, we need, on the one hand, records on regional environmental conditions and glaciation history over the Holocene and, on the other hand, a suit of observations on recent changes of the geometry, flow velocity and mass of the GrIS and its individual outlet glaciers as well as of bedrock displacement. The latter is controlled by, and therefore informs about, past and present-day ice-load changes. Moreover, it modulates the geometry of the ice-ocean interface and thereby feeds back to ice mass change processes. A special aspect is given by the hypothesis that an increased ice-mass loss and subsequent vertical rebound may lead to a considerably large seismic activity along the coastal regions.

These ice mass changes occurring over the course of glaciation history, especially since the last glacial maximum, cause a glacial isostatic adjustment (GIA) of the solid Earth (Whitehouse et al. 2018; Caron et al. 2018). Today, the GIA effect is reflected in a long-term linear trend, with the effective elastic lithosphere thickness and upper mantle viscosity being crucial for the focusing and decay behaviour, respectively. In addition, there is an instantaneous response to changes in ice loading on short time scales which can be in the same order as or even larger than the GIA effect. The combined effect of GIA and present-day deformation can be measured by permanent and/or repeated geodetic GNSS recordings with an accuracy at the level of 1 mm/a (Kappelsberger et al. 2021).

Thus, the main goal of this project is to realize geodetic GNSS observations at selected bedrock locations in north-east Greenland to enhance the observational basis for the subsequent analysis of the bedrock displacement. Resulting displacement time series (and rates) will serve as an important constraint to investigate the response of the solid Earth to present-day as well as to past ice-mass changes and, eventually, to refine the modelling of glacial isostatic adjustment (GIA). Furthermore, in conjunction with seismic investigations co-located with the GNSS sites we will contribute to the investigation of the nature and causes of present-day seismicity.

Work at sea

Three locations at land could successfully be visited, namely at Lambert Land West, at Holm Land and at Peary Land (see Fig. 5.2.2 and Tab. 5.2.1). At the new site Peary Land (PEAR, Fig. 5.2.1) and at the already existing marker at Lambert Land West (LAMW) GNSS equipment was installed to realize campaign measurements. Each campaign installation includes GNSS receiver and antenna, a sealed battery and solar modules to ensure power supply, and further electronics, all packed in a Zarges aluminium box (see Fig. 5.2.1). These installations shall be

run for about one year and will be recovered during cruise PS156 in 2026. At the location Lambert Land West, the already existing permanent GNSS site (LAP1, see Fig. 5.2.3) was visited for maintenance, to upgrade the receiver and to download data. GNSS campaign equipment was successfully recovered at Holm Land (HOLM), which was installed during *Polarstern* cruise PS109 in 2017 and could not be removed due to unfortunate sea ice and weather conditions. The deployment and re-initialization of a GNSS campaign installation at Holm Land was not possible since this region is now classified as a sensitive area.

Fig. 5.2.1: PEAR station. Zarges box on the left, two solar panels and GNSS antenna on the right

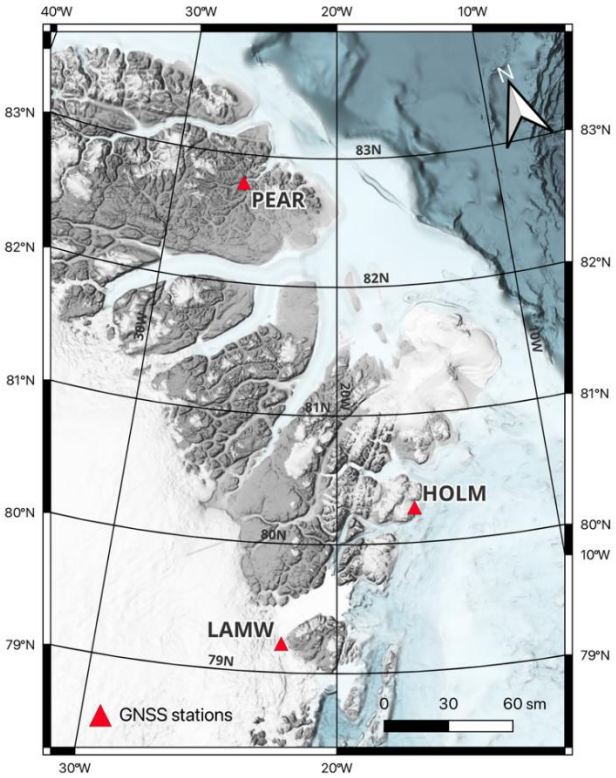

Fig. 5.2.2: Overview map of the area of investigation. The locations of the visited GNSS sites are plotted by red color (campaign sites PEAR, HOLM and LAMW, permanent site LAP1 is co-located with LAMW). Location PEAR is co-located with a seismometer (see Section 5.2.1).

Fig. 5.2.3: GNSS installations at Lambert Land West (LAP1, 2022, left) and Peary Land (PEAR, 2025, right). At LAP1 the GNSS antenna is mounted on top of a special pillar fixed to bedrock. Receiver, batteries and further equipment are stored in two Zarges aluminium boxes (mounted at the structure in the background), while four solar panels and a wind generator are used to recharge the batteries. At PEAR (right) the receiver and batteries are in the Zarges box (left), antenna and solar panels are mounted on bedrock (right).

Tab. 5.2.1: Locations and coordinates of the geodetic GNSS sites

ID	Location	Latitude (North) [°]	Longitude (West) [°]	Remark
LAP1	Lambert Land West	79° 13’ 35”	22° 18’ 22”	Upgrade and continuation of permanent recording
LAMW	Lambert Land West	79° 13’ 35”	22° 18’ 22”	Campaign sites: Setup during PS150, retrieval during PS156
PEAR	Peary Land	82° 46' 50''	25° 46' 7''	
HOLM	Holm Land	80° 16’ 23”	16° 25’ 54”	Recovering equipment

Preliminary (expected) results

During or right after the cruise PS150 we do not gain results right away. On the one hand, the GNSS campaign installations are planned to run for about one year and will be recovered in 2026 (during cruise PS156). The recovered data of the permanent GNSS site at Lambert Land West (LAP1) and campaign installation Holm Land (HOLM) will be processed at the home institution (so-called post-processing). For this, we will use the Bernese GNSS Software adopting up-to-date standards (e.g. consistent and precise realization of the reference frame, reduction of geodynamic and further effects). In the end, we will solve for time series of daily 3D coordinates from which displacement rates will finally be inferred.

Data management

The successfully recorded data are raw data and need to be processed at the home institutions. However, the GNSS raw data will be archived at TU Dresden in close coordination with a database which is being maintained in the frame of the SCAR Expert Group on Geodetic Infrastructure in Antarctica (GIANT). Resulting products from the GNSS processing will be published in conjunction with respective scientific papers and archived according to international standards by the World Data Center PANGAEA Data Publisher for Earth & Environmental Science; https://www.pangaea.de) within **two years** after the end of the expedition at the latest. Unless specified otherwise, a **CC-BY license** will apply.

In all publications based on this expedition, the **Grant No. AWI_PS150_4** will be quoted and the following publication will be cited:

Alfred-Wegener-Institut Helmholtz-Zentrum für Polar- und Meeresforschung (2017) Polar Research and Supply Vessel POLARSTERN Operated by the Alfred-Wegener-Institute. Journal of large-scale research facilities, 3, A119. http://dx.doi.org/10.17815/jlsrf-3-163.

References

Caron L, Ivins ER, Larour E, Adhikari S, Nilsson J & Blewitt G (2018) GIA model statistics for GRACE hydrology, cryosphere, and ocean science. Geophysical Research Letters 45:2203–2212. https://doi.org/10.1002/2017GL076644

Kanzow T, Humbert A, Mölg T, Scheinert M, Braun M, Burchard H, Doglioni F, Hochreuther P, Horwath M, Huhn O, Kappelsberger M, Kusche J, Loebel E, Lutz K, Marzeion B, McPherson R, Mohammadi-Aragh M, Möller M, Pickler C, Reinert M, Rhein M, Rückamp M, Schaffer J, Shafeeque M, Stolzenberger S, Timmermann R, Turton J, Wekerle C & Zeising O (2025) The system of atmosphere, land, ice and ocean in the region near the 79N Glacier in northeast Greenland: synthesis and key findings from the Greenland Ice Sheet–Ocean Interaction (GROCE) experiment, The Cryosphere 19:1789–1824. https://doi.org/10.5194/tc-19-1789-2025

Kappelsberger MT, Strößenreuther U, Scheinert M, Horwath M, Groh A, Knöfel C, Lunz S & Khan SA (2021) Validating surface-deformation predictions in north-east Greenland using refined estimates of contemporary ice-mass change and densified GNSS measurements. Journal of Geophysical Research Earth Surface. https://doi.org/10.1029/2020JF005860.

Mouginot J, Rignot E, Bjørk AA, van den Broeke M, Millan R, Morlighem M, Noël B, Scheuchl B & Wood M (2019) Forty-six years of Greenland Ice Sheet mass balance from 1972 to 2018. Proceedings of the National Acadamy of Sciences, 116(19): 9239–9244. https://doi.org/10.1073/pnas.1904242116.

The IMBIE Team (2020) Mass balance of the Greenland Ice Sheet from 1992 to 2018. Nature 579:233–239. https://doi.org/10.1038/s41586-019-1855-2.

Whitehouse PL (2018) Glacial isostatic adjustment modelling: historical perspectives, recent advances, and future directions. Earth System Dynamics 6(2):401–429. https://doi.org/10.5194/esurf-6-401-2018

5.3 Hydroacoustics

Catalina Gebhardt*[1], Simon Dreutter[1], Annie Lemire[1]

[1]DE.AWI

* catalina.gebhardt@awi.de

Objectives

Past glacier dynamics can be inferred from glacial features observed on the seafloor. These were formed by glacial processes during the maximum extent of the NEGIS during both the last glacial and stillstands of the deglacial. Targets for bathymetric and sediment-echosounding data collection are areas where moraines and grounding-zone wedges are encountered, helping to reconstruct past events of ice-sheet and ice-shelf retreat. In addition, accurate knowledge of seafloor topography is generally a basic information to understand marine processes, and reliable seafloor topography data is also needed as a boundary condition in modeling. However, as of June 2024, only 26.1% of the ocean are bathymetrically mapped (Seabed 2030 news of 21 June, 2024), and the target area of EGC-Sources is one of the under-investigated areas. We aim at collecting data of the seafloor and the upper sedimentary layers and contribute to international efforts to enhance seafloor topography resolution such as IBCAO (Jakobsson et al. 2025) as well as to provide information on subbottom acoustic facies (Mosher et al. 2015).

Work at sea

During PS150, bathymetric and sediment echosounder data were recorded simultaneously along the track. Bathymetry data was collected using the hull-mounted Teledyne Reson Hydrosweep DS3 multibeam echosounder, and sediment echosounder data was collected with the hullmounted Teledyne Reson Parasound P70 sub-bottom profiling system. The main task of the hydroacoustic group was to collect underway data during the cruise. Raw bathymetric data was corrected for sound velocity changes in the water column, and further processing and cleaning for erroneous soundings and artefacts was carried out in parallel to data acquisition. Sediment echosounder data was quality-checked and converted to standard SGY format. Acoustic measurements were continuously monitored during the survey.

Technical description

The HYDROSWEEP is a deep-water system for continuous mapping with the full swath potential. It operates on a frequency of ~14 kHz. On *Polarstern*, the MBES transducer arrays are arranged in a Mills cross configuration of 3 m (transmit unit) by 3 m (receive unit). The combined motion, position (Trimble GNSS), and time data comes from an iXBlue Hydrins system and the signal goes directly into the Processing Unit (PU) of the MBES to do real-time motion compensation in Pitch, Roll and Yaw. With a combination of phase and amplitude detection algorithms the PU computes the water depth from the returning backscatter signal. The system can cover a sector of up to 140° with each 70° per side.

The hull-mounted sub-bottom profiling system PARASOUND generates two primary frequencies, of which the lower frequency is selectable between 18 and 23.5 kHz transmitting in a narrow beam of 4° at high power (PHF). As a result of the non-linear acoustic behavior of water, the so-called “Parametric Effect”, two secondary harmonic frequencies are generated, one of which is the difference (e.g. 4 kHz, SLF) and the other the sum (e.g. 40 kHz, SHF) of the two primary frequencies, respectively. As a result of the longer wavelength, the difference parametric frequency allows sub-bottom penetration up to 200 m (depending on sediment conditions) with a vertical resolution of about 30-40 cm. The primary advantage of parametric echosounders is based on the fact that the sediment-penetrating pulse is generated within the

narrow beam of the primary frequencies, thereby providing a very high lateral resolution compared to conventional 4 kHz-systems.

Data acquisition and processing

Data acquisition was carried out throughout the entire cruise between Longyearbyen, Svalbard, and Bremerhaven, Germany, with the exception of two narwhal protection areas along the Greenland coast (for details, see Tab. 5.3.1 and Fig. 5.3.1).

PARASOUND was operated with Atlas Hydromap Control and the data was visualized in Atlas Parastore. Four different types of PARASOUND data files were stored:

- PHF data in ASD format
- PHF data in PS3 format (carrier frequency, lat.long)
- SLF data in ASD format
- SLF data in PS3 format (carrier frequency, lat.long)

SLF PS3 files were subsequently converted to standard SGY format with ps32sgy (Hanno Keil, University of Bremen), and UKOOA navigational files were created using PostProcessor v1.7 (Florian Riefstahl, AWI Bremerhaven). Files were then imported into S&P Global Kingdom for georeferenced visualization and quality check.

The MBES was operated with Sonar UI and for online data visualization and data logging, Teledyne PDS was used. The collected bathymetry was logged in S7K raw files. Subsequent data processing was performed using Caris HIPS and SIPS. For generating maps, the data were exported to Quantum GIS in the GeoTIFF raster format.

Tab. 5.3.1: Hydroacoustic event log for underway stations *PS150_0_Underway-2* (HYDROSWEEP) and *PS150_0_Underway-13* (PARASOUND)

Date Time	Action	Latitude	Longitude	Comment
2025-09-04 20:04	acquisition start	78° 02.963' N	011° 18.499' E	
2025-09-08 22:36	acquisition paused	82° 03.596' N	007° 15.223' W	entry narwhal protection area
2025-09-11 07:17	acquisition resumed	81° 51.273' N	012° 03.994' W	exit narwhal protection area
2025-09-29 11:55	acquisition paused	81° 44.895' N	012° 37.282' W	entry narwhal protection area
2025-10-03 10:10	acquisition resumed	81° 28.608' N	003° 48.766' W	exit narwhal protection area
2025-10-11 20:30	acquisition paused	79° 49.136' N	016° 17.377' W	entry narwhal protection area
2025-10-14 17:15	acquisition resumed	79° 50.579' N	016° 31.360' W	exit narwhal protection area
2025-10-17 18:40	acquisition paused	78° 04.155' N	011° 13.266' E	entry Svalbard territorial waters
2025-10-18 13:32	acquisition resumed	78° 06.214' N	013° 08.905' E	exit Svalbard territorial waters
2025-10-23 10:47	acquisition end	56° 04.387'N	006° 38.322'E	

Sound velocity profiles

For best survey results and to correct HYDROSWEEP depths for changes of the sound velocity (SV) in the water column, SV profiles were generated from CTD data that were collected and provided by the Oceanography group. SV correlates with the density of a water mass and thus is depending on pressure, temperature and salinity of the seawater in a given location at a given depth. Wrong or outdated SV profiles lead to refraction errors and reduced data quality and faulty depth measurements.

During PS150, a total of 136 SV profiles were applied to the MBES. They include 121 SV profiles from the CTD data. The remaining profiles were purely synthetic profiles generated during transit using the WOA23 (World Ocean Atlas 2023).

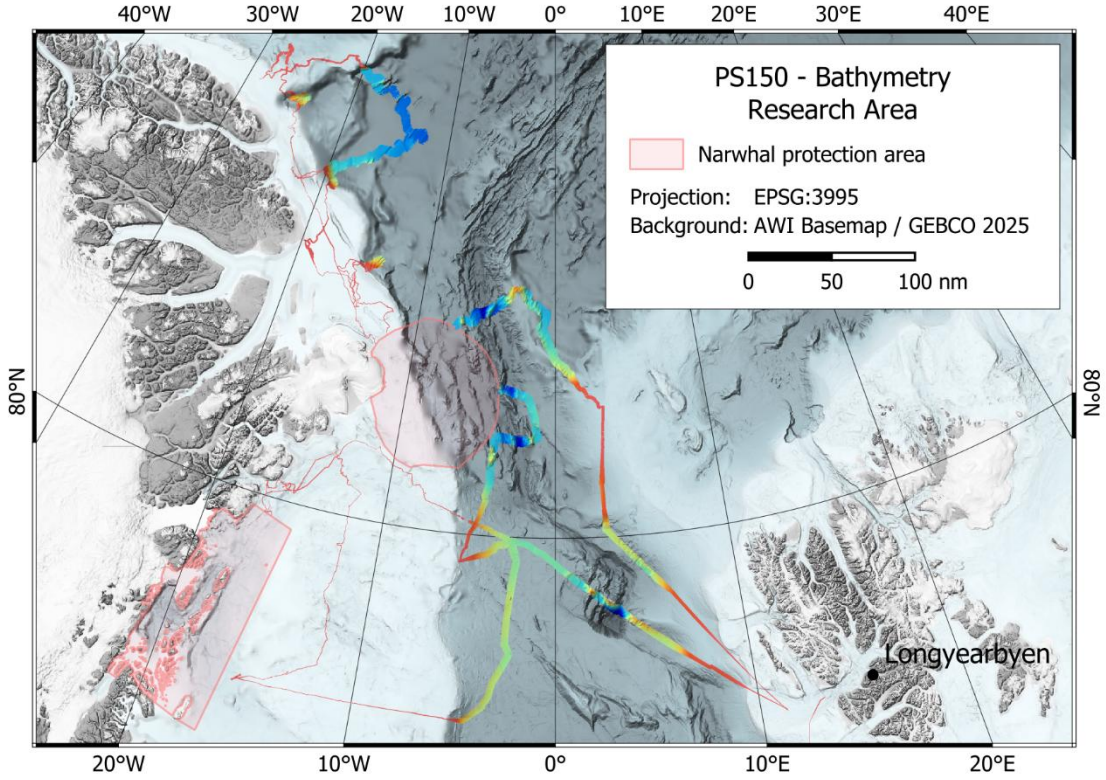

Fig. 5.3.1: Overview on the bathymetric data acquired in the main research area during PS150 (background digital elevation model is the AWI Basemap for the Arctic, based on IBCAO v5, Jakobsson et al. 2024, and GEBCO 2025)

Preliminary results

Parasound subbottom echosounding data often showed highly glacially overprinted signatures with characteristic low penetration of the signal. These signatures, in concert with bathymetry data, could be identified as glacial lineations of different style (Fig. 5.3.2). Due to the nature of this expedition, tracks often crossed slopes, resulting in low-quality sediment echosounder data. Ice conditions induced noise into the water column further lowering quality of data. When data were collected from small troughs on the shelf, they sometimes exhibited deeper penetration due to postglacial sedimentary infill. Deep-water areas were more variable, with areas close to the mid-ocean ridge exhibiting rough surface with low penetration, and those along the Svalbard-Norwegian margin during the transit from Longyearbyen to Bremerhaven displaying deep penetration into soft, well-layered sediments often intercalated by mass-failure deposits.

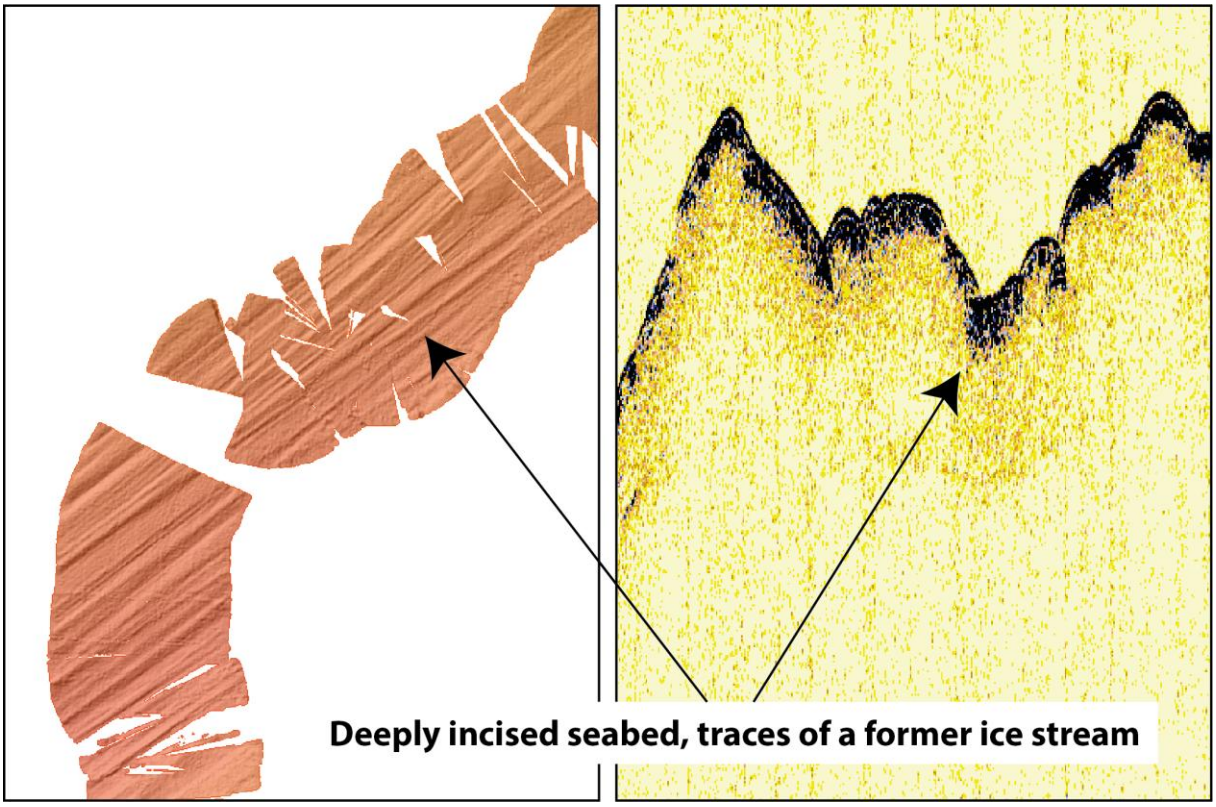

Fig. 5.3.2: Megascale glacial lineations off Independence Fjord. Left panel: Multibeam data; right panel: Parasound sediment-echosounder data.

During 43 days of survey, a track length of 4,266 nm (7,901 km) was surveyed by the swath bathymetry system, resulting in an area of 28,923 km2 of mapped seafloor. Fig. 5.3.2 shows the generated bathymetry grid. The raw data volume of bathymetric data (S7K format) was 197 GB broken up in 951 separated data files. Raw data volume of Parasound data (ASD and PS3 format) was 703 GB consisting of 46,861 single data files.

Data management

Bathymetry and sub-bottom data collected during the expedition will be archived, published and disseminated according to the international standards by the World Data Center PANGAEA Data Publisher for Earth & Environmental Science (https://www.pangaea.de) in accordance to the AWI research data guideline and directive (https://hdl.handle.net/10013/epic.be2ebee5-fb98-4144-9e74-aa1d38378c5e). The data will be made available upon request after a phase of restricted access of 4 years after data acquisition at the latest. By default, the CC-BY license will be applied. Furthermore, bathymetric data will be provided to the Nippon Foundation – GEBCO Seabed 2030 Project.

This expedition will contribute to the Helmholtz Research Programme "Changing Earth – Sustaining our Future" Topic 2, Subtopics 2.1 and 2.3.

In all publications based on this cruise, the Grant No. **AWI_PS150_04** will be quoted and the following article will be cited:

Alfred-Wegener-Institut Helmholtz-Zentrum für Polar- und Meeresforschung (2017) Polar research and supply Vessel POLARSTERN operated by the Alfred-Wegener-Institute. Journal of Large-Scale Research Facilities, 3, A119, http://dx.doi.org/10.17815/jlsrf-3-163.

References

GEBCO Compilation Group (2025) GEBCO 2025 Grid https://doi.org/10.5285/ 37c52e96-24ea-67c e-e063-7086abc05f29

Jakobsson M, Mohammad R, Karlsson M, Salas-Romero S, Vacek F, Heinze F, Bringensparr C, Castro CF, Johnson P, Kinney J, Cardigos S, Bogonko M, Accettella D, Amblas D, An L, Bohan A, Brandt A, Bunz S, Canals M, Casamor JL, Coakley B, Cornish N, Danielson S, Demarte M, Di Franco D, Dickson ML, Dorschel B, Dowdeswell JA, Dreutter S, Fremand AC, Hall JK, Hally B, Holland D, Hong JK, Ivaldi R, Knutz PC, Krawczyk DW, Kristofferson Y, Lastras G, Leck C, Lucchi RG, Masetti G, Morlighem M, Muchowski J, Nielsen T, Noormets R, Plaza-Faverola A, Prescott MM, Purser A, Rasmussen TL, Rebesco M, Rignot E, Rysgaard S, Silyakova A, Snoeijs-Leijonmalm P, Sorensen A, Straneo F, Sutherland DA, Tate AJ, Travaglini P, Trenholm N, van Wijk E, Wallace L, Willis JK, Wood M, Zimmermann M, Zinglersen KB & Mayer L (2024) The International Bathymetric Chart of the Arctic Ocean Version 5.0. Sci Data 11:1420. https://doi.org/10.1038/s41597-024-04278-w

Mosher DC, Courtney RC, Jakobsson M, Gebhardt AC & Mayer LA (2015) Mapping the surficial geology of the Arctic Ocean: A Layer for the IBCAO, Arctic Technology Conference. Offshore Technology Conference, Copenhagen, Denmark, p. OTC 25561.

Seabed 2030 news of June 21st, 2024, https://seabed2030.org/2024/06/21/seabed-2030-announces-latest-progress-on-world-hydrography-day/, accessed 12 June 2025.

6. MARINE GEOCHEMISTRY

Mara Rosmann[1] [1]DE.AWI

Not on board: Junjie Wu[1], Torben Gentz[1], Gesine Mollenhauer[1];

* mara.rosmann@awi.de

Grant-No. AWI_PS150_05

All components of the Marine Geochemistry research program have been incorporated into other programs, specifically 7. Chemistry (sections 7.6 and 7.7) and 8. Tracer Oceanography.

7. CHEMISTRY

Zoë Neumann[1], Klara Köhler[2], Sofia Kuzmina[3], Patrick Selle[4], Daniel Scholz[3], Mara Rosmann[3], Sinhué Torres-Valdés*[3];
not on board: Agneta Fransson[4, 5], Junjie Wu[3], Torben Gentz[3], Gesine Mollenhauer[3], Melissa Chierici[6];
* sinhue.torres-valdes@awi.de

[1]DE.CAU
[2]DK.AU
[3]DE.AWI
[4]NO.UNIS
[5]NO.NPI
[6]NO.IMR

Grant-No. AWI_PS150_06

Outline

The Chemistry/Biogeochemistry component of this research expeditions concerns *1)* the transport and water mass sources of nutrients associated with the East Greenland Current, *2)* the determination of the carbon/carbonate system, air-sea CO_2 exchange and ocean acidification state, and the impact of glacial water, in north east Greenland fjords and coast, and *3)* the release of nutrients and organic carbon from melting Greenland Glaciers into the adjacent fjord systems and coastal waters. Our aim was therefore to measure (biogeo)chemical properties in seawater, including dissolved oxygen, via the analyses – onboard and on land laboratories – of samples taken from CTD-Rosette casts, sediment and particle samples, as well as via the deployment of biogeochemical packages; consisting of Remote Access Samplers (RAS) equipped with multiple biogeochemical sensors.

Objectives

Our aims concerning nutrients and the carbon system are multiple. Given one of our main objectives is to compute nutrient and carbon transports (in collaboration with the Physical Oceanography Team) associated with the EGC, we sampled and/or carried out measurements along the transects across the Northeast Greenland Shelf (Ile_de_France, Norske_Trough, Holm, Westwind_Trough, Flade_1, Flade_2, Independence_Shelfbreak, Independence_Midshelf, Independence_Mouth, Wandel, Morris_Jesup_Rise, Morris_Jesup_Spit, Cape_Morris_Jesup, and Lincoln), the mouth of Independence Fjord and around the 79N Glacier. Measurements were done at the best vertical and horizontal resolution as conditions and/or water budget requirements allowed. This was so that we can characterise the nutrient and carbon contents of the source water masses leading to the formation of the EGC. Dissolved oxygen was measured onboard, in part to calibrate the CTD-O_2 sensor(s) and also because via the calculation of the apparent oxygen utilisation we can determine the proportion of regenerated and preformed nutrients, useful to determine biogeochemical signatures resulting from e.g., remineralisation or denitrification. We are also interested in constraining and quantifying temporal (seasonal) changes in nutrient content and their implication for nutrient transports. Therefore, we deployed three biogeochemical packages, which -all working well- should provide biogeochemical data at hourly to weekly resolution, for one year.

Our wider scope goal is to assess the role of the EGC in the balance of nutrient and carbon transports across Fram Strait (e.g., relative to the WSC), thereby allowing us to further assess

the role of Fram Strait in the context of nutrient transports at the pan-Arctic scale (i.e., the Arctic Ocean nutrient budget). Via the measurement of dissolved inorganic carbon and total alkalinity we will also estimate the ocean acidification state and the impact of glacial and sea ice meltwater input by dissolution as well as the contribution of carbonate from bedrock-derived minerals in the glacial water.

An additional aim was to collect snow samples during ice stations for the measurement of nutrients. The aim of this is to combine the data with data collected in previous expeditions (PS138 and PS144) to assess the potential role of snow as an external supply of nitrogen species. This work has been done in collaboration with the sea ice physics team.

Glacial Flour: In addition to the water and snow samples, sediment samples were taken to assess the role of glacial flour as a source of nutrients. Glaciers abrade underlying bedrock, producing fine sediments (glacial flour), which is then transported from beneath ice masses by glacial runoff. These fine sediments have greater potential for chemical weathering than the parent bedrock, due to the larger surface area available for chemical reactions and the release of reactive compounds from their crystalline silicate matrix, allowing them to participate in rock-water reactions (Sharp et al. 1995). Consequently, subglacial meltwater outflow is an important nutrient source to downstream rivers and oceans, supporting new primary production (Hawkings et al. 2015) by providing important macro-nutrients, such as silicon (Si; Meire et al. 2016; Hawkings et al. 2017), phosphorus (e.g. Hawkings et al. 2016) and dissolved inorganic nitrogen (DIN) species (e.g. Wadham et al. 2016) to the wider ecosystem. With the samples taken at PS150 we are aiming to further investigate whether we can directly attribute a significant nutrient source to the glacial flour feeding into the EGC, with a focus on a distinct δ30SiDSi signature.

Organic Carbon input from glaciers: Retreating glaciers expose subglacial till and the organic carbon (OC) it contains. The reactivity of this OC – how readily it degrades and releases carbon to the ocean and atmosphere – governs its climate impact (Wu et al. 2022). Nioghalvfjerdsfjorden Glacier (79NG) is among the largest floating ice tongues in the Arctic, and its retreat likely alters local OC cycling. Around Greenland, OC reactivity remains unresolved with contrasting views (Bhatia et al. 2013; Bröder et al. 2022). Sedimentary records near 79NG indicate marked shifts in carbon composition (Syring et al. 2020). To evaluate the reactivity and composition of OC remobilized by the current 79NG retreat, we collected surface sediment samples along a 79NG transect for subsequent analyses, including TOC, ^{13}C, ^{14}C, and ramped pyrolysis oxidation–^{14}C (RPO-^{14}C).

Work at sea

The next section is divided into the following subsections: Nutrients (Section 7.1), sensors and remote access samplers (Section 7.2), Dissolved Oxygen (Section 7.3), Glacial samples and sediments (Section 7.4) and DIC/TA (Section 7.5), Sediment sampling of organic and inorganic carbon (Section 7.6) and underway sampling for POM of surface water (Section 7.7).

7.1 Nutrients

Lab Set up

For PS150 a 7-channel Seal Analytical AA-500 autoanalyser was set up in the chemistry lab for the analysis of micro-molar concentrations of 1) dissolved inorganic nutrients: nitrate plus nitrite (NO_3^-+NO_2^-) - hereafter referred to as nitrate -, nitrite (NO_2^-), silicate ($Si(OH)_4$), phosphate (PO_4^{3-}), and ammonium (NH_4^+) and 2) total nutrients; total dissolved phosphorus (TDP) and total dissolved nitrogen (TDN). Installation of the AA-500 involved the fitting of new pump tubing and new cadmium columns for TDN and nitrate. The nutrient analyser was controlled by the Seal Analytical Software AACE version 8.04, which allows for automated and

simultaneous analysis of up to 7 channels. Following analyser set up, analytical reagents (stock and working solutions), standards (stock solutions and calibrants) and lab-made quality control solutions were prepared. 'Stocks' are concentrated solutions from which 'working' reagents/standards are prepared as required by solution stability or usage. Pump tubing in the analyser were replaced two times during the expedition. Analyses were carried out following current Seal Analytical Methods, which are based on standard and widely used colorimetric techniques for the analysis of nutrients in water and seawater. The methods are listed below:

1. Total dissolved nitrogen in seawater No. G-218-98 revision 14 (MT23).
2. Nitrate and nitrite in water and seawater No. A-044-19 revision 5 (MT519A).
3. Nitrite in water and seawater No. A-003-18 revision 3 (MT518).
4. Total dissolved phosphorus in seawater No. G-439-16 revision 2 (MT33).
5. Phosphate in water and seawater No. A-004-18 revision 4 (MT518).
6. Silicate in water and seawater No. A-006-19 revision 3 (MT519).
7. Ammonium in water and seawater No. G-327-05 revision 8

Best practices procedures for the analyses of nutrients in seawater following GO-SHIP recommendations, as described in Hydes et al. (2010) and Becker et al. (2020), were adopted. Due to the relatively early start of hydrographic work (~2.5 days upon leaving port), the lab was not fully set up as it typically takes 5 full days to do so, from unpacking to testing, before work can commence. Because of this, samples collected were stored frozen until analysis could take place. The first analysis run took place on the 11 September 2025, having previously carried out two test runs to ensure measurements yielded satisfactory results. From then on, samples stored frozen were taken out of the freezer and left to melt for at least 18 h before being analysed. Eventually, this included samples collected during PS148.

Calibrants

Calibration standards for the analysis were prepared using 1,000 mg/L NO_3^-, NO_2^-, PO_4^{3-}, Si and NH_4^+ MERCK solutions. An intermediate standard containing 4.032, 0.152, 3.560, 0.947 and 0.5266 µmol/mL of nitrate, nitrite, silicate, phosphate and ammonium was prepared in Milli-Q water using a 100 mL volumetric flask. Although working calibration standards are typically prepared in a saline solution or "artificial seawater" (35 g NaCl in 1 L of Milli-Q water), which is also used as a matrix for the analysis, in later years the so called "ultra clean or analytical grade reagents" have been found to be contaminated with a given nutrient (usually phosphate, nitrate and organic nitrogen, and even silicate). Therefore, standards and the analysis matrix were based on Milli-Q water instead. From the intermediate standards, five calibration standards were prepared regularly using 500 mL to yield the target concentrations shown in Table 7.1.1. These values were then input into an analysis template file in the AACE software, from which all consecutive runs are then built. For each analysis, standards were measured in triplicate, with the first measurement intended as preconditioning and thus ignored as a calibrant. It is good practice to adapt calibration concentration ranges for the particular system being measured, in this case, the Arctic Ocean. Here though, we used a rather high range for phosphate. This was imposed by the method to measure TP, which is designed to work efficiently with a top standard of 5 µmol L^{-1}. A calibration range with a top standard lower than this is likely to yield high noise in the signal.

Tab. 7.1.1: Set of calibration standards (Std) used for dissolved inorganic nutrient analysis. Concentration units are µmol L-1. Concentrations in the first column are the sum of NO_3^- and NO_2^-, hence $NO_3^-+NO_2^-$. This concentration, plus that of NH_4^+ give the concentrations for TDN. Likewise, the concentration range for phosphate applies to TDP.

	$NO_3^-+NO_2^-$	NO_2^-	$Si(OH)_4$	PO_4^{3-}	NH_4^+	TDN	TDP
Std 1	0.469	0.017	0.399	0.106	0.059	0.528	0.106
Std 2	6.209	0.226	5.284	1.406	0.782	6.991	1.406
Std 3	11.950	0.435	10.169	2.707	1.504	13.454	2.707
Std 4	17.961	0.643	15.054	4.007	2.227	19.917	4.007
Std 5	23.431	0.852	19.939	5.307	2.949	26.381	5.307

All primary, secondary and working standards, CRMs and quality control solutions were kept in moisturised and dark conditions within a high-quality grade cool box when not in use and right after preparations.

Figure 7.1.1 shows the run-to-run spread (noise) of calibration standards. This information was used to assess the precision of measurements at each concentration level. The cruise-mean, standard deviation and precision of the analysis at the different concentration levels are presented in Table 7.1.2. Calibration standards show good consistency throughout the expedition. As is common, precision is reduced at low concentration levels. The limits of detection, taken as twice the standard deviation of the lowest concentration standard (cruise-long standard deviation) were: 0.11, 0.014, 0.03, 0.01, 0.03, 0.10 and 0.02 µmol L^{-1} for $NO_3^-+NO_2^-$, NO_2^-, $Si(OH)_4$, PO_4^{3-}, NH_4^+, TDN and TDP, respectively.

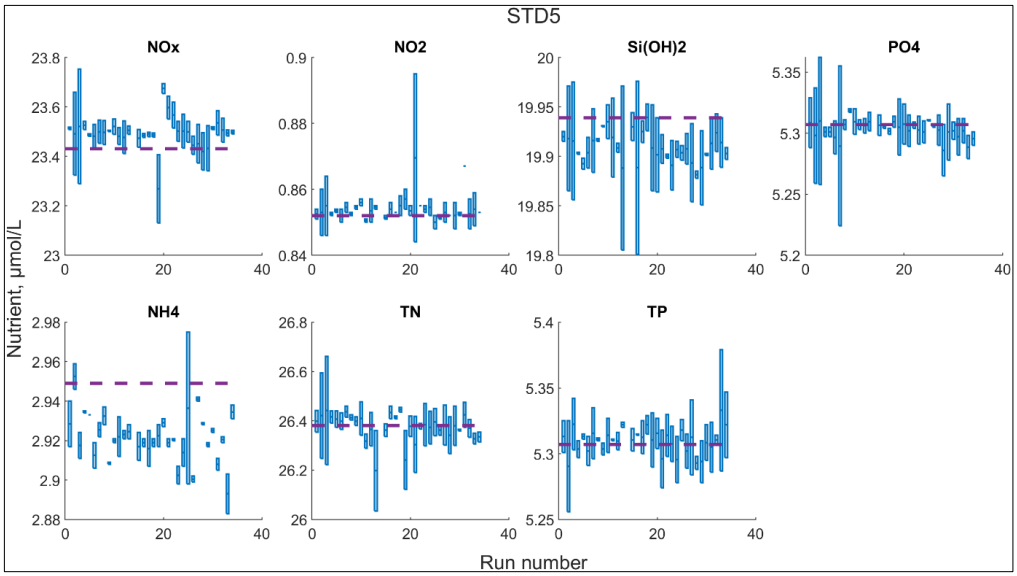

Fig. 7.1.1: Example of a time series box-and-whiskers plot for calibration standard 5 for each nutrient measured, showing the spread of data points on a run-by-run basis. Precision at the different concentration levels derives from this assessment. Purple dashed line indicates the target concentration.

Tab. 7.1.2: Cruise-mean, standard deviation and precision (%) of all calibration standards (Std). Concentration units are µmol L^{-1}.

Standard Number	$NO_3^-+NO_2^-$		NO_2^-		$Si(OH)_4$	
	Mean and Standard Deviation (µmol/L)	Precision (%)	Mean and Standard Deviation (µmol/L)	Precision (%)	Mean and Standard Deviation (µmol/L)	Precision (%)
1	0.569±0.059	10.51	0.019±0.007	37.5	0.38±0.01	3.3
2	6.133±0.032	0.52	0.224±0.007	3.4	5.29±0.01	0.3
3	11.864±0.070	0.59	0.431±0.004	1.0	10.17±0.02	0.2
4	17.688±0.055	0.32	0.642±0.003	0.5	15.08±0.02	0.2
5	23.494±0.091	0.39	0.854±0.006	0.7	19.90±0.03	0.2

Tab. 7.1.2: (Continued) Cruise-mean, standard deviation and precision (%) of all calibration standards (Std). Concentration units are µmol L^{-1}.

Standard Number	PO_4^{3-}		NH_4^+		TDN		TDP	
	Mean and Standard Deviation (µmol/L)	Precision (%)	Mean and Standard Deviation (µmol/L)	Precision (%)	Mean and Standard Deviation (µmol/L)	Precision (%)	Mean and Standard Deviation (µmol/L)	Precision (%)
1	0.107±0.006	6.1	0.044±0.018	42.3	0.558±0.053	9.5	0.120±0.011	9.8
2	1.402±0.007	0.5	0.776±0.024	3.1	6.961±0.049	0.7	1.390±0.010	0.7
3	2.705±0.011	0.4	1.529±0.020	1.3	13.420±0.054	0.4	2.695±0.014	0.5
4	4.014±0.013	0.3	2.247±0.012	0.5	19.954±0.068	0.3	4.016±0.018	0.5
5	5.303±0.020	0.4	2.921±0.014	0.5	26.337±0.094	0.3	5.309±0.019	0.4

Quality controls (QCs)

There are various products and lab-made solutions that are used for quality control of the analysis; low nutrient seawater, recovery standards and certified reference materials (CRMs). Below we describe how and what we used them for. All quality control standards and CRMs were measured in duplicate in every analysis run.

Low Nutrient Seawater (LNSW) from OSIL Scientific

LNSW can have multiple uses. It can be used as a saline matrix, as a low concentration standard, to prepare quality control standards or to determine whether contamination with any given nutrient occurs. It is expected that the signal produced is close to the baseline (i.e., blank) or above, and remain constant throughout analyses. LNSW is also useful in assessing the effect of measuring saline samples within a Milli-Q base. During PS150, LNSW measured for the various nutrients yielded consistent results within the expected analytical error associated with low nutrient concentrations and/or the precision as estimated for different concentration levels. Figure 7.1.2 shows time series of these measurements.

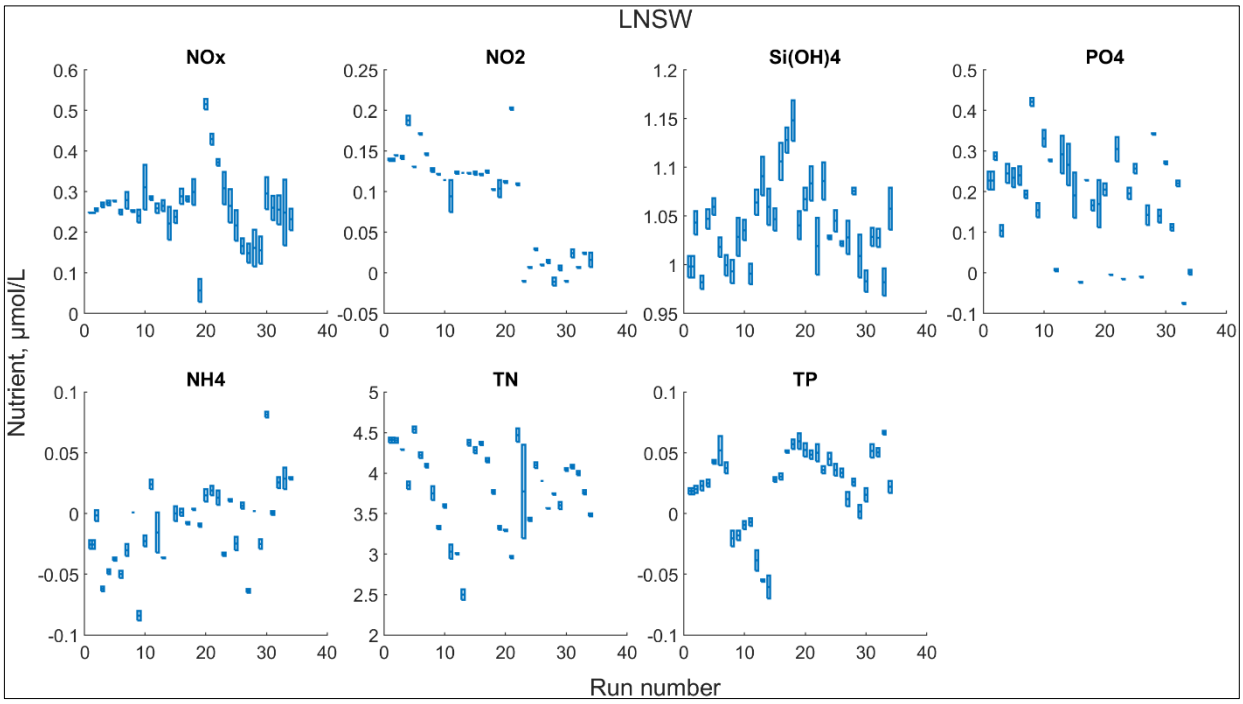

Fig. 7.1.2: Time series (shown as per run number) of OSIL Scientific certified Low Nutrient SeaWater measurements. This additional QC was measured in duplicate in every analysis run.

Recovery Standards: Cadmium coil and column reduction efficiency

The measurement of some nutrients such as NO_3^-+NO_2^- and TDN require continuous monitoring of the reduction efficiency of the Cadmium (Cd) column. The colorimetric method upon which the measurement of these two nutrients is based relies on the chemical reaction between reagents and NO_2^-. Thus, in order to measure NO_3^-, this has to be reduced to NO_2^- (the Cd is oxidised and the NO_3^- is reduced). In the case of TDN, the reaction is slightly more complex, as all dissolved nitrogen present in the water first needs to be oxidised to NO_3^-+NO_2^- and then reduced to NO_2^-. For TDN there is thus an extra step to monitor; the oxidation

efficiency, which is dealt with in the next subsection. In order to monitor the reduction efficiency, two lab-made standards containing only NO_2^- and only NO_3^- were prepared, both at a concentration of 23.31 µmol L^{-1}. The concentration yielded by measuring both recovery standards should be equal within the precision of the analyses. The reduction efficiency is presented as the ratio of the NO_3^- standard to the NO_2^- standard in percentage. As per best practice recommendations, the Cd columns were reactivated or replaced when the reduction efficiency reached or was close to 95%. Figure 7.1.3 shows time series of the Cd reduction efficiency of the NO_3^- + NO_2^- and TDN columns. Recovery standards were measured in duplicate at the beginning and at the end of each run. This is particularly useful as the efficiency can potentially be reduced during the analysis, in particular with long runs or when samples fixed with mercuric chloride are analysed (mercuric chloride reduces the efficiency of the Cd column). This way, we were able to assess whether the efficiency was still within expected values at the end of a given analysis run. Therefore, when required, we reactivated the column and tested its reduction efficiency before starting a new run. This was done by measuring -in duplicate- the top standard, the NO_3^- standard and the NO_2^- and making sure the resulting peaks were at the expected height.

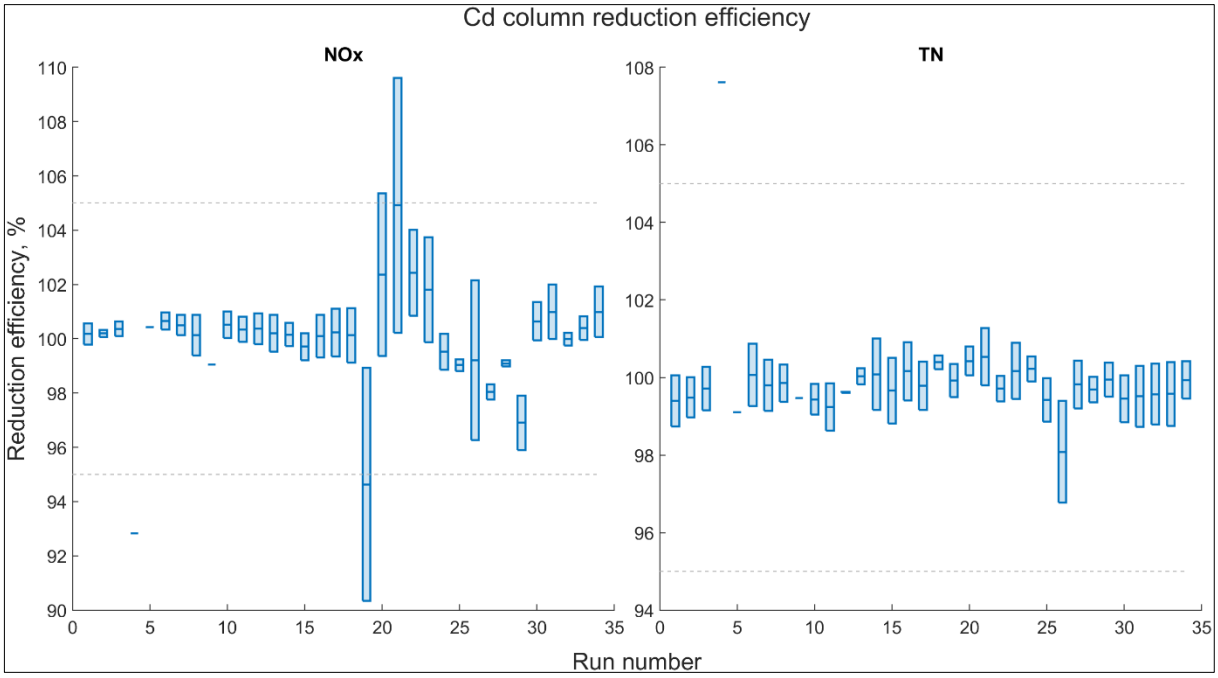

Fig. 7.1.3: Cd column reduction efficiency for the measurement of (a) NO_3^-+NO_2^- and (b) TN during PS150. Dash lines show the 95 and 105% thresholds.

Recovery Standards: TDN oxidation efficiency

As mentioned above, the measurement of TDN requires the oxidation of all nitrogenous compounds present in the sample. There are no certified reference materials available in the market to test the oxidation efficiency and the accuracy of the method. However, there are steps that can be taken. During PS150 we used an OSIL Scientific 10 mmol L^{-1} ammonium (NH_4^+) certified standard, from which we prepared a 15 µmol-NH_4^+ L^{-1} solution. This standard was measured in duplicate in every run. Although this standard is not an organic compound, it is most useful as the NH_4^+ first needs to be oxidised to NO_3^-+NO_2^- and then reduced to NO_2^-. Figure 7.1.4 shows time series of the oxidation efficiency and recovery of NH_4^+. The first standard prepared yielded lower than expected results, but having then prepared a second

solution, which indicated ~100% oxidation efficiency, we concluded that the first solution may have been accidently prepared at a lower concentration rather than the oxidation being low.

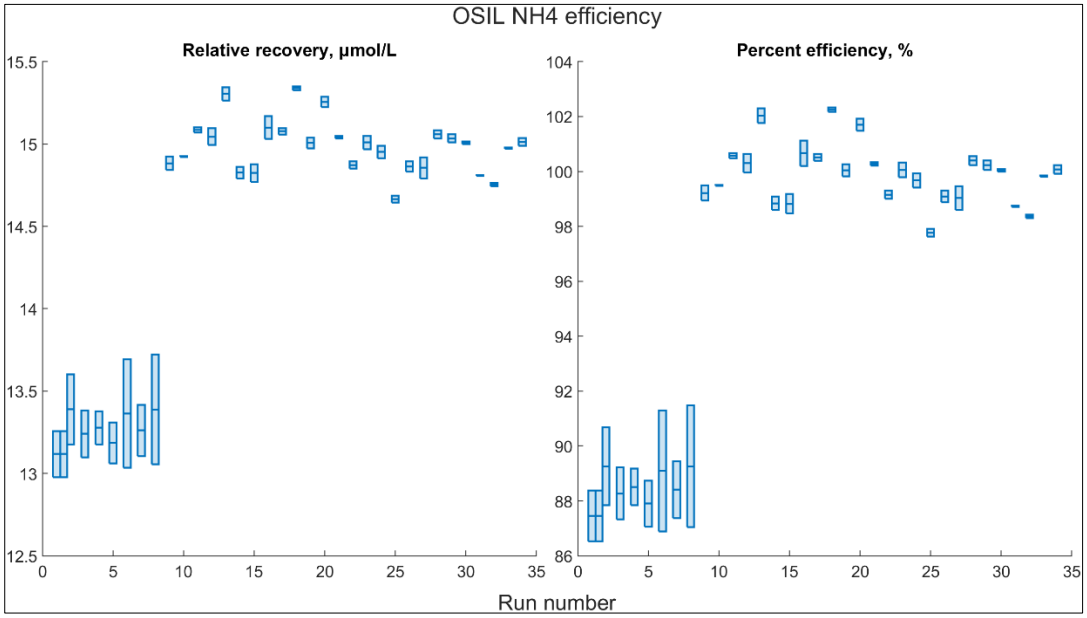

Fig. 7.1.4: Time series box-and-whiskers plot of the NH_4^+ recovery standard used during PS150 to test the oxidation efficiency of the TN channel. Recovery relative to the NH_4^+ standard prepared (15 µmol L^{-1}) and percent efficiency.

The oxidation efficiency also needs to be tested for TDP, as phosphorous bound to organic compounds has to be oxidised to PO_4^{3-} to be measured. There is a second way in which we monitored both, the oxidation efficiency of TDN and TDP, and we present this in the following section.

Certified reference materials (KANSO and OSIL Scientific)

In order to assess the accuracy and consistency of the methods employed, we used two types of certified reference materials (CRMs); 1) KANSO Technos Co., LTD, Japan, lots CS and CU, and 2) OSIL Scientific, UK, nutrient standards. KANSO are also known as 'RMNS or reference materials for the measurement of nutrients in seawater'. These are made from natural seawater, typically by combining deep and surface water from selected ocean regions to yield target concentrations, plus further processing (e.g., sterilisation). Certified values are reported in units of µmol kg^{-1}, so for our work we converted them to µmol L^{-1} using the reported CRM salinity and an average lab temperature of 22°C. KANSO CRM concentrations are shown in Table 7.1.3**.** The reported salinity of the CRMs is 34.520 for lot CS and 34.742 for lot CU.

For NO_3^-+NO_2^- we use the sum of NO_3^- and NO_2^-, with the uncertainty propagated from the respective uncertainties. OSIL Scientific standards are concentrated solutions distilled-water-based and certified to 100 µmol-PO_4^{3-} L^{-1}, 100 µmol-NO_2^- L^{-1}, 1,000 µmol-NO_3^- L^{-1}, 1,000 µmol-$Si(OH)_4$ L^{-1} and 1,000 µmol-NH_4 L^{-1}. These concentrated solutions were used to prepare an additional quality control standard with concentrations equal to our top calibration standard (STD 5, Tab. 7.1.1). We prepared two solutions of this quality control, one in Milli-Q water and another in LNSW. These standards were measured in duplicate at the beginning of each run. Table 7.1.4 shows the cruise-long-mean of measurements of certified materials and Figures 7.1.5 to 7.1.9 show time series of measurements, as carried out in individual runs.

KANSO CRMs are used to assess whether the methods used are accurate and whether data adjustments need to be applied. As these are internationally used CRMs, the aim is to provide traceability and render data comparable to measurements carried out by other laboratories. Data are adjusted based on the CRM measurements. A correction/adjusting/compensation factor (CF/AF) is obtained as $CRM_{certified}$:$CRM_{measured}$. Data is then multiplied by this correction factor. Corrections were applied on a run-by-run basis. The main assumption here is that the results of the CRM measured are representative of the whole run where it was analysed. Note that the implied CF is slightly different depending on the CRM Lot used. As per best practice procedures, a CRM with nutrient concentrations closest to the top calibration standards are to be used. However, sometimes (most times, indeed) this is constrained by the availability of lots with appropriate concentrations. For PS150 lot CS concentrations for NO_3^-+NO_2^-, PO_4^{3-}, $NH_4^+$and NO_2^- are appropriate and lot CU is appropriate for $Si(OH)_4$. The concentration for $Si(OH)_4$ is rather low (7.95 µmol L^{-1}), but this was the only CRM lot available with a concentration within our calibration range (top standard was 19.9 µmol L^{-1}).

Currently there are no CRMs with certified values for TDN and TDP. Thus, to standardise the data and avoid noise, we obtain the mean of all measurements carried out for a given CRM (excluding outliers), in particular those with concentrations closest to our top standards. Then each run is normalised to this mean. The OSIL standards were used as an additional and independent quality control to assess run-to-run noise. In the case of the OSIL standard prepared in Milli-Q water TDN concentration is given by the sum of NO_3^-+NO_2^- and NH_4^+ and the concentration of TDP is given by PO_4^{3-}. In the case of the standard prepared in LNSW, the concentrations of TDN and TDP are given, in addition, by any organic compounds contained in it.

Tab. 7.1.3: CRM certified nutrient concentrations (in µmol kg-1 and *µmol L-1)

CRM lot	NO_3^-	NO_2^-	NO_3^-+ NO_2^-	$Si(OH)_4$	PO_4^{3-}	NH_4^+
CS	16.65±0.16	0.18±0.07	16.83±0.17	33.8±0.4	1.069±0.019	0.73±0.06
CS*	17.04±0.164	0.184±0.072	17.231±0.179	34.606±0.41	1.095±0.019	0.747±0.061
CU	3.06±0.05	0.04±0.04	3.1±0.06	7.77±0.09	0.262±0.011	1.02±0.04
CU*	3.134±0.051	0.041±0.041	3.174±0.066	7.957±0.092	0.268±0.011	1.045±0.041

Tab. 7.1.4: Cruise-long-mean and standard deviation of measured CRMs for the 7 analyser channels (µmol L-1), including KANSO CRMs lots CS and CU, OSIL, prepared in Milli-Q water (MQ) and in low nutrient seawater (LNSW), and OSIL and MERCK combination CRM prepared in LNSW used after run 10. Shaded cells (as well as no "+" in the "QC" column) indicate that this CRM lot was not used for the quality adjustment procedure during this cruise, as it was not the closest to the top standard used for quality control procedures (STD 5). TDN and TDP are shaded in dark blue to indicate variables for which there are no KANSO CRM values reported. In the case of the OSIL CRM, TDN is given by NO_3^-+NO_2^- +NH_4^+ and TDP only by PO_4^{3-} (i.e., there is no organic nitrogen or organic phosphorus). All values given in µmol/L.

CRM / Variable	CS *std*	% std	QC	CU *std*	% std	QC	OSIL LNSW *std*	OSIL /MERCK LNSW *std*	OSIL MQ *std*
NO_3+NO_2	16,72 *0,86*	5	+	3,13 *0,17*	5		23,83 *0,84*	22,23 *2,13*	22,92 *1,38*
NO_2	0,18 *0,01*	7	+	0,03 *0,01*	28		0,99 *0,13*	0,89 *0,22*	0,81 *0,13*
$Si(OH)_4$	30,28 *0,11*	0		7,10 *0,03*	0	+	18,62 *0,15*	18,56 *0,12*	19,85 *0,32*
PO_4	1,10 *0,01*	1	+	0,35 *0,03*	9		5,31 *0,03*	5,23 *0,05*	5,27 *0,08*
NH_4	0,74 *0,04*	5		1,08 *0,05*	5	+	2,82 *0,10*	2,47 *0,44*	2,95 *0,30*
TDN	19,84 *0,81*	4	+	7,55 *0,36*	5		30,08 *1,22*	27,59 *2,30*	26,46 *0,59*
TDP	1,06 *0,06*	6	+	0,44 *0,03*	7		4,98 *0,12*	4,50 *0,26*	5,21 *0,21*

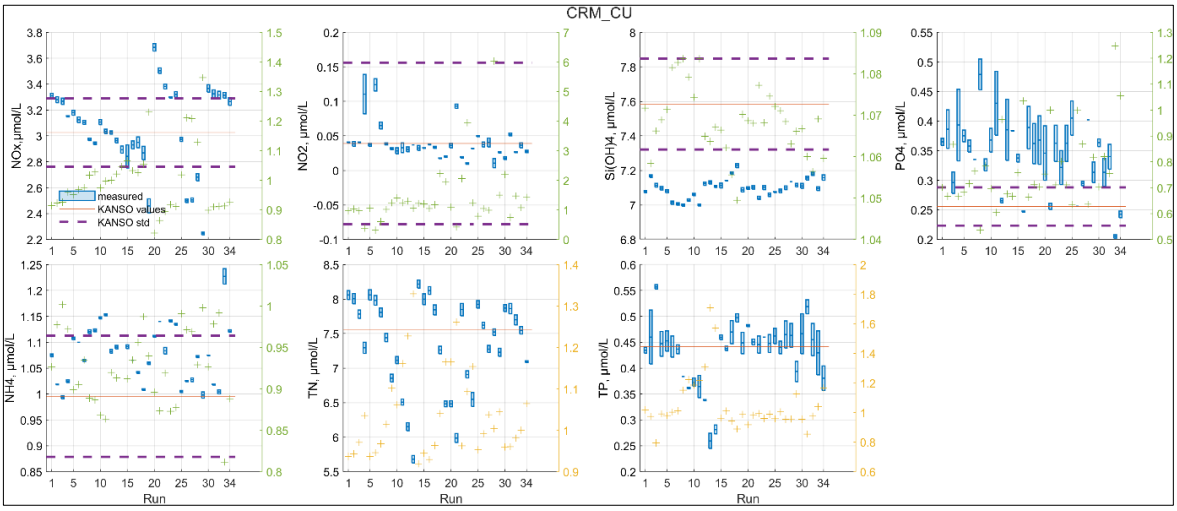

Fig. 7.1.5: Time series box-and-whiskers plot of KANSO CRM Lot CU measured on 34 runs during PS150. Solid and dashed lines show certified value and standard deviation respectively. Right hand y-axis shows the "compensation factor" (CF, in green and yellow "+" symbols) used in this particular run to compensate for the analyser's bias (i.e., accuracy).

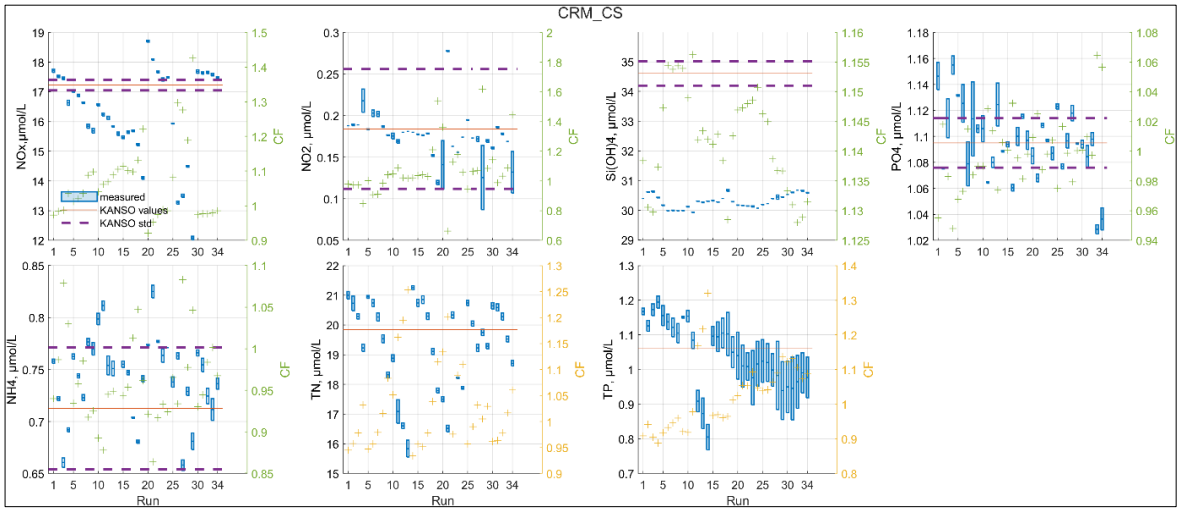

Fig. 7.1.6: Time series box-and-whiskers plot of KANSO CRM Lot CS measured on 34 runs during PS150. Solid and dashed lines show certified value and standard deviation respectively. Right hand y-axis shows the "compensation factor" (CF, in green and yellow "+" symbols) used in this particular run to compensate for the analyser's bias (i.e., accuracy).

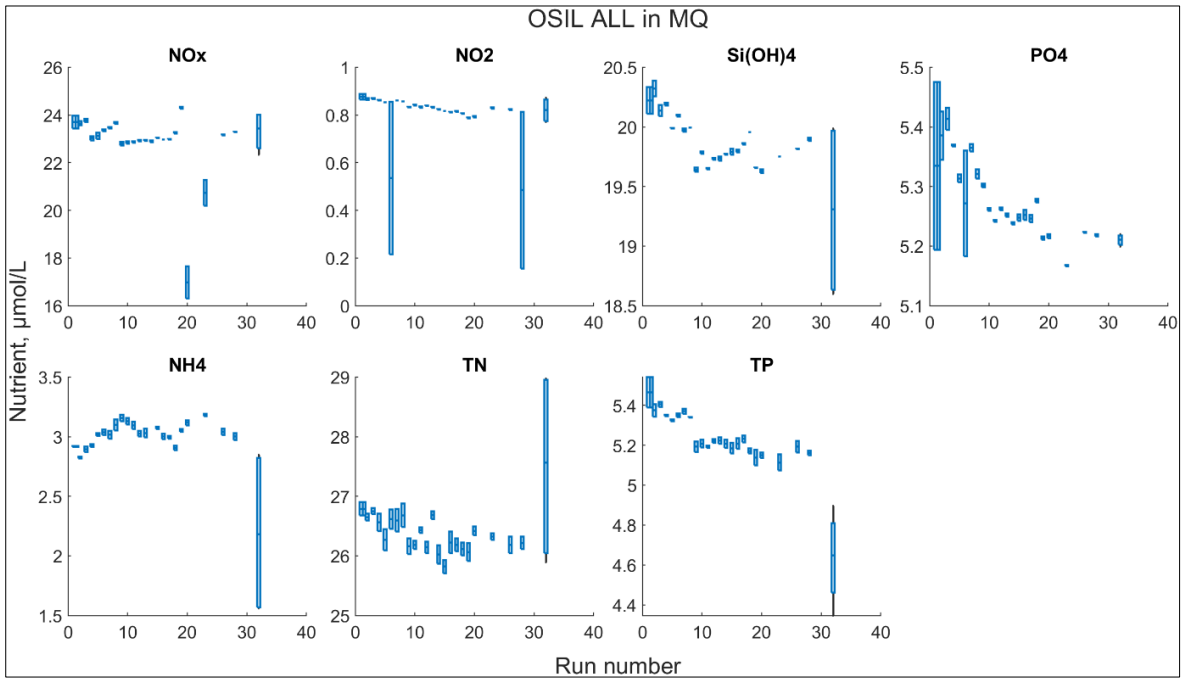

Fig. 7.1.7: Time series of standards prepared from OSIL Scientific concentrated CRMs in Milli-Q

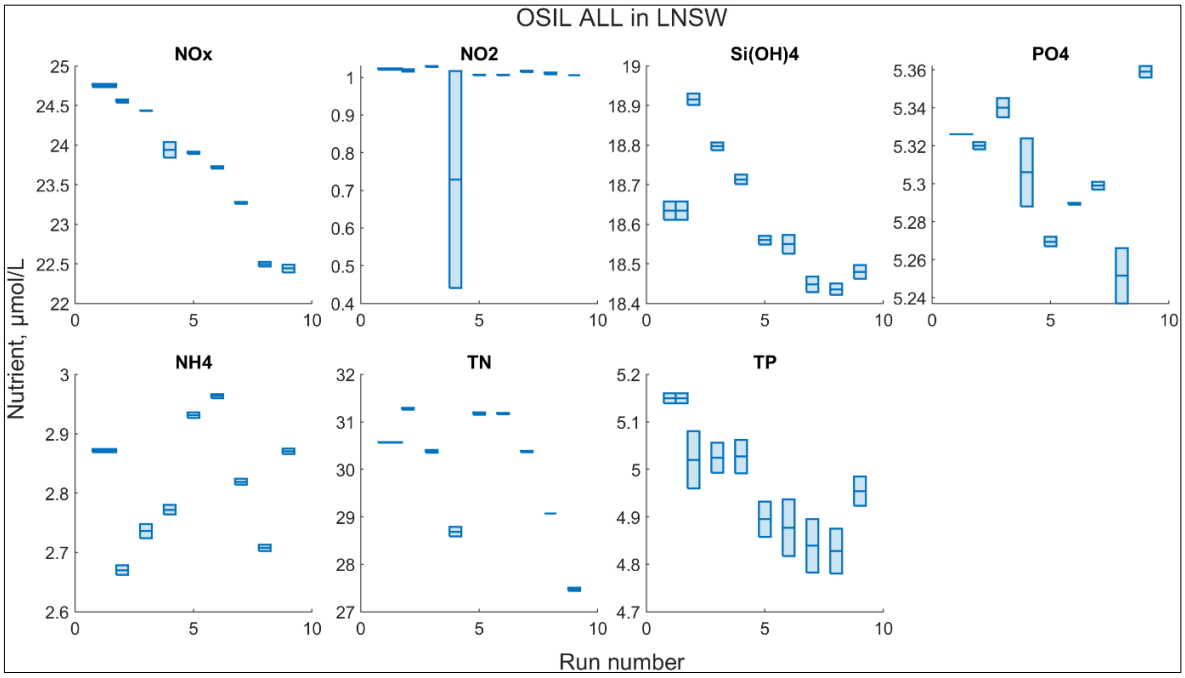

Fig. 7.1.8: Time series of standards prepared from OSIL Scientific concentrated CRMs in LNSW

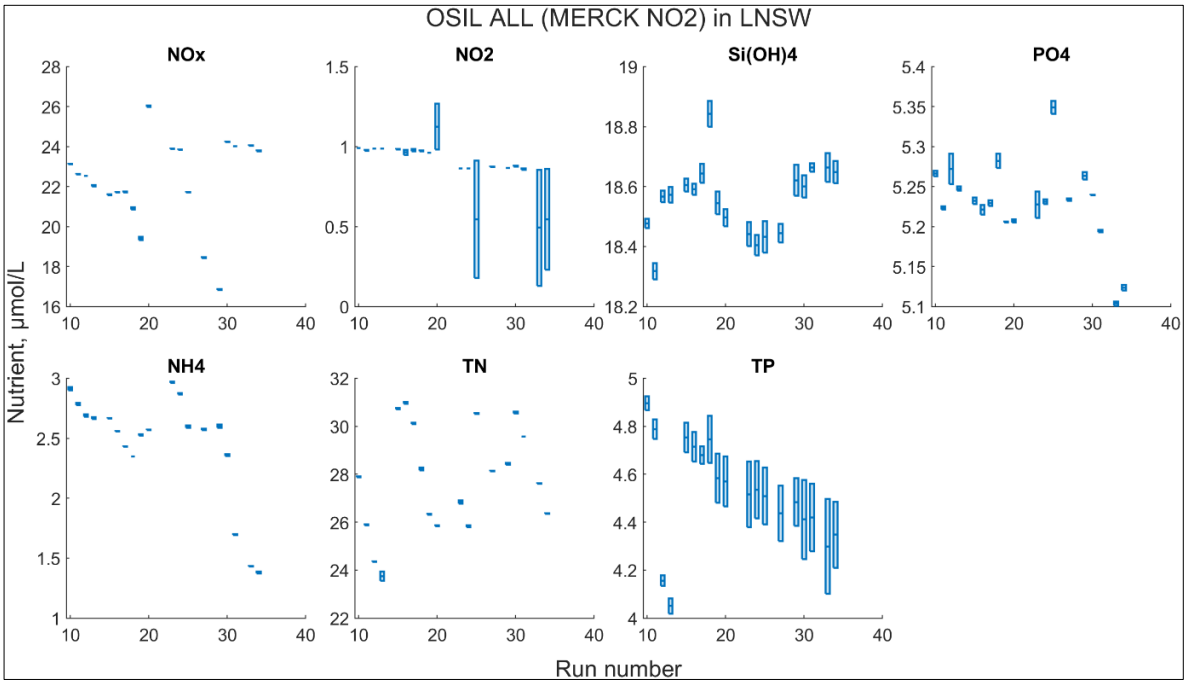

Fig. 7.1.9: Time series of standards prepared from OSIL Scientific concentrated CRMs in LNSW. Starting from Run 10, we used the MERCK CRM NO_2 instead of the OSIL CRM NO_2 here.

Sample collection and analysis

40 mL samples were collected directly into 50 mL sterile Falcon tubes for the analysis of nutrients. Tubes were rinsed three times with seawater before the sample was drawn. Two duplicate samples were randomly collected from each cast. In order to optimise lab work (e.g., number of samples analysed per run) and reduce the amount chemical waste produced, analyses were carried out when a minimum of 50-80 samples were available. Runs included samples from CTD casts, sea ice cores (Lisa W. von Friesen and Rebecca Duncan), CTD casts from PS148, remote access samplers from previous expeditions and snow samples. All samples were analysed in duplicate. All were sampled and analysed onboard. In some cases, when a given nutrient yielded results higher than our calibration range, the remaining sample was kept, diluted as deemed necessary, and reanalysed either by the end of the run or in the following run.

Snow samples at Ice and Heli Stations

During PS150 we collected snow samples at 4 ice stations (along the snow depth transect carried out by the sea ice physics team) and 1 Heli station. Samples were collected using 500 mL Nalgene polycarbonate or polyethylene cups. Cups were filled with Milli-Q water prior to sampling (several days before) and emptied only before going onto the ice.

The snow was collected by pressing the cup into the snow and filling it with snow, shaking, and emptying it three times – hence 'rinsing' the cup. After that, the actual snow sample was taken. Upon collection, samples were brought back to the lab and left to defrost in the dark. One cup was filled with Milli-Q water and brought on the field to serve as a blank.

Once the snow samples thawed, 40 mL were transferred into falcon tubes for nutrient analysis as described in the sections above.

Figure 7.1.10 shows the distribution of different nutrients in snow samples at the four ice stations. All snow station samples were rich in nitrogen species – relative to their water concentrations, the most abundant were NOx and NH_4, followed by TDN (the latter was higher than the sum of all inorganic N species, i.e., some dissolved organic nitrogen was present in the samples).

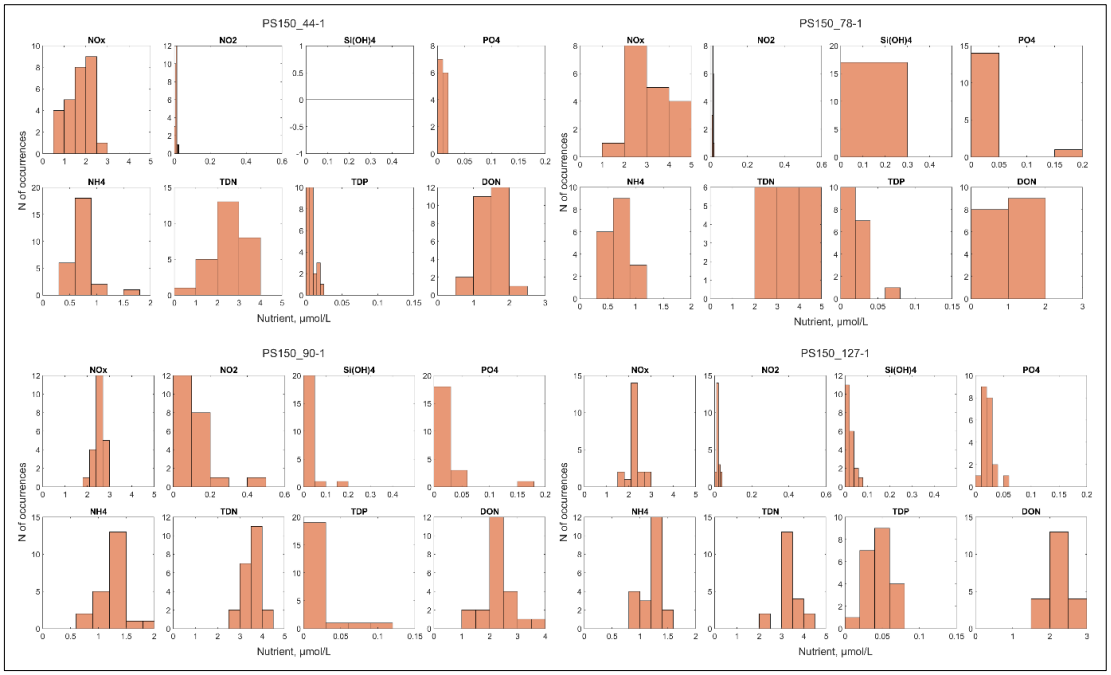

Fig. 7.1.10: Histogram of snow nutrient measurements taken at the different ice stations

Tab. 7.1.5: Overview of samples collected at ice and Heli stations during PS150

Label	Date	Ice station	Samples collected	Comment
PS150_44-1_snow-cup	13.09.2025	1	24	20 snow samples 2 frost flowers
PS150_78-1_snow-cup	21.09.2025	2	15	14 snow samples 1 frost flowers
PS150_90-1_snow-cup	25.09.2025	3	22	22 snow samples
PS150_121-1_snow-cup	10.10.2025	4	21	21 snow samples
PS150_heli_mooring_location_snow-cup	11.10.2025	---	5	5 snow samples 79NG fast ice snow sampling
PS150_heli_niskin_Independence_Fjord_1.5	26.09.2025	---	7	3 Nutrients 4 DIC
PS150_heli_niskin_Independence_Fjord_2.5	26.09.2025	---	6	3 Nutrients 3 DIC
PS150_heli_niskin_Independence_Fjord_5nm_from_station 6	28.09.2025	---	8	4 Nutrients 4 DIC

Problems encountered

As previously mentioned, because station work was able to start so soon after leaving Longyearbyen, we did not have the time to set up the analyser in time for the first sampling stations. This is why up until station PS150_029_01 the nutrient samples we took were frozen and analysed later on after defrosting. We always aimed to keep the samples defrosting for at least 18 hr to let the silicate fully dissolve.

Once we set the AA up, the autosampler was not recognised by the software (i.e., the signal from the SEAL software was not coming through to the AS). In the end we solved the issue: the AS needed reconfiguration because the config. file was corrupted.

Recurrent problems were mostly related to blockage of air lines, reagent lines and cadmium column lines. Most of the times they were solved simply by changing the tubing. However, there were some exceptions: it seems that the oxalic acid solution we use for $Si(OH)_4$ precipitates quite strongly – leading to the crystals blocking the tubing. The solution to that was using a 50% oxalic acid solution instead – i.e. instead of 95g/1L, the solution was now 47.5 g/L. Some other blockages were caused by Cd granules, rogue copepods and ice core and snow samples debris.

Other frequent problems include: wrongly prepared reagents causing no proper reaction to occur in the channels, reactions in the NH_4 channel not occurring properly because the N_2 valve was not open, backpressure in the valves causing reagent mixing, tubing wear-and-tear.

As mentioned above, the first OSIL NH_4 STD was not prepared properly, it seems it was prepared with a concentration of around 13-13.5 µmol/L, when it was supposed to contain 15 µmol/L. This can be deduced from the time series of the standard in question and the Cd column reduction efficiency: the latter never went below 95% for the TDN channel, while the former looks really low (below 95%) for runs 1-8.

Another problem encountered was leaving certain sample rack positions empty: this led to 1) noise in peaks if too much air was drawn in for the debubblers to manage, and more importantly 2) Cd columns drawing air and needing manual flushing with a syringe and the respective

buffer solution. In future expeditions it's important to always pay attention to the sample order and "empty" positions.

This year we tried to pay closer attention to the pH of Working Imidazole for the NOx channel and Ammonium Chloride for the TDN channel: the theory is that this buffer solution's pH can lead to run-to-run noise that we experienced during PS144, requiring further QC procedures down the line. The solution we came up with is as follows: 1) preferably have one person doing the pH adjustment during the cruise, and 2) wait at least 5 minutes between adjustments to let the pH signal stabilise.

TP efficiency went down throughout the cruise – will need further investigation during maintenance back on land. One can see quite easily that the CU lot CRM was semi-stable for the whole cruise, while the CS lot and OSIL CRMs went down gradually. That could be related to the fact that the TDP channel could only properly react with less than 1 µmol/L of phosphorus, while anything higher was not fully digested/oxidised/reacted with.

7.2 Sensors and remote access samplers

In order to investigate the nutrient and carbon content of the EGC and its biogeochemical activities (e.g., temporal variability), two biogeochemical sensor packages were deployed at the FI4-1 mooring at about 50 m and 245 m and one package at the FI2-1 mooring at 55 m. As a basis, each package utilizes a remote access sampler, capable of sampling and fixing 48 water samples with a volume of 500 mL throughout the deployment. While the deeper setup contains sensors to measure pH, pCO_2, nitrate, pressure, conductivity, temperature and oxygen, the shallower ones additionally include optical sensors to measure PAR, CDOM, *chl*-a and backscatter. Sensor and sampler information, including sensor type, parameter, measuring interval, serial number and start time are summarized in Tables 7.2.1 to 7.2.3. Unfortunately, a nitrate sensor was not available for the FI2-1 site due to a delivery problem.

Tab. 7.2.1: Deployment information for sensor package FI4-1 @ 50 m

sensor	parameter	interval	serial number	Start time UTC
Seabird Suna	NO_3	4h	1472	29.09.25 00:00
Wetlabs EcoTriplet	CDOM, chla, backscatter	2h	1425	30.09.25 22:00
Wetlabs EcoPar	PAR	1h	490	28.09.25 22:00
Seabird SBE37ODO	CTD, O_2	1h	20522	29.09.25 12:00
Sunburst Sami pH	pH	4h	0192	04.10.25 12:00
Sunburst Sami CO_2	CO_2	4h	0205	04.12.25 12:00
McLane remote access sampler (RAS)	500ml seawater	8d	13464_02	09.10.25 12:00

Tab. 7.2.2: Deployment information for sensor package FI4-1 @ 245 m

sensor	parameter	interval	serial number	Start time
Seabird Suna	NO_3	4h	1021	01.10.25 00:00
Seabird SBE37ODO	CTD, O_2	1h	16741	01.10.25 00:00
Sunburst Sami pH	pH	4h	0219	04.10.25 12:00
Sunburst Sami CO_2	CO_2	4h	0156	04.10.25 12:00
McLane remote access sampler (RAS)	500ml seawater	8d	14128_06	09.10.25 12:00

Tab. 7.2.3: Deployment information for sensor package FI2-1 @ 55 m

sensor	parameter	interval	serial number	Start time
Wetlabs EcoTriplet	CDOM, chla, backscatter	2h	1692	29.09.25 12:00
Wetlabs EcoPar	PAR	1h	491	29.09.25 12:00
Seabird SBE37ODO	CTD, O_2	1h	16389	29.09.25 12:00
Sunburst Sami pH	pH	4h	0165	01.10.25 00:00
Sunburst Sami CO_2	CO_2	4h	0184	01.10.25 00:00
McLane remote access sampler (RAS)	500ml seawater	8d	14128_07	01.10.25 00:00

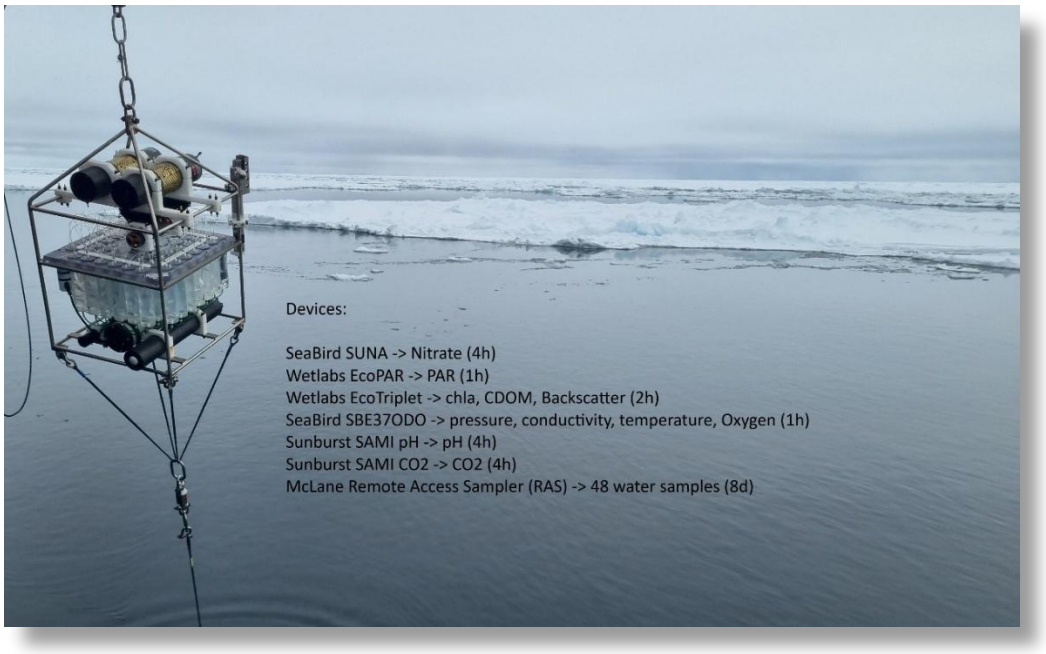

Fig. 7.2.1: Biogeochemical sensor package: SeaBird Suna (NO_3), Wetlabs Ecopar (PAR), Wetlabs EcoTriplet (CDOM, chla, backscatter), SeaBird SBE37ODO (CTD + O_2), Sunburst Sami pH (pH), Sunburst Sami CO_2 (CO_2), McLane remote access sampler (48 water samples)

Furthermore, 100 high resolution NO_3 profiles were recorded at stations shallower than 2000 m by deploying a SUNA sensor (SN 1166, calibrated Feb 2021) along with the ship's CTD system. The sensor was set up to record full spectral data internally, measuring at 1 Hz, taking a dark reference measurement every 60 s. Temperature and salinity data needed to apply data processing algorithms described in Sakamoto et al. 2009 are provided by the ship's CTD. Synchronizing the SUNA and CTD time stamp regularly is essential to match both datasets precisely. A profile pointing out the advantage of high-resolution sensor data combined with precise laboratory analysis for offset correction and reference is given in Figure 7.2.2. This figure shows the detailed vertical nitrate structure that is missed with discrete samples. One of our aims is to study the relevance of this finer structure in terms of the biogeochemical information it provides (e.g., density layers where shallow remineralisation takes place, water mass layering).

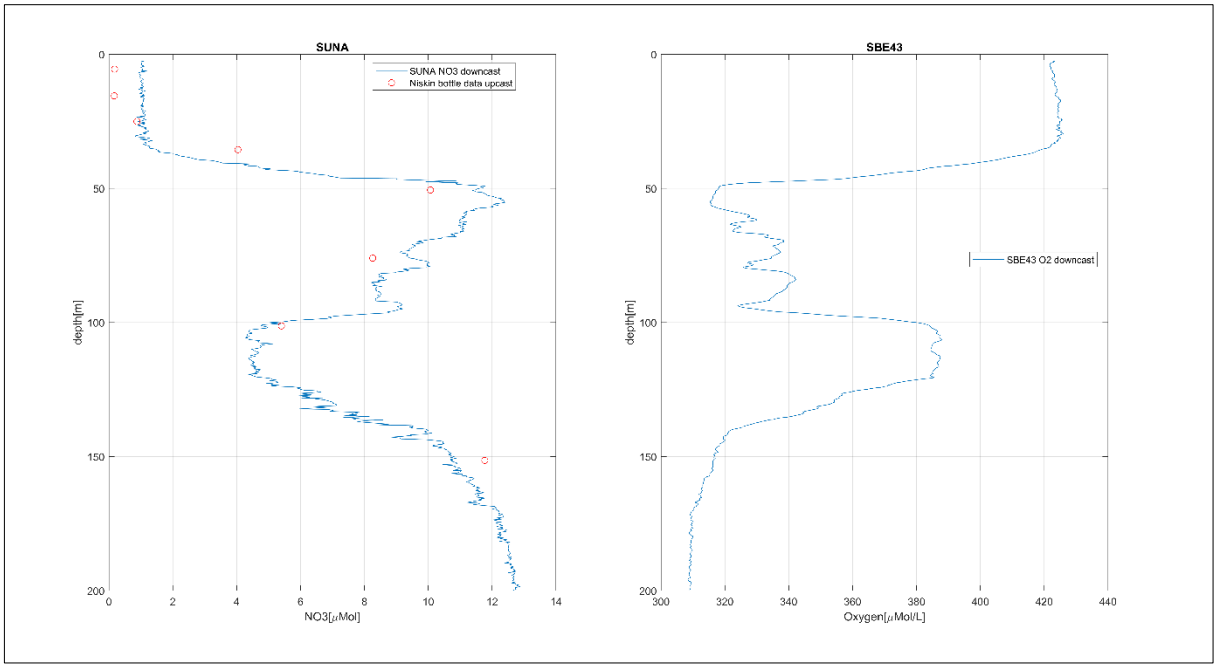

Fig. 7.2.2: This figure shows a Suna NO_3 downcast on the right-hand side and a SBE43 oxygen downcast on the left-hand side. The Suna plot also contains the Niskin bottle NO_3 data taken during the upcast. In this plot it only serves as an indicator for sampling depth in order to point out that some features in the water column would have been missed without using sensor-based investigations. The sensor's offset is calculated based on upcast data and later applied to the downcast data. NO_3 concentrations at the surface are below the sensor's detection limit and lead to falsified data which is flagged in the final dataset.

7.3 Dissolved oxygen

Samples were collected for the analysis of dissolved oxygen from the CTD-Rosette. Dissolved oxygen was measured as an important biogeochemical variable linked to nutrient cycling and also in order to calibrate the CTD-O_2 sensors in the Rosette and to have reference values for the CTD-O_2 sensors attached to moorings. Whenever samples for helium/CFCs and DIC were not collected, samples for dissolved oxygen were the first drawn from the Niskin bottles. Samples were collected using a tygon tube attached to the spigot of the Niskin bottles and placed directly into volume-calibrated borosilicate glass bottles with narrow necks. Care was taken to avoid bubbles inside the sampling tube and the sampling bottles. Water was left to

spill over approximately three or more times the volume of the sampling bottle before the sample was drawn. A hand-held thermometer was used to measure the temperature of the seawater at the time of sample collection (i.e., fixing temperature) using a relatively fast-response temperature probe. Samples were immediately fixed by dispensing 1 mL of manganese chloride, followed by 1 mL of alkaline iodide, and then mixed thoroughly. When sampling was completed, the precipitate of the sample was left to settle to about a third of the volume (~1-1.5 h). Then, samples were mixed thoroughly for a second time and the precipitate left to settle for a minimum of one hour more or until analysis. Analysis was carried out using a Metrohm Ti-Touch titration unit set up with the amperometric end point detection. Before analysis, 1 mL of 5 M sulphuric acid was added to a sample for titration. We followed the GO-SHIP method and best practices procedures as described by Langdon (2010). All hydrographic stations were sampled. Samples were collected at the same vertical resolution as for nutrients, including two random duplicates.

Soon after laboratory set up, 1 L of thiosulphate solution (titrant) was prepared (50 g/L), as it takes one to two days to stabilise. Thiosulphate calibrations were carried out using 1.667 mM OSIL Scientific certified Iodate Standards. Calibrations are done by first measuring 5 blanks (involving 2 x 1 mL additions of iodate standard, each titrated one at a time) and then 5 standards (each with 10 mL of iodate standard). After a first and second calibration, one day apart, further calibrations were carried out approximately every 4 days, with a total of 5 calibrations done for the first thiosulfate solution and 6 for the second thiosulfate solution (Tab 7.3.1) prepared during PS150. Calculation sheets were updated with the blank and standard titration volumes as new calibrations were done. Thus, the concentrations of dissolved oxygen for a given number of CTD casts were calculated with the most recent calibration results. Provided calibrations are consistent with each other and show no trend which may suggest degradation of reagents, results from calibrations represent analytical ‘noise’, that is, the combination of human, reagents and titration unit error associated with each analysis.

We present the results from each calibration in Table 7.3.1 and Figure 7.3.1. The first calibration yielded erroneous results, which we found were due to the dispensing tube from the thiosulfate burette not being properly connected. After this though, all calibrations were consistent for a given thiosulfate batch. CTD profiles from station PS150_5-1 to PS150_86-1 were analysed with the first thiosulfate solution. Stations PS150_89-1 to PS150_135-17 were analysed with the second thiosulfate solution. A plot showing all profiles and preliminary quality control assessment is show in Figure 7.3.2.

As mentioned above, on every cast, a minimum of two randomly selected Niskin bottles were sampled in duplicate to assess the cruise-long precision and uncertainty. The absolute difference between all duplicate samples taken during the expedition is shown in Figure 7.3.3. Absolute differences greater than 1µmol/L were considered outliers. The mean difference and standard deviation of all duplicates taken (n = 190) is 0.69 ±2.5 µmol/L, while without outliers (n=168) values are 0.32 ± 0.25 µmol/L.

Tab. 7.3.1: Thiosulfate solution calibrations (titrations) done for the determination of dissolved oxygen. Blank (Blk), Standard (STD), STD minus Blank (STD-Blk), titration volume (mL), and calculated thiosulfate molarity. During the first calibration the thiosulfate dispensing tube was not properly connected to the electronic burette, resulting in bad results, which were not used for dissolved oxygen calculations.

	Calibration	Date	Blank (mL)	Standard (mL)	STD-Blk	Thiosulfate Molarity
Thiosulfate Batch 1	1	06.09.2025	*0.0048*	*0.5423*	*0.5375*	*0.1861*
	2	07.09.2025	0.0024	0.4949	0.4925	0.2031
	3	11.09.2025	0.0036	0.4952	0.4916	0.2035
	4	15.09.2025	0.0024	0.4943	0.4919	0.2034
	5	21.09.2025	0.0027	0.4973	0.4946	0.2022
	Average		**0.0028**	**0.4954**	**0.4926**	**0.2030**
	Standard deviation		**0.0006**	**0.0013**	**0.0014**	**0.0006**
Thiosulfate Batch 2	6	24.09.2025	0.0032	0.4993	0.4961	0.2016
	7	30.09.2025	0.0023	0.4991	0.4968	0.2013
	8	03.10.2025	0.0032	0.4980	0.4948	0.2022
	9	07.10.2025	0.0031	0.4973	0.4942	0.2024
	10	11.10.2025	0.0018	0.4988	0.4970	0.2013
	11	13.10.2025	0.0031	0.4978	0.4947	0.2022
	Average		**0.0028**	**0. 4984**	**0.4956**	**0.2018**
	Standard deviation		**0.0006**	**0.0008**	**0.0012**	**0.0005**

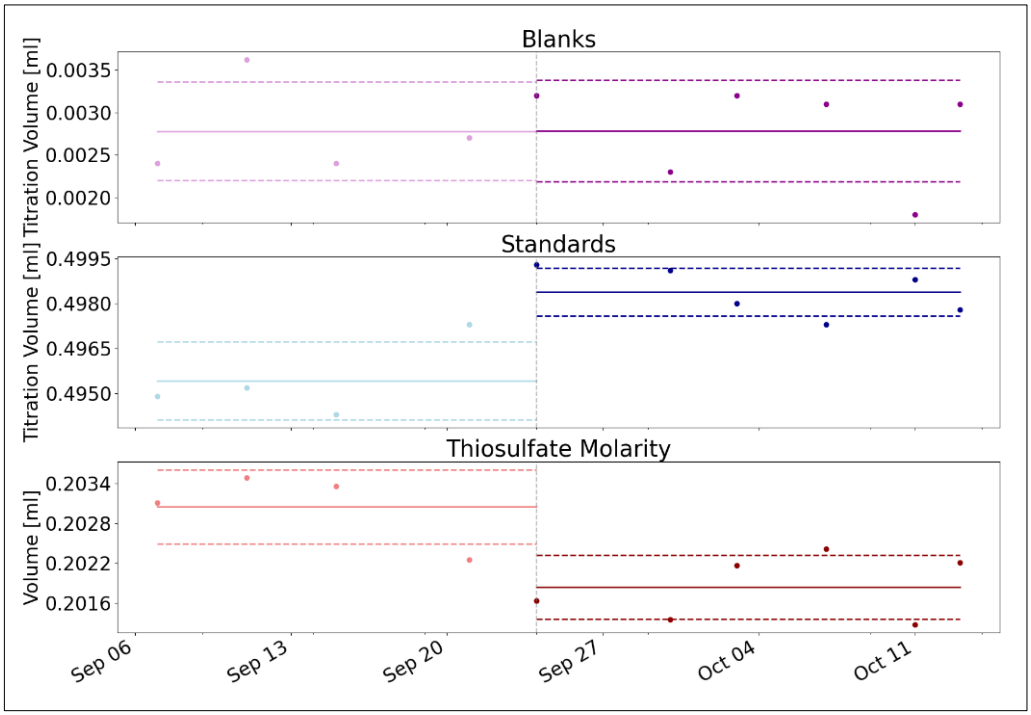

Fig. 7.3.1: Results from thiosulfate calibration carried out during PS150 for the determination of dissolved oxygen in seawater. The distribution of data over time does not show any significant trend that may suggest degradation/alteration of the reagents used. Solid and dashed horizontal lines show the mean and respective standard deviations, as indicated in the in Table 7.3.1. Vertical dashed line indicates swap from the first to second thiosulfate titre solution.

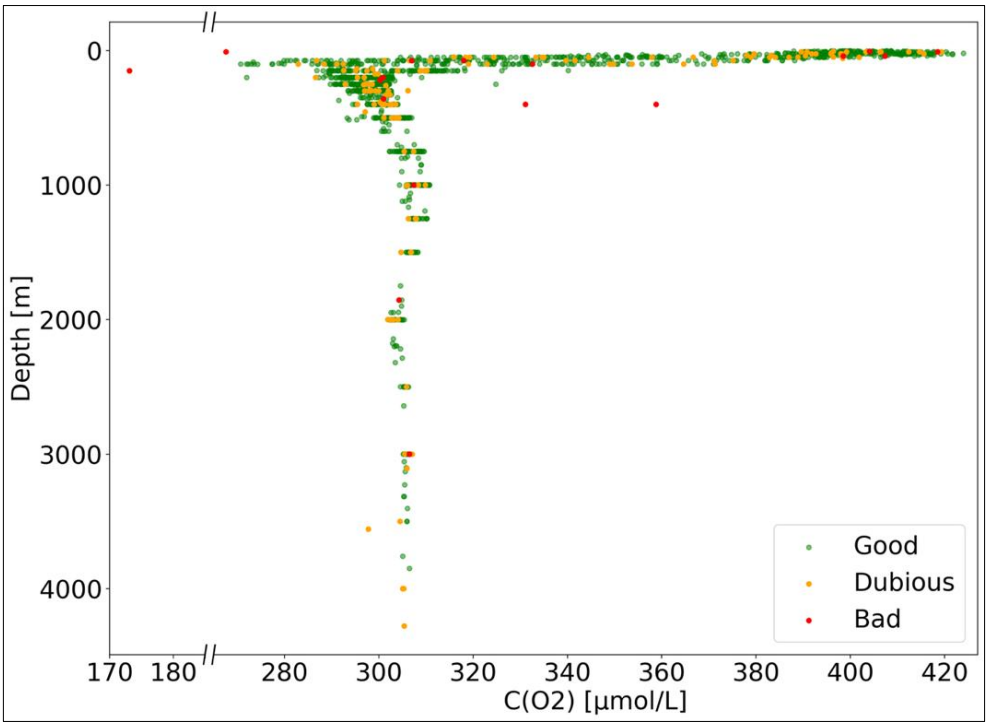

Fig. 7.3.2: (a) Dissolved oxygen profiles (data from all casts), showing preliminary quality control. Green dots indicate data deemed of good quality. Orange dots indicate data that need further inspection given we may have found tiny bubbles in oxygen bottles or had made notes about Niskin bottles being left opened by previous samplers. However, with s few exceptions, it will mostly be of good quality. Red dots show data deemed of bad quality).

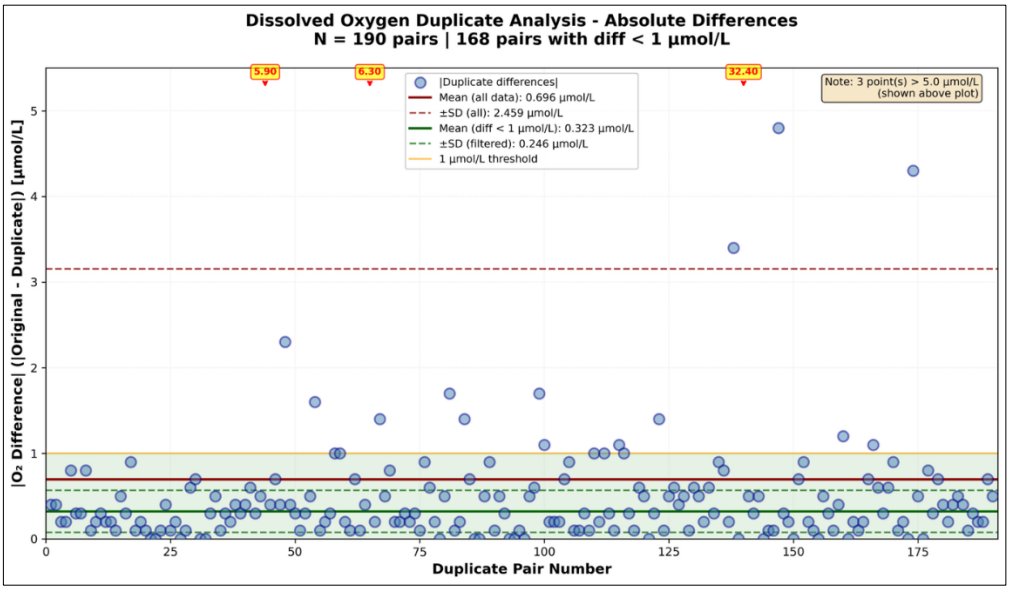

Fig. 7.3.3: Absolute difference between duplicate samples taken during PS150 (n=190, including outliers, differences in duplicates >1 µmol/L and shown by a solid yellow line). Purple solid and dashed lines show the mean difference of all duplicates taken (0.69±2.46 µmol/L). Green solid and dashed lines show the mean and standard deviation of the absolute difference between duplicates, without outliers (n=168) 0.32 ± 0.25 µmol/L. The latter is a simple estimate of the precision and uncertainty of our measurements.

7.4 Glacial Flour sampling

Due to problems with the MUC, it was not possible to sample as many stations as planned. Rapid ice cover prevented us from reaching the inner part of the fjords, so sampling was largely limited to the shelf sections. Four MUC stations were sampled on the shelf for pore water and nutrient extractions (Tab. 7.4.1, Fig. 7.4.1). The MUC station PS150_68-2 was only sampled by Ayla Murray (PEBCAO group) for eDNA samples, as the station was too deep (over 3,000 m) for glacial outflow sampling. t all other MUC stations listed in the table, the MUC did not close (problems with too cold temperatures led to ice accumulation inside the metal frame and blocking the release mechanism) or the ground was too rocky and not feasible the actual deployment. At each MUC station, a sample was taken from the overlying water and the upper 10 cm of sediment was divided into 1 cm slices, from which pore water was extracted. The water samples were filtered through 0.2 µm PES filters and stored at +4°C degrees for later $\delta^{30}Si_{DSi}$ analysis, while the sediment was frozen at -20°C degrees for later nutrient extraction.

Water samples (500 mL) were taken at 16 stations (Tab. 7.4.2) for later $\delta^{30}Si_{DSi}$ analyses. Three of the 16 stations were taken within Independence Fjord during a helicopter station, the rest with CTD rosette sampling. All samples were filtered through 0.2µm PES filter and stored at +4°C for later analysis on land.

Sampling for sediment particles from the surface was not carried out since we did not get far enough into the fjord and to the glacier itself, and the particle load in the water column was too low.

Tab. 7.4.1: MUC stations during PS150 (location and time since station start). Parameters marked with '/' indicate MUC stations where the sampler was not closed

Action number	Event Date Time	Latitude	Longitude	Sampled parameter
PS150_27-2	2025-09-10 13:29:55	81° 40.710' N	009° 54.190' W	Sediment for nutrient extractions
PS150_29-5	2025-09-10 18:22:41	81° 35.510' N	010° 10.323' W	Sediment for nutrient extractions Porewater and overlying water for $\delta^{30}Si_{DSi}$ analysis
'PS150_38-4	2025-09-12 12:17:57	82° 25.571' N	018° 54.384' W	/
'PS150_38-3'	2025-09-12 11:31:28	82° 25.545' N	018° 54.700' W	/
'PS150_42-2'	2025-09-12 21:49:04	82° 24.693' N	018° 51.301' W	/
'PS150_68-2'	2025-09-18 12:47:36	83° 53.244' N	012° 33.538' W	Station too deep station glacial outflow sampling
'PS150_81-2'	2025-09-22 20:23:19	84° 06.191' N	026° 27.442' W	/
'PS150_126-2'	2025-10-10 02:56:29	80° 27.736' N	014° 39.904' W	Sediment for nutrient extractions, TOC, ^{13}C, ^{14}C, and ramped pyrolysis oxidation–^{14}C (RPO-^{14}C) Porewater and overlying water for $\delta^{30}Si_{DSi}$, ^{14}C, ^{13}C and DIC concentration analysis

Action number	Event Date Time	Latitude	Longitude	Sampled parameter
'PS150_127-7'	2025-10-10 19:04:12	80° 10.168' N	015° 47.345' W	/
'PS150_129-4'	2025-10-11 04:28:33	80° 09.386' N	016° 02.717' W	/
'PS150_132-3'	2025-10-12 07:46:23	79° 25.464' N	017° 18.237' W	Sediment for nutrient extractions, TOC, ^{13}C, ^{14}C, and ramped pyrolysis oxidation–^{14}C (RPO-^{14}C) Porewater and overlying water for $\delta^{30}Si_{DSi}$, ^{14}C, ^{13}C and DIC concentration analysis

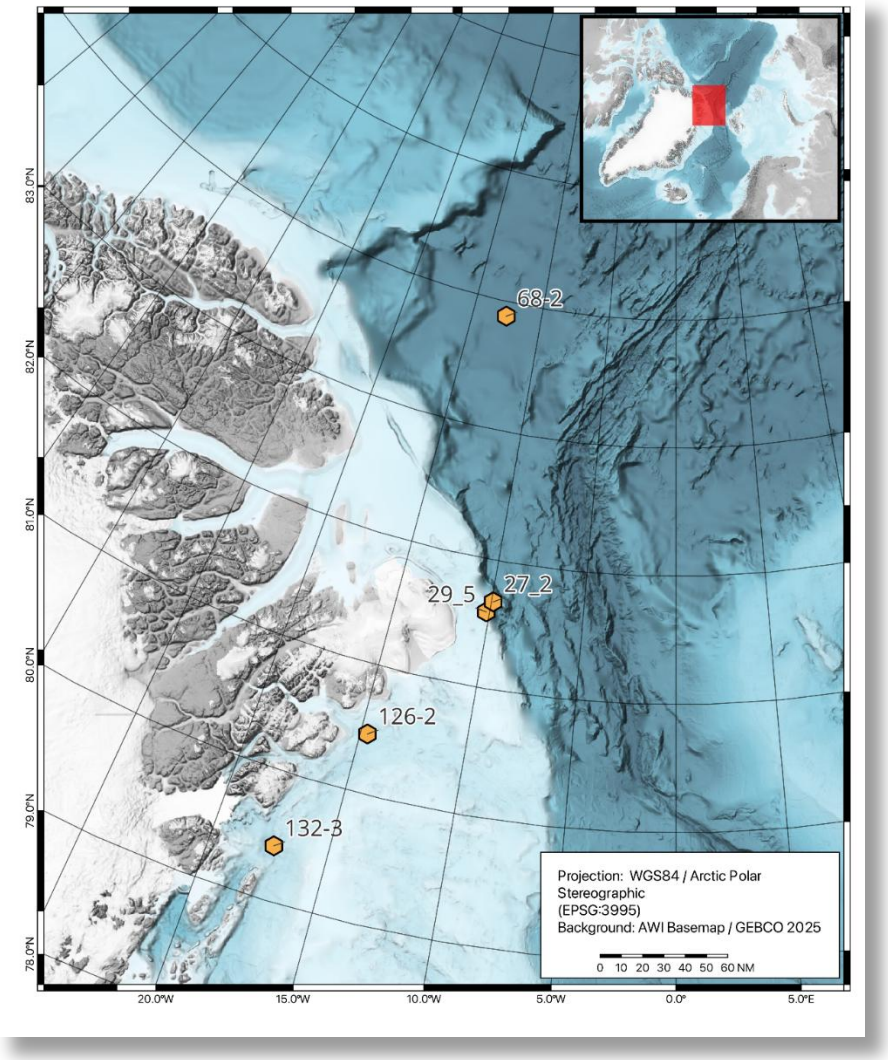

Fig 7.4.1: Map showing sampled MUC stations during PS150.

Tab. 7.4.2: CTD stations sampled for water samples for $\delta^{30}Si_{DSi}$ analysis (Location and Event time from station start)

Action number	Event Time	Latitude	Longitude
PS150_27-1	2025-09-10 12:30:08	81° 41,070' N	009° 55,448' W
PS150_29-1	2025-09-10 15:25:20	81° 36,755' N	010° 16,440' W
PS150_31-1	2025-09-10 23:46:22	81° 28,971' N	010° 58,527' W
PS150_38-1	2025-09-12 09:26:53	82° 25,787' N	018° 57,072' W
PS150_heli_Niskin _210909-01	2025-09-12 11:00:00	82.073268°N	27.809304°W
PS150_heli_Niskin _210909-02	2025-09-12 15:00:00	82.110433°N	23.961383°W
PS150_heli_Niskin _210909-03	2025-09-12 19:55:00	81.773583°N	24.20945°W
PS150_45-1	2025-09-14 10:59:00	83° 06,517' N	022° 22,175' W
PS150_46-1	2025-09-14 13:32:05	83° 09,910' N	021° 34,746' W
PS150_83-1	2025-09-23 02:55:45	83° 59,470' N	027° 40,567' W
PS150_85-6	2025-09-23 14:40:23	83° 51,475' N	028° 41,508' W
PS150_89-1	2025-09-24 03:40:53	84° 16,547' N	027° 32,393' W
PS150_126-1	2025-10-10 02:20:00	80° 27,720' N	014° 39,789' W
PS150_127-6	2025-10-10 18:20:07	80° 09,897' N	015° 48,768' W
PS150_129-1	2025-10-11 02:18:42	80° 09,421' N	016° 02,816' W
PS150_132-1	2025-10-12 06:00:01	79° 25,377' N	017° 18,196' W

7.5 DIC/TA

A total of 417 seawater samples were collected for the analysis of dissolved inorganic carbon (DIC) and total alkalinity (TA). The sampling was focused on the upper 400 m with standard sampling depths, plus the bottom depth sample. Additional samples were taken to match the sampling for radiocarbon ($DI^{14}C$). Samples were filled directly into 250 mL borosilicate bottles using tubing that was squeezed carefully to avoid air inside. During sampling, bottles were left to overflow by approximately 2x the sample volume to avoid air bubbles in the sample. Directly after sampling 50 µL of saturated mercuric chloride (HgCl) was added to the samples and samples were stored at +4°C. They will be sent to the CO_2 laboratory at the Institute of Marine Research in Tromsø, Norway, for further analysis. A list summarising our sampling program for nutrients, dissolved oxygen and DIC/TA is presented in the attached Table 7.5.1.

7.6 Sediment sampling of organic and inorganic carbon

A total of 2 MUC stations was sampled for sediment extractions, as well as for sediment porewater and overlying water analysis (Tab. 7.4.1, Fig. 7.4.1). The porewater was extracted from one core using rhizomes to collect three 2 mL aliquots for dissolved inorganic carbon (DIC) analysis. Aliquots were preserved by $HgCl_2$ (10µL) poisoning for later analysis for DIC concentration, $\delta^{13}C$, and $F^{14}C$. Additionally, duplicate samples of the overlying water from the same MUC core were collected into pre-combusted 12 mL Exetainer vials using syringes for subsequent radiocarbon analysis. Two additional cores were sliced into 1cm sections, stored in petri dishes and frozen at -20°C for further sediment extractions of TOC, ^{13}C, ^{14}C, and ramped pyrolysis oxidation–^{14}C (RPO-^{14}C) (Tab. 7.4.1) at AWI.

7.7 Underway sampling of POM from surface water

During expedition PS150, particulate organic matter (POM) was collected from surface seawater obtained via the ship's seawater inlet. Water was pumped through the internal pipeline system to the filtration unit and passed through pre-combusted glass fibre filters (Whatman GFF, 142 mm). Sampling was carried out during transits and on stations. In total, 50 filters were collected across the whole research area (Tab. 7.7.1), dried onboard and stored frozen (–20 °C) until biomarker extraction at AWI, Germany.

The POM samples will be used to calculate and calibrate biomarker-based proxies for sea-surface temperature (UK'_{37}, TEX_{86}) and sea-ice extent (PIP_{25}/$IPSO_{25}$). Simultaneous measurements of water temperature, salinity, sea-ice, and weather conditions will aid proxy evaluation and calibration.

Tab. 7.7.1: Ship stations and transits sampled for POM of surface water

Station / Transit ID	Latitude (Start)	Longitude (Start)	POM filter
PS150_46	83° 09,825' N	-021° 34,522' W	1
PS150_48 – 49	83° 15,533' N	-020° 25,474'W	1
PS150_52 – 53	83° 17,724' N	-019° 52,422'W	1
PS150_55 – 56	83° 17,912' N	-019° 26,908'W	1
PS150_56	83° 27,542' N	-019° 12,729'W	1
PS150_59	83° 21,842' N	-018° 03,080' W	1
PS150_63 – 64	83° 39,495'N	-014° 54,530'W	1
PS150_64	83° 39,684' N	-014° 46,337' W	1
PS150_65 – 66	83° 44,575' N	-014° 30,050' W	1
PS150_68	83° 53,837' N	-012° 35,265' W	1
PS150_70 – 71	84° 14,588' N	-018° 20,435' W	1
PS150_72 – 73	84° 21,424' N	-019° 31,845' W	1
PS150_74 – 75	84° 22,051' N	-019° 54,949' W	1
PS150_79	84° 13,309' N	-025° 23,629' W	1
PS150_80	84° 09,185' N	-025° 54,360' W	1
PS150_81 – 82	84° 04,390' N	-026° 32,130' W	1
PS150_83 – 84	83° 59,404' N	-027° 41,271' W	1
PS150_85 – 86	83° 51,493' N	-028° 41,437' W	1
PS150_89	84° 16,584' N	-027° 36,651' W	1
PS150_89 – 90	83° 52,482' N	-026° 44,581' W	1
PS150_90	83° 53,495' N	-024° 15,155' W	1
PS150_100 – 101	81° 46,524' N	-010° 38,193' W	1
PS150_104 – 105	81° 51,151' N	-009° 47,435' W	1
PS150_105	81° 53,131' N	-009° 20,618' W	1
PS150_107	81° 58,620' N	-008° 04,712' W	1
PS150_109 – 110	81° 53,200' N	-008° 18,166' W	1
PS150_112 – 113	80° 59,315' N	-001° 15,998' W	1
PS150_113 – 114	80° 58,229' N	-002° 46,909' W	1
PS150_114 – 115	80° 39,150' N	-004° 01,427' W	2
PS150_116 – 117	78° 10,564' N	-015° 44,245' W	1
PS150_117	78° 11,978' N	-015° 33,568' W	1

Station / Transit ID	Latitude (Start)	Longitude (Start)	POM filter
PS150_119 – 120	78° 30,179' N	-012° 00,406' W	3
PS150_122 – 123	80° 26,745' N	-013° 02,182' W	1
PS150_123	80° 29,071' N	-012° 58,540' W	1
PS150_129	80° 09,739' N	-016° 01,313' W	1
PS150_131	80° 05,789' N	-016° 59,956' W	1
PS150_132	79° 25,407' N	-017° 18,209' W	1
PS150_135	79° 10,018' N	-017° 04,983' W	1
PS150_135 – 136	79° 44,246' N	-015° 49,598' W	1
PS150_136 – End	80° 24,296' N	-008° 01,839' W	8

Preliminary (expected) results

Nutrients and dissolved oxygen

Dissolved nutrient and dissolved oxygen data was fully processed and quality controlled onboard. Results from this expedition will be used by Sofia Kuzmina for an AWI INSPIRES PhD project addressing ocean basin-scale nutrient biogeochemistry. Data will be eventually submitted to PANGAEA and a 2-year moratorium will be requested. Access will be granted to participants of the expedition upon request and agreement on data usage. Data will be made publicly available upon publication of research results.

Dissolved oxygen data will be shared with the physical oceanography team to calibrate the CTD sensors and will also be eventually submitted to PANGAEA and made publicly available.

The nutrient data was also fully processed and quality controlled before leaving *Polarstern*. An example is presented here below in Figure 7.1.11 and Figure 7.1.12, which show the distribution of NO_3^-+NO_2^-, TN, PO_4^{3-} and $Si(OH)_4$ across the Lincoln and Flade sections. Interesting features include the presumably Pacific water signal at around 75-100 m, as seen by the strong $Si(OH)_4$ presence (up to 35 µmol/L) not present in the Flade section further south. These differences, along with our previous results from FRAM cruises, indicate that Pacific waters entering the Atlantic Ocean from the Arctic do not reach Fram Strait and instead dissipate up north and/or reach the Atlantic through other circulation pathways (shelf?). The TS plot (Figure 7.1.13) further confirms our suspicions that the waters we trace here are of Pacific origin, based on their thermohaline properties.

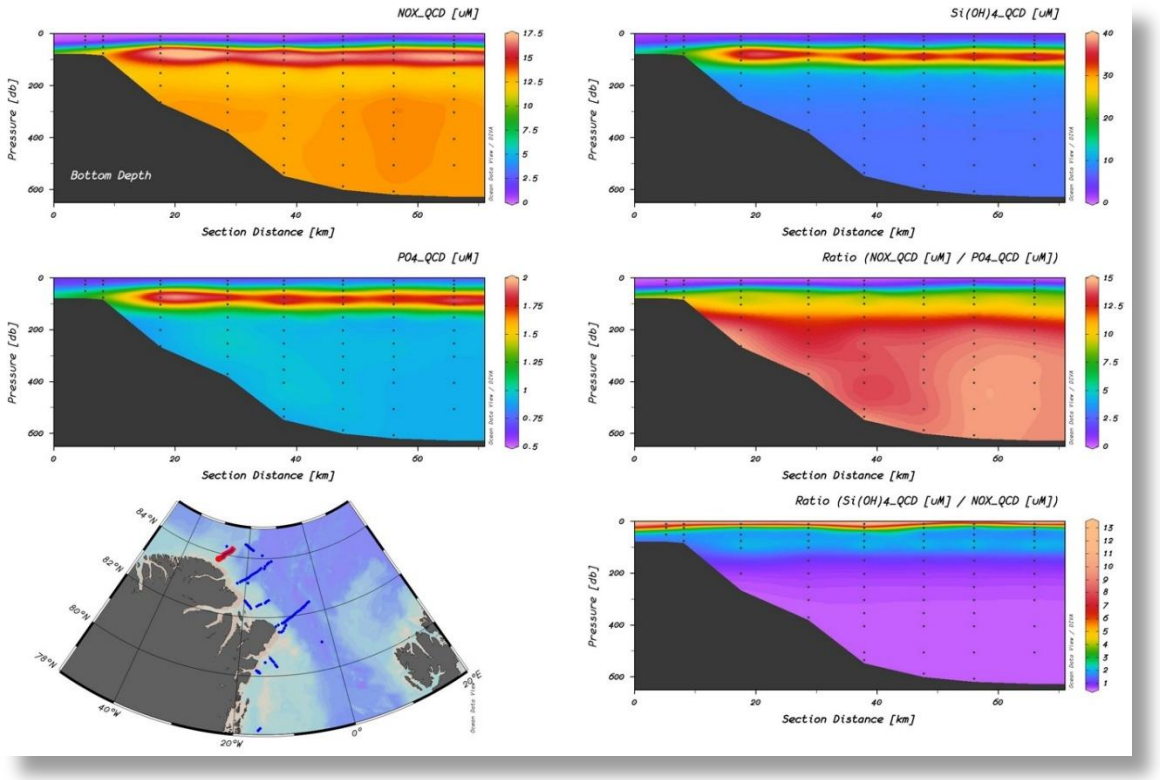

Fig. 7.1.11: Nutrient section plots across Lincoln line

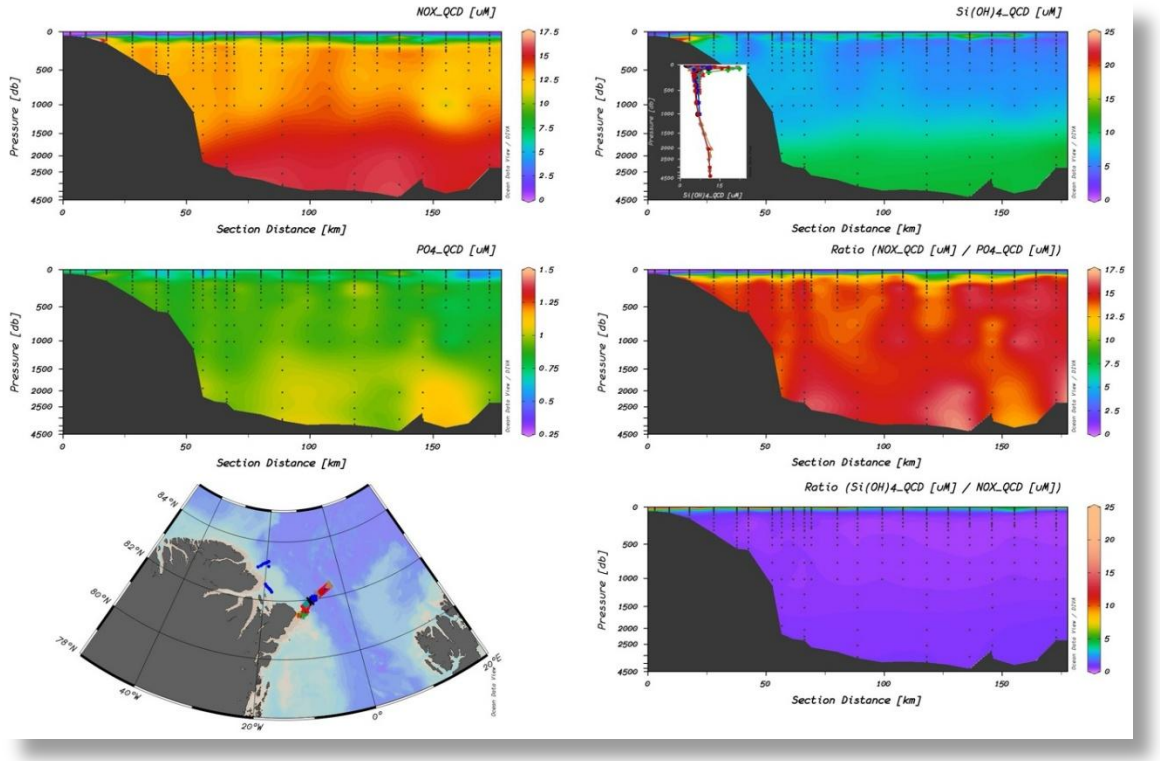

Fig. 7.1.12: Nutrient section plots across Flade line

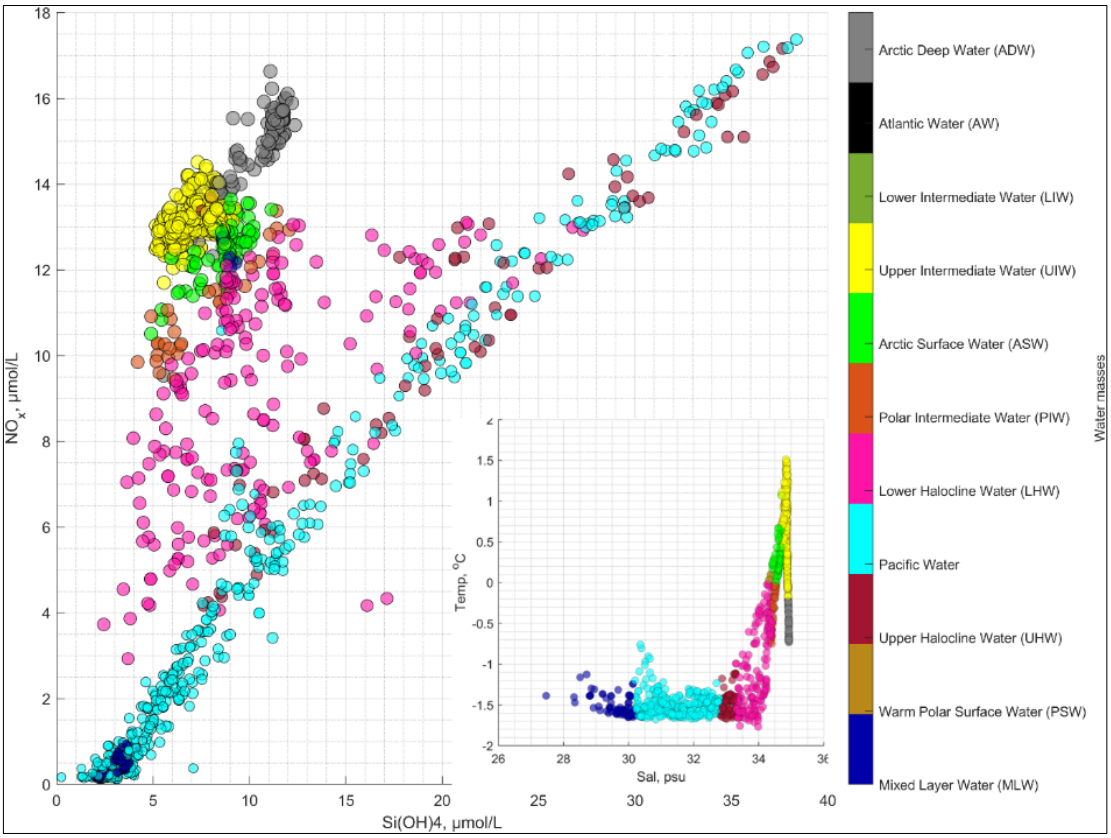

Fig. 7.1.13: N:Si plot showing different water masses using definitions from Aksenov et al. 2010. The insert shows a TS plot with the definitions of water masses used in the plot.

Data management

Environmental data will be archived, published and disseminated according to international standards by the World Data Centre PANGAEA Data Publisher for Earth & Environmental Science (https://www.pangaea.de) within two years after the end of the expedition at the latest. By default, the CC-BY license will be applied.

Any other data will be submitted to an appropriate long-term archive that provides unique and stable identifiers for the datasets and allows open online access to the data.

This expedition was supported by the Helmholtz Research Programme “Changing Earth – Sustaining our Future” Topics 2 and Topic 6, Subtopic 2.1 and Subtopic 6.3.

In all publications based on this expedition, the **Grant No. AWI_PS150_06** will be quoted and the following publication will be cited:

Alfred-Wegener-Institut Helmholtz-Zentrum für Polar- und Meeresforschung (2017) Polar Research and Supply Vessel POLARSTERN Operated by the Alfred-Wegener-Institute. Journal of large-scale research facilities, 3, A119. http://dx.doi.org/10.17815/jlsrf-3-163.

References

Aksenov Y, Bacon S, Coward AC & Holliday NP (2010) Polar outflow from the Arctic Ocean: A high-resolution model study. Journal of Marine Systems 83(1–2):14–37. https://doi.org/10.1016/j.jmarsys.2010.06.007

Becker S, Aoyama M, Woodward E M S, Coverly S, Mahaffey C & Tanhua T (2020) GO-SHIP Repeat Hydrography Nutrient Manual: the precise and accurate determination of dissolved inorganic

nutrients in seawater, using continuos flow analysis methods. Frontiers in Marine Science 7:581790. https://doi.org/10.3389/fmars.2020.581790

Bhatia MP, Das SB, Xu L, Charette MA, Wadham JL, & Kujawinski EB (2013) Organic carbon export from the Greenland ice sheet. Geochimica et Cosmochimica Acta 109:329–344.

Bröder L, Hirst C, Opfergelt S, Thomas M, Vonk JE, Haghipour N, Eglinton TI & Fouché J (2022) Contrasting Export of Particulate Organic Carbon From Greenlandic Glacial and Nonglacial Streams. Geophysical Research Letters 49(e2022GL101210).

Hawkings JR, Wadham, J.. Tranter M, Lawson E, Sole A, Cowton T, et al. (2015) The effect of warming climate on nutrient and solute export from the Greenland Ice Sheet. Geochem. Persp. Let. 94–104. https://doi.org/10.7185/geochemlet.1510

Hawkings J, Wadham J, Tranter M, Telling J, Bagshaw E, Beaton A, et al. (2016) The Greenland Ice Sheet as a hot spot of phosphorus weathering and export in the Arctic. Global Biogeochemical Cycles 30:191–210. https://doi.org/10.1002/2015GB005237

Hawkings J R, Wadham JL, Benning LG, Hendry KR, Tranter M, Tedstone A, et al. (2017) Ice sheets as a missing source of silica to the polar oceans. Nat Commun 8:14198. https://doi.org/10.1038/ncomms14198

Hydes D, Aoyama M, Aminot A, Bakker K & Becker S (2010) Recommendations for the determination of nutrients in seawater to high levels of precision and inter-comparability using continuous flow auotoanalysers. The GO-SHIP repeat hydrography manual: a collection of expert reports and guidelines.

Langdon C (2010) Determination of dissolved oxygen in seawater by Winkler titration using the amperometric technique. The GO-SHIP Repeat Hydrography Manual: A Collection of Expert Reports and Guidelines. IOCCP Report No. 14, ICPO Publication Series No. 134.

Meire L, Meire P, Struyf E, Krawczyk DW, Arendt KE, Yde JC, et al. (2016) High export of dissolved silica from the Greenland Ice Sheet. Geophysical Research Letters 43,_173–9182. https://doi.org/10.1002/2016GL070191

Sharp M, Tranter M, Brown GH & Skidmore M (1995) Rates of chemical denudation and CO2 drawdown in a glacier-covered alpine catchment. Geology 23:61–64. https://doi.org/10.1130/0091-7613

Syring N, Lloyd JM, Stein R, Fahl K, Roberts DH, Callard L & O'Cofaigh C (2020) Holocene Interactions Between Glacier Retreat, Sea Ice Formation, and Atlantic Water Advection at the Inner Northeast Greenland Continental Shelf. Paleoceanography and Paleoclimatology. 35(11):e2020PA004019.

Wadham JL, Hawkings J, Telling J, Chandler D, Alcock J, O'Donnell E, et al. (2016) Sources, cycling and export of nitrogen on the Greenland Ice Sheet. Biogeosciences 13:6339–6352. https://doi.org/10.5194/bg-13-6339-2016

Wu J, Mollenhauer G, Stein R, Köhler P, Hefter J, Fahl K, Grotheer H, Wei B, & Nam S (2022) Deglacial release of petrogenic and permafrost carbon from the Canadian Arctic impacting the carbon cycle. Nature Communications 13(7172).

8. TRACER OCEANOGRAPHY

Núria Casacuberta*[1], Anne-Marie Wefing[2], Stefan Pauls[3], Pia Sueltenfuss[3], Mara Rosmann[4]
Not on board: Oliver Huhn[3], Gesine Mollenhauer[4], Torben Gentz[4], Colin Stedmon[5], Mats Granskog[2], Agneta Fransson[2]
* cnuria@ethz.ch

[1]CH.ETHZ
[2]NO.NPI
[3]DE.UBREMEN
[4]DE.AWI
[5]DK.DTU

Grant-No. AWI_PS150_07

Outline

In recent years, transient tracers such as man-made gases (Tritium, CFC-12 and SF_6) and radionuclides of both natural and anthropogenic origin (e.g., ^{129}I, ^{236}U, ^{14}C, ^{39}Ar) have provided a rich dataset for studying ocean circulation in the Arctic Ocean (Tanhua et al. 2009; Wefing et al. 2021). These tracers are particularly effective because, first, they behave conservatively in the ocean (Casacuberta & Smith 2023). Second, their well-characterized input functions enable the estimation of circulation timescales, mixing processes along flow pathways, and deep-water ventilation rates.

Key findings to date indicate tracer ages of about 10–15 years for surface waters entering through the Barents Sea and West Spitsbergen Current before reaching the North Pole. At mid-depths, Atlantic-origin Arctic Water (AAW) circulates within the Arctic Ocean Boundary Current, reaching the Makarov Basin with mean tracer ages of around 20 years, and the Canada Basin with ages exceeding 25 years (Payne et al. 2024). Finally, AAW exits the Arctic Ocean through Fram Strait with mean ages of approximately 40 years (Wefing et al. 2021), continuing southward with the East Greenland Current (EGC). Recent results by Wefing et al. (2025) and (Gerke et al. 2024) provide a more detailed picture of tracer-based ages in the northern Fram Strait, extending to Eastern Makarov Basin, thus overlapping with the target area of expedition PS150, further underscoring the relevance of this region for understanding Arctic circulation and export pathways.

To date, radionuclide and gas-based transient tracers have typically been sampled and interpreted separately, often yielding slightly differing results (Raimondi et al. 2024). The goal of this project is to integrate these complementary tracer datasets to develop a more unified and robust understanding of transport timescales, mixing processes, and circulation pathways in the Arctic Ocean, and their outflow through the East Greenland Current.

One of the limitations of these tracers is their capability of tearing apart the composition of Polar Surface Waters. Sea ice melt or meteoric waters cannot be traced by neither radionuclide tracers nor gas tracers. Here is when complementary tracers such as $\delta^{18}O$ and CDOM can turn very useful to understand the composition of surface waters in the Arctic Ocean.

In addition to the gas Transient Tracers, oceanic measurement of low-solubility and stable noble-gases helium (^3He, ^4He) and neon (Ne) provide a useful tool to identify and to quantify basal glacial melt water (Huhn et al. 2018). Atmospheric air with a constant composition of these noble gases is trapped in the ice matrix during formation of the meteoric ice. Due to the enhanced hydrostatic pressure at the base of the floating ice, these gases are completely

dissolved, when the ice is melting from below. This leads to an excess of helium and neon in pure glacial melt water (He = 1,260%, Ne = 890%). Frontal or surface melt water would equilibrate quickly and not lead to any noble gas excess in the ocean water. With an accuracy of <0.5% for He and Ne measurements performed at the IUP Bremen, basal glacial melt water fractions of <0.05% are detectable. Helium has an additional oceanic source (primordial helium from hydrothermal vents with a distinct higher $^{3}He/^{4}He$ isotope ratio, and the alpha decay of tritium), which neon does not have. The latter ^{4}He addition can be assessed by tritium measurements. Moreover, tritium is discharged from Siberian rivers into the Arctic Ocean, and tritium observations might give insight into that source.

The combination of the transient tracer based “ages” and the noble gas-based melt water inventories allow estimate basal glacial melt rates (Heuzé et al. 2023).

Objectives

The main objective of our work during the PS150 cruise is to generate a comprehensive dataset of transient tracers along the different transects sampled during the expedition. Specifically, we aim to: i) identify the provenance and pathways of the main water masses; ii) estimate transport times and mixing processes of surface waters and Atlantic-derived Arctic Waters; and iii) constrain the ventilation times of deep and bottom waters outflowing from the Arctic Ocean. Additionally, noble gas isotopes (^{3}He, ^{4}He, total Ne) will be key to quantify submarine melt water (i.e., freshwater discharged from basal melting of Greenland ice shelfs and tide water glaciers) in North Greenland fjords and on the shelf. These transient tracer observations will be combined with other chemical tracers collected during PS150, particularly those used to quantify freshwater contributions (i.e. $\delta^{18}O$, nutrients, C-DOM), in order to better characterize water mass fractions and to assess the freshwater export through the East Greenland Current.

Work at sea

For all tracers, we collected seawater samples from the CTD rosette or from hand Niskin bottles when the work was not performed on the ship (i.e. work on sea ice and in the fjord). Stations sampled for the different parameters are detailed in Table 8.1 and illustrated in Figure 8.1 for the different parameters. Different symbols stand for the type of station (i.e. circles indicate the CTD casts from the ship, triangles and squares the samples taken on Independence fjord and ice stations, respectively, using hand Niskin bottles).

Tab. 8.1: Stations sampled for the different tracers. Table is subdivided in stations that were sampled from the ship using a CTD rosette (CTD casts from ship), samples that were taken using hand Niskin bottles in the ice stations (Samples from ice stations) and samples taken at the fjord, also using hand Niskin bottles (Samples from helicopter-based fjord sampling).

CTD casts from ship

Event	Station	Cast	Date (dd/mm/yyyy)	Time (UTC)	Latitude (N)	Longitude (E)	CFCs, SF6	Helium	Tritium	d18O, CDOM	I-129	U-236	C-14 (ETH)	Ar-39	C-14 (AWI, 12ml)	C-14 (AWI, 100ml)
ps150_001_01	1	1	05/09/2025	10:55	80.084	2.929	9	3	0	0	0	0	0	0	0	0
ps150_005_01	5	1	07/09/2025	02:50	82.388	-3.479	16	0	0	0	12	12	0	0	0	0
ps150_008_01	8	1	07/09/2025	03:00	82.253	-5.025	9	0	0	0	2	2	5	3	7	7
ps150_008_04	8	4	07/09/2025	08:38	82.237	-4.943	8	0	0	0	9	9	9	0	10	10
ps150_009_01	9	1	08/09/2025	01:19	82.212	-5.576	0	0	0	0	0	0	3	3	0	0
ps150_011_01	11	1	08/09/2025	11:01	82.124	-6.597	17	0	0	0	12	12	0	0	12	0
ps150_014_01	14	1	09/09/2025	01:51	81.984	-8.143	15	0	0	11	11	11	0	0	11	0
ps150_018_01	18	1	09/09/2025	12:59	81.876	-9.398	15	12	0	12	12	12	0	0	12	0
ps150_024_01	24	1	10/09/2025	01:46	81.807	-10.108	11	9	0	11	11	11	0	0	11	0
ps150_029_01	29	1	10/09/2025	03:27	81.613	-10.274	8	8	4	9	9	9	0	0	9	0
ps150_030_01	30	1	10/09/2025	08:47	81.523	-10.546	0	7	3	0	0	0	0	0	0	0
ps150_031_01	31	1	11/09/2025	12:00	81.479	-10.963	0	4	4	4	0	0	0	0	4	0
ps150_032_01	32	1	11/09/2025	01:55	81.49	-11.41	0	3	3	0	0	0	0	0	0	0
ps150_036_01	36	1	12/09/2025	06:29	82.305	-18.163	0	5	2	5	0	0	0	0	5	0
ps150_037_01	37	1	12/09/2025	07:56	82.366	-18.555	0	5	3	0	0	0	0	0	0	0
ps150_038_01	38	1	12/09/2025	09:46	82.429	-18.957	8	7	3	11	8	8	0	0	11	0
ps150_039_01	39	1	12/09/2025	01:46	82.48	-19.405	0	6	3	0	0	0	0	0	0	0
ps150_040_01	40	1	12/09/2025	05:02	82.548	-19.85	0	3	2	6	0	0	0	0	6	0
ps150_044_01	44	1	13/09/2025	12:16	83.158	-19.421	0	0	3	0	0	0	0	0	0	0
ps150_045_01	45	1	14/09/2025	11:05	83.109	-22.37	4	4	2	7	6	6	0	0	7	0
ps150_046_01	46	1	14/09/2025	01:35	83.165	-21.579	0	0	0	7	0	0	0	0	0	0
ps150_047_01	47	1	14/09/2025	06:29	83.227	-21.047	5	4	2	7	7	7	0	0	7	0
ps150_048_01	48	1	14/09/2025	08:13	83.258	-20.472	0	0	0	7	0	0	0	0	0	0
ps150_050_06	50	6	15/09/2025	06:55	83.29	-20.126	10	9	3	10	4	4	0	0	12	0
ps150_052_01	52	1	15/09/2025	12:56	83.31	-19.903	12	11	0	11	12	12	0	0	0	0
ps150_054_01	54	1	15/09/2025	04:57	83.335	-19.545	16	13	0	11	0	0	0	0	0	0
ps150_056_01	56	1	15/09/2025	11:57	83.362	-19.211	13	12	0	13	11	11	0	0	13	0
ps150_059_01	59	1	16/09/2025	09:49	83.465	-18.11	10	0	0	10	0	0	0	0	0	0
ps150_061_01	61	1	16/09/2025	10:29	83.56	-16.892	14	13	0	10	11	11	0	0	13	0
ps150_065_02	65	2	17/09/2025	06:54	83.749	-14.529	16	15	0	10	11	11	0	0	13	0
ps150_068_01	68	1	18/09/2025	09:21	83.911	-12.649	9	8	8	0	2	2	6	4	6	6
ps150_068_03	68	3	18/09/2025	07:15	83.904	-12.675	9	8	8	9	9	9	9	0	10	10
ps150_070_01	70	1	19/09/2025	03:22	84.259	-18.367	11	0	0	10	1	1	0	0	0	0
ps150_072_01	72	1	20/09/2025	02:30	84.351	-19.639	15	4	4	11	11	11	0	0	0	0
ps150_075_01	75	1	20/09/2025	06:22	84.39	-20.345	11	4	4	10	9	9	0	0	0	0
ps150_077_01	77	1	21/09/2025	02:29	84.436	-21.146	11	4	4	10	9	9	0	0	0	0

Event	Station	Cast	Date (dd/mm/yyyy)	Time (UTC)	Latitude (N)	Longitude (E)	CFCs, SF6	Helium	Tritium	d18O, CDOM	I-129	U-236	C-14 (ETH)	Ar-39	C-14 (AWI, 12ml)	C-14 (AWI, 100ml)
ps150_078_03	78	3	21/09/2025	01:00	84.471	-21.04	0	0	1	0	0	0	0	0	0	0
ps150_079_01	79	1	22/09/2025	07:07	84.222	-25.396	11	8	0	11	10	10	0	0	12	0
ps150_080_01	80	1	22/09/2025	12:54	84.153	-25.872	11	0	0	0	0	0	0	0	0	0
ps150_081_01	81	1	22/09/2025	07:21	84.104	-26.421	10	8	8	11	9	9	0	0	12	0
ps150_082_01	82	1	22/09/2025	11:00	84.044	-27.059	10	8	0	0	0	0	0	0	0	0
ps150_083_01	83	1	23/09/2025	02:58	83.991	-27.677	7	5	0	10	7	7	0	0	10	0
ps150_084_01	84	1	23/09/2025	05:45	83.908	-28.025	7	5	0	0	0	0	0	0	0	0
ps150_085_06	85	6	23/09/2025	02:46	83.858	-28.69	5	5	0	5	5	5	0	0	5	0
ps150_089_01	89	1	24/09/2025	03:47	84.276	-27.535	11	0	0	11	12	12	0	0	13	0
ps150_093_01	93	1	27/09/2025	04:09	82.502	-14.621	0	0	0	11	9	9	0	0	0	0
ps150_096_01	96	1	28/09/2025	05:41	82.422	-16.166	5	5	0	0	0	0	0	0	0	0
ps150_097_01	97	1	28/09/2025	07:15	82.38	-16.708	4	4	0	0	0	0	0	0	0	0
ps150_113_01	113	1	03/10/2025	11:42	80.955	-2.345	0	0	0	0	11	0	8	4	0	15
ps150_119_01	119	1	07/10/2025	02:07	78.142	-15.914	0	0	0	0	8	0	0	0	0	0
ps150_120_01	120	1	09/10/2025	02:41	80.313	-12.332	5	5	0	0	0	0	0	0	0	0
ps150_122_01	122	1	09/10/2025	06:33	80.394	-12.649	7	7	0	0	0	0	0	0	0	0
ps150_123_06	123	6	09/10/2025	06:30	80.478	-12.913	8	7	0	0	0	0	0	0	0	0
ps150_124_01	124	1	09/10/2025	09:12	80.543	-13.285	8	8	0	0	0	0	0	0	0	0
ps150_126_01	126	1	10/10/2025	02:23	80.462	-14.664	0	0	0	0	0	0	0	0	9	9
ps150_127_06	127	6	10/10/2025	06:30	80.166	-15.807	0	0	0	8	0	0	0	0	8	8
ps150_128_01	128	1	11/10/2025	12:07	80.115	-15.732	9	9	0	0	7	7	0	0	0	0
ps150_129_01	129	1	11/10/2025	02:28	80.158	-16.042	8	7	7	0	8	0	0	0	10	0
ps150_130_01	130	1	11/10/2025	06:41	80.177	-16.327	5	5	5	6	3	0	0	0	0	0
ps150_131_01	131	1	11/10/2025	08:16	80.194	-16.452	5	5	5	0	0	0	0	0	0	0
ps150_132_01	132	1	12/10/2025	06:12	79.423	-17.304	10	9	9	11	0	0	0	0	11	10
ps150_133_01	133	1	12/10/2025	11:23	79.209	-17.45	0	0	0	6	0	0	0	0	0	0
ps150_134_01	134	1	12/10/2025	04:15	79.208	-17.172	9	9	8	0	0	0	0	0	0	0
ps150_135_07	135	7	12/10/2025	11:06	79.159	-17.096	9	10	9	11	9	9	0	0	0	0

Samples from ice station

Event	Station	Cast	Date (dd/mm/yyyy)	Time (UTC)	Latitude (N)	Longitude (E)	CFCs, SF6	Helium	Tritium	d18O, CDOM	I-129	U-236	C-14 (ETH)	Ar-39	C-14 (AWI, 12ml)	C-14 (AWI, 100ml)
ps150_044_01	44	1	13/09/2025		83.141	-19.277	0	0	3	0	0	0	0	0	0	0
ps150_078_01	78	1	21/09/2025		84.471	-20.959	0	1	4	0	2	0	0	0	0	0
ps150_090_01	90	1	25/09/2025		83.884	-24.188	0	1	3	0	1	0	0	0	0	0

Samples from helicopter-based fjord sampling

Event	Station	Cast	Date (dd/mm/yyyy)	Time (UTC)	Latitude (N)	Longitude (E)	CFCs, SF6	Helium	Tritium	d18O, CDOM	I-129	U-236	C-14 (ETH)	Ar-39	C-14 (AWI, 12ml)	C-14 (AWI, 100ml)
PS150_heli_OZE_021_03	IF 1.5	1	26/09/2025	15:13	82.086	-27.042	0	1	1	1	1	0	0	0	1	0
PS150_heli_OZE_021_05	IF 1.5	2	26/09/2025	15:23	82.086	-27.042	0	3	3	3	3	0	0	0	3	0
PS150_heli_OZE_022_03	IF 2.5	1	26/09/2025	17:10	82.074	-24.837	0	2	2	3	3	0	0	0	3	0
PS150_heli_OZE_023_03	IF 6	1	28/09/2025	13:10	82.279	-19.559	0	4	4	4	4	0	0	0	8	0

Radionuclides ^{129}I and ^{236}U transient tracers

We collected a total 262 3L water samples to analyse ^{236}U and 313 250ml – 500 ml samples for the analysis of ^{129}I isotopes. Samples were collected in the different hydrographic sections North of Greenland (Flade 1, Wandel, Morris Jesup Rise, Cape Morris Jesup) and other single stations (e.g. Almost Lincoln, 79N area and Independent Fjord). See Figure 8.1a for details and exact location of the different stations and sections. In each station, about 10 – 15 samples were collected for the analysis of both isotopes, covering depths from 10 meters (surface) to 1500 m. No deep samples have been collected for these isotopes during this cruise, as our main target were Polar Surface Waters, Halocline Waters and Arctic-Atlantic waters. All samples have been stored in boxes and further analysis will take place at ETHZ (Switzerland) and Institute of Marine Sciences (Barcelona, Spain).

Radionuclides ^{14}C and ^{39}Ar transient tracers

Samples for the analysis of ^{14}C and ^{39}Ar were collected in a few selected stations, mostly targeting those having deep and bottom waters (see Figure 8.1b for details). A total of 14 samples were collected for ^{39}Ar, and a total of 40 for ^{14}C (same deep profiles, but with better resolution compared to ^{39}Ar samples). For ^{39}Ar samples were collected using 10L gas propane bottles, previously filled with N_2 gas to create overpressure and avoid any air coming into the bottle. Samples for ^{14}C were collected in 120 ml glass bottles, sealed with septum and poisoned with 50 ul with saturated $HgCl_2$. Samples for ^{39}Ar analysis will be sent to Heidelberg University for the gas extraction and measurements using Atom Trap Trace Analysis. Samples for ^{14}C analysis will be shipped together with to ETHZ for further extraction and measurement using Accelerator Mass Spectrometers.

A more extensive ^{14}C sampling was conducted by the group of Gesine Mollenhauer at AWI (Figure 8.1b, diamonds and cross symbols). A total of 287 samples were collected along 30 stations in Flade 1, Wandel, Cape Morris Jesup, Independence Fjord, Holm and 79N area. These samples, each with a comparably small volume of 12 mL, will undergo CO_2 gas extraction and subsequent measurement using the AMS MICADAS system at AWI. In addition, 75 samples, each with a volume of 100ml were collected in 6 individual stations, coinciding with the ^{14}C and ^{39}Ar samples collected by ETHZ group, with the aim to have a robust intercomparison between labs. The samples were also poisoned with 100 µl saturated $HgCl_2$ and will be converted to graphite before being measured with the AMS MICADAS system at AWI.

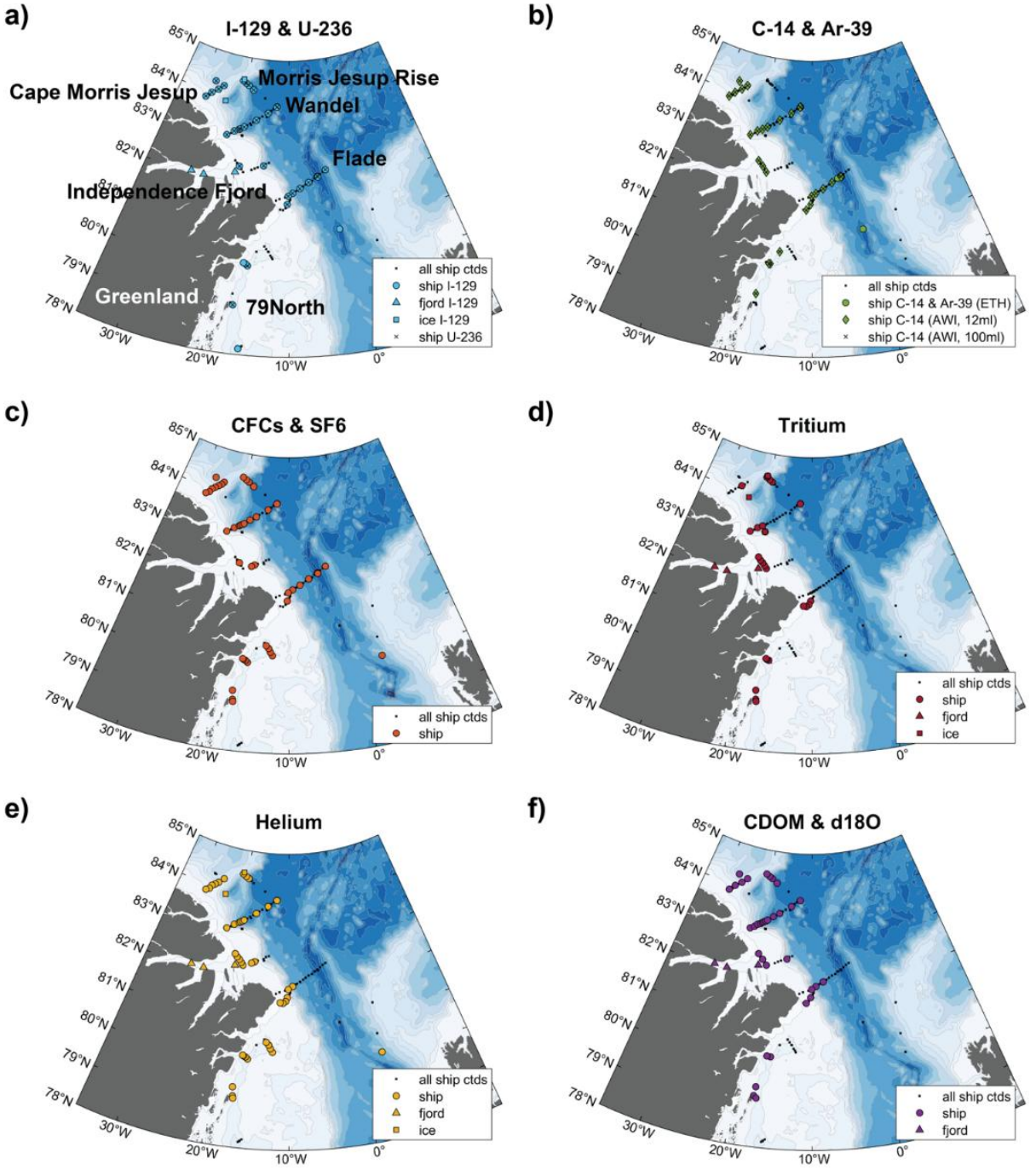

Fig. 8.1: Station maps for different tracers sampled during PS150. Different panels represent samples for: a) ^{236}U and ^{129}I, b) ^{14}C (both from ETHZ and AWI) and ^{39}Ar, c) CFCs and SF_6, d) Tritium, e) Helium (noble gases) and f) CDOM and $\delta^{18}O$.

Gas transient tracers: CFC-12, SF_6, Tritium

We collected a total amount of 446 CFC-12 and SF_6 water samples. The CFC samples are stored in 200 ml glass ampoules. After taking the samples, the headspace of the ampoules was filled with pure nitrogen to enable the flame sealing of the ampules. The ampoules were stored in cardboard boxes, staggered in aluminium boxes for its final shipment to Bremen. With

the aim of targeting the AAW layer of the EGC, water has been sampled at all sections (Flade 1, Independence Shelfbreak, Wandel, Morris Jesup Rise, Cape Morris Jesup, Almost Lincoln station, Westwind Trough, Holm and Norske Trough) as full depth profiles, at the shelf, but most importantly the slope and deeper ocean. For more details and the location of the different stations and sections see Figure 8.1c. The sampling location have been coordinated with those for ^{236}U and ^{129}I isotopes sampling. Per station, depending on the water depth, between 5 to 16 samples are taken, including approximately 10% of double samples. The samples will be later analyzed in the CFC-laboratory at the IUP Bremen using gas chromatography.

A total of 140 tritium samples were collected along the Flade 1, Independence Mouth, Wandel, Morris Jesup Rise, Cape Morris Jesup, Holm, and Norske Trough sections. For each sample, 500 ml of seawater was filled into plastic bottles and stored in aluminum boxes for transport. Per station 2 to 9 samples have been taken, at some stations the full depth profile. The latter with the aim of capturing the signature of the AAW layer. Some of the tritium samplings were aligned with the sampling of the radionuclides ^{129}I and ^{236}U to achieve a matching dataset. Moreover, tritium samples have been obtained at each ice station in form of one snow sample and a sample taken from an ice core, with the aim of doing research on the precipitation pattern. For this purpose, also snow on the ships deck has been collected three times. The tritium samples will be analyzed in the IUP Bremen noble gas mass spectrometry lab.

Noble gas tracers

We obtained 321 water samples for noble gas isotopes (^{3}He, ^{4}He, total Ne). The samples were collected in copper tubes with a total volume of about 40 ml, which are clamped off at both sides to ensure the samples to be gas tight. For the sampling of noble gas isotopes, we focused on the shelf of northern Greenland as well as the Independence Fjord and the program at the 79N glacier (including the sections: Flade 1, Independence Mouth, Independence Shelfbreak, Independence Fjord, Wandel, Morris Jesup Rise, Cape Morris Jesup, Almost Lincoln station, Westwind Trough, Holm and Norske Trough). See Figure 8.1e for the location of the different stations and sections sampled. Per station about 5 to 10 samples have been taken, targeting the glacial meltwater, for which each 50 m from the surface down to the shelf bottom is sampled. The noble gas samples are stored in wooden boxes for safe transport and will be analyzed in the IUP Bremen noble gas mass spectrometry lab.

CDOM and $\delta^{18}O$

A total of 344 seawater samples were collected for the analysis of coloured dissolved organic matter (CDOM) and stable oxygen isotopes ($\delta^{18}O$). Samples for both parameters were always collected combined, at the same stations and depths. We sampled along several sections (Flade 1, Wandel, Morris Jesup Rise, Cape Morris Jesup) and some individual stations along the mouth of Independence Fjord and in the area of the 79N glacier (Figure 8.1f). The sampling was focused on the upper 400m with standard sampling depths, plus the bottom depth sample. CDOM samples were filtered through an 0.22µm Millipore Opticap XL 4 Capsule directly into 40ml pre-combusted amber glass vials and stored at +4°C. They will be sent to DTU (Copenhagen, Denmark) for further analysis. Samples for $\delta^{18}O$ were filled directly into 30ml plastic vials, sealed with parafilm, and stored at room temperature. They will be sent to the Norwegian Polar Institute (Tromsø, Norway).

For the sampling in Independence Fjord using hand-held Niskins, seawater was filled in glass bottles and aliquots for CDOM and $\delta^{18}O$ were taken on the ship. The CDOM samples were filtered through a PALL Acrodisc PF syringe filter with a 0.8/0.2µm Supor Membrane.

Preliminary (expected) results

The combined analysis of gas and radionuclide transient tracers, together with the chemical tracers, is expected to significantly advance our understanding of the sources and composition of the East Greenland Current. In particular, we aim to determine the provenance of Polar Surface Waters and their freshwater contributions. For Atlantic-derived waters, both at the surface and intermediate depths (Atlantic-derived Arctic Waters), we expect to constrain transport times and mixing regimes more accurately.

For deep and bottom waters, the use of cosmogenic radionuclides such as ^{14}C and ^{39}Ar will provide new insights into ventilation timescales, helping to elucidate their origins and the specific Arctic basins from which they emerge. Furthermore, this dataset will offer an excellent opportunity to systematically compare Transit Time Distribution (TTD) estimates derived from gas tracers with those obtained from radionuclide tracers. By integrating these complementary approaches, we expect to overcome the individual limitations of each tracer type and develop optimized strategies for using transient tracers as tools to improve our understanding of Arctic Ocean circulation.

Data management

Environmental data will be archived, published and disseminated according to international standards by the World Data Center PANGAEA Data Publisher for Earth & Environmental Science (https://www.pangaea.de) within two years after the end of the expedition at the latest. By default, the CC-BY license will be applied.

Any other data will be submitted to an appropriate long-term archive that provides unique and stable identifiers for the datasets and allows open online access to the data.

In all publications based on this expedition, the **Grant No. AWI_PS150_07** will be quoted and the following publication will be cited:

Alfred-Wegener-Institut Helmholtz-Zentrum für Polar- und Meeresforschung (2017) Polar Research and Supply Vessel POLARSTERN Operated by the Alfred-Wegener-Institute. Journal of large-scale research facilities, 3, A119. http://dx.doi.org/10.17815/jlsrf-3-163.

References

Casacuberta N & Smith JN (2023) Nuclear Reprocessing Tracers Illuminate Flow Features and Connectivity Between the Arctic and Subpolar North Atlantic Oceans. Annual Review of Marine Science 15(1):203–221. https://doi.org/10.1146/annurev-marine-032122-112413

Gerke L, Arck Y & Tanhua T (2024) Temporal Variability of Ventilation in the Eurasian Arctic Ocean. Journal of Geophysical Research: Oceans 129(7): e2023JC020608. https://doi.org/https://doi.org/10.1029/2023JC020608

Heuzé C, Huhn O, Walter M, Sukhikh N, Karam S, Körtke W, Vredenborg M, Bulsiewicz K, Sültenfuß J, Fang YC, Mertens C, Rabe B, Tippenhauer S, Allerholt J, He H, Kuhlmey D, Kuznetsov I & Mallet M (2023) A year of transient tracers (chlorofluorocarbon 12 and sulfur hexafluoride), noble gases (helium and neon), and tritium in the Arctic Ocean from the MOSAiC expedition (2019 – 2020). Earth Syst. Sci. Data 15(12):5517–5534. https://doi.org/10.5194/essd-15-5517-2023

Huhn O, Hattermann T, Davis PED, Dunker E, Hellmer HH, Nicholls KW, Østerhus S, Rhein M, Schröder M & Sültenfuß J (2018) Basal Melt and Freezing Rates From First Noble Gas Samples Beneath an Ice Shelf. Geophysical Research Letters 45(16):8455–8461. https://doi.org/10.1029/2018GL079706

Payne A, Wefing A-M, Christl M, Vockenhuber C, Williams W, Smith JN & Casacuberta N (2024) Circulation Timescales and Pathways of Atlantic Water in the Canada Basin: Insights From Transient Tracers ^{129}I and ^{236}U. Journal of Geophysical Research: Oceans 129(6):e2023JC020813. https://doi.org/10.1029/2023JC020813

Raimondi L, Wefing A-M & Casacuberta N (2024) Anthropogenic Carbon in the Arctic Ocean: Perspectives From Different Transient Tracers. Journal of Geophysical Research: Oceans 129(1):e2023JC019999. https://doi.org/10.1029/2023JC019999

Tanhua T, Jones EP, Jeansson E, Jutterström S, Smethie WM, Wallace DWR & Anderson LG (2009) Ventilation of the Arctic Ocean: Mean ages and inventories of anthropogenic CO_2 and CFC-11. Journal of Geophysical Research: Oceans 114(C1). https://doi.org/10.1029/2008JC004868

Wefing AM, Casacuberta N, Christl M, Gruber N & Smith JN (2021) Circulation timescales of Atlantic Water in the Arctic Ocean determined from anthropogenic radionuclides. Ocean Sci. 17(1):111–129. https://doi.org/10.5194/os-17-111-2021

Wefing AM, Payne A, Scheiwiller M, Vockenhuber C, Christl M, Tanhua T & Casacuberta N (2025) Changes in Atlantic Water circulation in the central Arctic Ocean between 2011 and 2021 inferred from tracer observations. EGUsphere 2025:1–44. https://doi.org/10.5194/egusphere-2025-1322

APPENDIX

A.1 TEILNEHMENDE INSTITUTE / PARTICIPATING INSTITUTES

A.2 FAHRTTEILNEHMER:INNEN / CRUISE PARTICIPANTS

A.3 SCHIFFSBESATZUNG / SHIP'S CREW

A.4 STATIONSLISTE / STATION LIST

A.1 TEILNEHMENDE INSTITUTE / PARTICIPATING INSTITUTES

Affiliation	Address
On board / In the field	
CH.ETHZ	Eidgenössische Technische Hochschule Zürich Rämistraße 101 8092 Zürich Switzerland
DE.AWI	Alfred-Wegener-Institut Helmholtz-Zentrum für Polar- und Meeresforschung Postfach 120161 27515 Bremerhaven Germany
DE.CAU	Christian-Albrechts-Universität zu Kiel Ludewig-Meyn-Straße 10 24118 Kiel Germany
DE.DRF	DRF Luftrettung gAG Laal Avenue E312 77836 Rheinmünster Germany
DE.driftnoise	Drift + Noise Polar Services Stavendamm 17 28195 Bremen Germany
DE.DWD	Deutscher Wetterdienst Seewetteramt Bernhard Nocht Str. 76 20359 Hamburg Germany
DE.NHC	Northern HeliCopter Gmbh Gorch-Fock-Straße 103 26721 Emden Germany
DE.TU-Dresden	Technische Universität Dresden Dezernat 8 1062 Dresden Germany
DE.Uni-Bremen	Universität Bremern Otto-Hahn-Straße 1 28359 Bremen Germany
DE.UNI-Hamburg	Universität Hamburg Olbersweg 24 22767 Hamburg Germany
DE.UNI-Oldenburg	Carl von Ossietzky Universität Oldenburg Carl-von Ossietzky Straße 11l

Affiliation	Address
On board / In the field	
	2826129 Oldenburg Germany
DE.UNI-Potsdam	Universität Potsdam Karl-Liebknecht-Straße 24-25 14469 Potsdam Germany
DK.AU	Aarhus Universitet Frederiksborvey 399 4000 Roskilde Denmark
FR.LOCEAN.UPMC	Laboratoie d'Océanographie et du Climat: Expérimentations et Approches Numériques 4 place Jussieu 75005 Paris France
GL.Natur	Greenland Institut of Natural Resources Kivioq 2 3900 Nuuk Greenland
NL.NIOZ	Koninklijk Nederlands Instituut voor Onderzoek der Zee P.O. Box 59 1790 AB Den Burg Netherlands
NO.NPOLAR	Norsk Polarinstitutt Framsenteret Hjalmar Johansens gt. 14 9296 Tromsoe Norway
NO.UNIS	The University Centre in Svalbard P.O. Box 156 9170 Longyearbyen Norway
PL.UG	Uniwersytet Gdanski Al. Marszalka Pilsudskiego 46 81-378 Gdynia Poland
SE.LNU	Linnaeus University Stuvaregatan 4 39231 Kalmar Sweden
US.UD	University of Delaware Robinson Hall 19716 Newark DE USA

A.2 FAHRTTEILNEHMER:INNEN / CRUISE PARTICIPANTS

Name/ Last name	Vorname/ First name	Institut/ Institute	Beruf/ Profession	Fachrichtung/ Discipline
on board				
Aehle	Moritz	DE.UNI-Hamburg	Student (Master)	Biology
Brauer	Jens	DE.NHC	Pilot	Helikopter Service
Casacuberta	Nuria	CH.ETHZ	Scientist	Oceanography
Challet	Francois	FR.LOCEAN.UPMC	Student (PhD)	Oceanography
Detsch	Christian Willibald Guido	DE.UNI-Bremen	Student (Master)	Biology
Dreutter	Simon	DE.AWI	Technician	Geophysics
Duncan	Rebecca	SE.LNU	Scientist	Biology
Eggers	Neele	DE.UNI-Potsdam	Student (Master)	Physics
Engicht	Carina	DE.AWI	Technician	Oceanography
Franco Pire	Manuel	DE.AWI	Student (Master)	Oceanography
Fricke	Johannes	DE.TU-Dresden	Student (Master)	Other Geosciences
Gebhardt	Andrea Catalina	DE.AWI	Scientist	Geophysics
Gorniak	Rebecca	DE.UNI-Bremen	Student (Bachelor)	Biology
Harfst	Alicia Magdalena	DE.UNI-Oldenburg	Student (Master)	Oceanography
Hölzer	Martin	DE.DRF	Technician	Helikopter Service
Hoppmann	Mario Günther	DE.AWI	Scientist	Oceanography
Kanzow	Torsten	DE.AWI	Scientist	Oceanography
Köhler	Klara	DK.AU	Student (PhD)	Oceanography
Kuzmina	Sofia	DE.AWI	Student (PhD)	Oceanography
Lemire	Annie Catherine Juliette	DE.UNI-Bremen	Student (Master)	Geophysics
Makatun	Adam	PL.UG	Scientist	Oceanography
Mersch	Clara	DE.AWI	Student (PhD)	Biology
Monsees	Matthias	DE.AWI	Technician	Oceanography
Mortensen	John	GL.Natur	Scientist	Oceanography
Muenchow	Andeas	US.UD	Scientist	Oceanography
Murray	Ayla Rosina Cherrington Sealey	DE.AWI	Scientist	Biology
Neumann	Zoé	DE.CAU	Student (Bachelor)	Geology
Nicolaus	Marcel	DE.AWI	Scientist	Geophysics
Özkan	Ufuk	DE.AWI	Student (PhD)	Oceanography
Pauls	Stefan	DE.UNI-Bremen	Student (Master)	Physics
Pilot	Matthias	DE.UNI-Bremen	Student (PhD)	Geophysics
Rauschenbach	Quentin	DE.AWI	Student (PhD)	Oceanography
Regnery	Julia	DE.AWI	Scientist	Logistics

Name/ Last name	Vorname/ First name	Institut/ Institute	Beruf/ Profession	Fachrichtung/ Discipline
on board				
Rohling	Clemens Michel	DE.UNI-Hamburg	Stundent (Master)	Oceanography
Rosmann	Mara Lena	DE.AWI	Student (Bachelor)	Geochemistry
Schlindwein	Vera	DE.AWI	Scienist	Geophysics
Schmidt	Ina	DE.AWI	Technician	Physics
Schmitz	Bernhard	DE.driftnoise	Scientist	Other Geosciences
Scholz	Daniel Alexander	DE.AWI	Engineer	Chemistry
Seifert	Michael	DE.DRF	Technician	Helikopter Service
Selle	Patrick	NO.UNIS	Student (Bachelor)	Physics
Sueltenfuss	Pia	DE.UNI-Oldenburg	Student (Master)	Data
Suter	Patrick	DE.DWD	Scientist	Meteorology
Torres-Valdéz	Sinhué	DE.AWI	Scientist	Oceanography
Vaupel	Lars	DE.NHC	Pilot	Helikopter Service
Von Appen	Wilken	DE.AWI	Scientist	Oceanography
Wefing	Anne-Marie	NO.Npolar	Scientist	Oceanography
Wekerle	Claudia	DE.AWI	Scientist	Oceanography
Welsch	Andreas	DE.UNI-Hamburg	Technician	Oceanography
Winberg von Friesen	Lisa	SE.LNU	Scientist	Biology
Xi	Hongyan	DE.AWI	Scientist	Oceanography

A.3 SCHIFFSBESATZUNG / SHIP'S CREW

No	Dienstgrad	Rank	Nachname / Last name	Vorname / First name
1	Kapitän	Master	Schwarze	Stefan
2	1. Offizier	Chief Mate	Strauß	Erik
3	1. Offizier Ladung	Chief Mate Cargo	Eckenfels	Hannes
4	2. Offizier	2nd Mate	Weiß	Daniel
5	2. Offizier	2nd Mate	Heisterkamp	Ole Louca
6	Schiffsärztin	Doctor	Guba	Klaus
7	Leitender Ingenieur	Chief Engineer	Rusch	Torben
8	2. Ingenieur	2nd Engineer	Ehrke	Tom
9	2. Ingenieur	2nd Engineer	Krinfeld	Oleksandr
10	2. Ingenieur	2nd Engineer	Jassmann	Marvin
11	Schiffselektrotechniker Maschine	Ship Electrotechnical Officer Engine	Pommerencke	Bernd
12	Elektroniker Winden	Electrotechnical Engineer Winches	Krüger	Lars
13	Elektroniker Netzwerk/Brücke	Electrotechnical Engineer Netw./Bridge	Frank	Gerhard Ansgar Leon
14	Elektroniker Labor	Electrotechnical Engineer Labor	Ejury	René
15	Elektroniker System	Electrotechnical Engineer System	Winter	Andreas
16	Bootsmann	Bosun	Brück	Sebastian
17	Zimmermann	Carpenter	Keller	Jürgen
18	Schiffsmechaniker Deck	Multi Purpose Rating Deck	Buchholz	Joscha
19	Schiffsmechaniker Deck	Multi Purpose Rating Deck	Möller	Falko
20	Schiffsmechaniker Deck	Multi Purpose Rating Deck	Mahlmann	Oliver Karl-Heinz
21	Schiffsmechaniker Deck	Multi Purpose Rating Deck	Schade	Tom
22	Schiffsmechaniker Deck	Multi Purpose Rating Deck	Finkmann	Jan
23	Schiffsmechaniker Deck	Multi Purpose Rating Deck	Decker	Jens

No	Dienstgrad	Rank	Nachname / Last name	Vorname / First name
24	Schiffsmechaniker Deck	Multi Purpose Rating Deck	Deutschbein	Felix Maximilian
25	Schiffsmechaniker Deck	Multi Purpose Rating Deck	Siemon	Leon Anton
26	Decksmann/Matrose	Able Seaman	Niebuhr	Tim
27	Lagerhalter	Storekeeper	Plehn	Marco Markus
28	Schiffsmechaniker Maschine	Multi Purpose Rating Engine	Schröder	Paul
29	Schiffsmechaniker Maschine	Multi Purpose Rating Engine	Probst	Lorenz
30	Schiffsmechanikerin Maschine	Multi Purpose Rating Engine	Stubenrauch	Paula
31	Schiffsmechaniker Maschine	Multi Purpose Rating Engine	Buchholz	Karl Erik
32	Schiffsmechaniker Maschine	Multi Purpose Rating Engine	Cording	Bastian-Fynn
33	1. Koch	1st Cook	Skrzipale	Mitja
34	2. Köchin	2nd Cook	Fehrenbach	Martina
35	2. Köchin	2nd Cook	Loibl	Patrick
36	1. Stewardess	1st Stewardess	Witusch	Petra Gertrud Ramona
37	2. Stewardess	2nd Stewardess	Stocker	Eileen Sigourney
38	2. Steward	2nd Steward	Golla	Gerald
39	2. Stewardess	2nd Stewardess	Holl	Claudia
40	2. Stewardess / Krankenschwester	2nd Stewardess / Nurse	Ilk	Romy
41	2. Steward / Wäscherei	2nd Steward / Laundry	Shi	Wubo
42	2. Steward / Wäscherei	2nd Steward / Laundry	Chen	Jirong
43	2. Steward / Wäscherei	2nd Steward / Laundry	Chen	Quanlun
44	Auszubildender Schiffsmechaniker	Apprentice Multi Purpose Rating	Liedtke	Mattes

A.4 STATIONSLISTE / STATION LIST PS150

Station list of expedition PS150 from Longyearbyen – Bremerhaven; the list details the action log for all stations along the cruise track.
This list contains only stations taken onboard *Polarstern*. See https://www.pangaea.de/expeditions/events/PS150 to display the entire station (event) list for expedition PS150 including all stations taken on and from the ice.
This version contains Uniform Resource Identifiers for all sensors listed under https://sensor.awi.de. See https://www.awi.de/en/about-us/service/computing-centre/data-flow-framework.html for further information about AWI's data flow framework from sensor observations to archives (O2A).

Event label	Optional label	Date/Time	Latitude	Longitude	Depth [m]	Gear	Action	Comment *
PS150-track		2025-09-04T06:00:00	78.23584	15.61030		CT	Station start	Tromsø - Bremerhaven
PS150-track		2025-10-24T04:01:15	53.56374	8.55617		CT	Station end	Tromsø - Bremerhaven
PS150_0_Underway-1		2025-09-04T18:02:16	78.10728	13.01361	263.6	ADCP	Station start	
PS150_0_Underway-1		2025-10-23T18:11:42	54.72881	7.03104	18.7	ADCP	Station end	
PS150_0_Underway-2		2025-09-04T20:08:08	78.05030	11.25870	225.2	DS3	Station start	Event shows start/end point (date/time & coordinates) of first/last data record using Atlas Hydrographic Hydrosweep DS 3 multibeam…
PS150_0_Underway-2		2025-10-23T10:47:09	56.08190	6.64420	25.5	DS3	Station end	Event shows start/end point (date/time &

Event label	Optional label	Date/Time	Latitude	Longitude	Depth [m]	Gear	Action	Comment *
								coordinates) of first/last data record using Atlas Hydrographic Hydrosweep DS 3 multibeam…
PS150_0_Underway-6		2025-09-04T18:00:00	78.10826	13.04563	268.9	ICERAD	Station start	
PS150_0_Underway-6		2025-10-17T06:36:33	79.30905	3.01170	2582.4	ICERAD	Station end	
PS150_0_Underway-10		2025-09-04T18:00:15	78.10814	13.04187	267.5	CAME	Station start	
PS150_0_Underway-10		2025-10-24T03:59:22	53.56374	8.55617		CAME	Station end	
PS150_0_Underway-11		2025-09-04T18:01:21	78.10769	13.02654	265.3	pCO2	Station start	
PS150_0_Underway-11		2025-10-23T18:12:32	54.72619	7.03298	19.0	pCO2	Station end	
PS150_0_Underway-13		2025-09-04T20:04:00	78.04967	11.31534	227.3	PS	Station start	Entry Narwhal_summer_area; Outside Narwhal_summer_area
PS150_0_Underway-13		2025-10-23T10:50:46	56.07075	6.63718	26.3	PS	Station end	Entry Narwhal_summer_area; Outside Narwhal_summer_area
PS150_0_Underway-16		2025-09-04T17:57:32	78.10949	13.08041	272.5	TSG	Station start	
PS150_0_Underway-16		2025-10-23T18:14:22	54.72058	7.03711	19.9	TSG	Station end	

Event label	Optional label	Date/Time	Latitude	Longitude	Depth [m]	Gear	Action	Comment *
PS150_0_Underway-17		2025-09-04T17:57:58	78.10928	13.07436	271.5	TSG	Station start	
PS150_0_Underway-17		2025-10-23T18:13:49	54.72228	7.03587	19.6	TSG	Station end	
PS150_0_Underway-19		2025-09-04T09:11:43	78.23627	15.61034		SWEAS	Station start	
PS150_0_Underway-19		2025-10-24T04:00:17	53.56374	8.55617		SWEAS	Station end	
PS150_0_Underway-20		2025-09-04T17:59:35	78.10845	13.05148	270.6	FBOX	Station start	
PS150_0_Underway-20		2025-10-23T18:13:19	54.72377	7.03476	19.7	FBOX	Station end	
PS150_0_Underway-21		2025-09-04T18:00:00	78.10826	13.04563	268.9	MiRAC-P	Station start	
PS150_0_Underway-21		2025-10-14T12:21:16	79.73862	-15.83795	222.1	MiRAC-P	Station end	
PS150_0_Underway-22		2025-09-04T18:00:00	78.10826	13.04563	268.9	HATPRO	Station start	
PS150_0_Underway-22		2025-10-14T12:25:26	79.73860	-15.83806	221.0	HATPRO	Station end	
PS150_0_Underway-23		2025-09-04T18:00:00	78.10826	13.04563	268.9	CAME	Station start	
PS150_0_Underway-23		2025-10-24T03:59:55	53.56374	8.55617		CAME	Station end	
PS150_0_Underway-24		2025-09-06T15:44:00	81.70470	0.55688	2469.6	SPRA	Station start	

Event label	Optional label	Date/Time	Latitude	Longitude	Depth [m]	Gear	Action	Comment *
PS150_0_Underway-24		2025-10-16T09:15:13	80.40484	-8.02837	255.7	SPRA	Station end	
PS150_0_Underway-25		2025-09-06T16:20:00	81.72761	0.39639	2530.7	SIMS	Station start	
PS150_0_Underway-25		2025-10-07T10:00:48	78.36904	-13.08970	150.5	SIMS	Station end	
PS150_0_Underway-26		2025-09-07T09:20:15	82.34970	-3.97453	3287.4	ICEOBS	Station start	
PS150_0_Underway-26		2025-10-16T16:30:40	80.18144	-5.86179	389.4	ICEOBS	Station end	
PS150_0_Underway-28		2025-09-04T17:55:39	78.11035	13.10673	277.3	TSI	Station start	
PS150_0_Underway-28		2025-10-17T09:35:37	79.09425	4.56834	2049.4	TSI	Station end	
PS150_0_Underway-29		2025-09-04T18:00:59	78.10784	13.03150	266.3	FBOX	Station start	
PS150_0_Underway-29		2025-10-24T03:59:11	53.56374	8.55617		FBOX	Station end	
PS150_1-1		2025-09-05T11:47:50	80.08349	2.93017	2353.9	CTD-RO	max depth	RL max.:2317m
PS150_1-2		2025-09-05T12:54:08	80.08277	2.93067	2361.5	MSN	Station start	AWI004 RL max.: 50m
PS150_1-2		2025-09-05T13:19:16	80.08306	2.93149	2357.7	MSN	Station end	AWI004 RL max.: 50m
PS150_1-3		2025-09-05T13:21:43	80.08319	2.93134	2357.3	LIGHT	Station start	AWI004 RL max.: 100m

Event label	Optional label	Date/Time	Latitude	Longitude	Depth [m]	Gear	Action	Comment *
PS150_1-3		2025-09-05T13:56:07	80.08322	2.92962	2358.1	LIGHT	Station end	AWI004 RL max.: 100m
PS150_1-4		2025-09-05T14:45:37	80.08311	2.93090	2356.8	GC	max depth	AWI004 RL max = 2000m
PS150_2-1		2025-09-05T19:31:46	80.54112	2.82507	1516.1	CTD-RO	max depth	EL31; max SL: 1.510m
PS150_3-1		2025-09-06T04:34:21	81.27931	3.13975	791.3	CTD-RO	max depth	EL31 RL max = 782m
PS150_4-1		2025-09-06T05:30:48	81.31033	3.15975	793.3	MOOR	Station start	recovery UIB-Y8; top unit with 3 floats and 1 MicroCat on deck; 2nd float unit; 1 temperature logger; 1 current meter , 1 MicroCat…
PS150_4-1		2025-09-06T09:30:01	81.29245	3.01698	821.4	MOOR	Station end	recovery UIB-Y8; top unit with 3 floats and 1 MicroCat on deck; 2nd float unit; 1 temperature logger; 1 current meter , 1 MicroCat…
PS150_5-1		2025-09-07T03:43:10	82.38544	-3.46300	2332.2	CTD-RO	max depth	EL31 RL max.: 2312m
PS150_5-2		2025-09-07T05:14:25	82.38165	-3.43818	2368.9	MSN	Station start	AWI004 RL max = 1466m
PS150_5-2		2025-09-07T07:28:14	82.37489	-3.39766	2402.5	MSN	Station end	AWI004 RL max = 1466m
PS150_6-1		2025-09-07T09:14:03	82.34978	-3.97686	3292.4	CTD-RO	max depth	EL31 max. SL:L 995m

Event label	Optional label	Date/Time	Latitude	Longitude	Depth [m]	Gear	Action	Comment *
PS150_6-2		2025-09-07T10:04:37	82.34783	-3.96130	3275.0	LIGHT	Station start	Hand net at depth: 20m; Awi004, max SL.: 100m
PS150_6-2		2025-09-07T10:47:23	82.34614	-3.96313	3274.2	LIGHT	Station end	Hand net at depth: 20m; Awi004, max SL.: 100m
PS150_7-1		2025-09-07T12:57:23	82.30115	-4.48133	3631.4	CTD-RO	max depth	resp.: Von Appen; EL31 RL max.: 996m
PS150_8-1		2025-09-07T16:08:45	82.25080	-4.98534	3135.7	CTD-RO	max depth	resp.: von Appen; EL31 RL max = 3130m
PS150_8-2		2025-09-07T17:32:46	82.24554	-4.93706	2809.5	MSSP	Station start	resp.: Hoppmann; RL max = 366m
PS150_8-2		2025-09-07T18:22:00	82.24363	-4.90723	2727.8	MSSP	Station end	resp.: Hoppmann; RL max = 366m
PS150_8-3		2025-09-07T18:28:41	82.24090	-4.91228	2689.0	MSN	Station start	resp.: Murray; AWI004 RL max = 1468m
PS150_8-3		2025-09-07T20:21:45	82.23494	-4.89749	2820.6	MSN	Station end	resp.: Murray; AWI004 RL max = 1468m
PS150_8-4		2025-09-07T20:59:17	82.23575	-4.93379	2719.4	CTD-RO	max depth	Resp.: von Appen; EL31, max SL.: 747
PS150_9-1		2025-09-08T02:45:21	82.20912	-5.54294	4044.4	CTD-RO	max depth	resp.: Von Appen; EL31 RL max.:4026m
PS150_9-2		2025-09-08T04:36:42	82.21210	-5.53143	4107.0	LIGHT	Station start	resp.: Xi; AWI004 RL max = 100m
PS150_9-2		2025-09-08T05:29:35	82.21386	-5.50286	4213.6	LIGHT	Station end	resp.: Xi; AWI004 RL max = 100m
PS150_9-3		2025-09-08T04:48:30	82.21293	-5.52857	4150.8	HN	Station start	

Event label	Optional label	Date/Time	Latitude	Longitude	Depth [m]	Gear	Action	Comment *
PS150_9-3		2025-09-08T04:53:17	82.21293	-5.52798	4144.8	HN	Station end	
PS150_9-4		2025-09-08T06:00:32	82.21473	-5.47952	4261.8	CTD-RO	max depth	EL31 RL max = 97m
PS150_10-1		2025-09-08T08:29:48	82.15494	-5.99641	3601.1	CTD-RO	max depth	EL31, max SL.: 997m
PS150_11-1		2025-09-08T12:15:25	82.12546	-6.58033	3408.1	CTD-RO	max depth	EL31 RL max.:3396m
PS150_11-2		2025-09-08T14:07:19	82.12714	-6.59703	3402.2	MSN	Station start	AWI004 RL max.: 1467m
PS150_11-2		2025-09-08T16:01:38	82.12947	-6.63043	3291.4	MSN	Station end	AWI004 RL max.: 1467m
PS150_12-1		2025-09-08T18:30:55	82.07937	-7.13927	3344.6	LIGHT	Station start	AWI004 RL max = 100m
PS150_12-1		2025-09-08T19:31:19	82.07716	-7.13765	3343.2	LIGHT	Station end	AWI004 RL max = 100m
PS150_12-2		2025-09-08T18:51:43	82.07781	-7.14270	3343.0	HN	Station start	
PS150_12-2		2025-09-08T18:56:47	82.07766	-7.14184	3342.5	HN	Station end	
PS150_12-3		2025-09-08T20:08:15	82.07704	-7.13134	3342.9	CTD-RO	max depth	EL31, max SL.: 996m
PS150_12-4		2025-09-08T21:14:24	82.07525	-7.13951	3345.6	MSSP	Station start	Depth 400; Max depth: 400m; depth: 400m
PS150_12-4		2025-09-08T22:09:55	82.07126	-7.15502	3342.1	MSSP	Station end	Depth 400; Max depth: 400m; depth: 400m

Event label	Optional label	Date/Time	Latitude	Longitude	Depth [m]	Gear	Action	Comment *
PS150_13-1		2025-09-08T23:52:05	82.03088	-7.58693	3403.7	CTD-RO	max depth	EL31, max SL.: 996m
PS150_14-1		2025-09-09T02:56:24	81.98212	-8.16716	3121.0	CTD-RO	max depth	EL31 RL max.: 3049m
PS150_14-2		2025-09-09T04:29:40	81.97922	-8.19870	3159.0	MSSP	Station start	RL max = 390m; RL max = 393m
PS150_14-2		2025-09-09T05:20:07	81.97738	-8.21573	3177.8	MSSP	Station end	RL max = 390m; RL max = 393m
PS150_15-1		2025-09-09T06:40:51	81.94149	-8.63957	2789.7	CTD-RO	max depth	EL31 RL max = 995m
PS150_16-1		2025-09-09T09:16:10	81.88624	-9.22050	2596.3	CTD-RO	max depth	EL31, max SL.: 996m
PS150_16-2		2025-09-09T10:10:24	81.88366	-9.21827	2592.0	MSN	Station start	AWI004, max SL 489m
PS150_16-2		2025-09-09T10:56:37	81.88235	-9.21521	2588.9	MSN	Station end	AWI004, max SL 489m
PS150_16-3		2025-09-09T11:03:10	81.88171	-9.21666	2584.8	LIGHT	Station start	AWI004, max SL: 100m
PS150_16-3		2025-09-09T11:45:25	81.88057	-9.22209	2578.5	LIGHT	Station end	AWI004, max SL: 100m
PS150_16-4		2025-09-09T11:06:31	81.88136	-9.21659	2582.8	HN	Station start	
PS150_16-4		2025-09-09T11:09:12	81.88125	-9.21708	2582.5	HN	Station end	
PS150_16-5		2025-09-09T11:52:28	81.87993	-9.22465	2575.4	ICE	Station start	

Event label	Optional label	Date/Time	Latitude	Longitude	Depth [m]	Gear	Action	Comment *
PS150_16-5		2025-09-09T12:00:09	81.87949	-9.22784	2572.7	ICE	Station end	
PS150_17-1		2025-09-09T12:18:59	81.87851	-9.31893	2452.5	XCTD	Station start	1100m
PS150_17-1		2025-09-09T12:28:14	81.87819	-9.32282	2443.5	XCTD	Station end	1100m
PS150_18-1		2025-09-09T13:49:57	81.87574	-9.40033	2337.1	CTD-RO	max depth	EL31 RL max.: 2277m
PS150_18-2		2025-09-09T15:11:42	81.87560	-9.40787	2336.8	MSN	Station start	AWI004 RL max = 1466m
PS150_18-2		2025-09-09T17:08:22	81.87270	-9.41619	2310.2	MSN	Station end	AWI004 RL max = 1466m
PS150_18-3		2025-09-09T17:09:25	81.87260	-9.41649	2309.5	MSSP	Station start	RL max = 355m; RL max = 395m; RL max = 392m
PS150_18-3		2025-09-09T18:12:18	81.86915	-9.42280	2302.0	MSSP	Station end	RL max = 355m; RL max = 395m; RL max = 392m
PS150_19-1		2025-09-09T18:32:42	81.86183	-9.49127	2304.3	XCTD	Station start	RL = 1100m
PS150_19-1		2025-09-09T18:42:47	81.86022	-9.50686	2306.3	XCTD	Station end	RL = 1100m
PS150_20-1		2025-09-09T19:39:29	81.84908	-9.62885	2294.2	CTD-RO	max depth	EL31 RL max = 995m
PS150_21-1		2025-09-09T22:02:08	81.83895	-9.75201	2249.9	XCTD	Station start	
PS150_21-1		2025-09-09T22:14:43	81.83783	-9.74929	2247.1	XCTD	Station end	

Event label	Optional label	Date/Time	Latitude	Longitude	Depth [m]	Gear	Action	Comment *
PS150_22-1		2025-09-09T23:34:38	81.82211	-9.87930	2143.9	CTD-RO	max depth	EL31, max SL: 1.904m
PS150_23-1		2025-09-10T00:59:22	81.81951	-10.01002	1985.3	XCTD	Station start	1100m
PS150_23-1		2025-09-10T01:10:10	81.81869	-10.00394	1986.8	XCTD	Station end	1100m
PS150_24-1		2025-09-10T02:15:59	81.80432	-10.09052	1111.8	CTD-RO	max depth	EL31 RL max.: 1111m
PS150_24-2		2025-09-10T03:02:04	81.80106	-10.06231	1262.2	MSSP	Station start	RL max.: 367m; 2nd run; RL max.: 363m
PS150_24-2		2025-09-10T03:52:13	81.79787	-10.03225	1333.6	MSSP	Station end	RL max.: 367m; 2nd run; RL max.: 363m
PS150_24-3		2025-09-10T04:01:54	81.79670	-10.02704	1390.3	MSN	Station start	AWI004 RL max = 1259m
PS150_24-3		2025-09-10T05:38:40	81.78861	-9.97126	1317.4	MSN	Station end	AWI004 RL max = 1259m
PS150_24-4		2025-09-10T05:39:00	81.78858	-9.97098	1315.9	MSN	Station start	AWI004 Rl max = 1001m
PS150_24-4		2025-09-10T06:54:38	81.78131	-9.92998	1442.5	MSN	Station end	AWI004 Rl max = 1001m
PS150_24-5		2025-09-10T06:57:08	81.78107	-9.92824	1482.6	XCTD	Station start	RL 1100m
PS150_24-5		2025-09-10T07:14:21	81.77938	-9.91723	1385.4	XCTD	Station end	RL 1100m
PS150_25-1		2025-09-10T09:52:55	81.72085	-9.77627	577.4	CTD-RO	max depth	EL31, max SL: 549

Event label	Optional label	Date/Time	Latitude	Longitude	Depth [m]	Gear	Action	Comment *
PS150_25-2		2025-09-10T10:56:04	81.70685	-9.82104	565.2	LIGHT	Station start	AWI004, max SL: 100m
PS150_25-2		2025-09-10T11:35:53	81.70225	-9.80317	566.5	LIGHT	Station end	AWI004, max SL: 100m
PS150_25-3		2025-09-10T10:58:36	81.70654	-9.81997	564.9	HN	Station start	Depth: 20m
PS150_25-3		2025-09-10T11:00:42	81.70624	-9.81889	565.3	HN	Station end	Depth: 20m
PS150_26-1		2025-09-10T11:50:08	81.70128	-9.78764	574.8	XCTD	Station start	580m
PS150_26-1		2025-09-10T12:02:58	81.70032	-9.77989	575.7	XCTD	Station end	580m
PS150_27-1		2025-09-10T12:53:28	81.68174	-9.91645	558.5	CTD-RO	max depth	EL31 RL max.:530m
PS150_27-2		2025-09-10T13:53:52	81.67694	-9.89780	567.8	MUC	max depth	GE72.1 RL max.: 554m
PS150_28-1		2025-09-10T14:52:32	81.64326	-10.06843	1126.5	XCTD	Station start	1100m
PS150_28-1		2025-09-10T15:00:36	81.64134	-10.06724	1126.8	XCTD	Station end	1100m
PS150_29-1		2025-09-10T15:46:59	81.60944	-10.26070	351.1	CTD-RO	max depth	EL31 RL max.:350m
PS150_29-2		2025-09-10T16:18:01	81.60716	-10.24162	360.5	MSSP	Station start	RL max = 244m; RL max = 259m; RL max = 233m
PS150_29-2		2025-09-10T17:22:41	81.60018	-10.21565	287.1	MSSP	Station end	RL max = 244m; RL max = 259m; RL max = 233m

Event label	Optional label	Date/Time	Latitude	Longitude	Depth [m]	Gear	Action	Comment *
PS150_29-3		2025-09-10T17:23:00	81.60013	-10.21532	289.4	MSN	Station start	AWI004 RL max = 199m
PS150_29-3		2025-09-10T17:50:01	81.59671	-10.19694	289.4	MSN	Station end	AWI004 RL max = 199m
PS150_29-4		2025-09-10T17:50:24	81.59667	-10.19673	289.4	MSN	Station start	AWI004 RL max = 247m
PS150_29-4		2025-09-10T18:22:16	81.59187	-10.17230	276.3	MSN	Station end	AWI004 RL max = 247m
PS150_29-5		2025-09-10T18:48:32	81.58690	-10.14827	260.5	MUC	Station start	GE72.1 Rl max = 265m; RT max = 1,1t; GE72.1 Rl max = 245m
PS150_29-5		2025-09-10T19:30:02	81.57800	-10.11410	234.2	MUC	Station end	GE72.1 Rl max = 265m; RT max = 1,1t; GE72.1 Rl max = 245m
PS150_30-1		2025-09-10T20:56:22	81.52131	-10.53649	150.0	CTD-RO	max depth	EL31, max SL: 145m
PS150_30-2		2025-09-10T21:16:40	81.51736	-10.51518	152.8	LIGHT	Station start	AWI004, max. SL: 125m
PS150_30-2		2025-09-10T21:56:59	81.50964	-10.47077	163.1	LIGHT	Station end	AWI004, max. SL: 125m
PS150_30-3		2025-09-10T21:25:07	81.51572	-10.50609	155.2	HN	Station start	Max. depth: 20m
PS150_30-3		2025-09-10T21:28:27	81.51499	-10.50226	160.5	HN	Station end	Max. depth: 20m
PS150_30-4		2025-09-10T22:09:01	81.50679	-10.45543	165.8	MSC	max depth	AWI004, max. SL: 34m
PS150_31-1		2025-09-11T00:06:22	81.47722	-10.96085	73.6	CTD-RO	max depth	EL31 RL max.: 71m

Event label	Optional label	Date/Time	Latitude	Longitude	Depth [m]	Gear	Action	Comment *
PS150_32-1		2025-09-11T02:00:29	81.49004	-11.40858	54.7	CTD-RO	max depth	EL31 RL max.: 55m
PS150_33-1		2025-09-11T10:37:22	82.09964	-11.90068	247.2	OBS	Station start	
PS150_33-1		2025-09-11T11:07:29	82.09595	-11.90716	235.8	OBS	Station end	
PS150_34-1		2025-09-11T12:45:03	82.14102	-12.40912	224.7	OTTER_USV	Station start	short correction
PS150_34-1		2025-09-11T17:16:30	82.13173	-12.34841	227.3	OTTER_USV	Station end	short correction
PS150_35-1		2025-09-12T00:36:26	82.29115	-14.87993	214.7	OBS	Station start	
PS150_35-1		2025-09-12T01:01:04	82.29277	-14.87641	216.2	OBS	Station end	
PS150_36-1		2025-09-12T06:37:05	82.30488	-18.16173	120.0	CTD-RO	max depth	EL31 RL max = 117m
PS150_37-1		2025-09-12T08:13:06	82.36619	-18.55292	379.9	CTD-RO	max depth	EL31, max SL: 367m
PS150_38-1		2025-09-12T10:09:15	82.42760	-18.94535	510.5	CTD-RO	max depth	EL31, max SL: 499
PS150_38-2		2025-09-12T10:43:27	82.42666	-18.93134	505.2	MSN	Station start	AWI004, max SL: 479m
PS150_38-2		2025-09-12T11:30:51	82.42574	-18.91186	499.9	MSN	Station end	AWI004, max SL: 479m
PS150_38-3		2025-09-12T11:57:06	82.42607	-18.91370	499.9	MUC	max depth	GE72.1 RL max.: 497m

Event label	Optional label	Date/Time	Latitude	Longitude	Depth [m]	Gear	Action	Comment *
PS150_38-4		2025-09-12T12:38:17	82.42630	-18.90739	497.3	MUC	max depth	GE72.1 RL max.: 498m
PS150_39-1		2025-09-12T14:05:40	82.47999	-19.40472	465.7	CTD-RO	max depth	EL31 RL max.: 451m
PS150_39-2		2025-09-12T14:35:18	82.47974	-19.40396	465.7	LIGHT	Station start	AWI004 RL max.: 120m
PS150_39-2		2025-09-12T15:33:11	82.47999	-19.40573	465.7	LIGHT	Station end	AWI004 RL max.: 120m
PS150_39-3		2025-09-12T14:45:27	82.47997	-19.40336	465.7	HN	Station start	
PS150_39-3		2025-09-12T14:48:47	82.48001	-19.40337	465.7	HN	Station end	
PS150_40-1		2025-09-12T17:12:54	82.54774	-19.84957	121.7	CTD-RO	max depth	El31 RL amx = 135m
PS150_41-1		2025-09-12T19:15:22	82.49479	-19.47951	497.3	CTD-RO	max depth	EL31 RL max = 487m
PS150_42-1		2025-09-12T21:31:49	82.41207	-18.86429	526.3	CTD-RO	max depth	EL31, max SL: 512m
PS150_42-2		2025-09-12T22:17:11	82.41113	-18.85177	521.0	MUC	max depth	GE72.1, max SL: 519m
PS150_43-1		2025-09-13T02:17:05	82.57125	-18.97529	478.9	OBS	Station start	
PS150_43-1		2025-09-13T02:45:12	82.56946	-18.96950	471.0	OBS	Station end	
PS150_44-1		2025-09-13T10:20:00	83.16222	-19.45579	1040.7	ICE	Station start	

Event label	Optional label	Date/Time	Latitude	Longitude	Depth [m]	Gear	Action	Comment *
PS150_44-1		2025-09-13T19:43:13	83.14042	-19.27774	1039.0	ICE	Station end	
PS150_44-2		2025-09-13T12:47:12	83.15673	-19.41127	1058.7	CTD-RO	Station start	EL31 RL max.: 1040m; EL31 RL max.: 1066m
PS150_44-2		2025-09-13T13:40:23	83.15491	-19.39284	1078.3	CTD-RO	Station end	EL31 RL max.: 1040m; EL31 RL max.: 1066m
PS150_44-3		2025-09-13T14:14:26	83.15374	-19.38049	1075.7	LIGHT	Station start	AWI004 RL max.: 100m
PS150_44-3		2025-09-13T15:10:01	83.15179	-19.35953	1069.7	LIGHT	Station end	AWI004 RL max.: 100m
PS150_44-4		2025-09-13T15:47:05	83.15041	-19.34550	1071.3	CTD-RO	Station start	EL31 RL max.: 1054m; EL31 RL max = 1079m; EL31 RL max = 1066m; EL31 RL max = 1051m
PS150_44-4		2025-09-13T17:32:40	83.14616	-19.30871	1070.6	CTD-RO	Station end	EL31 RL max.: 1054m; EL31 RL max = 1079m; EL31 RL max = 1066m; EL31 RL max = 1051m
PS150_45-1		2025-09-14T11:17:33	83.10844	-22.36918	218.4	CTD-RO	max depth	EL31, max SL: 212m
PS150_45-2		2025-09-14T11:40:32	83.10775	-22.36762	221.0	MSN	Station start	AWI004 RL max.: 193m
PS150_45-2		2025-09-14T12:12:32	83.10683	-22.36630	218.7	MSN	Station end	AWI004 RL max.: 193m
PS150_46-1		2025-09-14T13:48:02	83.16456	-21.57370	223.6	CTD-RO	max depth	EL31 RL max.: 218m
PS150_46-2		2025-09-14T14:15:30	83.16363	-21.57476	223.6	MSSP	Station start	RL max.: 150m; at Surface; 2nd run; RL max.: 170m; 3rd run

Event label	Optional label	Date/Time	Latitude	Longitude	Depth [m]	Gear	Action	Comment *
PS150_46-2		2025-09-14T15:31:17	83.15955	-21.54213	228.9	MSSP	Station end	RL max.: 150m; at Surface; 2nd run; RL max.: 170m; 3rd run
PS150_46-3		2025-09-14T15:34:09	83.15909	-21.53969	226.9	LIGHT	Station start	AWI004 RL max.: 100m
PS150_46-3		2025-09-14T16:22:08	83.15448	-21.52447	239.4	LIGHT	Station end	AWI004 RL max.: 100m
PS150_46-4		2025-09-14T15:39:07	83.15830	-21.53671	231.5	HN	Station start	
PS150_46-4		2025-09-14T15:43:29	83.15807	-21.53543	231.5	HN	Station end	
PS150_46-5		2025-09-14T16:23:29	83.15430	-21.52333	239.4	MSN	Station start	AWI004 RL max = 196m
PS150_46-5		2025-09-14T16:57:00	83.15084	-21.51386	231.5	MSN	Station end	AWI004 RL max = 196m
PS150_47-1		2025-09-14T18:41:39	83.22538	-21.04434	205.2	CTD-RO	max depth	EL31 RL max = 202m
PS150_48-1		2025-09-14T20:26:07	83.25714	-20.46598	236.8	CTD-RO	max depth	El31, max RL: 232m
PS150_49-1		2025-09-14T21:17:06	83.27874	-20.32348	463.1	XCTD	Station start	Wire snapped at approx. 290 m; 2nd cast; snapped at 530 m
PS150_49-1		2025-09-14T21:41:08	83.27701	-20.30716	502.6	XCTD	Station end	Wire snapped at approx. 290 m; 2nd cast; snapped at 530 m
PS150_50-2		2025-09-14T23:20:42	83.28077	-20.13005	1077.1	HN	Station start	Depth: 20m

Event label	Optional label	Date/Time	Latitude	Longitude	Depth [m]	Gear	Action	Comment *
PS150_50-2		2025-09-14T23:28:20	83.27990	-20.12581	1081.0	HN	Station end	Depth: 20m
PS150_50-1		2025-09-14T23:44:45	83.27806	-20.11693	1094.3	CTD-RO	max depth	EL31, max RL: 1.068m
PS150_50-3		2025-09-15T00:34:50	83.27231	-20.09130	1116.2	MSSP	Station start	1st run ; 340m; 2nd run; 334m; 3rd run; 330m
PS150_50-3		2025-09-15T01:42:57	83.26407	-20.05424	1131.9	MSSP	Station end	1st run ; 340m; 2nd run; 334m; 3rd run; 330m
PS150_50-4		2025-09-15T01:50:35	83.26330	-20.05102	1137.3	MSN	Station start	AWI004 RL max.: 980m
PS150_50-4		2025-09-15T03:13:41	83.25282	-20.01155	1139.9	MSN	Station end	AWI004 RL max.: 980m
PS150_50-5		2025-09-15T03:13:43	83.25282	-20.01153	1139.6	MSN	Station start	AWI004 RL max.: 1104m
PS150_50-5		2025-09-15T04:42:03	83.24150	-19.96909	1142.6	MSN	Station end	AWI004 RL max.: 1104m
PS150_50-6		2025-09-15T07:25:57	83.28539	-20.10932	1159.0	CTD-RO	max depth	EL31 RL max = 1160m
PS150_51-1		2025-09-15T09:52:50	83.30339	-20.03874	1509.4	XCTD	Station start	At depth: 500m; 2. Cast; no data, connection lost; 3. Cast; at depth: 1.100
PS150_51-1		2025-09-15T10:28:50	83.29729	-20.00830	1510.7	XCTD	Station end	At depth: 500m; 2. Cast; no data, connection lost; 3. Cast; at depth: 1.100
PS150_52-1		2025-09-15T13:42:38	83.30167	-19.87175	1930.7	CTD-RO	max depth	EL31 RL max.: 1953m

Event label	Optional label	Date/Time	Latitude	Longitude	Depth [m]	Gear	Action	Comment *
PS150_53-1		2025-09-15T15:31:52	83.32294	-19.69496	2775.8	XCTD	Station start	Torn down; successfull 1100m
PS150_53-1		2025-09-15T16:09:34	83.31734	-19.62341	2788.5	XCTD	Station end	Torn down; successfull 1100m
PS150_54-1		2025-09-15T18:00:28	83.32347	-19.52305	2929.1	CTD-RO	max depth	resp.: v. Appen; EL31 RL max = 2946m
PS150_54-2		2025-09-15T19:39:43	83.30937	-19.49057	2864.2	MSSP	Station start	RL = 370m; 2. Cast; RL: 340m; 3. Cast ; RL: 370m; 4. Cast; RL: 375m; 5. Cast ; RL:375m; 6. Cast ; RL:374m
PS150_54-2		2025-09-15T21:20:03	83.29689	-19.44012	2803.1	MSSP	Station end	RL = 370m; 2. Cast; RL: 340m; 3. Cast ; RL: 370m; 4. Cast; RL: 375m; 5. Cast ; RL:375m; 6. Cast ; RL:374m
PS150_55-1		2025-09-15T22:57:49	83.35269	-19.37375	3053.7	XCTD	Station start	Depth: 1.100m
PS150_55-1		2025-09-15T23:05:09	83.35186	-19.36899	3046.0	XCTD	Station end	Depth: 1.100m
PS150_56-1		2025-09-16T01:03:28	83.35553	-19.17719	3106.3	CTD-RO	max depth	EL31, SL=3105m
PS150_57-1		2025-09-16T04:02:51	83.39335	-18.88601	3108.2	XCTD	Station start	1100m
PS150_57-1		2025-09-16T04:12:57	83.39233	-18.88180	3128.4	XCTD	Station end	1100m

Event label	Optional label	Date/Time	Latitude	Longitude	Depth [m]	Gear	Action	Comment *
PS150_58-1		2025-09-16T05:37:56	83.40798	-18.65745	3122.1	CTD-RO	max depth	EL31 RL max = 994m
PS150_58-2		2025-09-16T06:25:27	83.40372	-18.63901	3112.6	MSN	Station start	AWI004 RL max = 1472m
PS150_58-2		2025-09-16T08:17:43	83.39645	-18.60009	3096.8	MSN	Station end	AWI004 RL max = 1472m
PS150_59-2		2025-09-16T09:53:44	83.46438	-18.10757	3173.8	HN	Station start	Depth: 20m
PS150_59-2		2025-09-16T09:59:13	83.46411	-18.10478	3171.7	HN	Station end	Depth: 20m
PS150_59-1		2025-09-16T10:16:23	83.46324	-18.09566	3168.0	CTD-RO	max depth	EL31, max RL: 996m
PS150_59-3		2025-09-16T10:59:08	83.46096	-18.07128	3150.2	MSSP	Station start	1. Cast, 378m; 2. Cast; 3. Cast ; 4. Cast
PS150_59-3		2025-09-16T12:30:47	83.45501	-18.01315	3125.1	MSSP	Station end	1. Cast, 378m; 2. Cast; 3. Cast ; 4. Cast
PS150_59-4		2025-09-16T12:37:01	83.45454	-18.00904	3124.8	LIGHT	Station start	AWI004 RL max.: 100m
PS150_59-4		2025-09-16T13:18:20	83.45128	-17.98135	3118.6	LIGHT	Station end	AWI004 RL max.: 100m
PS150_59-5		2025-09-16T13:31:12	83.45044	-17.97419	3118.9	MSN	Station start	AWI004 RL max.: 1477m
PS150_59-5		2025-09-16T15:21:31	83.44063	-17.90296	3104.2	MSN	Station end	AWI004 RL max.: 1477m
PS150_59-6		2025-09-16T15:33:41	83.43945	-17.89578	3104.5	MSC	max depth	AWI004 RL max.: 77m

Event label	Optional label	Date/Time	Latitude	Longitude	Depth [m]	Gear	Action	Comment *
PS150_59-7		2025-09-16T16:49:55	83.43191	-17.85452	3090.7	CTD-RO	max depth	EL31 RL max = 997m
PS150_60-1		2025-09-16T19:28:29	83.50610	-17.46508	3189.3	CTD-RO	max depth	EL31 RL max = 996m
PS150_61-1		2025-09-16T23:40:35	83.55720	-16.86028	3234.6	CTD-RO	max depth	EL31, max RL: 3220m
PS150_62-1		2025-09-17T03:26:05	83.61152	-16.32644	3403.1	CTD-RO	max depth	EL31 RL max.: 995m
PS150_63-1		2025-09-17T06:28:18	83.66374	-15.73317	3485.8	CTD-RO	max depth	EL31 RL max = 996m
PS150_63-2		2025-09-17T07:11:48	83.66243	-15.72993	3485.8	LIGHT	Station start	AWI004 RL max = 100m
PS150_63-2		2025-09-17T08:09:36	83.66117	-15.72339	3487.9	LIGHT	Station end	AWI004 RL max = 100m
PS150_63-3		2025-09-17T07:28:17	83.66202	-15.72819	3483.9	HN	Station start	
PS150_63-3		2025-09-17T07:33:56	83.66189	-15.72754	3481.9	HN	Station end	
PS150_63-4		2025-09-17T08:10:15	83.66117	-15.72329	3488.2	MSSP	Station start	1. cast; RL: 396m; 2. Cast; RL: 397m; 2. Cast after technical problems
PS150_63-4		2025-09-17T09:28:01	83.66124	-15.71131	3487.7	MSSP	Station end	1. cast; RL: 396m; 2. Cast; RL: 397m; 2. Cast after technical problems
PS150_63-5		2025-09-17T09:00:16	83.66160	-15.71611	3483.7	MSN	Station start	AWI004, max RL: 1.466m
PS150_63-5		2025-09-17T11:31:57	83.65964	-15.68148	3483.7	MSN	Station end	AWI004, max RL: 1.466m

Event label	Optional label	Date/Time	Latitude	Longitude	Depth [m]	Gear	Action	Comment *
PS150_63-6		2025-09-17T11:34:15	83.65974	-15.68333	3482.4	LIGHT	Station start	AWI004, max RL: 100m
PS150_63-6		2025-09-17T12:17:58	83.65912	-15.67115	3489.2	LIGHT	Station end	AWI004, max RL: 100m
PS150_64-1		2025-09-17T14:14:09	83.66170	-14.77842	3533.9	CTD-RO	max depth	EL31 RL max.: 995m
PS150_64-2		2025-09-17T15:31:57	83.65733	-14.75460	3536.6	BONGO	Station start	AWI004 RL max = 500m
PS150_64-2		2025-09-17T16:07:01	83.65843	-14.74538	3538.1	BONGO	Station end	AWI004 RL max = 500m
PS150_65-1		2025-09-17T17:56:26	83.74946	-14.53306	3558.9	CTD-RO	max depth	EL31 Rl max = 97m
PS150_65-2		2025-09-17T20:08:23	83.74808	-14.52279	3562.8	CTD-RO	max depth	EL31, max RL: 3.547m
PS150_66-1		2025-09-18T01:08:22	83.81133	-13.86562	3644.9	CTD-RO	max depth	EL31 RL max.: 996m
PS150_66-2		2025-09-18T01:47:45	83.80919	-13.85203	3631.1	MSN	Station start	AWI004 RL max.: 1471m
PS150_66-2		2025-09-18T03:41:56	83.80108	-13.80823	3610.8	MSN	Station end	AWI004 RL max.: 1471m
PS150_67-2		2025-09-18T04:56:50	83.85823	-13.42808	3776.8	HN	Station start	
PS150_67-2		2025-09-18T05:14:42	83.85669	-13.42254	3777.3	HN	Station end	
PS150_67-1		2025-09-18T05:19:22	83.85629	-13.42109	3777.6	CTD-RO	max depth	EL31 RL max = 996m

Event label	Optional label	Date/Time	Latitude	Longitude	Depth [m]	Gear	Action	Comment *
PS150_67-3		2025-09-18T06:15:53	83.85313	-13.41507	3767.8	LIGHT	Station start	AWI004 RL max = 100m
PS150_67-3		2025-09-18T07:15:03	83.84781	-13.38874	3743.5	LIGHT	Station end	AWI004 RL max = 100m
PS150_68-1		2025-09-18T10:52:02	83.90140	-12.60422	3854.6	CTD-RO	max depth	EL31, max RL: 3.850m
PS150_68-2		2025-09-18T12:47:36	83.88741	-12.55897	3854.2	TVMUC	max depth	
PS150_68-3		2025-09-18T19:44:56	83.89926	-12.66951	3857.5	CTD-RO	max depth	EL31 RL max = 997m
PS150_69-1		2025-09-19T03:55:53	84.09309	-15.46346	3760.1	CTD-RO	max depth	EL31 RL max.: 998m
PS150_70-2		2025-09-19T15:29:17	84.25817	-18.36559	3153.3	HN	Station start	
PS150_70-2		2025-09-19T15:34:57	84.25786	-18.37005	3150.3	HN	Station end	
PS150_70-1		2025-09-19T15:47:53	84.25679	-18.37152	3155.6	CTD-RO	max depth	EL31 RL max = 997m
PS150_70-3		2025-09-19T16:27:17	84.25035	-18.34979	3178.5	LIGHT	Station start	AWI004 RL max = 100m
PS150_70-3		2025-09-19T17:23:45	84.24188	-18.33680	3197.1	LIGHT	Station end	AWI004 RL max = 100m
PS150_70-4		2025-09-19T17:24:10	84.24183	-18.33669	3198.2	BONGO	max depth	aborted due to ice conditions
PS150_71-1		2025-09-19T22:06:54	84.30394	-18.94523	3335.2	CTD-RO	max depth	EL31, max RL:996m

Event label	Optional label	Date/Time	Latitude	Longitude	Depth [m]	Gear	Action	Comment *
PS150_71-2		2025-09-19T22:45:06	84.29990	-18.95272	3335.0	MSSP	Station start	1. Cast ; 1. Cast at 373m; 2. Cast at depth: 377m; 3. Cast ; 3. Cast at depth: 372m
PS150_71-2		2025-09-19T23:53:56	84.29346	-18.96251	3332.9	MSSP	Station end	1. Cast ; 1. Cast at 373m; 2. Cast at depth: 377m; 3. Cast ; 3. Cast at depth: 372m
PS150_72-1		2025-09-20T03:38:41	84.34585	-19.63244	3320.2	CTD-RO	max depth	EL31 RL max.: 3308m
PS150_72-2		2025-09-20T05:24:03	84.33804	-19.61068	3322.7	MSN	Station start	AWI004 RL max = 1469m
PS150_72-2		2025-09-20T07:25:07	84.32849	-19.61109	3322.8	MSN	Station end	AWI004 RL max = 1469m
PS150_73-1		2025-09-20T10:23:34	84.37641	-20.12975	1115.9	CTD-RO	max depth	Technical problem with the ADCP; CTD out of the water, move away; EL31, max RL: 1.086
PS150_73-2		2025-09-20T11:22:37	84.37541	-20.14498	1180.2	MSSP	Station start	1. Cast ; 1. Cast at depth: 391m; 2. Cast; 397m;3.Cast; 401m
PS150_73-2		2025-09-20T12:38:01	84.37462	-20.16019	1241.3	MSSP	Station end	1. Cast ; 1. Cast at depth: 391m; 2. Cast; 397m;3.Cast; 401m
PS150_74-1		2025-09-20T14:15:38	84.36907	-19.91454	2448.3	CTD-RO	max depth	EL31 RL max.: 2382m
PS150_74-2		2025-09-20T15:24:46	84.36750	-19.91582	2508.6	LIGHT	Station start	AWI004 RL max = 100m
PS150_74-2		2025-09-20T16:23:00	84.36528	-19.92520	2654.3	LIGHT	Station end	AWI004 RL max = 100m

Event label	Optional label	Date/Time	Latitude	Longitude	Depth [m]	Gear	Action	Comment *
PS150_74-3		2025-09-20T15:37:38	84.36686	-19.91371	2582.0	HN	Station start	
PS150_74-3		2025-09-20T15:40:58	84.36687	-19.91393	2571.4	HN	Station end	
PS150_74-4		2025-09-20T16:23:31	84.36525	-19.92540	2665.0	ICE	Station start	
PS150_74-4		2025-09-20T17:02:13	84.36379	-19.91571	2810.1	ICE	Station end	
PS150_75-1		2025-09-20T18:46:36	84.38974	-20.35202	789.3	CTD-RO	max depth	EL31 RL max = 784m
PS150_76-1		2025-09-20T22:43:34	84.42744	-20.77481	776.6	CTD-RO	max depth	EL31, max RL: 779m
PS150_76-2		2025-09-20T23:14:27	84.42792	-20.78322	782.1	MSSP	Station start	1 Cast; 1 Cast at depth: 392m; 2. Cast; 2. Cast at depth: 393m; 3. Cast; 395m
PS150_76-2		2025-09-21T00:31:42	84.42878	-20.79913	753.6	MSSP	Station end	1 Cast; 1 Cast at depth: 392m; 2. Cast; 2. Cast at depth: 393m; 3. Cast; 395m
PS150_77-1		2025-09-21T02:48:49	84.43545	-21.14600	717.8	CTD-RO	max depth	EL31 RL max.: 714m
PS150_77-2		2025-09-21T03:20:03	84.43484	-21.14660	717.3	MSN	Station start	AWI004 RL max.: 686m
PS150_77-2		2025-09-21T04:32:33	84.43265	-21.15253	719.0	MSN	Station end	AWI004 RL max.: 686m
PS150_78-1		2025-09-21T07:34:26	84.47116	-20.94864	739.3	ICE	Station start	

Event label	Optional label	Date/Time	Latitude	Longitude	Depth [m]	Gear	Action	Comment *
PS150_78-1		2025-09-21T22:13:17	84.46322	-21.19233	716.3	ICE	Station end	
PS150_78-2		2025-09-21T11:14:22	84.47021	-21.02246	734.3	OTTER_USV	Station start	
PS150_78-2		2025-09-21T12:08:24	84.47069	-21.03370	732.3	OTTER_USV	Station end	
PS150_78-3		2025-09-21T13:21:21	84.47101	-21.04136	734.9	CTD-RO	max depth	EL31 RL max.: 728m
PS150_78-4		2025-09-21T13:54:33	84.47095	-21.04293	734.7	LIGHT	Station start	AWI004 RL max.: 100m
PS150_78-4		2025-09-21T14:43:17	84.47047	-21.04576	733.3	LIGHT	Station end	AWI004 RL max.: 100m
PS150_79-1		2025-09-22T07:28:41	84.22273	-25.39765	623.6	CTD-RO	max depth	EL31 RL max = 605m
PS150_79-2		2025-09-22T08:07:05	84.22210	-25.39037	621.0	MSSP	Station start	1. Cast ; 1. Cast at depth 350m; 2. Cast; 2. Cast at depth: 375m; 3. Cast ; 3. Cast at depth: 352m
PS150_79-2		2025-09-22T09:14:55	84.22356	-25.43867	620.9	MSSP	Station end	1. Cast ; 1. Cast at depth 350m; 2. Cast; 2. Cast at depth: 375m; 3. Cast ; 3. Cast at depth: 352m
PS150_79-3		2025-09-22T09:15:27	84.22359	-25.43920	621.0	LIGHT	Station start	AWI004, max RL: 100m
PS150_79-3		2025-09-22T10:10:12	84.22643	-25.47847	623.6	LIGHT	Station end	AWI004, max RL: 100m

Event label	Optional label	Date/Time	Latitude	Longitude	Depth [m]	Gear	Action	Comment *
PS150_79-4		2025-09-22T09:28:25	84.22425	-25.44862	618.5	HN	Station start	20m
PS150_79-4		2025-09-22T09:32:10	84.22466	-25.45118	621.0	HN	Station end	20m
PS150_79-5		2025-09-22T10:25:24	84.22353	-25.52130	613.1	BONGO	Station start	AWI004, max RL: 501m
PS150_79-5		2025-09-22T11:00:54	84.22348	-25.54079	613.1	BONGO	Station end	AWI004, max RL: 501m
PS150_80-1		2025-09-22T13:14:05	84.15286	-25.87953	615.7	CTD-RO	max depth	EL31 RL max.: 596m
PS150_80-2		2025-09-22T13:47:17	84.15306	-25.89262	618.4	MSN	Station start	AWI004 RL max.: 587m
PS150_80-2		2025-09-22T14:40:17	84.15299	-25.91325	615.7	MSN	Station end	AWI004 RL max.: 587m
PS150_80-4		2025-09-22T14:33:24	84.15304	-25.91048	615.7	SS	Station start	Frost-Flower sampling
PS150_80-4		2025-09-22T15:01:47	84.15279	-25.92212	621.0	SS	Station end	Frost-Flower sampling
PS150_80-3		2025-09-22T14:44:16	84.15296	-25.91486	615.7	MSN	Station start	AWI004 RL max.: 588m
PS150_80-3		2025-09-22T15:33:18	84.15238	-25.93581	621.0	MSN	Station end	AWI004 RL max.: 588m
PS150_81-1		2025-09-22T19:40:31	84.10383	-26.43565	597.3	CTD-RO	max depth	EL31 RLmax = 576m
PS150_81-2		2025-09-22T20:51:45	84.10279	-26.47324	600.0	TVMUC	max depth	GE52.2, max RL 587

Event label	Optional label	Date/Time	Latitude	Longitude	Depth [m]	Gear	Action	Comment *
PS150_82-1		2025-09-22T23:19:16	84.04414	-27.06593	544.7	CTD-RO	max depth	EL31, max RL: 525m
PS150_82-2		2025-09-22T23:53:10	84.04406	-27.07734	544.7	MSSP	Station start	1st run; 396m; 2nd run; 394m; 3rd run; 397m
PS150_82-2		2025-09-23T01:10:11	84.04378	-27.09905	539.4	MSSP	Station end	1st run; 396m; 2nd run; 394m; 3rd run; 397m
PS150_83-1		2025-09-23T03:12:32	83.99089	-27.67901	378.9	CTD-RO	max depth	EL31 RL max.: 363m
PS150_83-2		2025-09-23T03:35:08	83.99047	-27.68179	376.3	MSN	Station start	AWI004 RL max.:293m
PS150_83-2		2025-09-23T04:15:04	83.99009	-27.68752	378.9	MSN	Station end	AWI004 RL max.:293m
PS150_84-1		2025-09-23T05:57:42	83.90762	-28.02321	265.7	CTD-RO	max depth	EL31 RL max = 257m
PS150_85-1		2025-09-23T12:17:00	83.85809	-28.67067	84.2	CTD-RO	max depth	EL 31 RL max.: 90m
PS150_85-2		2025-09-23T12:50:09	83.85806	-28.67393	84.2	MSSP	Station start	Probe Cast; 80m; 1st Cast; 86m; 2nd Cast; 84m; 3rd Cast; 85m
PS150_85-2		2025-09-23T13:32:30	83.85790	-28.68263	94.7	MSSP	Station end	Probe Cast; 80m; 1st Cast; 86m; 2nd Cast; 84m; 3rd Cast; 85m
PS150_85-3		2025-09-23T13:37:21	83.85796	-28.68308	94.7	LIGHT	Station start	AWI004 RL max.: 85m
PS150_85-3		2025-09-23T14:22:58	83.85818	-28.68325	94.7	LIGHT	Station end	AWI004 RL max.: 85m
PS150_85-4		2025-09-23T13:41:09	83.85811	-28.68258	94.7	HN	Station start	

Event label	Optional label	Date/Time	Latitude	Longitude	Depth [m]	Gear	Action	Comment *
PS150_85-4		2025-09-23T13:47:47	83.85803	-28.68480	94.7	HN	Station end	
PS150_85-5		2025-09-23T14:25:27	83.85813	-28.68455	94.7	MSN	Station start	AWI004 RL max.: 82m
PS150_85-5		2025-09-23T14:39:36	83.85790	-28.69169	89.4	MSN	Station end	AWI004 RL max.: 82m
PS150_85-6		2025-09-23T14:54:11	83.85823	-28.69030	94.7	CTD-RO	max depth	EL31 RL max.: 90m
PS150_86-1		2025-09-23T16:18:25	83.83696	-28.84189	78.9	CTD-RO	max depth	EL31 RL max = 80
PS150_87-1		2025-09-23T17:14:46	83.85834	-28.67070	86.4	MOOR	Station start	Depl. Moor MJ1-1; Ankerstein, Releaser with Microcat, Aquadopp & 3 Floats
PS150_87-1		2025-09-23T17:40:07	83.85865	-28.66548	87.6	MOOR	Station end	Depl. Moor MJ1-1; Ankerstein, Releaser with Microcat, Aquadopp & 3 Floats
PS150_88-1		2025-09-23T19:08:39	83.91955	-28.49609	209.2	CTD-RO	max depth	EL31 RL max = 210m
PS150_88-2		2025-09-23T19:16:52	83.91969	-28.49462	210.3	MOOR	Station start	Moor depl MJ2-1.; Ankerstein, releaser with Microcat & 3 Floats
PS150_88-2		2025-09-23T19:24:17	83.91902	-28.49588	206.5	MOOR	Station end	Moor depl MJ2-1.; Ankerstein, releaser with Microcat & 3 Floats
PS150_89-1		2025-09-24T04:17:31	84.27574	-27.55069	1060.9	CTD-RO	max depth	EL31 RL max = 1057m

Event label	Optional label	Date/Time	Latitude	Longitude	Depth [m]	Gear	Action	Comment *
PS150_89-2		2025-09-24T05:04:42	84.27590	-27.58333	1070.2	MSSP	Station start	378m; 372m
PS150_89-2		2025-09-24T06:11:28	84.27724	-27.63677	1058.1	MSSP	Station end	378m; 372m
PS150_89-3		2025-09-24T06:11:54	84.27726	-27.63713	1058.0	MSN	Station start	AWI004 RL max = 989m
PS150_89-3		2025-09-24T07:43:16	84.28018	-27.70672	1051.6	MSN	Station end	AWI004 RL max = 989m
PS150_89-4		2025-09-24T07:45:17	84.28021	-27.70833	1051.0	MSN	Station start	AWI004, max RL: 1.022m
PS150_89-4		2025-09-24T09:19:27	84.28511	-27.79066	1023.9	MSN	Station end	AWI004, max RL: 1.022m
PS150_89-5		2025-09-24T09:15:49	84.28492	-27.78691	1026.9	LIGHT	max depth	100 m
PS150_89-6		2025-09-24T09:20:56	84.28516	-27.79190	1023.3	HN	Station start	
PS150_89-6		2025-09-24T09:26:48	84.28546	-27.79836	1019.6	HN	Station end	
PS150_89-7		2025-09-24T10:45:42	84.29092	-27.84394	1014.9	CTD-RO	max depth	EL31, max RL: 1.014m
PS150_89-8		2025-09-24T11:26:50	84.29394	-27.88425	1007.5	ICE	Station start	Ice sampled
PS150_89-8		2025-09-24T11:53:01	84.29454	-27.89715	1008.2	ICE	Station end	Ice sampled
PS150_90-1		2025-09-25T09:13:18	83.88363	-24.18754	2504.4	ICE	Station start	

Event label	Optional label	Date/Time	Latitude	Longitude	Depth [m]	Gear	Action	Comment *
PS150_90-1		2025-09-25T18:45:27	83.89143	-24.26239	2454.0	ICE	Station end	
PS150_90-2		2025-09-25T11:27:33	83.88486	-24.22009	2496.3	LIGHT	Station start	AWI004 RL max.: 100m
PS150_90-2		2025-09-25T12:16:20	83.88580	-24.22860	2493.8	LIGHT	Station end	AWI004 RL max.: 100m
PS150_90-3		2025-09-25T13:51:44	83.88820	-24.24007	2489.8	CTD-RO	max depth	EL 31 RL max.:2489m
PS150_90-4		2025-09-25T16:44:25	83.89146	-24.25124	2466.8	ZODIAC	Station start	
PS150_90-4		2025-09-25T17:05:17	83.89161	-24.25302	2465.6	ZODIAC	Station end	
PS150_91-1		2025-09-27T10:59:46	82.45274	-15.65005	174.7	CTD-RO	max depth	EL31, max RL: 167m
PS150_91-2		2025-09-27T11:21:50	82.44925	-15.64465	164.9	MSSP	Station start	Probecast; Probecast at depth 143m; 1 Cast ; The experiment is repeated; 136m; 2nd Cast 153m; 3rd Cast; 144m
PS150_91-2		2025-09-27T12:25:10	82.43991	-15.63429	168.0	MSSP	Station end	Probecast; Probecast at depth 143m; 1 Cast ; The experiment is repeated; 136m; 2nd Cast 153m; 3rd Cast; 144m
PS150_92-1		2025-09-27T13:23:39	82.48953	-15.17575	348.1	XCTD	Station start	350m

Event label	Optional label	Date/Time	Latitude	Longitude	Depth [m]	Gear	Action	Comment *
PS150_92-1		2025-09-27T13:29:57	82.48877	-15.17418	345.5	XCTD	Station end	350m
PS150_93-2		2025-09-27T16:26:34	82.49940	-14.61221	1300.3	HN	Station start	
PS150_93-2		2025-09-27T16:32:47	82.49842	-14.60937	1263.0	HN	Station end	
PS150_93-1		2025-09-27T16:38:58	82.49742	-14.60635	1214.8	CTD-RO	max depth	EL31 RL max = 1200m
PS150_93-3		2025-09-27T17:22:09	82.49033	-14.58481	1181.7	MSSP	Station start	339m; 329m
PS150_93-3		2025-09-27T18:34:23	82.47721	-14.54543	988.2	MSSP	Station end	339m; 329m
PS150_93-4		2025-09-27T18:34:43	82.47715	-14.54526	987.6	LIGHT	Station start	AWI004 RL max = 151m
PS150_93-4		2025-09-27T19:16:42	82.46922	-14.52286	853.1	LIGHT	Station end	AWI004 RL max = 151m
PS150_93-5		2025-09-27T19:50:27	82.46286	-14.50541	734.2	CTD-RO	max depth	EL31 RL max = 728m
PS150_94-1		2025-09-27T23:29:24	82.54575	-14.18336	1955.4	CTD-RO	max depth	EL31, max RL: 1.951m
PS150_95-1		2025-09-28T03:08:10	82.57356	-13.63293	2190.2	CTD-RO	max depth	Technical problem; EL31 RL max.: 2181m
PS150_95-2		2025-09-28T04:17:24	82.56628	-13.58260	2092.9	MSN	Station start	AWI004 RL max = 1489m
PS150_95-2		2025-09-28T06:18:55	82.55446	-13.50284	2153.6	MSN	Station end	AWI004 RL max = 1489m

Event label	Optional label	Date/Time	Latitude	Longitude	Depth [m]	Gear	Action	Comment *
PS150_96-1		2025-09-28T17:50:23	82.42116	-16.16539	186.8	CTD-RO	max depth	EL31 RL max = 183m
PS150_97-1		2025-09-28T19:24:12	82.38041	-16.70926	161.2	CTD-RO	max depth	EL31 RL max = 161m
PS150_98-1		2025-09-29T18:35:23	81.68882	-12.21754	103.2	MOOR	Station start	Depl. Ankerstein, Releaser, Microcat & 2 Floats
PS150_98-1		2025-09-29T18:47:52	81.68877	-12.21742	102.6	MOOR	Station end	Depl. Ankerstein, Releaser, Microcat & 2 Floats
PS150_98-2		2025-09-30T00:46:08	81.67905	-12.14775	136.8	RBR_CTD	Station start	Fishingrod CTD; 159m
PS150_98-2		2025-09-30T01:04:18	81.67851	-12.14269	136.9	RBR_CTD	Station end	Fishingrod CTD; 159m
PS150_98-3		2025-09-30T08:50:39	81.69879	-12.13873	128.7	CTD-RO	max depth	EL31, max RL: 120m
PS150_99-1		2025-09-30T13:10:42	81.73682	-11.55864	178.1	CTD-RO	max depth	EL31 RL max.: 173m
PS150_99-2		2025-09-30T13:37:47	81.73587	-11.55077	177.3	MOOR	Station start	MOOR/D PS150-99-2 FI1-1-; Ankerstein Doppelreleaser Microcat; 3 Floats; Temp.Logger; 2ADCP 1Temp.Logger; 2Floats 1Microcat Topeinh…
PS150_99-2		2025-09-30T14:43:04	81.73390	-11.53474	183.6	MOOR	Station end	MOOR/D PS150-99-2 FI1-1-; Ankerstein Doppelreleaser Microcat; 3 Floats; Temp.Logger; 2ADCP

Event label	Optional label	Date/Time	Latitude	Longitude	Depth [m]	Gear	Action	Comment *
								1Temp.Logger; 2Floats 1Microcat Topeinh…
PS150_100-1		2025-09-30T16:30:12	81.77812	-10.67600	185.3	MOOR	Station start	depl.: FI2-1; Ankerstein with Doppelreleaser, Microcat, 6 Floats, ADCP; Temperature logger; 4 Floats; Water collector, 4 floats; r…
PS150_100-1		2025-09-30T17:27:01	81.77829	-10.66458	196.1	MOOR	Station end	depl.: FI2-1; Ankerstein with Doppelreleaser, Microcat, 6 Floats, ADCP; Temperature logger; 4 Floats; Water collector, 4 floats; r…
PS150_100-2		2025-09-30T17:47:24	81.77532	-10.64677	200.5	CTD-RO	max depth	EL31 RL max = 197m
PS150_100-3		2025-09-30T18:07:37	81.77589	-10.64399	205.7	LIGHT	Station start	AWI004RL max = 150m
PS150_100-3		2025-09-30T19:00:05	81.77618	-10.63527	224.2	LIGHT	Station end	AWI004RL max = 150m
PS150_100-4		2025-09-30T18:20:44	81.77529	-10.64103	205.4	HN	Station start	
PS150_100-4		2025-09-30T18:37:02	81.77560	-10.63812	206.8	HN	Station end	
PS150_101-1		2025-09-30T19:36:30	81.79893	-10.35307	573.7	POS	Station start	AWI004 RL max = 480m
PS150_101-1		2025-09-30T20:27:48	81.79976	-10.34236	584.2	POS	Station end	AWI004 RL max = 480m

Event label	Optional label	Date/Time	Latitude	Longitude	Depth [m]	Gear	Action	Comment *
PS150_101-2		2025-09-30T20:50:19	81.79984	-10.33857	586.8	CTD-RO	max depth	EL31, max RL: 567m
PS150_102-1		2025-09-30T23:06:56	81.83379	-9.91010	2198.8	CTD-RO	max depth	EL31, max RL: 2.138m
PS150_103-1		2025-10-01T01:31:46	81.81192	-10.24752	1000.3	CTD-RO	max depth	EL31 RL max.: 999m
PS150_103-2		2025-10-01T02:15:27	81.81138	-10.23819	979.9	MSSP	Station start	1st Cast; 389m; 2nd Cast; 397m; 3rd Cast; 395m
PS150_103-2		2025-10-01T03:33:10	81.81015	-10.23080	927.3	MSSP	Station end	1st Cast; 389m; 2nd Cast; 397m; 3rd Cast; 395m
PS150_103-3		2025-10-01T06:00:21	81.80356	-10.12807	976.9	MOOR	Station start	Depl.: FI-3-1; Ankerstein, Doppelreleaser, 2 Floats; Aquadopp, Microcat; 6 Floats, 1 ADCP 1 MicroCat; SonoVault; 1 Temperature log…
PS150_103-3		2025-10-01T10:06:48	81.80339	-10.13299	956.5	MOOR	Station end	Depl.: FI-3-1; Ankerstein, Doppelreleaser, 2 Floats; Aquadopp, Microcat; 6 Floats, 1 ADCP 1 MicroCat; SonoVault; 1 Temperature log…
PS150_104-1		2025-10-01T11:53:53	81.84018	-9.74335	2260.8	CTD-RO	max depth	EL31, max RL: 2.194m

Event label	Optional label	Date/Time	Latitude	Longitude	Depth [m]	Gear	Action	Comment *
PS150_104-2		2025-10-01T13:11:41	81.83867	-9.75447	2248.1	MOOR	Station start	MOOR/D FI4-1; Ankerstein and Doppelreleaser; sediment trap; 5Floats; Microcat; 4Floats 1ADCP; 5Floats 1 RAS; Temp.Logger; 1Microca…
PS150_104-2		2025-10-01T16:18:00	81.83394	-9.79351	2225.4	MOOR	Station end	MOOR/D FI4-1; Ankerstein and Doppelreleaser; sediment trap; 5Floats; Microcat; 4Floats 1ADCP; 5Floats 1 RAS; Temp.Logger; 1Microca…
PS150_105-1		2025-10-01T18:15:25	81.88549	-9.33450	2499.9	CTD-RO	max depth	EL31 RL max = 996m
PS150_105-2		2025-10-01T18:51:56	81.88552	-9.35116	2475.2	ICE	Station start	sample taken; 2nd sample taken
PS150_105-2		2025-10-01T19:39:47	81.88579	-9.35434	2479.3	ICE	Station end	sample taken; 2nd sample taken
PS150_106-1		2025-10-01T22:52:53	81.91879	-8.99128	2704.8	CTD-RO	max depth	EL31, max RL: 2.639m
PS150_107-1		2025-10-02T06:00:06	81.99280	-7.99551	2975.1	MOOR	Station start	Depl.: FI-6-1; Ankerstein with Doppelreleaser, Microcat; 4 Floats; ADCP; 5 Floats; Temperature logger, Transponder; 1 Temperature …

Event label	Optional label	Date/Time	Latitude	Longitude	Depth [m]	Gear	Action	Comment *
PS150_107-1		2025-10-02T08:40:05	81.99066	-8.11172	3056.1	MOOR	Station end	Depl.: FI-6-1; Ankerstein with Doppelreleaser, Microcat; 4 Floats; ADCP; 5 Floats; Temperature logger, Transponder; 1 Temperature …
PS150_107-2		2025-10-02T09:36:44	81.97714	-8.07376	3045.6	CTD-RO	max depth	EL31, max RL: 997m
PS150_108-1		2025-10-02T11:08:06	81.95786	-8.39880	2931.6	XCTD	Station start	depth ca.800m
PS150_108-1		2025-10-02T11:19:48	81.95759	-8.40531	2927.2	XCTD	Station end	depth ca.800m
PS150_109-1		2025-10-02T12:52:58	81.92460	-8.87129	2726.6	MOOR	Station start	MOOR/D FI5-1; 1Ankerstein 1Doppelreleaser; 4Floats; Microcat; 1ADCP 1Microcat; SonoVault; 6Floats; Temp.Logger; 1Transponder 1Micr…
PS150_109-1		2025-10-02T15:36:28	81.92449	-8.92282	2720.1	MOOR	Station end	MOOR/D FI5-1; 1Ankerstein 1Doppelreleaser; 4Floats; Microcat; 1ADCP 1Microcat; SonoVault; 6Floats; Temp.Logger; 1Transponder 1Micr…

Event label	Optional label	Date/Time	Latitude	Longitude	Depth [m]	Gear	Action	Comment *
PS150_110-1		2025-10-03T05:00:03	81.53480	-5.40221	3176.2	OBS	Station start	Depl.: OBS-4; start Posidonia tracking; stop tracking.
PS150_110-1		2025-10-03T07:15:02	81.54117	-5.34786	3579.7	OBS	Station end	Depl.: OBS-4; start Posidonia tracking; stop tracking.
PS150_111-1		2025-10-03T13:09:41	81.40115	-1.82891	3066.0	OBS	Station start	OBS-5; start Posidonia tracking; stop tracking.
PS150_111-1		2025-10-03T15:09:11	81.39705	-1.83503	3064.5	OBS	Station end	OBS-5; start Posidonia tracking; stop tracking.
PS150_112-1		2025-10-03T19:21:31	81.00042	-1.09967	3189.0	OBS	Station start	Depl.: OBS-6; at depth 3.202m
PS150_112-1		2025-10-03T21:26:30	80.99294	-1.10178	3188.3	OBS	Station end	Depl.: OBS-6; at depth 3.202m
PS150_113-1		2025-10-04T01:11:18	80.95505	-2.40361	4271.3	CTD-RO	max depth	EL31, max RL: 4277m
PS150_114-1		2025-10-04T05:36:02	80.99751	-3.83313	3315.5	OBS	Station start	Depl.: OBS-7; in the water; start tracking; stop tracking
PS150_114-1		2025-10-04T07:42:08	80.99310	-3.79000	3316.9	OBS	Station end	Depl.: OBS-7; in the water; start tracking; stop tracking
PS150_115-1		2025-10-05T05:09:58	79.86731	-5.08437	1105.6	BUOY	Station start	cable
PS150_115-1		2025-10-05T07:08:36	79.79558	-5.31978	725.9	BUOY	Station end	cable
PS150_115-2		2025-10-05T07:54:52	79.73772	-5.36868	644.1	BUOY	Station start	S3_2025P276_ROV

Event label	Optional label	Date/Time	Latitude	Longitude	Depth [m]	Gear	Action	Comment *
PS150_115-2		2025-10-05T09:50:30	79.71987	-5.39252	618.6	BUOY	Station end	S3_2025P276_ROV
PS150_115-3		2025-10-05T10:10:24	79.71845	-5.41580	581.1	BUOY	Station start	3rd Buoy recovery
PS150_115-3		2025-10-05T10:29:31	79.71570	-5.41294	584.5	BUOY	Station end	3rd Buoy recovery
PS150_115-4		2025-10-05T12:54:34	79.81310	-3.86369	2008.4	BUOY	Station start	4th buoy recovery
PS150_115-4		2025-10-05T13:11:11	79.81243	-3.86399	2001.7	BUOY	Station end	4th buoy recovery
PS150_115-5		2025-10-05T20:00:14	78.93942	-2.65413	2525.1	BUOY_ADCP	Station start	
PS150_115-5		2025-10-05T20:31:11	78.92854	-2.67177	2521.6	BUOY_ADCP	Station end	
PS150_115-6		2025-10-06T01:50:52	78.29724	-3.63323	2336.4	BUOY_ADCP	Station start	no action, buoy spotted
PS150_115-6		2025-10-06T01:59:30	78.29399	-3.63742	2343.2	BUOY_ADCP	Station end	no action, buoy spotted
PS150_115-7		2025-10-06T04:36:37	78.13181	-4.58521	1822.2	10m Met tower	Station start	
PS150_115-7		2025-10-06T05:06:03	78.13195	-4.62491	1758.8	10m Met tower	Station end	
PS150_116-1		2025-10-06T19:32:44	78.16647	-15.69166	354.6	MOOR	Station start	recovery IdF3-2; Posidonia window open; deployed; 2nd buoyancy unit; Posidonia window closed; Am Dracken;

Event label	Optional label	Date/Time	Latitude	Longitude	Depth [m]	Gear	Action	Comment *
								Toppeinehit on crane; Mi…
PS150_116-1		2025-10-06T20:57:40	78.17216	-15.75958	367.8	MOOR	Station end	recovery IdF3-2; Posidonia window open; deployed; 2nd buoyancy unit; Posidonia window closed; Am Dracken; Toppeinehit on crane; Mi…
PS150_117-1		2025-10-06T22:01:17	78.20989	-15.53422	251.5	CTD-RO	max depth	EL31, max RL: 242m
PS150_118-2		2025-10-06T23:16:53	78.17596	-15.71477	361.0	HN	Station start	at depth: 20m
PS150_118-2		2025-10-06T23:19:55	78.17534	-15.71613	359.0	HN	Station end	at depth: 20m
PS150_118-1		2025-10-06T23:27:25	78.17438	-15.72185	356.8	CTD-RO	max depth	EL31, max RL: 346m
PS150_118-3		2025-10-06T23:47:27	78.17445	-15.73139	360.0	LIGHT	Station start	AWI004 RL max.: 150m
PS150_118-3		2025-10-07T00:26:15	78.17042	-15.75266	366.5	LIGHT	Station end	AWI004 RL max.: 150m
PS150_118-4		2025-10-07T01:01:31	78.16501	-15.76307	372.6	CTD-RO	max depth	EL31 RL max.:357m
PS150_119-1		2025-10-07T02:23:00	78.14168	-15.91354	406.9	CTD-RO	max depth	EL31 RL max.: 400m
PS150_120-2		2025-10-09T02:43:27	80.31249	-12.33249	172.6	HN	Station start	

Event label	Optional label	Date/Time	Latitude	Longitude	Depth [m]	Gear	Action	Comment *
PS150_120-2		2025-10-09T02:47:03	80.31193	-12.33208	174.4	HN	Station end	
PS150_120-1		2025-10-09T02:51:26	80.31140	-12.33039	171.6	CTD-RO	max depth	EL31 RL max.:164m
PS150_120-3		2025-10-09T03:05:11	80.30912	-12.32404	164.2	LIGHT	Station start	AWI004 RL max.:150m
PS150_120-3		2025-10-09T03:38:15	80.30329	-12.30671	154.7	LIGHT	Station end	AWI004 RL max.:150m
PS150_121-1		2025-10-09T05:06:28	80.35064	-12.45650	210.5	CTD-RO	max depth	EL31 RL31 RL max = 202m
PS150_122-1		2025-10-09T06:46:48	80.38993	-12.64987	258.9	CTD-RO	max depth	EL31 RL max = 250m
PS150_123-2		2025-10-09T15:54:24	80.48451	-12.98297	277.8	HN	Station start	
PS150_123-2		2025-10-09T15:57:42	80.48452	-12.98097	277.6	HN	Station end	
PS150_123-1		2025-10-09T16:03:18	80.48452	-12.97762	277.6	CTD-RO	max depth	EL31 RL max = 269m
PS150_123-3		2025-10-09T16:24:38	80.48435	-12.96495	277.7	LIGHT	Station start	AWI004 RL max = 150m
PS150_123-3		2025-10-09T17:18:18	80.48266	-12.93573	275.1	LIGHT	Station end	AWI004 RL max = 150m
PS150_123-4		2025-10-09T17:19:23	80.48261	-12.93522	274.9	MSN	Station start	AWI004 RL max = 263m
PS150_123-4		2025-10-09T17:49:00	80.48089	-12.92287	275.7	MSN	Station end	AWI004 RL max = 263m

Event label	Optional label	Date/Time	Latitude	Longitude	Depth [m]	Gear	Action	Comment *
PS150_123-5		2025-10-09T17:49:25	80.48086	-12.92274	275.7	MSN	Station start	AWI004 RL max = 246m
PS150_123-5		2025-10-09T18:20:51	80.47848	-12.91412	282.1	MSN	Station end	AWI004 RL max = 246m
PS150_123-6		2025-10-09T18:42:45	80.47650	-12.91108	282.0	CTD-RO	max depth	EL31 RL max = 270m
PS150_124-1		2025-10-09T21:25:47	80.54209	-13.29251	258.9	CTD-RO	max depth	EL31, max RL: 251m
PS150_124-2		2025-10-09T21:47:17	80.54075	-13.30601	258.3	MSSP	Station start	1. Cast to water; 1. Cast at depth: 233m; 2. Cast; 2. Cast at depth: 233m; 3. Cast ; 3. Cast at depth: 231m
PS150_124-2		2025-10-09T22:40:12	80.53835	-13.34072	259.9	MSSP	Station end	1. Cast to water; 1. Cast at depth: 233m; 2. Cast; 2. Cast at depth: 233m; 3. Cast ; 3. Cast at depth: 231m
PS150_125-1		2025-10-09T23:47:37	80.60452	-13.59198	134.9	CTD-RO	max depth	EL31, max RL: 129m
PS150_125-2		2025-10-10T00:03:32	80.60701	-13.59283	130.5	MSN	Station start	AWI004 RL max.: 116m
PS150_125-2		2025-10-10T00:22:06	80.60704	-13.59052	131.4	MSN	Station end	AWI004 RL max.: 116m
PS150_126-1		2025-10-10T02:37:35	80.46228	-14.66492	319.9	CTD-RO	max depth	EL31 RL max.:313m
PS150_126-2		2025-10-10T03:17:55	80.46182	-14.66456	318.9	MUC	Station start	GE52.2 RL max.:322m RT peak.: 1.2t; 2nd try (MUC did not work on

Event label	Optional label	Date/Time	Latitude	Longitude	Depth [m]	Gear	Action	Comment *
								first try); GE52.2 RL max.: 319m RL peak.:1.5t
PS150_126-2		2025-10-10T03:39:30	80.46110	-14.66314	319.9	MUC	Station end	GE52.2 RL max.:322m RT peak.: 1.2t; 2nd try (MUC did not work on first try); GE52.2 RL max.: 319m RL peak.:1.5t
PS150_127-1		2025-10-10T12:05:58	80.12711	-16.12066	257.9	ICE	Station start	
PS150_127-1		2025-10-10T17:49:00	80.16158	-15.83007	278.9	ICE	Station end	
PS150_127-2		2025-10-10T13:19:34	80.13091	-16.07000	223.6	LIGHT	Station start	AWi004 RL max.: 100m
PS150_127-2		2025-10-10T14:11:45	80.13538	-16.02531	218.4	LIGHT	Station end	AWi004 RL max.: 100m
PS150_127-3		2025-10-10T14:26:07	80.13688	-16.01085	219.1	CTD-RO	max depth	EL31 RL max.: 214m
PS150_127-4		2025-10-10T15:08:41	80.14184	-15.96422	206.5	OTTER_USV	Station start	
PS150_127-4		2025-10-10T16:55:17	80.15538	-15.86275	276.3	OTTER_USV	Station end	
PS150_127-5		2025-10-10T16:57:46	80.15567	-15.86107	276.3	ZODIAC	Station start	
PS150_127-5		2025-10-10T17:24:07	80.15875	-15.84457	278.9	ZODIAC	Station end	

Event label	Optional label	Date/Time	Latitude	Longitude	Depth [m]	Gear	Action	Comment *
PS150_127-6		2025-10-10T18:43:23	80.16743	-15.80011	305.2	CTD-RO	max depth	EL31 RL max = 298m
PS150_127-7		2025-10-10T19:26:28	80.17152	-15.77812	308.0	MUC	Station start	GE52.2 RL max = 317m; not released; 2nd attempt; GE52.2 RL max = 316m; GE52..2, max RL: 310m
PS150_127-7		2025-10-10T20:11:34	80.17483	-15.76016	297.3	MUC	Station end	GE52.2 RL max = 317m; not released; 2nd attempt; GE52.2 RL max = 316m; GE52..2, max RL: 310m
PS150_128-2		2025-10-11T00:07:07	80.11483	-15.73176	373.6	HN	Station start	
PS150_128-2		2025-10-11T00:19:11	80.11474	-15.73225	373.6	HN	Station end	
PS150_128-1		2025-10-11T00:20:54	80.11472	-15.73228	373.6	CTD-RO	max depth	EL31 RL max.: 359m
PS150_128-3		2025-10-11T00:44:37	80.11426	-15.73254	373.6	LIGHT	Station start	AWI004 RL max.:150m
PS150_128-3		2025-10-11T01:27:41	80.11415	-15.73053	376.3	LIGHT	Station end	AWI004 RL max.:150m
PS150_129-1		2025-10-11T02:42:12	80.15954	-16.03503	323.6	CTD-RO	max depth	EL31 RL max.: 311m
PS150_129-2		2025-10-11T03:04:51	80.16181	-16.02444	323.6	MSN	Station start	AWI004 RL max.: 308m

Event label	Optional label	Date/Time	Latitude	Longitude	Depth [m]	Gear	Action	Comment *
PS150_129-2		2025-10-11T03:39:10	80.16573	-16.00620	286.8	MSN	Station end	AWI004 RL max.: 308m
PS150_129-3		2025-10-11T03:40:16	80.16589	-16.00549	286.6	MSN	Station start	AWI004 RL max.: 245m
PS150_129-3		2025-10-11T04:09:35	80.16962	-15.98654	252.6	MSN	Station end	AWI004 RL max.: 245m
PS150_129-4		2025-10-11T05:21:17	80.15671	-16.04097	318.4	MUC	max depth	GE52.2 RL max = 320m; RT peak = 1,4t
PS150_130-1		2025-10-11T06:50:46	80.17793	-16.31879	154.2	CTD-RO	max depth	EL31 max = 145m
PS150_131-1		2025-10-11T08:27:24	80.19447	-16.44763	146.3	CTD-RO	max depth	Technical problem; EL31, max RL: 140m
PS150_131-2		2025-10-11T08:50:12	80.19575	-16.43755	143.6	LIGHT	Station start	Awi004, max RL 125m
PS150_131-2		2025-10-11T09:37:47	80.19736	-16.41681	137.1	LIGHT	Station end	Awi004, max RL 125m
PS150_131-3		2025-10-11T09:28:47	80.19718	-16.41990	137.3	HN	Station start	Depth: 20m
PS150_131-3		2025-10-11T09:31:30	80.19713	-16.41904	137.8	HN	Station end	Depth: 20m
PS150_131-4		2025-10-11T09:38:19	80.19739	-16.41645	136.8	MSN	Station start	AWi004, max RL: 119m
PS150_131-4		2025-10-11T10:06:39	80.19788	-16.40443	128.2	MSN	Station end	AWi004, max RL: 119m
PS150_131-5		2025-10-11T10:07:26	80.19790	-16.40431	128.4	ICE	Station start	Ice sampled

Event label	Optional label	Date/Time	Latitude	Longitude	Depth [m]	Gear	Action	Comment *
PS150_131-5		2025-10-11T10:24:38	80.19839	-16.40878	132.1	ICE	Station end	Ice sampled
PS150_132-1		2025-10-12T06:28:22	79.42369	-17.30347	413.1	CTD-RO	max depth	EL31 RL max = 396m
PS150_132-2		2025-10-12T06:55:40	79.42411	-17.30367	413.1	MSN	Station start	AWI004 RL max = 341m
PS150_132-2		2025-10-12T07:46:00	79.42441	-17.30397	413.1	MSN	Station end	AWI004 RL max = 341m
PS150_132-3		2025-10-12T08:19:04	79.42431	-17.30376	413.1	MUC	max depth	GE52,2 max RL: 411m
PS150_133-1		2025-10-12T11:32:35	79.20878	-17.44959	152.6	CTD-RO	max depth	EL31, max RL: 145m
PS150_133-2		2025-10-12T11:54:43	79.20875	-17.44913	152.6	LIGHT	Station start	AWI004 RL max.: 140m
PS150_133-2		2025-10-12T12:40:54	79.20804	-17.44977	154.7	LIGHT	Station end	AWI004 RL max.: 140m
PS150_133-3		2025-10-12T12:00:28	79.20871	-17.44899	152.7	HN	Station start	
PS150_133-3		2025-10-12T12:08:35	79.20868	-17.44857	153.6	HN	Station end	
PS150_133-4		2025-10-12T12:41:36	79.20802	-17.44979	154.7	MSN	Station start	AWI 004 RL max.: 141m
PS150_133-4		2025-10-12T13:19:16	79.20752	-17.44932	154.7	MSN	Station end	AWI 004 RL max.: 141m
PS150_134-1		2025-10-12T14:32:42	79.20856	-17.16739	370.5	MSSP	Station start	1st Cast; 343m; 2nd Cast ; 346m; 2nd Cast an Oberfläche; 3rd

Event label	Optional label	Date/Time	Latitude	Longitude	Depth [m]	Gear	Action	Comment *
								Cast; 3rd Cast an der Oberfläche
PS150_134-1		2025-10-12T15:59:30	79.20802	-17.17302	369.4	MSSP	Station end	1st Cast; 343m; 2nd Cast ; 346m; 2nd Cast an Oberfläche; 3rd Cast; 3rd Cast an der Oberfläche
PS150_134-2		2025-10-12T16:28:11	79.20831	-17.17165	369.4	CTD-RO	max depth	EL31 RL max = 354m
PS150_135-1		2025-10-12T18:00:05	79.17310	-17.03717	397.3	MOOR	Station start	Depl.: NT4-1; depl.: NT4-1; Ankerstein with Doppelreleaser, 4 Floats, ADCP, Temperature logger; Microcat; 5 Floats; Weaklink, sett…
PS150_135-1		2025-10-12T19:23:40	79.17321	-17.04780	398.0	MOOR	Station end	Depl.: NT4-1; depl.: NT4-1; Ankerstein with Doppelreleaser, 4 Floats, ADCP, Temperature logger; Microcat; 5 Floats; Weaklink, sett…
PS150_135-2		2025-10-12T20:07:20	79.16878	-17.08012	395.9	CTD-RO	max depth	EL31, max RL: 384m
PS150_135-3		2025-10-12T20:27:07	79.16812	-17.08043	396.8	MSSP	Station start	1. Cast ; 1. Cast at depth: 358m; 2. Cast ; 2. Cast at depth: 358m; 3. Cast ; 3. Cast at depth 364m

Event label	Optional label	Date/Time	Latitude	Longitude	Depth [m]	Gear	Action	Comment *
PS150_135-3		2025-10-12T21:41:31	79.16546	-17.08507	397.9	MSSP	Station end	1. Cast ; 1. Cast at depth: 358m; 2. Cast ; 2. Cast at depth: 358m; 3. Cast ; 3. Cast at depth 364m
PS150_135-4		2025-10-12T21:40:40	79.16549	-17.08501	397.9	MSN	Station start	AWI004, max RL: 344m
PS150_135-4		2025-10-12T22:21:53	79.16294	-17.08892	398.9	MSN	Station end	AWI004, max RL: 344m
PS150_135-5		2025-10-12T21:49:38	79.16504	-17.08558	397.9	HN	Station start	Depth: 20m
PS150_135-5		2025-10-12T21:52:31	79.16488	-17.08584	398.2	HN	Station end	Depth: 20m
PS150_135-6		2025-10-12T22:22:54	79.16285	-17.08907	398.9	MSN	Station start	AWI004, max RL: 369m
PS150_135-6		2025-10-12T22:54:56	79.16023	-17.09435	397.9	MSN	Station end	AWI004, max RL: 369m
PS150_135-7		2025-10-12T23:21:27	79.15763	-17.09939	397.3	CTD-RO	max depth	EL31, max RL: 382m

**Comments are limited to 130 characters. See https://www.pangaea.de/expeditions/events/PS150 to show full comments in conjunction with the station (event) list for expedition PS150.*

Abbreviation	Method/Device
ADCP	Acoustic Doppler Current Profiler
ARGOFL	Argo float
BUCKET	Bucket water sampling
CT	Underway cruise track measurements
CTD-RO	CTD/Rosette
DS3	Swath-mapping system Atlas Hydrosweep DS-3
FBOX	FerryBox
NEUMON	Neutron monitor
SD	Secchi disk
SNDVELPR	Sound velocity probe
SWEAS	Ship Weather Station
TSG	Thermosalinograph
WP2	WP-2 towed closing plankton net
XBT	Expendable bathythermograph
pCO2	pCO2 sensor

Die **Berichte zur Polar- und Meeresforschung** (ISSN 1866-3192) werden beginnend mit dem Band 569 (2008) als Open-Access-Publikation herausgegeben. Ein Verzeichnis aller Bände einschließlich der Druckausgaben (ISSN 1618-3193, Band 377-568, von 2000 bis 2008) sowie der früheren **Berichte zur Polarforschung** (ISSN 0176-5027, Band 1–376, von 1981 bis 2000) befindet sich im electronic Publication Information Center **(ePIC)** des Alfred-Wegener-Instituts, Helmholtz-Zentrum für Polar- und Meeresforschung (AWI); see https://epic.awi.de. Durch Auswahl “Reports on Polar- and Marine Research“ (via “browse”/”type”) wird eine Liste der Publikationen, sortiert nach Bandnummer, innerhalb der absteigenden chronologischen Reihenfolge der Jahrgänge mit Verweis auf das jeweilige pdf-Symbol zum Herunterladen angezeigt.

The **Reports on Polar and Marine Research** (ISSN 1866-3192) are available as open access publications since 2008. A table of all volumes including the printed issues (ISSN 1618-3193, Vol. 377-568, from 2000 until 2008), as well as the earlier **Reports on Polar Research** (ISSN 0176-5027, Vol. 1–376, from 1981 until 2000) is provided by the electronic Publication Information Center **(ePIC)** of the Alfred Wegener Institute, Helmholtz Centre for Polar and Marine Research (AWI); see URL https://epic.awi.de. To generate a list of all Reports, use the URL http://epic.awi.de and select “browse”/”type” to browse ”Reports on Polar and Marine Research”. A chronological list in declining order will be presented, and pdf-icons displayed for downloading.

Zuletzt erschienene Ausgaben:

Recently published issues:

809 (2026) The Expedition PS150 of the Research Vessel POLARSTERN to the Arctic Ocean in 2025, edited by Torsten Kanzow with contributions of the participants.

808 (2026) The Expedition PS149 of the Research Vessel POLARSTERN to the Arctic Ocean in 2025, edited by Marcel Nicolaus with contributions of the participants.

807 (2026) Expeditions to Antarctica: ANT-Land 2024/25 NEUMAYER STATION III, Kohnen Station and Field Campaigns. Edited by Julia Regnery, Peter Köhler, Thomas Matz and Christine Wesche with contributions of the participants.

806 (2026) The Expedition PS151 of the Research Vessel POLARSTERN to the Atlantic Ocean in 2025, edited by Karen H. Wiltshire, Peter Croot and Angelika Dummermuth with contributions of the participants.

805 (2026) The IsoPerm Project: Expedition to the Klondike (Yukon, Canada) in 2023, edited by Thomas Opel with contributions of the participants.

804 (2025) The Expeditions of the Research Vessels LITTORINA, LUDWIG PRANDTL and MYA II to the Elbe River, Elbe Estuary and German Bight in 2024, edited by Ingeborg Bussmann, Eric Achterberg, Holger Brix, Norbert Kamjunke, Björn Raupers and Tina Sanders with contributions of the participants.

803 (2025) The Expedition PS148 of the Research Vessel POLARSTERN to the Arctic Ocean in 2025. Edited by Jennifer Dannheim with contributions of the participants.

802 (2025) Arctic Land Expeditions in Permafrost Research in 2024. Edited by Anne Morgenstern, Lutz Schirrmeister and Milena Gottschalk with contributions of the participants.

801 (2025) The Expedition PS143/2 of the Research Vessel POLARSTERN to the Arctic Ocean in 2024. Edited by Katja Metfies with contributions of the participants.

800 (2025) The Expedition PS143/1 of the Research Vessel POLARSTERN to the Arctic Ocean in 2024. Edited by Frank Wenzhöfer with contributions of the participants.

ALFRED-WEGENER-INSTITUT
HELMHOLTZ-ZENTRUM FÜR POLAR-
UND MEERESFORSCHUNG

BREMERHAVEN

Am Handelshafen 12
27570 Bremerhaven
Telefon 0471 4831-0
Telefax 0471 4831-1149
www.awi.de

HELMHOLTZ